Synthesis of Polyoxometalates for Detailed Solution Reactivity Studies

Thompson Izuagie

A thesis submitted in partial fulfilment of the requirements for the award of

Doctor of Philosophy

School of Natural and Environmental Sciences
(Chemistry)
Newcastle University,
Newcastle upon Tyne, UK

December 2017

Abstract

Non-aqueous methodologies provide an opportunity to access a range of polyoxometalates that may not be stable in H_2O and enable mechanistic studies into hydrolytic and protonation behaviours, which are fundamental to polyoxometalate chemistry. ^{17}O-enriched $(TBA)_6[NaPW_{11}O_{39}]$ was prepared *via* an efficient non-aqueous route and shown to be a suitable precursor to $[(L)MPW_{11}O_{39}]^{n-}$ (M = Sn^{2+}, Pb^{2+}, Bi^{3+}, Sb^{3+}, Sn^{4+}, Ti^{4+}) for detailed systematic studies. Reactions were monitored by ^{31}P NMR while products were characterised by FT-IR, multinuclear NMR (^{1}H, ^{13}C, ^{17}O, ^{31}P, ^{119}Sn, ^{183}W and ^{207}Pb), solid state NMR, ESI-MS, CHN microanalysis, UV-Vis and/or single crystal XRD. Using this approach, the readily-hydrolysable tin derivatives, $(TBA)_4[(CH_3O)SnPW_{11}O_{39}]$ and $(TBA)_8[(\mu\text{-}O)(SnPW_{11}O_{39})_2]$ were prepared for the first time and the previously reported $(TBA)_4[(HO)TiPW_{11}O_{39}]$ was shown to be stable in DMSO for up to 3 months possibly due to interaction between HO- and DMSO. As a result of the more ionic character of Sn—OCH_3 bond compared with Ti—OCH_3, $(TBA)_4[(CH_3O)SnPW_{11}O_{39}]$ was observed to hydrolyse faster than $(TBA)_4[(CH_3O)TiPW_{11}O_{39}]$ whereas $(TBA)_4[ClTiPW_{11}O_{39}]$ with a large excess of H_2O hydrolysed more readily than $(TBA)_4[ClSnPW_{11}O_{39}]$. Although $(TBA)_4[(HO)TiPW_{11}O_{39}]$ underwent condensation to $(TBA)_8[(\mu\text{-}O)(TiPW_{11}O_{39})_2]$ easily in acetonitrile at room temperature, this reaction only occured for $(TBA)_4[(HO)SnPW_{11}O_{39}]$ at elevated temperature (~120^oC) in the presence of a water-scavenging agent such as N, N'-dicyclohexylcarbodiimide (DCC). These experimental observations were consistent with DFT calculations on the energetics of the hydrolysis and condensation of $(TBA)_4[(CH_3O)SnPW_{11}O_{39}]$ and $(TBA)_4[(CH_3O)TiPW_{11}O_{39}]$. Protonation studies on the ^{17}O-enriched POMs provided insights into protonation of the MOW sites in $(TBA)_4[(CH_3O)TiPW_{11}O_{39}]$, $(TBA)_4[ClM^{IV}PW_{11}O_{39}]$ (M = Sn, Ti), $(TBA)_5[M^{II}PW_{11}O_{39}]$ (M = Sn, Pb) and $(TBA)_4[M^{III}PW_{11}O_{39}]$ (M = Sb, Bi) and protonation at both TiOW and TiOTi sites in $(TBA)_8[(\mu\text{-}O)(TiPW_{11}O_{39})_2]$ whilst reactions between $(TBA)_8[(\mu\text{-}O)(TiPW_{11}O_{39})_2]$ and electrophiles indicated possible formation of adducts. Treatment of $(TBA)_4[(L)SnPW_{11}O_{39}]$ (L = Cl, HO) with $NaBH_4$ resulted in reduction of the tin heteroatom only whereas reaction between $(TBA)_5[Sn^{II}PW_{11}O_{39}]$ and halogens (Br_2 and I_2) or the molybdate $(TBA)_3[PMo_{12}O_{40}]$ showed oxidation of tin (II). Electrochemical studies in acetonitrile revealed no redox processes associated with the heterometals in $(TBA)_4[(L)Sn^{IV}PW_{11}O_{39}]$ and $(TBA)_5[Pb^{II}PW_{11}O_{39}]$ while redox waves assigned to Sn^{2+}/Sn^{4+} were observed for

Abstract

$(TBA)_5[Sn^{II}PW_{11}O_{39}]$ within the potential range studied. Finally, attempts to prepare Lindqvist-type derivatives, $[(L)MW_5O_{18}]^{n-}$ (M = Co^{2+}, Mo^{2+}, Sn^{2+}, Pb^{2+}, Fe^{2+}, Cu^{2+}, Cr^{3+}, Sb^{3+}, Bi^{3+}) from a tungstate precursor prepared by hydrolysis of a 3:2 mixture of $(TBA)_2WO_4$ and $WO(OMe)_4$ provided evidence that only in certain cases were the required heterometalates formed. Acetonitrile hydrolysis was observed under reaction conditions and the acetamide adduct $(TBA)_3[\{CH_3C(O)NH_2\}CoW_5O_{17}(OMe)]$ was characterised crystallographically. An attempt to prepare $[(L)Mo^{II}W_5O_{18}]^{4-}$ produced the crystallographically characterised, one-electron reduced $(TBA)_3[W_6O_{19}]$.

Dedication

To my beloved family!

"There is no such thing as a failed experiment, only experiments with unexpected outcomes"

~ Richard Buckminster Fuller

Acknowledgements

All praise to God Almighty for this unique opportunity and for seeing me through the accompanying travails.

My sincere gratitude to my supervisor, Dr. R. John Errington for his tutelage, guidance and immense support. He introduced me to the field of Polyoxometalate Chemistry and has greatly sharpened my skills in air-sensitive techniques and synthetic metalorganic chemistry. He has always ensured that I understood the underlying principles behind all techniques, apparatus and equipment that I employed and every opportunity to interact with him has been very enlightening. He has been very supportive in my difficult moments and has always ensured that I promptly regain my confidence whenever I am down. His door has always been opened to me and his humorous touch to everything (especially difficult cases) has seen me through the programme. He also provided me the opportunity to interact and network with leading scientists in the POM community. Thank you very much John – I will forever be indebted to you!

I greatly acknowledge the immeasurable guidance and contributions of Professor Walter G. Klemperer, who was very thorough with me during my interaction with him. He has insisted that I understand the operations and principles of all my working techniques and working with him has instilled a good degree of thoroughness in me – many thanks Prof.! I wish I had had a longer interaction with you.

I thank Dr. Corinne Wills and Prof. William McFarlane for NMR spectroscopy, which was a major characterisation technique in my thesis. You have simply been great to me! I thank Dr. Paul Waddell for Single Crystal X-ray Crystallography, Dr. D. C. Apperley (Durham University) for Solid State NMR and Drs. Jennifer Mathieson and Maria Diana Castro Spencer of the Cronin Group, University of Glasgow for ESI-MS analysis and advice on interpreting the spectra.

I equally would want to thank Prof. Pedro De Oliveira and Dr. Israël Mbomekalle of the electrochemistry and photochemistry team at Université Paris-Sud, Orsay, France for their wonderful supervision during my COST-Action visit to their Lab.

I thank Dr. Magda Boras Pascual and the group of Prof. Josep M. Poblet at the Universitat Rovira i Virgili, Tarragona, Spain for computational analysis.

My gratitude to academics in the Synthesis and Spectroscopy group of the School for their support and advice. Worthy of mentioning are Retired Prof. Richard Henderson, Dr. Keith Izod and Dr. Simon Doherty. I also thank Dr. Jerry Hagon for his superb IT support.

My warmest appreciations go to the technical staff of the School of Chemistry for their support during my time in the lab. I especially appreciate Geoffrey Reah and Christopher Burrow (Electrical workshop), John Corner and, Gary Day (Mechanical workshop), William McCormack and Robyn Hare (Glassblowers), Dr. Rachael Dack (ESIMS) and Dr. Mark Garner (IT support).

I acknowledge the research support staff of the School of Chemistry including Joanne Lakey, Claire Nicole, Kate Kirkpatrick and Jane of the School Office and Robin Ingleton retired stores officer.

A very big thank-you to former Head of School, Prof. Mike Green and his PA, Mrs. Isobel Lamb for their great assistance while applying for visa and during their time in office.

I am greatly indebted to the Niger Delta Development Commission (NDDC) for granting me PhD scholarship, Sokoto State University for granting me study fellowship, COST Action CM1203 for funding to attend workshops, conferences and an STSM visit to Orsay and the Royal Society of Chemistry for funding to attend a conference.

My sincere gratitude goes to my parents – Mr and Mrs. Paul Izuagie for their support (financially and otherwise) during the period of my studies. May the good Lord grant them good health and long life to reap the fruits of their labour. To my siblings, Clement, Juliet, Omoh, Aloaye, Ezekiel, Johnpaul, Peter and Louis – I say thank you for your support, spiritually and otherwise.

I also appreciate the contributions of Prof. G. V. Ardo, former Hon. Special Adviser, Department for Higher Education, Sokoto State; the family of Barr. and Mrs. Jibril O. Uwadiae and Late Prof. S. O. Eguare and his wife.

Also, I thank Very Rev. Fr. Nuhu Iliya, my spiritual director for his advice, spiritual and financial support while I was processing my NDDC application and all through my PhD programme. I equally thank all members of the Parish Pastoral Council, Our Lady of Perpetual Help Catholic Church, Old Airport, Sokoto for their prayers and support.

To Dr. Eimer Tuite and Niamh who have become a family to me, I say many thanks for making Newcastle a second home to me.

My gratitude also goes to the Vice-Chancellor, Sokoto State University; the Registrar, Hajiya Amina Yusuf Garba, MON (for her motherly support); the Dean, Faculty of Science and Head of Chemistry Department, Dr. Surajo and the entire staff of Chemistry Department for their assistance in one way or the other.

I would also want to express my indebtedness to my wonderful group members – Daniel Lebbie, Lan Feng and Kate Phipps and Einas Abood and Tom Backhouse of the SD group. And to my friends and compatriots in Newcastle – Dr. Thaer Al-Rammahi, Benafa Oyinkuro, Hector Oyem, Chinedu Nwali, Dr. Osa Ighodaro, Oshido Banabas, Dr. Steve Nomor, Charles Orji, Mansur Yahaya, Dr. Emmanuel Oriaifo – I say thank you for your time and company.

I acknowledge the support of the following either while pursuing my NDDC application or during my PhD study: Mustapha Musa, Lawrence Eruke Mukoro, Dr. D. M. Sahabi, Prof. L. G. Hassan, Dr. A. Uba, HRH Peter Osigbemeh, Dr. Hon. Chief Oshiobugie Ojor, Hon. Abdulmalik Suleiman Afegbua, Edoh Ayesemeh, Bro. Joe PH, Sunny, his wife and his dad, Babau, Mrs. Shittu of NDDC, Mustapha Mohammed, Mama Courage, I. I. Igbagbe, Amanda Tilley of Kings Gate, Fr. George Ehusani, Fr. Solomon Uko, Samson Thomas of UPS, my Mairuwa friend at Aloaye's house, Legion of Mary (in Sokoto and St. Charles Lwanga, Abuja), Eddy (Bishop), Modu, Afor, Dr. Natalia Maksimchuk, Dr. Sergey Adonin, Dr. Yan Duan, Cheryl, Mathei, Francisca Dixon, Prof. Terry and Gaby Wright, Mike Hannon, Fr. Shaun O'Neil and Anthony of St. Roberts and Bill from London.

Lastly, to all those who have contributed in one way or the other to the successful completion of my studies and whose names are not mentioned here, I say thank you.

Table of contents

List of Figures

List of Tables

List of Schemes

Abbreviations

^{119}Sn:	Tin-119
^{13}C:	Carbon-13
^{17}O:	Oxygen-17
^{183}W:	Tungsten-183
^{195}Pt:	Platinum-195
^{1}H:	Proton
^{207}Pb:	Lead-207
2D-INADEQUATE:	Two-dimensional Incredible natural-abundance double-quantum transfer experiment
^{31}P:	Phosphorus-31
3D:	Three-dimensional
Å:	Armstrong
ATR:	Attenuated Total Reflectance
CASSCF:	Complete Active Space Self Consistent Field
CHN:	Carbon, Hydrogen and Nitrogen
COST:	An intergovernmental framework for European Cooperation in Science and Technology
COSY:	Correlation Spectroscopy
CoTAPc:	Cobalt tetraaminophthalocyanine
CSI:	Cryospray Ionization
CV:	Cyclic Voltammetry
DCC:	N, N'-dicyclohexylcarbodiimide
DCM:	Dichloromethane

DFT: Density Functional Theory

DMF: Dimethylformamide

DMSO: Dimethyl sulfoxide

ECPB: Electron-coupled-proton buffer

EI: Electron Impact Ionization

ESI: Electrospray Ionization

Et_2O: Diethyl ether (ether)

EXSY: Exchange Spectroscopy

FAB: Fast Atom Bombardment

FTIR: Fourier Transformed Infrared

Fwhm: Full width at half maximum

GCE: Glassy carbon electrode

H_2biim: 2,29-biimidazole

HKUST-1: Hong Kong University of Science and Technology

H_xPOM: Protonated forms of Polyoxometalates

Hz: Hertz

ICP AES: Inductively Coupled Plasmas Atomic Emission Spectroscopy

KRS-5: Thallium Bromoiodide (TlBr-TlI)

LBL: Layer-by-Layer

LCAO: Linear Combination of Atomic Orbitals

LH_3: Tris(2-hydroxy-3,5-di-tert-butylbenzyl)amine

MALDI: Matrix-Assisted Laser Desorption/Ionization

MeCN: Acetonitrile

MeOH: Methanol

MOF: Metal Organic Framework

MR: Miolati- Rosenheim

MS: Mass Spectrometry

NLO: Non-linear optical

NMR: Nuclear Magnetic Resonance

PAH: Polyallylamine hydrochloride

PDDA: Poly(dimethyl diallyl ammonium chloride)

Phnz: Phenazine

POM: Polyoxometalate

ppm: Parts per million

PtNPs: Platinum nanoparticles

PXV: Poly(hexyl viologen)

RAM: Random Access Memory

RB: Rhodamine B

REDOX: Oxidation and Reduction

RF: Radio Frequency

rGO: Reduced graphene oxide

SAIL: Surface Active Ionic Liquid

SCF: Self-Consistent Field

SMM: Single Molecule Magnet

STSM: Short Term Scientific Mission

TBA: n-Tetrabutylammonium

THF: Tetrahydrofuran

TM: Transition metal

TMA: Tetramethylammonium

UV-Vis: Ultraviolet and Visible Spectroscopy

X_2M_{15}: $[X_2M_{15}O_{56}]^{n-}$

X_2M_{17}: $[X_2M_{17}O_{61}]^{n-}$

X_2M_{18}: $[X_2M_{18}O_{62}]^{n-}$

XM_{11}: $[XM_{11}O_{39}]^{n-}$

XM_{12}: $[XM_{12}O_{40}]^{n-}$

XM_9: $[XM_9O_{34}]^{n-}$

XRD: X-ray Diffraction

Chapter 1

Introduction

This chapter gives a brief background into polyoxometalates (POMs) and current interest in POM chemistry. It enumerates the objectives of the thesis highlighting the rationale for the projects contained in this thesis. Finally, it gives a summary of the thesis structure.

1. Introduction

1.1 Background to the Study

Polyoxometalates (POMs) are anionic molecular metal oxide clusters formed by early transition metals in their highest oxidation states.[1-5] The self-assembly, composition, structure, reactivity and applications of these clusters have been and still remain major areas of interest. They have been investigated in a wide range of applications including catalysis,[4] energy conversion and storage; magnetic, electronic and photonic devices and medicine.[6-9] Presently, specific uses of POMs include the use of POM-MOF hybrids for absorption and sensing applications;[10] catalysts for activation of C-H and C-O bonds, biomass conversion, photocatalytic water splitting and lithium ion batteries; POM-stabilised metal nanoparticles and POMs for molecular spintronics.[6,9,11,12] These applications stem from their uniquely versatile properties, based on their composition, size, shape, redox, magnetic, photophysical and chemical behaviours.[5] A thorough understanding of these properties especially in solution provides atomic-level control over properties and functions of materials based on these molecular metal oxides. Most studies on POMs have been *via* aqueous strategies, while much non-aqueous POM synthesis and reactivity remains unexplored. The implication of this, is a limited understanding of fundamental POM solution chemistry (*i.e.* self-organisation and assembly from complex mixtures of precursors, electronic properties and chemical reactivity). Therefore, there is great need for a corresponding development in reliable and flexible non-aqueous POM synthetic methods and detailed insights into associated chemistry in non-aqueous media. This, will facilitate the widespread adoption of POMs in the production of robust materials for challenging applications where precise control is of utmost importance.

1.2 Aims and Objectives

This thesis therefore aims to address some key questions in POM chemistry and contribute towards the development of a comprehensive understanding of the non-aqueous solution chemistry associated with POM synthesis and reactivity based on generic methods developed at Newcastle.

In this regard, the work discussed in this thesis addresses six main objectives organized across six chapters (Chapters 3 to 8). The objectives are to:

i. Establish a versatile platform (for developments in POM science), using non-aqueous methods developed in Newcastle, for targeted, efficient synthesis of a range of ^{17}O-enriched heterometallic POMs for systematic studies in protonolysis and hydrolysis.

ii. Design and synthesise multi-functional POMs that will show reactivity and/or properties that are crucial to advances in catalysis and molecular nanoscience.

iii. Gain insights into the protonation and hydrolytic behaviours of a series of ^{17}O-enriched heterometallic POMs.

iv. Establish the use of POMs as 'non-innocent' ligands in organometallic chemistry.

v. Gather data on POM families to enable an understanding of variations in properties through computational modelling.

vi. Develop some understanding of the electrochemistry and redox properties of a range of POMs in non-aqueous media.

1.3 Structure of the Thesis

This thesis is divided into ten chapters. Chapter 1 provides a brief background to the work contained in the thesis. It gives the thesis aims and objectives and outlines the general structure. Chapter 2 is a literature study, which discusses some relevant background including major historical developments in POM chemistry. It describes the classification, properties, synthesis, characterisation techniques and applications of POMs. Some early works on the chemistry of POM solutions and speciation are given at the end of the chapter.

Chapter 3 builds on previous work in the Errington group and discusses an efficient non-protic approach to a range of ^{17}O-enriched monosubstituted heterometallic Keggin POMs *via* non-aqueous substitution into $(TBA)_6[NaPW_{11}O_{39}]$.

Chapter 4 examines the hydrolysis and condensation of a series of tin- and titanium-substituted monolacunary Keggin POMs in acetonitrile and DMSO. It also discusses chemical reduction of $(TBA)_4[(L)Sn^{IV}PW_{11}O_{39}]$ (L = Cl, OH).

Chapter 5 discusses attempts to understand trends in surface oxygen basicity in the POM series $(TBA)_4[(L)M^{IV}PW_{11}O_{39}]$ (M = Ti, Sn; L = Cl, OH, CH_3O) and $(TBA)_8[(\mu\text{-}O)(TiPW_{11}O_{39})_2]$ and also investigate possible metal binding sites in $(TBA)_8[(\mu\text{-}O)(TiPW_{11}O_{39})_2]$ using ^{17}O and ^{31}P NMR and FT-IR techniques.

Chapter 6 describes protonolysis of $(TBA)_5[M^{II}PW_{11}O_{39}]$ (M = Sn and Pb) and $(TBA)_4[M^{III}PW_{11}O_{39}]$ (M = Sb and Bi). Furthermore, the chapter discusses the non-aqueous reactivity and redox properties of $(TBA)_5[M^{II}PW_{11}O_{39}]$ (M = Sn and Pb) with a range of reagents.

Chapter 7 discusses results from a COST Action Short-Term Scientific Mission (STSM) visit to the photo- and electrochemistry team of Prof. Pedro de Oliveira and Dr. Israël M. Mbomekalle at Laboratoire de Chimie Physique (LCP), Université Paris-Sud, Orsay, France. It examines the solution electrochemistry of a range of post-transition metal monosubstituted Keggin POMs in MeCN.

Chapter 8 describes attempts to extend the non-aqueous hydrolytic aggregation approach developed in the Errington group to a range of metal substituted Lindqvist-type polyoxotungstates , $[(L)MW_5O_{18}]^{n-}$ (M = Mo^{2+}, Co^{2+}, Sn^{2+}, Pb^{2+}, Fe^{2+}, Cu^{2+}, Cr^{3+}, Sb^{3+}, Bi^{3+}) *via* reactions between the 'virtual' pentatungstate anion, $[W_5O_{18}]^{6-}$ and metal salts.

Chapter 9 enumerates milestones achieved in the course of the works described in this thesis and provides a general conclusion to the findings of the thesis. Additionally, it highlights some possible areas for further studies.

Chapter 10 contains the experimental details and describes materials, instrumentation and methods (including synthesis and reactivity study) employed in carrying out the research work discussed in this thesis. Finally, full and simulated NMR spectra, expansions and simulated ESIMS spectra and crystallographic data are given in the appendices section.

REFERENCES

1. M. Ammam, *J. Mater. Chem. A*, 2013, **1**, 6291-6312.
2. P. W. Atkins, T. L. Overton, J. P. Rourke, M. T. Weller and F. A. Armstrong, *Shriver & Atkins' Inorganic Chemistry* Oxford University Press Oxford, 5th edn., 2010.
3. R. J. Errington, S. S. Petkar, P. S. Middleton, W. McFarlane, W. Clegg, R. A. Coxall and R. W. Harrington, *J. Am. Chem. Soc.*, 2007, **129**, 12181-12196.
4. I. Kozhevnikov, *Catalysis by Polyoxometalates*, John Wiley and Sons Ltd, England, 2002.
5. M. T. Pope, *Heteropoly and Isopoly oxometalates* Springer-Verlag Berlin, New York, 1983.
6. D. L. Long, R. Tsunashima and L. Cronin, *Angew Chem Int Ed Engl*, 2010, **49**, 1736-1758.
7. D.-L. Long, E. Burkholder and L. Cronin, *Chem. Soc. Rev.*, 2007, **36**, 105-121.
8. D.-L. Long and L. Cronin, *Chem. Eur. J.*, 2006, **12**, 3698-3706.
9. A. Proust, B. Matt, R. Villanneau, G. Guillemot, P. Gouzerh and G. Izzet, *Chem. Soc. Rev.*, 2012, **41**, 7605-7622.
10. Y. Yang, S. Liu, C. Li, S. Li, G. Ren, F. Wei and Q. Tang, *Inorg. Chem. Commun.*, 2012, **17**, 54-57.
11. D. Barats-Damatov, L. J. W. Shimon, L. Weiner, R. E. Schreiber, P. Jimenez-Lozano, J. M. Poblet, C. de Graaf and R. Neumann, *Inorg. Chem.*, 2014, **53**, 1779-1787.
12. M. T. Pope and A. Müeller, *Mol. Eng.*, 1993, **3**, 1-8.

Chapter 2

Background

This chapter discusses some relevant background including major historical developments in POM chemistry, POMs classification, properties, synthesis, characterisation techniques and applications. The chapter concludes by reviewing early studies on POM solution chemistry and speciation.

2. Background

2.1 Introduction

Polyoxometalates (POMs) are molecular metal oxoanions with nuclearities ranging up to 368 metal atoms per molecule, making them nanoscale in dimension.[1] They are formed by early transition metals especially members of Group 5 and 6 (V, Nb, Ta, Mo and W) in their highest oxidation states. Derivatives of heavier 4d and 5d metals (Mo and W) are most common because of a suitable mix of ionic radius and charge and accessibility of empty d orbitals for π bonding with oxygen.[2] These properties make the 4d and 5d metals easily share oxido ligands between vertices or edges (or rarely between faces) in their polyhedral framework as opposed to their 3d congeners, which can only share oxido ligands between vertices (due to their smaller size).[3] The oxoanions may also contain a wide variety of heteroelements such as P, As, Si and Ge.[1]

Although the history of POM chemistry can be traced to 1783, when the D´Elhuyar brothers discovered a yellow spicy/bitter tasting salt, now known as ammonium 12-phosphomolybdate, $(NH_4)_3[PMo_{12}O_{40}]$ from the reaction between ammonium molybdate and phosphoric acid;[4] the field is still very fertile with several groups around the world working actively to understand fundamental aspects and further explore their application in areas such as catalysis, nanoscience, sensing, energy systems and medicine. Pope[5] and Baker[6] have given historical accounts on the field and some major developments are highlighted in **Table 2.1**. Today over ten thousand publications on various aspects of POM chemistry are indexed in the Web of Science.

Table 2.1. Timeline of some major developments in POM chemistry.

Scientist	Year	Contributions	Ref
Juan José D´Elhuyar (Logroño, 1754) and Fausto D´Elhuyar (Logroño, 1755)	1783	Discovered a yellow spicy/bitter tasting salt, now known as ammonium 12-phosphomolybdate, $(NH_4)_3[PMo_{12}O_{40}]$ from the reaction of ammonium molybdate with phosphoric acid.	4
J. J. Berzelius	1826	Serendipitously also made a yellowish ammonium 12-molybdophosphate $[(NH_4)_3PM_{12}O_{40}]$ from reaction of phosphoric acid and ammonium molybdate.	7
L. Svanberg and H. Struve	1848	Initiated the use of ammonium 12-molybdophosphate in analytical chemistry.	8
C. Marignac	1862	Discovered tungstosilicic acids and their salts.	9,10
A. Miolati R. Pizzighelli A. Rosenheim	1908	Formulated the Miolati- Rosenheim (MR) theory, which stated that the structure of heteropolyacids was based on 6-co-ordinate heteroatoms with MO_4^{2-} or $M_2O_7^{2-}$ anions as ligands or bridging groups.	5,11
L. Pauling	1929	Proposed that 12:1 complexes were based on the arrangement of 12 MoO_6 or WO_6 corner sharing octahedral around a central XO_4 tetrahedron.	12
J. F. Keggin	1933	Solved the structure of $H_3PW_{12}O_{40}.5H_2O$ by X-ray diffraction and noted that it was based on WO_6 octahedral units connected by shared edges as well as corners as opposed to Pauling's proposal.	13
A. J. Bradley and J. W. Illingworth	1936	Confirmed the structure of $H_3PW_{12}O_{40.}29H_2O$	14
J. S. Anderson	1937	Suggested possible structures for 6:1 heteropolyanions and for para(hepta)molybdate anion $[Mo_7O_{24}]^{6-}$	15
H. T Evans	1948	Reported the structure of $[TeMo_6O_{24}]^{6-}$	16
I. Lindqvist	1950	Reported structure of $[Mo_7O_{24}]^{6-}$	17
I. Lindqvist	1952	Reported structure of $[Nb_6O_{19}]^{8-}$	18
P. Souchay	1969	Provided support for dimerization in the Dawson POM.	19

2.2 Classification

POMs have been classified in different ways. One form of classification is based on their basic structure, that is Lindqvist, Keggin, Dawson, etc.[1,20,5] Another is based on whether they possess a central heteroatom or not, i.e. heteropolyanion or isopolyanion.[5] In 2010, Cronin and co-workers provided a polyoxometalates periodic table, which broadly captures all the different classes of POMs, showing the nuclearities, types and the broad range of known structures. The table (**Figure 2.1**[21]) also highlighted already isolated generic building blocks (structures in boxes with solid lines) and proposed structural building blocks that were yet to be isolated as clusters but could be identified as building blocks for POMs with high-nuclearity (structures in dash lines). Though the table highlights all forms of POMs classification, the following sections will briefly discuss the structural-based classification only.

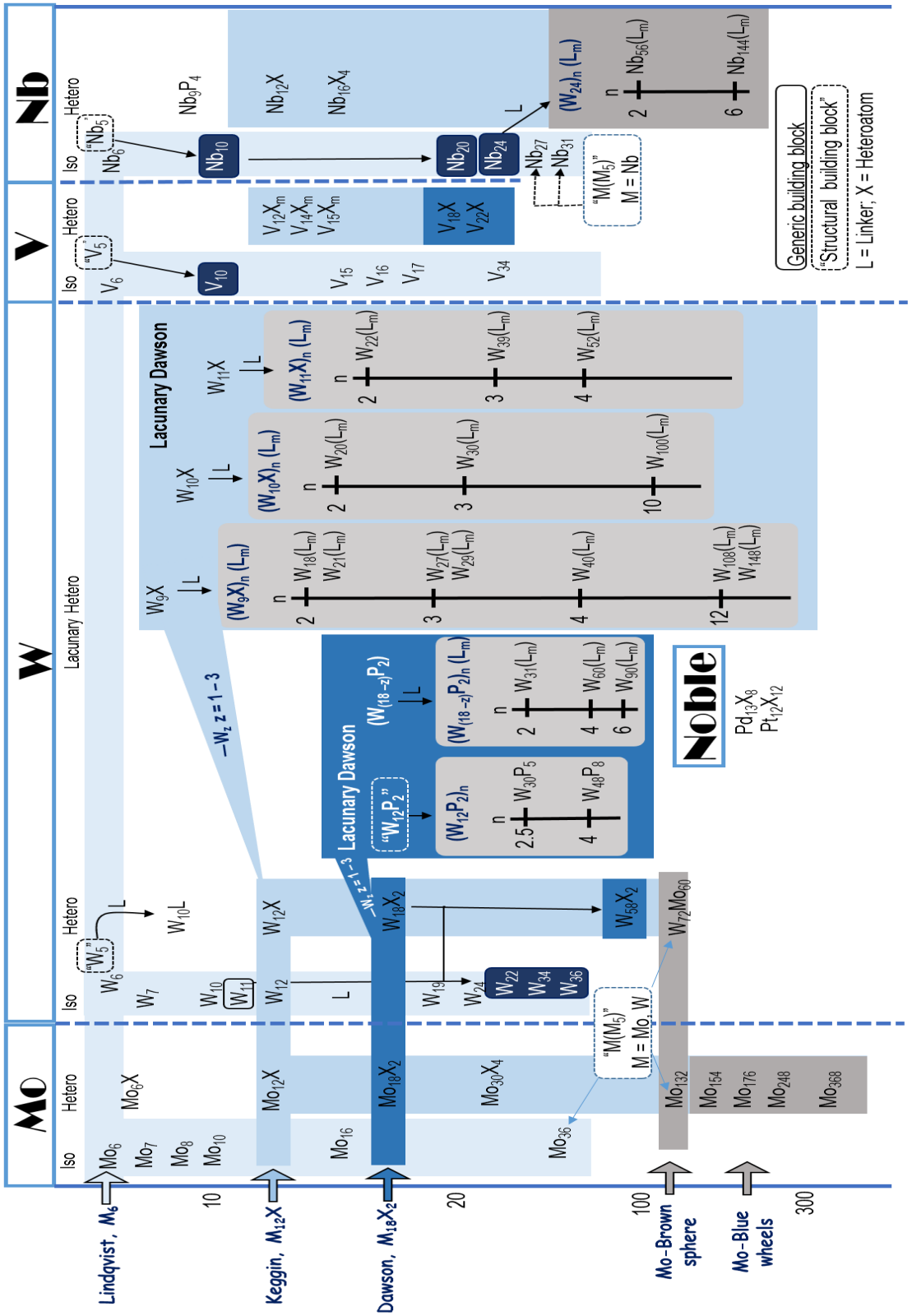

Figure 2.1: A periodic table of POMs adapted from Cronin and co-workers.[21]

2.2.1 Lindqvist structure

The Lindqvist or hexametalate POM is perhaps the simplest POM family. Members of this class possess an O_h symmetry and have six edge-shared octahedral with a central octahedrally-coordinated oxido ion. The structure is thus considered as a neutral metal-oxygen cage encapsulating an oxido ion as shown in **Figure 2.2**. Polyanions with this structure include the basic structures $[Mo_6O_{19}]^{2-}$, $[W_6O_{19}]^{2-}$, $[Nb_6O_{19}]^{8-}$ and $[Ta_6O_{19}]^{8-}$ and the heterometallic derivatives $[V_2W_4O_{19}]^{4-}$, $[Nb_3W_3O_{19}]^{5-}$,[5] $[(L)TiW_5O_{18}]^{3-}$,[22] $[(L)SnW_5O_{18}]^{3-}$[23] and $[(py)CoTiW_5O_{18}H]^{3-}$.[24] They usually contain terminal O atoms (O_T), which are seen as projecting out from a single metal atom and two types of bridging O atoms: one that bridges two-metals (M-O-M) (O_B), and another hyper-coordinated O atom in the centre of the structure that is common to all six metal atoms (O_C).[5]

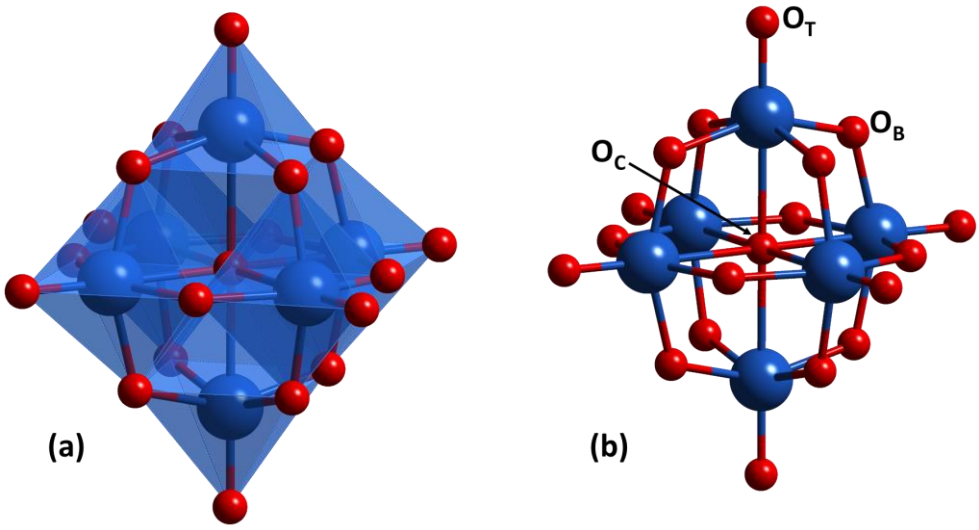

Figure 2.2: (a) Polyhedral representation and (b) Ball and stick representation of Lindqvist POM; oxygen (red), metal (royal blue); O_T, terminal oxygens; O_B, bridging OM_2 oxygens and O_C, central OM_6 oxygens

2.2.2 Keggin structure

POMs with the Keggin structure are the most widely studied and used. They have the general formula $[XY_mM_{(12-m)}O_{40}]^{(3+m)-}$, where X is the central heteroatom and M and Y are the addenda atoms. The heteroatom X is bonded to four oxygen atoms to form a tetrahedron, XO_4 (X = P, As, Si, Ge) at the centre of the structure, which links twelve MO_6 and YO_6 octahedra units (M =V, Nb, Ta, Mo, W; Y = V, Cr, Mn, Co, Fe, etc) *via* corner or edge sharing oxygen atoms.[5,25] In the parent Keggin structure (m = 0, i.e. $[XM_{12}O_{40}]^{3-}$; M = Mo, W, X = P,

As), the octahedra assemble to form trimetallic groups, (M_3O_{13}) (triads) and the four triads surround the central heteroatom X to form (XO_4)$M_{12}O_{36}$ with twelve (M=O) terminal oxygens, twenty-four (MOM, 1 and 2) bridging oxygens (1 connecting edge-sharing octahedra and 2 connecting corner-sharing octahedra) and four internal oxygens (M_3OP) [see **Figure 2.3 (a)** and **(b)**]. Like other POM structures, it is convenient to represent them as XM_{12}.[5] Keggin POMs are widely applied as catalysts because of their many attractive properties, which include: strong Brønsted acidity of the H_xPOM forms, high proton mobility, fast multielectron transfer, high solubility in various solvents and pH dependent resistance against hydrolytic/oxidative degradations in solution.[5,25]

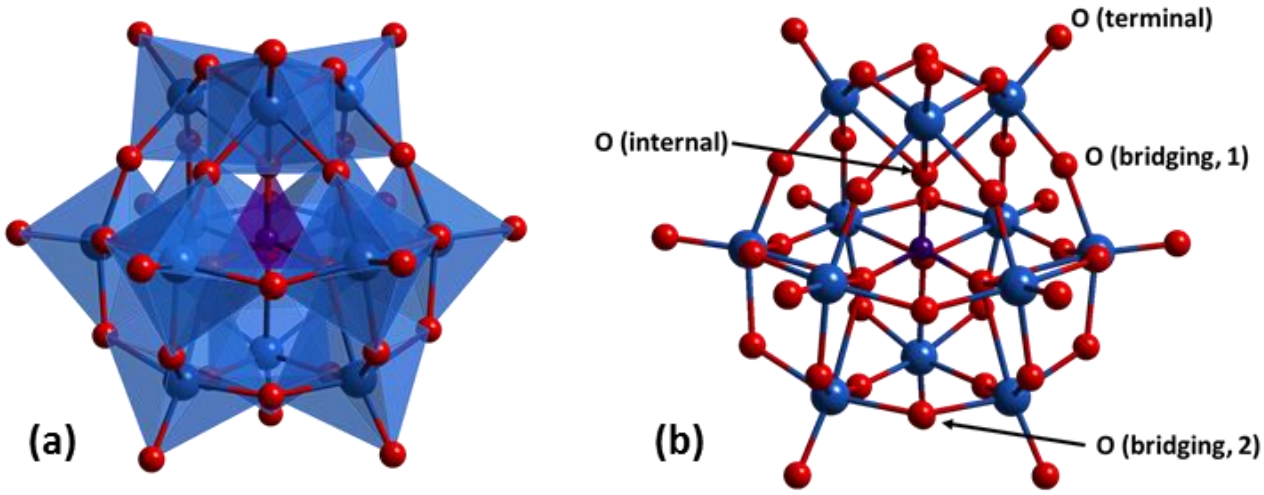

Figure 2.3: (a) Polyhedral and (b) ball and stick model of Keggin structure; oxygen (red), metal (royal blue), central heteroatom (purple).

The Keggin family of POMs exhibit isomerism with five known isomers. The first isomer corresponds to the α-isomer, which is the most stable Keggin form. It has a T_d symmetry and isomerism in the Keggin anion is due to rotation of one or more M_3O_{13} group about the C_3 axes of the T_d symmetry (see **Figure 2.4**).[1,5] Rotation of one of the four M_3O_{13} groups by 60° yields the β-isomer with a C_{3v} symmetry. The third isomer, γ-isomer with a C_{2v} symmetry is formed by rotation of two of the four M_3O_{13} groups by 60° while rotation of three of the four M_3O_{13} groups by 60° produces the δ isomer with a C_{3v} symmetry. The fifth isomer (ε-isomer) having a T_d symmetry arises from rotation of all the M_3O_{13} groups by 60°.

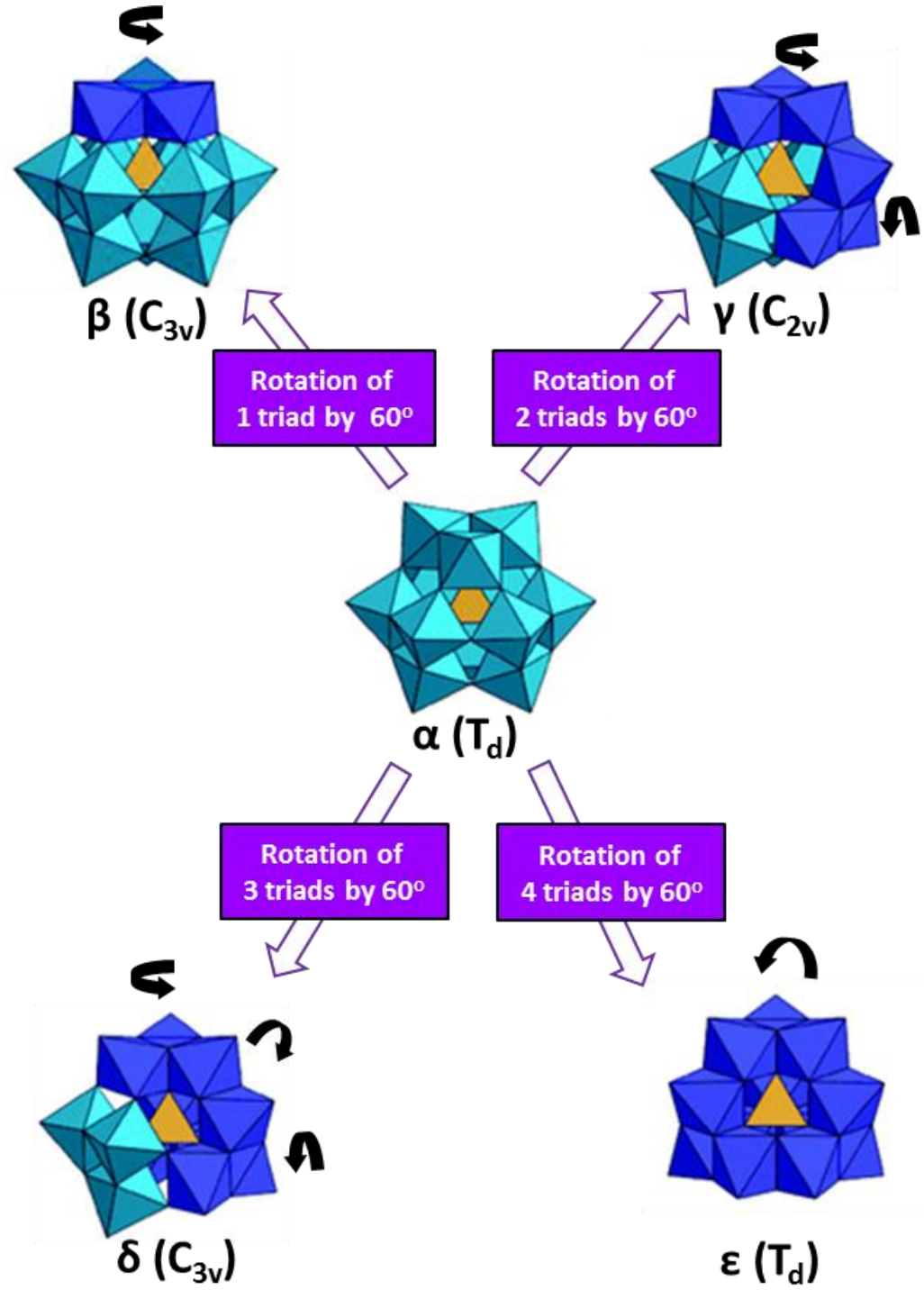

Figure 2.4. Isomerism in Keggin POMs (the five Baker-Figgis isomers)

Keggin POMs form lacunary or defect polyanions such as $XW_{11}O_{39}^{y-}$ and $XW_9O_{34}^{z-}$ by the loss of one or more of the addenda atoms.[5]

2.2.3 Wells-Dawson structure

Wells-Dawson (also called Dawson) POMs are formed as a result of the dimerization of two lacunary Keggin monomers, $XW_9O_{34}^{z-}$. In the Dawson structure, $X_2M_{18}O_{64}^{p-}$, two distinguishable structural arrangements are possible: (i) dimetallic groups (M_2O_{10}) resulting from the condensation of two octahedra of which the centres are occupied by metal atoms and the vertices by oxygen atoms and (ii) trimetallic groups (M_3O_{13}) resulting from the combination of three MO_6 octahedra as earlier explained in the Keggin structure. Each group is connected to the heteroatom, X and the two $XW_9O_{34}^{Z-}$ fragments are joined together *via* M-(μ-O)-M bridges to give the Dawson structure ($X_2M_{18}O_{64}^{p-}$).[1] As shown in **Figure 2.5**, the MOM linkages are almost linear.

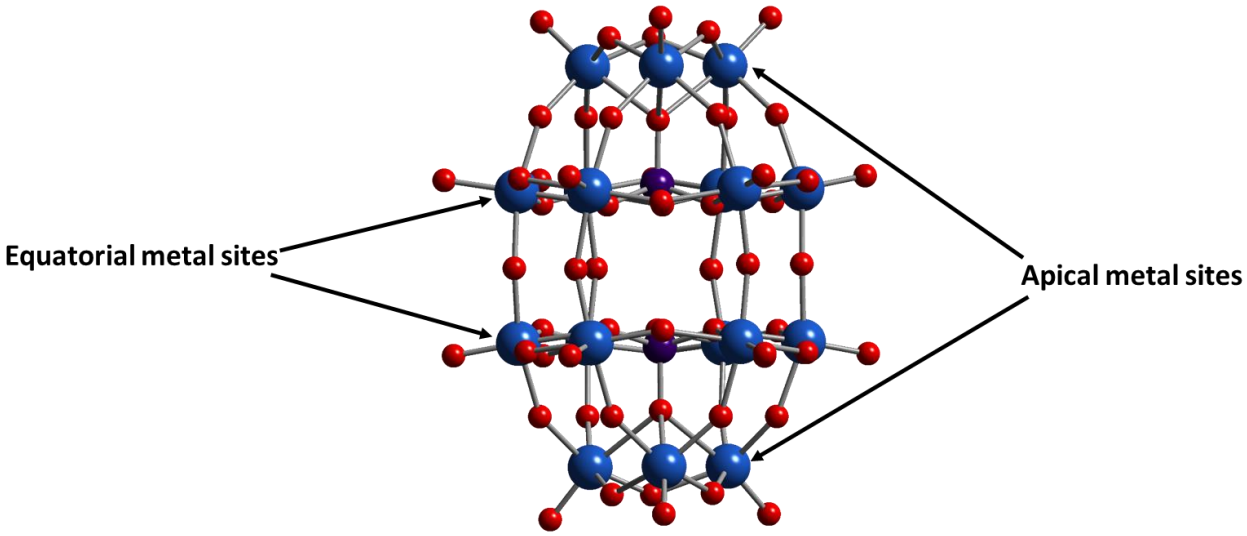

Figure 2.5: A ball and stick representation of Wells-Dawson POM; oxygen (red), metal (royal blue), central heteroatom (purple).

Dawson POMs are conveniently represented by X_2M_{18} and they possess two principal metal atom positions in the structure: six apical and twelve equatorial sites (see **Figure 2.5**). They also show isomerism and Constant and Thouvenot identified six possible isomers of the Dawson family as α, β, γ, α*, β* and γ*.[1] The α isomer has a D_{3h} symmetry and a rotation around its C_3 symmetry axis by 60° results in the β isomer with a lowered C_{3v} symmetry due to the loss of the symmetry plane which divides the Dawson molecule into two equivalent parts. The third isomer, γ with a restored D_{3h} symmetry, is formed by the recovery of the symmetry plane in the Dawson unit from a second rotation of the α isomer around the C_3 symmetry axis by 60°. The isomers α*(D_{3d}), β*($C3_v$) and γ*(D_{3d}) are formed by similar

rotations as for α, β and γ but in the presence of an inversion centre between the two $XW_9O_{34}^{z-}$ units.[1] Dissymmetrical Dawson POMs in which the ratio X/M = 1/18 also exist. In this class, the second heteroatom X of the Dawson structure is often replaced by a hydrogen atom.

2.2.4 Other classes of POMs

Other structural classes of POMs (see **Figure 2.6**) exist and include: the planar Anderson-Evans structure (XM_6) with a D_{3d} symmetry observed in $[TeMo_6O_{24}]^{6-}$;[16] the bent heptametalate structure with C_{2v} symmetry observed in $[Mo_7O_{24}]^{6-}$;[17] the icosahedral heteroatom structure ($XM_{12}O_{42}$) coordinated by six face-shared pairs of MO_6 octahedra which are linked together by corners with I_h symmetry and observed in $(NH_4)_2H_6[CeMo_{12}O_{42}].12H_2O$[26] and combined or complex structures formed by the combination of lacunary Keggin or Dawson POMs such as sandwich type POMs (e.g. $K_{10}Co_4(H_2O)_2(PW_9O_{34})_2$[27], Crown or Wheel type POMs (e.g. $K_{28}Li_5H_7P_8W_{48}O_{184}$)[28] and fullerenes (e.g. {Mo_{132}}-type cluster).[29]

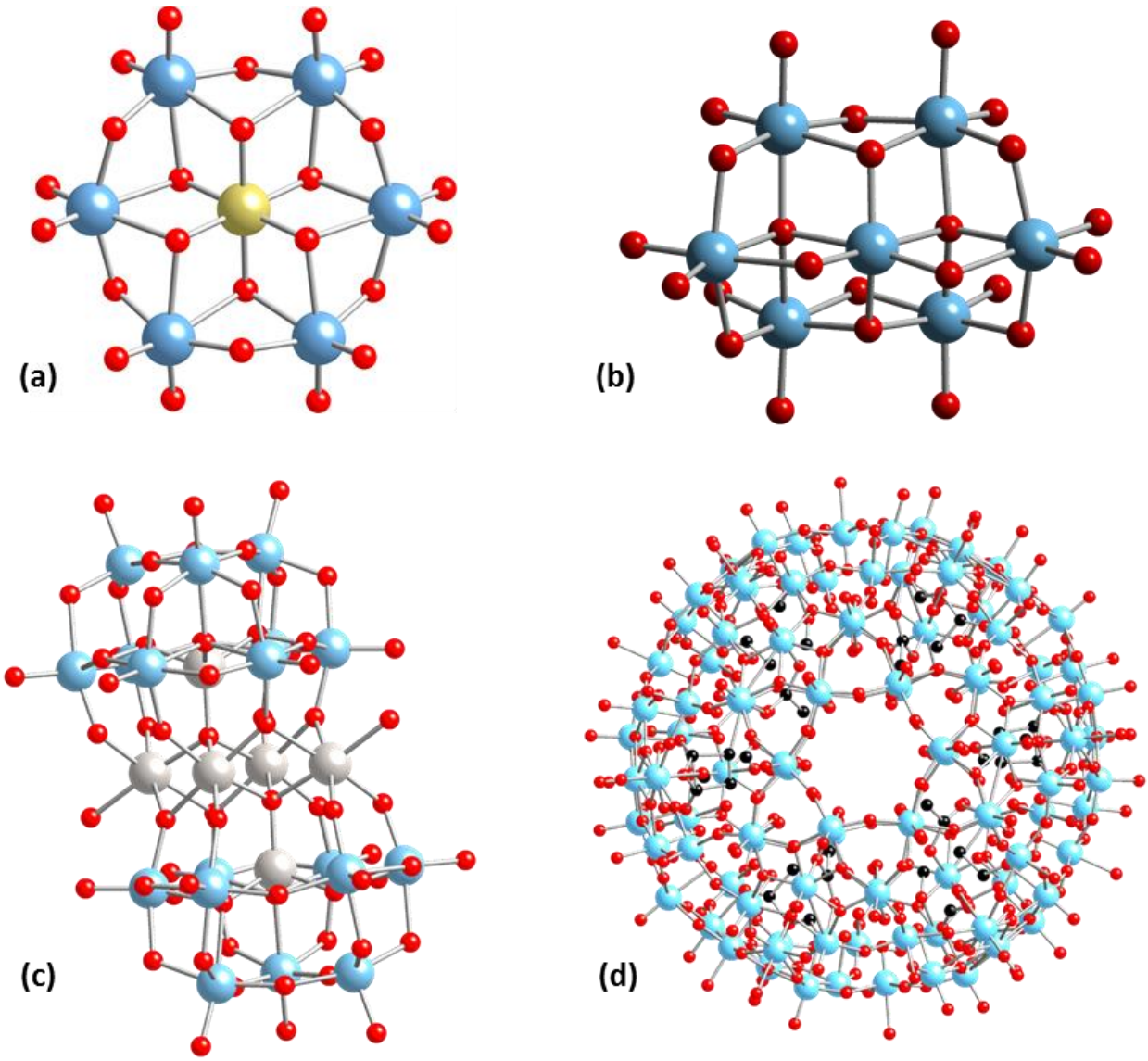

Figure 2.6. Ball and stick representations of (a) planar Anderson-Evans structure, $[TeMo_6O_{24}]^{6-}$; (b) *heptamolybdate structure, $[Mo_7O_{24}]^{6-}$*; (c) *a sandwich $[Zn_4(ZnW_9O_{34})_2]^{16-}$ structure and (d) an {Mo_{132}} -type cluster*; oxygen (red), molybdenum and tungsten (light blue); central tellurium (orange), zinc (grey) and carbon (black)

2.3 Properties

The versatile range of POM sizes, shapes, structures and compositions have endowed them with numerous properties, which can be greatly tuned by the incorporation of certain components into their framework. POMs have large sizes (6 – 25 Å) with large ionic weights (ca. 1000 – 10, 000).[5] They exhibit good stability to heat and oxidation and have the ability to accept and release several number of electrons without decomposition or structural changes thus making them good electron reservoirs.[1] POMs have varying solubility in a range of solvents with different polarities depending on their counter ions.[30] With inorganic cations

like sodium, potassium or proton, they are generally soluble in aqueous medium and behave like acids but are only soluble in organic solvents when they possess organic counter ions like TBA. Water-soluble POMs are generally stable to water and air while acid salts of POMs show Brønsted acidity in both solution and solid state.[20] Base treatment of POMs may lead to loss of one or more addenda atoms yielding lacunary POM species. For example, XM_9 and XM_{11} lacunary Keggin species are formed by the degradation of XM_{12} Keggin structure while X_2M_{15}, X_2M_{16} and X_2M_{17} lacunary Dawson species result from the degradation of X_2M_{18} Dawson structure (see **Figure 2.1**). These lacunary species are still relatively stable and are widely used in subsequent syntheses.[1] The lacunary forms also show unique ligand properties and can react with transition elements (e.g. Fe^{II}, Mn^{II}, Co^{II}, Ni^{II}, Zn^{II}, W^{VI}, Mo^{V}, V^{V}) to fill out the vacant sites and form substituted species.[1,20,30] Depending on the composition, POMs may also possess luminescent; ferromagnetic; chirality[1], biological and medicinal properties.[30]

2.4 Synthetic Routes to POMs

POMs are most often synthesised *via* aqueous routes or to a lesser extent *via* nonaqueous strategies. A mixture of aqueous and organic solvent (e.g. H_2O/CH_3CN) has also been used as medium for POM preparation.[21] In aqueous syntheses, aqueous solutions of simple oxoanions such as MoO_4^{2-} and WO_4^{2-} and the required heteroatoms (e.g. SiO_3^{2-} and HPO_4^{2-}) are acidified to produce polyoxoanions.[5] It is noted that the nuclearity of the metal oxide fragments generally increases as the pH of the solution decreases.[21] Non-aqueous methods may involve the careful hydrolysis of metal alkoxides (e.g. $WO(OMe)_4$ and $VO(OBu^t)_3$) with organic bases (e.g. NR_4OH and Bu^n_4NOH) or the dissolution of metal oxides in organic bases and subsequent precipitation and recrystallization from non-aqueous solution.[5] Both aqueous and nonaqueous POM syntheses may adopt a one-pot approach to produce new POMs.[21] This approach involves the addition of all the required reagents in a defined sequence and proportion with the right adjustment of parameters (see **Figure 2.7**). The key variables in POM synthesis are: type and concentration of metal oxide anion, type and concentration of heteroatom, pH for aqueous systems, temperature of reaction, method of processing (e.g. microwave, hydro/solvothermal, refluxing), ionic strength, presence of additional ligands or reducing agents.[21] Because of the moisture sensitive nature of most of the POM samples that are handled in our lab, our non-aqueous synthetic approach involves

manipulations using anaerobic techniques such as standard Schlenk techniques and the glovebox. A handy guide to these anaerobic techniques is provided by Errington.[31]

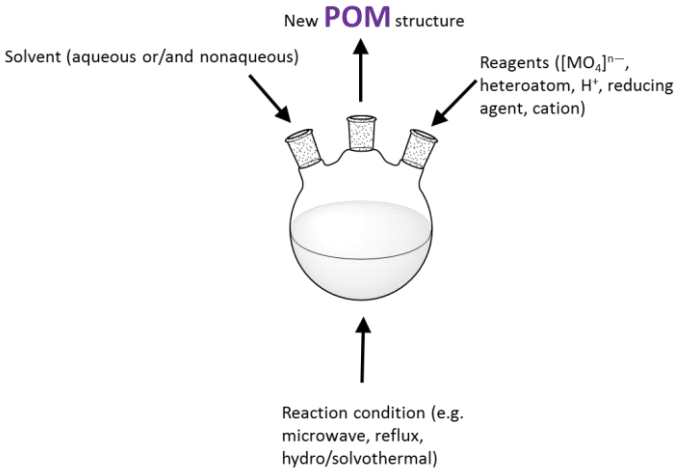

Figure 2.7. Parameters that are often adjusted in the synthesis/isolation of new POM clusters using the multi-parameter one-pot method.

2.5 Characterization techniques

A thorough study of POM structure, compositions and properties usually requires a combination of techniques including: elemental microanalysis; x-ray diffraction (XRD) analysis; vibrational spectroscopy (IR and Raman); nuclear magnetic resonance (NMR) spectroscopy; mass spectrometry; electronic spectroscopy (UV-Vis); equilibrium analysis, polarography and voltammetry; salt cryoscopy; diffusion and dialysis; ultracentrifugation and computational analysis. Weller and Young[32] provide a handy guide on some of the techniques applied in this thesis and a brief overview is given below.

2.5.1 Elemental analysis

CHN microanalysis and ICP AES are two techniques employed in this regard. CHN microanalysis was important for this thesis as all the samples studied had TBA counter ions and thus the number of TBA ion deduced from CHN microanalysis provided support for predicted formulas of prepared POMs. CHN analysis employs instruments to determine the carbon, hydrogen, nitrogen, oxygen and sulphur content of a sample by high-temperature decomposition. The sample is heated to 900 ^{o}C in oxygen leading to the production of a mixture of carbon dioxide, carbon monoxide, water, nitrogen and nitrogen oxides. A stream of helium gas is used to push the products into a tube furnace at 750 ^{o}C, where copper

reduces nitrogen oxides to nitrogen and removes oxygen. Also, carbon monoxide is converted to carbon dioxide by copper oxide. Subsequently, a series of three thermal conductivity detectors are used to analyse the resulting mixture as it passes through them. The first detector measures hydrogen and then water is removed in a trap. At the second detector the carbon is measured by oxidation to carbon dioxide, which is removed in a second trap. The remaining nitrogen is measured at the third detector. The data obtained from this technique are reported as mass percentage of C, H and N. Sulphur can be measured if the sample is oxidized in a tube filled with copper oxide.[3]

2.5.2 Multinuclear NMR spectroscopy

Multinuclear-NMR is arguably one of the most powerful tools at the disposal of POM chemists, which enables determination of structures, mostly in solution and on solid samples in some instances. The physical foundation of the non-destructive technique lies in the magnetic properties of atomic nuclei. NMR uses the interaction between nuclear magnetic moment and an external magnetic field, B_0, to create discrete nuclear energy states. A radiofrequency (RF) transmitter is used to initiate transitions between these states and the absorption of energy, which is recorded as a resonance signal is detected in an RF receiver (**Figure 2.8**). This allows a spectrum to be generated for a molecule containing atoms whose nuclei have non-zero magnetic moments (e.g. ^{1}H, ^{11}B, ^{13}C, ^{17}O, ^{19}F, ^{31}P, ^{119}Sn, ^{183}W etc). The size of nuclear magnetic moment and the abundance of the isotope determine the sensitivity of NMR.[33] The frequency of an NMR transition in relation to a reference is expressed as the chemical shift, δ (ppm) in the spectrum. This characterizes the chemical environment of the nucleus responsible for the transition and is given by the equation below as the difference between the resonance frequency of nuclei (υ) in the sample and that of the reference compound (υ_o):

$$\delta = \frac{v - v_o \; x \; 10^6}{v_o}$$

Spectrum integration may enable determination of the relative numbers of nuclei present whereas spin-spin coupling data may allow the establishment of positional relationship between nuclei.[33] These information allow the use of NMR to deduce shape and symmetry

with greater certainty than is possible with other spectroscopic techniques like IR and Raman spectroscopy.[3] NMR can also provide reaction mechanistic details such as the rate and nature of the interchange of ligands in fluxional molecules and can be used to follow reactions.[33] **Figure 2.9** displays pictures of some of the spectrometers used for this thesis.

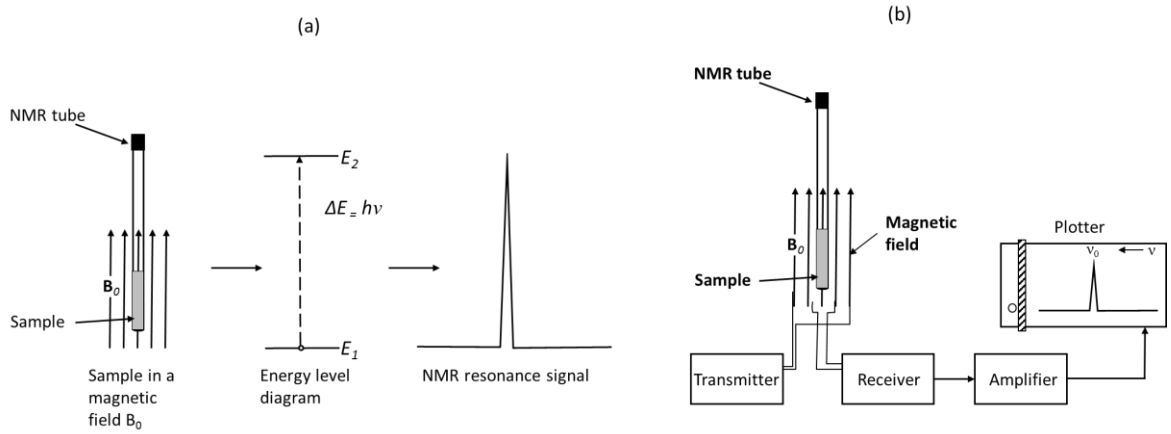

Figure 2.8. (a) Formation of an NMR signal and (b) schematic diagram of an NMR spectrometer with an electromagnet and separate transmitter and receiver coil (cross coils) adapted from Gunther (2013).[33]

Figure 2.9. Pictures of NMR spectrometers (300, 500 and 700 MHz) at Newcastle NMR Laboratory.

2.5.3 Fourier transformed infrared (FT-IR) spectroscopy

IR spectroscopy is a non-destructive technique which can be performed on virtually any state of a sample. It is based on change in the electric dipole moment of a compound during vibration and infrared spectra are obtained by passing infrared radiation through a sample

and determining what fraction of the incident radiation is absorbed at a particular energy.[34] Vibrations which do not result in a change in dipole moment are not IR active. Fourier-Transform Infrared spectrometers have succeeded traditional dispersive spectrometers and they work according to the principle of interference of radiation between two beams to yield an interferogram, a signal produced as a function of the change of path length between two beams. Fourier-transformation method is then used to interconvert the domains of time and frequency.[34] **Figure 2.10** displays the fundamental components of an FT-IR spectrometer while **Figure 2.11 (a)** and **(b)** are pictures of a Bruker Alpha FT-IR spectrometer with an ATR module set-up in a glove box in our lab for measurements in inert atmosphere.

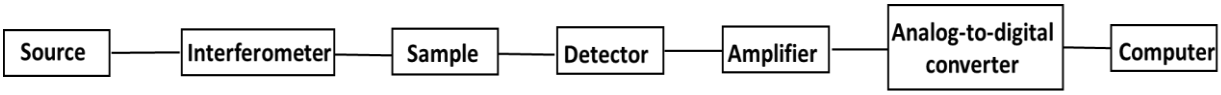

Figure 2.10. Fundamental components of an FT-IR Spectrometer.

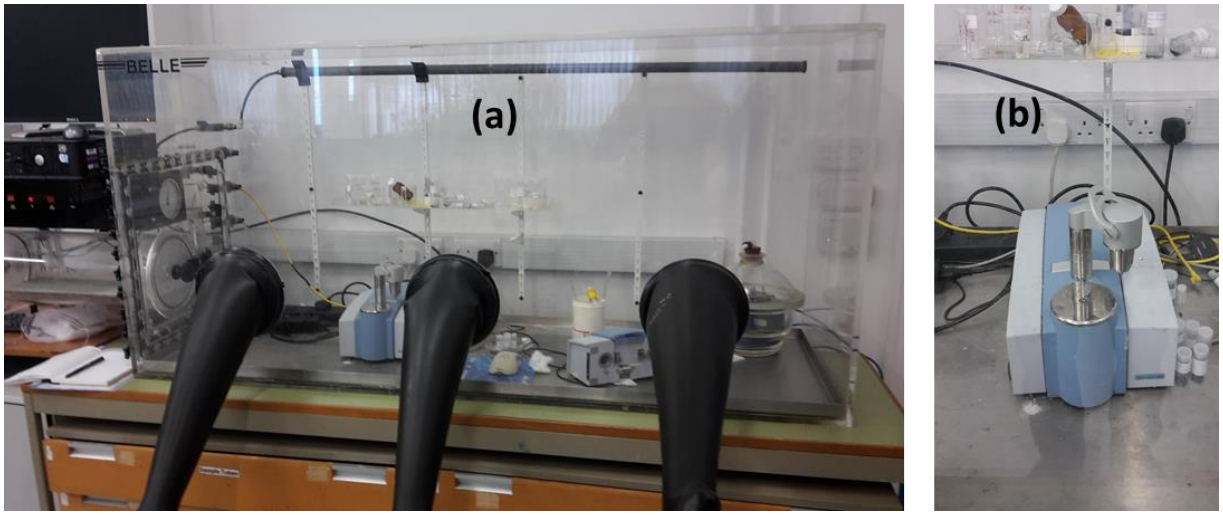

Figure 2.11. (a) A glove box set-up containing a Bruker Alpha FT-IR spectrometer (b) a Bruker Alpha FT-IR spectrometer with an ATR module.

An IR spectrum usually has a range between 4000 and 250 cm^{-1} (2.5 and 40 µm) but the most characteristic region of the spectrum for polyoxometalates is *ca.* 1000 – 400cm^{-1} where absorptions due to metal-oxygen stretching vibrations occur.[5] Thus, identical spectral band positions, shapes and relative intensities for two complexes strongly indicate that they have similar structures while good agreement between the spectra of crystalline and dissolved POMs is taken to prove that the structure of the solute anion is the same as that observed in the crystal.[5] The applications of FT-IR in inorganic chemistry includes: to detect the presence of known compounds, that is, fingerprinting; to determine the components, shape and likely

structure of an unknown compound; to monitor changes in the concentration of a species during a reaction; to measure properties of bonds (their force constants). IR methods include transmission and reflectance e.g. attenuated total reflectance (ATR). The ATR, which was applied in this thesis utilizes the phenomenon of total internal reflection.[34] In ATR spectroscopy, a beam of radiation entering a crystal will undergo total internal reflection when the angle of incidence at the interface between the sample and crystal is greater than the critical angle. The critical angle is dependent on the refractive indices of the two surfaces. The beam penetrates a fraction of a wavelength beyond the reflecting surface and when a material that selectively absorbs radiation is in close contact with the reflecting surface, the beam loses energy at the wavelength where the material absorbs. The resultant attenuated radiation is measured and plotted as a function of wavelength by the spectrometer and produces the absorption spectral characteristics of the sample. The depth of penetration, d_p in ATR spectroscopy is a function of the wavelength, λ, the refractive index of the crystal, n_2, and the angle of incident radiation, θ. For a non-absorbing medium, d_p is given by

$$d_p = (\lambda/n_1)/ \{2\pi[\sin \theta - (n_1/n_2)^2]^{1/2}\}$$

where n_1 is the refractive index of the sample.

The crystals used in ATR cells are made from materials with high refractive index and low solubility in water. Such materials include zinc selenide (ZnSe), germanium (Ge) and thallium-iodide (KRS-5).[34]

2.5.4 Cyclic voltammetry (CV)

Cyclic voltammetry is an electrochemical technique that measures electrical currents due to reduction and oxidation of electroactive species in solution.[3] It gives first-hand information on reduction potentials and the stabilities of different products of oxidation or reduction.[3] The technique gives rapid qualitative insight into the redox properties of an electroactive species like POMs and reliable quantitative information on its thermodynamic and kinetic properties. It usually involves an electrochemical cell having three electrodes, i.e. working (W), reference (R) and counter or auxiliary electrode (C) all immersed in a liquid and connected to a potentiostat, which allows the current flowing between W and R to be

measured as the potential difference is changed cyclically. The working electrode at which the electrochemical reaction of interest occurs is usually constructed from platinum, silver, gold, graphite or glassy carbon, etc. The reference electrode is normally a silver/silver-chloride or saturated calomel electrode and the counter electrode is normally platinum.[3,35]

2.5.5 X-ray diffraction analysis (XRD)

X-ray diffraction techniques have become very important[36] and have been applied widely in the determination of POM crystal structures.[13,14,16-18] It is non-destructive and measures the variation of intensity of radiation (X-ray) with direction at fixed wavelength. This information is used to determine positions of atoms that make up a crystal and hence provides a complete description of crystal structures in terms of features such as bond lengths, bond angles, and the relative positions of atoms in a unit cell. The structural information also enable chemists to predict structures and explain trends in properties such as bonding and possible protonation sites.[3,37] **Figure 2.12** is a schematic representation of a single-crystal X-ray diffractometer consisting of three basic units: the X-ray tube, which is the X-rays source; a sample holder, which holds the crystal sample and a detector, which records and processes diffracted X-ray signal and output it to a computer. Filters are required to produce monochromatic X-rays needed for diffraction while collimators help to provide parallel beam of X-rays.

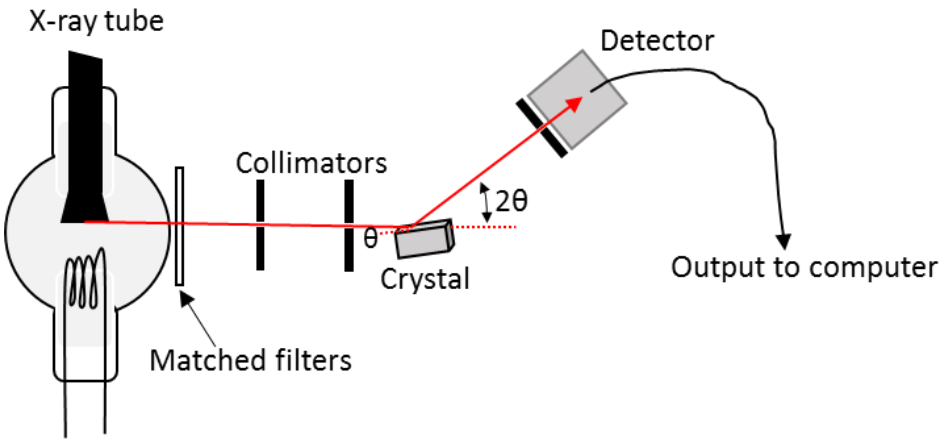

Figure 2.12. Schematic representation of a single-crystal X-ray diffractometer.

XRD involves the scattering or diffraction of X-rays that occurs as a result of an object in their path, resulting in interference. X-rays are usually diffracted elastically (with no change in

energy) by the electrons in atoms, and this scattering can occur for a periodic arrangement of scattering centres separated by distances similar to the wavelength of the radiation (about 100 pm), such as is found in a crystal. If the scattering is taken to be equivalent to reflection from two adjacent parallel planes of atoms separated by a distance, d, then the angle at which constructive interference occurs (to produce a diffraction intensity maximum) between waves of wavelength, λ, is given by Bragg's equation: $2d\sin\theta = n\lambda$. Where n is an integer. Thus an X-ray beam impinging on a crystalline compound with an ordered array of atoms will give a set of diffraction maxima, termed a diffraction pattern, with each maximum, or reflection, occurring at an angle θ corresponding to a different separation of planes of atoms, d, in the crystals.[3]

Also, an atom or ion scatters waves or X-rays in proportion to the number of electrons it possesses and the intensities of the measured diffraction maxima are proportional to the square of this number. Thus, the diffraction pattern produced is characteristic of the positions and types (in terms of their number of electrons) of atom present in the crystalline compound and the measurement of X-ray diffraction angles and intensities provides structural information. Because of its dependence on the number of electrons, X-ray diffraction is particularly sensitive to any electron-rich atoms in a compound.[3]

There are two principal X-ray techniques: (i) the powder diffraction method, in which the materials being studied are in polycrystalline form and is used mainly for phase identification and the determination of lattice parameters and lattice type and (ii) the single-crystal diffraction method, in which the sample is a single crystal of dimensions of several tens of micrometers or larger and it enables the full determination of the structure.[3] Only single-crystal diffraction method was applied in this thesis.

2.5.6 Electronic spectroscopy (UV-Vis)

Ultraviolet-visible spectroscopy (UV-Vis) deals with the absorption of electromagnetic radiation in the UV and visible region of the spectrum. It is also known as electronic spectroscopy because it involves electronic excitations to higher energy levels.[3]

Though gas and solid samples may be studied, UV-Vis samples are usually solutions. A gas or liquid is contained in a cell known as a cuvette, which is made of an optically transparent

material like glass or pure silica for UV spectra at wavelengths below 320 nm. The principle usually involves the beam of incident radiation being split into two, one passing through the sample and the other through a reference that is a cell that is similar except for the absence of the sample. The emerging beams are compared at the detector (a photodiode) and the absorption is obtained as a function of wavelength. Conventional spectrometers sweep the wavelength of the incident beam by changing the angle of a diffraction grating.[3,36] The intensity of absorption is measured as the absorbance, A, defined as

$$A = \log_{10} (I_o/I)$$

Where, I_o is the intensity of incident ray and I is the measured intensity of emergent ray, after passing through the sample. The empirical Beer-Lambert law is used to relate the absorbance to the molar concentration (J) of the absorbing species J and optical path length L:

$$A = \varepsilon[J]L$$

Where ε (epsilon) is the molar absorption coefficient (still commonly referred to as the 'extinction coefficient' and sometimes the 'molar absorptivity').[3]

2.5.7 Mass spectrometry (MS)

Mass spectrometry is a destructive technique used to determine the mass of a molecule or an ion and of its fragments. It measures the mass-to-charge ratio of gaseous ions, which can be either positively or negatively charged. Several ionization methods are employed including Electron Impact Ionization (EI), Fast Atom Bombardment (FAB), Matrix-Assisted Laser Desorption/Ionization (MALDI), Electrospray Ionization (ESI) and Cryospray Ionization (CSI).[3] Finke and co-workers were the first to use FABMS to record mass spectra of polyanions.[38,39] Cronin and co-workers also noted the versatility of ESI-MS and CS-MS in monitoring the self-assembly and discovering of new clusters of POMs. They emphasized the application of CSI-MS in the investigation of unstable POM complexes and examining reaction mechanism.[21]

2.5.8 Computational analysis

Computational techniques are increasingly being used to complement experimental techniques in POMs studies[40-45], and involve the use of numerical models for exploring the structures and properties of individual POM molecules and materials. Methods employed are either **ab initio** (rigorous and computationally very time-consuming, treatments) based on the solution of the Schrodinger equation for the system or parametized **semi-empirical** methods (more rapid and necessarily less detailed), which use approximate or effective functions to calculate the properties of POM molecules and solids especially the forces between their particles. These two methods of resolving the Schrodinger equation for many-electron polyatomic systems typically adopt a self-consistent field (SCF) procedure, in which an initial guess about the composition of the linear combination of atomic orbitals (LCAO) used to model molecular orbitals is successively refined until the composition and the corresponding energy remains unchanged in a cycle of calculation.[3] These have been applied in many studies on POMs and a currently popular alternative to the *ab initio* method is Density Functional Theory (DFT), in which the total energy is expressed in terms of the total electron density, $p = |\psi|^2$, rather than the wave function, ψ, itself and the results are displayed using graphical techniques.[3]

2.6 Applications of Polyoxometalates

The robust and versatile properties (size, shape, composition, bonding etc) of POMs have resulted in their use in a host of applications, from catalysis to nanoscience, biology to medicine, magnetic devices to material science and photochemistry.

2.6.1 Catalysis

The use of POMs as catalysts has been and remains a major area of POM application.[30] At an industrial scale, this arises mainly from their acidic properties (i.e. acid catalysts especially in the solid state) or their ability to act as electron reservoirs (i.e. oxidation catalysts) or sometimes due to their photoactivity. They have been investigated as homogeneous, heterogeneous, photo and electrocatalysts for many conversions including oxidation of alkenes and aromatic hydrocarbons, olefin polymerization, Friedel-Crafts alkylation,

acylation, sulfonation of aromatics, C-H bond activation, water oxidations and reduction of CO_2.[5,46,30,47-50]

A catalytic study by Habibi *et al.* in 2001 demonstrated the use of potassium dodecatungstocobaltate trihydrate ($K_5CoW_{12}O_{40}{\cdot}3H_2O$) as a catalyst for a mild and efficient conversion of epoxides and acetone to 1, 3-dioxolanes with high to excellent yields.[51] Rafiee *et al.* in 2005 also showed that $K_5CoW_{12}O_{40}{\cdot}3H_2O$ catalyst was reusable several times without loss of activity with higher yield and selectivity in an experiment for the addition of trimethylsilyl cyanide to carbonyl compounds.[52] Additionally, Sheshmani *et al.* in a study to prepare and examine the reactivity of some POMs established that $K_3[PMo_6W_6O_{40}]$ showed the best reactivity and efficiency as catalysts in the esterification of phthalic anhydride and 1-butanol to dibutylphtalate among the various acid catalysts tested.[53] The study contributed to the catalytic efficiency of Keggin-type POMs particularly with tungsten addenda.

Furthermore, while investigating the catalytic activity of the Keggin-type heteropolyoxometalates of general formula $[PW_{11}MO_{39}]^{(7-n)-}$ with M = Co(II), Ni(II), and Fe(III) on the partial oxidation of methane by molecular oxygen and nitrous oxide, Mansori *et al.* in 2013 found that there was good selectivity for oxygenates (CH_3OH and HCHO) with yields as high as 48%. They also showed that cobalt and iron doped polyoxometalates were the most active and selective catalysts.[54] The work further supported the catalytic efficiency of early transition metal substituted Keggin-type POMs.

A major challenge in the currently interesting field of artificial photosynthesis, which is aimed at producing fuels and oxygen from water and CO_2 is the availability of robust catalysts. Boncho and co-workers, propelled by a desire to contribute towards tackling this challenge, reported the synthesis of $M_{10}[Ru_4(H_2O)_4(\mu\text{-}O)_4(\mu\text{-}OH)_2(\gamma\text{-}SiW_{10}O_{36})_2]$ (M = Cs, Li), which was applied in water oxidation in the presence of an excess of Ce(IV) with high turnover frequencies (>450 cycles·h^{-1}) and no catalyst deactivation.[55,56] In the same vein, Hill and co-workers reported the application of $[Co_4(H_2O)_2(PW_9O_{34})_2]^{10-}$ and $[Co_4(H_2O)_2(VW_9O_{34})_2]^{10-}$ as water oxidation catalysts[57,58] while Galan-Mascaros and co-workers showed that the catalytic activity of an insoluble salt of the cobate polyoxometalate ($[Co_9(H_2O)_6(OH)_3(HPO_4)_2(PW_9O_{34})_3]^{16-}$)($Co_9$) used to modify amorphous carbon paste was not

affected as water oxidation catalysts. The result revealed that good catalytic rates were reached at reasonable over potentials and that Co_9 showed a remarkable long-term stability in turnover conditions. The study also showed that oxygen evolution rate remained constant for hours without the appearance of any sign of fatigue or decomposition in a large pH range, including acidic conditions, where many metal oxides are unstable.[59]

Similarly, Symes and Cronin in a landmark study in 2013 demonstrated that by using $H_3PMo_{12}O_{40}$ POM as an electron-coupled-proton buffer (ECPB), O_2 and H_2 could be produced at different times during water electrolysis to prevent them from mixing. The study was significant because it tackled the safety problem and electrolyser degradation and also allowed greater flexibility as regards the membranes and electrodes that could be used in electrolytic water splitting with possible advantages for the future of hydrogen economy.[60]

Yang *et al.* in 2013 were equally able to design a catalytic system with exceptional catalytic ability by encapsulating vanadium-doped Keggin polyoxometalates ($PMo_{12}–nV_n$) into a MOF (HKUST-1 framework). This system proved very effective for hydroxylation of benzene into phenol[61] and the study contributed to the extended area of doping POMs with MOFs for catalytic applications.

Additionally, in a bid to optimize the homogeneous catalysts for selective oxidation of biomass to formic acid using oxygen as an oxidant and p-toluenesulfonic acid as an additive, Albert *et al.* in 2014 synthesized and characterized several vanadium (number of V = 0 to 6) substituted Keggin-type polyoxometalates with molybdenum addenda. The study showed that ($H_8[PV_5Mo_7O_{40}]$) was the best system, which enabled higher space-time-yields compared to other systems investigated. Therefore, it allowed a reduced reactor size and lower pressure of operation. It also provided an insight into the chemistry of the process which it noted was due to the formation of the pervanadyl species (VO_2^+) which was only discernible for the higher V-substituted species.[25]

Incorporating reactive sites on POMs has been shown to greatly influence their properties.[62-64] In this regard, Lan *et al.* investigated the reactive transition metal site in a Keggin polyoxometalates pillared on metal-organic co-ordination polymer sheet in the construction of two new 3D porous frameworks $[Co(bix)_2][VW_{12}O_{40}]\cdot(H_2bix)\cdot H_2O$ (see **Figure 2.13**) and

$[Ni(bix)_2][VW_{12}O_{40}]\cdot(H_2bix)\cdot 2H_2O$ (bix = 1,4-bis(imidazol-1-ylmethyl)-benzene). The study revealed the structural integrity of the framework in aqueous solution with a wide pH range of 1 to 11, and in common organic solvents (methanol, ethanol and DMF) and indicated that both compounds were not only active photocatalysts for degradation of rhodamine B (RB), but were very stable and easily separated from the photocatalytic system for reuse.[65] This shows the importance of transition metal reactive sites in the assembly of 3D structures using POMS. This was also supported by Iwanowa and co-workers in their IR spectroscopic investigation of the surface acid-base properties of modified Keggin polyoxometalates activated by supported gold nanoparticle ($Au/Cs_5PW_{11}TiO_{40}.nH_2O$) for catalysis.[66]

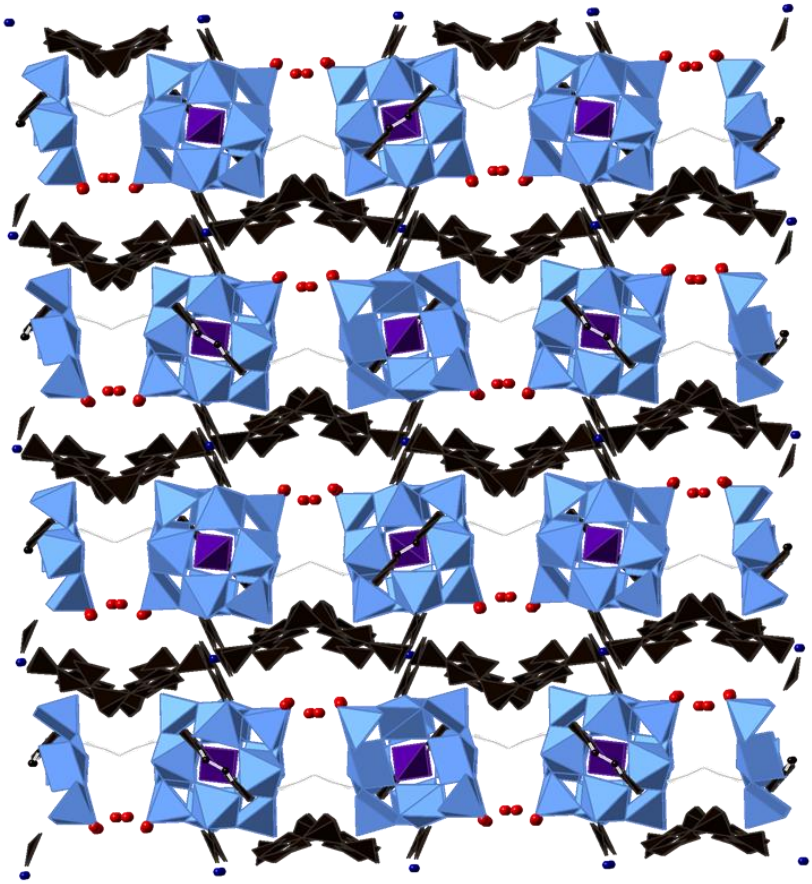

Figure 2.13. 3D layered structure of $[Co(bix)_2][VW_{12}O_{40}]\cdot(H_2bix)\cdot H_2O$; tungsten (royal blue), oxygen, (red), vanadium (purple), nitrogen (orange), cobalt (blue), hydrogen (white) and carbon (black).

A catalytic study by Balaska *et al.* in 2013 showed that Dawson anions of Cs and Co possess the ability to accept or release electrons through an external potential or upon exposure to

UV radiation (photochemical reactions) and that the Cs salt was a better catalyst for phenol degradation.[67]

Yang *et al.* had earlier reported electrocatalytic oxidation and reduction of chlorate anion in acid buffer media by a nanocomposite films containing water-insolvable cobalt tetraaminophthalocyanine (CoTAPc) and Dawson-type tungstophosphate anions (P_2W_{18}). The film was assembled by electrostatic layer-by-layer (LbL) method in nonaqueous (DMF) media.[68]

Also, Neumann and co-workers in 2014 in a bid to gain a better understanding of the mechanism of oxygen transfer reactions with high-valent Co-O intermediates reported the isolation and characterization of a dicobalt(IV)-μ-oxo polyoxometalate compound $[(\alpha_2\text{-}P_2W_{17}O_{61}Co)_2O]^{14-}$ $[(POMCo)_2O]$, by the oxidation of a monomeric $[\alpha_2\text{-}P_2W_{17}O_{61}Co^{II}(H_2O)]^{8-}$, $[POMCo^{II}H_2O]$, with ozone in water. They were able to show that the isolated POM was an active compound in the oxidation of H_2O to O_2. The study also implicated $[(POMCo)_2O]$ in the indirect epoxidation of alkenes *via* a Mn porphyrin; the direct oxygen transfer to water-soluble sulfoxides and phosphines and the selective oxidation of alcohols by carbon–hydrogen bond activation *via* a hydrogen atom transfer mechanism. The report used Density Functional and CASSCF calculations to provide some insight into the oxygen transfer reactions.[46] This study was consequent upon previous reports that had stressed the intermediacy of reactive metals oxo species (e.g. Fe, Cu and Mn) in metalloenzymes which enabled them to undertake C-H activation and water oxidation and highlighted the importance of these metallic systems in important conversions like the oxidation of methane to liquid methanol (e.g. iron- and copper-based catalysts)[69] and oxidation of water to hydrogen gas (e.g. ruthenium- and manganese-based catalysts).[70]

While examining the photoelectrocatalytic properties of two films of Keggin-type polyoxotungstates, $[TBA]_4[PW_{11}O_{39}SnC_6H_4C{\equiv}CCH_2SC(O)CH_3]$ and $[TBA]_4[PW_{11}O_{39}SnC_6H_4C{\equiv}C(CH_2)_4SC(O)CH_3]$ on gold electrodes , Forster and co-workers showed that the films exhibited well defined POM based redox processes and were stable to electrochemical cycling. They noted that the surface coverage of both materials was less than that anticipated for a dense monolayer while the rate of heterogeneous electron transfer across linker lengths for both POM based redox processes were in the range of 100 -

200 s^{-1} suggesting that the redox state of the film could be switched within a few milliseconds and this they noted was important for applications like catalysis, solar energy conversion and sensing.[71]

Recently, Mizuno and co-workers applied $TBA_4H_4[\gamma\text{-}SiW_{10}O_{36}]$ as catalyst for the visible-light photoredox interconversions (oxygenation/deoxygenation) between sulfur-containing compounds (sulphides and sulfoxides).[72] Mizuno and co-workers have been very active in the field of catalysis by Polyoxometalates and have written some reviews on the field.[73-75] Also, Wu and Ye in their 2016 review summarised some applications of immobilised POM-based materials in oxidation, hydrolysis, cyanosilylation, photocatalysis and electrocatalysis.[47] Additionally, a hybrid of the Keggin-type POM ($H_3PW_{12}O_{40}$) and an oppositely charged COOH-functionalized surface active ionic liquid (SAIL), N-decyl-N-carboxymethyl imidazolium bromide was recently applied as catalyst for dye degradation.[76]

2.6.2 Sensing

POMs deposited on electrode surfaces have been applied in sensing. A POM based sensor is an analytical device, having an immobilized layer of POM on a transducer (solid support) with the ability to recognize and catalyse the analyte if its structure and properties are retained upon deposition. The chemical reaction induced from recognition between the immobilized POM and the analyte will then be converted into an electrical signal, which will be amplified and changed into a display converted by the signal processing equipment. A good POM-based sensor should have good sensitivity, selectivity, linear range, response time, detection limit and stability.[1] A number of studies have been conducted on POM sensors.[77,78] One of such studies was by Xu *et al.* who reported the fabrication of a multiple-coloured electrochromic composite film of Dawson-type polyoxometalates (P_2W_{18}) and poly(hexyl viologen) (PXV) by layer-by-layer (LbL) self-assembly method. The report noted that the P_2W_{18}/PXV composite film could be used as a pH sensor as its electrochemical response depended on pH and undergoes a colourless to blue to violet transition over the potential range from +0.1 to −0.9 V.[77]

Additionally, Anwar *et al.* reported the use of a conducting polymer for the immobilization of various transition metal ion-substituted Dawson-type polyoxometalates (POMs) onto glassy carbon electrodes. They noted that the immobilized POMs showed good response on

investigation as sensor for hydrogen peroxide. Their report also revealed that voltammetric responses of films of different thicknesses were stable within the pH domain 2–7 and showed that redox processes were associated with the conducting polymer, the entrapped POMs and incorporated metal ions. The resulting POM doped polypyrrole films were found to be extremely stable towards redox switching between the various redox states associated with the incorporated POM.[78] Another study by Li *et al.* in 2013 showed that the electrocatalytic efficiency and amperometric response of a vanadium-substituted molybdophosphate $H_6[PMo_9V_3O_{40}]$ (PMo_9V_3) decorated by platinum nanoparticles (Pt) composite film towards oxidation of dopamine at physiological conditions were greatly enhanced by the synergistic contributions of the components, PMo_9V_3 and Pt. It also showed that the film exhibited high sensitivity, fast response time (<1s), low detection limit and a wide linear range for dopamine sensing and no interference from the common interfering species such as ascorbic acid, glucose, uric acid and 1-cysteine.[79] Also, Liu *et al.* in an important study on POM immobilization, employed layer-by-layer self-assembly method in developing electrochromic multilayer films consisting of $K_6[P_2W_{18}]\cdot 14H_2O$ (P_2W_{18}) POM clusters, TiO_2 and polyallylamine hydrochloride (PAH) on quartz, silicon wafer and ITO substrates. The study further demonstrated the application of the POM films in sensing as the multilayer films exhibit high optical contrast, suitable response time and low operation potential.[80]

Furthermore, two reports in 2016 demonstrated the application of POM-based materials for sensing. One is a sensor of platinum nanoparticles (PtNPs) functionalized on POM/multi-walled carbon nanotube for analysis of the herbicide, Simazine in wastewater samples and this showed good selectivity and stability.[81] The other is a sensor made of polyoxometalate ($H_3PW_{12}O_{40}$) functionalized reduced graphene oxide on modified glassy carbon electrode (POM-rGO/GCE) for the simultaneous determination of L-tyrosine (L-Tyr) and L-tryptophan (L-Trp).[82]

2.6.3 Nanoscience and molecular spintronics

POMs are also very attractive building blocks for the assembly of metal-oxide based systems in nanoscience. They have been used to assemble particles/dots, micelles, wire/fibre, tubes and films in the zero, one and two dimensions for a host of other applications. POMs with

pentagonal building blocks have being explored to produce curved and spherical architectures in a similar fashion to the architectures of carbon nanostructures.[21] POMs with redox active templates have been explored for utilization in molecular flash RAM.[21] In Spintronics, several magnetic POMs particularly those with redox-active core have been explored for application in devices.[83] For instance, Coronado and co-workers have reported and published on POM-based magnetic materials.[84-86] Also, Cronin and co-workers reported a polyoxometalate-mediated single-molecule magnet (SMM), $[(GeW_9O_{34})_2[Mn^{III}_4Mn^{II}_2O_4(H_2O)_4]]^{12-}$ in which a central cationic mixed-valance hexameric manganese core is stabilized by two POM ligands. Other SMMs have also been reported.[20,21]

Equally, Gam Derouich *et al.* in a bid to develop POM-based materials for molecular electronics (hybrid memories) by the controlled immobilization of POMs on surfaces reported the controlled formation of monolayers or sub-monolayers of covalently grafted POMs on glassy carbon (GC) and Au that were stable with time or potential. This they noted was a requirement in the design of molecular memories.[87] Further still, Andreev *et al.* established that both $[Co_4Mo_{12}]$ and the Ni analogue exhibited a complex magneto-optical response in fields of up to 33 T at energies characteristic for formally spin-forbidden d−d transitions.[88] The study in a way contributed to the understanding of the magnetic behaviour of the compounds. Similarly, Zhang *et al.* in the early part of 2014 reported a new crown inorganic–organic hybrid material with ferromagnetic interactions. The material, which was composed of the Keggin polyoxometalates $[PW_{12}O_{40}]$ and transition metal-amino acid coordination complexes, $K_2\{[KCu_4(gly)_4(OH)_2(H_2O)_2Cl][PW_{12}O_{40}]\}n_2.19H_2O$, was made in an attempt to functionalize POM by making a system with POM as building block and metal-amino acid complex as linkers.[89] Additionally, a study in 2016 on the tunnel conductivity of POMs and their organic derivatives showed them to be viable as molecular diodes in nanoelectronics.[90]

2.6.4 Energy

The potential for redox catalysis, including proton-coupled electron-transfer has been employed in energy applications for CO_2 activation and splitting of water to produce hydrogen to help in the capture and storage of sunlight energy.[46,59,91] In this regard, Hu *et al.* reported new hybrid materials based on Keggin polyoxometalates and transition metal

complexes with a lower positive charge. The hybrid materials showed some unprecedented properties for many applications including energy systems.[92] Also, Poly(dimethyl diallyl ammonium chloride) functionalized graphene composite materials based on tungsten addenda mixed heteropolymolybdate ($PMo_{12-x}W_xO_{40}^{3-}$) (PMoW–PDDA–RGO) were reported as good candidates for high capacitance aqueous supercapacitors.[93]

2.6.5 Medicine and Biology

POMs with anti-viral, anti-bacterial and anti-fungal activities have been applied in medicine.[2,5,30,94] Rhule *et al.* have written a review on such medicinal POMs.[95] Two POM hybrid materials ((tris(vanadyl)-substituted tungsto-antimonate(III) and tris-butyltin-21-tungsto-9-antimonate(III) anions) were also reported to have significant biological activity as active stimuli for differentiation of stem cells into insulin-producing cells.[96]

2.6.6 Photochemistry

In photochemistry, several POMs have been reported that show photochemical properties and have been explored for applications in eletrochromic and photochromic devices.[5,30,77,97] In this direction, Shi *et al.* in their work noted that by introducing a polycyclic aromatic ligand phnz to the Ag/POM/H_2biim system, two unusual compounds with argentophilic $\{Ag_5\}^{5+}$–$\{Ag_4\}^{4+}$/$\{Ag_2\}^{2+}$ clusters were hydrothermally synthesized; $\{[Ag_7(H_2biim)_5][PW_{11}O_{39}]\}.Cl.H_2O$ and $\{[Ag_2(H_2biim)_2][Ag(phnz)](PW_{12}O_{40})\}.H_2O$ (H_2biim = 2,29-biimidazole, phnz = phenazine). The compounds were reported to have some electrocatalytic, electrochemical and luminescent behaviour.[98] Additionally, a photochemical study on La-substituted POMs reported the moisture responsiveness and high energy UV radiation reduction of a composite films of $Na_9[EuW_{10}O_{36}].32H_2O$ (EuW10) and agarose, which the study noted could open the way for their application as luminescent POM-based materials.[99] In photophysics, Zhang *et al.* showed that the molecular NLO activity of lacunary Keggin POM derivatives could be modified by replacing the central heteroatom (X) and the substituted addenda metal atom (M). This further supports the activity of the heteroatom and revealed the general rules to design a system with large optical nonlinearity.[100]

2.6.7 Analytical Chemistry

Since their first application in analytical chemistry in 1848 by Svanberg and Struve, POMs have been used to determine a range of elements including Ti, Zr, Hf, Th, Nb, Ce and Sb. They have also been applied in the gravimetric determination of P, As, Si or Ge based on the formation and subsequent precipitation of $[XMo_{12}O_{40}]^{n-}$.[5,30]

2.7 Early work on POM solution properties, speciation and reactivity

Since the discovery of POMs, much work has been conducted with a view to understanding, their structure, composition, mechanism of formation, solution properties and speciation. In this context, Weakley and Malik in an attempt to understand the structures of a range of Keggin-type heteropolyanions (HPAs) reported the synthesis of POMs of the series, $XZW_{11}O_{40}H_2^{n-}$ (X, Z = Si, Co(III); Ge, Co(II); Ge, Co(III); Si, Ni(II); Ge, Ni(II); P, Ni(II)) and the unstable anion $SiCoMo_{11}O_{40}H_2^{6-}$. The report noted that Co(III) species are the most resistant to acid and base attack and also gave an insight into their ligand-field spectra.[101] A further solution study by Malik and Weakley reported the first HPA with Mn^{III} heteroatom when they prepared eleven heteropolytungstate anions, $X_2ZW_{17}O_{62}H_2^{n-}$ (X = P or As; Z = Mn, Co, Ni, or Zn) and investigated their stabilities towards acids and bases. The study also gave an insight into the redox and magnetic properties of the POMs.[102]

Tourne *et al.* reported the synthesis of triheteropolyanions containing Cu^{II}, Mn^{II} and Mn^{III} [$XZW_{11}O_{40}H_2^{n-}$ (X = B, Zn, P, Si, Ge; Z = Cu^{II}, Mn^{II}, Mn^{III}), $XZMo_{11}O_{40}H_2^{n-}$ (X = P, Si, Ge; Z = Mn^{II}, Cu^{II}), and $X_2'CuW_{17}O_{62}H_2^{8-}$ (X' = P, As)]. They noted that the POMs were degraded slowly by bases and that though the very stable free acids of the $XMn^{III}W_{11}O_{40}H_2^{n-}$ anions can be prepared, acid attack on the Cu^{II} and Mn^{II} anions was rapid. Their report also indicated that the molybdate analogues were much less stable than the tungstates and that the manganese complexes were high-spin.[103] While investigating heteropolyanions containing two different heteroatoms, Weakley furthermore in 1973 showed that the diffuse reflectance UV-Vis spectra of cobalt (II) complexes were cation-dependent and noted that salts whose reflectance and solution spectra differ markedly are dichroic. He further observed that the distortion of the CoO_6 chromophore by crystal packing is accompanied by

preferential orientation of the heteropolyanion and concluded that such salts should be suitable for X-ray studies of the detailed structure of the anion.[27]

In their systematic study on the relationship between cation-size and the vibrational spectra of α- and β-$XM_{12}O_{40}^{n-}$ polyoxometalates (X = B^{III}, Si^{IV} Ge^{IV}, P^{V}, As^{V}; M = Mo^{V1}, W^{VI}), Rocchiccioli-Deltcheff *et al.* demonstrated that the terminal metal oxygen stretching frequencies decrease as the cation size increases and attributed the observation to a weakening of anion-anion interactions of the electrostatic type. They reported that for these polyanions, the approximation for the isolated anion strictly holds with large counter ions such as TBA, that is, these interactions vanish for only interanionic oxygen-oxygen distances as long as 6 Å [when the cation is tetrabutylammonium (TBA) salts].[104] Another insightful piece of work into speciation in solution over a wide pH range (0 to 12) was carried out by McGarvey and Moffat in 1991 and their work revealed that Keggin POM of 12-tungstphospate anions produces several species as the pH of the solution is changed while vanadate-phosphate or chromate-phosphate system did not show such behaviours. Thus the report provided a basis for an optimum pH range for working to minimize speciation in aqueous medium.[105]

Also, Hill and Combs-Walker in 1991 while studying the stability characteristics and metalation chemistry of the lacunary ion ($PMo_{11}O_{39}^{7-}$) stressed its significance in the development of POMs chemistry and its applications.[106] They noted the importance of the addition of TBA ion in the kinetic stabilization of the $PMo_{11}O_{39}^{7-}$ ion and that in contrast to aqueous solution, $PMo_{11}O_{39}^{7-}$ in MeCN solution showed some interesting solution chemistry. They stated that the $PMo_{11}O_{39}^{7-}$ polyanion could be (1) highly purified by recrystallization with no generation of other polymolybdophosphates. (2) reversibly protonated to $H_4PMo_{11}O_{39}^{3-}$ which slowly decomposes to $PMo_{12}O_{40}^{3-}$, $P_2Mo_{18}O_{62}^{6-}$ and $P_2Mo_5O_{23}^{6-}$ and is reversibly deprotonated to $H_2PMo_{11}O_{39}^{5-}$ and converted to α-A-$PMo_9O_{31}(OH)_3^{6-}$ with the requisite amount of OH^- and (3) metalated with several divalent d^n ($n \neq 0$) transition-metal (TM) ions to form the corresponding TM^{II}-substituted polymolybophosphates $[(TM^{II})PMo_{11}O_{39}]^{5-}$.[106] This study was fundamental because it further highlighted the importance of non-aqueous medium in understanding POMs metalation and solution chemistry. It also provided a basis for high yield preparations, rigorous purification by

crystallization, controlled stability and protonation studies of d^n ($n \neq 0$) transition metal substituted complexes $[(TM^{II})PMo_{11}O_{39}]^{5-}$.

While investigating polymorphism in a number of tetra-n-butylammonium salts of Keggin-type polyoxotungstates, namely α-$[PW_{11}O_{39}]^{7-}$, α-$[PW_{11}M(H_2O)O_{39}]^{5-}$ (M = Mn, Co, N)i, α-$[PW_{11}CuO_{39}]^{5-}$, α-$[PW_{11}Fe(H_2O)O_{39}]^{4-}$ and α-$[PW_{11}Fe(OH)O_{39}]^{5-}$, with the general formula $[(C_4H_9)_4N]_4H_x[anion].nH_2O$, Gamelas *et al.* in 2003 showed that solids with the less distorted anions ($PW_{11}M$, M = Co, Ni, Fe) crystallize in the same body-centered cubic structure whereas compounds with the anions PW_{11}, $PW_{11}Cu$ and $PW_{11}FeOH$ constitute a new isomorphic series, with a body-centered tetragonal lattice.[107] This showed how important the nature of the anion affects crystallization of Keggin POMs. Additionally, a study on Keggin mono-titanium (IV)-substituted POMs acid catalysis conducted by Matsuki *et al.* in 2013 reported the preparation and characterization of the monomeric Keggin POM $(Et_2NH_2)_5[\alpha\text{-}PW_{11}TiO_{40}]\cdot 2H_2O$ (EtN-**1**) and the μ-oxo Keggin dimer $(Et_2NH_2)_8[(\alpha\text{-}PW_{11}TiO_{39})_2O]\cdot 6H_2O$ (EtN-**2)**. The study showed that the monomer and dimer were strongly dependent upon pH in solution and that their interconversion could be controlled by the pH of the solutions. It also showed that unlike the Dawson analogues, the mono-protonated species of the dimer was not found in the pH range of 3.2–0.5.[108]

The Errington group at Newcastle has carried out fundamental studies aimed at developing nonaqueous strategies to Lindqvist POMs and understanding their nonaqueous solution properties. Building on the alkaline hydrolysis of metal alkoxides first investigated by Jahr and Fuchs, the Group in 1996 reported a nonaqueous hydrolytic synthetic method to early transition metal-substituted Lindqvist POMs.[109] It successfully showed that by the hydrolysis reaction of mixtures of metal alkoxides and mononuclear WO_4^{2-}, the hexametalates $[MW_5O_{19}]^{n-}$ or their methoxide derivatives $[(MeO)MW_5O_{18}]^{(n-1)-}$ (M = Ti, Zr, V, Nb, Ta, Mo or W), could be obtained with very good selectivities in some cases especially, where M = Ti or Zr. These results provided a way to overcoming the complex equilibria during aqueous acidification of MO_4^{2-} (M = W, Mo) as it showed that only simple nonaqueous species could be produced in the system as opposed to aqueous systems with a wide variety of complex species. The study also provided a simple and straightforward route to ^{17}O-enriched samples for the study of solution dynamics and reactivity.[109]

The newly developed synthetic strategy led to the covalent immobilization of a TiW_5 hexametalate by reaction with alkanol surface monolayers to single-crystal and porous silicon.[110] This was achieved due to the presence of robust, alkanol-derivatized silicon surfaces from hydrogen-terminated silicon, which provided the means to attach the hexametalates to the surface through covalent M-O-C alkoxide bonds by alcoholysis of the M-OR bond in $[(RO)MW_5O_{18}]^{n-}$.[110] As the reactivity of the T-O-Me bond presents a way for functionality manipulation in the titanotungstates $[XTiW_5O_{18}]^{3-}$, the tetra-*n*-butylammonium (TBA) salt of $[(MeO)TiW_5O_{18}]^{3-}$ was subsequently, protonated in a reactivity study by reactions with alcohols (ROH) to give primary, secondary and tertiary alkoxide derivatives $[(RO)TiW_5O_{18}]^{3-}$ (R = Et , ^{i}Pr, ^{t}Bu and Ar) while hydrolysis with water yielded the $[(\mu\text{-}O)(TiW_5O_{18})_2]^{6-}$.[63] The reactions showed that the titanium was six-coordinate in all cases and possibly demonstrated its reluctance to attain seven co-ordination. These studies showed that the heterometalates $[LM\text{-}M_5O_{18}]^{n-}$ contained labile M-L bond and that they had higher surface basicity than the parent $[M_6O_{19}]^{n-}$, thus opening up access to reactivity at the heterometal site.

Driven by the fact that some studies had shown that oxides of metals like zirconium and tungsten supported on the metals are strongly acidic and coupled with interesting postulations that Brønsted acid activity in WO_3/ZrO_2 and WO_3/TiO_2 catalytic systems was associated with the formation of polynuclear oxotungsten aggregates with incorporated heterometal surfaces,[111] further research by Errington and co-workers on zirconium hexametalate system, led to the successful synthesis of the dimeric methoxo-bridged, Zr^{IV}-substituted hexametalates $(^{n}Bu_4N)_6\text{-}[\{(\mu\text{-}MeO)ZrW_5O_{18}\}_2$ by stoichiometric hydrolysis of $Zr(O^{n}Pr)_4$, $[\{Zr(O^{i}Pr)_3(\mu\text{-}O^{n}Pr)(^{i}PrOH)\}_2]$, or $[\{Zr(O^{i}Pr)_4(^{i}PrOH)\}_2]$ and $[\{WO(OMe)_4\}_2]$ in the presence of $(^{n}Bu_4N)_2WO_4$. The study was the first to provide an avenue for the study of the systematic nonaqueous chemistry of ZrW_5 POMs and it also revealed that the coordination number of Zr was restricted to six in aryloxide systems while seven coordination was achieved in the alkoxides and chelate complexes. It further proposed the protonation of ZrOW sites as a possible step in reactions with HX, thus showing the flexibility of the $[ZrW_5O_{18}]^{2-}$ core as a molecular platform for modelling catalysis by tungstate zirconia surfaces.[111]

In a bid to extending the nonaqueous hydrolytic method to Lindqvist derivatives containing late 3d transition elements such as iron and cobalt, Errington and co-workers reported the successful synthesis and structurally characterization of two CoW_5 heterometalates and provided evidence for the formation of an analogous FeW_5 species using a two-step procedure that involved preliminary preparation of a "virtual" $W_5O_{18}^{6-}$ precursor.[24] The report further showed that the precursor behaves in a constitutionally dynamic fashion in solution, forming Lindqvist-type $[(L)\text{-}MW_5O_{18}]^{n-}$ heterometalates when treated with MCl_x or labile complexes of M^{x+} and that the dimeric compound$[(CoW_5O_{18}H)_2]^{6-}$ was obtained from $[Co(MeCN)_4(H_2O)_2]^{2+}$ or $CoCl_2$.

Errington and co-workers have also studied molybdate POMs. One of its pioneering studies in this area revealed the synthesis and characterization of the tetrabutylammonium (TBA) salt of the alkoxido-titanium pentamolybdate $[(^iPrO)TiMo_5O_{18}]^{3-}$ by hydrolysis of a mixture containing $(TBA)_2[Mo_2O_7]$, $(TBA)_4[Mo_8O_{26}]$ and $Ti(O^iPr)_4$ in MeCN.[22] The study proved that the insertion of $[Ti(O^iPr)]^{3+}$ into the pentamolybdate framework provided a reactive site for the systematic manipulation of functionality in $[(L)TiMo_5O_{18}]^{3-}$ POM systems and this subsequently lead to further exploration of the solution dynamics of the system. For instance, reaction of the pentamolybdate POM towards a range of protic reagents, resulted in the synthesis of a range of alkoxido and aryloxido-derivatised titanomolybdates as well as the oxido-bridged condensation product obtained by hydrolysis.[112] This provided some indication of ligand (L) effects on charge distribution within $[LTiMo_5O_{18}]^{3-}$ and highlighted the relative abilities of $[LTi]^{3+}$ to withdraw charge from the different oxometalate ligand $[M_5O_{18}]^{6-}$. It further exposed slight differences in protonolysis behaviour of Ti-OR when incorporated in different $[M_5O_{18}]^{6-}$ lacunary structures (M = W, Mo) and demonstrated that systematic access to closely related series of derivatised POMs was important for studies that can shed light on fundamental details of mixed-metal molecular oxide reactivity.[112]

Furthermore, Errington and co-workers applied their nonaqueous strategy in the synthesis of the Lindqvist-type $\{SnW_5\}$ POM, $[(MeO)SnW_5O_{18}]^{3-}$.[23] The study was very significant as it opened up the field to a number of SnW_5 derivatives, i.e. $[(HO)SnW_5O_{18}]^{3-}$, $[(\mu\text{-}O)(SnW_5O_{18})_2]^{6-}$, $[ClSnW_5O_{18}]^{3-}$, etc.

References

1. M. Ammam, *J. Mater. Chem. A*, 2013, **1**, 6291-6312.
2. M. T. Pope and A. Müeller, *Mol. Eng.*, 1993, **3**, 1-8.
3. P. W. Atkins, T. L. Overton, J. P. Rourke, M. T. Weller and F. A. Armstrong, *Shriver & Atkins' Inorganic Chemistry* Oxford University Press Oxford, 5th edn., 2010.
4. J. J. De Luyart Lubice and F. C. De Luyar Lubic, *Extractos de las Juntas Generales celebradas or la Real Sociedad Bascongada*, 1783, **46**.
5. M. T. Pope, *Heteropoly and Isopoly oxometalates* Springer-Verlag Berlin, New York, 1983.
6. L. C. W. Baker and D. C. Glick, *Chem. Rev.*, 1998, **98**, 3-49.
7. J. J. Berzelius, *Pogg. Ann.*, 1826, **6**, 369-380.
8. L. Svanberg and H. Struve, *J. Prakt. Chem.*, 1848, **44**, 257 - 291.
9. C. Marignac, *C. R. Acad. Sci.*, 1862, **55**, 888.
10. C. Marignac, *Ann. Chim.*, 1862, **25**, 362.
11. A. Miolati and R. Pizzighelli, *J. Prakt. Chem.*, 1908, **77**, 417.
12. L. Pauling, *J. Am. Chem. Soc.*, 1929, **51**, 2868-2880.
13. J. F. Keggin, *Nature*, 1933, **132**, 351.
14. A. J. Bradley and J. W. Illingworth, *Proc. Roy. Soc., A*, 1936, **157**, 113.
15. J. S. Anderson, *Nature*, 1937, **140**, 850.
16. H. T. Evans, Jr., *J. Am. Chem. Soc.*, 1948, **70**, 1291-1292.
17. I. Lindqvist, *Arkiv Kemi*, 1950, **2**, 349.
18. I. Lindqvist, *Arkiv Kemi*, 1952, **5**, 245.
19. P. Souchay, *Ions Mineraux Condenses*, Masson, Paris, 1969.
20. A. Proust, B. Matt, R. Villanneau, G. Guillemot, P. Gouzerh and G. Izzet, *Chem. Soc. Rev.*, 2012, **41**, 7605-7622.
21. D.-L. Long, R. Tsunashima and L. Cronin, *Angew. Chem., Int. Ed.*, 2010, **49**, 1736-1758.
22. R. J. Errington, L. Coyle, P. S. Middleton, C. J. Murphy, W. Clegg and R. W. Harrington, *J. Cluster Sci.*, 2010, **21**, 503-514.
23. B. Kandasamy, C. Wills, W. McFarlane, W. Clegg, R. W. Harrington, A. Rodriguez-Fortea, J. M. Poblet, P. G. Bruce and R. J. Errington, *Chem. Eur. J.*, 2012, **18**, 59-62.
24. R. J. Errington, G. Harle, W. Clegg and R. W. Harrington, *Eur. J. Inorg. Chem.*, 2009, 5240-5246.
25. J. Albert, D. Lueders, A. Boesmann, D. M. Guldi and P. Wasserscheid, *Green Chem.*, 2014, **16**, 226-237.
26. D. D. Dexter and J. V. Silverton, *J. Amer. Chem. Soc.*, 1968, **90**, 3589-3590.

27. T. J. R. Weakley, *J. Chem. Soc., Dalton Trans.*, 1973, 341-346.

28. R. Contant and A. Teze, *Inorg. Chem.*, 1985, **24**, 4610-4614.

29. A. Müller, E. Krickemeyer, H. Bögge, M. Schmidtmann and F. Peters, *Angew. Chem. Int. Ed. Engl.*, 1998, **37**, 3359-3363.

30. M. T. Pope and A. Mueller, *Angew. Chem. Int. Ed. Engl.*, 1991, **30**, 34 - 48.

31. R. J. Errington, *Advanced Practical Inorganic and Metalorganic Chemistry*, Blackie Academic & Professional, London, 1997.

32. M. T. Weller and N. A. Young, *Characterisation Methods in Inorganic Chemistry*, Oxford University Press, Oxford, 2017.

33. H. Günther, *NMR Spectroscopy: Basic Principles, Concepts, and Applications in Chemistry*, Wiley-VCH, Germany, 3rd edn., 2013.

34. B. H. Stuart, *Infrared Spectroscopy: Fundamentals and Applications*, John Wiley & Sons, Ltd., Australia, 2004.

35. F. Marken, A. Neudeck and A. M. Bond, in *Electrochemical methods: Guides to Experiments and Applications*, ed. F. Scholz, Springer, 2002, ch. 11.I, pp. 51-93.

36. D. A. Skoog, F. J. Holler and T. A. Nieman, *Principles of Instrumental Analysis*, Saunders College Publishing, United Statates of America, 5th edn., 1998.

37. W. Clegg, *X-ray Crystallography*, Oxford University Press, Oxford, 2nd edn., 2015.

38. R. G. Finke, M. W. Droege, J. C. Cook and K. S. Suslick, *J. Am. Chem. Soc.*, 1984, **106**, 5750-5751.

39. K. S. Suslick, J. C. Cook, B. Rapko, M. W. Droege and R. G. Finke, *Inorganic Chemistry*, 1986, **25**, 241-243.

40. F. A. Bagherjeri, M. Vonci, E. A. Nagul, C. Ritchie, R. W. Gable, M. B. Taylor, G. Bryant, S.-X. Guo, J. Zhang, P. A. Aparicio, X. López, J. M. Poblet and C. Boskovic, *Inorg. Chem.*, 2016, **55**, 12329-12347.

41. M. Pascual-Borras, X. Lopez, A. Rodriguez-Fortea, R. J. Errington and J. M. Poblet, *Chem. Sci.*, 2014, **5**, 2031-2042.

42. P. Jiménez-Lozano, J. J. Carbó, A. Chaumont, J. M. Poblet, A. Rodríguez-Fortea and G. Wipff, *Inorg. Chem.*, 2014, **53**, 778-786.

43. L. Vilà-Nadal, J. P. Sarasa, A. Rodríguez-Fortea, J. Igual, L. P. Kazansky and J. M. Poblet, *Chem. Asian J*, 2010, **5**, 97-104.

44. X. López, I. A. Weinstock, C. Bo, J. P. Sarasa and J. M. Poblet, *Inorg. Chem.*, 2006, **45**, 6467-6473.

45. O. A. Kholdeeva, T. A. Trubitsina, R. I. Maksimovskaya, A. V. Golovin, W. A. Neiwert, B. A. Kolesov, X. López and J. M. Poblet, *Inorg. Chem.*, 2004, **43**, 2284-2292.

46. D. Barats-Damatov, L. J. W. Shimon, L. Weiner, R. E. Schreiber, P. Jimenez-Lozano, J. M. Poblet, C. de Graaf and R. Neumann, *Inorg. Chem.*, 2014, **53**, 1779-1787.

47. J.-J. Ye and C.-D. Wu, *Dalton Trans.*, 2016, **45**, 10101-10112.

48. S. J. Folkman and R. G. Finke, *ACS Catal.*, 2017, **7**, 7-16.

49. J. J. Stracke and R. G. Finke, *ACS Catal.*, 2014, **4**, 79-89.

50. Y. Ren, M. Wang, X. Chen, B. Yue and H. He, *Materials*, 2015, **8**, 1545.

51. M. H. Habibi, S. Tangestaninejad, V. Mirkhani and B. Yadollahi, *Catal. Lett.*, 2001, **75**, 205-207.

52. E. Rafiee, S. Tangestaninejad, M. H. Habibi and V. Mirkhani, *Bull. Korean Chem. Soc.*, 2005, **26**, 1585-1587.

53. S. Sheshmani, M. A. Fashapoyeh, M. Mirzaei, B. A. Rad, S. N. Ghortolmesh and M. Yousefi, *Indian J. Chem., Sect. A: Inorg., Bio-inorg., Phys., Theor. Anal. Chem.*, 2011, **50A**, 1725-1729.

54. S. Mansouri, O. Benlounes, C. Rabia, R. Thouvenot, M. M. Bettahar and S. Hocine, *J. Mol. Catal. A: Chem.*, 2013, **379**, 255-262.

55. A. Sartorel, M. Carraro, G. Scorrano, R. D. Zorzi, S. Geremia, N. D. McDaniel, S. Bernhard and M. Bonchio, *J. Am. Chem. Soc.*, 2008, **130**, 5006-5007.

56. A. Sartorel, P. Miró, E. Salvadori, S. Romain, M. Carraro, G. Scorrano, M. D. Valentin, A. Llobet, C. Bo and M. Bonchio, *J. Am. Chem. Soc.*, 2009, **131**, 16051-16053.

57. H. Lv, J. Song, Y. V. Geletii, J. W. Vickers, J. M. Sumliner, D. G. Musaev, P. Kögerler, P. F. Zhuk, J. Bacsa, G. Zhu and C. L. Hill, *J. Am. Chem. Soc.*, 2014, **136**, 9268-9271.

58. Q. Yin, J. M. Tan, C. Besson, Y. V. Geletii, D. G. Musaev, A. E. Kuznetsov, Z. Luo, K. I. Hardcastle and C. L. Hill, *Science*, 2010, **328**, 342-345.

59. J. Soriano-Lopez, S. Goberna-Ferron, L. Vigara, J. J. Carbo, J. M. Poblet and J. R. Galan-Mascaros, *Inorg. Chem.*, 2013, **52**, 4753-4755.

60. M. D. Symes and L. Cronin, *Nat. Chem.*, 2013, **5**, 403-409.

61. H. Yang, J. Li, L. Wang, W. Dai, Y. Lv and S. Gao, *Catal. Commun.*, 2013, **35**, 101-104.

62. R. J. Errington, S. S. Petkar and P. S. Middleton, Boston, MA, United States., 2007.

63. R. J. Errington, S. S. Petkar, P. S. Middleton, W. McFarlane, W. Clegg, R. A. Coxall and R. W. Harrington, *Dalton Trans.*, 2007, 5211-5222.

64. R. J. Errington, S. S. Petkar, P. S. Middleton, W. McFarlane, W. Clegg, R. A. Coxall and R. W. Harrington, *J. Am. Chem. Soc.*, 2007, **129**, 12181-12196.

65. Q. Lan, J. Zhang, Z.-M. Zhang, Y. Lu and E.-B. Wang, *Dalton Trans.*, 2013, **42**, 16602-16607.

66. X. Iwanowa, J. Strunk, E. Loeffler, M. Muhler and K. Merz, *Phys. Status Solidi B*, 2013, **250**, 1165-1173.

67. A. Balaska, R. Belghiche, M. H. Samar, T. Chouchane and R. Haseneder, *MATEC Web Conf.*, 2013, **5**, 04011-04015.

68. Y. Yang, L. Xu, B. Xu, X. Du and W. Guo, *Mater. Lett.*, 2009, **63**, 608-610.

69. L. Que, Jr. and W. B. Tolman, *Nature*, 2008, **455**, 333-340.

70. X. Liu and F. Wang, *Coord. Chem. Rev.*, 2012, **256**, 1115-1136.

71. M. Yaqub, J. J. Walsh, T. E. Keyes, A. Proust, C. Rinfray, G. Izzet, T. McCormac and R. J. Forster, *Langmuir*, 2014, **30**, 4509-4516.

72. K. Suzuki, J. Jeong, K. Yamaguchi and N. Mizuno, *New J. Chem.*, 2016, **40**, 1014-1021.

73. N. Mizuno and M. Misono, *Chem. Rev.*, 1998, **98**, 199-218.

74. T. Okuhara, N. Mizuno and M. Misono, in *Advances in Catalysis*, eds. W. O. H. D.D. Eley and G. Bruce, Academic Press, 1996, vol. Volume 41, pp. 113-252.

75. T. Okuhara, N. Mizuno and M. Misono, *Appl. Catal., A.*, 2001, **222**, 63-77.

76. Y. Gong, Y. Guo, Q. Hu, C. Wang, L. Zang and L. Yu, *ACS Sustain. Chem. Eng.*, 2017, **5**, 3650-3658.

77. B. Xu, L. Xu, G. Gao, Y. Yang, W. Guo, S. Liu and Z. Sun, *Electrochim. Acta*, 2009, **54**, 2246-2252.

78. N. Anwar, M. Vagin, F. Laffir, G. Armstrong, C. Dickinson and T. McCormac, *Analyst* 2012, **137**, 624-630.

79. S. Li, H. Ma, K. P. O'Halloran, H. Pang, H. Ji and C. Zhou, *Electrochim. Acta*, 2013, **108**, 717-726.

80. S. Liu, L. Xu, G. Gao, B. Xu and W. Guo, *Mater. Chem. Phys.*, 2009, **116**, 88-93.

81. B. Ertan, T. Eren, İ. Ermiş, H. Saral, N. Atar and M. L. Yola, *J. Colloid Interface Sci.*, 2016, **470**, 14-21.

82. Ö. A. Yokuş, F. Kardaş, O. Akyıldırım, T. Eren, N. Atar and M. L. Yola, *Sens. Actuators, B*, 2016, **233**, 47-54.

83. S.-T. Zheng and G.-Y. Yang, *Chem. Soc. Rev.*, 2012, **41**, 7623-7646.

84. J. J. Baldoví, S. Cardona-Serra, A. Gaita-Ariño and E. Coronado, in *Advances in Inorganic Chemistry*, eds. E. Rudi van and C. Leroy, Academic Press, 2017, vol. Volume 69, pp. 213-249.

85. E. Coronado and C. J. Gómez-García, *Chemical Reviews*, 1998, **98**, 273-296.

86. J. Lehmann, A. Gaita-Arino, E. Coronado and D. Loss, *Nat. Nanotechnol.*, 2007, **2**, 312-317.

87. S. Gam Derouich, C. Rinfray, G. Izzet, J. Pinson, J.-J. Gallet, F. Kanoufi, A. Proust and C. Combellas, *Langmuir*, 2014, **30**, 2287-2296.

88. I. V. Andreev, A. L. Tchougreeff, P. Kogerler and R. C. Rai, *Inorg. Chem.*, 2014, **53**, 2892-2898.

89. J. Zhang, Q. Lan, Z.-M. Zhang, Z.-J. Liu, Y. Liang and E.-b. Wang, *J. Cluster Sci.*, 2014, **25**, 253-259.

90. F. I. Dalidchik, S. A. Kovalevskii, E. M. Balashov and B. A. Budanov, *Nanotechnologies in Russia*, 2016, **11**, 331-336.

91. J. J. Stracke and R. G. Finke, *ACS Catal.*, 2014, **4**, 79-89.

92. Y.-Y. Hu, L.-N. Xiao, Y. Wang, D.-C. Zhao, L.-M. Wang, H.-Y. Guo, X.-B. Cui and J.-Q. Xu, *Polyhedron*, 2013, **56**, 152-159.

93. Y.-H. Ding, J. Peng, H.-Y. Lu, Y. Yuan and S.-U. Khan, *RSC Adv.*, 2016, **6**, 81085-81091.

94. T. Yamase, H. Fujita and K. Fukushima, *Inorg. Chim. Acta.*, 1988, **151**, 15-18.

95. J. T. Rhule, C. L. Hill, D. A. Judd and R. F. Schinazi, *Chem. Rev.*, 1998, **98**, 327-358.

96. Ş. Bâlici, S. Şuşman, D. Rusu, G. Z. Nicula, O. Soriţău, M. Rusu, A. S. Biris and H. Matei, *J. Appl. Toxicol.*, 2016, **36**, 373-384.

97. X.-X. Li, S.-T. Zheng, W.-H. Fang and G.-Y. Yang, *Inorg. Chem. Commun.*, 2011, **14**, 1541-1545.

98. Z.-y. Shi, J. Peng, Y.-g. Li, Z.-y. Zhang, X. Yu, K. Alimaje and X. Wang, *CrystEngComm*, 2013, **15**, 7583-7588.

99. Y.-F. Qiu, H. Liu, J.-X. Liu, C. Zhang, Z. Ma, P.-A. Hu and G.-G. Gao, *J. Mater. Chem. C*, 2015, **3**, 6322-6328.

100. T. Zhang, N. Ma, L. Yan, S. Wen and Z. Su, *Chem. Phys. Lett.*, 2013, **557**, 123-128.

101. T. J. R. Weakley and S. A. Malik, *J. Inorg. Nucl. Chem.*, 1967, **29**, 2935-2944.

102. S. A. Malik and T. J. R. Weakley, *J. Chem. Soc. A*, 1968, 2647-2650.

103. C. Tourne, G. Tourne, S. A. Malik and T. J. R. Weakley, *J. Inorg. Nucl. Chem.*, 1970, **32**, 3875-3890.

104. C. Rocchiccioli-Deltcheff, M. Fournier, R. Franck and R. Thouvenot, *Inorg. Chem.*, 1983, **22**, 207-216.

105. G. B. McGarvey and J. B. Moffat, *J. Mol. Catal.*, 1991, **69**, 137-155.

106. L. A. Combs-Walker and C. L. Hill, *Inorg. Chem.*, 1991, **30**, 4016-4026.

107. J. A. F. Gamelas, M. R. Soares, A. Ferreira and A. M. V. Cavaleiro, *Inorg. Chim. Acta*, 2003, **342**, 16-22.

108. Y. Matsuki, Y. Mouri, Y. Sakai, S. Matsunaga and K. Nomiya, *Eur. J. Inorg. Chem.*, 2013, **2013**, 1754-1761.

109. W. Clegg, M. R. J. Elsegood, R. J. Errington and J. Havelock, *J. Chem Soc., Dalton Trans.*, 1996, 681-690.

110. R. J. Errington, S. S. Petkar, B. R. Horrocks, A. Houlton, L. H. Lie and S. N. Patole, *Angew. Chem., Int. Ed.*, 2005, **44**, 1254-1257.

111. R. J. Errington, S. S. Petkar, P. S. Middleton, W. McFarlane, W. Clegg, R. A. Coxall and R. W. Harrington, *J. Am. Chem. Soc.*, 2007, **129**, 12181-12196.

112. L. Coyle, P. S. Middleton, C. J. Murphy, W. Clegg, R. W. Harrington and R. J. Errington, *Dalton Trans.*, 2012, **41**, 971-981.

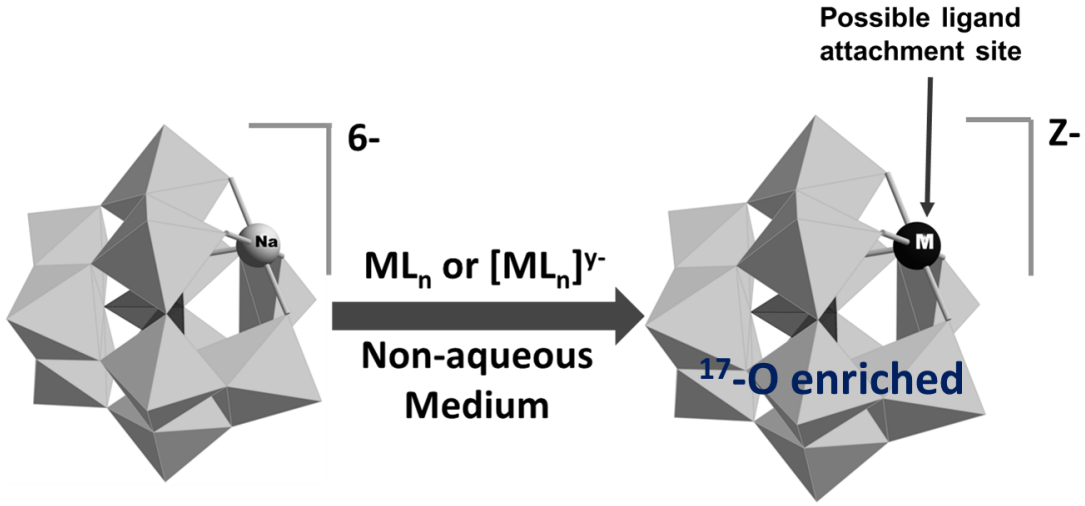

Chapter 3

Protonation and non-aqueous studies of substitution into $[NaPW_{11}O_{39}]^{6-}$

The present chapter builds on previous work by Dr. R. L. Wingad, a former PhD student in the Errington group, who developed a non-aqueous synthetic route to the sodium-monosubstituted Keggin polyoxometalate (POM), $(TBA)_6[NaPW_{11}O_{39}]$. Our group has extensive expertise and interest in applying ^{17}O NMR technique to fundamental and mechanistic studies on non-aqueous aggregation, speciation and reactivity of POMs especially those of the Lindqvist family. The work describe in this chapter is an extension to Keggin species and describes an efficient non-protic approach to a range of ^{17}O-enriched monosubstituted heterometallic Keggin POMs *via* non-aqueous substitution into $[NaPW_{11}O_{39}]^{6-}$. The enriched POMs are important as models for mechanistic studies and provide an avenue for extending available theoretical models for predicting ^{17}O NMR chemical shifts of POMs.

3. Protonation and non-aqueous studies of substitution into $[NaPW_{11}O_{39}]^{6-}$

3.1. Introduction

The availability of POMs with ^{17}O-enriched oxygen sites provides a unique opportunity for ^{17}O NMR studies that allow for better understanding of their reactivity. Such studies have resulted in the identification of novel POM species in solutions[1,2] and offered more insights into their catalytic reaction mechanisms. They have also facilitated the use of POMs as models for understanding both homogenous and heterogeneous processes[3-6] which are important in catalysis and sensing applications. In the mid 1970's, Klemperer pioneered the application of ^{17}O NMR spectroscopy to study the speciation, structure and behaviour of POMs in solution and has published widely in this area.[1,7-16] The Errington group also has published several papers on ^{17}O NMR studies on a range of Lindqvist polyoxometalates, prepared *via* non-aqueous hydrolytic aggregation with minimum amounts of ^{17}O-enriched H_2O.[17-31] Quite recently, two papers were published on models for predicting ^{17}O NMR chemical shifts of polyoxometalates.[5,32] However, these works were mainly on Lindqvist POMs, with limited information on Keggin species. To our knowledge, available ^{17}O NMR literature on Keggin POMs includes works on the anions, α-$[PW_{12}O_{40}]^{3-}$, α-$[PMo_{12}O_{40}]^{3-}$, α-$[SiW_{12}O_{40}]^{4-}$ α-$[SiMo_{12}O_{40}]^{4-}$, α-$[SiMoW_{11}O_{40}]^{4-}$,[11,13] α-$[(\eta^5\text{-}C_5H_5)Ti(PW_{11}O_{39})]^{4-}$ prepared *via* nonaqueous reactions of $(TBA)_4H_3[PW_{11}O_{39}]$,[11] $H_8[(TiPW_{11}O_{39})_2O]$, $[(TiPW_{11}O_{39})_2OH]^{7-}$ and $[TiPW_{11}O_{40})]$[5-33,34] and the series $[Ln^{III}(PW_{11}O_{39})_2]^{11-}$ (Ln = La, Ce, Pr, Nd, Sm, Eu, Gd, Tb, Dy, Ho, Er, Tm, Yb)[35] prepared *via* aqueous strategies. Non-aqueous POM synthesis has been shown to have the advantage of accessing compounds which are not stable in aqueous medium[19,22,23,28,36] and provides a cheaper and more efficient route to ^{17}O-enriched POMs for recording of well-resolved spectra in the shortest possible time.[13] However, products of non-aqueous reactions of $(TBA)_4H_3[PW_{11}O_{39}]$ are prone to trace impurities of $[PW_{12}O_{40}]^{3-}$, which arise from reactions with acids in solution produced by free protons.[37,38] Hence, the motivation for a convenient non-protic alternative route to a range of ^{17}O-enriched heterometallic POMs, $[(L)MPW_{11}O_{39}]^{n-}$ (M = Sn^{2+}, Pb^{2+}, Co^{2+}, Ni^{2+}, Bi^{3+}, Sb^{3+}, Ir^{3+}, Rh^{3+}, Sn^{4+} Ti^{4+},Ce^{4+}, Ir^{4+}, Pt^{4+}) for mechanistic studies in hydrolysis and protonation reactions. In this chapter therefore, the synthesis, characterization and protonolysis of ^{17}O-enriched

$(TBA)_6[NaPW_{11}O_{39}]$ are described. Additionally, non-aqueous substitution reactions between $(TBA)_6[NaPW_{11}O_{39}]$ and a range of metal salts are discussed.

3.2. Results and Discussion

3.2.1. Synthesis and characterization of ^{17}O-enriched $(TBA)_6[NaPW_{11}O_{39}]$

^{17}O-enriched $(TBA)_6[NaPW_{11}O_{39}]$ was prepared by a post-enrichment strategy, which involves preparation of unenriched $(TBA)_6[NaPW_{11}O_{39}]$ and then enrichment with minimum ^{17}O-enriched H_2O. A previously reported method[20,30,31,39] was adopted in preparing the unenriched POM species. The method involves reaction of 1 mole-equivalent of $Na_3[PW_{12}O_{40}].8H_2O$ with 6 mole-equivalents of methanolic TBAOH in dry acetonitrile at -30 ^oC. The isolated product was then enriched by adding ~ 0.5 weight percent of ^{17}O-enriched H_2O in an acetonitrile solution of the POM and stirring the solution at 80 ^oC for 12 h. The isolated product showed a single ^{31}P NMR peak at -10.40 ppm (the unenriched POM had a minor peak (1.9%) at -10.11 ppm in addition to the major peak (98.1%) at -10.40 ppm). ^{17}O-enrichment of samples is usually achieved either by preparing the sample with ^{17}O-enriched H_2O as reactant or by heating prepared unenriched samples in ^{17}O-enriched H_2O.[5] We were also able to achieve enrichment by stirring at room temperature. The solution of ^{17}O-enriched H_2O was recovered from the enriched POM by vacuum transfer into a solvent trap and was reused for up to 2 subsequent POM enrichments. Characterization of the product was by single crystal XRD analysis, FT-IR, multinuclear NMR (^{1}H, ^{17}O, ^{31}P and ^{183}W), ESI-MS and CHN elemental microanalysis.

3.2.1.1. Single crystal X-ray diffraction analysis of $(TBA)_6[NaPW_{11}O_{39}]$

Previous X-ray diffraction analysis on a crystalline sample obtained by cooling an acetonitrile/diethyl ether solution of the POM over several weeks showed disorder in the six tetrabutylammonium cations with the sodium atom statistically disordered over nine of the twelve metal sites.[39] Disorder is a well-known phenomenon in the crystal structures of monosubstituted Keggin polyanions[40] and our efforts to crystallize $(TBA)_6[NaPW_{11}O_{39}]$ were to provide extra support for the presence of sodium in the lacuna. In this direction, we thought that crystallizing the POM in the presence of a stronger co-ordinating ligand might introduce an interaction with the sodium and prevent or reduce disorder. Thus,

$(TBA)_6[NaPW_{11}O_{39}]$ was crystallized over 3 weeks by slow vapour diffusion of diethyl ether into an acetonitrile solution of the sample to which 2 drops of DMSO were added. Single crystal X-ray diffraction analysis revealed that the sample crystallizes in the monoclinic *Cc* space group and, though there was evidence of interaction with DMSO, the sodium atom was still statistically disordered across two of the twelve metal positions (see **Figure 3.1** for crystal structure and experimental section for the refinement method). These data provide further evidence for the incorporation of Na into the POM as there is not sufficient electron density for a fully-occupied W atom at the sites modelled as partially-occupied Na and W. There is also some evidence of solvation with DMSO at one Na site though there appears to have been significant solvent loss prior to the mounting of the crystal which has also led to partial-occupation of the MeCN sites. The disorder of the TBA cations has been modelled over multiple sites but there are still some very close contacts between them suggesting that the electron density associated with these cations is more spread out than the model might suggest.

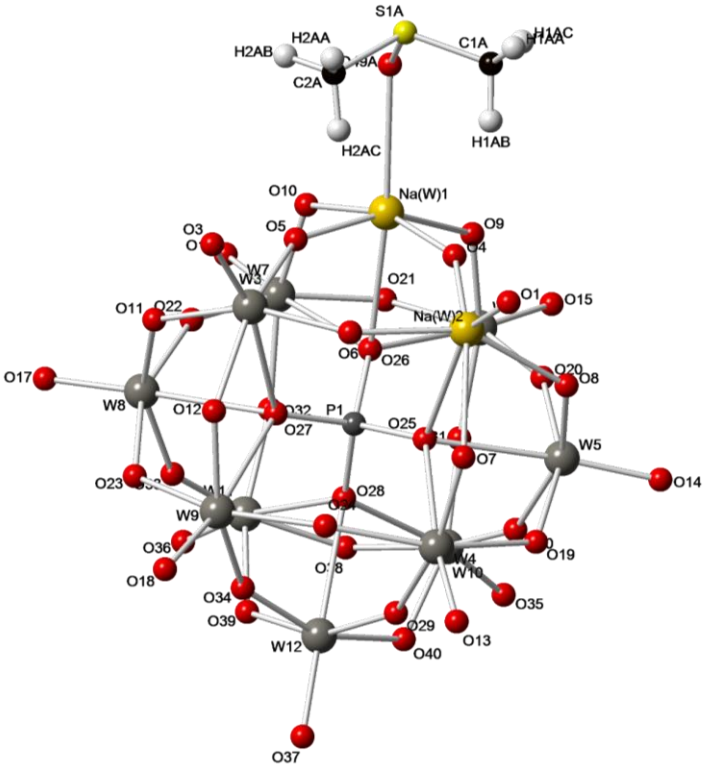

Figure 3.1. Ball and stick representation of the crystal structure of $[(dmso)NaPW_{11}O_{39}]^{6-}$ obtained from slow vapour diffusion of diethyl ether into an MeCN/DMSO solution of a TBA salt of the POM.

3.2.1.2. FT-IR spectroscopy

The FT-IR spectrum of the enriched $(TBA)_6[NaPW_{11}O_{39}]$ (**Figure 3.2**) showed no significant difference from that of the unenriched POM and compares well with that reported previously[39] though slight differences exist in wavenumber values and this is most likely due to the different methods of measurement (ATR in our case and transmission previously). Based on previous work,[39] peak assignments are 1070 and 1034 cm^{-1} for ν_{as}(P-O), 933 cm^{-1} for ν_{as}(W-O_t), 880 and 843 cm^{-1} for ν_{as}(W-O_b) between W_3 groups, 804 and 714 cm^{-1} for ν_{as}(W-O_b) within W_3 groups, 589 cm^{-1} for δ (O-P-O) and 504 cm^{-1} for δ (W-O-W). The observed vibrations around the POM characteristic region (1200 – 400 cm^{-1}) are well-established for substituted lacunary Keggin POMs.[41-43] Comparison of the IR parameters of the Keggin series presented in **Table 3.1** is quite informative. Firstly, it shows that the terminal W=O vibration of $[NaPW_{11}O_{39}]^{6-}$ was 24 and 38 cm^{-1} lower than values for $H_3[PW_{11}O_{39}]^{4-}$ and $[PW_{12}O_{40}]^{3-}$ respectively supporting the proposal of a higher charge (6-). Secondly, the loss of symmetry in the lacunary POM, $[PW_{11}O_{39}]^{7-}$ (due to loss of WO^{4+} unit from $[PW_{12}O_{40}]^{3-}$) is restored more in $[NaPW_{11}O_{39}]^{6-}$ than in $H_3[PW_{11}O_{39}]^{4-}$ based on its smaller ν_3 P-O asymmetric stretch frequency splitting. The degree of splitting, ν_3 Δ(P-O) has been linked to the symmetry of the substituted polyanion and the strength of the interaction of heterometal-O(PO_3).[41,42] This result is thus indicative of a strong interaction between the sodium atom and the central phosphorus tetrahedron (PO_4) in $[NaPW_{11}O_{39}]^{6-}$ and such interaction seems to be absent or weak in $H_3[PW_{11}O_{39}]^{4-}$ where there is no metal.

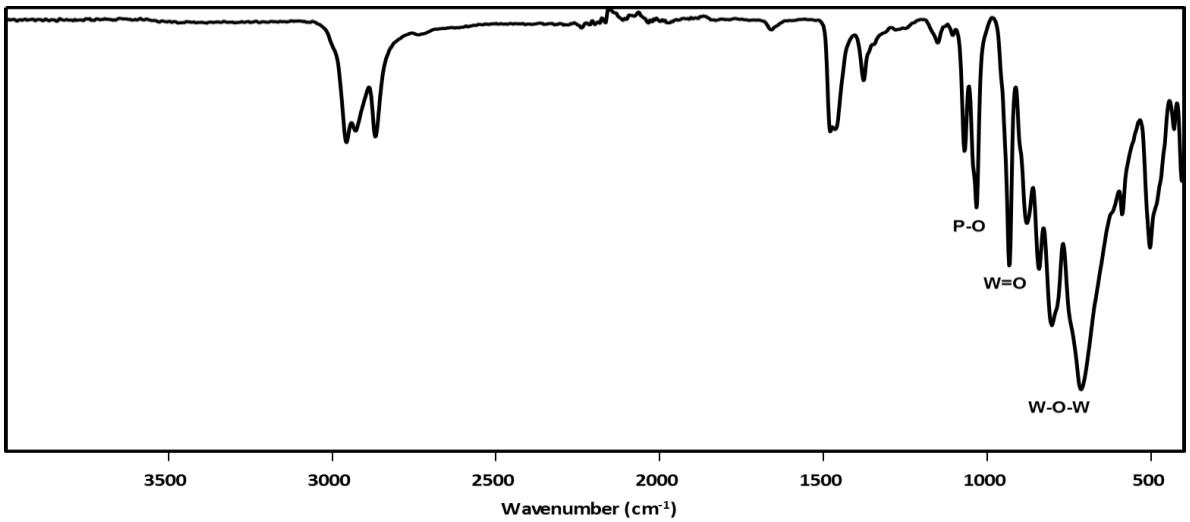

Figure 3.2. FT-IR spectrum of ^{17}O-enriched $(TBA)_6[NaPW_{11}O_{39}]$ before crystallization in DMSO/MeCN.

Table 3.1. FT-IR parameters in cm^{-1} for $[NaPW_{11}O_{39}]^{6-}$, $[H_3PW_{11}O_{39}]^{4-}$ and $[PW_{12}O_{40}]^{3-}$ anions[a]

Anion	ν (W=O)	ν (WOW)	ν (P-O)	Δν (P-O)	Reference
$[PW_{11}O_{39}]^{7-}$	[b]	[b]	1085, 1040	45	41
$[NaPW_{11}O_{39}]^{6-}$	933	880, 843, 804, 714	1070, 1034	36	This work
$[H_3PW_{11}O_{39}]^{4-}$	957	887, 805, 750	1105, 1055	50	44
$[PW_{12}O_{40}]^{3-}$	971	900, 765	1072	0	This work

[a] measured as solid powder of TBA salts on an ATR module; [b] not reported.

3.2.1.3. Multinuclear NMR (^1H, ^{17}O, ^{31}P, ^{183}W) spectroscopy

In contrast to $[PW_{12}O_{40}]^{3-}$, which has four sets of symmetry-equivalent oxygens (four central W_3OP oxygens, twelve WOW bridging oxygens each linked to two metals *via* corner-sharing octahedra, twelve WOW bridging oxygens each linked to two metals *via* edge-sharing octahedra and twelve W=O terminal oxygens), the monosubstituted heterometallic POMs are expected to have at least seven sets of symmetry-equivalent oxygens. As shown in **Figure 3.3**, these are due to three W_3OP oxygens (O_A), ten WOW oxygens bridging two tungsten metals *via* edge-sharing octahedra (O_B), ten WOW oxygens bridging two tungsten metals *via* corner-sharing octahedra (O_C), eleven W=O terminal oxygens (O_D), one W_2MOP oxygen (O_E), two M-O-W oxygens with larger M-O-W bond angle (O_F) and two MOW oxygens with smaller M-O-W bond angle (O_G). Chemical shifts, line widths and intensities of ^{17}O NMR resonances may generally provide structural and dynamic information but the assignment of ^{17}O NMR resonances in this thesis is based only on the established correlation between downfield chemical shifts and increasing oxygen π-bond order (with decreasing number of metals bonded to oxygen).[8,12,13] Relative peak intensities were not informative as differential enrichment of oxygen sites might lead to erroneous assignment of peaks. Also, due to line broadness and our inability to resolve peaks in some cases, no attempt was made to assigned peaks to individual WOW and MOW oxygens. The ^{17}O NMR spectrum (**Figure 3.4**) of ^{17}O-enriched $(TBA)_6[NaPW_{11}O_{39}]$ showed a major broad peak with shoulders and two minor peaks in the range 707 – 644 ppm, which were assigned to W=O oxygens. These oxygens with greater π-bond order are expected to appear further downfield.[12,13] The resonances were shifted upfield by >63 ppm from the value of $[PW_{12}O_{40}]^{3-}$ W=O terminal oxygens (770 ppm), signifying an extensive delocalisation of the extra negative charge (6- vs. 3-) on the polyanion (see **Table 3.4**). Two unresolved peaks at 438 and 433 ppm were assigned to Na-O-W oxygens consistent with XRD evidence of sodium in the crystal structure.

The presence and position of these peaks further support the existence of NaOW bonding, which is consistent with sodium in the lacuna in place of tungsten. Two broad peaks (and shoulders) at 397 and 363 ppm were assigned to W-O-W oxygens based on a smaller π-bond order and increasing number of metals to which oxygen is bonded.[8] These resonances were also at lower chemical shifts than those of $[PW_{12}O_{40}]^{3-}$ (432 and 405 ppm) due to the greater negative charge. The absence of a resonance at about 90 ppm in the ^{17}O NMR spectrum (**Figure 3.4**) indicates that no enrichment was achieved for the less accessible central PO_4 (W_3OP and W_2NaOP) oxygens by our method. Although Filowitz *et al.* were also not able to enrich these oxygens in $[PW_{12}O_{40}]^{3-}$ previously,[13] the ^{17}O NMR resonance is predicted to occur at 91 ppm.[32]

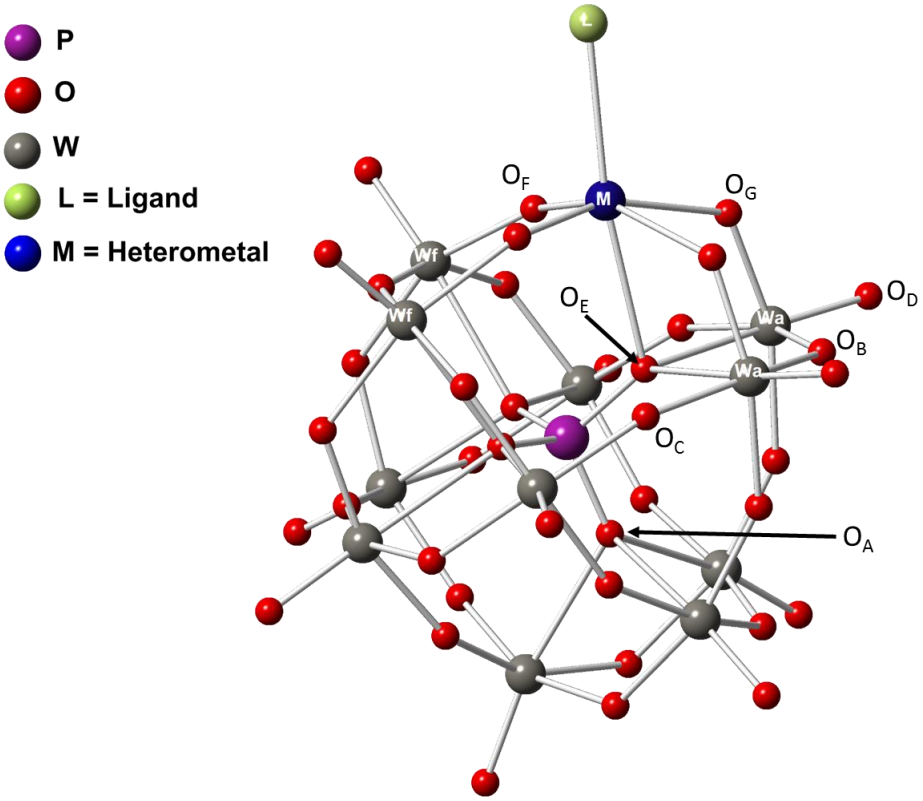

Figure 3.3. Ball and stick representation of monosubstituted heterometallic POMs, $[(L)MPW_{11}O_{39}]^{n-}$ ($M = Na^{+}$, Sn^{2+}, Pb^{2+}, Co^{2+}, Ni^{2+}, Bi^{3+}, Sb^{3+}, Ir^{3+}, Rh^{3+}, Sn^{4+}, Ti^{4+}, Ce^{4+}, Ir^{4+}, Pt^{4+}; $L = Cl^{-}$, NO_3^{-}, CH_3COO^{-}, CH_3CN) showing seven sets of symmetry-equivalent oxygens (O_A, O_B, O_C, O_D, O_E, O_F and O_G) and two types of MOW bond angles (M-O-W_a and M-O-W_f).

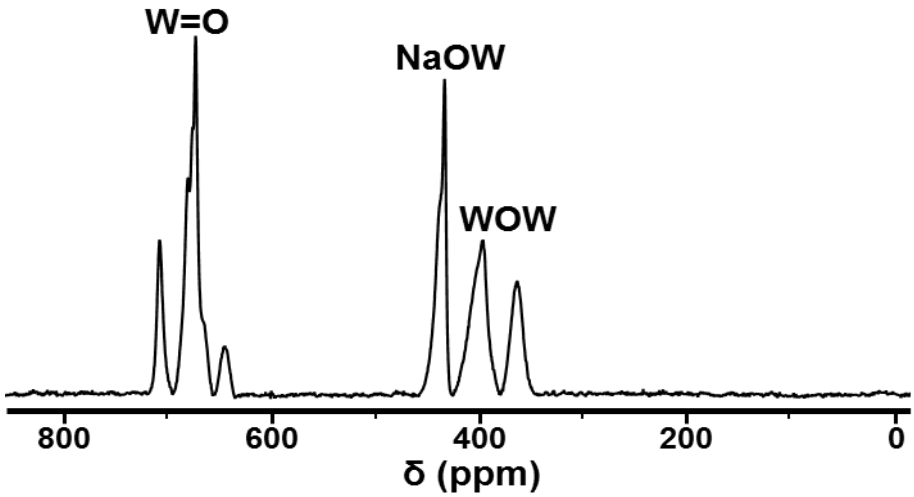

Figure 3.4. ^{17}O NMR spectrum of enriched $(TBA)_6[NaPW_{11}O_{39}]$ in MeCN

The ^{1}H NMR spectrum of both unenriched and enriched POMs (see **Appendix A3.1**) showed only peaks assigned to the TBA cation. The ^{31}P NMR spectrum, on the other hand of the unenriched $(TBA)_6[NaPW_{11}O_{39}]$ showed a major peak at -10.40 ppm (98.1%) and a minor peak at -10.11 ppm (1.9%), which Wingad had earlier assigned to an isomer.[39] Both peaks were still present in the spectrum when the POM was enriched at room temperature for up to 72 h. However, only the single peak at -10.40 ppm was observed when enrichment was done at elevated temperature (80 ^{o}C) for 12 h. This might suggests conversion of the minor less stable isomer to the more stable one at elevated temperature.

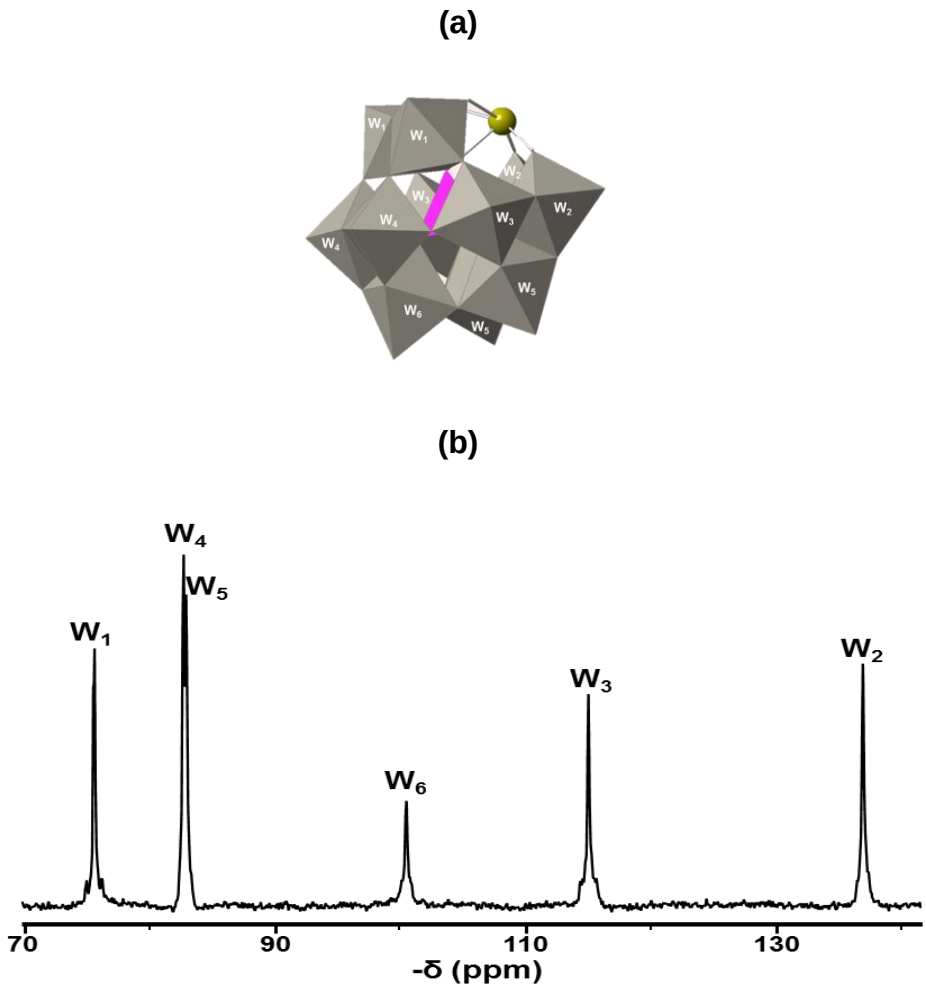

Figure 3.5. (a) Polyhedral model of $(TBA)_6[NaPW_{11}O_{39}]$ with numbering on tungsten octahedral (b) ^{183}W NMR spectrum of $(TBA)_6[NaPW_{11}O_{39}]$ with assignment of resonances.

The ^{183}W NMR spectrum of $(TBA)_6[NaPW_{11}O_{39}]$ as expected had six peaks at -75.6, -82.7, -82.9, -100.5, -115.1 and -137.0 ppm in the ratio 2:2:2:1:2:2 [see **Figure 3.5 (b)** and **Table 3.6**]. Although the two-dimensional NMR techniques, COSY and 2D-INADEQUATE are the best approach to completely and unequivocally assign tungsten resonances of POMs[40], the assignment in **Figure 3.5** was based on analysis of W-O-W satellite peaks[37,45] and previous assignment of the ^{183}W NMR spectrum of $Na_7[PW_{11}O_{39}]$ (in D_2O), which is expected to also contain the $[NaPW_{11}O_{39}]^{6-}$ polyanion. The observed peaks in the ^{183}W NMR spectrum of $(TBA)_6[NaPW_{11}O_{39}]$ have been attributed to the symmetry of the POM due to the presence of one distinctive tungsten atom and five inequivalent pairs.[40]

3.2.1.4. Electrospray Ionization Mass Spectrometry

Though the negative ESI-MS analysis of $(TBA)_6[NaPW_{11}O_{39}]$ in the region 0 – 2500 m/z showed a high degree of fragmentation with several unassigned species, some observed minute peaks could be assigned to $NaPW_{11}O_{39}^{6-}$ plus cation-compensating charges $[(C_{16}H_{36}N)_2HNaPW_{11}O_{39}]^{3-}$ and $[(C_{16}H_{36}N)_3HNaPW_{11}O_{39}]^{2-}$ [see **Appendix** (**Figure A3.2** for full ESI-MS spectrum and **Figure A3.3** for peaks expansion and simulation)]. Peaks were also assigned to $[H_3PW_{11}O_{39}]^{4-}$, $[NaW_6O_{19}]^-$ and $[HWO_4]^-$ (see **Table 3.2**) that have been observed in the ESI-MS spectrum of $Na_7PW_{11}O_{39}$.[46] The high fragmentation pattern might be ascribed to the high lability of the polyanion.

Table 3.2. ESI-MS data collected for $[NaPW_{11}O_{39}]^{6-}$

Formula	**m/z**	
	Observed	**Calculated**
$[W_2O_7]^{2-}$	239.9	239.84
$[HWO_4]^-$ / $[WO_3(OH)]^-$	248.9	248.85
$[W_3O_{10}]^{2-}$	355.9	355.76
$[W_4O_{13}]^{2-}$	471.9	471.68
$[HW_2O_7]^-$	480.9	480.68
$Na[W_2O_7]^-$	502.9	502.67
$[PW_2O_9]^-$	542.9	542.65
$[PW_2O_8(OH)_2]^-$	560.8	560.66
$[W_5O_{16}]^{2-}$	587.9	587.60
$[H_3PW_{11}O_{39}]^{4-}$	670.86	670.05
$[W_6O_{19}]^{2-}$	703.9	703.51
$[PW_3O_{12}]^-$	774.8	774.49
$[(C_{16}H_{36}N)_2HNaPW_{11}O_{39}]^{3-}$	1062.03	1062.04
$[NaW_6O_{19}]^-$	1430.6	1430.02
$[(C_{16}H_{36}N)_3PW_9O_{32}]^{2-}$	1462.42	1462.46
$[(C_{16}H_{36}N)_3HNaPW_{11}O_{39}]^{2-}$	1714.22	1714.30

3.2.1.5. CHN Elemental Microanalysis

The formulation, $(TBA)_6[NaPW_{11}O_{39}](MeCN)_{0.4}$ which agrees well with the proposed formula, $(TBA)_6[NaPW_{11}O_{39}]$, was deduced from CHN microanalysis results on sample crystallized by cooling from an acetonitrile/diethyl ether solution (See Experimental Section). This further supports the proposed charge of 6- for the anion due to the presence of a sodium atom in the POM lacuna.

3.2.2. Protonation study on $(TBA)_6[NaPW_{11}O_{39}]$ using $HBF_4.Et_2O$

In an attempt to understand its behaviour in the presence of protons and determine the protonation sites, $[NaPW_{11}O_{39}]^{6-}$ was protonated with varying amounts of $HBF_4.Et_2O$ in acetonitrile. Generally, addition of protons to POMs is expected to result in a slight downfield movement of the ^{17}O NMR peaks of non-protonated oxygens due to reduction of the overall negative charge whereas peaks of protonated oxygens are expected to shift upfield (lower chemical shift)[32] due to greater shielding of the nucleus.[47] The ^{17}O NMR spectra [**Figure 3.6 (a)**] showed that addition of 0.25 equiv. of H^+ to $[NaPW_{11}O_{39}]^{6-}$ gave fewer W=O peaks, which might indicate some restoration of symmetry in the acidified species with corresponding increase in chemical shifts from (707 – 644) to (722 – 688), expected due to decrease in the overall polyanion charge. Interestingly, the unresolved NaOW resonances at 438 – 433 gave two sharp peaks at 445 and 428 ppm. The upfield peak might indicate protonation at one of the NaOW oxygens. As mentioned above, ^{17}O NMR resonances of protonated oxygens have been proposed to move upfield while the non-protonated ones slightly move downfield when proton-exchange occurs between chemically similar or equivalent oxygen sites.[32] A new peak, which was not assigned was observed at 616 ppm. Subsequent protonation showed step-wise chemical shift changes in the NaOW resonances (456 and 428 ppm at 0.5 equiv. H^+ and 455 and 445 ppm at 0.75 equiv. of H^+). These changes could not be interpreted as protonation of NaOW sites as they were downfield. However, the changes generally support a decreasing overall polyanion charge. Also, a general downfield shift (723 – 700 at 0.5 H^+, 724 – 704 at 0.75 H^+ and 732 – 711 ppm at 1.0 H^+) was observed in the terminal W=O peaks as expected. A minor terminal W=O chemical shift assigned to $[PW_{12}O_{40}]^{3-}$ appeared at 0.75 H^+ and increased upon further protonation. ^{31}P NMR studies provided more information on the protonation chemistry and revealed formation of multiple species upon protonation. **Figure 3.6 (b)** shows that addition of 0.25 equiv. of H^+ to $[NaPW_{11}O_{39}]^{6-}$ resulted in the disappearance of the single ^{31}P NMR resonance at -10.40 ppm and appearance of three peaks at -11.15 (95.72%), -9.88 (1.74%) and -10.87 ppm (2.54%). An upfield shift of the major resonance to -11.38 ppm with appearance of six other minor peaks (totalling 44%) at -9.89, -10.02, -10.90, -10.96, -12.94 and -15.03 ppm was observed with 0.5 equiv. of H^+. The spectrum became more complex with the addition of 0.75 equiv. of H^+ showing a more upfield major peak at -11.73 ppm with

ten other peaks including ~2% of a peak at -15.36 ppm assigned to $[PW_{12}O_{40}]^{3-}$ as earlier indicated by ^{17}O NMR. Again, no concrete explanation is available for the general upfield shift of the major ^{31}P NMR resonance upon protonation and though He *et al.* reported the structure of a Na-O-Na bridged dimer, $Na_{12}H_4[A\text{-}\beta\text{-}PW_9O_{34}Na(H_2O)]_2{\cdot}38H_2O$ prepared by recrystallization of $Na_9[A\text{-}PW_9O_{34}]$ from acidic solution[48] and a DFT study had predicted dimerization for a number of heterometallic Lindqvist and Keggin POMs upon protonation,[49] we could not ascribe this observation to dimerization of $[NaPW_{11}O_{39}]^{6-}$ *via* protonation of Na-O-W sites. Moreover, protonation at the M-O-W oxygen (M = V[50], Ti[33]) has been shown to result in a downfield shift of ^{31}P NMR. We did not attempt isolation of any species because of the complex nature of the spectrum although most of the species are suspected to be lacunary anions based on their ^{31}P chemical shift range (9- to 13- ppm)[51]. One conclusion, however is that $[NaPW_{11}O_{39}]^{6-}$ is very sensitive to protons, which is quite surprising in view of the existence of the tri-protonated anion, $H_3[PW_{11}O_{39}]^{3-}$ and $[NaPW_{11}O_{39}]^{6-}$ with a higher overall charge of 6- would be expected to accept at least 2 mole-equivalents of protons without decomposing. The high sensitivity of $[NaPW_{11}O_{39}]^{6-}$ to protons might be linked to the presence of sodium in the lacuna.

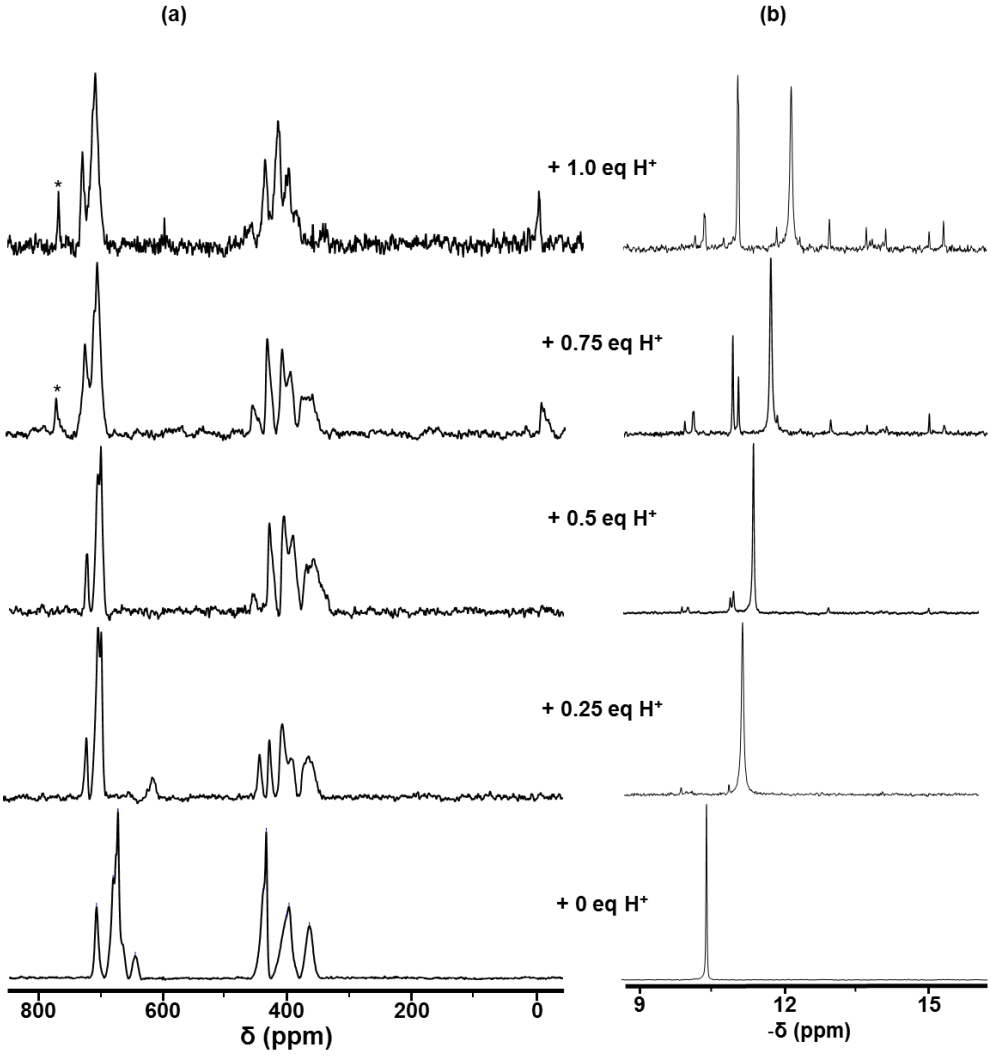

Figure 3.6. (a) ^{17}O and (b) ^{31}P NMR spectra of protonation of $(TBA)_6[NaPW_{11}O_{39}]$ with $HBF_4.Et_2O$ in CD_3CN. Peaks marked with an asterisk are assigned to $[PW_{12}O_{40}]^{3-}$ polyanion.

3.2.3. Non-aqueous studies of substitution into $[NaPW_{11}O_{39}]^{6-}$

Reactions between mono-lacunary Keggin species and suitable reactive heterometal compounds provide routes to heterometallic Keggin POMs of the $[(L)MPW_{11}O_{39}]^{n-}$ series. These reactions have mostly been in aqueous solution with alkali metal salts of $M_7[PW_{11}O_{39}]$ (M = K, Na, Cs),[52,53] or to a lesser extent in non-aqueous media with $(TBA)_4[H_3PW_{11}O_{39}]$.[37,38,53] In a bid to establish the previously reported highly organic-soluble mono-sodium-substituted polyanion, $(TBA)_6[NaPW_{11}O_{39}]$[20,30,31] as a suitable non-aqueous precursor to a range of ^{17}O-enriched heterometallic Keggin POMs (see **Figure 3.3**), substitution reactions with labile heterometallic salts were attempted based on **Scheme 3.1**. The reactions were monitored by

^{31}P NMR while products were characterized by FT-IR (**Table 3.3**), multinuclear NMR (^{17}O, ^{31}P, ^{119}Sn, ^{183}W, ^{207}Pb) and ESI-MS.

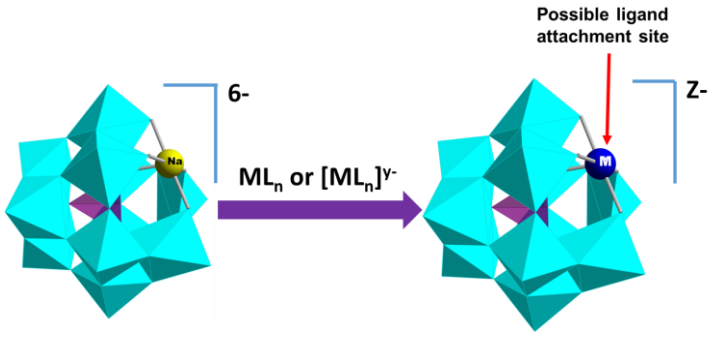

Scheme 3.1. Polyhedral representation of synthesis of [(L)MPW$_{11}$O$_{39}$]$^{n-}$ (M = Sn^{2+}, Pb^{2+}, Co^{2+}, Ni^{2+}, Bi^{3+}, Sb^{3+}, Ir^{3+}, Rh^{3+}, Sn^{4+}, Ti^{4+}, Ce^{4+}, Ir^{4+}, Pt^{4+}; L = Cl$^-$, NO$_3^-$, CH$_3$COO$^-$) from (TBA)$_6$[NaPW$_{11}$O$_{39}$].

Table 3.3. FT-IR data for {MPW$_{11}$} Keggin anions.[a]

Anion	Wavenumber (cm^{-1})			
	ν(W=O)	ν(WOW)	ν(P-O)	Δν(P-O)
[NaPW$_{11}$O$_{39}$]$^{6-}$	933	880, 843, 804	1070 1034	36
[Sn^{II}PW$_{11}$O$_{39}$]$^{5-}$	942	872, 787	1097 1046	51
[Pb^{II}PW$_{11}$O$_{39}$]$^{5-}$	940	873, 787	1083 1040	43
[Co^{II}PW$_{11}$O$_{39}$]$^{5-}$	946	873, 792	1065	-
[Ni^{II}PW$_{11}$O$_{39}$]$^{5-}$	946	875, 793	1062	-
[Sb^{III}PW$_{11}$O$_{39}$]$^{4-}$	955	880, 787	1101 1061	40
[Bi^{III}PW$_{11}$O$_{39}$]$^{4-}$	952	879, 784	1084 1053	31
[ClTiPW$_{11}$O$_{39}$]$^{4-}$	962	883, 787,	1071	-
[ClSn^{IV}PW$_{11}$O$_{39}$]$^{4-}$	962	880, 787, 702	1079 1056	23
[PW$_{12}$O$_{40}$]$^{3-}$	971	900, 765	1072	-

[a] recorded as ^{n}Bu$_4$N$^+$ salts on an ATR module.

Table 3.4. ^{17}O NMR data for {MPW_{11}} Keggin anions.[a]

Anion	^{17}O chemical shift/ppm		
	W=O	MOW	WOW
$[NaPW_{11}O_{39}]^{6-}$	707 – 644	438, 433	402 - 363
$[Sn^{II}PW_{11}O_{39}]^{5-}$	720 – 701	527, 522	426 - 379
$[Pb^{II}PW_{11}O_{39}]^{5-}$	718 – 694	566	426 - 372
$[Sb^{III}PW_{11}O_{39}]^{4-}$	750 – 730		427 – 384
$[Bi^{III}PW_{11}O_{39}]^{4-}$	743 – 719	487	425 - 384
$[ClTiPW_{11}O_{39}]^{4-}$	747 – 743	585, 565	427 - 386
$[ClSn^{IV}PW_{11}O_{39}]^{4-}$	749 – 737		429 - 372
$[PW_{12}O_{40}]^{3-}$	770	-	432, 405

[a] recorded as $^{n}Bu_4N^+$ salts in MeCN.

Table 3.5. ^{31}P, ^{119}Sn, and ^{207}Pb NMR data for {MPW_{11}} Keggin anions[a]

Anion	^{31}P		^{119}Sn		^{207}Pb
	δ (ppm)	$^2J_{Sn\text{-}P}$ (Hz)	δ (ppm)	$^2J_{Sn\text{-}W}$ (Hz)	δ (ppm)
$[NaPW_{11}O_{39}]^{6-}$	-10.40	-			-
$[Sn^{II}PW_{11}O_{39}]^{5-}$	-13.22	-	-684.38	91[b]	-
				131[c]	
$[Pb^{II}PW_{11}O_{39}]^{5-}$	-11.99	-	-	-	-355.52
$[Co^{II}PW_{11}O_{39}]^{5-}$	330.92	-	-	-	-
$[Ni^{II}PW_{11}O_{39}]^{5-}$	-12.78				-
$[Sb^{III}PW_{11}O_{39}]^{4-}$	-14.22	-	-	-	-
$[Bi^{III}PW_{11}O_{39}]^{4-}$	-12.54	-	-	-	-
$[ClTiPW_{11}O_{39}]^{4-}$	-14.36				-
$[ClSn^{IV}PW_{11}O_{39}]^{4-}$	-12.90	37	-578.08	63[b]	-
				157[c]	
$[PW_{12}O_{40}]^{3-}$	-15.35	-	-	-	-

[a] recorded as $^{n}Bu_4N^+$ salts in CD_3CN; [b] $^2J(^{119}Sn^{183}W_A)$; [c] $^2J(^{119}Sn^{183}W_F)$.

Table 3.6. ^{183}W NMR data for {MPW_{11}} Keggin anions.[a]

Anion	δ, ppm (Integral)					
$[NaPW_{11}O_{39}]^{6-}$	-75.6(2)	-82.7(2)	-82.9(2)	-100.5(1)	-115.1 (2)	-137.0(2)
$[Sn^{II}PW_{11}O_{39}]^{5-}$	-62.8(2)	-96.3 (2)	-106.1(2)	-106.9 (1)	-115.9 (2)	-127.2(2)
$[Pb^{II}PW_{11}O_{39}]^{5-}$	-48.9(2)	-77.5 (2)	-92.6(2)	-97.8(1)	-116.2 (2)	-129.9(2)
$[Sb^{III}PW_{11}O_{39}]^{4-}$[b]	-82.0(2)	-96.5(2)	-105.0(1)	-111.9(2)	-115.0 (2)	-142.3 (2)
$[Bi^{III}PW_{11}O_{39}]^{4-}$	-40.6(2)	-60.4(2)	-92.5(2)	-102.3(1)	-115.7 (2)	-121.2 (2)
$[ClSn^{IV}PW_{11}O_{39}]^{4-}$	-76.8(2)	-91.4(2)	-108.4(2)	-114.8(2)	-130.7(1)	-174.5(2)

[a] recorded as $^{n}Bu_4N^+$ salts in CD_3CN; [b] recorded in DMSO-d_6.

Synthesis of $(TBA)_5[SnPW_{11}O_{39}]$: Reaction between $[NaPW_{11}O_{39}]^{6-}$ and 1 mole-equivalent of $SnCl_2$ in MeCN led to an instant colour change from colourless to deep orange-yellow, fading to pale yellow and the reaction was completed within 30 mins at room temperature. The ^{31}P NMR spectrum of the isolated yellow solid showed a single resonance at -13.22 ppm with no

P-Sn coupling. The ^{17}O NMR spectrum (**Figure 3.7**) showed three peaks at 720 – 701 ppm assigned to the terminal W=O oxygens based on the correlation between downfield peaks and greater oxygen π-bond order discussed in **Section 3.2.1.3**. A peak and a shoulder at 527 – 522 ppm were assigned to SnOW oxygens based on previously reported experimental (395 – 562 ppm)[22,23,28,54,55] and theoretical (376 – 570 ppm)[32] ^{17}O NMR chemical shifts for MOW (M = Ta, Nb, V, Sn, Ti, Zr) oxygens in POMs while peaks at 426 – 379 ppm were assigned to the WOW oxygens based on the relationship between upfield resonances and increasing number of tungsten metals bonded to oxygen also discussed in **Section 3.2.1.3**. It is worth noting that peaks in the ^{17}O NMR spectra of other heterometallic POMs were assigned in a similar fashion. The ^{119}Sn NMR spectrum (**Figure 3.8**) showed a peak at -684.38 ppm with no P-Sn coupling but with Sn-W couplings of 131 and 91 Hz respectively [see **Appendix (Figure A3.21)** for simulations of ^{119}Sn NMR spectrum]. The absence of P-Sn coupling in the ^{31}P and ^{119}Sn NMR spectra shows that there is no P-O-Sn^{II} bonding, which suggests that the tin in its +2 state does not fit into the POM lacuna very well.[38] The ^{183}W NMR spectrum [**Figure 3.16 (b)**] gave six lines at -62.78, -96.30, -106.06, -106.89, -115.94 and -127.12 ppm in the ratio: 2:2:2:1:2:2 indicative of the C_s symmetry of the POM. It was however difficult to resolve the Sn-W couplings. This allows only assignment of the unique tungsten peak (C). The FT-IR data presented in **Table 3.3** show a terminal W=O vibrational frequency of 942 cm^{-1} suggestive of an overall polyanion charge of 5- whereas the large $\Delta\nu_3$ (P-O) (51 cm^{-1}) also confirms the weak or none existing interaction between the tin atom and the central PO_4 tetrahedron. These results led to the formulation, $(TBA)_5[SnPW_{11}O_{39}]$ for the product. Pope had earlier prepared $(TMA)_5[SnPW_{11}O_{39}]$ by adding excess $(CH_3)_4NCl$ to an aqueous buffered solution of the product of the reaction between α-$K_7PW_{11}O_{39}.xH_2O$ and $SnSO_4$ at 70 – 80 ^oC and pH 4.[38] However, even though the FT-IR spectra of $(TBA)_5[SnPW_{11}O_{39}]$ and $(TMA)_5[SnPW_{11}O_{39}]$ were similar and their ^{31}P NMR spectra showed no P-Sn coupling, there was a marked difference in the ^{119}Sn NMR chemical shift, -684.38 ppm (in CD_3CN) for $(TBA)_5[SnPW_{11}O_{39}]$ and -43.9 (in D_2O) to -45.7 ppm (in 10 M LiCl) for $(TMA)_5[SnPW_{11}O_{39}]$. Pope had suggested the variation in δ (^{119}Sn) in the presence of Li^+ in D_2O to be due to formation of ion-paired complexes. The even larger difference in weakly coordinating MeCN may suggest different Sn environment in MeCN and H_2O. ESI-MS data (see **Table 3.7**) provided more evidence for $(TBA)_5[SnPW_{11}O_{39}]$. The data showed peaks that were assigned to $[(C_{16}H_{36}N)_4(Sn^{II}PW_{11}O_{39})]^-$,

$[(C_{16}H_{36}N)_3(Sn^{II}PW_{11}O_{39})]^{2-}$, $[(C_{16}H_{36}N)(Sn^{II}PW_{11}O_{39})]^{2-}$, $[(C_{16}H_{36}N)_2(Sn^{II}PW_{11}O_{39})]^{3-}$, $[(C_{16}H_{36}N)H(Sn^{II}PW_{11}O_{39})]^{3-}$ and $[H_2Sn^{II}PW_{11}O_{39}]^{3-}$ [see **Appendix** (**Figure A3.2** for full ESI-MS spectrum and **Figure A3.4** for peaks expansion and simulation)]. Other peaks could be assigned to $[(HO)Sn^{IV}PW_{11}O_{39}]^{4-}$ plus compensating cation (a product of the easy oxidation of Sn^{II} to Sn^{IV}), but there was no proof of any species with chloride ion present.

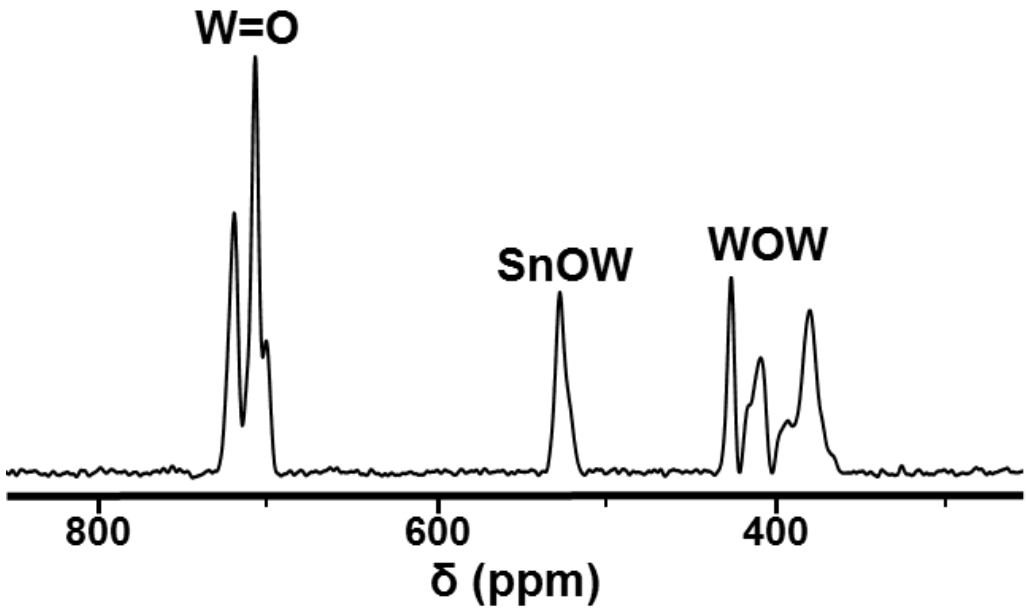

Figure 3.7. ^{17}O NMR spectrum of $(TBA)_5[SnPW_{11}O_{39}]$ in MeCN.

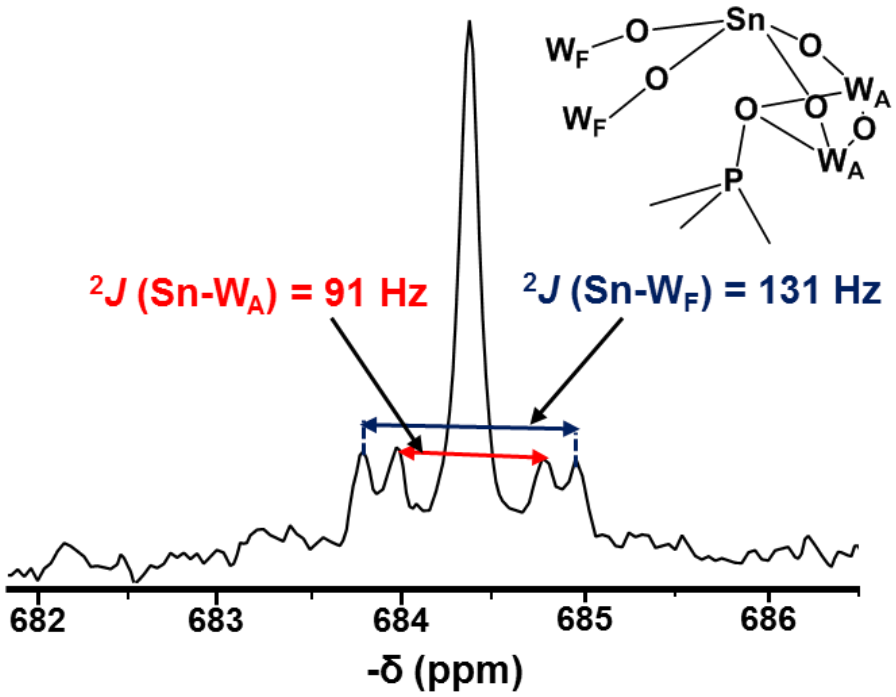

Figure 3.8. ^{119}Sn NMR spectrum of $(TBA)_5[SnPW_{11}O_{39}]$ in CD_3CN.

Table 3.7. ESI-MS data for $(TBA)_5[SnPW_{11}O_{39}]$

Formula	m/z	
	Observed	Calculated
$[(HO)SnPW_{11}O_{39}]^{4-}$	703.3	703.23
$[H_2SnPW_{11}O_{39}]^{3-}$	932.6	932.64
$[H((HO)SnPW_{11}O_{39})]^{3-}$	937.9	937.97
$[(C_{16}H_{36}N)H(SnPW_{11}O_{39})]^{3-}$	1013.1	1013.13
$[(C_{16}H_{36}N)_2(SnPW_{11}O_{39})]^{3-}$	1093.5	1093.61
$[H_2(HO)SnPW_{11}O_{39})]^{2-}$	1407.1	1406.96
$[(C_{16}H_{36}N)(SnPW_{11}O_{39})]^{2-}$	1519.1	1519.19
$[(C_{16}H_{36}N)H((HO)SnPW_{11}O_{39})]^{2-}$	1528.2	1528.19
$[(C_{16}H_{36}N)_2((HO)SnPW_{11}O_{39})]^{2-}$	1648.7	1648.92
$[(C_{16}H_{36}N)_3(SnPW_{11}O_{39})]^{2-}$	1761.4	1761.65
$[(C_{16}H_{36}N)_3((HO)SnPW_{11}O_{39})]^{-}$	3539.9	3540.31
$[(C_{16}H_{36}N)_4(SnPW_{11}O_{39})]^{-}$	3765.3	3765.78

Synthesis of $(TBA)_5[PbPW_{11}O_{39}]$: Treatment of $[NaPW_{11}O_{39}]^{6-}$ with 1 mole-equivalent of $Pb(OOCCH_3)_2$ in MeCN gave a cloudy solution within ~5 mins. NMR and FT-IR spectra of the isolated white solid after an hour of reaction showed some similarity to $[Sn^{II}PW_{11}O_{39}]^{5-}$: (1) The ^{31}P NMR resonance was at -11.99 ppm with no observed P-Pb coupling also consistent with Pb(II) and no P-O-Pb bonding. (2) The ^{17}O NMR spectrum (**Figure 3.9**) showed peaks at

718 – 694 ppm assigned to the terminal W=O oxygens, a peak at 566 ppm assigned to PbOW oxygens and peaks at 426 – 372 ppm assigned to the WOW oxygens. The more downfield resonance of Pb^{II}-O-W (566 ppm) than Sn^{II}-O-W (527, 522 ppm) suggests it possesses more π character. (3) The ^{183}W NMR spectrum [**Figure 3.16 (c)**] also suggests a C_s symmetry with six lines at -48.92, -77.53, -92.57, -97.77, -116.18 and -129.90 ppm in the ratio: 2:2:2:1:2:2. (4) In the FT-IR spectrum, the terminal W=O vibration of 940 cm^{-1} and the large P-O splitting (43 cm^{-1}) equally provide evidence for an overall polyanion charge of 5- and Pb^{2+} heteroatom respectively (see **Table 3.1**). In addition, the ^{207}Pb NMR spectrum (**Figure 3.10**) showed a very broad peak at -355.52 ppm ($\nu_{1/2}$ = 3109 Hz), which did not allow for resolution of any P-Pb or Pb-W couplings. The reason for this is not clear as ^{207}Pb nucleus is not quadrupolar (I = ½), however, it might be due to some dynamic process (i.e. solvent association) happening in solution. ESI-MS analysis (see **Table 3.8**) showed a high degree of fragmentation though some peaks in the spectrum could be assigned to $[(C_{16}H_{36}N)H(PbPW_{11}O_{39})]^{3-}$, $[(C_{16}H_{36}N)(PbPW_{11}O_{39})]^{4-}$, $[H(PbPW_{11}O_{39})]^{4-}$, $[(C_{16}H_{36}N)_2(PbPW_{11}O_{39})]^{3-}$, $[(C_{16}H_{36}N)_3(PbPW_{11}O_{39})]^{2-}$, $[Na_2(PbPW_{11}O_{39})]^{3-}$ and $[Na_3(PbPW_{11}O_{39})]^{2-}$ [see **Appendix** (**Figure A3.2** for full ESI-MS spectrum and **Figure A3.5** for peaks expansion and simulation)]. The Na observed in the fragments are due to Na ions picked up by the polyanion as its goes through a glass capillary to the detector in the ESI-MS. The polyanion was as a result characterized as $(TBA)_5[Pb^{II}PW_{11}O_{39}]$.

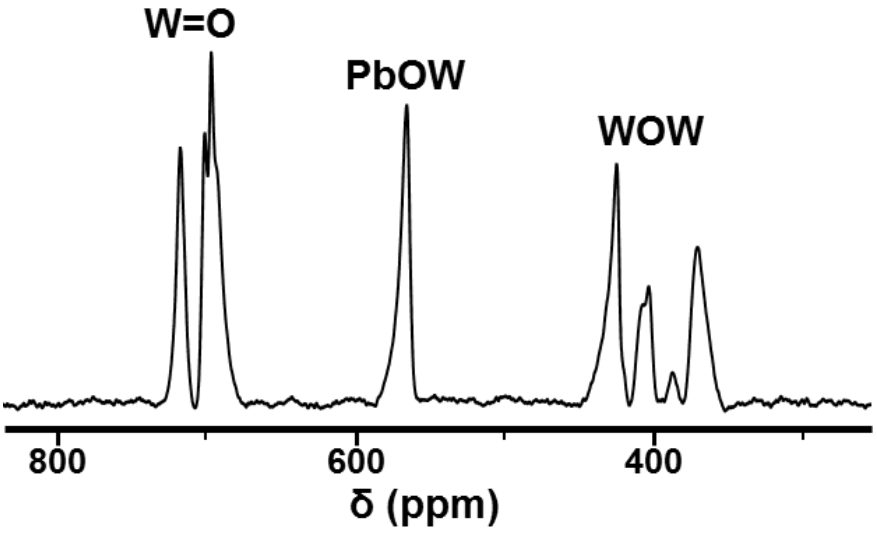

Figure 3.9. ^{17}O NMR spectrum of $(TBA)_5[PbPW_{11}O_{39}]$ in MeCN.

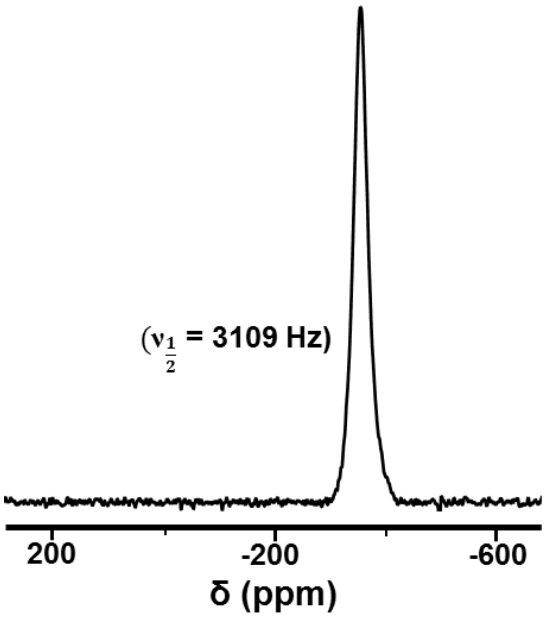

Figure 3.10. ^{207}Pb NMR spectrum of (TBA)$_5$[PbPW$_{11}$O$_{39}$] in CD$_3$CN.

Table 3.8. ESI-MS data for (TBA)$_5$[PbPW$_{11}$O$_{39}$]

Formula	**m/z**	
	Observed	**Calculated**
$[WO_3]^-$	231.9	
$[W_2O_7]^{2-}$	239.9	239.84
$[HWO_4]^-$	248.9	248.9
$[W_3O_{10}]^{2-}$	355.9	355.76
$[W_4O_{13}]^{2-}$	471.9	471.68
$[W_2O_7H]^-$	480.8	480.68
$[NaW_2O_7]^-$	502.9	502.67
$[W_5O_{16}]^{2-}$	587.8	587.60
$[W_6O_{19}]^{2-}$	703.8	703.51
$[Na_2(PbPW_{11}O_{39})]^{3-}$	976.9	976.79
$[(C_{16}H_{36}N)_2(PbPW_{11}O_{39})]^{3-}$	1122.9	1123.11
$[Na_3(PbPW_{11}O_{39})]^{2-}$	1476.6	1476.68
$[(C_{16}H_{36}N)(PbPW_{11}O_{39})]^{4-}$	781.89	781.72
$[H(PbPW_{11}O_{39})]^{4-}$	721.31	721.35
$[(C_{16}H_{36}N)H(PbPW_{11}O_{39})]^{3-}$	1042.52	1042.62
$[(C_{16}H_{36}N)_3(PbPW_{11}O_{39})]^{2-}$	1805.5	1805.90

Synthesis of (TBA)$_4$[SbPW$_{11}$O$_{39}$]: Treatment of $[NaPW_{11}O_{39}]^{6-}$ with 1 mole-equivalent of $SbCl_3$ in MeCN immediately gave a cloudy solution with blueish tinge. The ^{31}P NMR spectrum of the isolated white product gave a single peak at -14.22 ppm. The ^{17}O NMR spectrum (**Figure 3.11**) of the product gave four peaks at 750 – 730 ppm assigned to W=O oxygens and peaks at 427 – 384 ppm assigned to SbOW and WOW oxygens. We were not able to unambiguously assign peaks to these oxygens as the Sb^{III}-O-W resonance was shifted more

upfield into the W-O-W region. When compared to those of other polyanions (see **Table 3.4**), the chemical shifts of terminal W=O oxygens give an idea of the overall charge of the polyanion. **Table 3.4** shows that it compares more with polyanions of overall charge of 4-, suggesting that no chloride ligand is attached to the Sb atom. Also, when compared with the terminal W=O resonances of the series $[Ln^{III}(PW_{11}O_{39})_2]^{11-}$ (Ln = La, Ce, Pr, Nd, Sm, Eu, Gd, Tb, Dy, Ho, Er, Tm, Yb) (717 – 670 ppm)[35], it is safe to infer a formulation of $[Sb^{III}PW_{11}O_{39}]^{4-}$ where the antimony is coordinated to four oxygens of $PW_{11}O_{39}^{7-}$ in a square pyramidal geometry with no P-O-Sb interaction. The ^{183}W NMR spectrum [**Figure 3.16(d)**] gave six lines at -82.04, -96.46, -105.00, -111.88, -114.96 and -142.33 ppm in the ratio: 2:2:1:2:2:2 indicative of a C_s symmetry. The pattern is similar to that observed in Sn^{2+} and Pb^{2+} polyanions though the unique tungsten peak appeared at a different position. The FT-IR data (**Table 3.3**) showed a terminal W=O vibration of 955 cm^{-1}, also supporting an overall polyanion charge of 4- and a large P-O splitting of 40 cm^{-1} indicating no or some sort of weak interaction between antimony heteroatom and the central PO_4 tetrahedron. ESI-MS analysis provided sound proof of the absence of a chloride ligand. **Table 3.9** shows peaks assigned to $[Sb^{III}PW_{11}O_{39}]^{4-}$, $[HSb^{III}PW_{11}O_{39}]^{3-}$, $[(C_{16}H_{36}N)Sb^{III}PW_{11}O_{39}]^{3-}$ and $[(C_{16}H_{36}N)_2Sb^{III}PW_{11}O_{39}]^{2-}$ [see **Appendix** (**Figure A3.2** for full ESI-MS spectrum and **Figure A3.6** for peaks expansion and simulation)]. $(TBA)_4[SbPW_{11}O_{39}]$ was treated with methanolic MeONa in a bid to further confirm the presence or absence of chloride ligand on the polyanion. MeO- is expected to substitute any chloride ligand on the POM to give the methoxyl derivative as shown in **Equation 3.1**. Only degradation products and some unreacted starting material resulted from the reaction [as shown by ^{31}P and ^{1}H NMR, see **Appendix (Figure A3.10)**] confirming the absence of a chloride ligand.

$$?[ClSbPW_{11}O_{39}]^{5-} + NaOMe \longrightarrow [(MeO)SbPW_{11}O_{39}]^{5-} + NaCl \qquad (3.1)$$

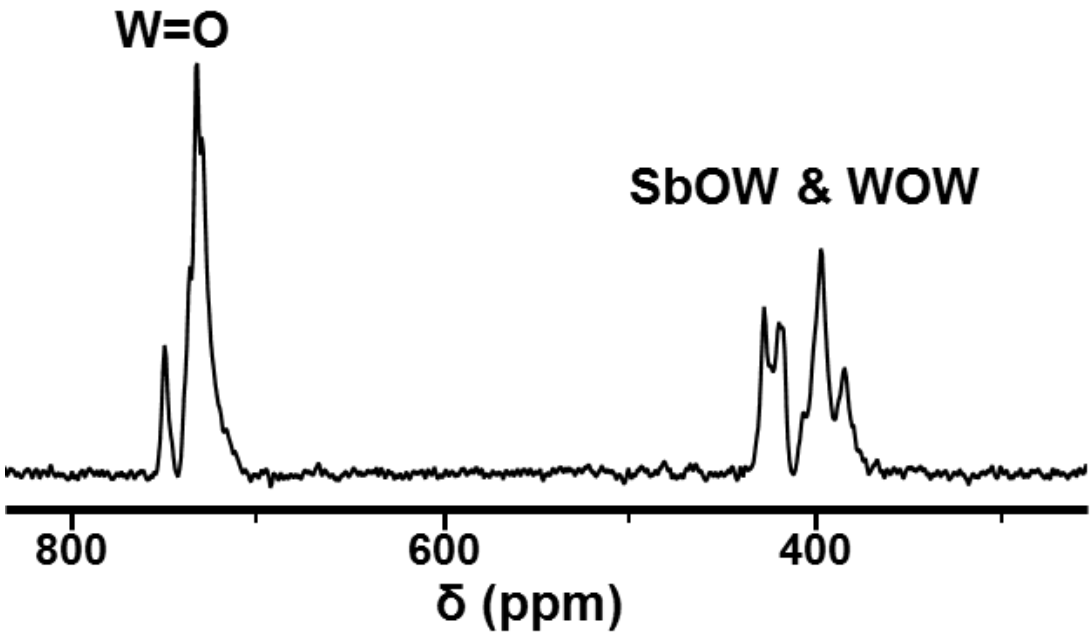

Figure 3.11. ^{17}O NMR spectrum of $(TBA)_4[SbPW_{11}O_{39}]$ in MeCN

Table 3.9. ESI-MS data for $(TBA)_4[SbPW_{11}O_{39}]$

Formula	m/z	
	Observed	Calculated
$[NaW_2O_7]^-$	502.9	502.67
$[Sb^{III}PW_{11}O_{39}]^{4-}$	699.56	699.74
$[HSb^{III}PW_{11}O_{39}]^{3-}$	933.08	933.32
$[(C_{16}H_{36}N)Sb^{III}PW_{11}O_{39}]^{3-}$	1013.84	1013.81
$[(C_{16}H_{36}N)_2Sb^{III}PW_{11}O_{39}]^{2-}$	1641.92	1641.94

Synthesis of $(TBA)_4[BiPW_{11}O_{39}]$: The reaction between $[NaPW_{11}O_{39}]^{6-}$ and 1 mole-equivalent of $BiCl_3$ in MeCN gave a cloudy solution after ~10 mins. The ^{31}P NMR spectrum of the product showed a single peak at -12.54 ppm. The ^{17}O NMR spectrum (**Figure 3.12**) showed one major peak and two minor peaks at 743 – 719 ppm assigned to W=O oxygens; a broad peak at 487 ppm assigned to BiOW oxygens and two broad peaks with shoulders at 425 – 384 ppm assigned to WOW oxygens. As in the ^{17}O NMR spectrum of $(TBA)_4[SbPW_{11}O_{39}]$, the terminal W=O chemical shift is suggestive of an overall charge of 4-. However, the chemical shift for Bi^{III}-O-W oxygens is downfield of the Sb^{III}-O-W resonance. This trend is consistent with that observed for Sn^{2+} and Pb^{2+} substituted polyanions. Generally, the peaks in the ^{17}O NMR spectrum of $(TBA)_4[BiPW_{11}O_{39}]$ were observed to be more broadened than those of $(TBA)_4[SbPW_{11}O_{39}]$. The ^{183}W NMR spectrum[**Figure 3.16 (e)**] also suggested a C_s symmetry with six lines at -40.61, -60.35, -92.49, -102.31, -115.70 and -121.22 ppm similar to Sn^{2+} and

Pb^{2+} substituted polyanions (2:2:2:1:2:2). FT-IR data (**Table 3.3**) indicated a terminal W=O vibrational frequency of 952 cm^{-1} in the region expected for a polyanion with an overall charge of 4- as was observed for $(TBA)_4[SbPW_{11}O_{39}]$ but with a smaller P-O splitting of 31 cm^{-1} which indicates a better interaction of the bismuth heteroatom with the central PO_4 tetrahedron than was observed for antimony and might suggest a co-ordination number of 5 for bismuth in $(TBA)_4[BiPW_{11}O_{39}]$. It is not clear why this is as Bi^{3+} is larger than Sb^{3+} and is expected to have a lesser interaction. It is however consistent with observation for Sn^{2+} and Pb^{2+} polyanions. Also, ESI-MS data (**Table 3.10**) showed peaks that could be assigned to $[Bi^{III}PW_{11}O_{39}]^{4-}$, $[HBi^{III}PW_{11}O_{39}]^{3-}$, $[NaBi^{III}PW_{11}O_{39}]^{3-}$, $[(C_{16}H_{36}N)Bi^{III}PW_{11}O_{39}]^{3-}$, $[Na_2Bi^{III}PW_{11}O_{39}]^{2-}$, $[(C_{16}H_{36}N)NaBi^{III}PW_{11}O_{39}]^{2-}$ and $[(C_{16}H_{36}N)_2Bi^{III}PW_{11}O_{39}]^{2-}$ [see **Appendix** (**Figure A3.2** for full ESI-MS spectrum and **Figure A3.7** for peaks expansion and simulation)]. The ESI-MS showed no evidence of peaks that could either be assigned to $[Bi(PW_{11}O_{39})_2]^{11-}$ or its fragments or even the chloride derivative. Additionally, as with $(TBA)_4[SbPW_{11}O_{39}]$, $(TBA)_4[BiPW_{11}O_{39}]$ was treated with methanolic MeONa and the ^1H and ^{31}P NMR spectra of the reaction product [see **Appendix (Figure A.3.11)**] showed no evidence for the formation of a methoxido derivative suggesting no chloride ligand is attached to the polyanion.

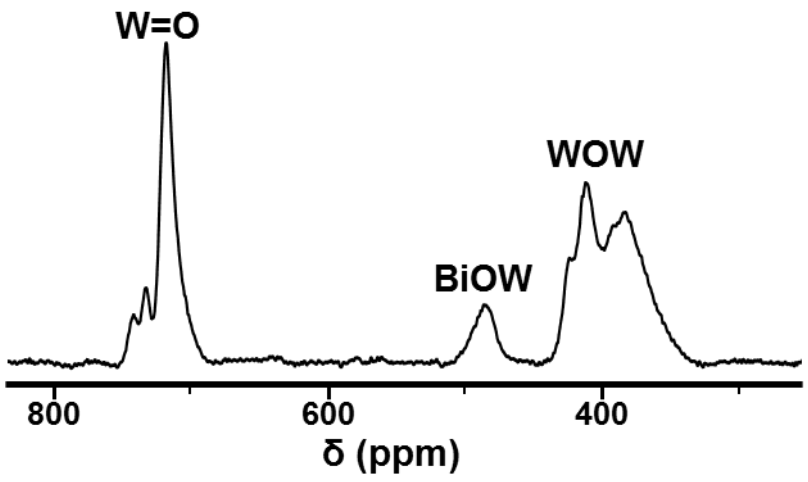

Figure 3.12. ^{17}O NMR spectrum of $(TBA)_4[BiPW_{11}O_{39}]$ in MeCN

Table 3.10. ESI-MS data for $(TBA)_4[BiPW_{11}O_{39}]$

Formula	m/z	
	Observed	Calculated
$[W_2O_7]^{2-}$	239.93	239.84
$[Bi^{III}PW_{11}O_{39}]^{4-}$	721.57	721.54
$[HBi^{III}PW_{11}O_{39}]^{3-}$	962.09	962.39
$[NaBi^{III}PW_{11}O_{39}]^{3-}$	969.76	969.72
$[(C_{16}H_{36}N)Bi^{III}PW_{11}O_{39}]^{3-}$	1042.85	1042.88
$[Na_2Bi^{III}PW_{11}O_{39}]^{2-}$	1466.15	1466.08
$[(C_{16}H_{36}N)NaBi^{III}PW_{11}O_{39}]^{2-}$	1575.79	1575.81
$[(C_{16}H_{36}N)_2Bi^{III}PW_{11}O_{39}]^{2-}$	1685.45	1685.55

Synthesis of $(TBA)_4[ClSnPW_{11}O_{39}]$: The reaction between $[NaPW_{11}O_{39}]^{6-}$ and 1 mole-equivalent of $SnCl_4$ in dry MeCN immediately gave a cloudy solution, which gave a white solid characterized as $(TBA)_4[ClSnPW_{11}O_{39}]$ upon work-up. A single resonance at -12.92 ppm with P-Sn coupling of 37 Hz was observed in the ^{31}P NMR spectrum. The ^{17}O NMR spectrum (**Figure 3.13**) contained peaks at 749 – 737 ppm assigned to W=O oxygens. The peaks at 429 – 372 ppm were assigned to SnOW and WOW oxygens but it was difficult to unambiguously assign individual peaks. This suggests an increasing sigma-character[47] in the Sn^{IV}-O-W bonding due to tin in the +4 oxidation state and possibly the electronegativity of the Cl^- ligand, thus causing an upfield shift into the region for W-O-W compared to the Sn^{2+} substituted polyanion. The ^{119}Sn NMR spectrum showed both P-Sn and Sn-W couplings [see **Figure 3.14** and **Appendix (Figure A3.22)**]. The ^{183}W NMR spectrum [**Figure 3.16 (f)**] is consistent with a C_s symmetry with six lines at -76.78, -91.41, -108.35, -114.80, -130.65 and -174.49 ppm in the ratio: 2:2:2:2:1:2. It was possible to resolve the Sn-W couplings and this enabled assignment of three of the peaks, A, C and F (see **Figure 3.15** and **Figure 3.16**). The unique tungsten (C) is observed at a different position from that of $(TBA)_5[Sn^{II}PW_{11}O_{39}]$, $(TBA)_5[Pb^{II}PW_{11}O_{39}]$, $(TBA)_4[Sb^{III}PW_{11}O_{39}]$ and $(TBA)_4[Bi^{III}PW_{11}O_{39}]$. The FT-IR data (**Table 3.3**) showed a vibrational frequency of 962 cm^{-1} for the terminal W=O, which is evidence of an overall polyanion charge of 4- and a P-O splitting of 23 cm^{-1} , which demonstrates a stronger interaction of the tin with the central PO_4 tetrahedron than in the Sn^{2+} polyanion. The ESI-MS showed little fragmentation with the most intense peaks assigned to $[ClSnPW_{11}O_{39}]^{4-,}$ $[(C_{16}H_{36}N)ClSnPW_{11}O_{39}]^{3-}$ and $[(C_{16}H_{36}N)_2ClSnPW_{11}O_{39}]^{2-}$ and peaks assigned to $[(HO)SnPW_{11}O_{39}]^{4-}$ (**Table 3.11**) [see **Appendix** (**Figure A3.2** for full ESI-MS spectrum and **Figure A3.8** and **Figure A3.9** for peaks expansion and simulation)]. Knoth had earlier prepared $(TBA)_4[ClSn^{IV}PW_{11}O_{39}]$ from $(Bu_4N)_4H_3[PW_{11}O_{39}]$ and $SnCl_4$ with 61% yield and

$W_{12}PO_{40}^{3-}$ as trace impurity.[52] Our method gave a pure product (by ^{31}P NMR) with a yield of 79%.

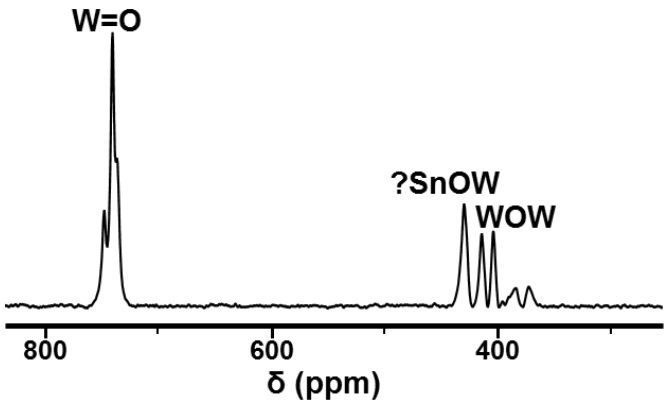

Figure 3.13. ^{17}O NMR spectrum of $(TBA)_4[ClSnPW_{11}O_{39}]$ in MeCN

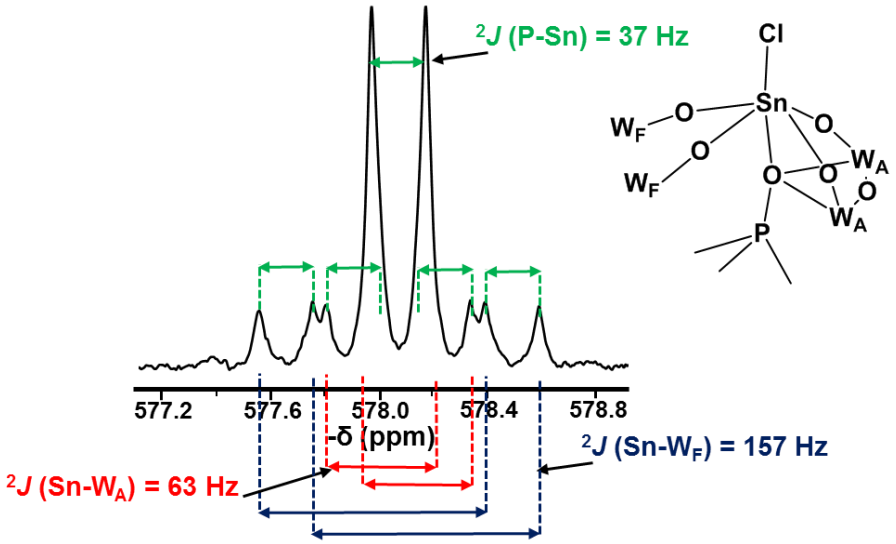

Figure 3.14. ^{119}Sn NMR spectrum of $(TBA)_4[ClSnPW_{11}O_{39}]$ in CD_3CN

Table 3.11. ESI-MS data for $(TBA)_4[ClSnPW_{11}O_{39}]$

Formula	m/z	
	Observed	Calculated
$[(HO)SnPW_{11}O_{39}]^{4-}$	703.30	703.23
$[ClSnPW_{11}O_{39}]^{4-}$	707.79	707.84
$[(C_{16}H_{36}N)ClSnPW_{11}O_{39}]^{3-}$	1024.48	1024.61
$[(C_{16}H_{36}N)_2ClSnPW_{11}O_{39}]^{2-}$	1657.87	1658.15

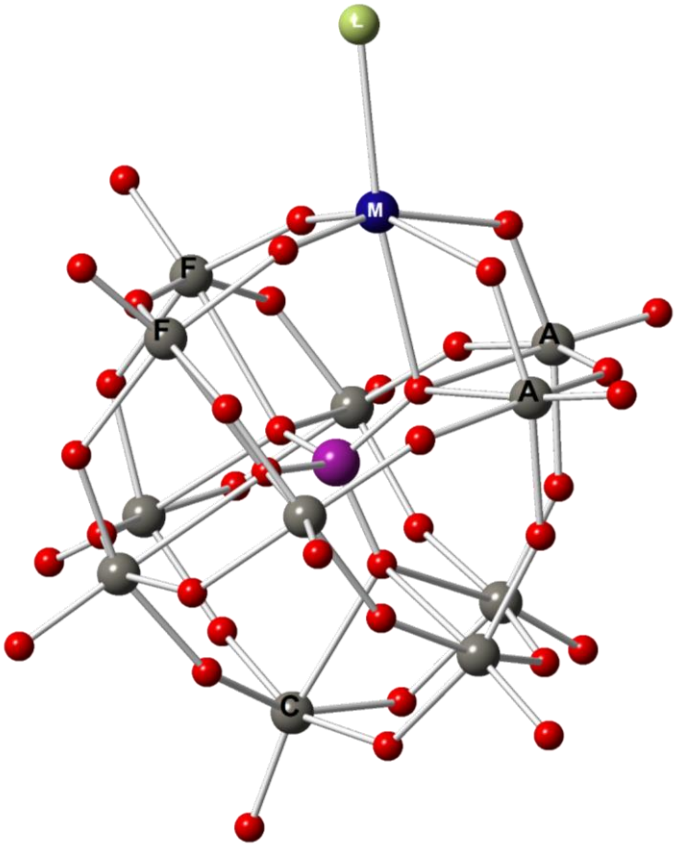

Figure 3.15. Ball and stick structure of $[(L)MPW_{11}O_{39}]^{n-}$ ($M = Sn^{2+}, Pb^{2+}, Bi^{3+}, Sb^{3+}, Sn^{4+}$, $L = Cl^{-}$) showing assignments of tungstens, A, C and F only.

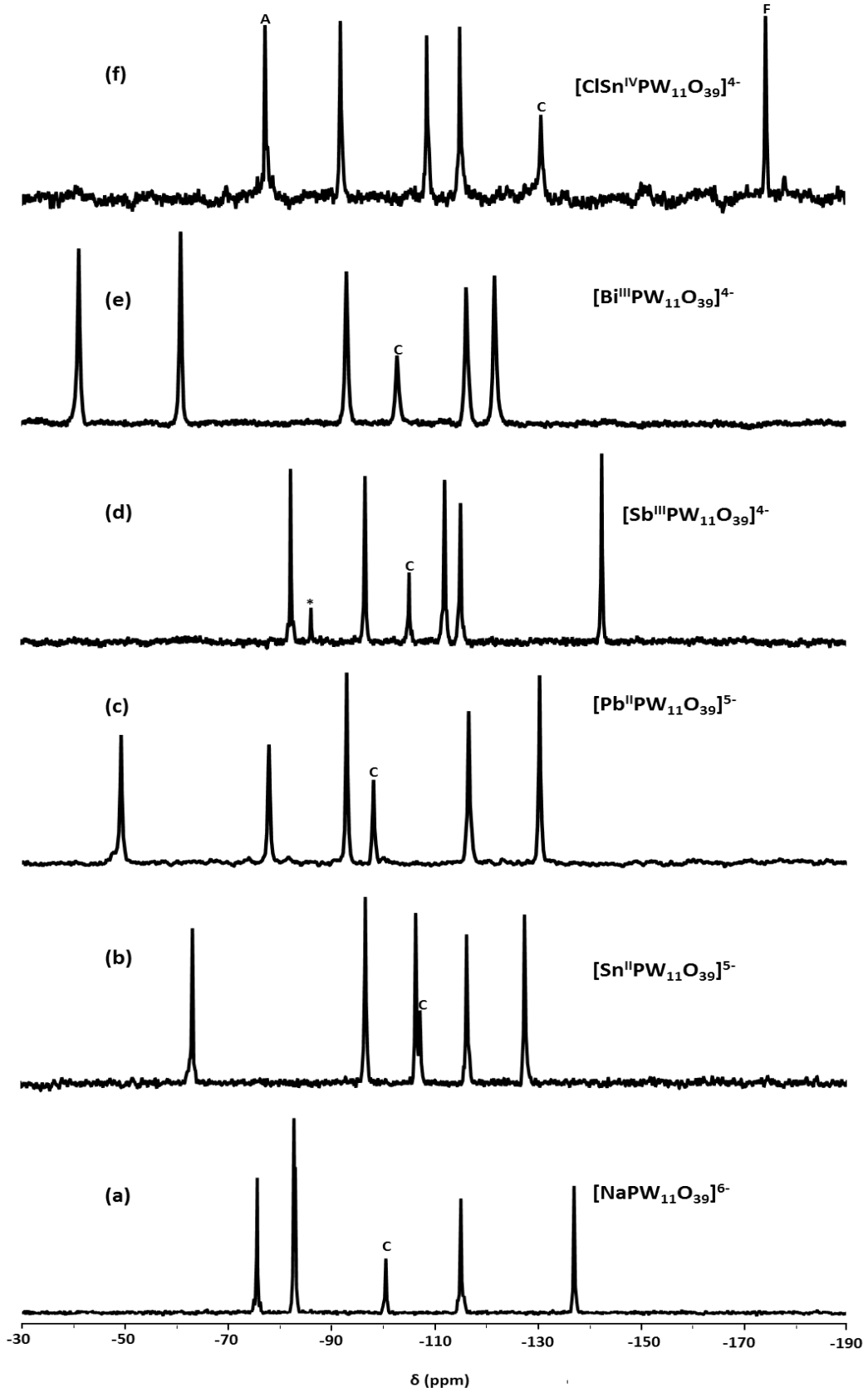

Figure 3.16. ^{183}W NMR spectra of (a) $[NaPW_{11}O_{39}]^{6-}$ (b) $[Sn^{II}PW_{11}O_{39}]^{5-}$ (c) $[Pb^{II}PW_{11}O_{39}]^{5-}$ (d) $[SbPW_{11}O_{39}]^{4-}$ (in DMSO-d_6) (e) $[BiPW_{11}O_{39}]^{4-}$ and (f) $[ClSn^{IV}PW_{11}O_{39}]^{4-}$ in CD_3CN. Peak asterisked is assigned to $[PW_{12}O_{40}]^{3-}$.

Synthesis of $(TBA)_4[ClTiPW_{11}O_{39}]$: Reaction of $[NaPW_{11}O_{39}]^{6-}$ and 1 mole-equivalent of $TiCl_4$ in DCM immediately gave a cloudy yellow solution, which was allowed to settle down and the top yellow solution filtered off. The white solid residue was washed several times with DCM until the solution became clear. The isolated white solid had a single ^{31}P NMR peak at -14.36 ppm. The ^{17}O NMR spectrum (**Figure 3.17**) showed peaks at 747 – 743 ppm assigned to W=O oxygens, two sharp peaks at 585 and 565 ppm assigned to TiOW oxygens and broad peaks with shoulders at 427 – 386 ppm assigned to WOW oxygens. The $Ti^{IV}OW$ resonance is shifted more downfield than was observed for $Sn^{IV}OW$ indicating stronger bonding in Ti^{IV}-O-W. As in $(TBA)_4[ClSnPW_{11}O_{39}]$, FT-IR data showed a vibrational frequency of 962 cm^{-1} for terminal W=O, however no P-O splitting was observed. This is consistent with Knoth's observation when he prepared $(TBA)_4[ClTi^{IV}PW_{11}O_{39}]$ from $(Bu_4N)_4H_3[PW_{11}O_{39}]$ and $TiCl_4$.[52]

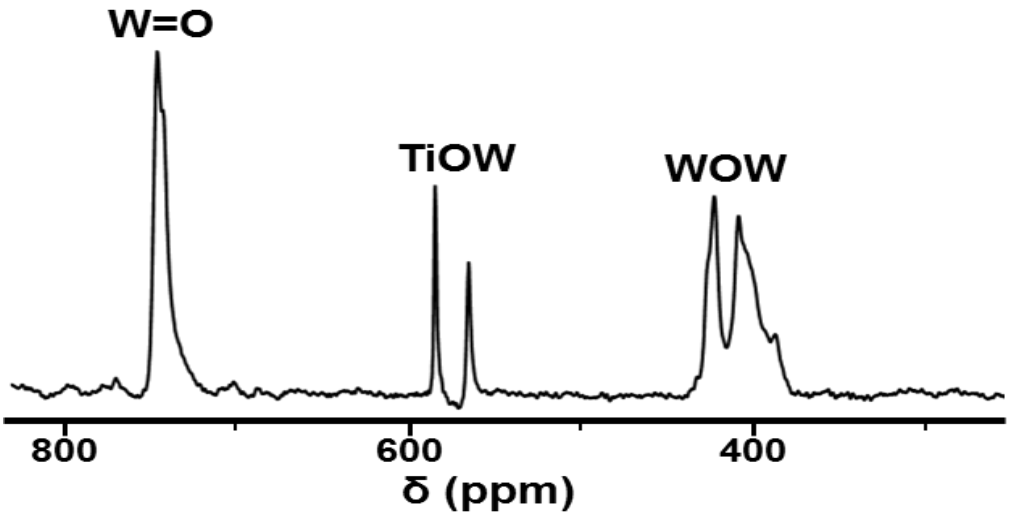

Figure 3.17. ^{17}O NMR spectrum of $(TBA)_4[ClTiPW_{11}O_{39}]$ in MeCN.

Synthesis of $(TBA)_5[CoPW_{11}O_{39}]$: The reaction between $[NaPW_{11}O_{39}]^{6-}$ and 1 mole-equivalent of $[Co(H_2O)_6](NO_3)_2$ in MeCN gave a cloudy purple solution, which was filtered and dried before purifying by washing a DCM solution of the product severally with water to remove any nitrate impurity and drying to give a green solid. The ^{31}P NMR spectrum of a purple solution of the product in CH_3CN gave a broad peak that is paramagnetically shifted to 331 ppm while the spectrum of a green solution of the product in CH_2Cl_2 showed a broad peak at 273 ppm [see **Appendix (Figure A3.12**)]. The POM was observed to be purple in the presence of a coordinating solvent (CH_3CN or H_2O) and green in a non-coordinating solvent (CH_2Cl_2). The purple colour has been proposed to be due to 6-coordinate Co and the green

colour due to 5-coordinate Co (with no co-ligand).[56] The FT-IR spectrum of the green solid had a terminal W=O vibrational frequency of 946 cm^{-1} which is indicative of an overall polyanion charge of 5-. No P-O vibration splitting was observed. No enrichment of this product was attempted because of its paramagnetism.

Synthesis of $(TBA)_5[NiPW_{11}O_{39}]$: Treatment of $[NaPW_{11}O_{39}]^{6-}$ with 1 mole-equivalent of $NiBr_2.3H_2O$ in MeCN gave a light green solution which was filtered and dried before purifying by washing a DCM solution of the product several times with water to remove any bromide salts and drying to give a light green solid. The ^{31}P NMR of the product gave a peak at -12.78 ppm [see **Appendix (Figure A3.13**)]. No P-O vibration splitting was observed and the terminal W=O vibration at 946 cm^{-1} is indicative of an overall polyanion charge of 5-. No enrichment of this product was attempted.

Attempted synthesis of $(TBA)_8[(Mo^{II}PW_{11}O_{39})_2]$: Attempts to synthesize $(TBA)_8[(Mo^{II}PW_{11}O_{39})_2]$, containing a Mo≡Mo bond was motivated by the compound, $[Re_2(PW_{11}O_{39})_2]^{8-}$ (with a central Re_2 quadruple bonded core) reported by Sokolov *et al.* in 2009.[57] Treatment of $[NaPW_{11}O_{39}]^{6-}$ with ½ mole-equivalent of $[Mo_2(NCCH_3)_8(ax\text{-}CH_3CN)_{0.5}][BF_4]_4$ in MeCN resulted in an immediate colour change to dark green. The ^{31}P NMR spectrum of the product after ~30 mins showed four resonances, a major peak at -11.14 ppm (79%) and three minor peaks at -10.08, -11.54 and -14.07 ppm. The spectrum became more complex with the appearance of more lacunary species (-9.90 to -10.05 ppm) and $[PW_{12}O_{40}]^{3-}$ at -15.30 ppm after stirring the solution for 12 h [see **Appendix (Figure A3.14)**]. The FT-IR of the product after ~30 mins of reaction showed that the major product has a terminal W=O vibrational frequency of 943 cm^{-1} and P-O splitting of 11 cm^{-1}. Thus, in addition to products due to degradation of the molybdenum quadruple bond, these results and a structure obtained from a similar study on the Lindqvist analogue (see **Chapter 8 Section 8.22**) suggest degradation of $[NaPW_{11}O_{39}]^{6-}$ into multiple species including $[PW_{12}O_{40}]^{3-}$, which was then possibly reduced by electrons from molybdenum in $[Mo_2(NCCH_3)_8(ax\text{-}CH_3CN)_{0.5}][BF_4]_4$.

Attempted synthesis of $(TBA)_n[ClMPW_{11}O_{39}]$ (M = Rh^{III}, Ir^{III}, Ir^{IV}): Rhodium and iridium substituted Keggin POMs have been prepared *via* hydrothermal methods.[58-60] Our attempts to synthesise related POMs were stimulated by the need for a milder more efficient

approach to enrich these POMs for protonation study. Treatment of $(TBA)_6[NaPW_{11}O_{39}]$ with 1 mole-equivalent of $RhCl_3$ in DMSO gave an orange solution with two broad ^{31}P NMR chemical shifts at -10.10 and -10.87 ppm after ~10 mins at room temperature. Heating at 120 ^oC for ~ 5 h gave three ^{31}P NMR peaks at -10.36 (36.5%), -11.48 (1.5%) and -11.84 ppm (62.0%) ppm. After heating the solution for up to 30 h, the solution became dark orange with the broad peak at -10.36 shifted to -10.73 and the appearance of a new peak at -10.45 ppm. Beyond this time, the spectrum became more complicated [see **Appendix (Figure A3.15)**]. The reaction between $(TBA)_6[NaPW_{11}O_{39}]$ and 1 mole-equivalent of $IrCl_3$ in DMSO gave a dark solution with a broad ^{31}P NMR chemical shift at -10.70 ppm which apparently contained some starting material at -10.59 ppm. Heating at 150 ^oC for ~ 18 h gave multiple products as shown by the ^{31}P NMR spectrum with peaks at -10.49 (33.8%), -10.76 (2.4%), -11.01 (60.5%), -12.06 (0.9%) and -15.64 (2.4%) ppm. The peak at -15.64 was assigned to $(TBA)_3[PW_{12}O_{40}]$. After heating the solution for 48 h, the ^{31}P NMR peaks observed were -10.67 (10.2%), -11.01 (85.1%), -12.06 (1.9%) and -15.64 (2.8%) ppm. Beyond this time, the peak at -11.01 ppm broadened with formation of more $(TBA)_3[PW_{12}O_{40}]$ [see **Appendix (Figure A3.16)**]. Treatment of $(TBA)_6[NaPW_{11}O_{39}]$ with 1 equivalent of $Na_2IrCl_6.xH_2O$ in DMSO at 150 ^oC led to a change in colour from dark brown to greenish yellow after ~ 50 mins and gave a broad ^{31}P NMR peak at -10.81 ppm. The solution became dark green after ~ 2 h with the appearance of a new ^{31}P NMR peak at -11.33 ppm. Two sharp peaks at -10.42 (26.3%) and -10.97 ppm (71.9%) and a peak at -15.64 ppm (1.9%) assigned to $(TBA)_3[PW_{12}O_{40}]$ were observed after 20 h. Only the peak at -10.97 ppm (98%) was observed with some $(TBA)_3[PW_{12}O_{40}]$ at -15.64 ppm (2%) after heating for ~44 h. The ^{31}P NMR spectrum of the product became complex after workup, suggesting further transformation [see **Appendix (Figure A3.17)**].

Attempted synthesis of $(TBA)_4[ClPt^{IV}PW_{11}O_{39}]$: Klemperer *et al.* reported the successful incorporation of platinum in a silicon-centred monolacunary Keggin POM, which stimulated our study on the phosphorus-centred analogue.[61] Our reaction of $(TBA)_6[NaPW_{11}O_{39}]$ with 1 mole-equivalent of Na_2PtCl_6 in DMSO gave an orange solution which showed two broad peaks at -10.60 and -11.51 ppm after ~ 10 mins at room temperature. After 11 h at room temperature two sharp peaks were observed. One at -10.59(68%) assigned to the starting material and the other at -11.58 ppm (32%). Heating the solution at 100 ^oC for 1 h gave a

broad peak at -11.58 ppm, which became sharper after 3 h. After 4 h, a peak assigned to $(TBA)_3[PW_{12}O_{40}]$ appeared in the ^{31}P NMR spectrum and at about 18 h, a broad peak at -13.41 was observed with more $(TBA)_3[PW_{12}O_{40}]$ [see **Appendix (Figure A3.18)**]. The FT-IR spectrum of an orange solid isolated from a second reaction between $(TBA)_6[NaPW_{11}O_{39}]$ and 1 mole-equivalent of Na_2PtCl_6 in DMSO after 5 h of heating at 100 ^oC showed a W=O vibrational frequency of 941 cm^{-1} and a P-O splitting of 48 cm^{-1} indicating very little or no interaction between the central PO_4 and the heterometal. The ^{31}P NMR spectrum of the orange solid showed a major peak (85%) at -11.55 ppm while the ^{195}Pt NMR spectrum showed the disappearance of the starting peak at -109.6 and appearance of new peaks at -2956 and -2960 ppm [see **Appendix (Figure A3.19)**]. Also, when only Na_2PtCl_6 was heated at 100 ^oC, the ^{195}Pt NMR peaks showed the same changes as when both Na_2PtCl_6 and $[NaPW_{11}O_{39}]^{6-}$ were heated together. This indicates that the changes in the ^{195}Pt NMR spectra were not due to incorporation of Pt into the polyanion. This is further supported by the absence of any P-Pt coupling in the ^{31}P NMR spectrum of the reaction products [see **Figure A3.18 (h)**].

Attempted synthesis of $(TBA)_4[(L)Ce^{IV}PW_{11}O_{39}]$ ($L=NO_3^-$, DMSO): Reaction between $(TBA)_6[NaPW_{11}O_{39}]$ and 1 equivalent of $(NH_4)_2[Ce(NO_3)_6]$ in MeCN immediately gave a cloudy green solution and the ^{31}P NMR spectrum showed four peaks at -12.32 ppm (72.6%), -13.58 (21.8%), -11.85 ppm (4.1%) and -12.87 ppm (1.6%). After stirring for 18 h, the ^{31}P NMR spectrum showed that only two species remained in solution at -12.32 ppm (96.5%) and -11.85 ppm (3.5%). The isolated greenish yellow solid gave a peak at -12.30 ppm [see **Appendix (Figure A3.20)**] and the FT-IR spectrum showed a vibrational frequency of 952 cm^{-1} for ν(W=O) and 1049 cm^{-1} for the triply degenerate ν(P-O). These values compare well with values reported for $(TBA)_{11}[Ce^{III}(PW_{11}O_{39})_2]$ and $(TBA)_{10}[Ce^{IV}(PW_{11}O_{39})_2]$.[62] In a bid to prevent dimerization by introducing a strong co-ordinating ligand like DMSO for possible interaction with the cerium heterometal, $(TBA)_6[NaPW_{11}O_{39}]$ was treated with 1 mole-equivalent of $(NH_4)_2[Ce(NO_3)_6]$ and 4 mole-equivalents of DMSO in MeCN with immediate formation of an orange red precipitate. A ^{31}P NMR spectrum after 1 hour showed only one peak at -12.73 ppm. The ^{31}P NMR spectrum of the isolated yellow solid showed a peak at -12.34 ppm [see **Figure A3.20 (d)** and **(e)**] while the FT-IR spectrum showed the same bands obtained previously at 952 and 1048 cm^{-1} for ν(W=O) and ν_3(P-O) respectively. Attempts to crystallise

this product resulted in a by-product, $(TBA)_3[Ce(NO_3)_6]$ (see **Figure 3.18** for structure). These results suggest Ce^{4+} ion preference for formation of the dimer, $(TBA)_{10}[Ce^{IV}(PW_{11}O_{39})_2]$ even in the presence of strongly co-ordinating ligands. Also, reaction between 2 mole-equivalents of $(TBA)_6[NaPW_{11}O_{39}]$ and 1 mole-equivalent of $(NH_4)_2[Ce(NO_3)_6]$ in MeCN gave a major peak at -12.32 (90%) assigned to the dimer, $(TBA)_{10}[Ce^{IV}(PW_{11}O_{39})_2]$ and an unassigned minor peak at -13.63 ppm (10%) in the ^{31}P NMR spectrum [see **Figure A3.19 (f)**].

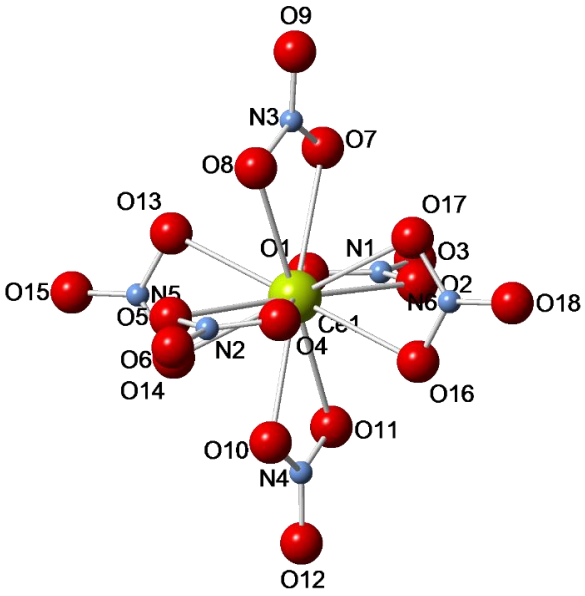

Figure 3.18. Crystal structure of $[Ce(NO_3)_6]^{3-}$ anion from slow diethyl ether diffusion into an MeCN solution of product of reaction of $(TBA)_6[NaPW_{11}O_{39}]$, 1 mole-equivalent of $(NH_4)_2[Ce(NO_3)_6]$ and 4 mole-equivalents of DMSO

3.3. ^{17}O-enrichment of monosubstituted heterometallic Keggin POMs

Attempts were made to post-enrich the monosubstituted heterometallic Keggin POMs, $(TBA)_4[ClSn^{IV}PW_{11}O_{39}]$ and $(TBA)_4[(HO)Sn^{IV}PW_{11}O_{39}]$. Both were chosen as models because of their resistance to hydrolysis. ^{17}O NMR studies showed no significant enrichment after heating an acetonitrile solution of $(TBA)_4[ClSn^{IV}PW_{11}O_{39}]$ with ~1% (w/w) ^{17}O-enriched H_2O at 80 ^oC for up to 72 h. $(TBA)_4[(HO)Sn^{IV}PW_{11}O_{39}]$ only showed enrichment of the OH group attached to tin. When compared with $(TBA)_6[NaPW_{11}O_{39}]$, which was enriched even at room temperature, this demonstrated the increased rigidity upon addition of a metal to the lacuna. Thus, $(TBA)_4[ClSn^{IV}PW_{11}O_{39}]$ and $(TBA)_4[(HO)Sn^{IV}PW_{11}O_{39}]$ are more inert to

enrichment than $(TBA)_6[NaPW_{11}O_{39}]$, and hence ^{17}O-enriched derivatives were prepared by substitution of Sn(IV) into enriched $(TBA)_6[NaPW_{11}O_{39}]$. It is worth noting also that hydrolysis of un-enriched $(TBA)_4[(CH_3O)Ti^{IV}PW_{11}O_{39}]$ with minimum ^{17}O-enriched H_2O (discussed in Chapter 4) showed no enrichment of the POM cage.

3.4. Conclusions

The chapter has described the synthesis and characterization of ^{17}O-enriched $(TBA)_6[NaPW_{11}O_{39}]$. The POM was further shown to be very sensitive to protonation. Though attempts with noble metals are not yet successful, it has shown that $(TBA)_6[NaPW_{11}O_{39}]$ can be used as a convenient precursor to ^{17}O-enriched heterometallic POMs of the series, $[(L)MPW_{11}O_{39}]^{n-}$ (M = Sn^{2+}, Pb^{2+}, Bi^{3+}, Sb^{3+}, Sn^{4+}, Ti^{4+}). This is important as these enriched POMs can serve as models for mechanistic studies in homogenous and heterogeneous processes such as catalysis and sensing. They can also provide an experimental basis for extending the theoretical analysis of ^{17}O NMR chemical shifts for a wide variety of POMs.

REFERENCES

1. W. G. Klemperer and K. A. Marek, *Eur. J. Inorg. Chem.*, 2013, **2013**, 1762-1771.
2. R. I. Maksimovskaya and G. M. Maksimov, *Inorg. Chem.*, 2011, **50**, 4725-4731.
3. C. A. Ohlin, E. M. Villa, J. R. Rustad and W. H. Casey, *Nat Mater*, 2010, **9**, 11-19.
4. J. R. Rustad and W. H. Casey, *Nat Mater*, 2012, **11**, 223-226.
5. R. Sharma, J. Zhang and C. A. Ohlin, *Phys. Chem. Chem. Phys.*, 2016, **18**, 8235-8241.
6. S. R. Bajpe, C. E. A. Kirschhock, A. Aerts, E. Breynaert, G. Absillis, T. N. Parac-Vogt, L. Giebeler and J. A. Martens, *Chem. Eur. J.*, 2010, **16**, 3926-3932.
7. A. D. English, J. P. Jesson, W. G. Klemperer, T. Mamouneas, L. Messerle, W. Shum and A. Tramontano, *J. Am. Chem. Soc.*, 1975, **97**, 4785-4786.
8. M. Filowitz, W. G. Klemperer, L. Messerle and W. Shum, *J. Am. Chem. Soc.*, 1976, **98**, 2345-2346.
9. V. W. Day, M. F. Fredrich, W. G. Klemperer and W. Shum, *J. Am. Chem. Soc.*, 1977, **99**, 952-953.
10. M. Filowitz and W. G. Klemperer, *J. Chem. Soc., Chem. Commun.*, 1977, 201-202.
11. R. K. C. Ho and W. G. Klemperer, *J. Am. Chem. Soc.*, 1978, **100**, 6772-6774.
12. W. G. Klemperer, *Angew. Chem. Int. Ed. (English).* 1978, **17**, 246-254.
13. M. Filowitz, R. K. C. Ho, W. G. Klemperer and W. Shum, *Inorg. Chem.*, 1979, **18**, 93-103.
14. V. W. Day and W. G. Klemperer, *Science*, 1985, **228**, 533-541.
15. T. M. Che, V. W. Day, L. C. Francesconi, C. M. F. Fredrich, W. G. Klemperer and W. Shum, *Inorg. Chem.* , 1985, **24**, 4055-4062.
16. V. W. Day, W. G. Klemperer and D. J. Maltbie, *J. Am. Chem. Soc.*, 1987, **109**, 2991-3002.
17. William Clegg, R. John Errington, P. Kraxner and C. Redshaw, *J. Chem. Soc., Dalton Trans.*, 1992, 1431-1438.
18. R. J. Errington, C. Lax, D. G. Richards, W. Clegg and K. A. Fraser, in *Polyoxometalates: From Platonic Solids to Anti-Retroviral Activity*, eds. M. T. Pope and A. Müller, Springer Netherlands, 1994, vol. 10, pp. 105-114.
19. W. Clegg, M. R. J. Elsegood, R. J. Errington and J. Havelock, *J. Chem Soc., Dalton Trans.*, 1996, 681-690.
20. R. J. Errington, in *Polyoxometalate Chemistry: From Topology via Self-Assembly to Applications*, eds. M. T. Pope and A. Müller, Springer, Dordrecht, 2001, pp. 7-22.
21. R. J. Errington, S. S. Petkar and P. S. Middleton, Boston, MA, United States., 2007.
22. R. J. Errington, S. S. Petkar, P. S. Middleton, W. McFarlane, W. Clegg, R. A. Coxall and R. W. Harrington, *Dalton Trans.*, 2007, 5211-5222.

23. R. J. Errington, S. S. Petkar, P. S. Middleton, W. McFarlane, W. Clegg, R. A. Coxall and R. W. Harrington, *J. Am. Chem. Soc.*, 2007, **129**, 12181-12196.

24. R. J. Errington, G. Harle, W. Clegg and R. W. Harrington, *Eur. J. Inorg. Chem.*, 2009, 5240-5246.

25. J. Errington, L. Coyle, G. Harle, B. Kandasamy and P. Middleton, Honolulu, HI, United States., 2010.

26. R. J. Errington, L. Coyle, P. S. Middleton, C. J. Murphy, W. Clegg and R. W. Harrington, *J. Cluster Sci.*, 2010, **21**, 503-514.

27. L. Coyle, P. S. Middleton, C. J. Murphy, W. Clegg, R. W. Harrington and R. J. Errington, *Dalton Trans.*, 2012, **41**, 971-981.

28. B. Kandasamy, C. Wills, W. McFarlane, W. Clegg, R. W. Harrington, A. Rodriguez-Fortea, J. M. Poblet, P. G. Bruce and R. J. Errington, *Chem. Eur. J.*, 2012, **18**, 59-62.

29. R. J. Errington, in *Advances in Inorganic Chemistry*, eds. R. v. Eldik and L. Cronin, 2017, vol. 69, pp. 287-336.

30. R. J. Errington, in *NATO Sci. Ser., II*, eds. J. J. Borrás-Almenar, E. Coronado, A. Müller and M. Pope, Springer, Netherlands, 2003, vol. 98, ch. Polyoxometalate Molecular Science, pp. 55-78.

31. R. J. Errington, in *Comprehensive Coordination Chemistry II: From Biology to Nanotechnology*, ed. J. A. McCleverty, Meyer, T.J., Elsevier Ltd., Oxford, UK, 2003, vol. 2, pp. 759-773.

32. M. Pascual-Borras, X. Lopez, A. Rodriguez-Fortea, R. J. Errington and J. M. Poblet, *Chem. Sci.*, 2014, **5**, 2031-2042.

33. O. A. Kholdeeva, G. M. Maksimov, R. I. Maksimovskaya, L. A. Kovaleva, M. A. Fedotov, V. A. Grigoriev and C. L. Hill, *Inorg. Chem.*, 2000, **39**, 3828-3837.

34. G. M. Maksimov, R. I. Maksimovskaya, O. A. Kholdeeva, M. A. Fedotov, V. I. Zaikovskii, V. G. Vasil'ev and S. S. Arzumanov, *J. Struct. Chem.*, 2009, **50**, 618-627.

35. M. A. Fedotov, B. Z. Pertsikov and D. K. Danovich, *Polyhedron*, 1990, **9**, 1249-1256.

36. L. A. Combs-Walker and C. L. Hill, *Inorg. Chem.*, 1991, **30**, 4016-4026.

37. W. H. Knoth, P. J. Domaille and D. C. Roe, *Inorg. Chem.*, 1983, **22**, 198-201.

38. G. S. Chorghade and M. T. Pope, *J. Am. Chem. Soc.*, 1987, **109**, 5134-5138.

39. R. L. Wingad, PhD Thesis, The University of Newcastle upon-Tyne, 1999.

40. C. Brevard, R. Schimpf, G. Tourne and C. M. Tourne, *J. Am. Chem. Soc.*, 1983, **105**, 7059-7063.

41. F. Zonnevijlle, C. M. Tourne and G. F. Tourne, *Inorg. Chem.*, 1982, **21**, 2742-2750.

42. F. Zonnevijlle, C. M. Tourne and G. F. Tourne, *Inorg. Chem.*, 1982, **21**, 2751-2757.

43. C. Rocchiccioli-Deltcheff, M. Fournier, R. Franck and R. Thouvenot, *Inorg. Chem.*, 1983, **22**, 207-216.

44. R. K. C. Ho, PhD Thesis, Columbia University, 1979.

45. P. J. Domaille and W. H. Knoth, *Inorg. Chem.*, 1983, **22**, 818-822.

46. M. Bonchio, O. Bortolini, V. Conte and A. Sartorel, *Eur. J. Inorg. Chem.*, 2003, 699-704.

47. H. Gunther, *NMR Spectroscopy: Basic Principles, Concepts, and Applications in Chemistry*, Wiley-VCH Verlag GmbH & Co, Germany, 3rd edn., 2013.

48. J. He, Y. Chen, X. Wang, X. Fang and J. Liu, *J. Mol. Struct.*, 2002, **641**, 159-164.

49. X. López, I. A. Weinstock, C. Bo, J. P. Sarasa and J. M. Poblet, *Inorg. Chem.*, 2006, **45**, 6467-6473.

50. O. A. M. Kholdeeva, R. I., *Zh. Neorg. Khim.*, 1992, **37**, 6.

51. R. Massart, R. Contant, J. M. Fruchart, J. P. Ciabrini and M. Fournier, *Inorg. Chem.*, 1977, **16**, 2916-2921.

52. W. H. Knoth, *J. Am. Chem. Soc.*, 1979, **101**, 759-760.

53. F. Zonnevijlle and M. T. Pope, *J. Am. Chem. Soc.*, 1979, **101**, 2731-2732.

54. C. J. Besecker, W. G. Klemperer, D. J. Maltbie and D. A. Wright, *Inorg. Chem.*, 1985, **24**, 1027-1032.

55. W. G. Klemperer and W. Shum, *J. Am. Chem. Soc.*, 1978, **100**, 4891-4893.

56. A. Dannenhoffer, J. Baker, N. Pantano, J. Stachowski, D. Zemla, W. Swanson, E. Zurek, S. Szczepankiewicz and M. Kozik, *J. Coord. Chem.*, 2014, **67**, 2830-2842.

57. M. N. Sokolov, V. S. Korenev, N. V. Izarova, E. V. Peresypkina, C. Vicent and V. P. Fedin, *Inorg. Chem.*, 2009, **48**, 1805-1807.

58. M. N. Sokolov, S. A. Adonin, D. A. Mainichev, P. L. Sinkevich, C. Vicent, N. B. Kompankov, A. L. Gushchin, V. A. Nadolinny and V. P. Fedin, *Inorg. Chem.*, 2013, **52**, 9675-9682.

59. M. N. Sokolov, S. A. Adonin, D. A. Mainichev, C. Vicent, N. F. Zakharchuk, A. M. Danilenko and V. P. Fedin, *Chem. Commun.* , 2011, **47**, 7833-7835.

60. M. N. Sokolov, S. A. Adonin, P. L. Sinkevich, C. Vicent, D. A. Mainichev and V. P. Fedin, *Z. Anorg. Allg. Chem.*, 2014, **640**, 122-127.

61. P. Klonowski, J. C. Goloboy, F. J. Uribe-Romo, F. Sun, L. Zhu, F. Gandara, C. Wills, R. J. Errington, O. M. Yaghi and W. G. Klemperer, *Inorg. Chem.*, 2014, **53**, 13239-13246.

62. J. Iijima, E. Ishikawa, Y. Nakamura and H. Naruke, *Inorg. Chim. Acta*, 2010, **363**, 1500-1506.

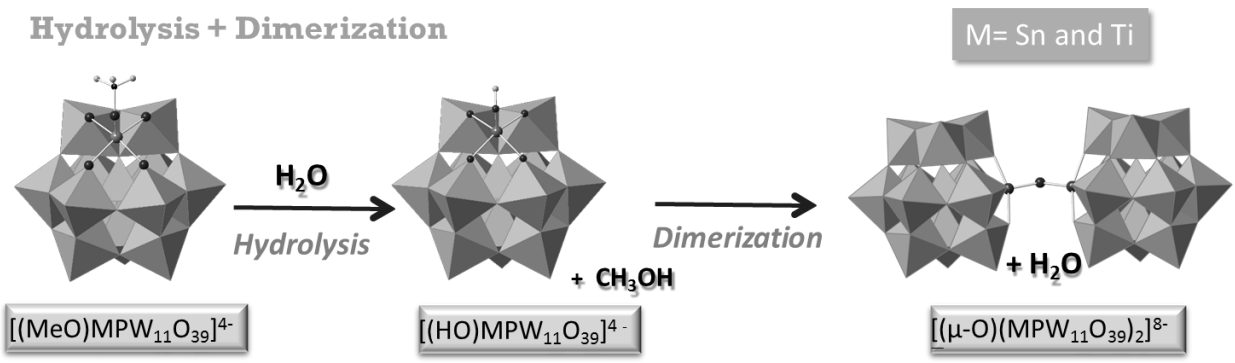

Chapter 4

Hydrolysis, condensation and reduction of $(TBA)_4[(L)M^{IV}PW_{11}O_{39}]$ (M = Sn, Ti; L = Cl, CH_3O, HO)

This chapter examines the hydrolysis and condensation of a series of tin- and titanium-monosubstituted Keggin polyoxometalates (POMs). Although, several publications have described derivatives of the titanium-substituted POMs, this study uses a comparative approach to offer some mechanistic insights into reactions of the tin (IV) analogue, which was first described by Knoth in 1983.[1] For the first time, the readily-hydrolysable $(TBA)_4[(CH_3O)SnPW_{11}O_{39}]$ and $(TBA)_8[(\mu\text{-}O)(SnPW_{11}O_{39})_2]$ are isolated and characterized by FT-IR, Multinuclear NMR (^1H, ^{13}C, ^{17}O, ^{31}P, ^{119}Sn and ^{183}W) and solid state NMR (^1H, ^{13}C and ^{31}P). Also the previously reported unstable $(TBA)_4[(HO)TiPW_{11}O_{39}]$ is shown to exist in solution for up to 3 months without dimerising when prepared *via* hydrolysis of $(TBA)_4[(CH_3O)TiPW_{11}O_{39}]$ in DMSO. The chapter ends with a discussion on the treatment of $(TBA)_4[(L)Sn^{IV}PW_{11}O_{39}]$ (L = Cl, HO) with reducing agents.

4. Hydrolysis, condensation and reduction of $(TBA)_4[(L)M^{IV}PW_{11}O_{39}]$(M = Sn, Ti; L = Cl, CH_3O, HO)

4.1 Introduction

Halo derivatives of titanium, tin and aluminium mono-substituted Keggin polyoxotungustates were first prepared by Knoth in the early 80s.[1] Since then, several groups have reported various alkoxido and dimeric species of the Ti-substituted POMs and their subsequent application in H_2O_2-oxidation catalysis.[2-8] Kholdeeva's group for instance, reported three monomeric Ti-substituted POMs, with the formula, $[(L)TiPW_{11}O_{39}]^{4-}$, where L = OH , OMe and OAr [ArOH = 2,3,6-trimethylphenol (TMP)] and the μ-oxo and μ-hydroxo dimers, $[(\mu\text{-}O)(PTiW_{11}O_{39})_2]^{8-}$ and $[(\mu\text{-}OH)(PTiW_{11}O_{39})_2]^{7-}$.[2] As molecular models of metal oxides, the POMs were shown to be effective catalysts for H_2O_2 oxidation of organic substrates, like thioethers,[9] 2,3,6-trimethylphenol[3] and alkenes.[10]

The tin analogue however, has received very little attention. Among the few studies on tin POMs are works by Pope,[11,12] Krebs,[13] Proust[14] and Hasenknopf.[15] As far as we know, there are no reported works on the alkoxido and dimeric derivatives of tin-monosubstituted Keggin POMs. Tin alkoxides and dimers have been implicated in several tin catalysed reactions including acetallization of ketones and deactivated aldehydes,[16] urethane synthesis[17] and transesterification reactions.[18-20] Our group had previously reported the synthesis of a range of titanium-substituted Lindqvist POMs (TiW_5) including $[(CH_3O)TiW_5O_{18}]^{3-}$ and $[(\mu\text{-}O)(TiW_5O_{18})_2]^{6-}$ *via* non-aqueous strategies.[21] In 2012, the same approach was successfully applied in the synthesis of the methoxido-tin-substituted Lindqvist POM, $[(CH_3O)SnW_5O_{18}]^{3-}$($SnW_5$)[22] and we have strong evidence for the μ-oxo-dimer, $[(\mu\text{-}O)(SnW_5O_{18})_2]^{6-}$.[23,24] These studies revealed some interesting variations in the hydrolytic and protonation behaviours of the TiW_5 and SnW_5 systems. The observed disparities were appropriately accounted for by a blend of experimental observations and DFT calculations and this stimulated our interest for similar study on the Keggin analogue. Such a study affords a better understanding of these systems by examining how the type of heterometal and POM structure (Lindqvist and Keggin) influence trends in hydrolysis and protonation.

Thus, in this chapter, the synthesis of $(TBA)_4[(CH_3O)M^{IV}PW_{11}O_{39}]$ (M = Sn, Ti) is discussed. Also, hydrolysis and condensation of $(TBA)_4[(CH_3O)M^{IV}PW_{11}O_{39}]$ and $(TBA)_4[(Cl)M^{IV}PW_{11}O_{39}]$ in MeCN and DMSO are investigated as routes to $(TBA)_4[(HO)M^{IV}PW_{11}O_{39}]$ and $(TBA)_8[(M^{IV}PW_{11}O_{39})_2O]$ (M = Sn, Ti). In addition, results on alcohol-alkoxide exchange of methanol and $(TBA)_4[(CH_3O)M^{IV}PW_{11}O_{39}]$ (M = Sn, Ti) and alkanolysis of $(TBA)_4[(HO)Sn^{IV}PW_{11}O_{39}]$ with alcohols and phenols are presented. Lastly, reduction of $(TBA)_4[(L)Sn^{IV}PW_{11}O_{39}]$ (L = Cl, HO) with $H_2NNH_2.HCl$ and $NaBH_4$ is examined. The fundamental knowledge gained from this work could lead to the potential application of the tin-POM species as catalysts in processes such as urethane synthesis and transesterification.

4.2 Results and Discussion

4.2.1. Syntheses of Sn- and Ti- Keggin POMs

$(TBA)_4[(CH_3O)M^{IV}PW_{11}O_{39}]$ (M = Sn, Ti): Though the preparation of $(TBA)_4[(CH_3O)TiPW_{11}O_{39}]$ was achieved quite easily following Knoth's approach of treating $(TBA)_4[ClTiPW_{11}O_{39}]$ with $NaOCH_3$[1], reaction of $(TBA)_4[ClSnPW_{11}O_{39}]$ and $NaOCH_3$ as a route to $(TBA)_4[(CH_3O)SnPW_{11}O_{39}]$, was however not as straightforward. Firstly, ^{31}P NMR studies showed that a slight excess of $NaOCH_3$ was required to push the reaction to completion. Secondly, the initially isolated product was found to be a mixture of two species (see **Figure 4.1**), which were later identified as $(TBA)_4[(CH_3O)SnPW_{11}O_{39}]$ and $(TBA)_4[(HO)SnPW_{11}O_{39}]$. Furthermore, addition of a drop of H_2O to an NMR solution of the product mixture gave $(TBA)_4[(HO)SnPW_{11}O_{39}]$ as a single species in solution whereas addition of excess MeOH was required to obtain $(TBA)_4[(CH_3O)SnPW_{11}O_{39}]$ as the only species in solution (**Figure 4.2**). This shows that the product, $(TBA)_4[(CH_3O)SnPW_{11}O_{39}]$ very readily hydrolyses in the presence of trace amount of H_2O and this may explain why it has not been reported previously. $(TBA)_4[(CH_3O)SnPW_{11}O_{39}]$ was therefore isolated by stirring the reaction product in a 1:1 (v/v) mixture of acetonitrile/methanol for ~10 min before vacuum drying to obtain a white solid (see Experimental for full characterization).

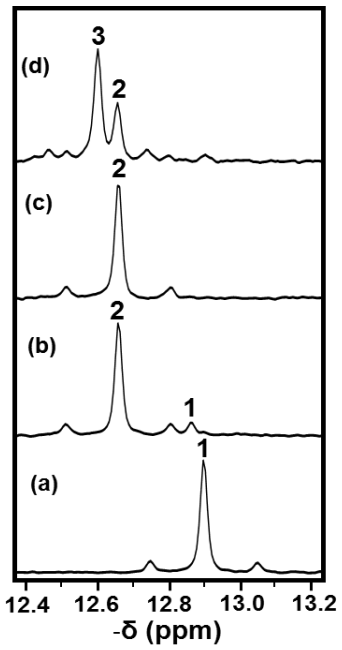

*Figure 4.1. ^{31}P NMR spectra in CD_3CN of (a) $(TBA)_4[ClSnPW_{11}O_{39}]$ (**1**) and reactions with (b) 1 mole-equivalent amount of $NaOCH_3$ (c) a slight excess of $NaOCH_3$ and (d) isolated product showing mixture of $(TBA)_4[(CH_3O)SnPW_{11}O_{39}]$ (**2**) and $(TBA)_4[(HO)SnPW_{11}O_{39}]$(**3**).*

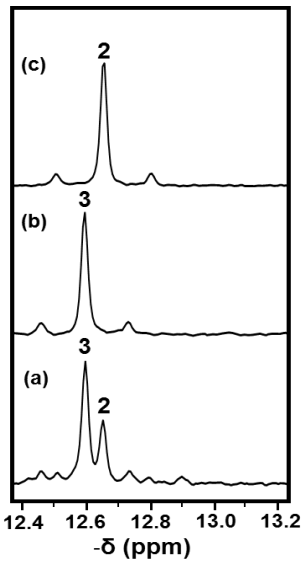

*Figure 4.2. ^{31}P NMR spectra in CD_3CN of (a) a mixture of $(TBA)_4[(CH_3O)SnPW_{11}O_{39}]$ (**2**) and $(TBA)_4[(HO)SnPW_{11}O_{39}]$ (**3**); (b) after addition of a drop of water and (c) after addition of an excess of methanol.*

$(TBA)_4[(HO)M^{IV}PW_{11}O_{39}]$ (M = Sn, Ti): These compounds were prepared *via* hydrolysis of the corresponding methoxides. As shown earlier, $(TBA)_4[(HO)SnPW_{11}O_{39}]$ was readily isolated as a single product from the hydrolysis of $(TBA)_4[(CH_3O)SnPW_{11}O_{39}]$. Attempts were also made to prepare $(TBA)_4[(DO)SnPW_{11}O_{39}]$ by deutrolysis (with D_2O). Though the product was characterised as $(TBA)_4[(DO)SnPW_{11}O_{39}]$ (see Experimental for ^{31}P and ^{119}Sn NMR and FTIR

data), it was also observed to readily hydrolyse to $(TBA)_4[(HO)SnPW_{11}O_{39}]$ in the presence of trace amount of H_2O in MeCN. The preparation of $(TBA)_4[(DO)SnPW_{11}O_{39}]$ was in a bid to compare its condensation with that of $(TBA)_4[(HO)SnPW_{11}O_{39}]$ and possibly use both as precursors to $(TBA)_8[(\mu\text{-}O)(SnPW_{11}O_{39})_2]$.

$(TBA)_4[(HO)TiPW_{11}O_{39}]$ was prepared by hydrolysis of $(TBA)_4[(CH_3O)TiPW_{11}O_{39}]$ in MeCN and DMSO (A detailed discussion on the hydrolysis is given in **Section 4.2.5**). Kholdeeva's group had previously reported the preparation of $(TBA)_4[(HO)TiPW_{11}O_{39}]$ by vapour diffusion of wet acetone into an acetonitrile solution of $(TBA)_8[(\mu\text{-}O)(TiPW_{11}O_{39})_2]$. They also showed that hydrolysis of $(TBA)_4[(CH_3O)TiPW_{11}O_{39}]$ leads to both $(TBA)_4[(HO)TiPW_{11}O_{39}]$ and $(TBA)_8[(\mu\text{-}O)(TiPW_{11}O_{39})_2]$ in solution and were able to push the equilibrium towards $(TBA)_8[(\mu\text{-}O)(TiPW_{11}O_{39})_2]$ using 3Å molecular sieves.[2] They however, were not able to isolate $(TBA)_4[(HO)TiPW_{11}O_{39}]$ from the hydrolysis reaction and did not report the characteristic HO-Ti IR vibration frequency of the crystals from the wet acetone vapour diffusion. Our study sought to better control the hydrolysis in order to isolate $(TBA)_4[(HO)TiPW_{11}O_{39}]$ and monitor its dimerization in a separate step.

In MeCN, $(TBA)_4[(HO)TiPW_{11}O_{39}]$ was prepared by repeated hydrolysis of $(TBA)_4[(CH_3O)TiPW_{11}O_{39}]$ with a 2000-fold excess of H_2O for ~1 h. The process was repeated 6 times for complete hydrolysis of $(TBA)_4[(CH_3O)TiPW_{11}O_{39}]$. The large excess of water and short stirring time in solution served to minimize dimerization. The product was 91% pure by ^{31}P NMR with only 6% of the $(TBA)_8[(\mu\text{-}O)(TiPW_{11}O_{39})_2]$ and 3% of $(TBA)_3[PW_{12}O_{40}]$ (which was present in the starting material) as impurity. In DMSO, however, only one hydrolysis with a 200-fold excess of H_2O was required for complete hydrolysis of $(TBA)_4[(CH_3O)TiPW_{11}O_{39}]$ in ~1 h.

$(TBA)_8[(\mu\text{-}O)(M^{IV}PW_{11}O_{39})_2O]$ (M = Sn, Ti): Synthesis of $(TBA)_8[(\mu\text{-}O)(SnPW_{11}O_{39})_2]$ was attempted *via* condensation of $(TBA)_4[(HO)SnPW_{11}O_{39}]$ at ~120 ^oC according to the equilibrium reaction in **Equation 4.1**.

$$2(TBA)_4[(HO)SnPW_{11}O_{39}] \xrightleftharpoons{120\ ^oC} (TBA)_8[(\mu\text{-}O)(SnPW_{11}O_{39})_2] + H_2O \quad (4.1)$$

$$2(TBA)_4[(HO)SnPW_{11}O_{39}] + (C_6H_{11}N)_2C \xrightleftharpoons{120\ ^oC} (TBA)_8[(\mu\text{-}O)(SnPW_{11}O_{39})_2O] + (C_6H_{11}NH)_2CO \quad (4.2)$$

The reaction system was slowly evacuated at intervals to gradually eliminate the product water vapour to prevent rehydrolysis of $(TBA)_8[(\mu\text{-}O)(SnPW_{11}O_{39})_2]$. ^{31}P NMR studies showed over 35% condensation of $(TBA)_4[(HO)SnPW_{11}O_{39}]$ after about 12 h (see **Figure 4.3**). It was however difficult to push the equilibrium further as most of the reaction solvents (MeCN) had evaporated (MeCN with a lower boiling point than water also evaporates during evacuation) and addition of fresh solvent readily pushes the equilibrium backwards due to trace amount of water in the solvents (it is difficult to obtain 100% water-free dry acetonitrile). MeCN dried over 3Å molecular sieves (20% m/v) for up to 120 h is reported to have 10.5±0.9 ppm residual water content.[25] We therefore decided to introduce a dehydrating agent to remove water from the system. Two dehydrating agents were tried: (1) 3Å molecular sieves and (2) *N, N'*-dicyclohexylcarbodiimide (DCC), which reacts according to **Equation 4.2**. The former had no significant effect on the reaction even when left in the POM solution for up to 2 weeks while the later proved to be effective. **Figure 4.4** shows that ~14 mole-equivalents of DCC was needed to push the reaction to completion after ~48 h with trace amount of two unidentified peaks at -13.4 ppm (5.5%) and -14.00 ppm (1%). The impurities are possibly due to reactions between $(TBA)_4[(HO)SnPW_{11}O_{39}]$ and DCC and all the species were observed to readily hydrolyse upon addition of H_2O. The white solid product was isolated by filtration to remove insoluble side products like urea, vacuum-drying and washing severally with dry THF. The FT-IR spectra in **Figure 4.5** shows dry THF washing to be effective in removing any excess DCC.

$(TBA)_8[(\mu\text{-}O)(TiPW_{11}O_{39})_2]$ was obtained by a slight modification of the hydrolytic method shown previously by Kholdeeva.[2] After three repeated hydrolysis of ^{17}O-enriched $(TBA)_4[(CH_3O)TiPW_{11}O_{39}]$ with 80 mole-equivalents of H_2O, the product was vacuum-dried and allowed to stand in 3Å molecular sieves in MeCN solution for 2 d. In a separate experiment, this approach was used to selectively enrich the Ti-O-Ti oxygen of the POM by using minimum ^{17}O-enriched H_2O (~0.06%) for hydrolysis of unenriched

$(TBA)_4[(CH_3O)TiPW_{11}O_{39}]$ (see experimental) and this enabled a more informed protonation study using samples with and without Ti-O-Ti enrichment (see **Chapter 5 Section 5.2.1.4**).

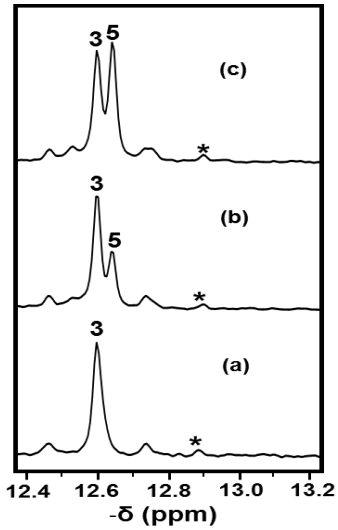

*Figure 4.3. ^{31}P NMR spectra in CD_3CN of (a) $(TBA)_4[(HO)SnPW_{11}O_{39}]$ (**3**) (b) mixture of $(TBA)_4[(HO)SnPW_{11}O_{39}]$ **(3)** and $(TBA)_8[(\mu\text{-}O)(SnPW_{11}O_{39})_2]$ (**5**) in equilibrium after heating to ~120 °C for 6 h and (c) mixture of $(TBA)_4[(HO)SnPW_{11}O_{39}]$ (**3**) and $(TBA)_8[(\mu\text{-}O)(SnPW_{11}O_{39})_2]$ (**5**) in equilibrium after condensation at ~120 °C for 12 h. Peaks asterisked indicate $(TBA)_4[ClSnPW_{11}O_{39}]$ impurity.*

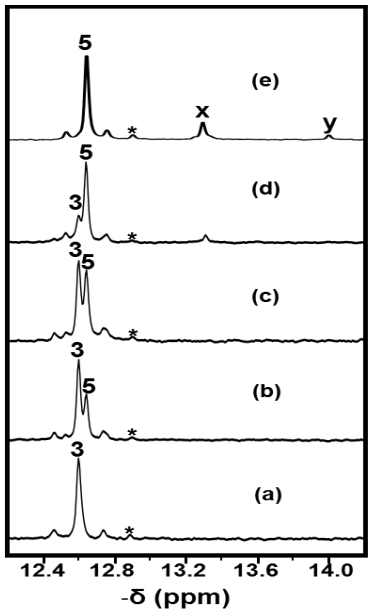

*Figure 4.4. ^{31}P NMR spectra in CD_3CN of (a) $(TBA)_4[(HO)SnPW_{11}O_{39}]$ (**3**) and mixture of $(TBA)_4[(HO)SnPW_{11}O_{39}]$ (**3**) and $(TBA)_8[(\mu\text{-}O)(SnPW_{11}O_{39})_2]$ (**5**) in equilibrium after heating to ~120 °C with (b) 5 equiv. of DCC for 12 h (c) 10 equiv. for 24 h. and (d) 14 equiv. for 48 h. Peaks asterisked indicate $(TBA)_4[ClSnPW_{11}O_{39}]$ impurity.*

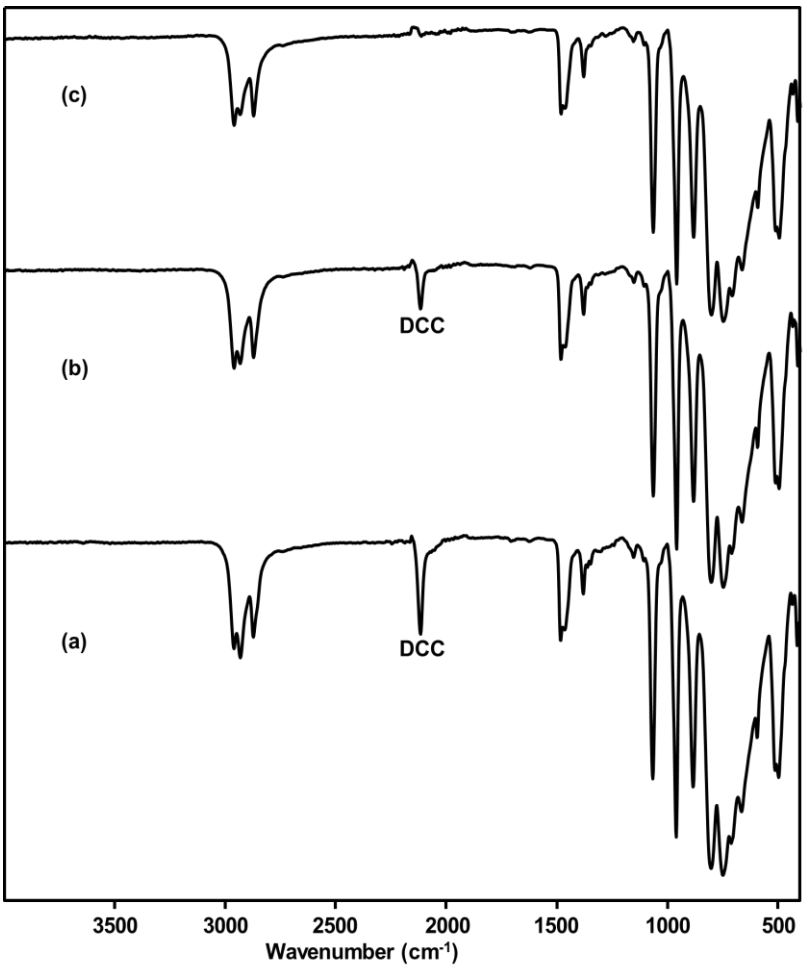

Figure 4.5. IR spectra of (a) crude $(TBA)_8[(\mu\text{-}O)(SnPW_{11}O_{39})_2]$ (b) after washing twice with THF (10 ml) and (c) after washing four times with THF (10 ml).

4.2.2. FT-IR spectroscopy

FT-IR data for Ti-substituted POMs (see **Table 4.1**) were in the range reported in the literature.[2] Slight differences are due to different modes of measurement i.e. ATR vs. transmission (see Experimental). **Figure 4.6** shows that the IR spectra of $(TBA)_4[ClSnPW_{11}O_{39}]$, $(TBA)_4[(CH_3O)SnPW_{11}O_{39}]$ and $(TBA)_4[(HO)SnPW_{11}O_{39}]$ are very similar in the region 1200 – 400 cm^{-1}. A weak band at 2819 cm^{-1} was assigned to the ν_{CH} of the OMe group of $(TBA)_4[(CH_3O)SnPW_{11}O_{39}]$ [see **Figure 4.6 (d)**]. Weak bands in the 2860-2800 cm^{-1} IR region are characteristic of methoxyl group.[26] **Table 4.1** gives a weak sharp band at 3638 cm^{-1} [see also **Figure 4.6 (c)**] and at 3633 cm^{-1} for the ν(OH) of $(TBA)_4[(HO)SnPW_{11}O_{39}]$ and $(TBA)_4[(HO)TiPW_{11}O_{39}]$ respectively. Also, a weak sharp band at 2684 cm^{-1} in the IR spectrum of $(TBA)_4[(DO)SnPW_{11}O_{39}]$ [**Figure 4.6 (b)**] was assigned to the ν(OD) band (see Experimental). As expected, other important bands associated with the Keggin POMs [ν(P-

O), ν(W=O) and ν(W-O-W)] were very similar. The FT-IR spectrum [**Figure 4.6 (a)**] of $(TBA)_8[(\mu\text{-}O)(SnPW_{11}O_{39})_2]$ however showed some marked differences. Firstly, the IR vibration at 3638 cm^{-1} for OH was absent, indicating the formation of a new species different from the starting POM. Secondly, the ν(P-O) vibration showed no splitting [$\Delta\nu$(P-O) = 0 cm^{-1}] as against the three monomeric species with splitting from 19 to 23 cm^{-1}. This is indicative of symmetry restoration in the central PO_4 tetrahedron of the dimeric product. Kholdeeva had earlier reported a similar high symmetry ν(P-O) vibration for $[Bu_4N]_7[(\mu\text{-}OH)(PTiW_{11}O_{39})_2]$ and $[Bu_4N]_8[(\mu\text{-}O)(PTiW_{11}O_{39})_2]$.[2] Finally, two new bands at 748 and 495 cm^{-1} assigned to Sn-O-Sn asymmetric (ν_{asym}) and symmetric (ν_{sym}) vibrations respectively were observed in the spectrum. Bridged metal-oxygen IR vibrations are reported to occur at the region ca. 850 – 200 cm^{-1} and Sn-O-Sn ν_{asym} and ν_{sym} for $Sn_2OF_{10}^{4-}$ have been assigned 833 and 452 cm^{-1} respectively.[27] Sn-O-Sn ν_{asym} vibrations of bis-(triethyltin) oxide (778 cm^{-1}), bis-(tributyltin) oxide (775 cm^{-1}), bis-(triisobutyltin) oxide (772 cm^{-1}), bis-(di-n-propyl-n-octyltin) oxide (781 cm^{-1}) and bis-(triphenyltin) oxide (774 cm^{-1}) have also been reported.[28] The low Sn-O-Sn ν_{asym} of $(TBA)_8[(\mu\text{-}O)(SnPW_{11}O_{39})_2]$ and appearance of a high ν_{sym} band are indications of a bent Sn-O-Sn bond. This has been attributed to a lower degree of metal-oxygen pi-bonding interaction.[27,29,30] Fe-O-Fe bands have been reported at 795[31] and 837.5 cm^{-1} .[32] Whereas Bent Cr-O-Cr ν_{asym} and ν_{sym} bands at 772 and 558 cm^{-1} respectively for $(Cr_2O_7)^{2-}$ and W-O-W ν_{asym} and ν_{sym} bands at 790 and 556 cm^{-1} respectively for the peroxy complex $[W_2O_{11}(H_2O)_2]^{2-}$ have also been reported.[29]

Table 4.1. FT-IR data for Sn- and Ti-Keggin polyanions.[a]

	IR parameter (cm^{-1})					
Anion	v(HO)	v(W=O)	v(WOW)	v(MOM)	v(P-O)	Δv(P-O)
$[ClSnPW_{11}O_{39}]^{4-}$	-	962	880	-	1079	23
			787		1056	
			702			
$[(MeO)SnPW_{11}O_{39}]^{4-}$	-	961	881	-	1077	19
			791		1058	
			708			
$[(HO)SnPW_{11}O_{39}]^{4-}$	3639	961	882	-	1077	19
	(w)		789		1058	
			705			
$[(\mu\text{-}O)(SnPW_{11}O_{39})_2]^{8-}$	-	959	882	748	1065	-
			802	495		
$[ClTiPW_{11}O_{39}]^{4-}$	-	962	883	-	1071	-
			787			
$[(MeO)TiPW_{11}O_{39}]^{4-}$	-	959	882	-	1068	-
			784			
$[(HO)TiPW_{11}O_{39}]^{4-}$	3633	960	884	-	1070	-
	(w)		791			
$[(\mu\text{-}O)(TiPW_{11}O_{39})_2]^{8-}$	-	959[b]	882	630[b]	1065	-
		958[c]	792	635[c]		

[a] as solid $^nBu_4N^+$ salts [b] for ^{17}O-enriched sample; [c] for unenriched sample.

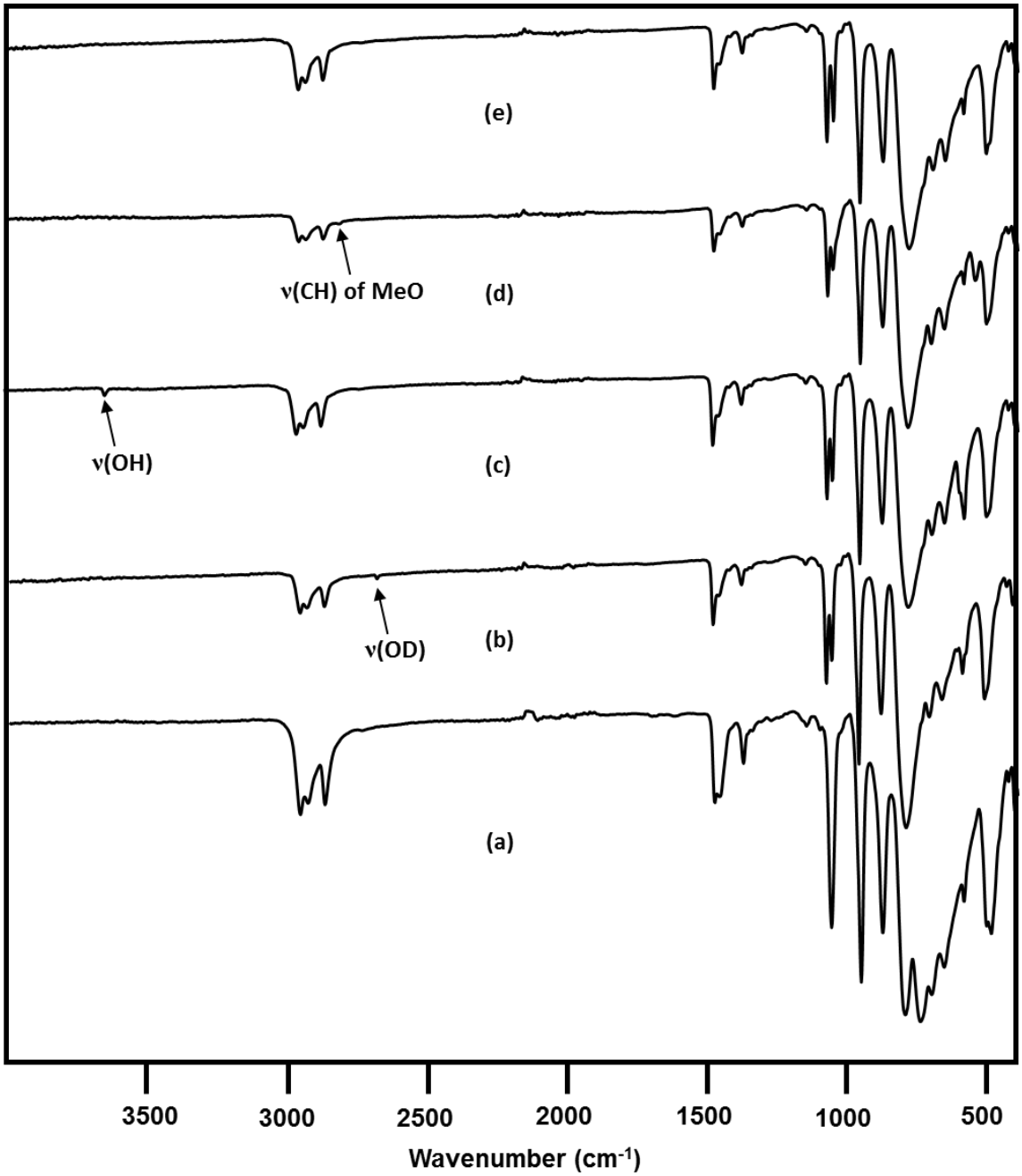

Figure 4.6. IR spectra of (a) $(TBA)_8[(\mu\text{-}O)(SnPW_{11}O_{39})_2O]$ (b) $(TBA)_4[(DO)SnPW_{11}O_{39}]$ (c) $(TBA)_4[(HO)SnPW_{11}O_{39}]$ (d) $(TBA)_4[(CH_3O)SnPW_{11}O_{39}]$ and (e) $(TBA)_4[ClSnPW_{11}O_{39}]$.

4.2.3. Multinuclear (^{1}H, ^{13}C, ^{17}O, ^{119}Sn and ^{183}W) NMR spectroscopy

The presence of phosphorous and tin as primary and secondary heteroatoms respectively in the Sn-substituted POMs were quite useful for elucidating speciation in solutions of these anions based on ^{31}P, ^{119}Sn and ^{119}Sn {^{1}H} NMR data (see **Table 4.2**). ^{1}H and ^{31}P NMR parameters recorded for Ti-substituted POMs (see **Table 4.2**) were in the range reported in literature.[2,9]

^{31}P NMR spectroscopy: ^{31}P NMR chemical shift of $(TBA)_4[ClSnPW_{11}O_{39}]$ appeared farthest upfield perhaps due to the high electronegativity of the chloride ligand on the tin heteroatom. The ^{31}P NMR shifts of $(TBA)_4[(CH_3O)SnPW_{11}O_{39}]$, $(TBA)_4[(HO)SnPW_{11}O_{39}]$, $(TBA)_4[(DO)SnPW_{11}O_{39}]$ and $(TBA)_8[(\mu\text{-}O)(SnPW_{11}O_{39})_2]$ were quite similar differing by 0.02 to 0.06 ppm. ^2J(Sn-P) was similar for $(TBA)_4[ClSnPW_{11}O_{39}]$ and $(TBA)_4[(CH_3O)SnPW_{11}O_{39}]$ (37 Hz) but was interestingly smallest for $(TBA)_8[(\mu\text{-}O)(SnPW_{11}O_{39})_2]$ (28 Hz). The small Sn-P coupling is possibly due to weaker P-Sn interaction in $(TBA)_8[(\mu\text{-}O)(SnPW_{11}O_{39})_2]$.

Table 4.2. ^{1}H, ^{13}C, ^{31}P and ^{119}Sn NMR data for Sn- and Ti-Keggin polyanions.[a]

Anion	^{31}P		^{119}Sn		^{1}H		^{13}C	
	δ (ppm)	$^2J_{Sn\text{-}P}$ (Hz)	δ (ppm)	$^2J_{Sn\text{-}W}$ (Hz)	δ (ppm)	$J_{H\text{-}Sn}$ (Hz)	δ (ppm)	$^2J_{C\text{-}Sn}$ (Hz)
$[ClSnPW_{11}O_{39}]^{4-}$	-12.90	37	-578.08	63[b] 157[c]				
$[(MeO)SnPW_{11}O_{39}]^{4-}$	-12.66	37	-622.09	58[b] 149[c]	3.68	81[d] 78[e]	53.82	39
$[(HO)SnPW_{11}O_{39}]^{4-}$	-12.60	34	-600.24	56[b] 149[c]	1.98 3.98[f]	48 42[f]	-	-
$[(\mu\text{-}O)(SnPW_{11}O_{39})_2]^{8-}$	-12.64	28	-620.42	67[b] 164[c]				
$[ClTiPW_{11}O_{39}]^{4-}$	-14.36	-	-	-				
$[(MeO)TiPW_{11}O_{39}]^{4-}$	-14.05 -14.25[f]	-	-	-	4.31			
$[(HO)TiPW_{11}O_{39}]^{4-}$	-14.14 -14.35[f]	-	-	-	12.04[f]			
$[(\mu\text{-}O)(TiPW_{11}O_{39})_2]^{8-}$	-14.07 -14.28[f]	-	-	-				

[a] *as $^nBu_4N^+$ salts in CD_3CN;* [b] *$J_{Sn\text{-}W}$ between ^{119}Sn and $^{183}W_A$;* [c] *$J_{Sn\text{-}W}$ between ^{119}Sn and $^{183}W_F$;* [d] *$^3J(^1H\text{-}^{119}Sn)$.* [e] *$^3J(^1H\text{-}^{117}Sn)$;* [f] *NMR was done in DMSO-d_6. See labelling of $^{183}W_A$ and $^{183}W_F$ in* ***Figure 4.18.***

^{1}H and ^{13}C NMR spectroscopy: ^{1}H and ^{13}C NMR spectra were used to confirm the presence of CH_3O- and HO- groups in the POMs. The ^{1}H NMR spectrum of $(TBA)_4[(CH_3O)SnPW_{11}O_{39}]$ [**Figure 4.8 (a)**] showed a peak for methoxido protons at 3.68 ppm with $^3J(^1H\text{-}^{119}Sn)$ and $^3J(^1H\text{-}^{117}Sn)$ of 81 and 78 Hz respectively. The ratio of the integral of CH_3O- protons to CH_2N protons in the TBA cation was however found to be 1:13 instead of the expected 1:11. This is most likely because some of the CH_3O- protons had been hydrolysed to methanol and the integral of the methanol peak in the spectrum accounted for the lost protons. The ^{13}C NMR spectrum [**Figure 4.8 (b)**] showed a peak at 53.82 assigned to CH_3O- carbon with $^2J(^{13}C\text{-}^{117/119}Sn)$ of 39 Hz. The ^{1}H NMR spectrum of $(TBA)_4[(CH_3O)TiPW_{11}O_{39}]$ (see Experimental) showed a peak at 4.31 ppm for methoxido protons. The ratio of methoxido protons to CH_2N protons was 1:12 (calculated 1:11). The ^{1}H NMR spectrum of $(TBA)_4[(HO)SnPW_{11}O_{39}]$ **[Figure**

4.9 (a)] showed a peak at 1.98 ppm for the OH proton with ^2J (^1H-^{119}Sn) of 48 Hz in CD_3CN and 3.98 ppm with ^2J (^1H-$^{117/119}Sn$) of 42 Hz in (DMSO-d_6) [**Figure 4.9 (b)**]. The OH signal was not always detected in the proton NMR spectrum in CD_3CN solvent most likely due to exchange with H_2O hence the use of DMSO-d_6. The advantage of DMSO-d_6 in investigating spin-spin interactions of groups like –OH and the slight dependence of spin-spin coupling on solvent are well known.[33] To minimize dimerization, the ^1H NMR of $(TBA)_4[(HO)TiPW_{11}O_{39}]$ was recorded in DMSO-d_6 and the spectrum [**Figure 4.10 (a)**] showed a peak significantly shifted downfield at 12.04 ppm assigned to the –OH group. The high downfield shift of the -OH group of $(TBA)_4[(HO)TiPW_{11}O_{39}]$ in DMSO could be linked to an association with the solvent (see **Section 4.2.5**). DMSO is a better ligand than MeCN so will compete in the associative step of condensation (**Figure 4.7**). This might explain why $(TBA)_4[(HO)TiPW_{11}O_{39}]$ is more stable in DMSO solvent than in acetonitrile where there is little or no solvent interaction and hence $(TBA)_4[(HO)TiPW_{11}O_{39}]$ dimerizes easily. The ratio of hydroxyl proton to CH_2N protons was 1:34 (calculated 1:32). The NMR sample of $(TBA)_4[(HO)TiPW_{11}O_{39}]$ in DMSO-d_6 was treated with excess D_2O and a ^1H NMR study showed the disappearance of the –OH peak due to substitution by -OD further confirming $(TBA)_4[(HO)TiPW_{11}O_{39}]$ as the product [**Figure 4.10 (b)**].

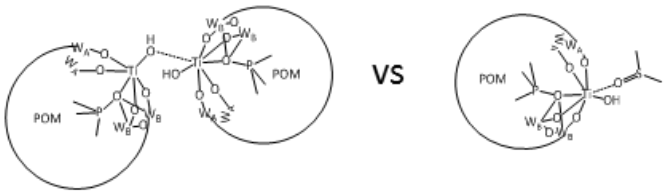

Figure 4.7. Diagram of competitive associative step between $(TBA)_4[(HO)TiPW_{11}O_{39}]$ and DMSO solvent.

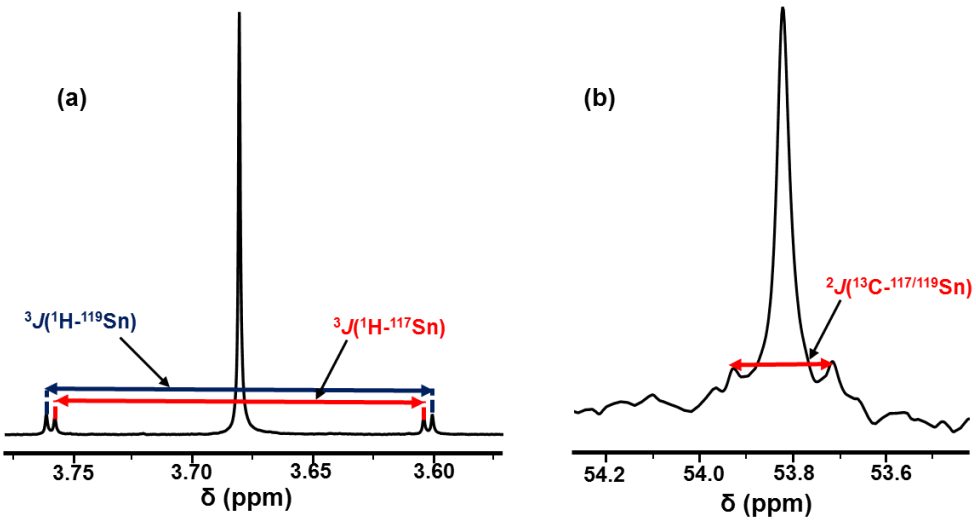

Figure 4.8. (a) ^1H NMR spectrum of $(TBA)_4[(CH_3O)SnPW_{11}O_{39}]$ in CD_3CN showing $^3J(^1H^{119}Sn)$ and $^3J(^1H^{117}Sn)$ couplings and (b) ^{13}C NMR spectrum of $(TBA)_4[(CH_3O)SnPW_{11}O_{39}]$ in CD_3CN showing $^2J(^{13}C\text{-}^{117/119}Sn)$ coupling.

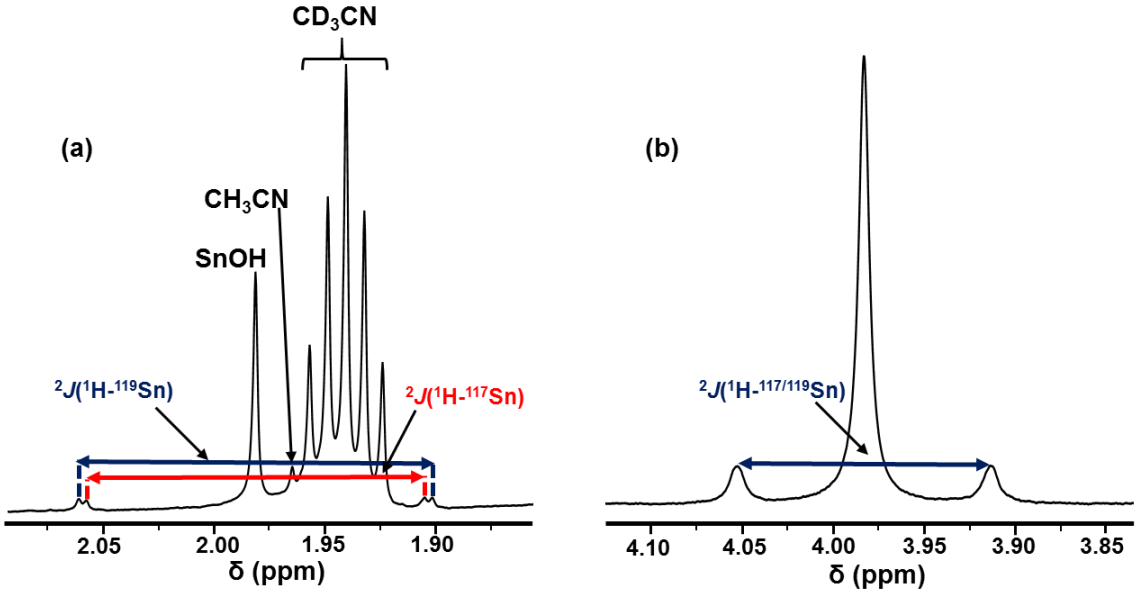

Figure 4.9. ^1H NMR spectra of $(TBA)_4[(HO)SnPW_{11}O_{39}]$ showing $^2J(^1H^{119}Sn)$ and $^2J(^1H^{117}Sn)$ couplings in (a) CD_3CN and (b) DMSO-d_6.

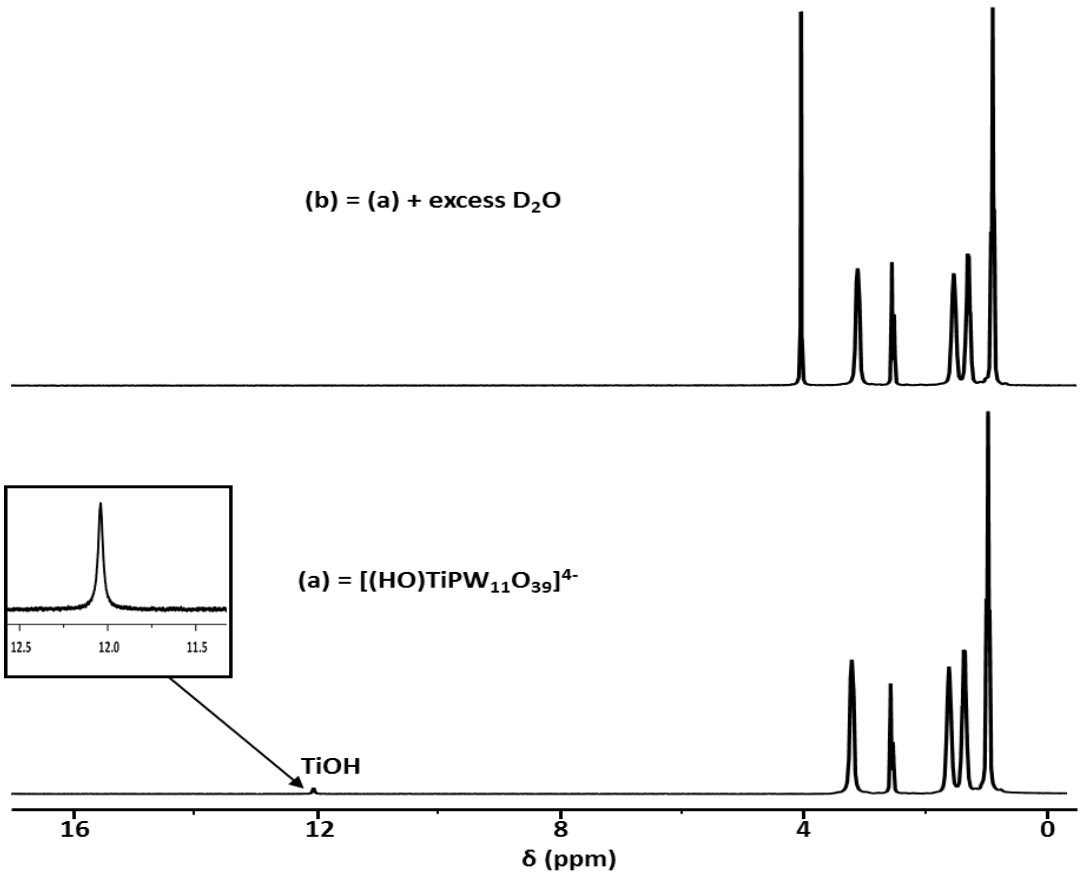

Figure 4.10. ^1H NMR spectra of (a) $(TBA)_4[(HO)TiPW_{11}O_{39}]$ in DMSO-d_6 showing TiOH peak at -12.02 ppm and (b) after treating with excess of D_2O resulting in the disappearance of the TiOH peak.

^{17}O NMR *spectroscopy*: ^{17}O NMR chemical shifts are summarized in **Table 4.3**. The spectrum for $(TBA)_4[(CH_3O)SnPW_{11}O_{39}]$ [**Figure 4.11(a)**] showed three peaks at 745 – 731 ppm assigned to W=O. The unresolved peaks at 427 – 333 ppm were assigned to SnOW and WOW as it was not possible to unambiguously assigned peaks to them individually. The spectrum of $(TBA)_4[(CH_3O)TiPW_{11}O_{39}]$ [**Figure 4.11(b)**] showed two peaks at 740 – 738 ppm for W=O, two sharp peaks at 559 and 534 ppm assigned to TiOW and broad peaks at 424 – 382 ppm assigned to WOW. There is literature precedence for upfield shift of the SnOW ^{17}O NMR resonance in the Lindqvist POM, $(TBA)_3[(MeO)SnW_5O_{18}]$ towards the WOW region compared to the TiOW resonance for the analogous titanium species, $(TBA)_3[(MeO)TiW_5O_{18}]$.[22]

The ^{17}O NMR spectrum of $(TBA)_4[(HO)SnPW_{11}O_{39}]$ [**Figure 4.12(a)**] showed three peaks at 746 – 733 ppm assigned to W=O and the peaks at 427 – 340 ppm were also assigned to SnOW and WOW. The spectrum of $(TBA)_4[(HO)TiPW_{11}O_{39}]$ [**Figure 4.12(b)**] on the other hand showed two peaks at 739 – 736 ppm assigned to W=O, two sharp peaks at 559 and 536 ppm

assigned to TiOW and broad peaks at 424 – 401 ppm assigned to WOW. The spectrum of $(TBA)_8[(\mu\text{-}O)(SnPW_{11}O_{39})_2]$ (**Figure 4.13**) showed three broad peaks at 740 – 732 assigned to W=O and several peaks at 429 – 374 assigned to SnOW and WOW. The peak for SnOSn could not be assigned and the present synthetic approach to $(TBA)_8[(\mu\text{-}O)(SnPW_{11}O_{39})_2]$, which involves heating at ~120 ^oC did not allow for selective enrichment of the SnOSn site. At this temperature, enrichment is likely to occur at all the oxygens in the POM. In contrast, the method of $(TBA)_8[(\mu\text{-}O)(TiPW_{11}O_{39})_2]$ synthesis enabled the selective enrichment of the TiOTi site as discussed in **Section 4.2.1**. **Figure 4.14** shows the ^{17}O NMR spectra of $(TBA)_8[(\mu\text{-}O)(TiPW_{11}O_{39})_2]$ with ^{17}O enrichment only at the TiOTi site (a), with no TiOTi site enrichment (b) and with enrichment at all oxygen sites (c). Peak assignments are W=O resonances at 742 – 738, TiOTi resonance at 712 ppm, TiOW resonances at 572 and 544 ppm and WOW resonances at 423 – 404 ppm.

Table 4.3. ^{17}O NMR data for $[MPW_{11}]$ Keggin anions.[a]

Anion	^{17}O chemical shift/ppm			
	W=O	MOM	MOW	WOW
$[ClSn^{IV}PW_{11}O_{39}]^{4-}$	749 – 737	-	429 - 372	
$[(MeO)Sn^{IV}PW_{11}O_{39}]^{4-}$	745 – 731	-	427 - 333	
$[(HO)Sn^{IV}PW_{11}O_{39}]^{4-}$	746 – 733	-	427 - 334	
$[(\mu\text{-}O)(Sn^{IV}PW_{11}O_{39})_2]^{8-}$	740 – 732	*b*	429 - 374	
$[ClTiPW_{11}O_{39}]^{4-}$	747 – 743	-	585, 565	427 - 386
$[(MeO)TiPW_{11}O_{39}]^{4-}$	740 – 738	-	559, 534	423 - 382
$[(HO)TiPW_{11}O_{39}]^{4-}$	739 – 736	-	559, 536	424 - 384
$[(\mu\text{-}O)(TiPW_{11}O_{39})_2]^{8-}$	742 – 738	712	572, 544	423 - 404

[a] as $^nBu_4N^+$ salts in CD_3CN; [b] not observed

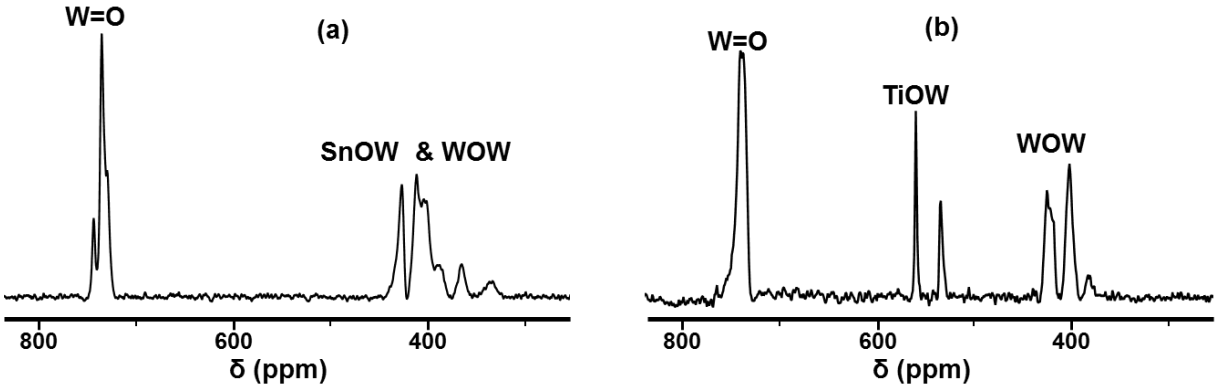

Figure 4.11. ^{17}O NMR spectra of (a) $(TBA)_4[(CH_3O)SnPW_{11}O_{39}]$ and (b) $(TBA)_4[(CH_3O)TiPW_{11}O_{39}]$ in CD_3CN.

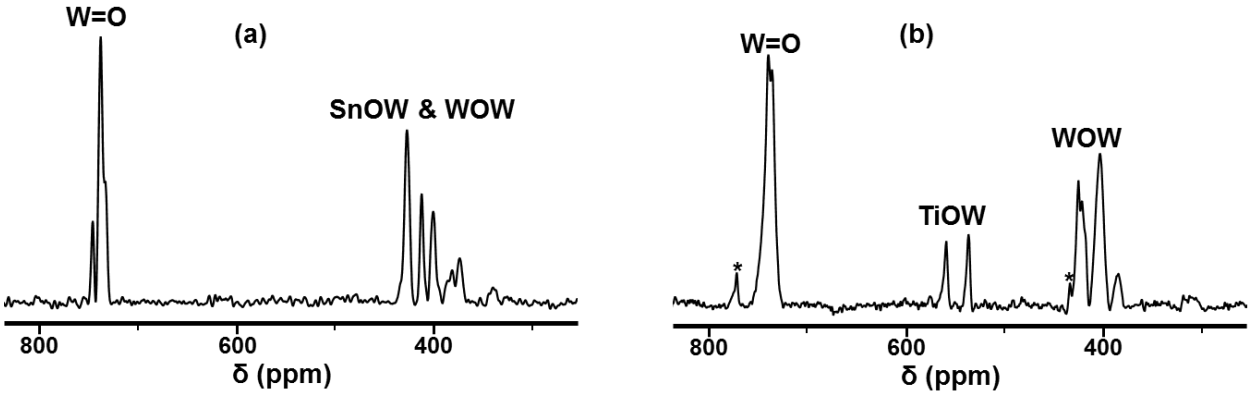

Figure 4.12. ^{17}O NMR spectra of (a) $(TBA)_4[(HO)SnPW_{11}O_{39}]$ and (b) $(TBA)_4[(HO)TiPW_{11}O_{39}]$ in CD_3CN. Peaks marked with asterisk (*) are assigned to $[PW_{12}O_{40}]^{3-}$.

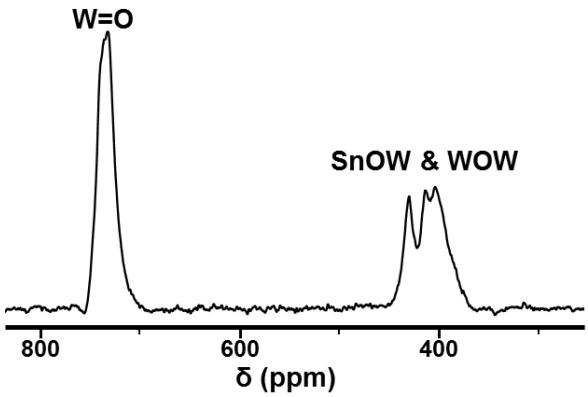

Figure 4.13. ^{17}O NMR spectrum of $(TBA)_8[(\mu\text{-}O)(SnPW_{11}O_{39})_2]$ in CD_3CN.

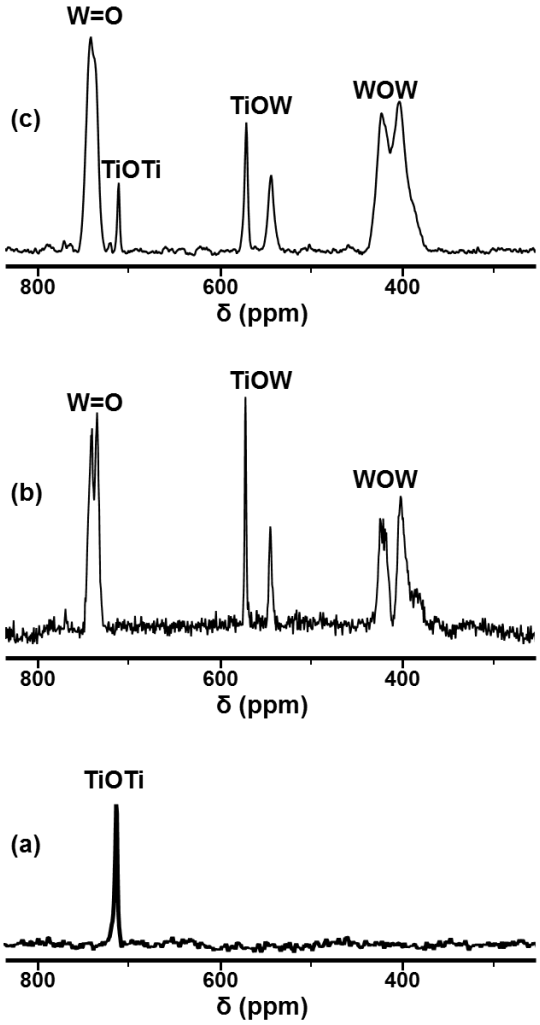

Figure 4.14. ^{17}O NMR spectra of $(TBA)_8[(\mu\text{-}O)(TiPW_{11}O_{39})_2]$ in CD_3CN (a) with enrichment only at TiOTi site (b) without TiOTi site enrichment and (c) with enrichment at all oxygen sites.

^{119}Sn NMR spectroscopy: As expected, there was no difference between the peak patterns for ^{119}Sn and ^{119}Sn {^{1}H} NMR spectra of $(TBA)_4[ClSnPW_{11}O_{39}]$ and $(TBA)_8[(\mu\text{-}O)(SnPW_{11}O_{39})_2]$ [see **Figure 4.15 (a) and (d)**] confirming the absence of a direct or indirect attachment of proton to the tin atoms of the POMs. The ^{119}Sn and ^{119}Sn {^{1}H} NMR spectra of $(TBA)_4[(CH_3O)SnPW_{11}O_{39}]$ however were different [see **Figure 4.15 (b)**]. A quartet of doublets in the ratio 1:3:3:1 was observed in the ^{119}Sn NMR spectrum confirming the direct or indirect attachment of 3H atoms, i.e. the CH_3O- group to the tin atom [see **Appendix (Figure A3.23)** for simulation of the spectrum]. The ^{119}Sn NMR spectrum of $(TBA)_4[(HO)SnPW_{11}O_{39}]$ [**Figure 4.15 (c)**] also showed different spectra for both ^{119}Sn and ^{119}Sn {^{1}H}. The ^{119}Sn spectrum had a 1:1 doublet of doublets as expected confirming the

bonding of the OH group to the tin atom [see **Appendix (Figure A3.24)** for simulation of the spectrum].

Unfortunately, it was not possible to resolve any $^{2}J(^{119}Sn\text{-}^{117}Sn)$ coupling in the ^{119}Sn NMR spectrum of $(TBA)_8[(\mu\text{-}O)(SnPW_{11}O_{39})_2]$. This was surprising as $^{2}J(^{119}Sn\text{-}^{117}Sn)$ coupling of 300 Hz has previously been observed for the Lindqvist POM, $(TBA)_6[(\mu\text{-}O)(SnW_5O_{18})_2]$.[23,24] We therefore attempted to simulate the ^{119}Sn NMR spectrum for $(TBA)_8[(\mu\text{-}O)(SnPW_{11}O_{39})_2]$ using the obtained experimental NMR (^{31}P, ^{119}Sn and ^{183}W) parameters while varying $^{2}J(^{119}Sn\text{-}^{117}Sn)$ from 0 to 350 Hz [**see Appendix (Figure A4.1)**]. The best fits between the experimental and theoretical spectra were obtained for $^{2}J(^{119}Sn\text{-}^{117}Sn)$ = 60 Hz and 110 Hz (**Figure 4.16**). Thus, it was not possible to resolve $^{2}J(^{119}Sn\text{-}^{117}Sn)$ for $(TBA)_8[(\mu\text{-}O)(SnPW_{11}O_{39})_2]$ as these lower values were smaller than the line width of the ^{119}Sn peaks and would be hidden under the peaks. The lower coupling constant might be due to a bent Sn-O-Sn bond with a smaller bond angle in the Keggin POM, $(TBA)_8[(\mu\text{-}O)(SnPW_{11}O_{39})_2]$ than in the Lindqvist POM, $(TBA)_6[(\mu\text{-}O)(SnW_5O_{18})_2]$. This reduces the sigma type character in the Sn-O bond interaction, which in turn lowers the $^{119}Sn\text{-}O\text{-}^{117}Sn$ coupling constant.[33] Attempts to run $^{119}Sn\ \{^{31}P\}$ or $^{117}Sn\ \{^{31}P\}$ NMR were not successful.

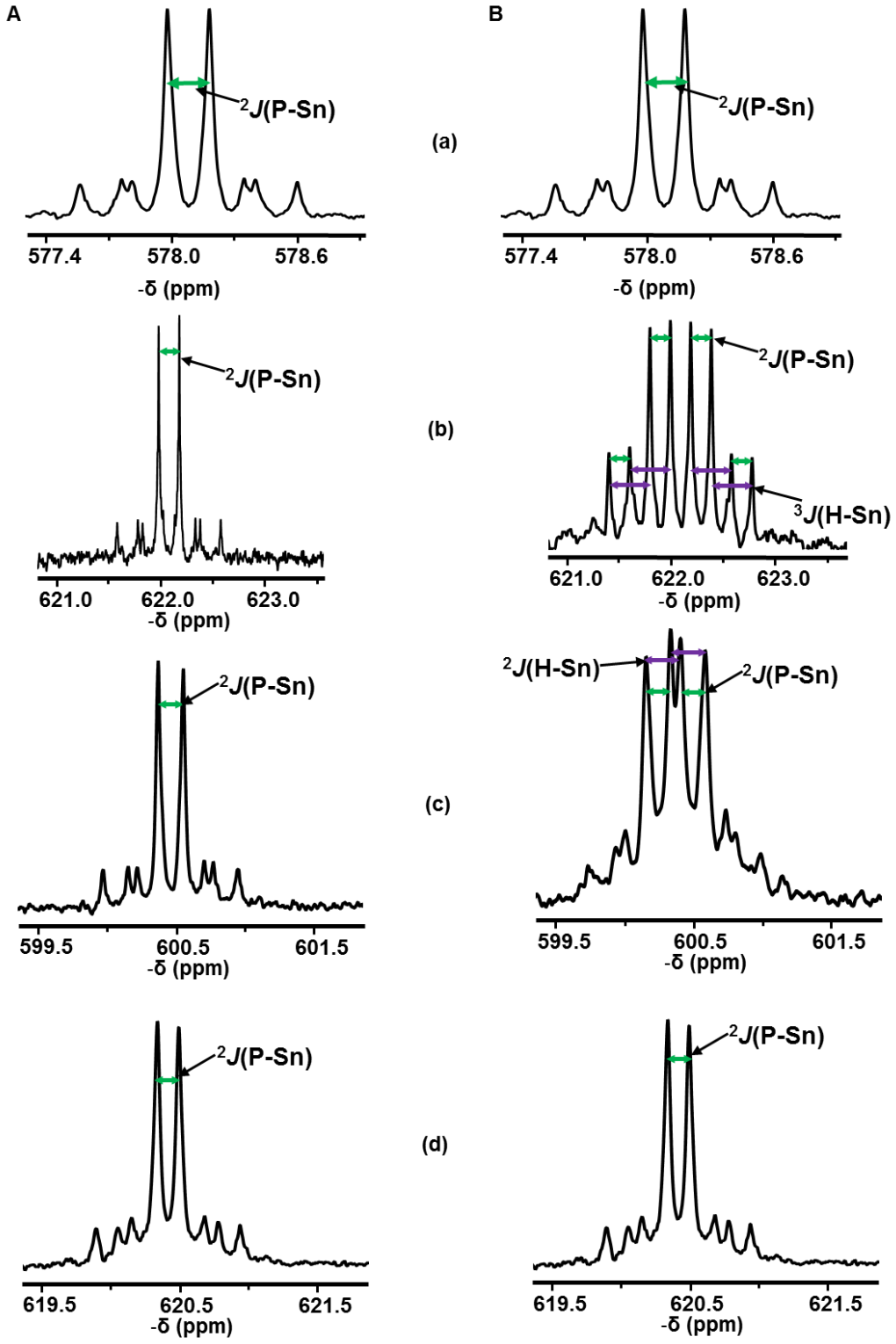

Figure 4.15. (A) ^{119}Sn {^1H} and (B) ^{119}Sn NMR spectra showing P-Sn and H-Sn couplings of (a) $(TBA)_4[ClSnPW_{11}O_{39}]$ (b) $(TBA)_4[(CH_3O)SnPW_{11}O_{39}]$ (c) $(TBA)_4[(HO)SnPW_{11}O_{39}]$ and (d) $(TBA)_8[(\mu\text{-}O)(SnPW_{11}O_{39})_2]$ in CD_3CN.

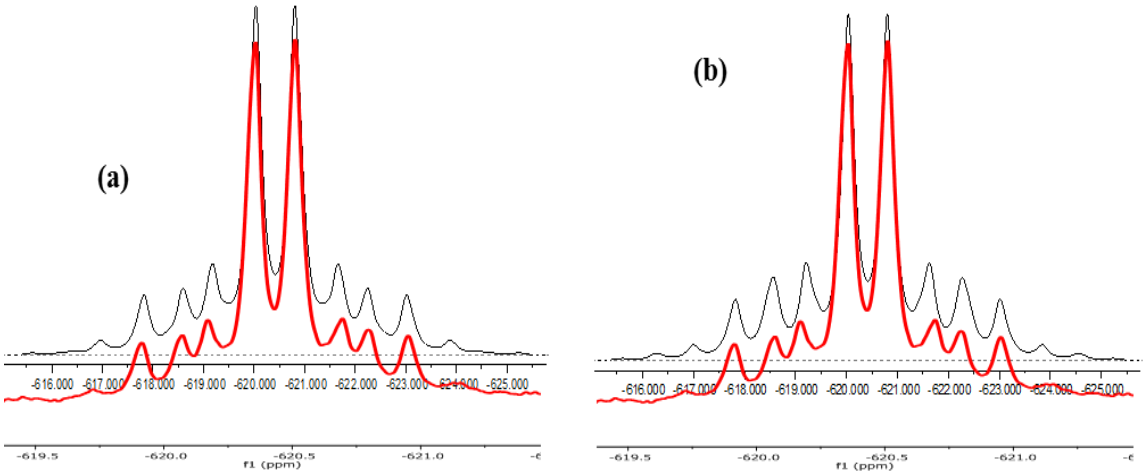

Figure 4.16. ^{119}Sn NMR simulated spectrum (top or black) and experimental spectrum (bottom or red) of $(TBA)_8[(\mu\text{-}O)(SnPW_{11}O_{39})_2]$ at $^2J(^{119}Sn\text{-}^{117}Sn)$ = 60 Hz (a) and $^2J(^{119}Sn\text{-}^{117}Sn)$ = 110 Hz (b).

^{183}W NMR spectroscopy: **Figure 4.17** gives the ^{183}W NMR spectra of $(TBA)_8[(\mu\text{-}O)(TiPW_{11}O_{39})_2]$ and $(TBA)_4[(HO)TiPW_{11}O_{39}]$. The pattern of the peaks were similar except for the 6th peak in $(TBA)_4[(HO)TiPW_{11}O_{39}]$, which was broaden. No concrete explanation is available as to why this is. The ^{183}W NMR spectra of all the tin-substituted POMs (**Figure 4.19**) indicated similar number of peaks and pattern. As predicted, 6 peaks in the ratio 2:2:2:2:1:2 were present revealing a C_s symmetry for the monomers and possibly C_{2v} or C_{2h} symmetry for the dimer. The spectra also showed that the monomeric structural symmetry was retained in the dimer. The peaks were assigned as shown in **Figure 4.18**. A and F were assigned based on Sn-W couplings. E was assigned based on peak intensity ratio. C was assigned after assigning B and D, which were assigned based on W-O-W couplings, peak height and broadness.[1,34,35] Peaks B, C, D and E are quite similar for all POMs. Interestingly however, peaks A and F for the dimer were shifted more upfield. This movement in chemical shift might be due to the influence of each monomer on the electron clouds of tungsten A and F of the other resulting in more shielding. This is likely as tungsten A and F are the closest to the oxo-bridge between the monomers in $(TBA)_8[(\mu\text{-}O)(SnPW_{11}O_{39})_2]$.

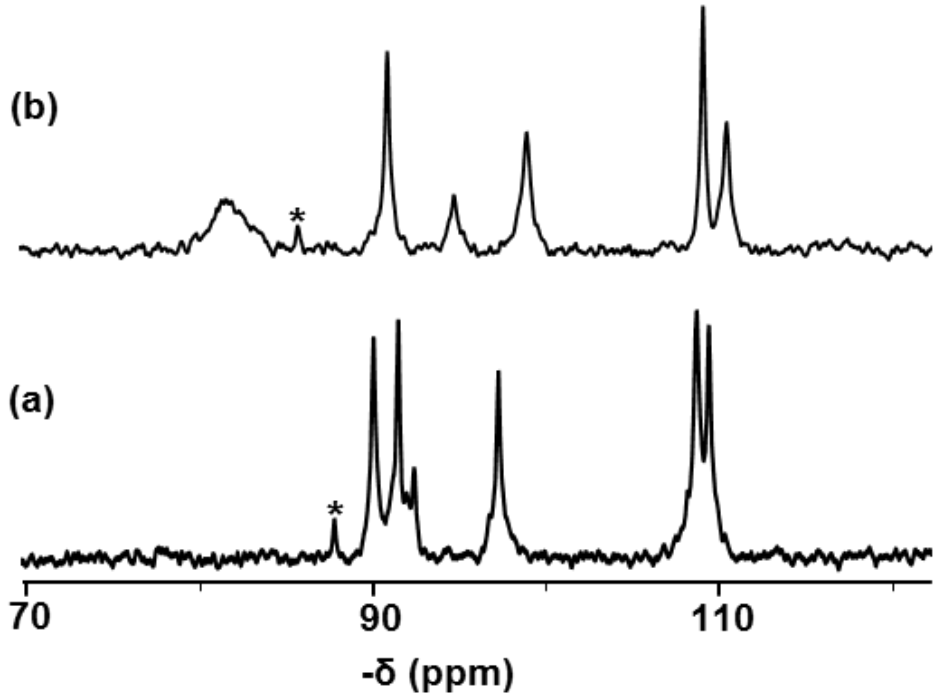

Figure 4.17. ^{183}W NMR spectra of (a) $(TBA)_8[(\mu\text{-}O)(TiPW_{11}O_{39})_2]$ in CD_3CN and (b) $(TBA)_4[(HO)TiPW_{11}O_{39}]$ in DMSO-D_6. Peaks asterisked (*) are due to $[PW_{12}O_{40}]^{3-}$ impurities.

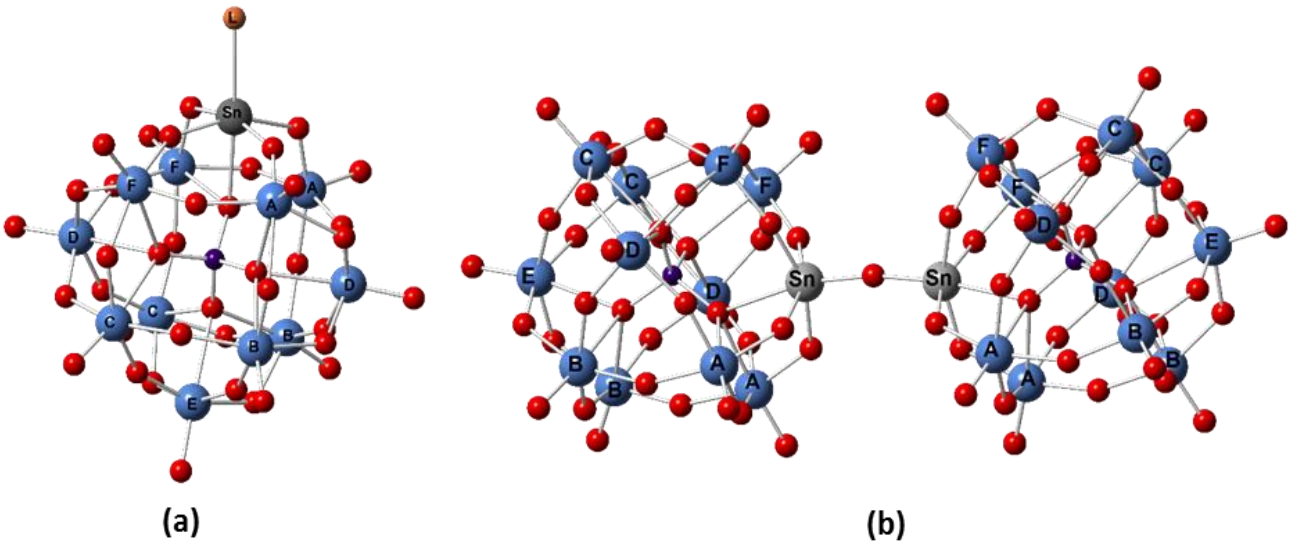

Figure 4.18. Proposed structures with W-atoms labelling of tin-substituted Keggin POMs (a) monomer (L = Cl, OH, MeO) and (b) dimer.

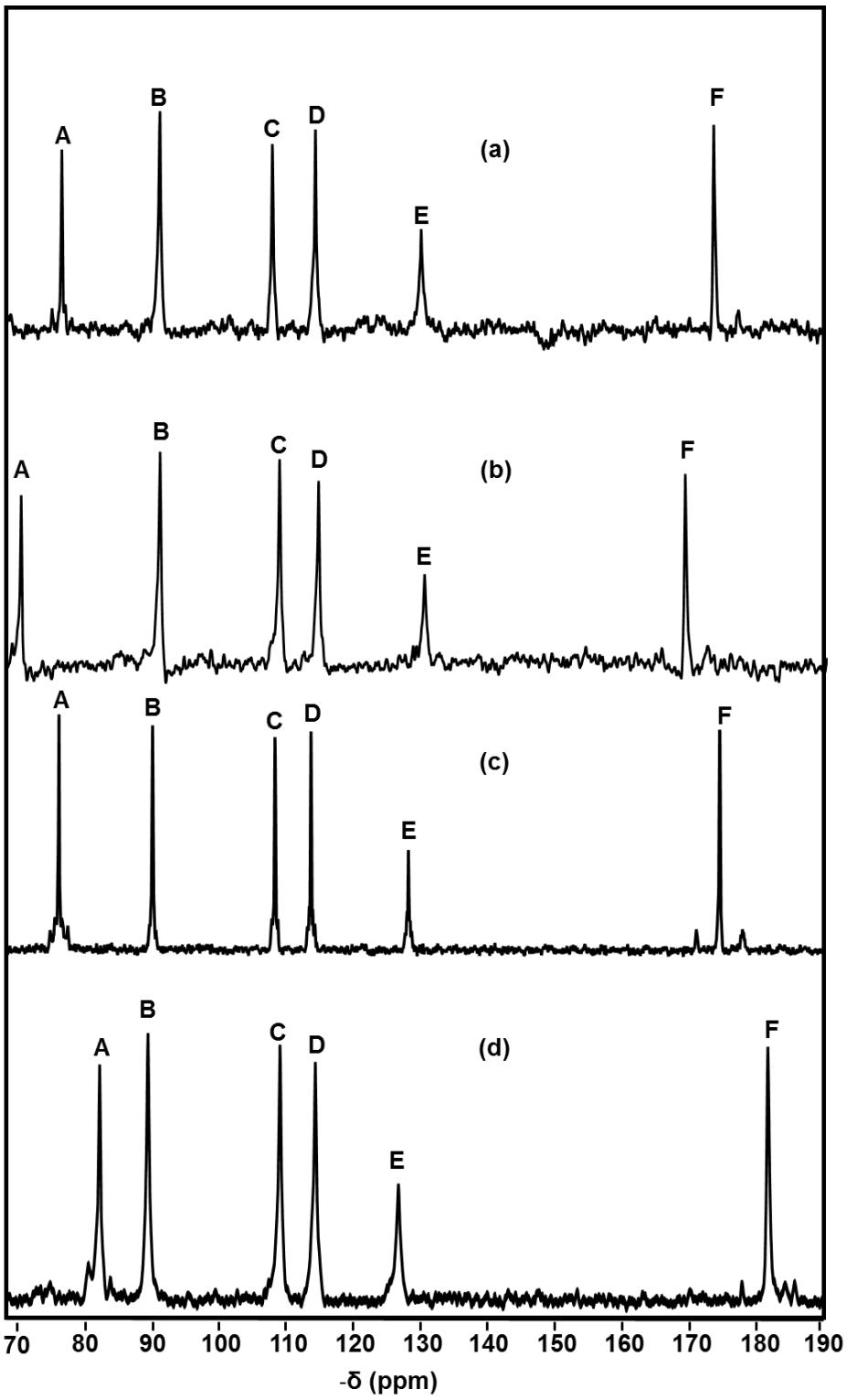

Figure 4.19. ^{183}W NMR spectra of (a) $(TBA)_4[ClSnPW_{11}O_{39}]$ (b) $(TBA)_4[(CH_3O)SnPW_{11}O_{39}]$ (c) $(TBA)_4[(HO)SnPW_{11}O_{39}]$ and (d) $(TBA)_8[(\mu\text{-}O)(SnPW_{11}O_{39})_2]$ in CD_3CN.

4.2.4. Solid state NMR spectroscopy

Solid State NMR (^{1}H, ^{13}C and ^{31}P) spectra were recorded for $(TBA)_4[(CH_3O)SnPW_{11}O_{39}]$ in a bid to further confirm the nature of the product in the solid state. The ^{31}P spectrum had one peak at -12.2 ppm. The linewidth was however too high to resolve any coupling to tin. The spectrum confirmed the purity of $(TBA)_4[(CH_3O)SnPW_{11}O_{39}]$**.** The Sn-OMe bond seemed to be intact at 55.3 ppm in the ^{13}C NMR spectrum but again, the linewidth was too high to resolve the tin satellites. The ^{1}H NMR was not very helpful as is typical for a solid sample. Although it did seem as though the protons were all methyls, a faint shoulder was observed around 3 ppm that could arise from the OMe protons [see **Appendix (Figure A4.2**)].

4.2.5. Hydrolysis of $(TBA)_4[(CH_3O)M^{IV}PW_{11}O_{39}]$ (M = Sn and Ti)

Hydrolysis of $(TBA)_4[(CH_3O)SnPW_{11}O_{39}]$ with 4 mole-equivalents of H_2O was fast and had almost reached equilibrium after about 3 mins with only 31% of $(TBA)_4[(CH_3O)SnPW_{11}O_{39}]$ left in solution (see **Figure 4.20** and **Figure 4.21**). The fast reaction rate did not allow determination of a hydrolytic rate constant. Hydrolysis of $(TBA)_4[(CH_3O)TiPW_{11}O_{39}]$ was however slower, even with a larger excess of H_2O (2.5 times or 10 mole-equivalents). After ~ 60 min about 96% of $(TBA)_4[(CH_3O)TiPW_{11}O_{39}]$ was still in solution (see **Figure 4.21**). The faster hydrolysis rate of $(TBA)_4[(CH_3O)SnPW_{11}O_{39}]$ is attributed to the more ionic character in the Sn—OCH_3 bond than in Ti—OCH_3. The greater covalency in the Ti—O bond results from the availability of Ti 3d orbitals for π-bonding with oxygen. This is absent in the Sn—O bond.[36] Kholdeeva previously studied $(TBA)_4[(CH_3O)TiPW_{11}O_{39}]$ hydrolysis and proposed that it results in a mixture of $(TBA)_4[(HO)TiPW_{11}O_{39}]$ and $(TBA)_8[(\mu\text{-}O)(TiPW_{11}O_{39})_2]$.[2] This work sought to exercise better control over the process so as to isolate $(TBA)_4[(HO)TiPW_{11}O_{39}]$ as the only product. As a result, further studies with a greater excess of H_2O (50 mole equivalents) in MeCN and in DMSO were carried out. **Figure 4.22** shows that the hydrolysis rate increases with the amount of H_2O and that it was fastest in DMSO as solvent, with only about 25% of $(TBA)_4[(CH_3O)TiPW_{11}O_{39}]$ left in solution after 110 min. The fast reaction in DMSO is probably due to the different pK_a of H_2O in MeCN and DMSO. DMSO is more polar than MeCN and thus ionization of H_2O is faster in DMSO. Also when the ^{31}P NMR of the hydrolysis product was recorded, the peak for the oxobridge dimer was not observed. These

results prompted the synthesis of $(TBA)_4[(HO)TiPW_{11}O_{39}]$ with a large excess of H_2O in MeCN and in DMSO as described in **Section 4.2.1.**

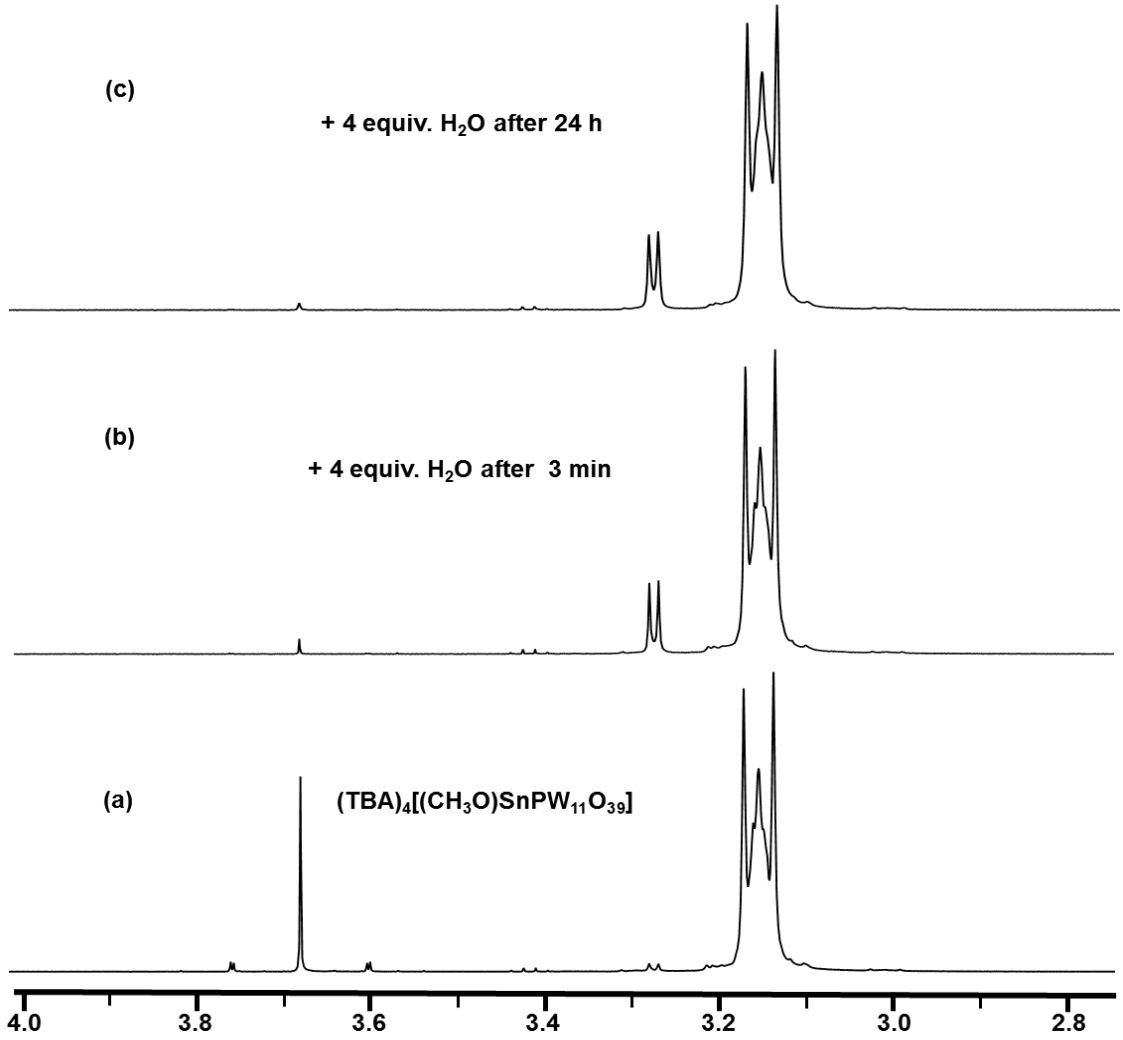

Figure 4.20. ^1H NMR spectra of (a) $(TBA)_4[(CH_3O)SnPW_{11}O_{39}]$ in CD_3CN plus (b) 4 equiv. of H_2O after 3 min at room temperature and (c) 4 equiv. of H_2O after 24 h at room temperature.

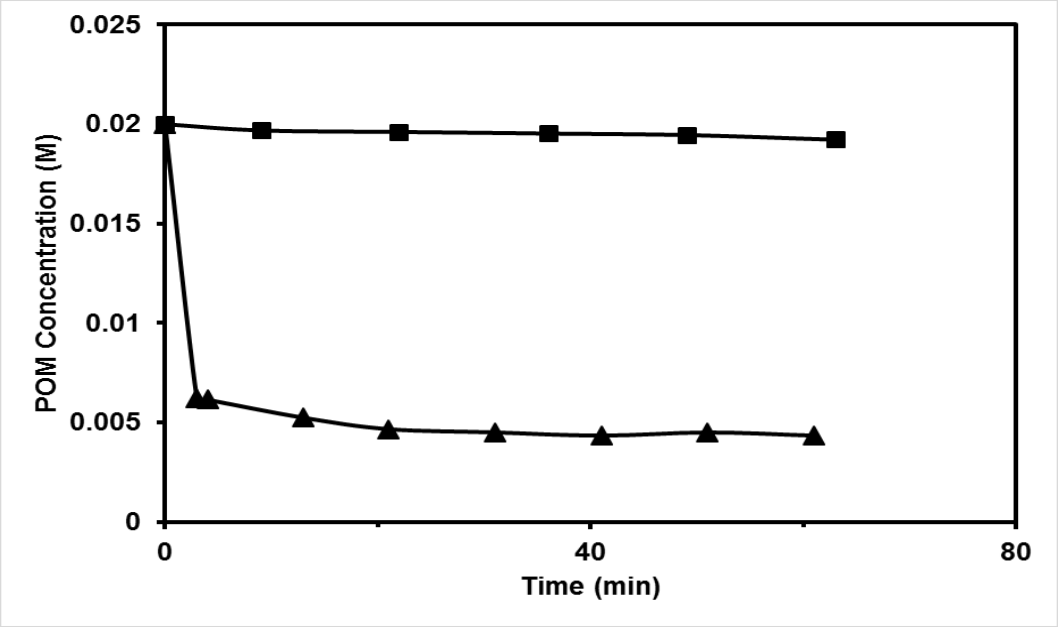

Figure 4.21. Plots of change in concentration of $(TBA)_4[(CH_3O)M^{IV}PW_{11}O_{39}]$ (M = Sn, Ti) during hydrolysis. Conditions: $[POM]_0$ = 0.02 M, H_2O = 4 equiv. (Sn-POM) and 10 equiv. (Ti-POM), MeCN, 295 K:▲- $(TBA)_4[(CH_3O)Sn^{IV}PW_{11}O_{39}]$, ■ - $(TBA)_4[(CH_3O)Ti^{IV}PW_{11}O_{39}]$.

z\z

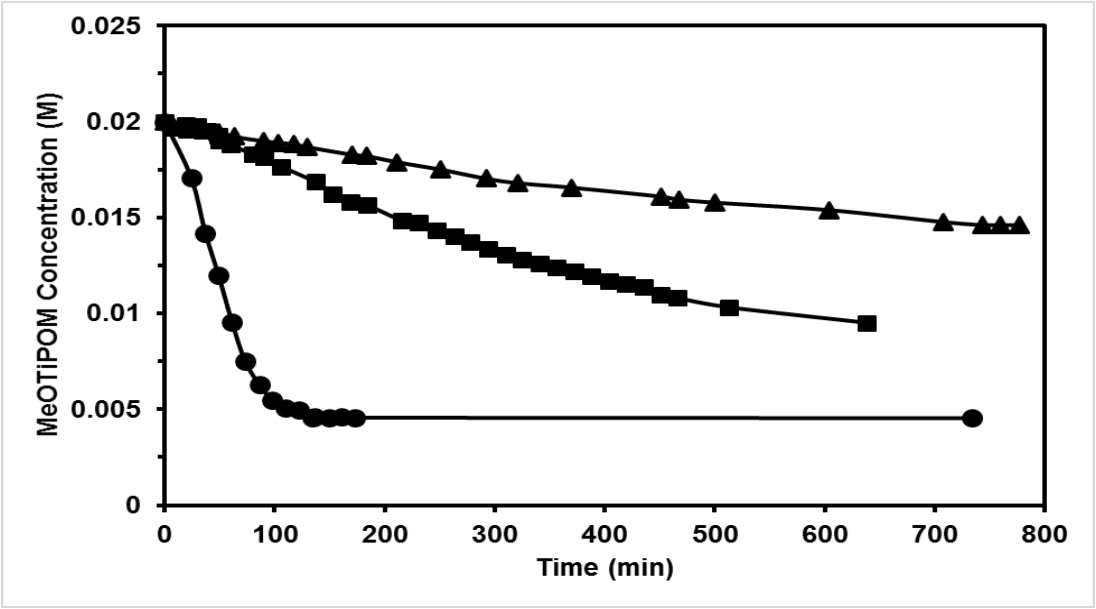

Figure 4.22. Plots of change in concentration of $(TBA)_4[(CH_3O)TiPW_{11}O_{39}]$ during hydrolysis. Conditions:$[POM]_0$ = 0.02 M, 295 K :▲- H_2O = 10 equiv. , MeCN; ■ - H_2O = 50 equiv. , MeCN; ● - H_2O = 10 equiv. , DMSO.

4.2.6. Alcohol-alkoxide exchange

Addition of alcohol R'OH to $[(RO)MPW_{11}O_{39}]^{4-}$ was expected to result in alkoxido exchange so attempts were made to detect exchange in $[(CH_3O)M^{IV}PW_{11}O_{39}]^{4-}$ (M = Sn, Ti) by ^{1}H EXSY. Though off-diagonal SnOMe/MeOH cross-peaks with an exchange constant of 2.946 s^{-1} were observed for MeOH/$[(MeO)SnPW_{11}O_{39}]^{4-}$, no TiOMe/MeOH cross-peaks were observed for

MeOH/[(MeO)TiPW$_{11}$O$_{39}$]$^{4-}$, even after addition of water at 60 °C. Small peaks with an exchange constant of 0.043 s^{-1} did appear upon addition of small amounts of HBF$_4$ (see **Figure 4.23**). This was surprising as our group had previously reported exchange peaks for MeOH/[(MeO)TiW$_5$O$_{18}$]$^{3-}$. To further investigate this process, a second exchange study between [(CH$_3$O)M^{IV}PW$_{11}$O$_{39}$]$^{4-}$ (M = Sn, Ti) and CD$_3$OD was attempted by ^{1}H NMR and the results are presented in **Figure 4.24**. In agreement with the EXSY results, the figure shows that the exchange with [(MeO)SnPW$_{11}$O$_{39}$]$^{4-}$ was faster compared with that of [(MeO)TiPW$_{11}$O$_{39}$]$^{4-}$. After ~4 min, [(MeO)SnPW$_{11}$O$_{39}$]$^{4-}$ exchange was almost completed with ~22% of starting POM left in solution while about 71% of [(MeO)TiPW$_{11}$O$_{39}$]$^{4-}$ was still in solution after 74 min. These observations are consistent with our general findings that alkoxido-tin(IV)-substituted POMs are much more moisture-sensitive than their titanium analogues.

(a)

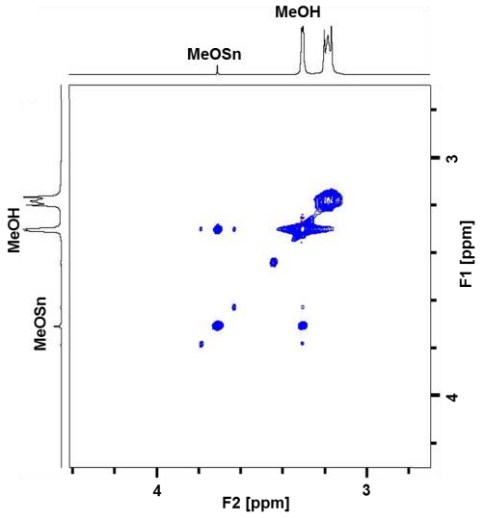

(b)

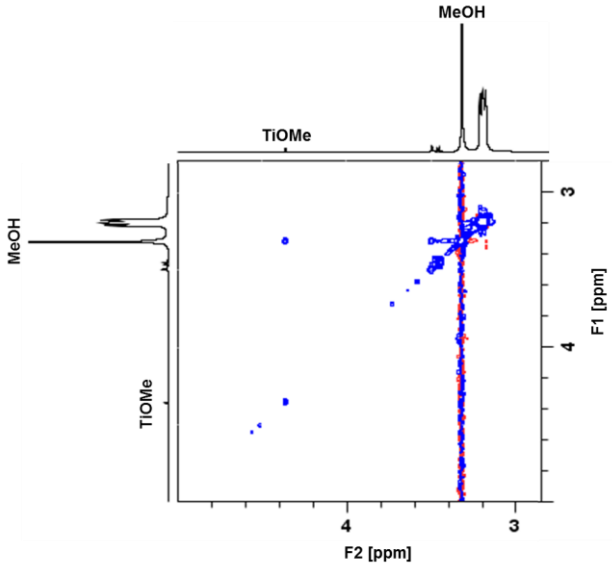

Figure 4.23. 2D EXSY spectra for alcohol-alkoxide exchange in CD_3CN between CH_3OH and (a) $(TBA)_4[(MeO)SnPW_{11}O_{39}]$ and (b) $(TBA)_4[(MeO)TiPW_{11}O_{39}]$ after addition of $HBF_4.Et_2O$. See experimental for experimental conditions.

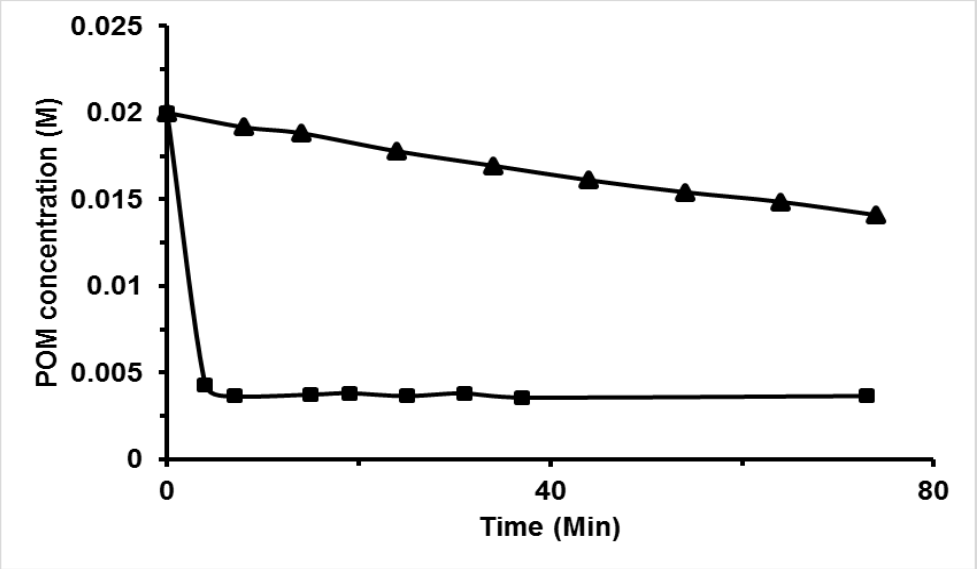

Figure 4.24. Plots of change in concentration of $(TBA)_4[(CH_3O)M^{IV}PW_{11}O_{39}]$ (M = Sn, Ti) after addition of CD_3OD. Conditions: $[POM]_0$ = 0.02 M, CD_3OD = 0.6 µl, MeCN, 295 K:■ - $(TBA)_4[(CH_3O)Sn^{IV}PW_{11}O_{39}]$, ▲ - $(TBA)_4[(CH_3O)Ti^{IV}PW_{11}O_{39}]$.

4.2.7. Alkanolysis of $(TBA)_4[(HO)Sn^{IV}PW_{11}O_{39}]$

The exchange experiments inspired further attempts to treat the easily-formed $[(HO)Sn^{IV}PW_{11}O_{39}]^{4-}$ anion with a range of alcohols and phenols. This was firstly in a bid to ascertain trends in stability of the POMs as R substituents becomes bulkier and also to possibly obtain less disordered crystal structures for potentially more stable bulky-R derivatives. The monomeric titanium (IV) complex, $LTi(O^tBu)$ [LH_3 = tris(2-hydroxy-3,5-di-tert-butylbenzyl)amine] was reported to be very stable to hydrolysis due to stronger metal-oxygen bonding in tert-butoxide than in the hydroxide and also due to the bulky peripheral tert-butyl substituents.[37] Equally, the stability of $R_3SnCl.S$ complexes (S = pyridine, dimethylsulphoxide, hexamethylphosphortriamide and R = n-butyl, benzyl, phenyl) in solution have been shown to increase in the pattern: n-butyl < benzyl < phenyl.[38] The alkanolysis reactions generally followed **Equation 4.3** and an excess of ROH was required to push the equilibrium to the right. The ^1H, ^{31}P and ^{119}Sn NMR parameters for the reaction products are summarized in

$$(TBA)_4[(HO)SnPW_{11}O_{39}] \underset{-ROH}{\overset{ROH}{\rightleftharpoons}} (TBA)_4[(RO)SnPW_{11}O_{39}] + H_2O \qquad (4.3)$$

Table 4.4. No reaction was observed with 2, 4, 6-tributylphenol, most likely due to steric hindrance between SnOW and tert-butyl substituents in ortho positions which did not allow access to the HOSn site of $[(HO)Sn^{IV}PW_{11}O_{39}]^{4-}$. Attempts to isolate and crystallize the products resulted in rehydrolysis to $[(HO)Sn^{IV}PW_{11}O_{39}]^{4-}$ further highlighting the very moisture sensitive nature of the Keggin tin-POMs compared to the Lindqvist analogue, where the series $[(R)SnW_5O_{18}]^{3-}$ (R = MeO, EtO, ^{i}PrO, ^{t}BuO, PhO, *p*-CH_3-C_6H_4O, *p*-$C(CH_3)_3$-C_6H_4O), *m*-OH-C_6H_4O, *p*-OH-C_6H_4O, 2-CHO-C_6H_4O, Me_3SiO) have been isolated and characterized.[23]

$$(TBA)_4[(HO)SnPW_{11}O_{39}] \underset{-ROH}{\overset{ROH}{\rightleftharpoons}} (TBA)_4[(RO)SnPW_{11}O_{39}] + H_2O \qquad (4.3)$$

Table 4.4. NMR parameters of products of alkanolysis of $(TBA)_4[(HO)SnPW_{11}O_{39}]$[a].

R	^{31}P		^{119}Sn		^{1}H	
	δ (ppm)	$^{2}J_{Sn\text{-}P}$ (Hz)	δ (ppm)	$^{2}J_{Sn\text{-}W}$ (Hz)	δ (ppm)	$J_{H\text{-}Sn}$ (Hz)
Me	-12.66	37	-622.09	58[b]	3.68	81[d]
				149[c]		78[e]
Et	-12.64	35	-623.72	60[b]		72
				147[c]		
^{n}Bu	-12.64	34	-625.00	[f]		67
Ph	-12.74	38	-646.67	66[b]		
				157[c]		
4-^{t}BuPh	-12.80	37	-647.17	[f]		
2,6-Me_2Ph	-12.83	37	-647.34	66[b]		
				157[c]		
2, 4, 6-tri-^{t}BuPh[g]	-	-	-	-	-	-

*[a] NMR spectra were recorded in CD_3CN; [b] is $^{2}J(Sn\text{-}W_A)$coupling; [c] is $^{2}J(Sn\text{-}W_F)$ coupling (see labelling in **Figure 4.18**); [d] is $^{3}J(^{1}H\text{-}^{119}Sn)$ coupling; [e] is $^{3}J(^{1}H\text{-}^{117}Sn)$ coupling; [f] could not be resolved due low spectrum resolution; [g] no observed reaction.*

4.2.8. Dimerization of $(TBA)_4[(HO)M^{IV}PW_{11}O_{39}]$ (M = Sn and Ti)

Figure 4.25 shows results from ^{31}P NMR studies, which confirm that $(TBA)_4[(HO)TiPW_{11}O_{39}]$ is more susceptible to dimerization than $(TBA)_4[(HO)SnPW_{11}O_{39}]$. At room temperature, no dimerization occurs with $(TBA)_4[(HO)SnPW_{11}O_{39}]$ even when left in solution for up to 1 month, it only dimerizes at elevated temperature, typically ~120 ^{o}C in the presence of a water-scavenging agent (e.g. DCC). The Lindqvist analogue, $(TBA)_3[(HO)SnW_5O_{18}]$ on the other hand, was observed to form a minor condensation product at ambient temperature.[39]

In contrast, $(TBA)_4[(HO)TiPW_{11}O_{39}]$, is prone to dimerization in MeCN reaching ~ 94% of the dimer after ~ 20 h. Interestingly, no dimerization was observed when $(TBA)_4[(HO)TiPW_{11}O_{39}]$ was left in DMSO solution for up to three months possibly due to interaction between the HO- and DMSO solvent.

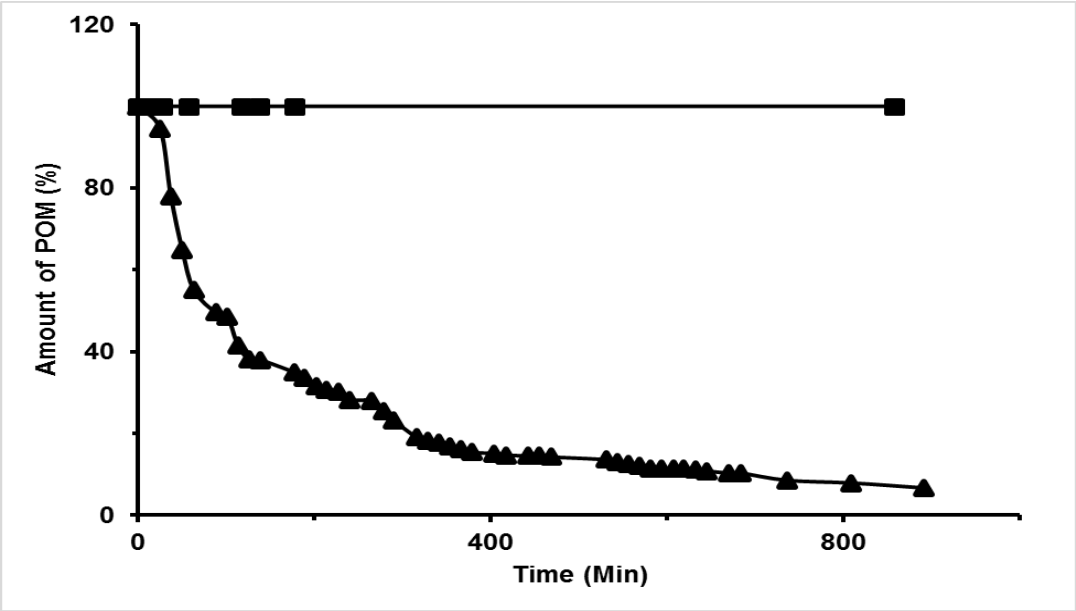

Figure 4.25. Plots of change in amount of $(TBA)_4[(HO)M^{IV}PW_{11}O_{39}]$ (M = Sn, Ti) during dimerisation. Conditions: 295 K, MeCN,:■ - $(TBA)_4[(CH_3O)Sn^{IV}PW_{11}O_{39}]$, ▲ - $(TBA)_4[(CH_3O)Ti^{IV}PW_{11}O_{39}]$.

4.2.9. Hydrolysis studies on $(TBA)_4[ClM^{IV}PW_{11}O_{39}]$ (M = Sn and Ti)

Hydrolysis of $(TBA)_4[ClSnPW_{11}O_{39}]$ and $(TBA)_4[ClTiPW_{11}O_{39}]$ were expected to follow **Equations 4.4** and **4.5** respectively and could serve as alternative routes to the hydroxides and dimers. As shown in **Figure 4.26**, addition of up to 800-fold excess (892 mole-equivalents) of H_2O to $(TBA)_4[ClSnPW_{11}O_{39}]$ gave only ~5% hydrolysis to $(TBA)_4[(HO)SnPW_{11}O_{39}]$ at room temperature. Only ~ 25% of the hydrolysis product was obtained when more H_2O (another 800-fold excess) was added. There was no further change in the species in solution even when the solution was left to stir for 48 h. The peaks for $(TBA)_4[(HO)SnPW_{11}O_{39}]$ and $(TBA)_4[ClSnPW_{11}O_{39}]$ were shifted to -12.74 and -12.98 ppm respectively due to change in the solution magnetic susceptibility as a result of the addition of H_2O and the species in solution were further confirmed by ^{119}Sn NMR and FTIR.

In contrast, **Figure 4.27** shows that addition of 172 mole-equivalents of H_2O to $(TBA)_4[ClTiPW_{11}O_{39}]$ caused only slight hydrolysis to occur after 30 mins, ~ 19% of hydrolysis

products {$(TBA)_4[(HO)TiPW_{11}O_{39}]$ and $(TBA)_8[(\mu\text{-}O)(TiPW_{11}O_{39})_2]$} and ~13% of a new peak at -13.68 ppm, which was not assigned. Addition of 1720 mole-equivalents of H_2O to the solution, led to an immediate change to a cloudy solution, which became clear again after ~10 min and ^{31}P NMR studies showed complete hydrolysis to give a mixture of $(TBA)_4[(HO)TiPW_{11}O_{39}]$ {~62%) and $(TBA)_8[(\mu\text{-}O)(TiPW_{11}O_{39})_2]$ (~38%) as the only products. The isolated product however showed the presence of some $(TBA)_4[ClTiPW_{11}O_{39}]$ impurity (~19%), which was most likely due to re-chlorination of some of the product during work-up by HCl in solution. A series of repeated hydrolysis was required to minimize the $(TBA)_4[ClTiPW_{11}O_{39}]$ impurity in the product. These results show a case where titanium-substituted Keggin POM is more moisture sensitive than the tin-substituted Keggin species.

$$(TBA)_4[ClTiPW_{11}O_{39}] \underset{+HCl\ (-H_2O)}{\overset{Excess\ H_2O\ (-HCl)}{\rightleftharpoons}} (TBA)_4[(HO)TiPW_{11}O_{39}] \underset{+{}^1/_2H_2O}{\overset{-{}^1/_2H_2O}{\rightleftharpoons}} {}^1/_2(TBA)_8[(TiPW_{11}O_{39})_2O] \quad (4.4)$$

$$(TBA)_4[ClSnPW_{11}O_{39}] \underset{-H_2O}{\overset{Excess\ H_2O}{\rightleftharpoons}} (TBA)_4[(HO)SnPW_{11}O_{39}] + HCl \quad (4.5)$$

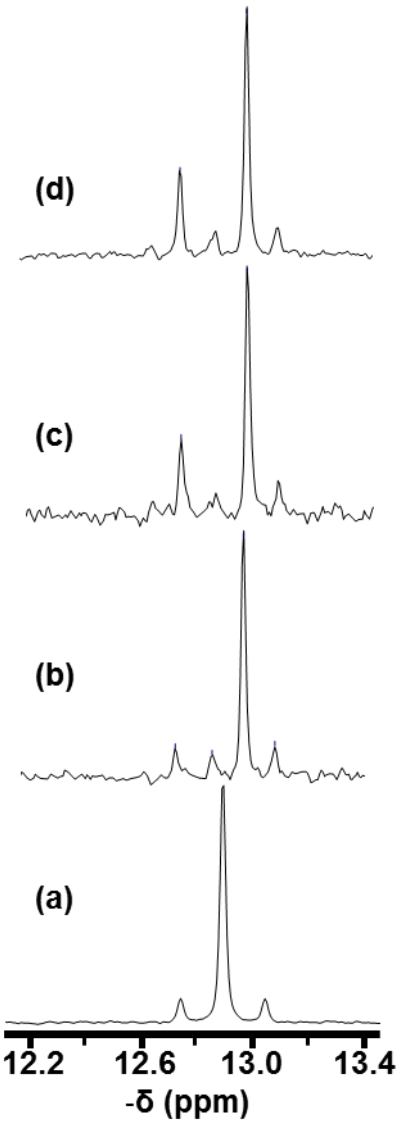

Figure 4.26. ^{31}P NMR spectra of (a) $(TBA)_4[ClSn^{IV}PW_{11}O_{39}]$ in CD_3CN (b) after addition of 800-fold excess of H_2O (c) after addition of 1600-fold excess of H_2O and (d) after stirring (c) for 48 h.

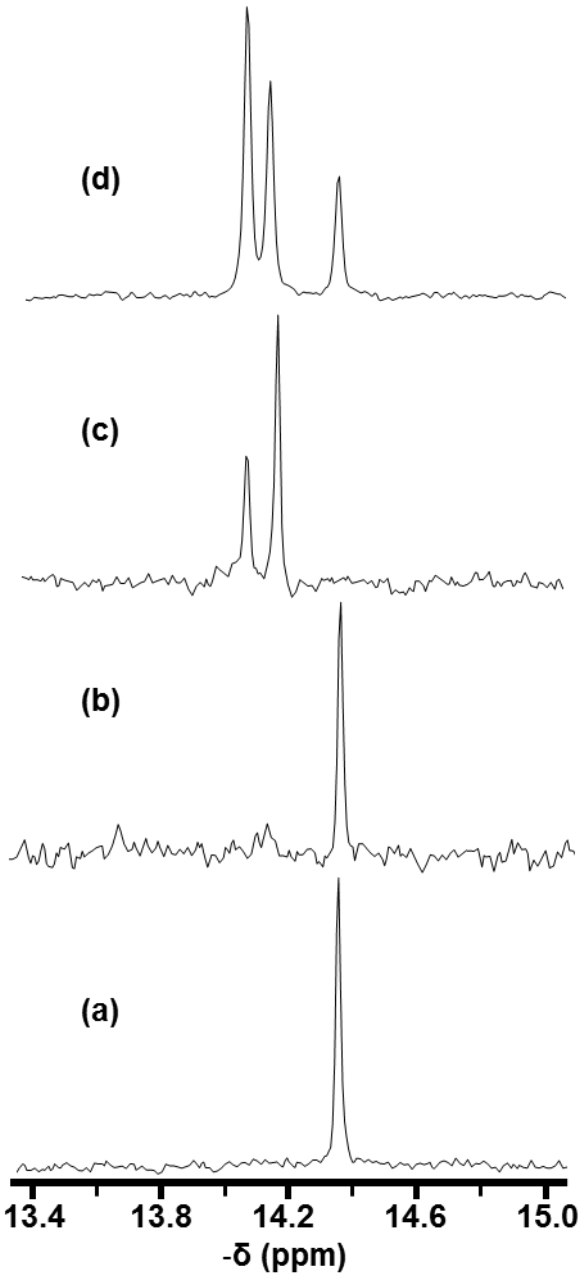

Figure 4.27. ^{31}P NMR spectra of (a) $(TBA)_4[ClTi^{IV}PW_{11}O_{39}]$ in CD_3CN (b) after addition of 100-fold excess of H_2O (c) after addition of 1000-fold excess of H_2O and (d) Isolated hydrolysis product.

4.2.10. Computational studies

DFT calculations on methanol exchange and hydrolysis reactions for $[(MeO)MPW_{11}O_{39}]^{4-}$ anions (M = Ti, Sn) were carried out in collaboration with the Poblet group at URV, Tarragona.[39-41] The results indicated that methanol exchange occurs *via* probably an initial attack of MeOH at the methoxido oxygen at M and the formation of a symmetrical transition state with a seven-coordinate heteroatom and hydrogen bridging between the two OMe groups, followed by proton transfer and elimination of methanol. The activation energies for

this concerted process were calculated to be higher for $[(MeO)TiPW_{11}O_{39}]^{4-}$ than for $[(MeO)SnPW_{11}O_{39}]^{4-}$, which is consistent with results from EXSY NMR experiments, where exchange cross-peaks were observed for $[(MeO)SnPW_{11}O_{39}]^{4-}$ but not for $[(MeO)TiPW_{11}O_{39}]^{4-}$. Calculations on the hydrolysis of $[(MeO)MPW_{11}O_{39}]^{4-}$ anions (**Scheme 4.1**) predicted a similar concerted mechanism for reactions leading to hydroxido derivatives, with a lower activation energy for the tin anion and greater stability for $[(HO)SnPW_{11}O_{39}]^{4-}$(**Figure 4.28**), which is consistent with the faster hydrolysis rate observed for the tin compound and the facile isolation of $(TBA)_4[(HO)SnPW_{11}O_{39}]$. The preferred condensation reaction pathways for both hydroxido anions involve nucleophilic attack by the OH group of one $[(HO)MPW_{11}O_{39}]^{4-}$ anion at the heterometal M of an adjacent anion with subsequent hydrogen transfer and elimination of a water molecule. However, the pathways for Ti and Sn differ slightly in that an extra transition state for the initial Sn–O bond formation was found in the case of the $[(MeO)SnPW_{11}O_{39}]^{4-}$ anion, while hydrogen transfer and loss of water was found to occur in a second step (**Figure 4.29**). This might explain why DMSO was observed to inhibit the condensation of $(TBA)_4[(HO)TiPW_{11}O_{39}]$. Similar values were obtained for the highest energy transition state in each of these condensation reactions, but the titanium oxo-bridged product $(TBA)_8[(\mu\text{-}O)(TiPW_{11}O_{39})_2]$ was predicted to be significantly more stable than the tin analogue. Again, this is consistent with the experimental observations, where it was more difficult to prepare pure samples of $(TBA)_8[(\mu\text{-}O)(SnPW_{11}O_{39})_2]$.

Calculations on the Lindqvist anions $[(MeO)MW_5O_{18}]^{3-}$ (M = Ti, Sn) gave similar results to the corresponding Keggin anions, and predicted that $[(MeO)SnW_5O_{18}]^{3-}$ should hydrolyse more readily than $[(MeO)TiW_5O_{18}]^{3-}$, as observed experimentally. As in the case of the Keggin anions, separate steps were predicted for Sn–O bond formation and water elimination in the $[(MeO)SnW_5O_{18}]^{3-}$ condensation reaction but not for $[(MeO)TiW_5O_{18}]^{3-}$. Comparison of the Lindqvist $[(MeO)MW_5O_{18}]^{3-}$ and Keggin $[(MeO)MPW_{11}O_{39}]^{4-}$ hydrolysis reaction profiles shows that the highest energy barrier is for $[(MeO)TiPW_{11}O_{39}]^{4-}$ and the lowest for $[(MeO)SnPW_{11}O_{39}]^{4-}$, and the most stable products are the tin-substituted anions in each family. A similar comparison of condensation reaction profiles shows that the highest energy barrier is for the $SnPW_{11}$ Keggin anion and the lowest is for the SnW_5 Lindqvist anion. The most stable oxo-bridged product is $[(\mu\text{-}O)(TiW_5O_{18})_2]^{6-}$ and the least stable is $[(\mu\text{-}O)(SnPW_{11}O_{39})_2]^{8-}$. This reflects the observed extreme moisture-sensitivity of $(TBA)_8[(\mu\text{-}$

O)($SnPW_{11}O_{39}$)$_2$], which readily reverts to (TBA)$_4$[(HO)$SnPW_{11}O_{39}$] in the presence of traces of water.

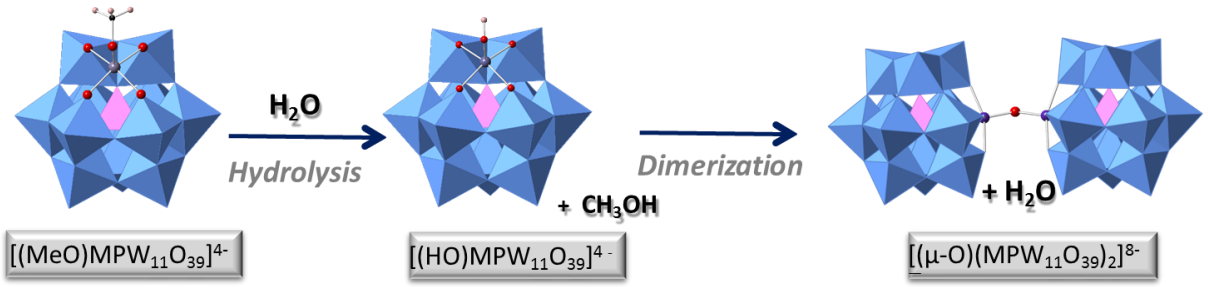

Scheme 4.1. Hydrolysis and condensation of [(L)$MPW_{11}O_{39}$]$^{4-}$ (M = Ti, Sn; L = MeO, HO)

Table 4.5. Thermodynamic parameters for hydrolysis and condensation of [(L)$MPW_{11}O_{39}$]$^{4-}$ (M = Ti, Sn; L = MeO, HO)

Metal	$\Delta E_{hydrolysis}$ (kcal/mol)	$\Delta E_{condensation}$ (kcal/mol)	ΔE_{total} (kcal/mol)
Ti	7.50 (10.3)	-74.0 (-54.8)	**-66.4 (-44.5)**
Sn	5.70 (2.39)	**-65.0 (-43.6)**	**-59.3 (-41.21)**

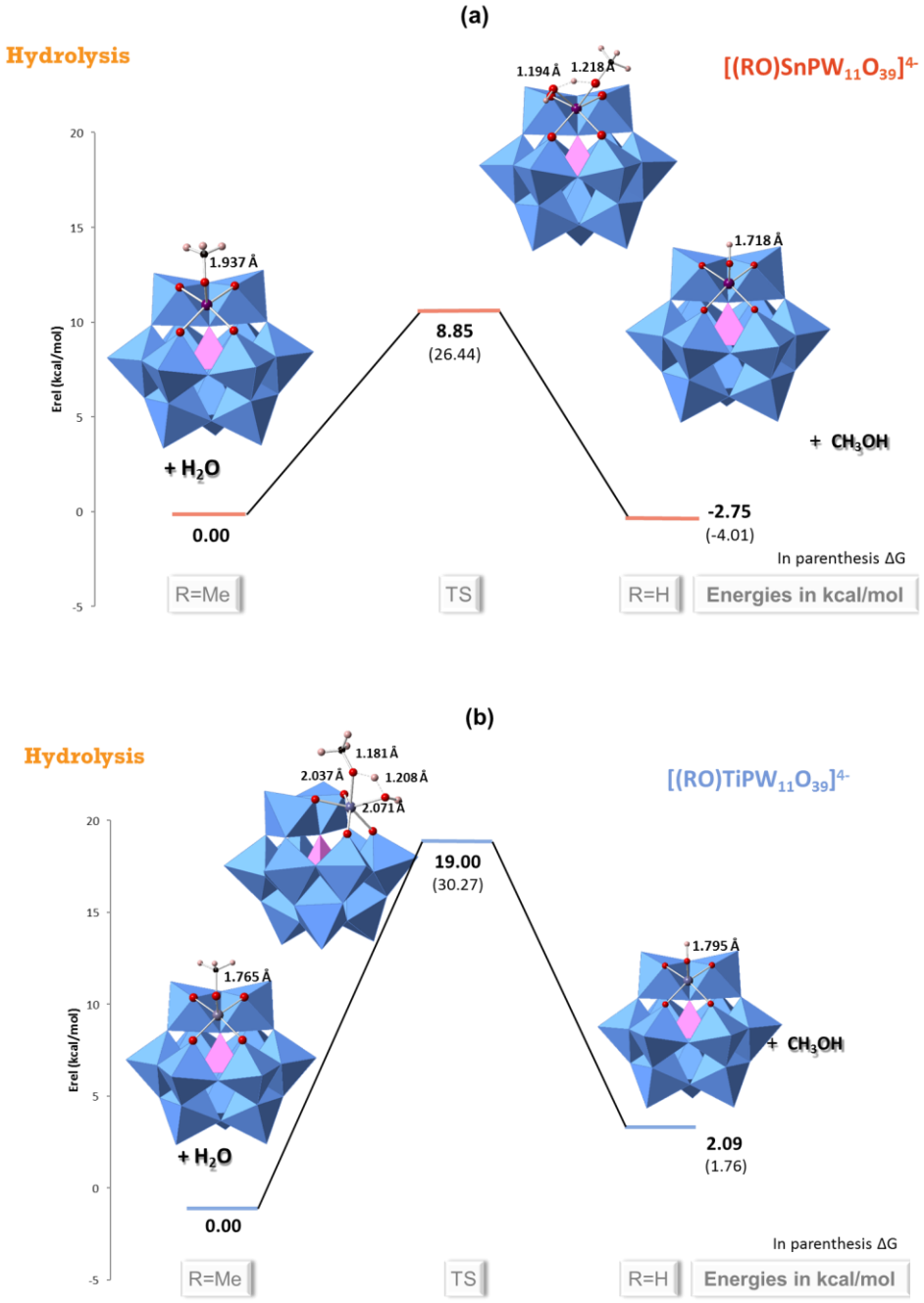

Figure 4.28. Reaction profiles for hydrolysis of (a) $[(MeO)SnPW_{11}O_{39}]^{4-}$ and (b) $[(MeO)TiPW_{11}O_{39}]^{4-}$

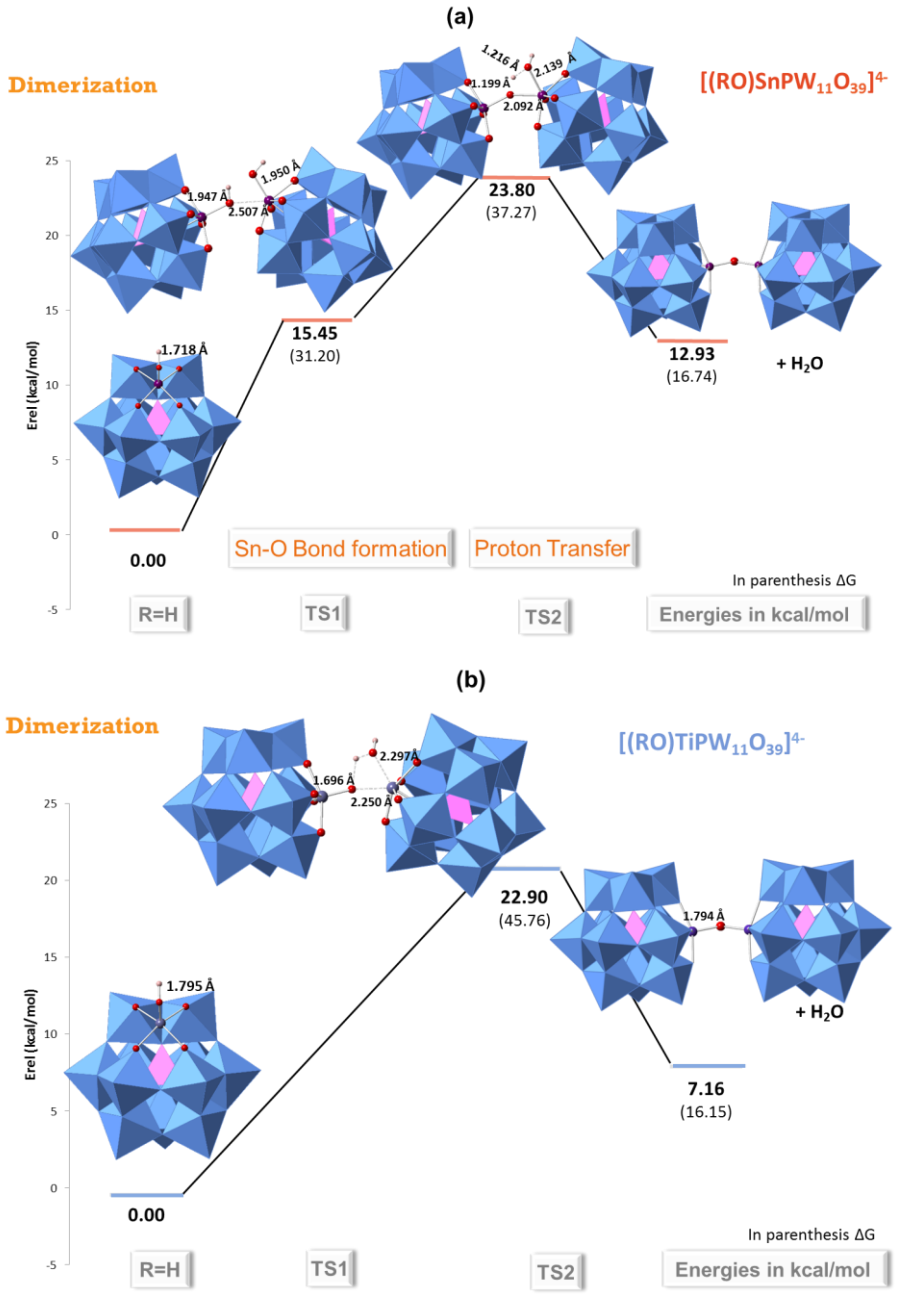

Figure 4.29. Reaction profiles for dimerization of (a) $[(HO)SnPW_{11}O_{39}]^{4-}$ and (b) $[(HO)TiPW_{11}O_{39}]^{4-}$

4.2.11. Reduction of $(TBA)_4[(L)Sn^{IV}PW_{11}O_{39}]$ (L = Cl^-, OH^-) with $H_2NNH_2.HCl$ and $NaBH_4$

Treatment of $(TBA)_4[(L)Sn^{IV}PW_{11}O_{39}]$ (L = Cl^-, OH^-) with reducing agents such as $H_2NNH_2.HCl$ and $NaBH_4$ was expected to result in reduction of either the tin heterometal or the tungstate cage. ^{31}P NMR studies showed no observable change in the reaction of $(TBA)_4[(HO)SnPW_{11}O_{39}]$ and $(TBA)_4[ClSnPW_{11}O_{39}]$ with $H_2NNH_2.HCl$ even when heated at 50 ^oC for 1 h. In contrast, reaction of the POMs with 1 mole-equivalent of $NaBH_4$ at room

temperature showed a change in colour of the solution from colourless to pale yellow while ^{31}P NMR studies showed a new peak at -13.06 ppm for $(TBA)_4[ClSnPW_{11}O_{39}]$ (94%) and -13.12 ppm for $(TBA)_4[(HO)SnPW_{11}O_{39}]$ (83%) (see **Figure 4.30**). The colour and chemical shifts of the products were similar to that observed for $(TBA)_5[Sn^{II}PW_{11}O_{39}]$ (-13.23 ppm). There was also a loss of the P-Sn coupling. The ^{119}Sn NMR spectrum also showed a broad peak at -698 ppm with no observable P-Sn coupling (**Figure 4.31**). This compares with the peak observed in the ^{119}Sn NMR spectrum of $(TBA)_5[Sn^{II}PW_{11}O_{39}]$ (-684 ppm). These results indicate a possible reductive elimination process with no reduction of the tungstate cage but a reduction of the tin heteroatom from +4 to +2 oxidation state by $NaBH_4$.

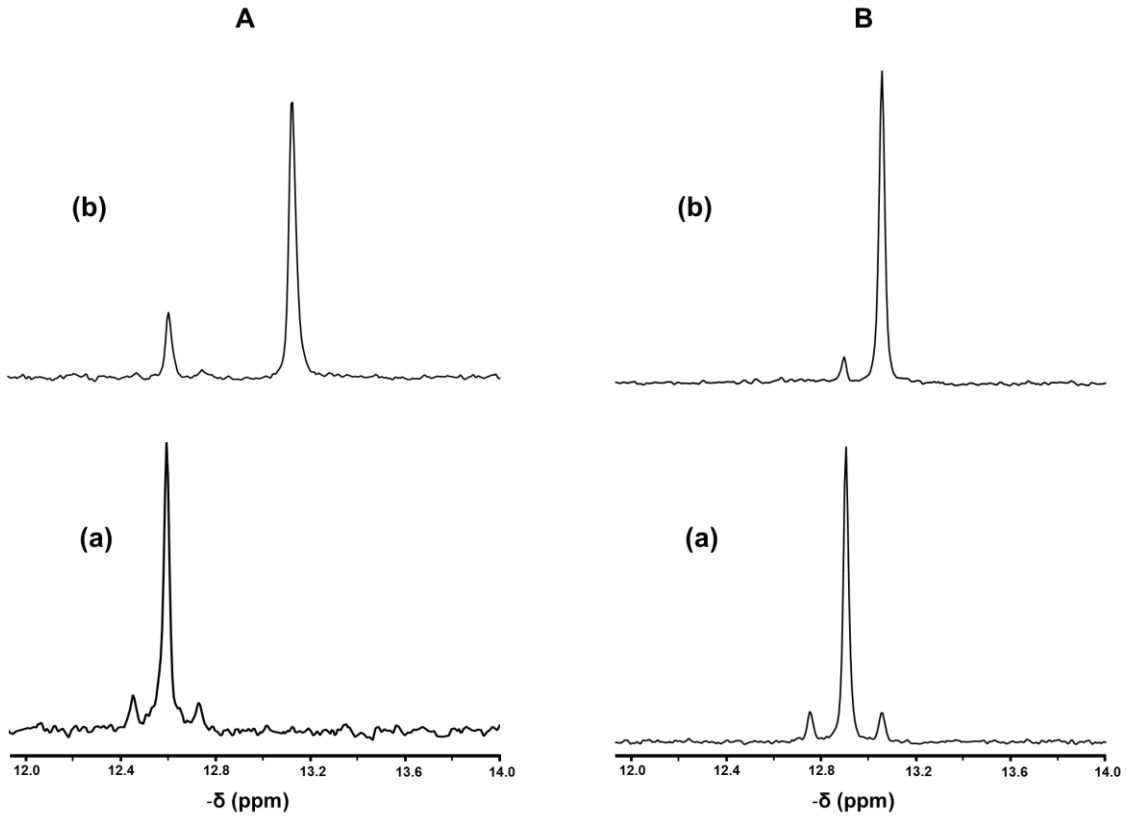

Figure 4.30. (A) ^{31}P NMR spectra in CD_3CN of (a) $(TBA)_4[(HO)SnPW_{11}O_{39}]$ and (b) after adding 1 mole-equivalent of $NaBH_4$ and (B) ^{31}P NMR spectra in CD_3CN of (a) $(TBA)_4[ClSnPW_{11}O_{39}]$ and (b) after adding 1 mole-equivalent of $NaBH_4$.

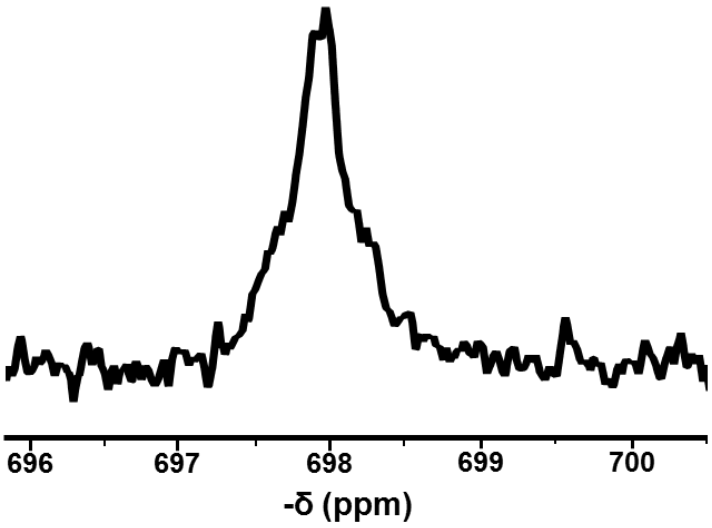

Figure 4.31. ^{119}Sn NMR spectrum of the product of the reaction between $(TBA)_4[ClSnPW_{11}O_{39}]$ and 1 mole-equivalent of $NaBH_4$ in CD_3CN.

4.3 Conclusions

In conclusion, this chapter has demonstrated the successful isolation and characterization of the readily-hydrolysable, tin-substituted POMs, $(TBA)_4[(CH_3O)SnPW_{11}O_{39}]$ and $(TBA)_8[(\mu\text{-}O)(SnPW_{11}O_{39})_2]$ for the first time. It has shown that the previously reported unstable $(TBA)_4[(HO)TiPW_{11}O_{39}]$ can exist in DMSO solution for up to 3 months without dimerising. The chapter also showed that the Sn(II)-substituted Keggin POM can be prepared by treatment of $(TBA)_4[(L)Sn^{IV}PW_{11}O_{39}]$ (L = Cl, HO) with $NaBH_4$. Though more studies are required to fully harness the potential of the tin-POMs as efficient catalysts, the results discussed in the chapter have generally provided some fundamental insights into the hydrolytic behaviours of these POMs.

REFERENCES

1. W. H. Knoth, P. J. Domaille and D. C. Roe, *Inorg. Chem.*, 1983, **22**, 198-201.
2. O. A. Kholdeeva, T. A. Trubitsina, G. M. Maksimov, A. V. Golovin and R. I. Maksimovskaya, *Inorg. Chem.*, 2005, **44**, 1635-1642.
3. T. A. Trubitsyna and O. A. Kholdeeva, *Kinet. Catal.*, 2008, **49**, 371-378.
4. G. M. Maksimov, R. I. Maksimovskaya, O. A. Kholdeeva, M. A. Fedotov, V. I. Zaikovskii, V. G. Vasil'ev and S. S. Arzumanov, *J. Struct. Chem.*, 2009, **50**, 618-627.
5. Y. Matsuki, Y. Mouri, Y. Sakai, S. Matsunaga and K. Nomiya, *Eur. J. Inorg. Chem.*, 2013, **2013**, 1754-1761.
6. K. Nomiya, M. Takahashi, J. A. Widegren, T. Aizawa, Y. Sakai and N. C. Kasuga, *J. Chem Soc., Dalton Trans.*, 2002, 3679-3685.
7. K. Hayashi, M. Takahashi and K. Nomiya, *Dalton Trans.*, 2005, 3751-3756.
8. Y. Matsuki, Y. Mouri, Y. Sakai, S. Matsunaga and K. Nomiya, *Eur. J. Inorg. Chem.*, 2013, **2013**, 1754-1761.
9. O. A. Kholdeeva, G. M. Maksimov, R. I. Maksimovskaya, L. A. Kovaleva, M. A. Fedotov, V. A. Grigoriev and C. L. Hill, *Inorg. Chem.*, 2000, **39**, 3828-3837.
10. O. A. Kholdeeva, *Top. Catal.*, 2006, **40**, 229-243.
11. G. S. Chorghade and M. T. Pope, *J. Am. Chem. Soc.*, 1987, **109**, 5134-5138.
12. G. Sazani and M. T. Pope, *Dalton Trans.*, 2004, 1989-1994.
13. B. Krebs, E. Droste, M. Piepenbrink and G. Vollmer, *Comptes Rendus de l'Académie des Sciences - Series IIC - Chemistry*, 2000, **3**, 205-210.
14. B. Matt, J. Moussa, L.-M. Chamoreau, C. Afonso, A. Proust, H. Amouri and G. Izzet, *Organometallics*, 2012, **31**, 35-38.
15. J. Rieger, T. Antoun, S.-H. Lee, M. Chenal, G. Pembouong, J. Lesage de la Haye, I. Azcarate, B. Hasenknopf and E. Lacote, *Chem. - Eur. J.*, 2012, **18**, 3355-3361.
16. J. Otera, T. Mizutani and H. Nozaki, *Organometallics*, 1989, **8**, 2063-2065.
17. J. Otera, T. Yano and R. Okawara, *Organometallics*, 1986, **5**, 1167-1170.
18. J. Otera, T. Yano, A. Kawabata and H. Nozaki, *Tetrahedron Lett.*, 1986, **27**, 2383-2386.
19. J. Otera, *Acc. Chem. Res.*, 2004, **37**, 288-296.
20. B. Jousseaume, C. Laporte, M.-C. Rascle and T. Toupance, *Chem. Commun.*, 2003, 1428-1429.
21. R. J. Errington, S. S. Petkar, P. S. Middleton, W. McFarlane, W. Clegg, R. A. Coxall and R. W. Harrington, *Dalton Trans.*, 2007, 5211-5222.
22. B. Kandasamy, C. Wills, W. McFarlane, W. Clegg, R. W. Harrington, A. Rodriguez-Fortea, J. M. Poblet, P. G. Bruce and R. J. Errington, *Chem. Eur. J.*, 2012, **18**, 59-62.
23. B. Kandasamy, PhD Thesis, University of St. Andrews, 2011.

24. D. Lebbie, unpublished work.

25. D. B. G. Williams and M. Lawton, *J. Org. Chem.*, 2010, **75**, 8351-8354.

26. I. A. Degen, *Appl. Spectrosc.*, 1968, **22**, 164-166.

27. R. M. Wing and K. P. Callahan, *Inorg. Chem.*, 1969, **8**, 871-874.

28. B. Kushlefsky, I. Simmons and A. Ross, *Inorg. Chem.*, 1963, **2**, 187-189.

29. D. J. Hewkin and W. P. Griffith, *J. Chem. Soc. A. Inorg. phys. theor.*, 1966, 472-475.

30. F. A. Cotton and R. M. Wing, *Inorg. Chem.*, 1965, **4**, 867-873.

31. S. M. Nelson, P. Bryan and D. H. Busch, *Chem. Commun.*, 1966, 641-642.

32. H. J. Schugar, G. R. Rossman, C. G. Barraclough and H. B. Gray, *J. Amer. Chem. Soc.*, 1972, **94**, 2683-2690.

33. H. Gunther, *NMR Spectroscopy: Basic Principles, Concepts, and Applications in Chemistry*, Wiley-VCH Verlag GmbH & Co, Germany, 3rd edn., 2013.

34. L. P. Kazansky, *Chem. Phys. Lett.*, 1994, **223**, 289-296.

35. N. N. Sveshnikov and M. T. Pope, *Inorg. Chem.*, 2000, **39**, 591-594.

36. B. Kandasamy, P. G. Bruce, W. Clegg, R. W. Harrington, A. Rodríguez-Fortea, M. Pascual-Borrás and R. J. Errington, *In Preparation.*, 2017.

37. V. Ugrinova, G. A. Ellis and S. N. Brown, *Chem. Commun.*, 2004, 468-469.

38. J. Holeček, K. Handlír¸, V. Černý, M. Nádvorník and A. Lyčka, *Polyhedron*, 1987, **6**, 1037-1039.

39. R. J. Errington, in *Advances in Inorganic Chemistry*, eds. R. v. Eldik and L. Cronin, 2017, vol. 69, pp. 287-336.

40. M. Pascual-Borrás, PhD Thesis, Universitat Rovira i Virgili 2017.

41. M. Pascual-Borrás, J. M. Poblet and R. J. Errington, unpublished work.

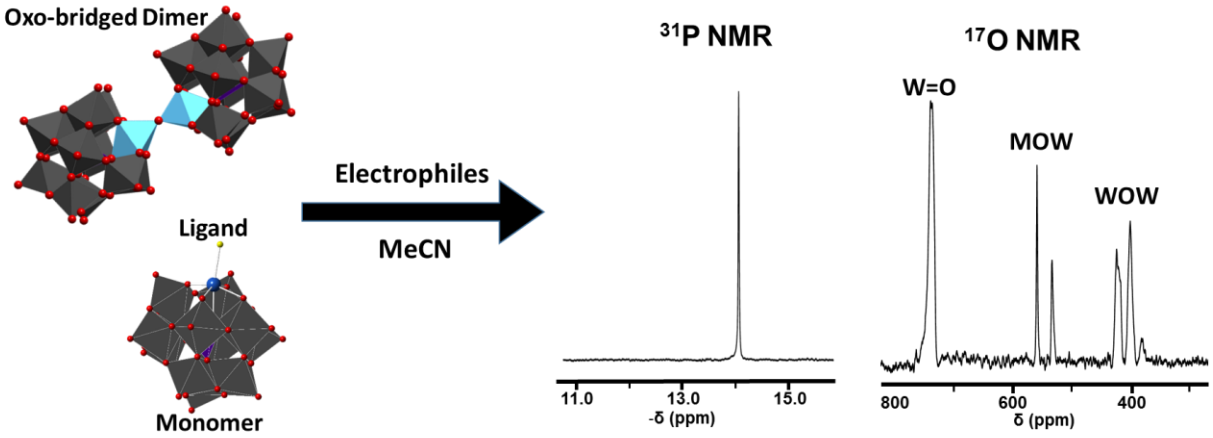

Chapter 5

Studies on protonolysis of tin- and titanium-monosubstituted Keggin POMs and possible metal binding sites in $(TBA)_8[(\mu\text{-}O)(TiPW_{11}O_{39})_2]$

The research discussed in this chapter involves firstly an attempt to understand the trends in surface oxygen basicity in the POM series $(TBA)_4[(L)M^{IV}PW_{11}O_{39}]$ (M = Ti, Sn; L = Cl, HO, CH_3O) and $(TBA)_8[(\mu\text{-}O)(TiPW_{11}O_{39})_2]$ and secondly an investigation of possible metal binding sites in $(TBA)_8[(\mu\text{-}O)(TiPW_{11}O_{39})_2]$ using ^{17}O and ^{31}P NMR techniques. In this direction, the protonation sites and mechanisms of the POMs were probed. Furthermore, reactions of $(TBA)_8[(\mu\text{-}O)(TiPW_{11}O_{39})_2]$ and a range of electrophiles were examined. Reaction products were also characterized by FT-IR, ^1H and ^{119}Sn NMR spectroscopy. The study contributes to the possibility of POM 'pincer complexes' with likely implications for POM catalysis.

5. Studies on protonolysis of tin- and titanium-monosubstituted Keggin POMs and possible metal binding sites in $(TBA)_8[(TiPW_{11}O_{39})_2O]$ – a POM "Pincer Ligand"?

5.1 Introduction

A sound knowledge of proton-attachment centres and mechanisms in POMs is key to understanding their catalytic activity.[1-4] In the parent Keggin anion (e.g. $[PW_{12}O_{40}]^{3-}$) with only two types of outer oxygens, it is well-established that the more basic bridging oxygens (W-O-W) are protonated in preference to the terminal oxygens (W=O).[1,5,6] In substituted derivatives however such as $[(L)MPW_{11}O_{39}]^{4-}$ and the oxobridged dimer, $[(\mu\text{-}O)(MPW_{11}O_{39})_2]^{8-}$ [M = Ti, Sn; L = Cl, RO (R = alkyl)], the replacement of a $[WO]^{4+}$ with an $[ML]^{n+}$ group generates M-O-W, ROM, or/and M-O-M as additional basic sites for possible proton attachment. Based on previous proposals for $[(RO)TiMo_5O_{18}]^{3-}$ and $[(RO)TiW_5O_{18}]^{3-}$,[7-9] protonation of $(TBA)_4[(RO)M^{IV}PW_{11}O_{39}]$ is expected to follow either of the mechanisms in **Scheme 5.1**. Thus, addition of a protic reagent, HL to $(TBA)_4[(RO)M^{IV}PW_{11}O_{39}]$ (M = Ti, Sn) is expected to result in HL either attacking the ROM^{IV} or $M^{IV}OW$ site depending on their relative basicities. In contrast however, proton attack at TiOTi site has been proposed for $(TBA)_8[(\mu\text{-}O)(TiPW_{11}O_{39})_2]$[10] whilst study on the Lindqvist analogue, $(TBA)_6[(\mu\text{-}O)(TiW_5O_{18})_2]$ and structure of the protonated dimer, $(TBA)_4[(\mu\text{-}O)(TiW_5O_{18}H)_2]$ revealed protonation at Ti-O-W sites instead.[11,12] These studies seem to create an ambiguity as to whether the Ti-O-Ti or a TiOW site is protonated in the oxo-bridged compound. To clarify this and ascertain a better understanding of the protonolysis of these polyanions, a detailed study on the series is necessary. If indeed protonation is possible at both Ti-O-W and Ti-O-Ti sites in $(TBA)_8[(\mu\text{-}O)(TiPW_{11}O_{39})_2]$ as the results seem to suggest then this will open up the possibility of $(TBA)_8[(\mu\text{-}O)(TiPW_{11}O_{39})_2]$ forming POM 'pincer complexes' with electrophiles. Pincer complexes have huge applications in catalysis, medicine, sensing and nanoscience.[13-16]

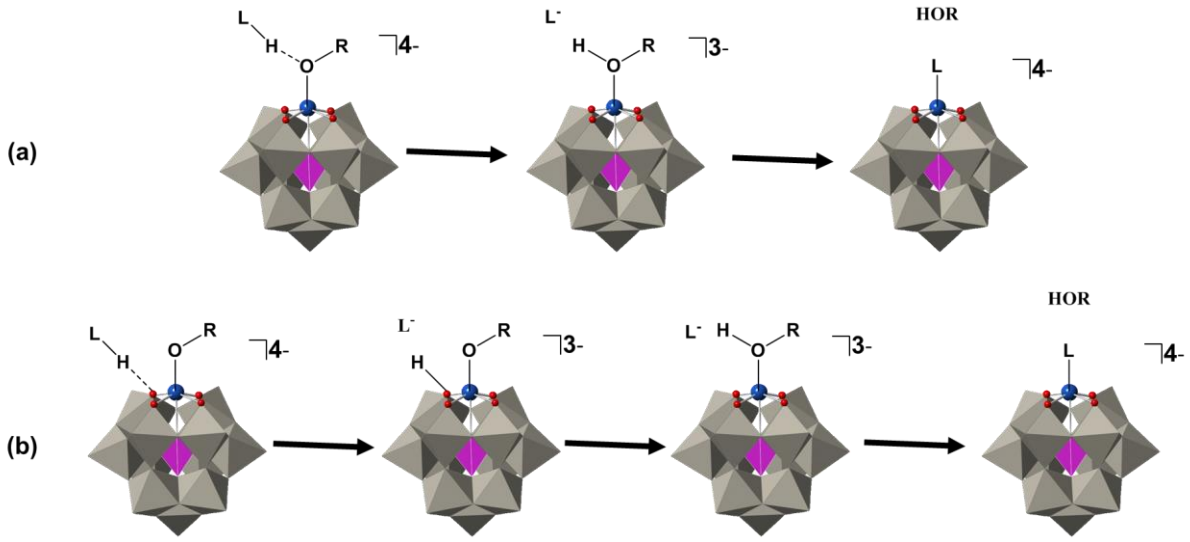

Scheme 5.1. Polyhedral representations of proposed mechanisms for protonation of $[(RO)M^{IV}PW_{11}O_{39}]^{4-}$ with HL via either (a) direct protonation of the alkoxido ligand or (b) protonation of the oxometalate cage at $M^{IV}OW$ with subsequent proton transfer to the alkoxido ligand.

In this chapter therefore, results on protonation of $(TBA)_4[(L)M^{IV}PW_{11}O_{39}]$ (M = Ti, Sn; L = Cl, HO, CH_3O) and $(TBA)_8[(\mu\text{-}O)(TiPW_{11}O_{39})_2]$ with $HBF_4.Et_2O$ are presented to determine protonation sites and mechanisms. Furthermore, reactions between $(TBA)_8[(\mu\text{-}O)(TiPW_{11}O_{39})_2]$ and $AgBF_4$, $SnCl_2$, $FeCl_2$, $Co(CH_3CN)_4(H_2O)_2][BF_4]_2$, $[Mo_2(NCCH_3)_8(ax\text{-}CH_3CN)_{0.5}][BF_4]_4$, $BiCl_3$, $SbCl_3$, Me_2SnCl_2, $SnCl_4$ and $TiCl_4$ are examined to determine potential metal binding sites and possibly isolate mixed-metal POM species of the type, $(TBA)_n[(L)M(\mu\text{-}O)(TiPW_{11}O_{39})_2]$ (M = Ag, Sn, Fe, Co, Mo, Bi, Sb, Ti) with new reactive sites. Thus, establishing $(TBA)_8[(\mu\text{-}O)(TiPW_{11}O_{39})_2]$ as a POM 'pincer ligand' with implications for catalysis by POM 'pincer complexes'.

5.2 Results and Discussion

5.2.1 Protonation studies with $HBF_4.Et_2O$

5.2.1.1 Protonation study on $(TBA)_4[(CH_3O)TiPW_{11}O_{39}]$

Protonolysis was attempted on $(TBA)_4[(CH_3O)TiPW_{11}O_{39}]$ and $(TBA)_4[(HO)SnPW_{11}O_{39}]$ (see **Section 5.2.1.2**) only. This was because of the tendencies of $(TBA)_4[(CH_3O)SnPW_{11}O_{39}]$ to hydrolyse and $(TBA)_4[(HO)TiPW_{11}O_{39}]$ to dimerise in MeCN. As indicated above, the mechanisms in **Scheme 5.1** were proposed. The ^{31}P NMR spectra [**Figure 5.1 (a)**] showed that addition of 0.5 equiv. H^+ to $(TBA)_4[(CH_3O)TiPW_{11}O_{39}]$ gave a major peak (66%) shifted

downfield from -14.05 to -13.49 ppm and several minor peaks. Subsequent additions of acid continuously moved the peaks downfield until the addition of 2 equiv. of H^+ when they collapsed into a major peak at -13.02 (93%) and two minor doublets (7%) centred at -12.11 and -12.51 ppm. Beyond this, only one doublet, which gradually increased in intensity at the expense of the major peak existed. The ^{17}O NMR spectra [**Figure 5.1 (b)**] showed an increase from 740 – 735 ppm to 764 – 758 ppm after adding 2.0 equiv. of H^+ whereas the TiOW resonances at 559 and 535 disappeared and a new minor peak which vanished gradually upon further addition of protons was observed at 539 ppm after 0.5 equiv. of H^+. The POM did not seem to degrade even after adding 4 equiv. of H^+ as the species in solution by ^{31}P NMR were a major peak at -12.58 (75%), a doublet centred at -12.05(24%) and trace impurity of $[PW_{12}O_{40}]^{3-}$ at -15.35 (1%) from starting material. The general increase in the terminal W=O resonance upon protonation was expected because of the decrease in overall polyanion charge. While the downfield shift of the ^{31}P NMR peaks and the upfield movement and subsequent disappearance of the TiOW resonances both indicate protonation of the TiOW sites. As noted in **Chapter 3**, it has been shown that when proton-exchange occurs between chemically equivalent sites in POMs, the ^{17}O NMR resonances of protonated oxygens move upfield whereas resonances of non-protonated oxygens (such as the W=O) move slightly downfield.[17] Also, protonation at TiOW site has been reported to result in a downfield shift of ^{31}P NMR resonance.[10,18] Thus, these results are consistent with mechanism **(b)** in **Scheme 5.1** and suggest a stronger basicity at TiOW than CH_3OTi site of $(TBA)_4[(CH_3O)TiPW_{11}O_{39}]$. Several unsuccessful attempts were made to obtain a crystal structure of the major species in solution at 2 equiv. H^+. This species remained stable even after adding 4 equiv. H^+.

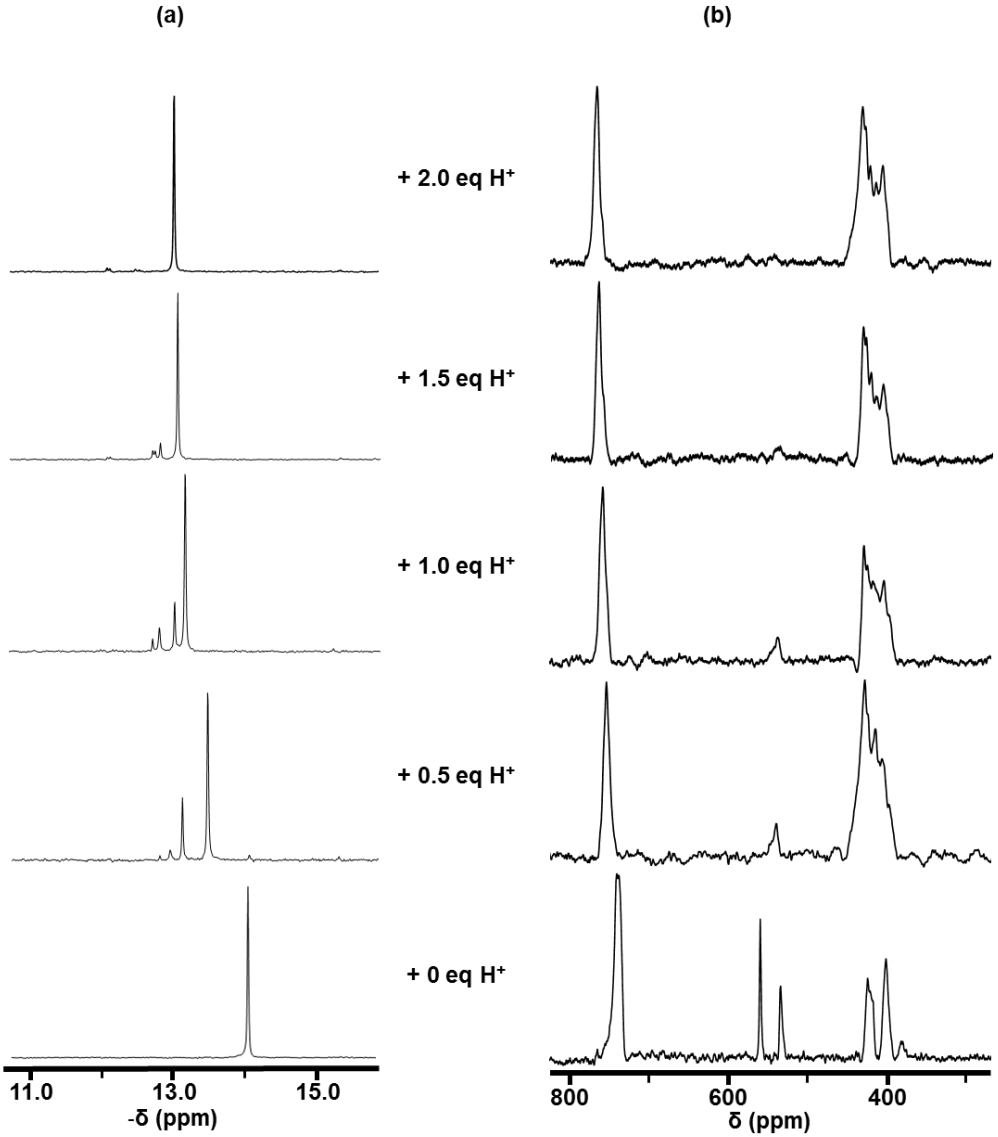

Figure 5.1. (a) ^{31}P and (b) ^{17}O NMR spectra of $(TBA)_4[(CH_3O)TiPW_{11}O_{39}]$ protonation in CD_3CN.

5.2.1.2 Protonation study on $(TBA)_4[(HO)SnPW_{11}O_{39}]$

Although our inability to unambiguously assign SnOW and WOW resonances did not allow for an explicit interpretation of the ^{17}O NMR spectra of $(TBA)_4[(HO)SnPW_{11}O_{39}]$ protonation, ^{31}P NMR parameters showed some interesting changes. Addition of 0.5 equiv. of H^+ resulted in two upfield peaks. The major peak at -12.82 ppm (~78 %) with an increased $^2J_{Sn\text{-}P}$ from 34 to 36 Hz and a new peak at -13.01 ppm (~ 22 % by ^{31}P NMR, it was difficult to resolve its $^2J_{Sn\text{-}P}$). Subsequent additions of protons led to growth of the new peak with the resonances of both continuously moving downfield whilst their coupling constants ($^2J_{Sn\text{-}P}$) decreased. At 2 equiv. H^+, the major species resonated at -12.00 ppm with $^2J_{Sn\text{-}P}$ of 34 Hz while the second peak was at -12.23 ppm with $^2J_{Sn\text{-}P}$ of 38 Hz. Only these two species remained in solution

with no evidence of formation of $[PW_{12}O_{40}]^{3-}$ upon addition of up to 4 mole-equivalents of protons (the major species at -11.83 ppm (58%) with $^{2}J_{Sn\text{-}P}$ = 32 Hz and the second species at -12.09 ppm (42%) with $^{2}J_{Sn\text{-}P}$ = 37 Hz). While it is difficult to clearly understand how protonation affects $^{2}J_{Sn\text{-}P}$, the results generally showed higher $^{2}J_{Sn\text{-}P}$ for the protonated species at low proton concentration and lower values at high proton concentrations. The dependence of spin-spin coupling constants on specific factors such as hybridization of atoms and presence of lone pairs of electrons is sometimes difficult to predict.[19] The ^{17}O NMR spectra [**Figure 5.2 (b)**] showed a steady increase in the terminal W=O resonances from 746 – 733 at 0.5 equiv. H^+ to 763 – 753 ppm at 2.0 equiv. H^+ and 766 – 755 ppm at 4.0 equiv. H^+. The SnOW and WOW chemical shift changed from 427 – 334 to 435 – 390 ppm at 2.0 equiv. H^+ and 437 to 396 ppm at 4.0 equiv. H^+. Even though only a general decrease in the overall negative charge of the species in solution can be inferred from the ^{17}O NMR data, these results suggest both mechanisms **(a)** and **(b)** in **Scheme 5.1** taking place in the protonation of $(TBA)_4[(HO)SnPW_{11}O_{39}]$. The initial upfield shift of ^{31}P NMR resonance points to protonation at $HOSn^{IV}$ site whilst subsequent downfield shifts of the ^{31}P NMR resonance suggest the protic agent attacking the $Sn^{IV}OW$ sites. This might imply $Ti^{IV}OW$ as more basic than $Sn^{IV}OW$ in $[(RO)M^{IV}PW_{11}O_{39}]^{4-}$ possibly because Ti has OMe (more electron donating) whereas Sn has the less electron donating OH. The ^{119}Sn NMR signals of both species were greatly shifted as no signal was observed within the normal region of the unprotonated POM species (500 – 700 ppm).

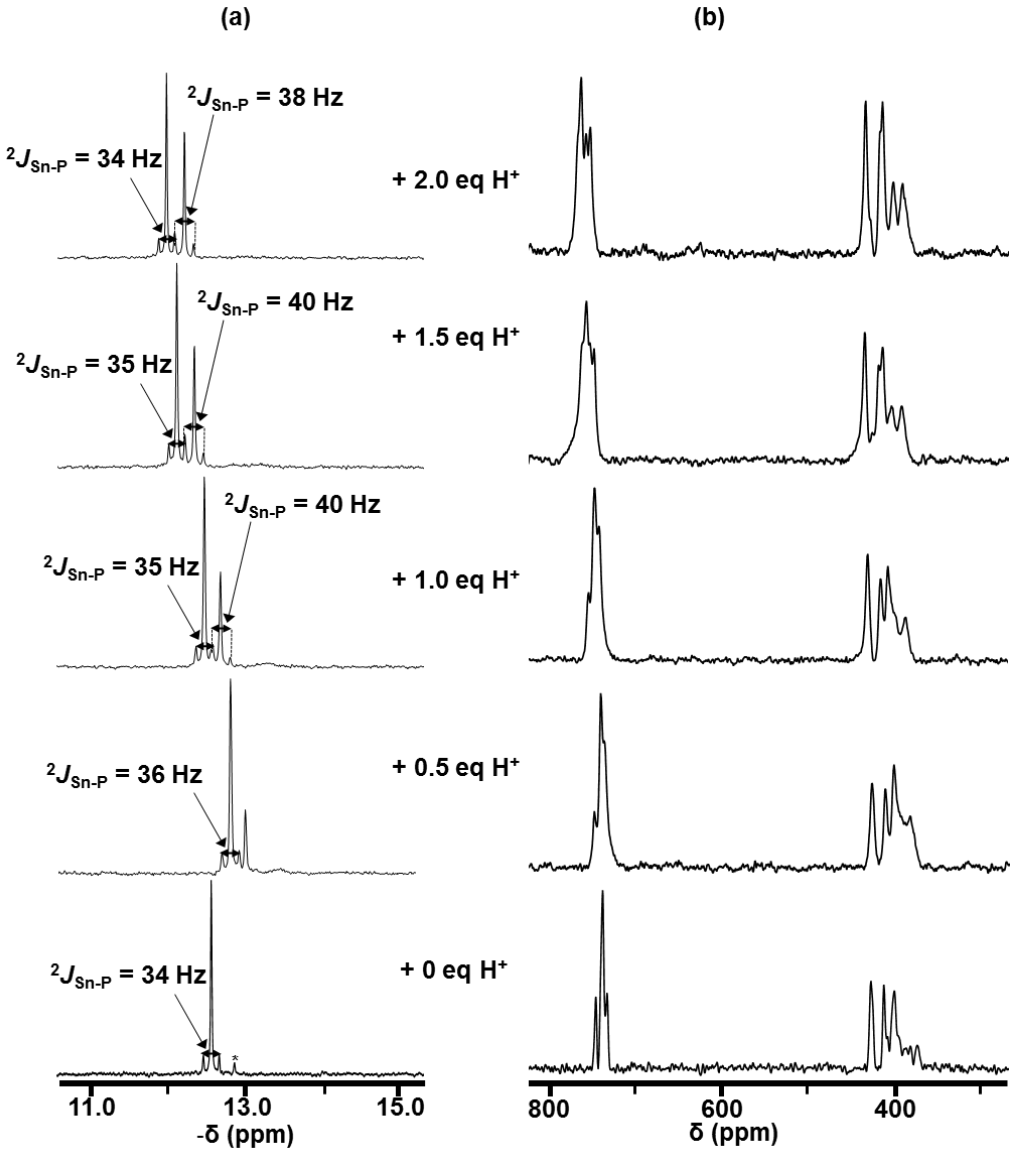

Figure 5.2. (a) ^{31}P and (b) ^{17}O NMR spectra of $(TBA)_4[(HO)SnPW_{11}O_{39}]$ protonation in CD_3CN.

5.2.1.3 Protonation of $(TBA)_4[ClM^{IV}PW_{11}O_{39}]$ (M = Sn and Ti)

To further investigate the basicities of $Ti^{IV}OW$ and $Sn^{IV}OW$, protonolysis was attempted on $(TBA)_4[ClM^{IV}PW_{11}O_{39}]$ (M = Sn, Ti) even though the low basicity of Cl^- compared to RO was expected to favour mechanism **(b)**. The results for protonation of $(TBA)_4[ClSnPW_{11}O_{39}]$ are presented in **Figure 5.3** whilst that of $(TBA)_4[ClTiPW_{11}O_{39}]$ are presented in **Figure 5.4**. Addition of 0.5 equiv. of H^+ to $(TBA)_4[ClSnPW_{11}O_{39}]$ caused a downfield shift in the ^{31}P NMR resonance from -12.90 to -12.00 ppm with a simultaneous decrease in $^2J_{Sn-P}$ from 37 to 32 Hz. Further acidification to 1.0 equiv. H^+ resulted in a further downfield shift to -11.64 ppm and an additional decrease in $^2J_{Sn-P}$ to 30 Hz. Also, trace amounts of two new species at -

11.94 and -12.45 ppm were observed. A slight change in the major peak to -11.58 ppm and $^{2}J_{Sn\text{-}P}$ to 29 Hz was observed upon addition of 1.5 equiv. H^+. And though the spectrum became more complex with multiple species after 2 equiv. of H^+, $^{2}J_{Sn\text{-}P}$ of the major species in the clear solution remained unchanged and there was no evidence of formation of $[PW_{12}O_{40}]^{3-}$ even after adding 4 mole-equivalents of H^+. These results differ from observations for $(TBA)_4[(HO)SnPW_{11}O_{39}]$ and, as in the case of $(TBA)_4[(CH_3O)TiPW_{11}O_{39}]$ are consistent with protonation at the SnOW sites. Also, results of both $(TBA)_4[ClSnPW_{11}O_{39}]$ and $(TBA)_4[(HO)SnPW_{11}O_{39}]$ protonation studies suggest a decrease in the $^{2}J_{Sn\text{-}P}$ with protonation at SnOW sites. The ^{17}O NMR spectra showed the expected increase in terminal W=O chemical shifts to 781 – 764 due to a decrease in the overall anionic charge after adding 1.5 equiv. H^+, whilst the peaks at 428 and 412 initially increase to 436 and 417 ppm and were at 437 and 423 ppm after adding 1.5 H^+.

The ^{31}P NMR spectra for $(TBA)_4[ClTiPW_{11}O_{39}]$ likewise showed that addition of protons resulted in a downfield shift of the resonance, though new peaks appeared which continued to grow at the expense of original peak. No attempt was made to isolate any of the species because of the complex spectrum that developed upon protonation even though the solution generally remained clear after adding up to 5 equiv. H^+. The ^{17}O NMR spectra showed a consistent increase in the terminal W=O resonance from 747 – 743 ppm to 759 – 754 ppm at 0.5 H^+ and 775 to 764 ppm at 2 equiv. H^+. As in the case of $(TBA)_4[(CH_3O)TiPW_{11}O_{39}]$, the TiOW peaks at 585 and 565 disappeared and a broad bump centred at 568 was seen after adding 0.5 equiv. H^+. This moved to unresolved peaks at 431 and 428 ppm after 1 equiv. H^+ while unresolved peaks at 433 ppm and 435 ppm were observed upon addition of 1.5 and 2.0 mole-equivalents of protons respectively. Again, these results support protonation at the Ti-O-W sites.

A mechanism of type **(b)** is therefore proposed for protonation of $(TBA)_4[ClM^{IV}PW_{11}O_{39}]$ (M = Sn, Ti) with step-wise addition of protons to the M^{IV}-O-W sites resulting in several species in solution. Though the low basicity of Cl^- might make it less prone to protonation than $M^{IV}OW$ in $[ClM^{IV}PW_{11}O_{39}]^{4-}$ (M = Sn, Ti), these results indicate more resistance to degradation upon protonation in the tin-substituted POMs than in the titanium analogues. Also, the small line width (i.e. narrow lines) in the spectra generally suggest fast proton exchange between POM species in solution. Slow exchange would result in broadened peaks.

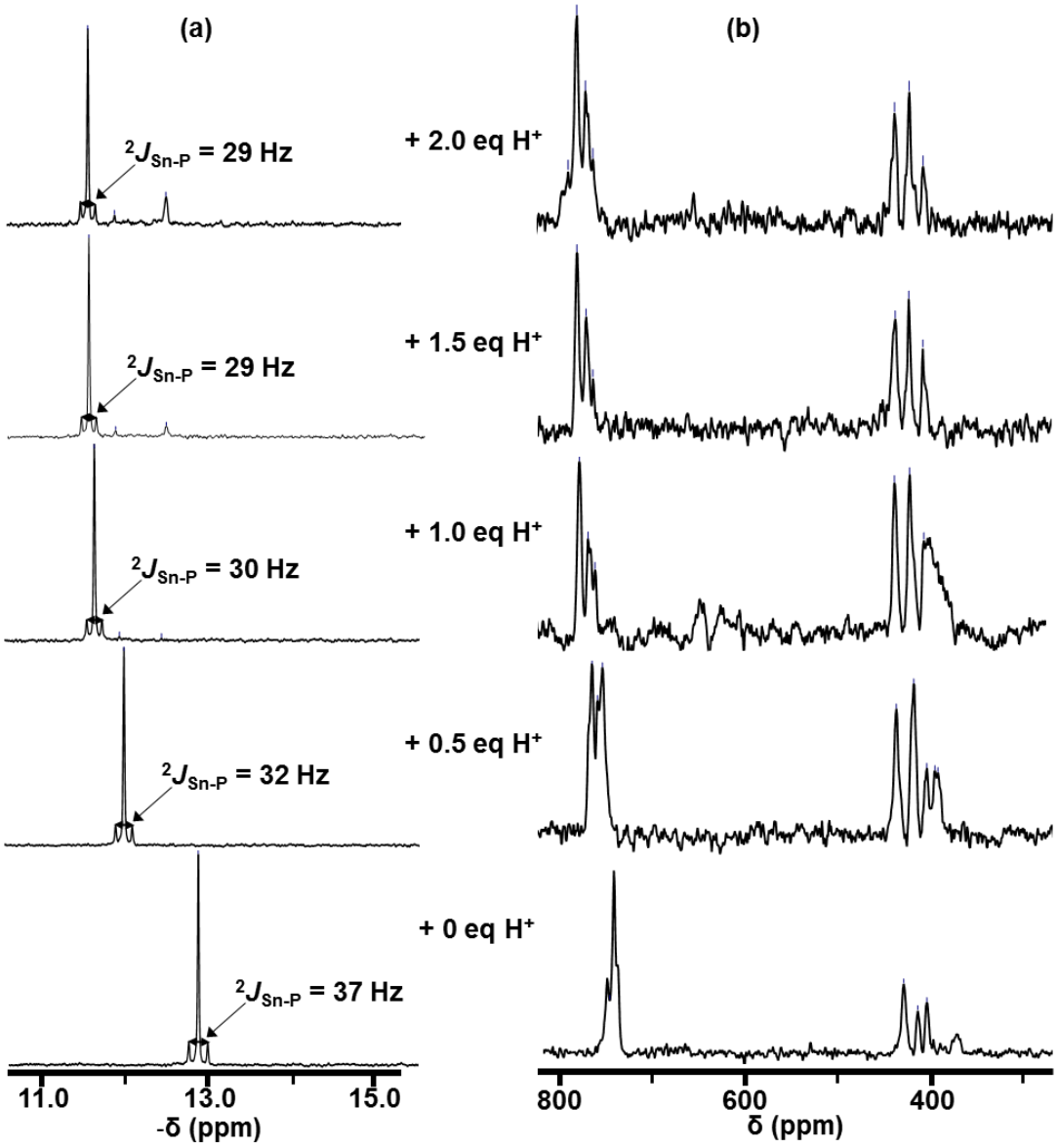

Figure 5.3. (a) ^{31}P and (b) ^{17}O NMR spectra of $(TBA)_4[ClSnPW_{11}O_{39}]$ protonation in CD_3CN.

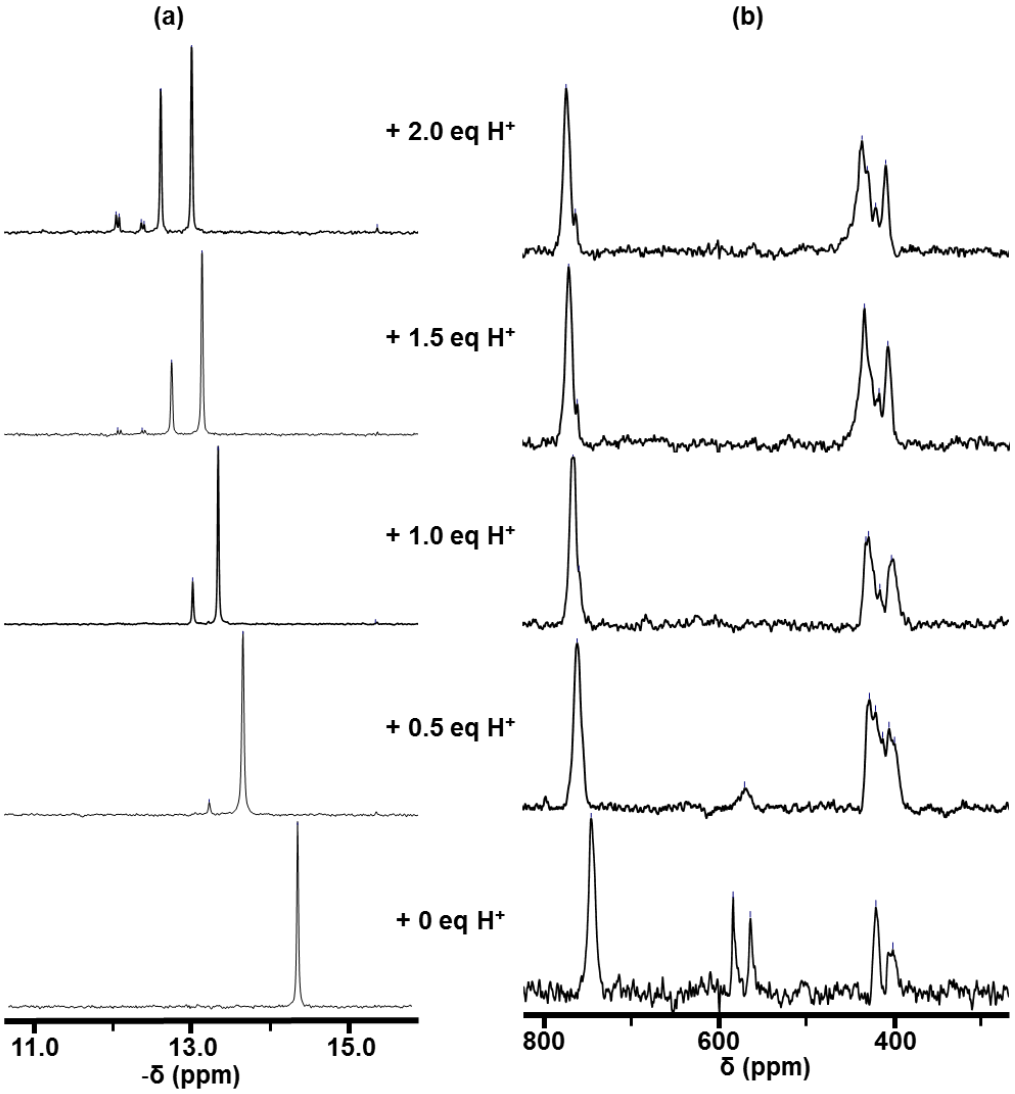

Figure 5.4. (a) ^{31}P and (b) ^{17}O NMR spectra in CD_3CN of $(TBA)_4[ClTiPW_{11}O_{39}]$ protonation.

5.2.1.4 Protonation study on $(TBA)_8[(\mu\text{-}O)(TiPW_{11}O_{39})_2]$

Kholdeeva proposed previously that protonation of $(TBA)_5[TiPW_{11}O_{40}]$ resulted in $(TBA)_7[(\mu\text{-}OH)(TiPW_{11}O_{39})_2]$ *via* an initial protonation of Ti=O to form $(TBA)_4[(HO)TiPW_{11}O_{39}]$, which then dimerised into $(TBA)_8[(\mu\text{-}O)(TiPW_{11}O_{39})_2]$ before a final protonation at Ti-O-Ti site.[10] However, studies on the Lindqvist analogue, $(TBA)_6[(\mu\text{-}O)(TiW_5O_{18})_2]$ and structural characterisation of the protonated dimer, $(TBA)_4[(\mu\text{-}O)(TiW_5O_{18}H)_2]$ revealed that protonation occurs at Ti-O-W sites.[11,12] To understand if this was as a result of variation due to different POM frameworks or a misinterpretation of previous results for $(TBA)_8[(\mu\text{-}O)(TiPW_{11}O_{39})_2]$, protonation of $(TBA)_8[(\mu\text{-}O)(TiPW_{11}O_{39})_2]$ was studied using two different samples: Sample A with ^{17}O enrichment at only Ti-O-Ti oxygen site and sample B with enrichment at all oxygen sites of the POM except Ti-O-Ti.

The ^{31}P NMR spectra (**Figure 5.5**) of sample B showed a consistent downfield shift of the resonance upon protonation. Addition of 0.25 equiv. protons to $(TBA)_8[(\mu\text{-}O)(TiPW_{11}O_{39})_2]$ gave a new peak at -14.01 ppm while the original peak was now centred at -14.06 ppm and broadened. Addition of 0.5 equiv. H^+ led to almost complete disappearance of the original resonance with the appearance of a broad peak centred at -13.76 ppm and a minor peak at -13.22 ppm. At least two major peaks existed in solution upon further protonation until at 3.0 equiv. H^+ where the spectrum showed a major peak at -13.02 ppm (83%) with two minor peaks including a doublet which grew with further acidification.

The ^{17}O NMR spectra [**Figure 5.6 (a)**] showed a slight upfield shift from 571 and 544 to 566 and 541 ppm on the TiOW resonances upon addition of 0.25 equiv. H^+ to $(TBA)_8[(\mu\text{-}O)(TiPW_{11}O_{39})_2]$ (sample B). These resonances remained virtually unchanged until at 1.0 equiv. H^+ when an extra peak was observed at 548 ppm. Also, no significant change was observed in the chemical shifts of W=O peaks at 1.0 equiv. H^+. The small changes observed in the ^{17}O NMR chemical shifts upon protonation might be due to the presence of a number of similar/equivalent oxygen sites that can accept an itinerant proton.[17] This is supported by a simultaneous effect observed on the TiOTi resonance upon protonation of sample A [see **Figure 5.6 (b)]**. A downfield shift from 712 to 730 ppm and appearance of two other new peaks at 7 ppm (53.7%) and 48 ppm (9.5 %) were observed upon addition of 0.5 equiv. H^+. Addition of 1.0 equiv. H^+ led to a decrease in the intensity of the peak at 730 ppm to ~19.9 % of the spectrum with corresponding increase in the other peaks at 7 (to 67.6%) and 48 ppm (to 12.5%). Further protonation of the samples generally led to downfield shift in the terminal W=O resonances as expected while TiOW and TiOTi resonances gradually decreased in intensities. The TiOW peaks (sample B) disappeared completely after 3.0 equiv. H^+ [**Figure 5.6 (a)**] while the TiOTi peak (sample A) disappeared completely after 2.0 equiv. H^+ with the new peaks now centered at -4.17 (10.7%) and 39.7 ppm (89.3%) [see **Figure 5.6 (b)**]. To ascertain if the peaks were due to formation of H_2O, 1 µL of ^{17}O enriched H_2O was added to the NMR solution of sample A and the peak at 39.7 ppm was now observed at 42.59 ppm while a peak assigned to H_2O was observed at -3.16 ppm. Thus, the major peak at 39.7 ppm was not due to H_2O.

FT-IR analysis on solid protonated products provided more information (**Table 5.1**). It showed an increase in TiOTi vibration from 630 to 640 cm^{-1} upon addition of 1 equiv. of H^+ and the wavenumber difference compares well with that reported by Kholdeeva for $(TBA)_8[(\mu\text{-}O)(TiPW_{11}O_{39})_2]$ and $(TBA)_7[(\mu\text{-}OH)(TiPW_{11}O_{39})_2]$ (15 cm^{-1}).[20] This again points to protonation at TiOTi site of $(TBA)_8[(\mu\text{-}O)(TiPW_{11}O_{39})_2]$ to form $(TBA)_7[(\mu\text{-}OH)(TiPW_{11}O_{39})_2]$. Addition of 2 equiv. of H^+ on the other hand, results in a decrease in TiOTi vibration from 640 to 634 cm^{-1} and this could be linked to protonation at TiOW site. Protonation at TiOW site of $(TBA)_6[(\mu\text{-}O)(TiW_5O_{18})_2]$ was observed to results in a decrease in TiOTi FT-IR vibration from 670 to 656 cm^{-1}.[12] It is worth mentioning that the frequency of the terminal W=O vibration increases gradually as expected upon protonation. From 959 cm^{-1} for the unprotonated species to 963 cm^{-1} at 1 equiv. H^+, 966 cm^{-1} at 2 equiv. H^+ and 971 cm^{-1} at 5 equiv. H^+. Generally, these results suggest that protonation of $(TBA)_8[(\mu\text{-}O)(TiPW_{11}O_{39})_2]$ leads to multiple species formed by simultaneous proton attacks on both TiOW and TiOTi sites. The major product formed after addition of 3 equiv. H^+ is likely the tri-protonated POM, $(TBA)_5[(\mu\text{-}OH)(TiPW_{11}O_{39}H)_2]$ with both TiOW and TiOTi sites protonated. These results inspired further studies on $(TBA)_8[(\mu\text{-}O)(TiPW_{11}O_{39})_2]$ as a possible POM pincer ligand. Details of the investigations are presented in **Section 5.2.2**.

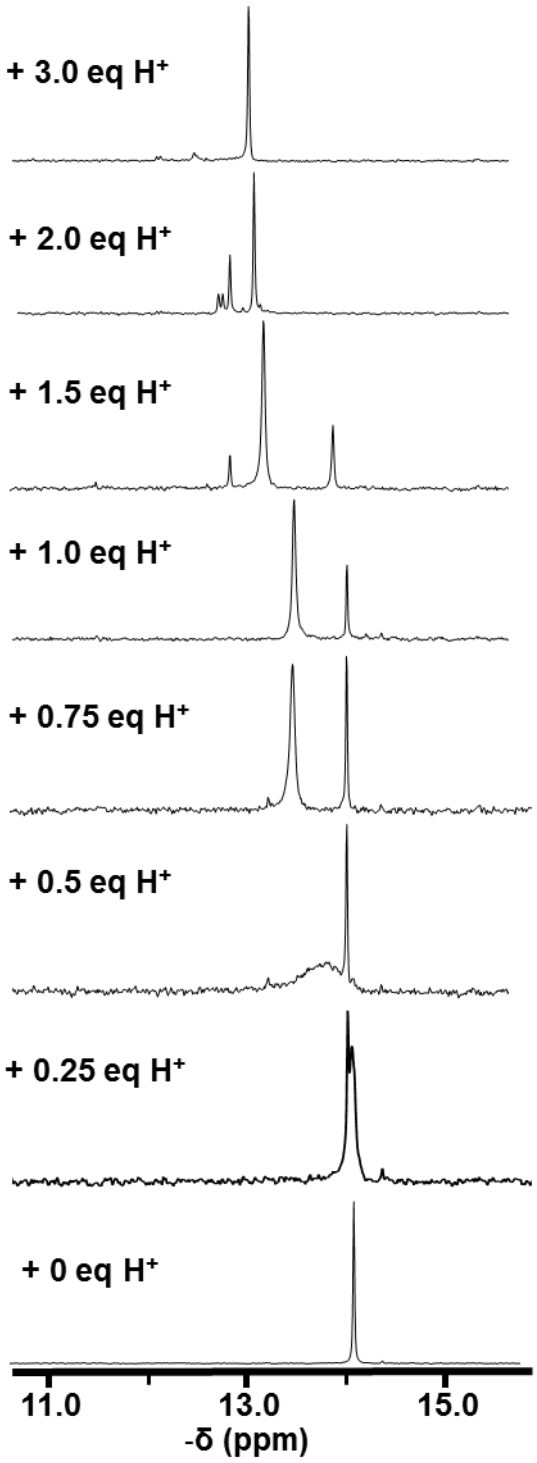

Figure 5.5. ^{31}P NMR spectra of $(TBA)_8[(\mu\text{-}O)(TiPW_{11}O_{39})_2]$ (Sample B) protonation in CD_3CN.

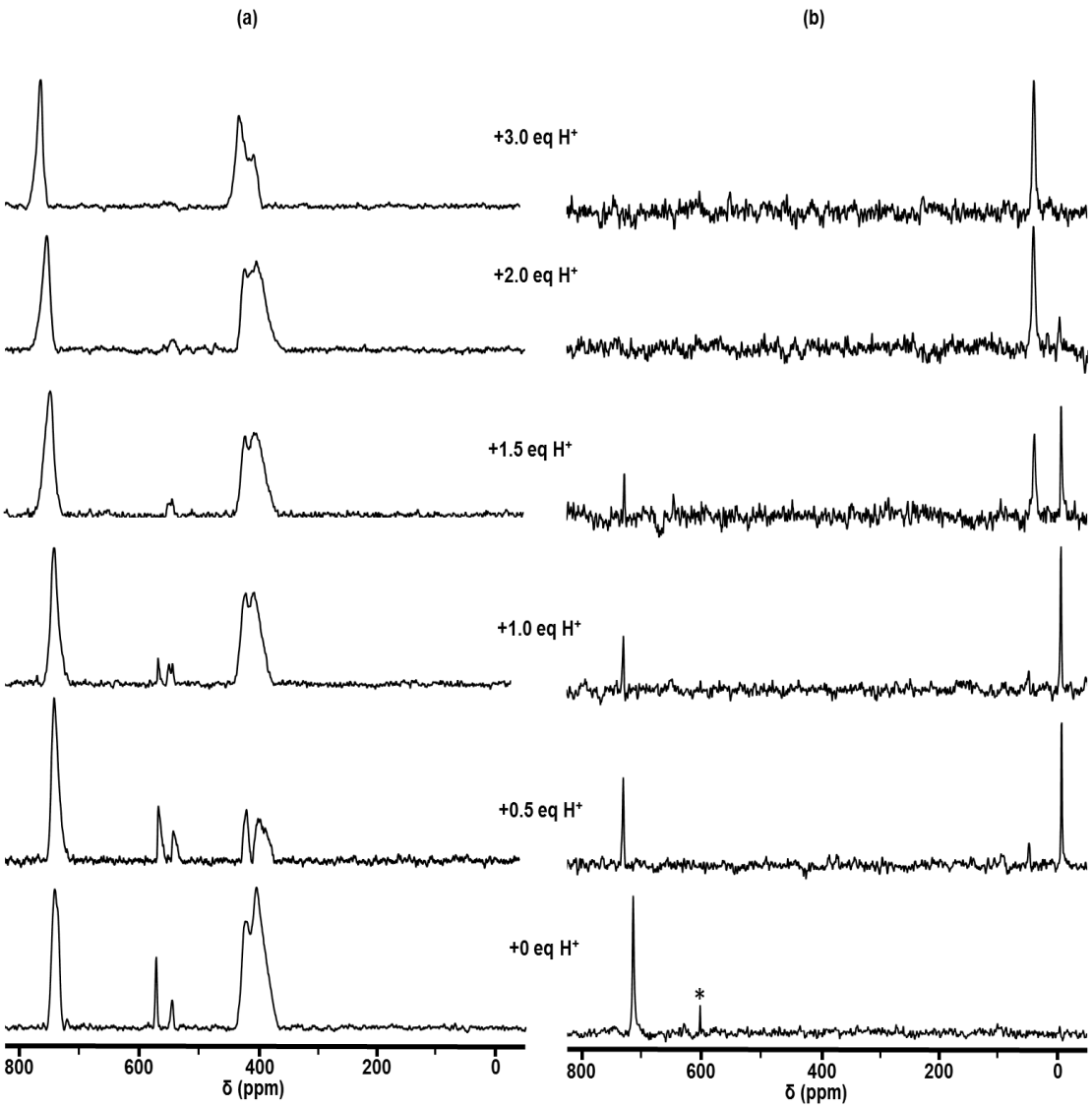

Figure 5.6. ^{17}O NMR spectra of $(TBA)_8[(\mu\text{-}O)(TiPW_{11}O_{39})_2]$ protonation in CD_3CN (a) with no ^{17}O TiOTi enrichment and (b) with only TiOTi enrichment

5.2.2 Investigation of possible metal binding sites in $(TBA)_8[(\mu\text{-}O)(TiPW_{11}O_{39})_2]$

Reactions of $(TBA)_8[(\mu\text{-}O)(TiPW_{11}O_{39})_2]$ and a range of electrophiles, $AgBF_4$, $SnCl_2$, $FeCl_2$, $Co(MeCN)_4(H_2O)_2][BF_4]_2$, $[Mo_2(NCCH_3)_8(ax\text{-}CH_3CN)_{0.5}][BF_4]_4$, $BiCl_3$, $SbCl_3$, Me_2SnCl_2, $SnCl_4$ and $TiCl_4$ were studied using ^{17}O and ^{31}P NMR spectroscopy to determine possible metal binding sites with the aim of isolating mixed-metal POM species, with new reactive sites as shown in **Scheme 5.2**. Protonolysis results suggest the possibility of such systems and in fact a structure, $(TBA)_4[(\mu\text{-}O)(TiW_5O_{18})_2Sn(CH_3)_2]$ (see **Figure 5.7**) with the Lindqvist POM framework has been isolated previously.[11,12] This inspired similar study on the Keggin analogue, $(TBA)_8[(\mu\text{-}O)(TiPW_{11}O_{39})_2]$. Pictures of some NMR samples of the reactions are

given in **Figure 5.8**. For no specific reason other than sample availability, $(TBA)_8[(\mu\text{-}O)(TiPW_{11}O_{39})_2]$ with ^{17}O enrichment at all the oxygen sites of the POM was used for reactions with $AgBF_4$ while $(TBA)_8[(\mu\text{-}O)(TiPW_{11}O_{39})_2]$ with no TiOTi enrichment was used for other reactions.

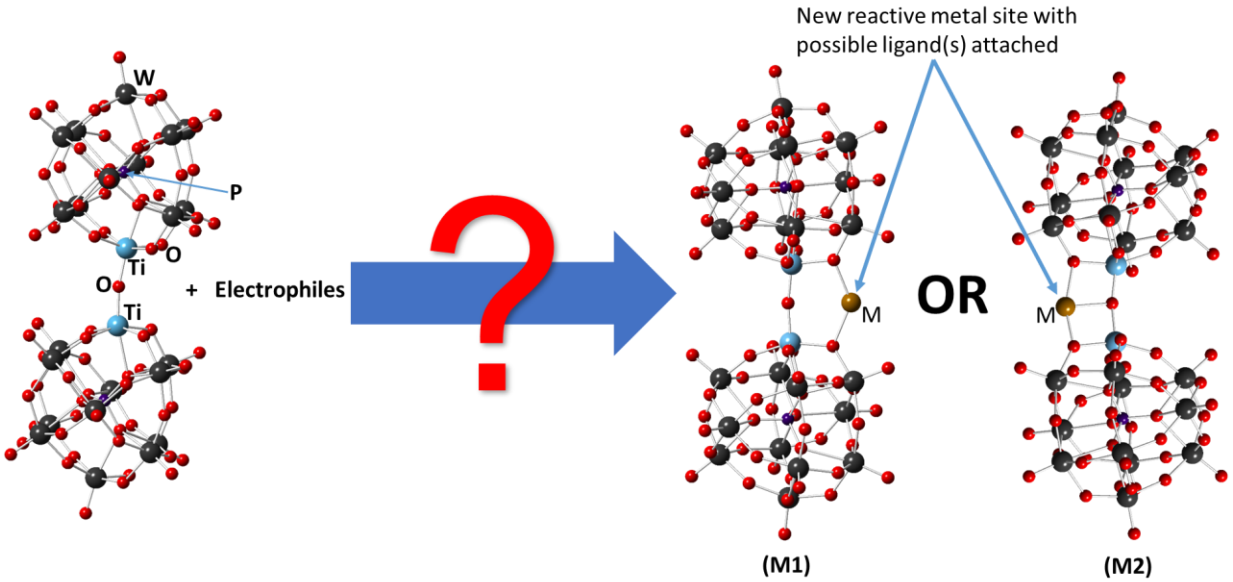

Scheme 5.2. Proposed interactions between $[(TiPW_{11}O_{39})_2O]^{8-}$ and a range of electrophiles (M = Ag^+, Sn^{2+}, Fe^{2+}, Co^{2+} Mo^{2+}, Bi^{3+}, Sb^{3+}, Sn^{4+}, and Ti^{4+})

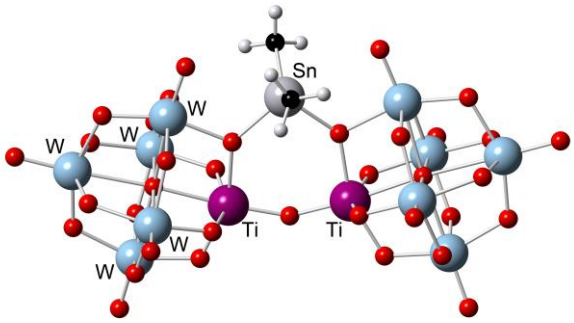

Figure 5.7. Structure of $(TBA)_4[(\mu\text{-}O)(TiW_5O_{18})_2Sn(CH_3)_2]$ obtained from reaction of $(TBA)_6[(\mu\text{-}O)(TiW_5O_{18})_2]$ and 1 mole-equivalent $(CH_3)_2SnCl_2$.[11,12]

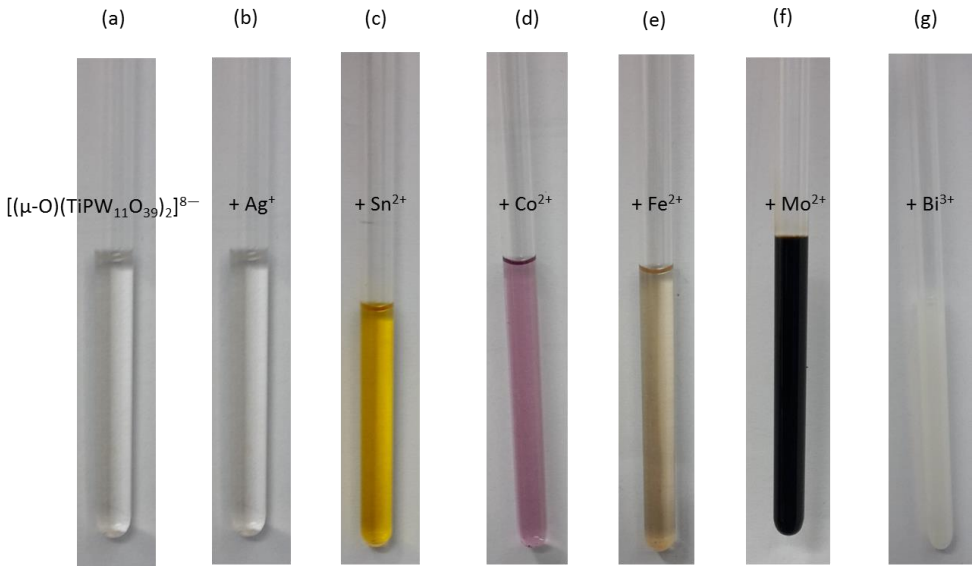

Figure 5.8. NMR samples of (a) $[(TiPW_{11}O_{39})_2O]^{8-}$ and reactions with 1 mole-equivalent of (b) $AgBF_4$ (c) $SnCl_2$ (d)$[Co(CH_3CN)_4(H_2O)_2][BF_4]_2$ (e) $FeCl_2$ (f) $[Mo_2(NCCH_3)_8(ax\text{-}CH_3CN)]_{0.5}[BF_4]_4$ and (g) $BiCl_3$

5.2.2.1 Reaction between $(TBA)_8[(\mu\text{-}O)(TiPW_{11}O_{39})_2]$ and $AgBF_4$

Figure 5.9. (A). shows a small downfield shift in the ^{31}P NMR resonance upon addition of $AgBF_4$ to $(TBA)_8[(\mu\text{-}O)(TiPW_{11}O_{39})_2]$. The observed movements were from -14.07 to -14.05 ppm with 1 equiv. of Ag^+ and -14.04 ppm with 2 equiv. of Ag^+. As with addition of H^+, this shift is likely due to metal binding at TiOW sites though Ag^+ causes a smaller ^{31}P NMR resonance movement. Whilst **Figure 5.9. (B)**. shows no significant change in the terminal W=O ^{17}O NMR resonance, a slight movement was observed in the TiOW peaks. Addition of 1 equiv. of Ag^+ caused an upfield shift from 572, 544 to 566, 543 ppm. These remain virtually unchanged at 565, 543 ppm upon addition of 2 equiv. of Ag^+. The slight movements in the TiOW resonances further suggests possible silver binding at the TiOW sites. A slight movement from 712 to 709 ppm is also observed in the TiOTi resonance after 2 equiv. of Ag^+. Again, like with protons, these small changes in ^{17}O resonances might be attributed to the presence of a number of equivalent oxygen sites that can accept Ag^+. Additionally, **Table 5.1** shows an increase from 630 to 635 cm^{-1} in the TiOTi vibrational frequency whilst the terminal W=O vibration change from 959 to 960 cm^{-1}. The movements in the FT-IR vibration and ^{17}O resonance of TiOTi suggest metal binding at the TiOTi site as well. The results are consistent with observations for protonolysis of $(TBA)_8[(\mu\text{-}O)(TiPW_{11}O_{39})_2]$ with $HBF_4.Et_2O$ and points to formation of **(M2)**-type complex based on **Equation 5.1** where L might be MeCN, BF_4^- or F^-.

$$(TBA)_8[(\mu\text{-}O)(TiPW_{11}O_{39})_2] + AgBF_4 \longrightarrow (TBA)_8[(\mu\text{-}O)TiPW_{11}O_{39})_2Ag(L)] \quad (5.1)$$

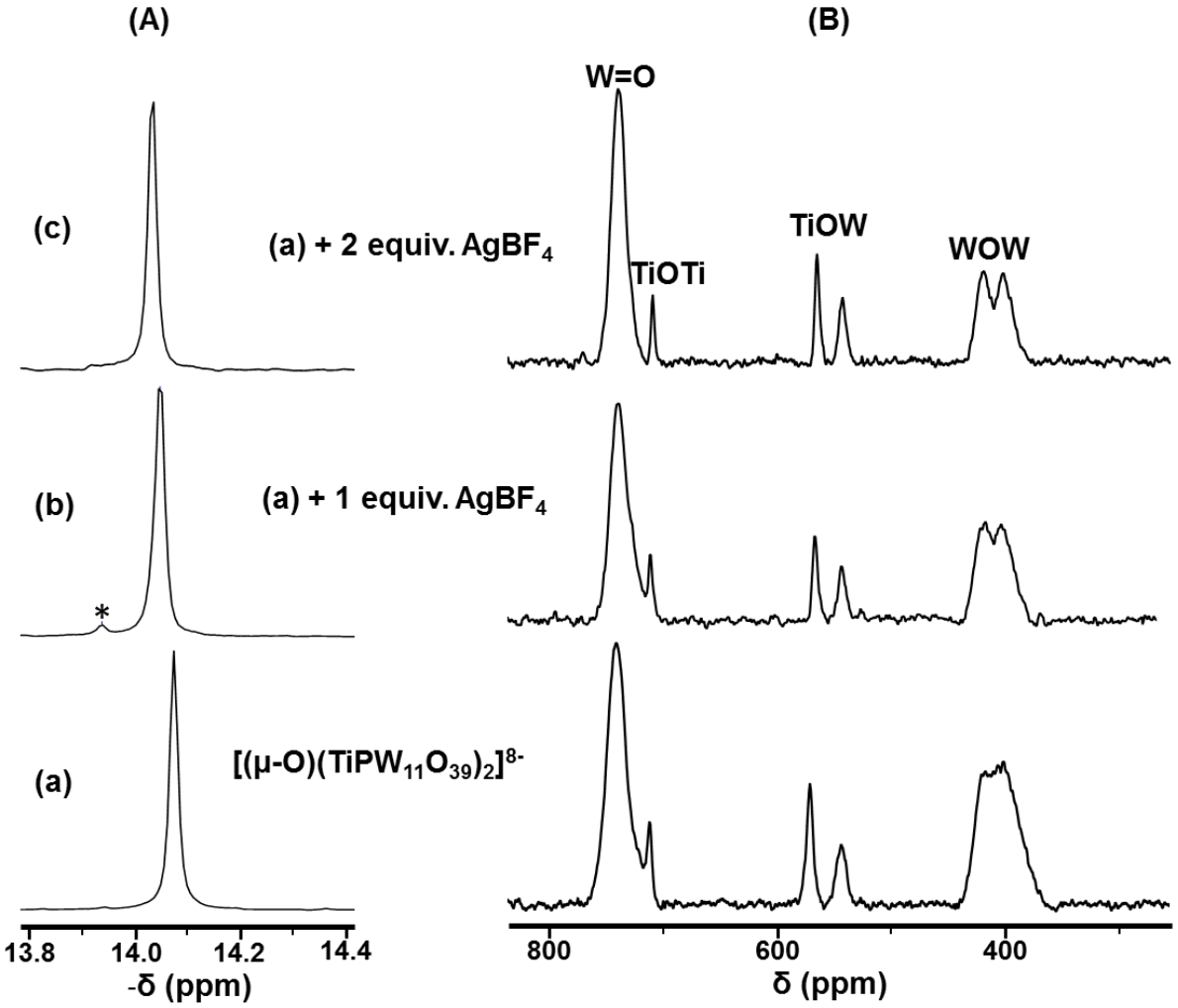

Figure 5.9. (A). ^{31}P and (B). ^{17}O NMR spectra of (a) (TBA)$_8$[(TiPW$_{11}$O$_{39}$)$_2$O] in CD$_3$CN plus (b) 1 mole-equivalent and (c) 2 mole-equivalents of AgBF$_4$. Peak asterisked is unassigned.

Table 5.1. FT-IR data (cm-[1]) of solid products from reactions between $(TBA)_8[(\mu\text{-}O)(TiPW_{11}O_{39})_2]$ and a range of Lewis acid reagents.

Lewis acid reagents	ν(W=O)	ν (WOW)	ν (TiOTi)	ν (P-O)
[a]	959	882, 792	630	1065
$HBF_4.Et_2O$ (1 equiv.)	963	882, 781	640	1068
$HBF_4.Et_2O$ (2 equiv.)	966	883, 772	634	1071
$HBF_4.Et_2O$ (5 equiv.)	971	887, 777	663	1074
$AgBF_4$ (1 equiv.)	960	883, 791	635	1066
$AgBF_4$ (2 equiv.)	962	884, 791	636	1067
$SnCl_2$	963	883, 782	620	1068
$FeCl_2$	959	883, 790	625	1065
$[Co(CH_3CN)_4(H_2O)_2][BF_4]_2$	964	885, 789	634	1065
$[Mo_2(NCCH_3)_8(ax\text{-}CH_3CN)]_{0.5}[BF_4]_4$	964	887, 774	629	1060
$SbCl_3$	962	882, 785	634	1068
$BiCl_3$	962	883, 784	631	1067
Me_2SnCl_2	962	883, 782	631	1066
$SnCl_4$	961 917 (minor)	881, 775	634	1068
$TiCl_4$	963	883, 797	-	1070

[a] FT-IR data for $(TBA)_8[(\mu\text{-}O)(TiPW_{11}O_{39})_2]$.

Table 5.2. ^{17}O NMR data of products from reactions between $(TBA)_8[(\mu\text{-}O)(TiPW_{11}O_{39})_2]$ and Lewis acid reagents

Lewis acid reagents	^{17}O chemical shift/ppm			
	W=O	MOM	MOW	WOW
[a]	742 - 738	712	572, 544	423 - 404
$AgBF_4$	739 – 726	710	566, 543	421- 404
	739 – 729	709	565, 543	419 - 402
$SnCl_2$	757 – 742		565, 537	427 - 408
$FeCl_2$	739 – 737		570, 543	419 - 401
$[Co(CH_3CN)_4(H_2O)_2][BF_4]_2$	756	714	582, 568, 560	426 - 408
$[Mo_2(NCCH_3)_8(ax\text{-}CH_3CN)]_{0.5}[BF_4]_4$	742		580, 574, 567	417 - 397
$SbCl_3$	743		585, 566, 554, 534	422 - 404
$BiCl_3$	737		570, 541	416 - 400
Me_2SnCl_2	743-737		572, 543	426 - 403
$SnCl_4$	748		585, 565, 548	422 - 408
$TiCl_4$	754		585, 567	426 - 404

[a] ^{17}O NMR data for $(TBA)_8[(\mu\text{-}O)(TiPW_{11}O_{39})_2]$.

5.2.2.2 Reaction between $(TBA)_8[(\mu\text{-}O)(TiPW_{11}O_{39})_2]$ and $SnCl_2$

The reaction of $(TBA)_8[(\mu\text{-}O)(TiPW_{11}O_{39})_2]$ and $SnCl_2$ instantly led to a colour change from colourless to yellow. The ^{31}P NMR spectrum of the product showed a broaden peak [line width (fwhm) = 13.53 Hz] downfield at -13.89 ppm [**Figure 5.10. (a)**]. Also, the ^{17}O NMR data in **Table 5.2** and **Figure 5.10. (b)** show the terminal W=O resonance downfield at 757 - 742 ppm indicating decrease in the overall negative charge. This is expected if one or both chloride ions in $SnCl_2$ are lost upon reaction with $(TBA)_8[(\mu\text{-}O)(TiPW_{11}O_{39})_2]$ as illustrated in **Equation 5.2** (x = 1 or 2).

$$(TBA)_8[(\mu\text{-}O)(TiPW_{11}O_{39})_2] + SnCl_2 \longrightarrow (TBA)_{8-x}[(\mu\text{-}O)TiPW_{11}O_{39})_2SnCl_{2-x}] + xTBACl \qquad (5.2)$$

The Ti-O-W resonances appeared upfield at 565, 537 ppm while the WOW resonances appeared at 427 - 408 ppm. The movements of the ^{31}P and Ti-O-W ^{17}O NMR resonances are consistent with metal binding at the Ti-O-W sites. The ^{119}Sn NMR spectrum of the yellow product showed a very broad peak at -20.13 ppm [**Figure 5.10 (c)**]. The broadness of the peak [line width (fwhm) = 558 Hz] did not allow for resolution of any Sn-W couplings, which was expected to confirm Sn-O-W interactions in the POM. Pure $SnCl_2$ is not soluble in MeCN and no ^{119}Sn signal was observed when a suspension of $SnCl_2$ in MeCN was recorded. FT-IR data of the isolated product after washing with $CHCl_3$ (see **Table 5.1**) gave a terminal W=O band of 963 cm^{-1} indicating a reduction in the overall negative charge of the polyanion as shown in **Equation 5.2** while the TiOTi band decreased from 630 to 620 cm^{-1}. This might suggest an (**M1**)-type of complex with no interaction between TiOTi and the Sn atom (see **Scheme 5.2**). As noted earlier, protonation at TiOTi site in $[(\mu\text{-}O)(TiPW_{11}O_{39})_2]^{8-}$ has been proposed to result in an increase in its wavenumber by 15 cm^{-1},[20] whilst interaction of electrophiles with oxygens of TiOW sites of $[(\mu\text{-}O)(TiW_5O_{18})_2]^{6-}$ has resulted in a reduction in TiOTi vibrational frequency.[11] Additionally, the broad peaks observed in both the ^{31}P and ^{119}Sn NMR spectra are likely due to some sort of fluxional behaviour, which are not yet understood.

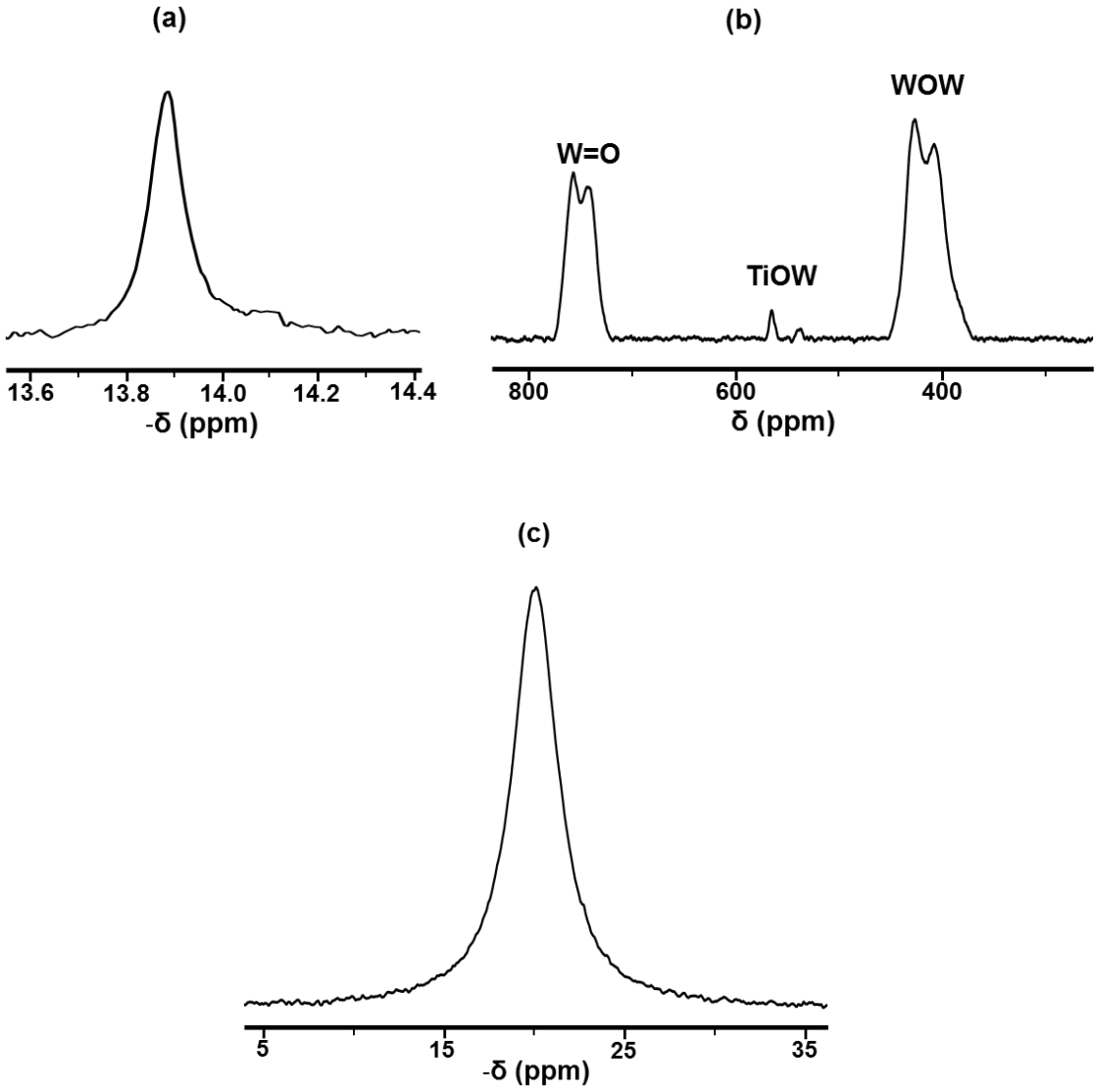

Figure 5.10. (a) ^{31}P (b) ^{17}O and (c) ^{119}Sn NMR spectra of the product from the reaction between $(TBA)_8[(TiPW_{11}O_{39})_2O]$ and 1 mole-equivalent of $SnCl_2$ in CD_3CN.

5.2.2.3 Reaction between $(TBA)_8[(\mu\text{-}O)(TiPW_{11}O_{39})_2]$ and $FeCl_2$

Treatment of $(TBA)_8[(\mu\text{-}O)(TiPW_{11}O_{39})_2]$ with $FeCl_2$ produced a brown coloured solution. The ^{31}P NMR spectrum gave a broadened downfield resonance at -13.90 ppm [line width (fwhm) = 10.33 Hz]. The ^{17}O NMR data in **Table 5.2** and **Figure 5.11 (b)** show an upfield movement of the terminal W=O resonance to 739 -737 ppm whilst the TiOW resonances showed only a slight shift upfield to 570, 543 and the WOW resonances appeared at 419 – 401 ppm. Also, **Table 5.1** shows only a slight change to 625 cm^{-1} in the TiOTi FT-IR vibration while the terminal W=O vibration was unchanged. These results suggest an **(M1**)-type of complex based on **Equation 5.3**.

$$(TBA)_8[(\mu\text{-}O)(TiPW_{11}O_{39})_2] \quad + \quad FeCl_2 \longrightarrow (TBA)_8[(\mu\text{-}O)TiPW_{11}O_{39})_2FeCl_2] \qquad (5.3)$$

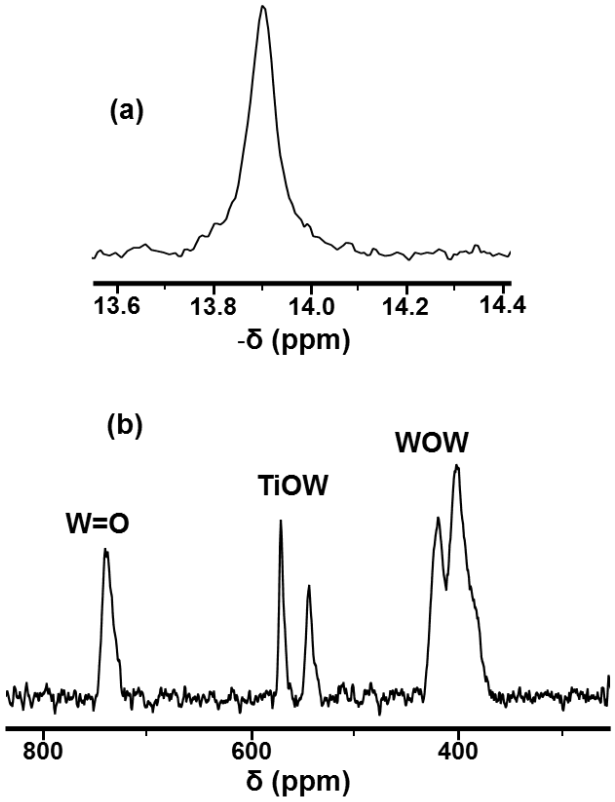

Figure 5.11. (a) ^{31}P and (b) ^{17}O NMR spectra of the product from the reaction of $(TBA)_8[(TiPW_{11}O_{39})_2O]$ and 1 equiv. $FeCl_2$ in CD_3CN.

5.2.2.4 Reaction between $(TBA)_8[(\mu\text{-}O)(TiPW_{11}O_{39})_2]$ and $[Co(CH_3CN)_4(H_2O)_2][BF_4]_2$

The ^{31}P NMR spectrum of the purple solution obtained from reaction between $(TBA)_8[(\mu\text{-}O)(TiPW_{11}O_{39})_2]$ and $[Co(CH_3CN)_4(H_2O)_2][BF_4]_2$ showed a very broad peak centered at 2.03 ppm [line width (fwhm) = 418 Hz]. The ^{17}O NMR data in **Table 5.2** and **Figure 5.12. (b)** show broadened peaks. The terminal W=O resonances were at 756 and 791 ppm whilst the TiOW resonances showed three peaks at 582, 568, 560 and the WOW resonances were at 426 – 408 ppm. Also, **Table 5.1** shows increase in the frequency of the W=O terminal band to 964 whilst the TiOTi vibration increased slightly to 634 cm^{-1}. Though the presence of a paramagnetic Co^{2+} makes it difficult to interpret the NMR spectra, these results suggest an **(M2)**-type complex based on **Equation 5.4** where L is likely CH_3CN or H_2O. Though it is not very clear why and how the Co^{2+} exhibits the greatest paramagnetic effect on the terminal W=O ^{17}O NMR resonances.

$$(TBA)_8[(\mu\text{-}O)(TiPW_{11}O_{39})_2] + [Co(CH_3\overset{+}{C}N)_4(H_2O)_2[BF_4]_2 \longrightarrow (TBA)_6[(\mu\text{-}O)TiPW_{11}O_{39})_2Co(L)] + 2TBA[BF_4] \quad (5.4)$$

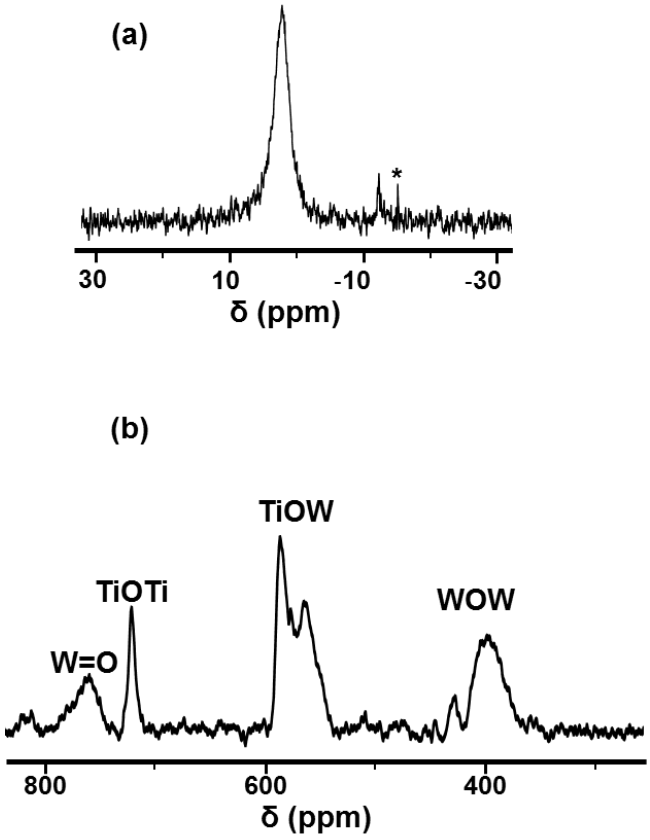

Figure 5.12. (a) ^{31}P and (b) ^{17}O NMR spectra of the product from the reaction between $(TBA)_8[(TiPW_{11}O_{39})_2O]$ and 1 mole-equivalent $[Co(CH_3CN)_4(H_2O)_2][BF_4]_2$ in CD_3CN.

5.2.2.5 Reaction between $(TBA)_8[(\mu\text{-}O)(TiPW_{11}O_{39})_2]$ and $[Mo_2(NCCH_3)_8(ax\text{-}CH_3CN)]_{0.5}[BF_4]_4$

The reaction between $(TBA)_8[(\mu\text{-}O)(TiPW_{11}O_{39})_2]$ and 0.5 mole-equivalents of the Mo≣Mo quadruply-bonded $[Mo_2(NCCH_3)_8(ax\text{-}CH_3CN)]_{0.5}[BF_4]_4$ at -30 °C gave a green solution which gradually became dark brown as the solution warmed up gently to room temperature. **Figure 5.13. (a)** shows a mixture of species in the ^{31}P NMR spectrum with a major upfield peak (55%) at -14.27 ppm. There was no significant change in the spectrum when the solution of the mixture was allowed to stir for up to 24 h and the spectrum became more complex upon heating. The ^{17}O NMR spectrum [**Figure 5.13. (b)**] showed a terminal W=O peak centered at 742 and WOW at 417 – 397 ppm. Three resonances were observed for the

TiOW oxygens at 580, 574 and 567 ppm. **Table 5.1** gives a terminal W=O IR band of 964 cm^{-1}, a P-O band at 1060 cm^{-1} and TiOTi vibration at 629 cm^{-1}. Generally, at least one major and 6 minor species were present in solution (from ^{31}P NMR spectrum) and though ^{17}O NMR is not able to differentiate between them, it is likely that among these species are products from both degradation of Mo≡Mo quadruple bond and reduction of tungsten.

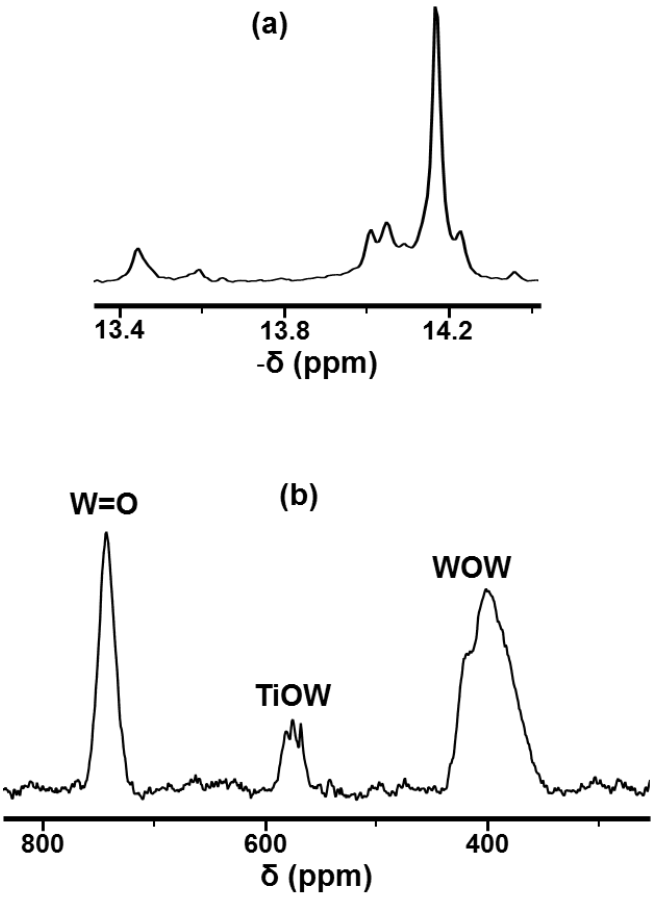

Figure 5.13. (a) ^{31}P and (b) ^{17}O NMR spectra of the product from the reaction between $(TBA)_8[(TiPW_{11}O_{39})_2O]$ and 0.5 mole-equivalents of $[Mo_2(NCCH_3)_8(ax\text{-}CH_3CN)]_{0.5}[BF_4]_4$ in CD_3CN.

5.2.2.6 Reaction between $(TBA)_8[(\mu\text{-}O)(TiPW_{11}O_{39})_2]$ and $SbCl_3$

Treatment of $(TBA)_8[(\mu\text{-}O)(TiPW_{11}O_{39})_2]$ with $SbCl_3$ gave a major broadened peak [line width (fwhm) = ~41 Hz] in the ^{31}P NMR spectrum centered at -14.01, a sharp peak at -14.13 and 15% of $[ClTiPW_{11}O_{39}]^{4-}$ at -14.37 ppm. In addition to peaks for $[ClTiPW_{11}O_{39}]^{4-}$, the ^{17}O NMR spectrum showed peaks at 554 and 534 and a shoulder at 540 ppm for TiOW oxygens (see **Figure 5.14**). These are indication of metal binding at the TiOW sites. Also, FT-IR data in **Table 5.1** show an increase in terminal W=O and TiOTi vibrational frequencies to 962 and

634 cm^{-1} respectively. Thus, in addition to chlorination, these results might suggest formation of an **(M2)**-type complex based on **Equation 5.5** (x = 1 to 3).

$$(TBA)_8[(\mu\text{-}O)(TiPW_{11}O_{39})_2] + SbCl_3 \longrightarrow (TBA)_{8-x}[(\mu\text{-}O)TiPW_{11}O_{39})_2SbCl_{3-x}] + xTBACl \qquad (5.5)$$

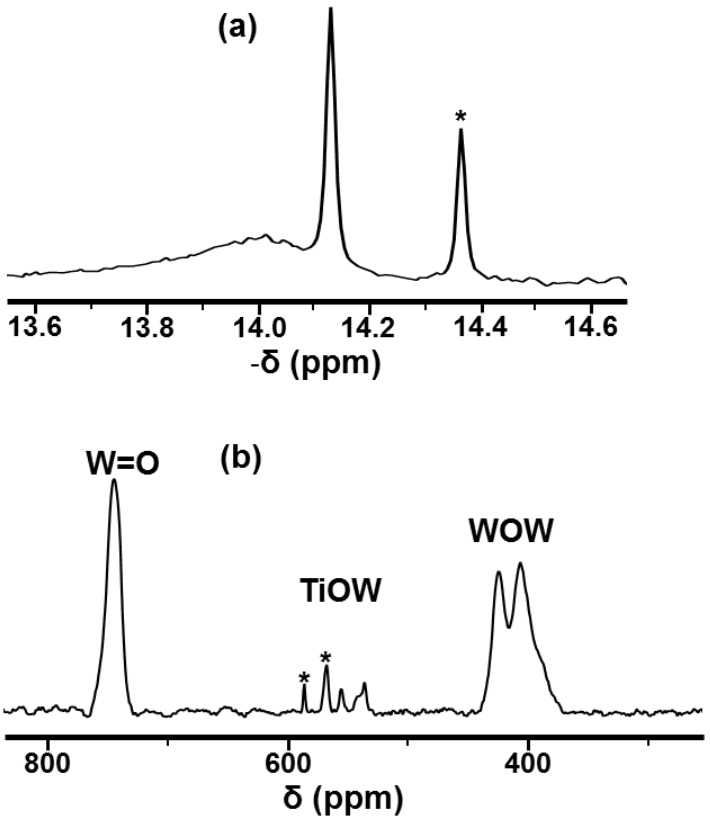

Figure 5.14. (a) ^{31}P and (b) ^{17}O NMR spectra of the product from the reaction of $(TBA)_8[(TiPW_{11}O_{39})_2O]$ and 1 mole-equivalent $SbCl_3$ in CD_3CN. Peaks asterisked are assigned to $[ClTiPW_{11}O_{39}]^{4-}$.

5.2.2.7 Reaction between $(TBA)_8[(\mu\text{-}O)(TiPW_{11}O_{39})_2]$ and $BiCl_3$

The reaction between $(TBA)_8[(\mu\text{-}O)(TiPW_{11}O_{39})_2]$ and $BiCl_3$ gave a major product (95%) with a broadened ^{31}P NMR peak at -14.03 ppm (line width fwhm = 20.71 Hz) and 5 % of impurities including $[ClTiPW_{11}O_{39}]^{4-}$. The ^{17}O NMR spectrum showed the terminal W=O resonances at 737 ppm while WOW peaks appeared at 416 – 400 ppm. A slight upfield shift to 570, 541 ppm was observed in the TiOW resonances (**Figure 5.15**). These are indicative of metal binding at the TiOW sites. FT-IR data showed the W=O band at 962 cm^{-1} with no substantial change in the ν(TiOTi) vibration (see **Table 5.1**). These results points to formation of an **(M1)**-type complex based on **Equation 5.6** (x = 1 to 3).

$$(TBA)_8[(\mu\text{-}O)(TiPW_{11}O_{39})_2] + BiCl_3 \longrightarrow (TBA)_{8-x}[(\mu\text{-}O)TiPW_{11}O_{39})_2BiCl_{3-x}] + xTBACl \quad (5.6)$$

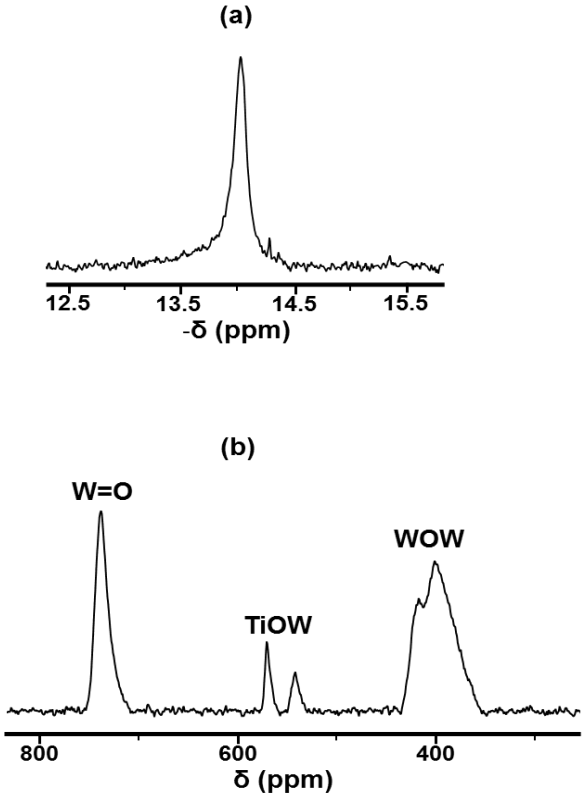

Figure 5.15. (a) ^{31}P and (b) ^{17}O NMR spectra of the product from the reaction of $(TBA)_8[(TiPW_{11}O_{39})_2O]$ and 1 mole-equivalent $BiCl_3$ in CD_3CN.

5.2.2.8 Reaction between $(TBA)_8[(\mu\text{-}O)(TiPW_{11}O_{39})_2]$ and $SnCl_4$

^{31}P NMR studies (**Figure 5.16**) showed that reaction between $(TBA)_8[(\mu\text{-}O)(TiPW_{11}O_{39})_2]$ and $SnCl_4$ at room temperature gave a mixture of species including some unreacted $(TBA)_8[(\mu\text{-}O)(TiPW_{11}O_{39})_2]$. After heating the reaction mixture at 60 ^oC for 8 h, the products by ^{31}P NMR were a species (94%) with a broadened peak at -13.61 ppm [line width (fwhm) = 15.17 Hz] and 6 % of $[ClTiPW_{11}O_{39}]^{4-}$. In addition to peaks for $[ClTiPW_{11}O_{39}]^{4-}$, the ^{17}O NMR spectrum (**Figure 5.17**) of the product showed a peak at 548 ppm for the TiOW oxygen suggesting metal binding at these sites. Also, the terminal W=O resonances was observed at 748 ppm. The ν(TiOTi) IR band also increased slightly from 630 to 634 cm^{-1}. Thus, in addition to chlorination, these results are consistent with formation of an **(M2)**-type complex based on **Equation 5.7** (x = 1 to 4).

$$(TBA)_8[(\mu\text{-}O)(TiPW_{11}O_{39})_2] + SnCl_4 \longrightarrow (TBA)_{8-x}[(\mu\text{-}O)TiPW_{11}O_{39})_2SnCl_{4-x}] + xTBACl \quad (5.7)$$

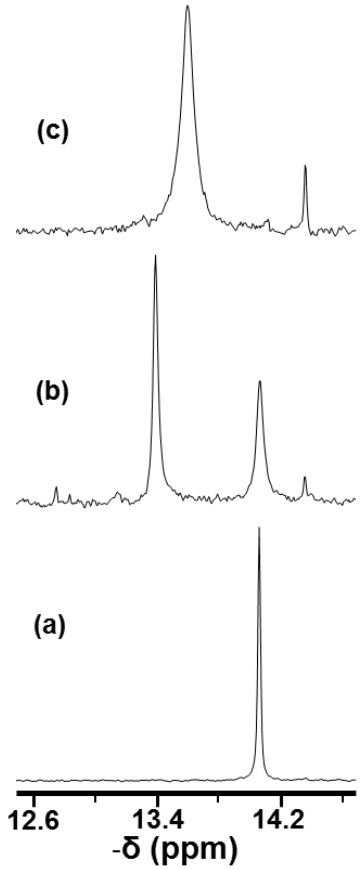

Figure 5.16. ^{31}P NMR spectra of $(TBA)_8[(TiPW_{11}O_{39})_2O]$ in CD_3CN (a) and product from the reaction with 1 mole-equivalent of $SnCl_4$ at room temperature (c) and after string at 60 ^oC for 8 h (c).

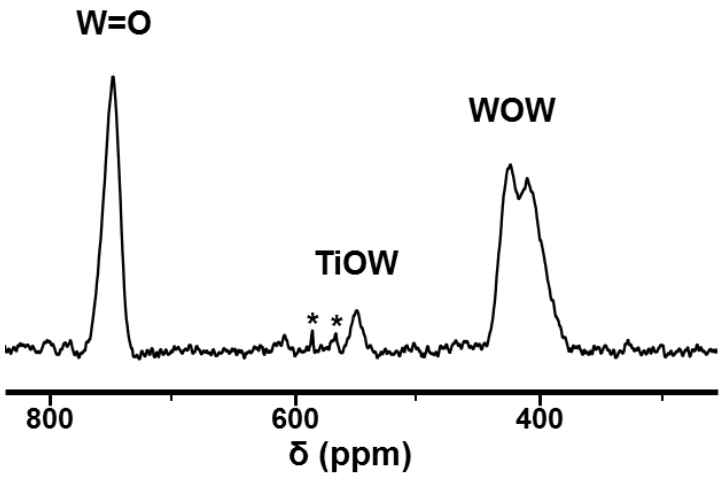

Figure 5.17. ^{17}O NMR spectrum of the product of the reaction of $(TBA)_8[(TiPW_{11}O_{39})_2O]$ and 1 mole-equivalent of $SnCl_4$ in CD_3CN at room temperature.

5.2.2.9 Reaction between $(TBA)_8[(\mu\text{-}O)(TiPW_{11}O_{39})_2]$ and $TiCl_4$

In contrast to the reaction with $SnCl_4$, ^{17}O and ^{31}P NMR studies showed that treatment of $(TBA)_8[(\mu\text{-}O)(TiPW_{11}O_{39})_2]$ with $TiCl_4$ gave $[ClTiPW_{11}O_{39}]^{4-}$ as the only product. Thus, $TiCl_4$ acts as a chlorinating agent to the POM.

5.2.2.10 Reaction between $(TBA)_8[(\mu\text{-}O)(TiPW_{11}O_{39})_2]$ and $(CH_3)_2SnCl_2$

To eliminate any side-reaction due to chlorination in the reaction with $SnCl_4$, $(TBA)_8[(\mu\text{-}O)(TiPW_{11}O_{39})_2]$ was treated with $(CH_3)_2SnCl_2$ (which is less Lewis acidic). And though the ^{17}O and ^{31}P NMR spectra of the reaction product in **Figure 5.18** showed no significant difference from those of the starting $(TBA)_8[(\mu\text{-}O)(TiPW_{11}O_{39})_2]$, ^1H NMR of the isolated product after washing three times with $CHCl_3$ to remove any unreacted $(CH_3)_2SnCl_2$ still showed a methyl peak at 1.2 ppm with tin satellites. The ratio of the methyl protons to CH_2N protons was 1:7.8 (calculated 1:8) suggesting the attachment of $(CH_3)_2SnCl_2$ to the POM. Also, IR data in **Table 5.1** showed an increase in the terminal W=O vibration from 959 to 962cm^{-1} also suggesting decrease in the overall polyanion charge due to the attachment of $(CH_3)_2Sn^{2+}$ group to the POM. The TiOTi vibration remained unchanged. In addition, the $^{119}Sn\{^1H\}$ spectrum in **Figure 5.19** shows an upfield shift in the resonance from 45.3 ppm for $(CH_3)_2SnCl_2$ to -18.6 ppm for the reaction product. This is expected due to replacement of Sn-Cl bonds with new Sn-O interactions and electronic influence on tin from the POM cage, which causes increased ^{119}Sn nuclear shielding. A number of factors including change in substituent, coordination, temperature and solvents are known to affect ^{119}Sn nuclear shielding.[21-23] The peak also broadens from 49 to 233 Hz and this did not allow for resolution of any $^2J(^{119}Sn^{183}W)$ couplings. These results are consistent with formation of an **(M1)**-type complex based on **Equation 5.8.** This type of complex has been structurally characterised for the Lindqvist POM, $(TBA)_6[(\mu\text{-}O)(TiW_5O_{18})_2]$ (see **Figure 5.7**).[11,12]

$$\begin{matrix}(TBA)_8[(\mu\text{-}O)(TiPW_{11}O_{39})_2] \\ + \\ (CH_3)_2SnCl_2\end{matrix} \longrightarrow \begin{matrix}(TBA)_6[(\mu\text{-}O)TiPW_{11}O_{39})_2Sn(CH_3)_2] \\ + \\ 2TBACl\end{matrix} \qquad (5.8)$$

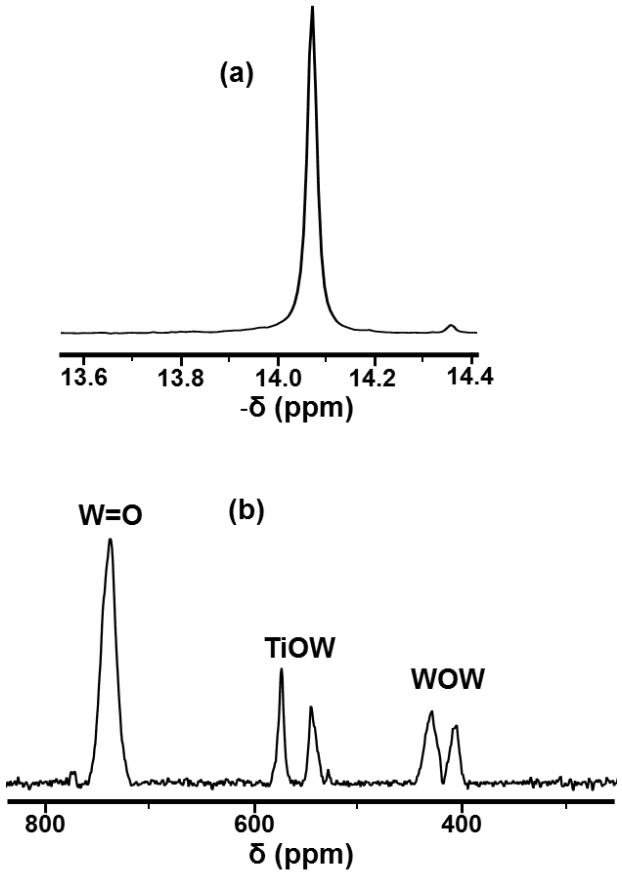

Figure 5.18. (a) ^{31}P and (b) ^{17}O NMR spectra of the product from the reaction of $(TBA)_8[(TiPW_{11}O_{39})_2O]$ and 1 mole-equivalent of Me_2SnCl_2 in CD_3CN.

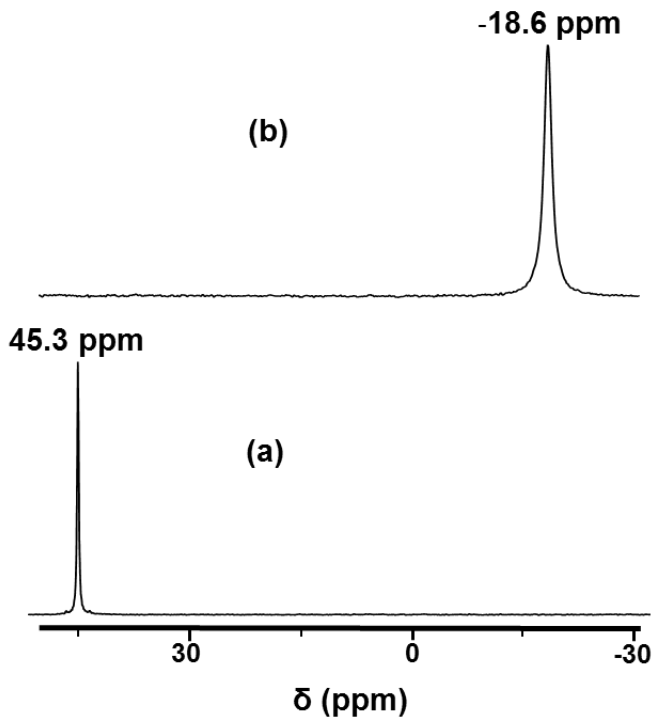

Figure 5.19. $^{119}Sn\{^1H\}$ NMR spectra of (a) Me_2SnCl_2 at 298K and (b) product from the reaction of $(TBA)_8[(TiPW_{11}O_{39})_2O]$ and 1 mole-equivalent of Me_2SnCl_2 at 298K in CD_3CN.

5.2.3 Crystallization of POMs

Several attempts to crystallize the products of protonolysis of the tin- and titanium-substituted POMs and the products from the reactions between $(TBA)_8[(\mu\text{-}O)(TiPW_{11}O_{39})_2]$ and electrophiles have so far been unsuccessful. Methods employed for crystallization include slow vapour diffusion of diethyl ether into acetonitrile solutions of the POMs, cooling saturated solutions of POMs over several days and layering acetonitrile solutions of POMs with diethyl ether.

5.3 Conclusions

The results discussed in this chapter have provided evidence for protonation at TiOW sites in $(TBA)_4[(CH_3O)TiPW_{11}O_{39}]$ and an initial proton attack at ROSn before subsequent protonation of SnOW sites in $(TBA)_4[(HO)SnPW_{11}O_{39}]$ implying that $Ti^{IV}OW$ sites are more basic than $Sn^{IV}OW$ sites in $(TBA)_4[(RO)M^{IV}PW_{11}O_{39}]$ possibly because of the more electron donating OMe bonded to Ti. Protonation of $(TBA)_4[ClM^{IV}PW_{11}O_{39}]$ (M = Sn, Ti) was shown to result in several species *via* possible step-wise proton attack at M^{IV}-O-W sites, whereas protonation at both TiOW and TiOTi sites was observed in $(TBA)_8[(\mu\text{-}O)(TiPW_{11}O_{39})_2]$. Furthermore, preliminary results for reactions between $(TBA)_8[(\mu\text{-}O)(TiPW_{11}O_{39})_2]$ and $AgBF_4$, $[Co(CH_3CN)_4(H_2O)_2][BF_4]_2$, $SbCl_3$ and $SnCl_4$ provide evidence for metal binding at Ti-O-W and TiOTi sites whilst reactions with $SnCl_2$, $FeCl_2$, $BiCl_3$ and $(CH_3)_2SnCl_2$ point to metal binding at only TiOW sites of the POM. Finally, reactions with $SbCl_3$, $SnCl_4$ and $TiCl_4$ have been shown to give varying amounts of chlorinated products. Further attempts to obtain crystal structures are required to fully elucidate the nature of the bonding in these adducts.

References

1. I. Kozhevnikov, *Catalysis by Polyoxometalates*, John Wiley and Sons Ltd, England, 2002.
2. I. V. Kozhevnikov, *Chem. Rev.*, 1998, **98**, 171-198.
3. I. V. Kozhevnikov and K. I. Matveev, *Appl. Catal.*, 1983, **5**, 135-150.
4. M. Misono, *Chem. Commun.*, 2001, 1141-1152.
5. B. B. Bardin, S. V. Bordawekar, M. Neurock and R. J. Davis, *J. Phys. Chem. B*, 1998, **102**, 10817-10825.
6. J. B. Moffat, *J. Mol. Catal.*, 1984, **26**, 385-396.
7. L. Coyle, P. S. Middleton, C. J. Murphy, W. Clegg, R. W. Harrington and R. J. Errington, *Dalton Trans.*, 2012, **41**, 971-981.
8. R. J. Errington, S. S. Petkar, P. S. Middleton, W. McFarlane, W. Clegg, R. A. Coxall and R. W. Harrington, *Dalton Trans.*, 2007, 5211-5222.
9. T. M. Che, V. W. Day, L. C. Francesconi, C. M. F. Fredrich, W. G. Klemperer and W. Shum, *Inorg. Chem.* , 1985, **24**, 4055-4062.
10. O. A. Kholdeeva, G. M. Maksimov, R. I. Maksimovskaya, L. A. Kovaleva, M. A. Fedotov, V. A. Grigoriev and C. L. Hill, *Inorg. Chem.*, 2000, **39**, 3828-3837.
11. R. J. Errington, in *Advances in Inorganic Chemistry*, eds. R. v. Eldik and L. Cronin, 2017, vol. 69, pp. 287-336.
12. D. Lebbie, unpublished work.
13. D. Morales-Morales, *Rev. Soc. Quím. Méx.*, 2004, **48**, 338-346.
14. K. J. Szabó, in *Organometallic Pincer Chemistry*, eds. G. v. Koten and D. Milstein, Springer Berlin Heidelberg, 2013, vol. 40, pp. 203-241.
15. K. J. Szabo and O. F. Wendt, *Pincer and Pincer-Type Complexes: Applications in Organic Synthesis and Catalysis*, Wiley-VCH, 2014.
16. M. Albrecht and G. van Koten, *Angew. Chem., Int. Ed.*, 2001, **40**, 3750-3781.
17. M. Pascual-Borras, X. Lopez, A. Rodriguez-Fortea, R. J. Errington and J. M. Poblet, *Chem. Sci.*, 2014, **5**, 2031-2042.
18. O. A. M. Kholdeeva, R. I., *Zh. Neorg. Khim.*, 1992, **37**, 6.
19. J. E. Del Bene, J. Elguero and I. Alkorta, *J. Phys. Chem. A*, 2004, **108**, 3662-3667.
20. O. A. Kholdeeva, T. A. Trubitsina, G. M. Maksimov, A. V. Golovin and R. I. Maksimovskaya, *Inorg. Chem.*, 2005, **44**, 1635-1642.
21. J. Holeček, K. Handlír¸, V. Černý, M. Nádvorník and A. Lyčka, *Polyhedron*, 1987, **6**, 1037-1039.
22. B. Wrackmeyer, in *Annual Reports on NMR Spectroscopy*, ed. G. A. Webb, Academic Press, London, 1999, vol. 38, pp. 203 - 251.
23. J. D. Kennedy, W. McFarlane, P. J. Smith, R. F. M. White and L. Smith, *J. Chem. Soc., Perkin Trans. 2*, 1973, 1785-1788.

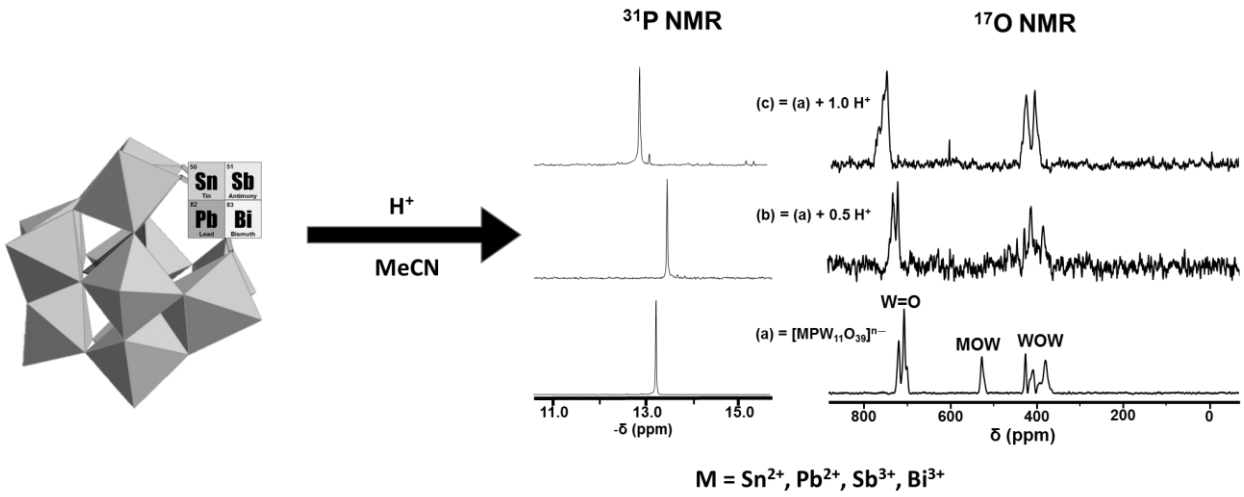

Chapter 6

Protonolysis and non-aqueous studies on heavier group 14 and 15 monosubstituted Keggin POMs

This chapter is a continuation of the project discussed in Chapter 5. It explores the surface oxygen basicity of heavier group 14 and 15 monosubstituted Keggin POMs. Furthermore, the reactivity of tin(II) - and lead (II)-substituted Keggin POMs in non-aqueous media is investigated.

6. Protonolysis and non-aqueous studies on heavier group 14 and 15 monosubstituted Keggin POMs

6.1 Introduction

Protonolysis of post-transition metal-substituted Keggin POMs was investigated to complement results described in Chapter 5 and provide more insights into protonation sites and mechanisms in this class of POMs. This is important in the light of recent studies which have shown the potential of salts and electrode materials of post-transition metals as catalyst candidates for the reduction of CO_2.[1,2] The mechanisms in aqueous medium were proposed to involve a protonation step, whereby lead oxide surface was protonated in the lead electrode whereas pure metallic bismuth surface was protonated in the bismuth electrode (detail mechanisms is discussed in **Chapter 7**).[2] This made us wonder the possible protonation sites and mechanisms of the series $(TBA)_5[M^{II}PW_{11}O_{39}]$ (M = Sn and Pb) and $(TBA)_4[M^{III}PW_{11}O_{39}]$ (M = Sb and Bi) in acetonitrile and their possible application as catalyst materials for CO_2 reduction. In this direction therefore, results are presented herein on the protonolysis of $(TBA)_5[M^{II}PW_{11}O_{39}]$ (M = Sn and Pb) and $(TBA)_4[M^{III}PW_{11}O_{39}]$ (M = Sb and Bi). Additionally, the non-aqueous reactivity and redox properties of $(TBA)_5[M^{II}PW_{11}O_{39}]$ (M = Sn and Pb) are studied with a range of reagents.

6.2 Results and Discussion

6.2.1 Protonation of $(TBA)_5[M^{II}PW_{11}O_{39}]$ (M = Sn and Pb) with $HBF_4.Et_2O$

The results from ^{31}P and ^{17}O NMR studies of $(TBA)_5[Sn^{II}PW_{11}O_{39}]$ and $(TBA)_5[Pb^{II}PW_{11}O_{39}]$ protonation are given in **Figure 6.1** and **Figure 6.2** respectively. An initial upfield shift from -13.22 to -13.46 ppm was observed for the ^{31}P NMR resonance of $(TBA)_5[Sn^{II}PW_{11}O_{39}]$ upon addition of 0.5 equiv. H^+. Subsequent additions of acids resulted in a more intensely coloured solution with downfield movement of the ^{31}P NMR resonances and broadening of the major peak. Trace amounts of other species including $[PW_{12}O_{40}]^{3-}$ appeared at 1.0 equiv. H^+. The ^{17}O NMR spectra on the other hand revealed that in addition to the expected downfield movements of the terminal W=O resonances,[3] the SnOW resonance disappeared

after adding 0.5 equiv. H^+. A peak, which was not assigned appeared at -6.4 ppm in the ^{17}O NMR spectrum after adding 1.5 equiv. H^+. Also, in addition to the terminal W=O and bridging WOW resonances, at least three broadened peaks appeared at -3.26, 17.18 and 38.70 ppm in the ^{17}O NMR spectrum at 2.0 equiv. H^+. Although it is difficult to interpret, the initial upfield movement of the ^{31}P NMR chemical shift, these results are consistent with protonation at the SnOW sites and formation of multiple species with increasing proton concentration. The broadened linewidth of the ^{31}P NMR peak might suggest slow proton exchange between these species at high acid concentration.

As with $(TBA)_5[Sn^{II}PW_{11}O_{39}]$, addition of 0.5 equiv. H^+ to $(TBA)_5[Pb^{II}PW_{11}O_{39}]$ caused an initial upfield shift from -11.99 to -12.18 ppm in the ^{31}P NMR spectrum. Also, in addition to the major peak (82%), two minor peaks existed at -11.32 (3%) and -11.72 ppm (15%). The ^{17}O NMR spectrum equally showed an upfield movement of the PbOW peak from 565 to 552 ppm. This also is suggestive of protonation at the PbOW sites. Addition of 1.0 equiv. H^+ resulted in multiple species including $[PW_{12}O_{40}]^{3-}$ (2%) with a downfield movement of the major ^{31}P NMR peak to -11.96 ppm (74%). The ^{17}O NMR spectrum at 1.0 equiv. H^+ showed the disappearance of the PbOW resonance. The POM is almost completely degraded to $[PW_{12}O_{40}]^{3-}$ at 1.5 equiv. H^+. Though both POMs seem to follow a similar protonation mechanism, the results generally show $(TBA)_5[Sn^{II}PW_{11}O_{39}]$ to be more stable to protonation than $(TBA)_5[Pb^{II}PW_{11}O_{39}]$.

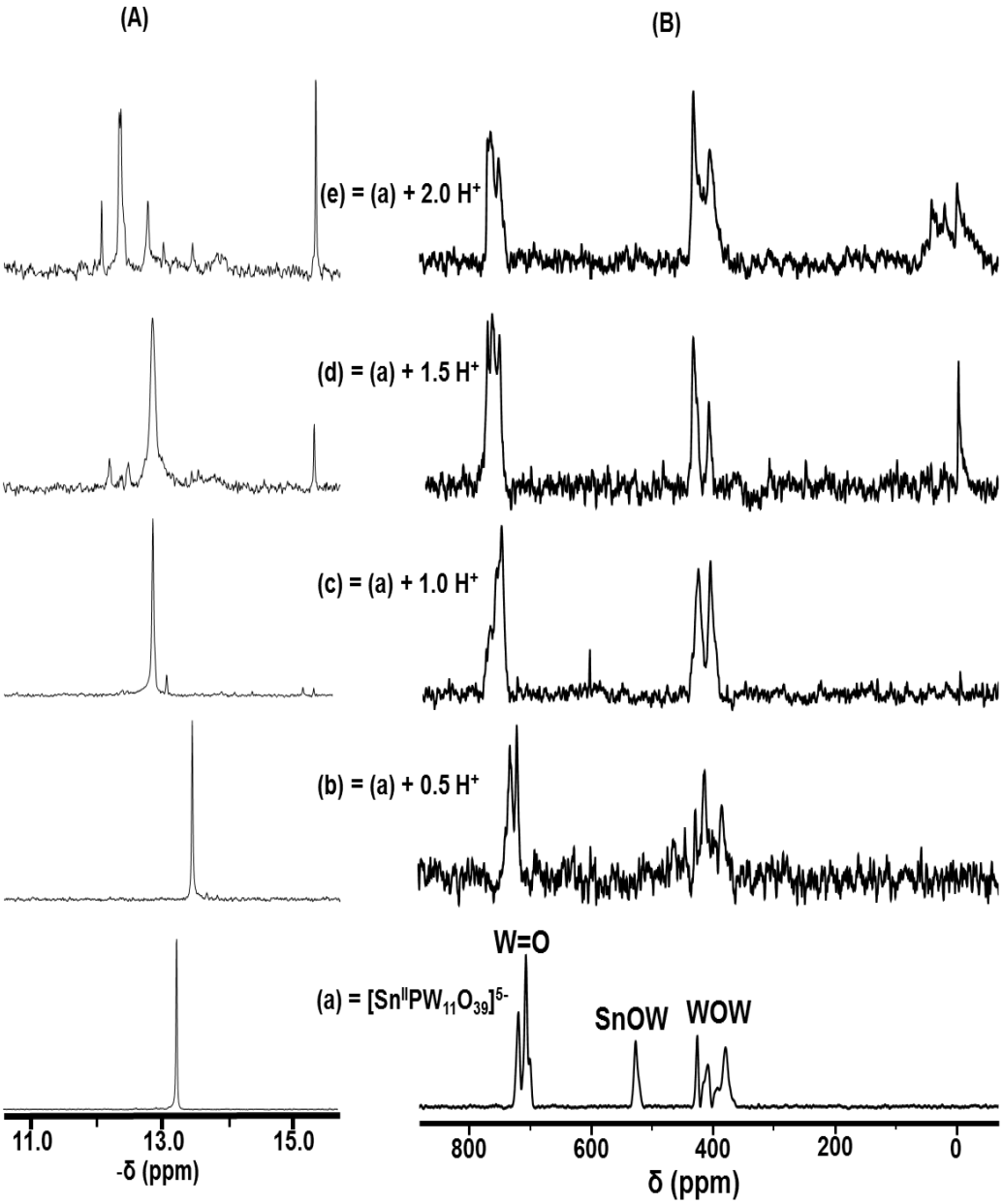

Figure 6.1. (A) ^{31}P NMR and (B) ^{17}O NMR spectra of (a) $(TBA)_5[Sn^{II}PW_{11}O_{39}]$ in CD_3CN plus (b) 0.5 (c) 1.0 (d) 1.5 and (e) 2.0 equiv. H^+.

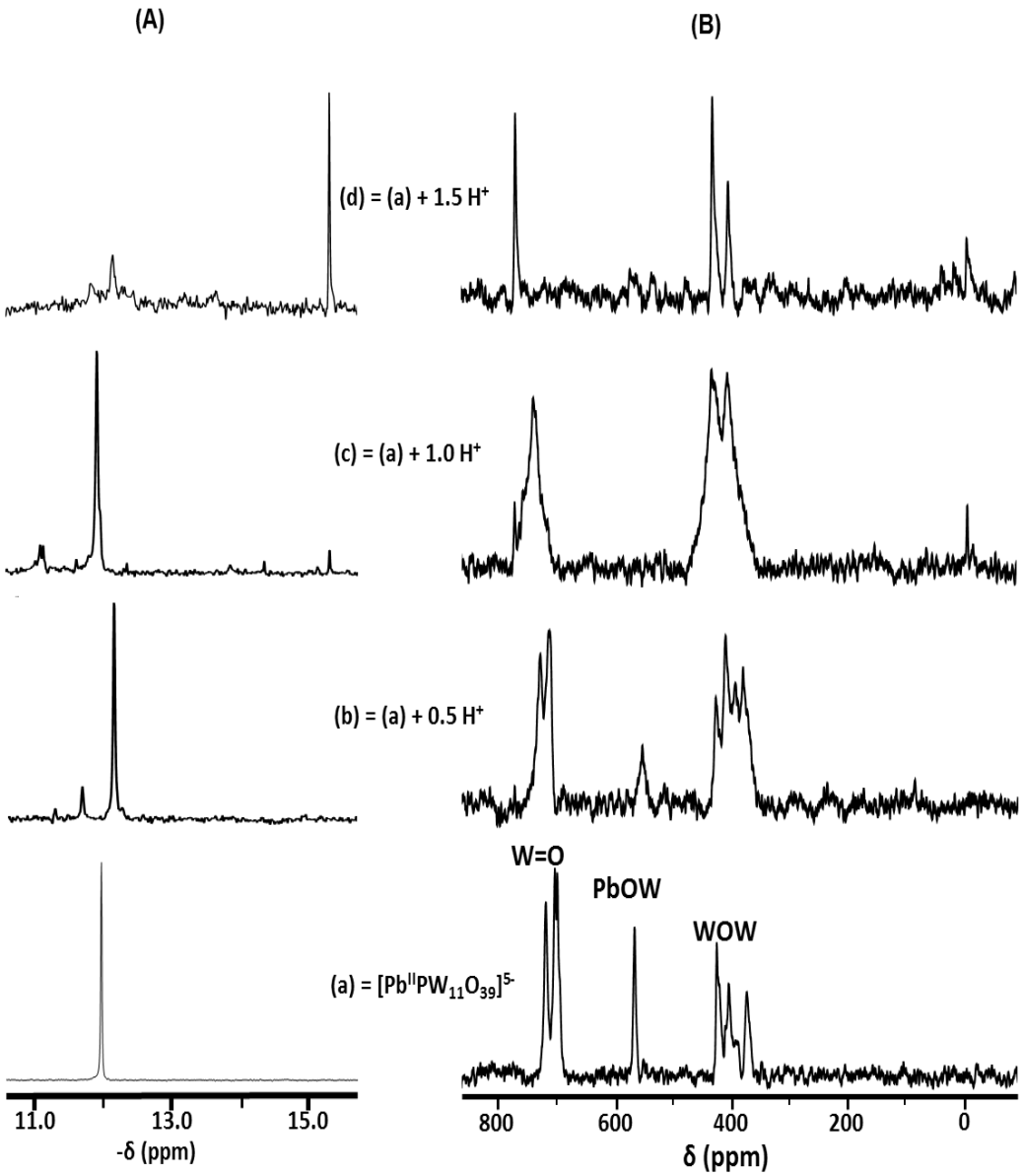

Figure 6.2. (A) ^{31}P NMR and (B) ^{17}O NMR spectra of (a) $(TBA)_5[Pb^{II}PW_{11}O_{39}]$ in CD_3CN plus (b) 0.5 (c) 1.0 and (d) 1.5 equiv. H^+.

6.2.2 Protonation of $(TBA)_4[M^{III}PW_{11}O_{39}]$ (M = Sb and Bi) with $HBF_4.Et_2O$

The ^{31}P and ^{17}O NMR spectra for protonation of $(TBA)_4[Sb^{III}PW_{11}O_{39}]$ and $(TBA)_4[Bi^{III}PW_{11}O_{39}]$ are given in **Figure 6.3** and **Figure 6.4** respectively. Although, it was not possible to unambiguously assign peaks to SbOW and WOW oxygens, protonolysis of $(TBA)_4[Sb^{III}PW_{11}O_{39}]$ caused a consistent shift in the ^{31}P NMR resonance from -14.22 to -14.02 (0.5 equiv. H^+) to -13.96 ppm (1.0 equiv. H^+) to -13.86 ppm (1.5 equiv. H^+) with a gradual peak broadening. Also, a gradual downfield shift is observed in the terminal W=O ^{17}O

NMR resonance upon protonation indicating decreasing overall negative charge of the polyanion. And in line with previous arguments, the ^{31}P NMR data might suggest protonation at the SbOW sites. Multiple species are observed at 2.0 equiv. H^+.

Protonation of $(TBA)_4[Bi^{III}PW_{11}O_{39}]$ also showed a steady downfield shift in the ^{31}P NMR resonance from -12.54 to -12.43 (at 0.5 equiv. H^+) to -12.33 ppm (at 1.0 equiv. H^+) and -12.11 ppm (at 1.5 equiv. H^+) with a steadily increasing broadening of the peak. Additionally, the ^{17}O NMR spectra showed a disappearance of the BiOW resonance after adding 0.5 equiv. H^+ with a gradual downfield shift of the terminal W=O resonance upon further protonation. These results are consistent with protonation at the BiOW sites and also support earlier proposition for protonation at SbOW sites in $(TBA)_4[Sb^{III}PW_{11}O_{39}]$.

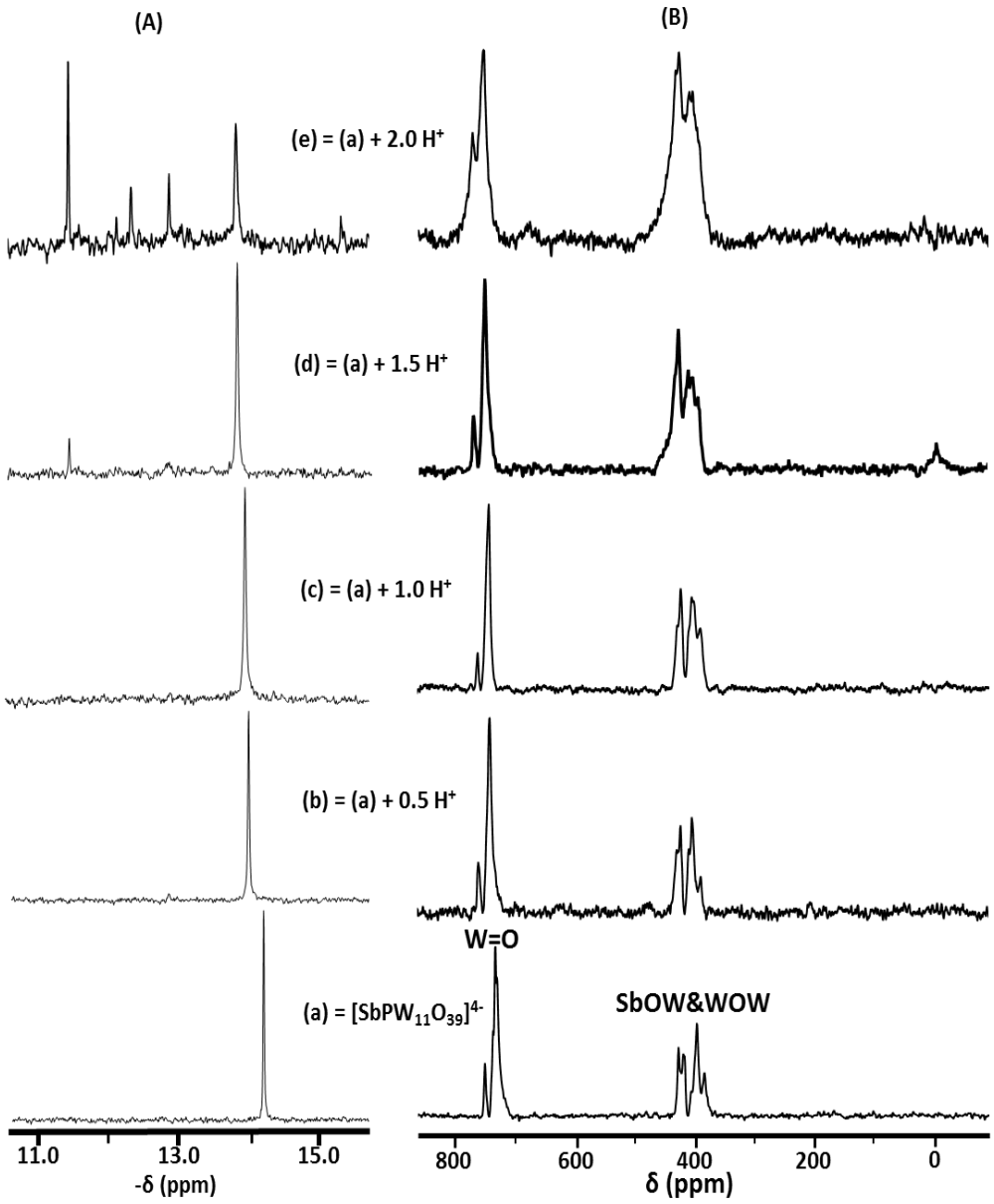

Figure 6.3. (A) ^{31}P NMR and (B) ^{17}O NMR spectra of (a) $(TBA)_4[Sb^{III}PW_{11}O_{39}]$ in CD_3CN plus (b) 0.5 (c) 1.0 (d) 1.5 and (e) 2.0 equiv. H^+.

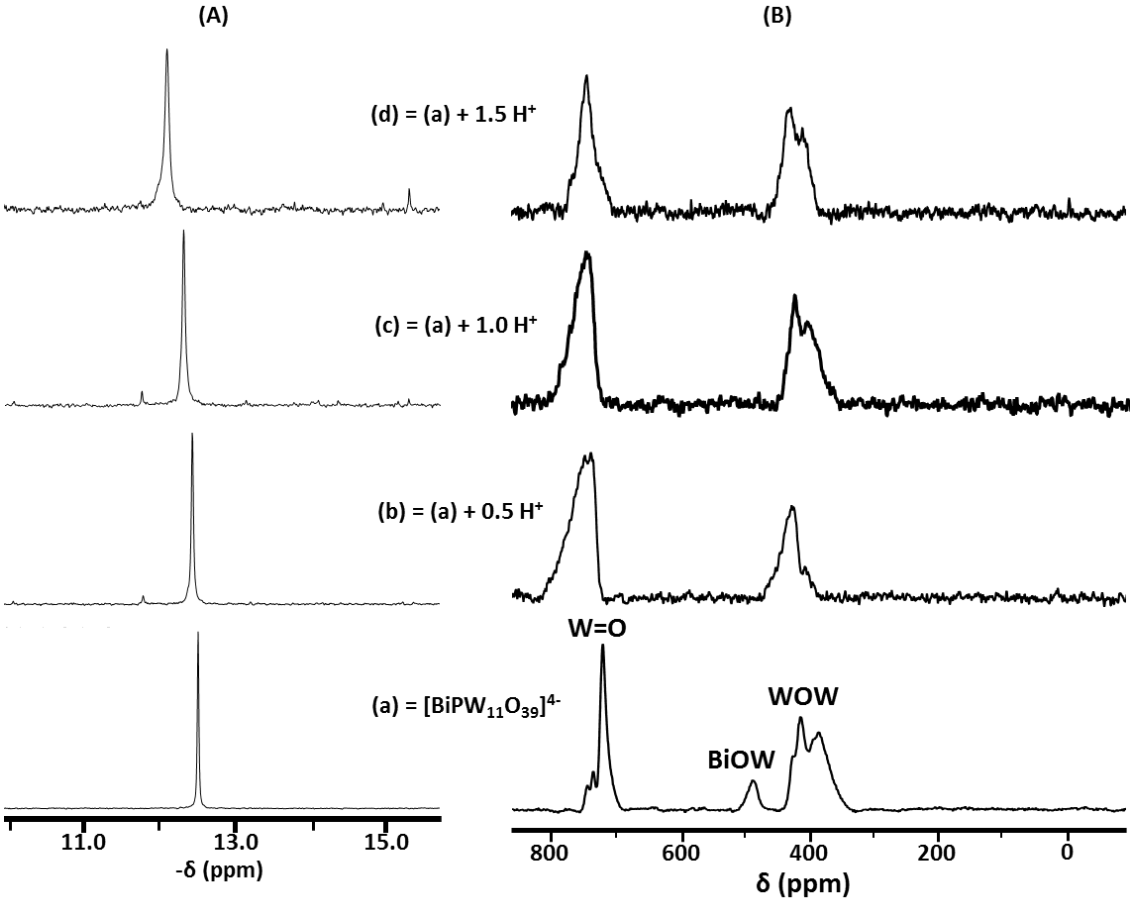

Figure 6.4. (A) ^{31}P NMR and (B) ^{17}O NMR spectra of (a) $(TBA)_4[Bi^{III}PW_{11}O_{39}]$ in CD_3CN plus (b) 0.5 (c) 1.0 and (d) 1.5 equiv. H^+.

6.2.3 Reaction of $(TBA)_5[M^{II}PW_{11}O_{39}]$ (Sn, Pb) with Br_2, I_2 and 1-bromobutane

Possible oxidation of $(TBA)_5[Sn^{II}PW_{11}O_{39}]$ and $(TBA)_5[Pb^{II}PW_{11}O_{39}]$ were investigated by reactions with Br_2, I_2 and 1-bromobutane. The ^{31}P and ^{17}O NMR spectra for the reactions of $(TBA)_5[Sn^{II}PW_{11}O_{39}]$ are given in **Figure 6.5**. It showed that reaction between $(TBA)_5[Sn^{II}PW_{11}O_{39}]$ and I_2 resulted in a downfield ^{31}P NMR resonance at -12.77 and an upfield ^{119}Sn NMR peak at -812 ppm with $^2J_{Sn\text{-}P}$ of 33 Hz whilst reaction with Br_2 gave a downfield ^{31}P peak at -12.85 ppm and ^{119}Sn NMR peak at -643.1 ppm with $^2J_{Sn\text{-}P}$ of 35 Hz. This implies that $(TBA)_5[Sn^{II}PW_{11}O_{39}]$ readily undergoes oxidative addition with Br_2 and I_2 according to **Equations 6.1** and **6.2** to form halogenated tin (IV) products. The ^{31}P NMR parameters of the species compared well with those of $[ClSn^{IV}PW_{11}O_{39}]^{4-}$ (δ = -12.91 and $^2J_{Sn\text{-}P}$ of 37 Hz). No reaction was observed with 1-bromobutane. In contrast, reaction of $(TBA)_5[Pb^{II}PW_{11}O_{39}]$ with I_2 gave multiple species at -11.24, -11.71, -12.40, -12.63 ppm with no evidence of Pb-P coupling whilst reaction with Br_2 gave a major peak at -12.90 (74%) with

$^2J_{Pb\text{-}P}$ = 32 Hz and a broaden peak at -12.14 ppm (26%). This might suggest oxidative addition occurring only with Br_2 as shown in **Equation 6.3**.

$$[Sn^{II}PW_{11}O_{39}]^{5-} + Br_2 \xrightarrow[MeCN]{RT} [BrSn^{IV}PW_{11}O_{39}]^{4-} + Br^- \quad (6.1)$$

$$[Sn^{II}PW_{11}O_{39}]^{5-} + I_2 \xrightarrow[MeCN]{RT} [ISn^{IV}PW_{11}O_{39}]^{4-} + I^- \quad (6.2)$$

$$[Pb^{II}PW_{11}O_{39}]^{5-} + Br_2 \xrightarrow[MeCN]{RT} [BrPb^{IV}PW_{11}O_{39}]^{4-} + Br^- \quad (6.3)$$

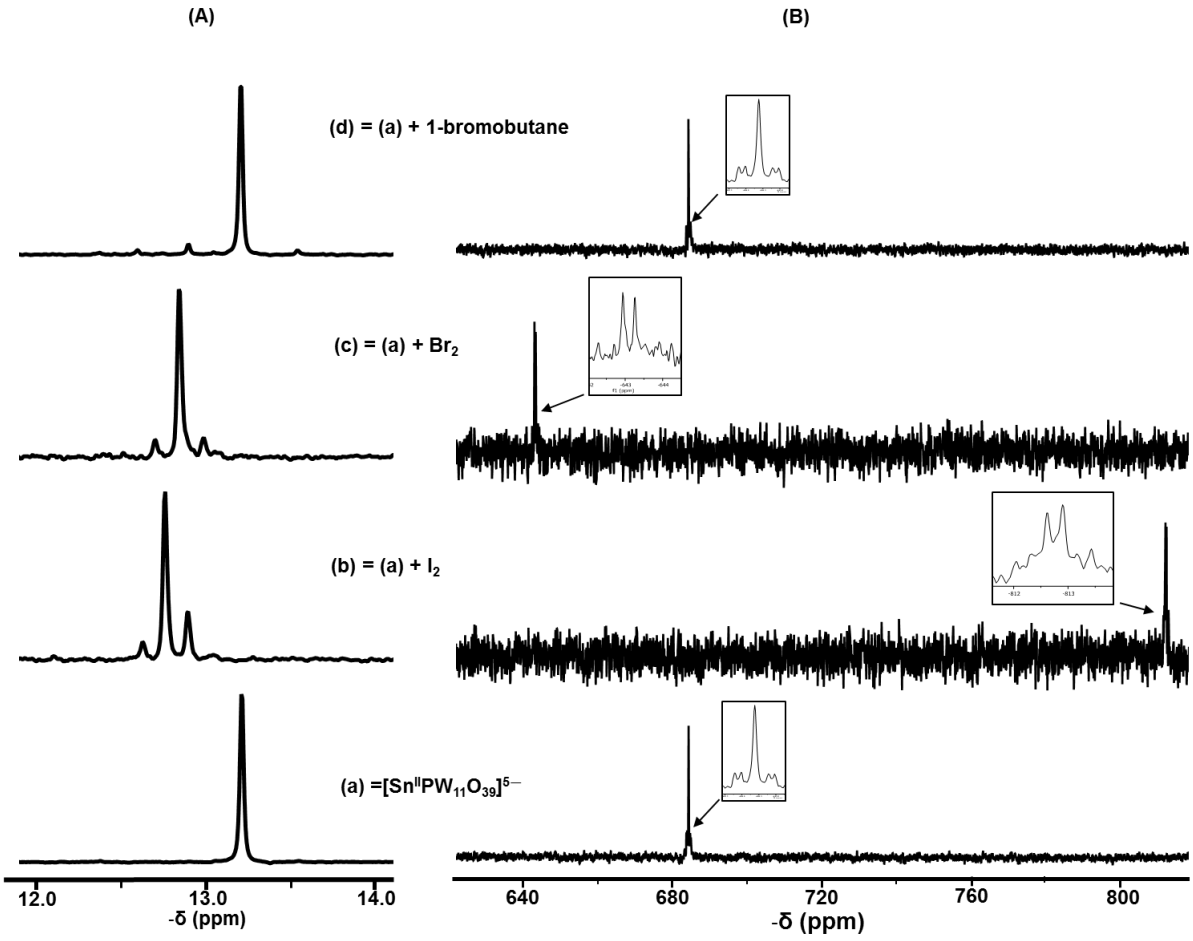

Figure 6.5. (A) ^{31}P NMR and (B) ^{119}Sn NMR spectra of (a) $[Sn^{II}PW_{11}O_{39}]^{5-}$ in CD_3CN plus (b) I_2 (c) Br_2 and (d) 1-bromobutane.

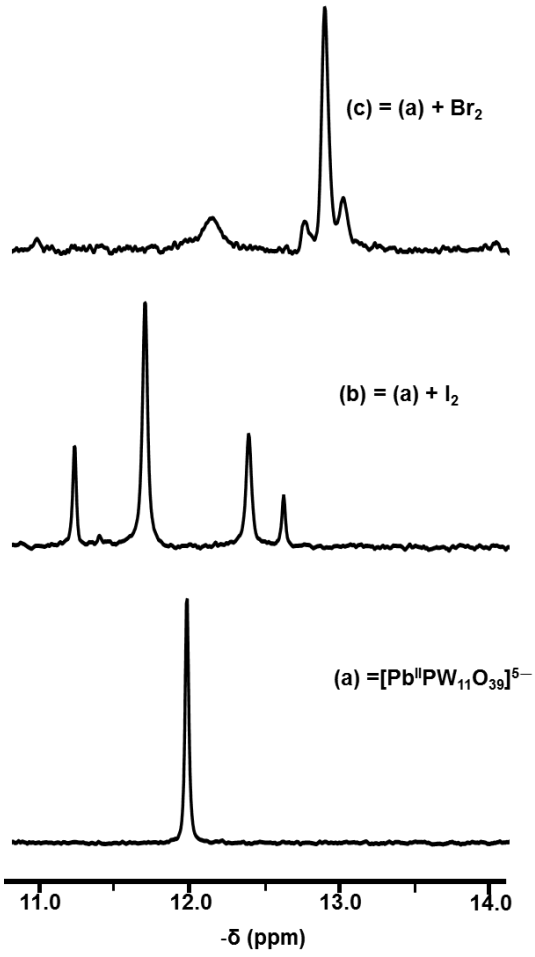

Figure 6.6. ^{31}P NMR spectra of (a) $[Pb^{II}PW_{11}O_{39}]^{5-}$ in CD_3CN plus (b) I_2 and (c) Br_2.

6.2.4 Redox behaviour of $(TBA)_5[M^{II}PW_{11}O_{39}]$ (Sn, Pb) with $(TBA)_3[PMo_{12}O_{40}]$

Previous reductive studies on the synthesis of capped Keggin anions $(TBA)_3[PMo_{12}O_{40}(ML_m)_n]$ *via* reactions of $(TBA)_3[PMo_{12}O_{40}]$ and sodium-mercury amalgam in the presence of metal halides[4] made us wonder whether treatment of $(TBA)_5[Sn^{II}PW_{11}O_{39}]$ and $(TBA)_5[Pb^{II}PW_{11}O_{39}]$ with $(TBA)_3[PMo_{12}O_{40}]$ would result in any electron transfer between the POMs and possibly produce systems where $(TBA)_3[PMo_{12}O_{40}]$ is capped by either $[Sn^{IV}PW_{11}O_{39}]^{4-}$ or $[Pb^{IV}PW_{11}O_{39}]^{4-}$. In the mono-capped POM, $[PMo_{12}O_{40}\{Co(MeCN)_2]^{3-}$, the single Co is bonded to two MeCN ligands and four bridging surface oxygen atoms in one of the six tetragonal sites on the Keggin anion whereas in bicapped systems (e.g. $[PMo_{12}O_{40}Sb_2]^{3-}$) two mutually trans tetragonal sites are occupied.[4] The reaction between $(TBA)_5[Sn^{II}PW_{11}O_{39}]$ and 0.5 mole-equivalents of $(TBA)_3[PMo_{12}O_{40}]$ was aimed at $4e^-$ reduction of $(TBA)_3[PMo_{12}O_{40}]$ and the ^{31}P (**Figure 6.8**) and ^{119}Sn (**Figure 6.9**) NMR spectra showed that the reaction resulted in a dark

blue solution of 2 electron reduced $[PMo_{12}O_{40}]^{5-}$ at -6.92 ppm with oxidation of $[Sn^{II}PW_{11}O_{39}]^{5-}$ to two tin (IV) species (majorly $[(HO)Sn^{IV}PW_{11}O_{39}]^{4-}$ and $[ClSn^{IV}PW_{11}O_{39}]^{4-}$ possibly due to chloride impurities in the starting material). Reaction with 1.0 mole-equivalent of $[PMo_{12}O_{40}]^{3-}$ also resulted in a 2 electron reduced $[PMo_{12}O_{40}]^{5-}$ whereas addition of 2.0 mole-equivalents of $[PMo_{12}O_{40}]^{3-}$ gave a dark green solution containing predominantly the 1 electron reduced $[PMo_{12}O_{40}]^{4-}$ (97%) at -0.31 ppm with only trace amount of 2 electron reduced $[PMo_{12}O_{40}]^{4-}$ (3%) at -7.18 ppm (see **Figure 6.7**). On the other hand, although minor peaks appeared at -1.32 and -2.26 ppm in the ^{31}P NMR spectra (**Figure 6.10**), no change in colour was observed when $(TBA)_5[Pb^{II}PW_{11}O_{39}]$ was treated with up to 2.0 mole-equivalents of $(TBA)_3[PMo_{12}O_{40}]$ suggesting that no electron transfer occurred. $(TBA)_5[Pb^{II}PW_{11}O_{39}]$ was observed to degrade into multiple species when heated at 70 ^oC for 10 mins to facilitate the reaction. Thus, electron transfer to $(TBA)_3[PMo_{12}O_{40}]$ from tin (II) is observed with $(TBA)_5[Sn^{II}PW_{11}O_{39}]$ but not with $(TBA)_5[Pb^{II}PW_{11}O_{39}]$ and this reflects the reduction potentials of Sn vs. Pb.

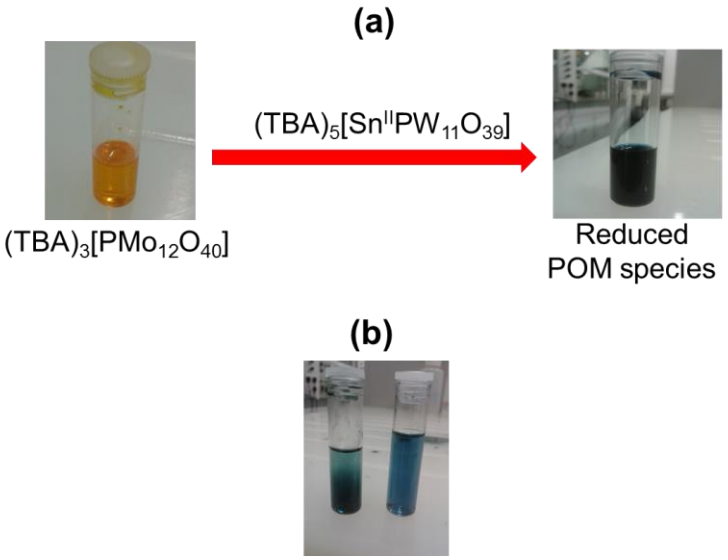

Figure 6.7. (a) Reduction of $(TBA)_3[PMo_{12}O_{40}]$ with $(TBA)_5[Sn^{II}PW_{11}O_{39}]$ and (b) diluted samples of 2-electrons reduced (blue) and 1-electron reduced (green) $(TBA)_3[PMo_{12}O_{40}]$.

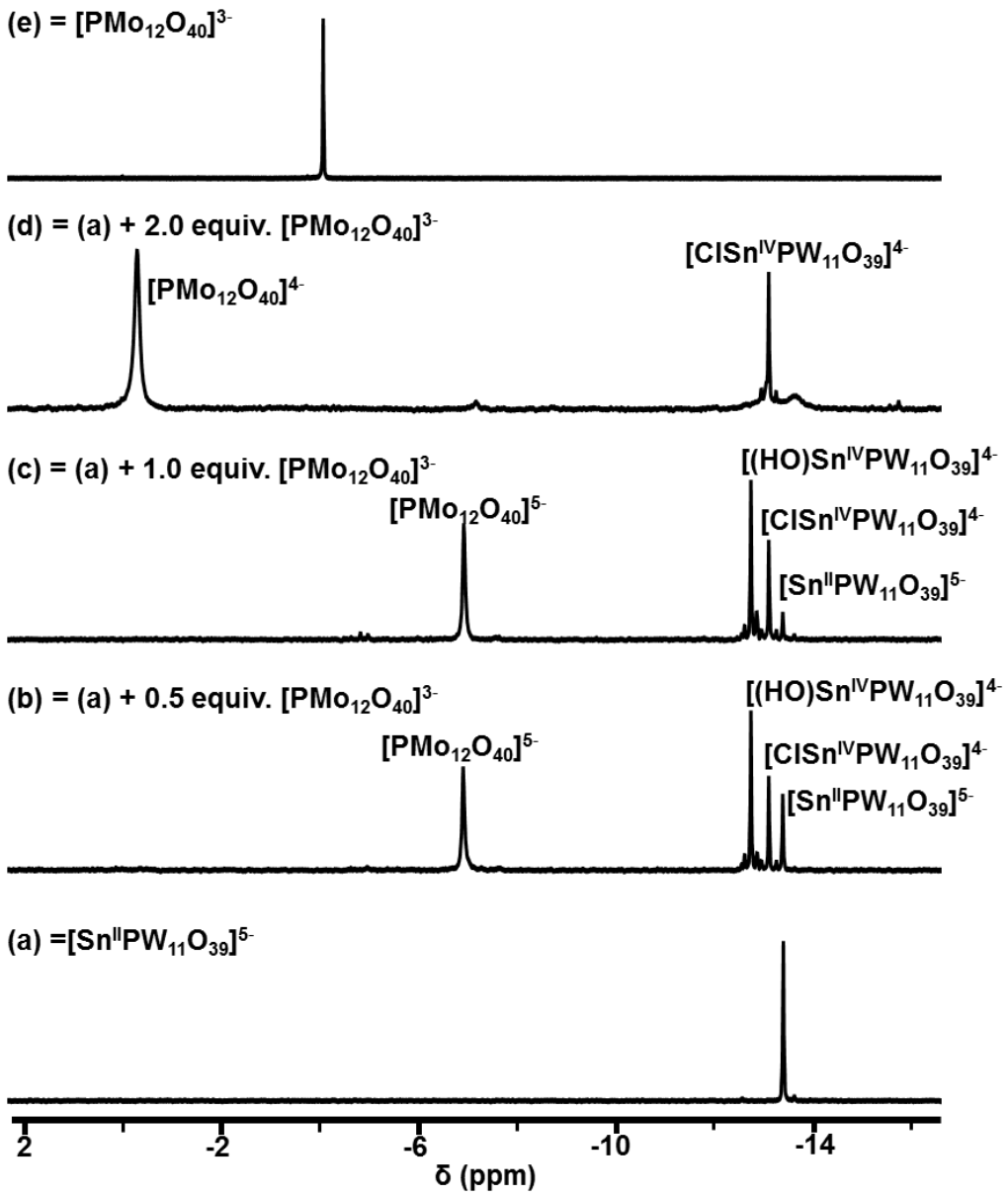

Figure 6.8. ^{31}P NMR spectra of (a) $[Sn^{II}PW_{11}O_{39}]^{5-}$ in CD_3CN plus (b) 0.5 (c) 1.0 and (d) 2.0 equiv. $[PMo_{12}O_{40}]^{3-}$ and (e) pure $[PMo_{12}O_{40}]^{3-}$.

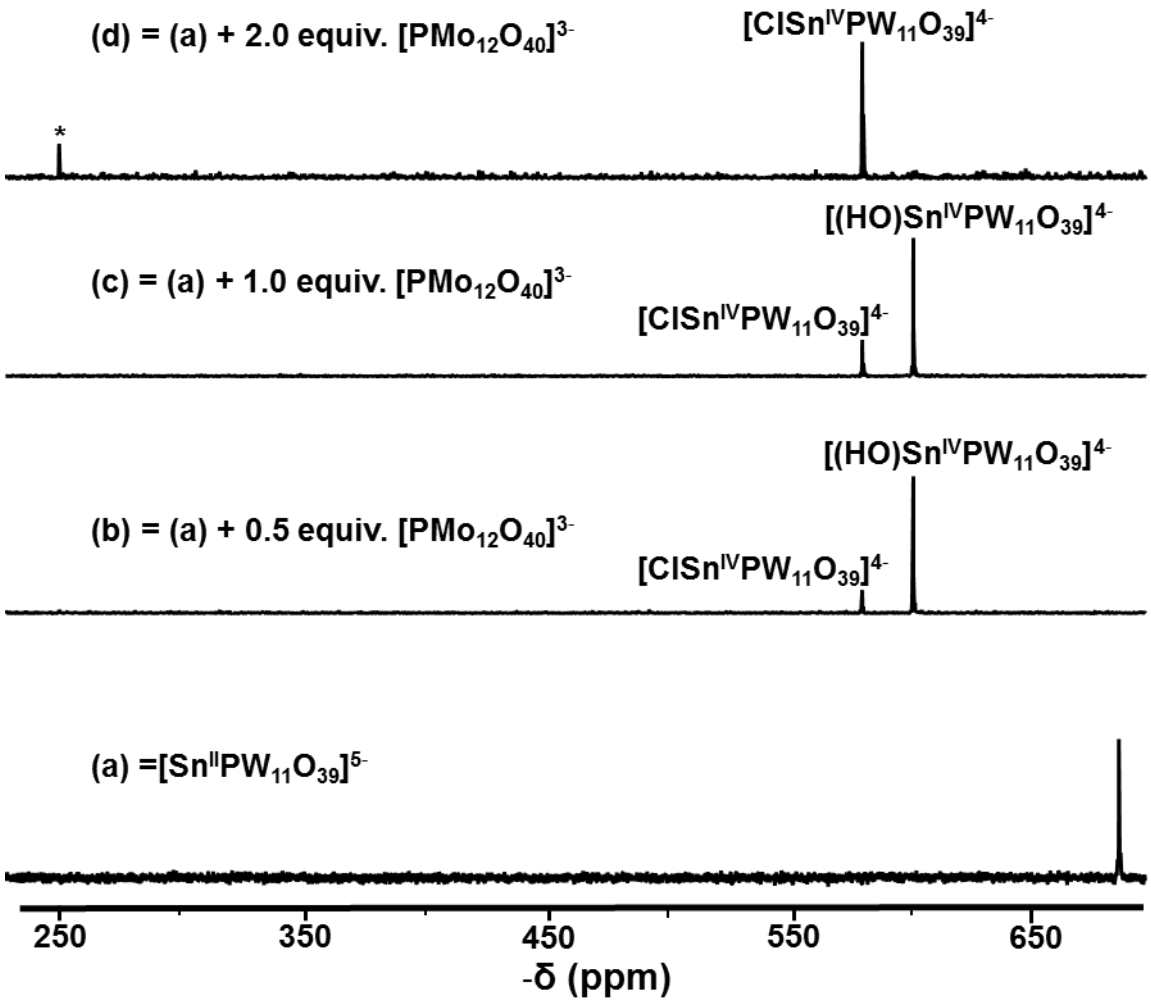

Figure 6.9. ^{119}Sn NMR spectra of (a) $[Sn^{II}PW_{11}O_{39}]^{5-}$ in CD_3CN plus (b) 0.5 (c) 1.0 and (d) 2.0 equiv. $[PMo_{12}O_{40}]^{3-}$. Peak asterisked was not assigned.

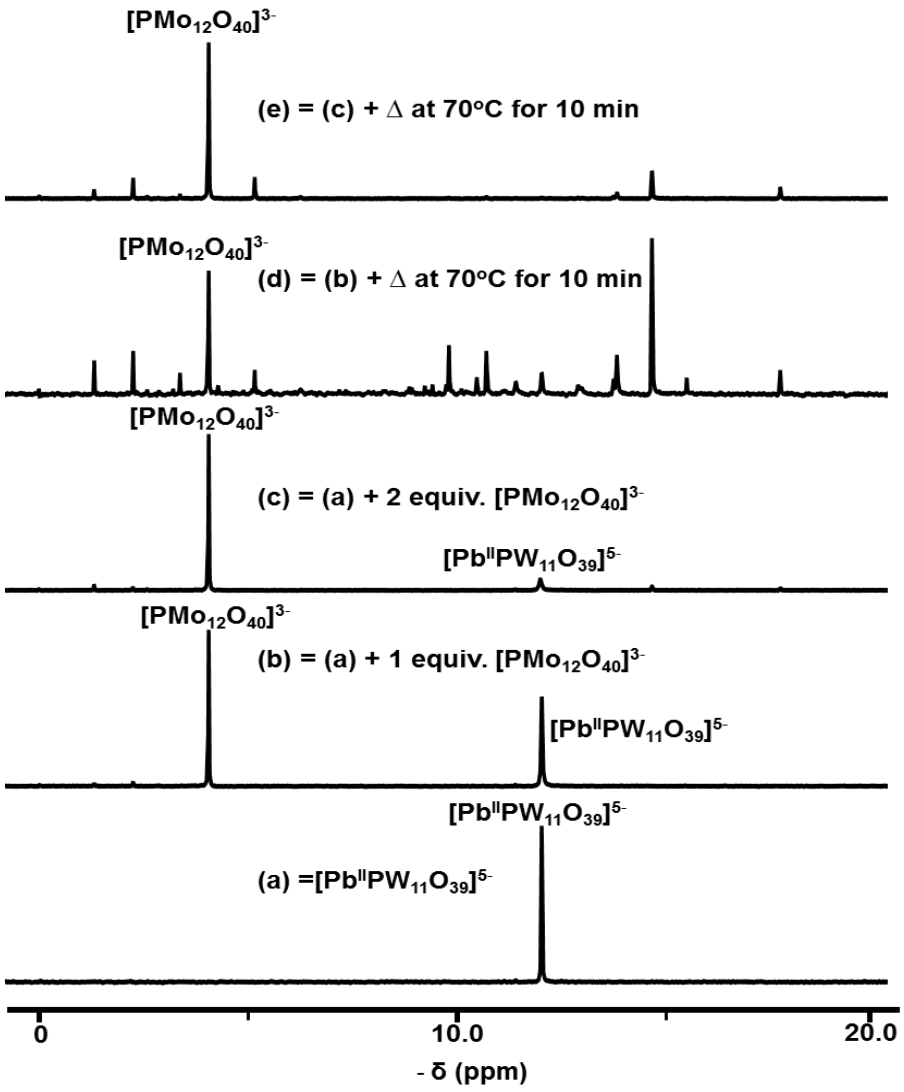

Figure 6.10. ^{31}P NMR spectra of (a) $[Pb^{II}PW_{11}O_{39}]^{5-}$ in CD_3CN plus (b) 1.0 and (c) 2.0 equiv. $[PMo_{12}O_{40}]^{3-}$ (d) (b) after heating at 70 °C for 10 min. and (e) after heating at 70 °C for 10 min.

6.2.5 Reaction of $(TBA)_5[SnPW_{11}O_{39}]$ with methanolic NaOMe

$(TBA)_5[SnPW_{11}O_{39}]$ was treated with methanolic MeONa in a bid to further confirm the presence or absence of chloride ligand on the polyanion. MeO- is expected to substitute any chloride ligand on the POM to give the methoxyl derivative as shown in **Equation 6.4**.

$$?[ClSnPW_{11}O_{39}]^{6-} + NaOMe \longrightarrow [(MeO)SnPW_{11}O_{39}]^{6-} + NaCl \qquad (6.4)$$

Treatment of $(TBA)_5[SnPW_{11}O_{39}]$ with methanolic NaOMe did not result in any change in the colour of the solution. However, in addition to trace peaks at -10.41 and -12.16 ppm, there were movements in the NMR chemical shifts. The ^{31}P NMR resonance moved from -13.23 to

-13.08 ppm (**Figure 6.11**) while ^{119}Sn NMR resonance moved from -684 to -700 ppm (**Figure 6.12**). When the solution was worked up, FT-IR, ^{1}H, ^{13}C (not shown), ^{31}P and ^{119}Sn NMR (**Figure 6.11** and **Figure 6.12**) of the isolated product showed no evidence of attachment of methoxido group to the POM indicating that the starting material was unchanged and that only some degradation products were formed. The change in chemical shift was therefore due to the magnetic susceptibility of the solvent. This reaction further supports the proposition that no chloride ligand is attached to tin (II) in the POM. These degradation products were also observed when $(TBA)_5[SnPW_{11}O_{39}]$ was treated with methanolic TBAOH.

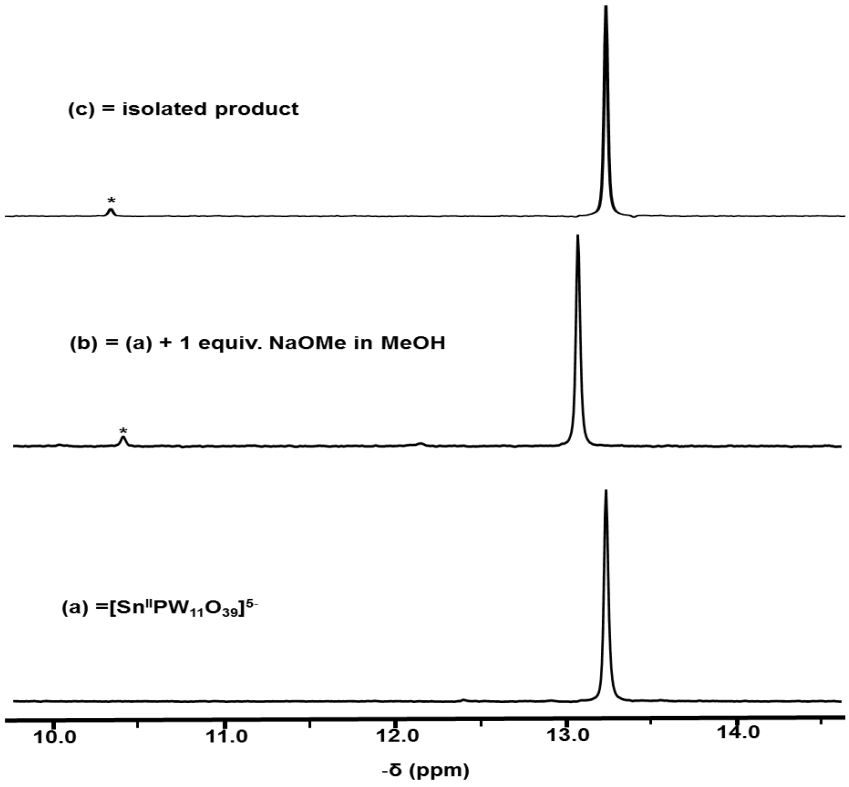

Figure 6.11. ^{31}P NMR spectra of (a) $(TBA)_5[Sn^{II}PW_{11}O_{39}]$ in CD_3CN plus (b) 1 equiv. NaOMe in MeOH and (c) isolated product of reaction. Peaks asterisked are species due to degradation of $(TBA)_5[Sn^{II}PW_{11}O_{39}]$ by NaOMe.

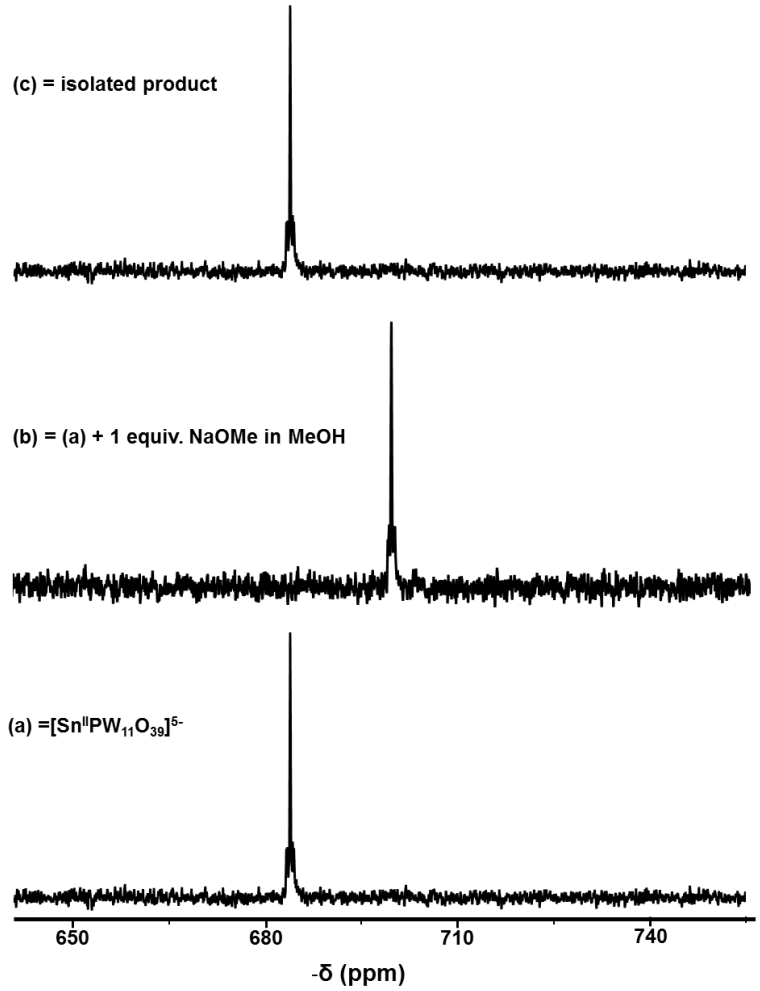

Figure 6.12. ^{119}Sn NMR spectra of (a) (TBA)$_5$[Sn^{II}PW$_{11}$O$_{39}$] in CD$_3$CN plus (b) 1 equiv. NaOMe in MeOH and (c) isolated product of reaction.

6.2.6 Reaction of (TBA)$_5$[SnPW$_{11}$O$_{39}$] with HCl

Treatment of (TBA)$_5$[SnPW$_{11}$O$_{39}$] with aqueous HCl was observed to result in the growth of a peak at -12.91 assigned to [ClSn^{IV}PW$_{11}$O$_{39}$]$^{4-}$ possibly due to oxidative addition. After 3 equiv. of HCl only ~34% of [SnPW$_{11}$O$_{39}$]$^{5-}$ was left in solution with no evidence of degradation to [PW$_{12}$O$_{40}$]$^{3-}$ (**Figure 6.13**). When compared with protonation with HBF$_4$.Et$_2$O in acetonitrile where the POM started degrading after 1.0 mole-equivalent of H$^+$, it demonstrates the stronger acidity of HBF$_4$.Et$_2$O in acetonitrile than HCl in water.

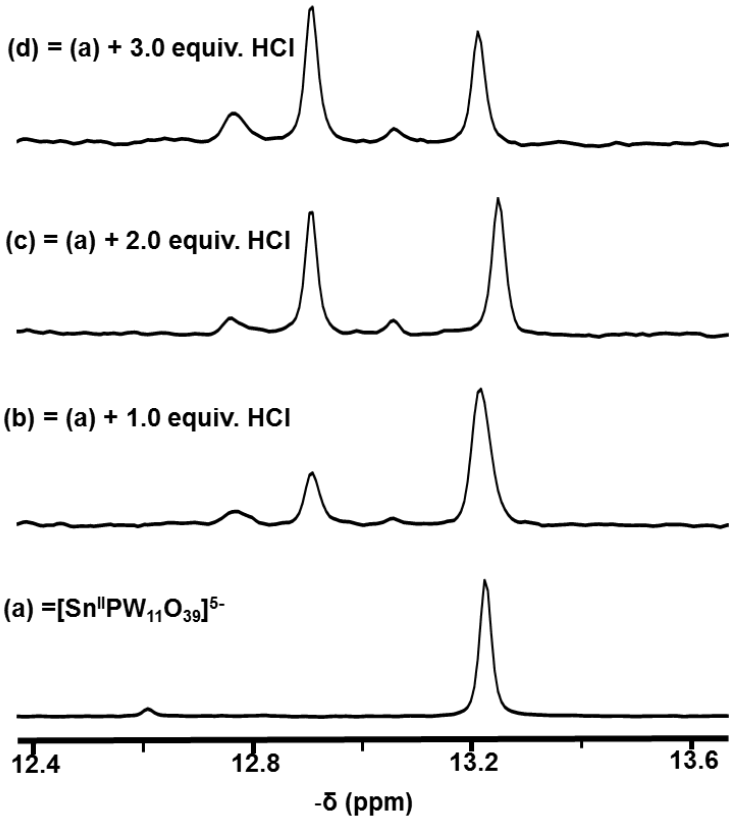

Figure 6.13. ^{31}P NMR spectra of (a) (TBA)$_5$[Sn^{II}PW$_{11}$O$_{39}$] in CD$_3$CN plus (b) 1.0 (c) 2.0 and (c) 3.0 equiv. HCl.

6.3 Conclusions

This chapter has provided evidence supporting protonation of the MOW sites in $[M^{II}PW_{11}O_{39}]^{5-}$ (M = Sn, Pb) and $[M^{III}PW_{11}O_{39}]^{4-}$ (M = Sb and Bi). It has also shown that $[Sn^{II}PW_{11}O_{39}]^{5-}$ readily undergoes oxidative addition with Br_2, I_2 and aqueous HCl to form halogenated tin (IV) products whilst $[Pb^{II}PW_{11}O_{39}]^{5-}$ only undergoes oxidative addition with Br_2. Furthermore, electron transfer was observed from $[Sn^{II}PW_{11}O_{39}]^{5-}$ to $[PMo_{12}O_{40}]^{3-}$ to form only 1 and 2 electrons reduced phosphomolybdates ($[PMo_{12}O_{40}]^{4-}$ and $[PMo_{12}O_{40}]^{5-}$). This was not observed with $[Pb^{II}PW_{11}O_{39}]^{5-}$.

REFERENCES

1. J. Medina-Ramos, R. C. Pupillo, T. P. Keane, J. L. DiMeglio and J. Rosenthal, *J. Am. Chem. Soc.*, 2015, **137**, 5021-5027.
2. J. E. Pander, M. F. Baruch and A. B. Bocarsly, *ACS Catal.*, 2016, **6**, 7824-7833.
3. M. Pascual-Borras, X. Lopez, A. Rodriguez-Fortea, R. J. Errington and J. M. Poblet, *Chem. Sci.*, 2014, **5**, 2031-2042.
4. R. Bakri, A. Booth, G. Harle, P. S. Middleton, C. Wills, W. Clegg, R. W. Harrington and R. J. Errington, *Chem. Commun.*, 2012, **48**, 2779-2781.

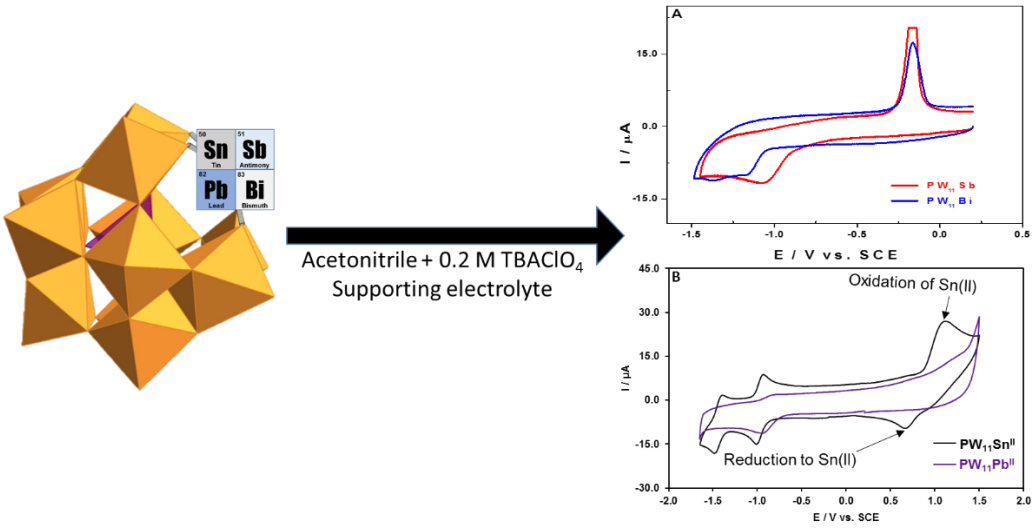

Chapter 7

Electrochemical Behaviour of Post-Transition Metal Substituted Keggin Polyoxotungstates

This chapter describes results from a COST Action Short-Term Scientific Mission (STSM) visit to the team of Prof. Pedro de Oliveira and Dr. Israel M. Mbomekalle at LCP, Universite Paris-Sud, Orsay, France. The group has developed a long-standing reputation in the electrochemistry and photochemistry of polyoxometalates. This collaborative work was therefore first aimed at acquainting me with best practices in non-aqueous POM electrochemistry. Additionally, it was meant to facilitate joint studies for a better understanding of the solution electrochemistry of a range of mono-substituted Keggin POMs in non-aqueous media.

7. Electrochemical Behaviour of Post-Transition Metal Substituted Keggin Polyoxotungstates

7.1 Introduction

Mono-substituted Keggin polyoxometalates (POMs) have been studied greatly because of their broad applications in fields such as catalysis, energy systems, nanoscience and medicine.[1-3] Electrochemical studies on these POMs have mostly been on aqueous solutions[4-6] with only a few reports in non-aqueous media.[7-9] Our non-aqueous studies of POMs is partly aimed at developing a fuller understanding of their non-aqueous redox chemistry in order to tune their properties for applications in catalysis and molecular nanoscience. A report in 2015 showed that inexpensive post-transition metal (Sn^{2+}, Pb^{2+}, Sb^{3+} and Bi^{3+}) salts in the presence of a promoter (1,3-dialkyl substituted imidazolium based ionic liquid) served as efficient electrocatalysts for CO_2 reduction to CO in MeCN.[10] Recently also, the mechanisms of aqueous CO_2 reduction on post-transition metal electrodes were discussed.[11] The mechanisms were proposed to involve interactions of CO_2 with metal oxide surfaces for tin and indium electrodes and pure metallic sites for lead and bismuth electrodes.[11-13] As shown in **Equations 1** to **4**, the overall mechanism for lead electrode involves (1) protonation of the lead oxide surface, (2) reduction of the proton to an adsorbed hydrogen atom and (3) reaction of the adsorbed hydrogen atom with other species. This reaction is likely the coupling of the surface hydrogen either with another surface hydrogen to form H_2 gas through the Volmer reaction or reaction of the surface hydrogen with CO_2 to form formate. It was proposed that reduction of CO_2 most likely occurred at a metallic site, while the formation of hydrogen occurred at the oxide surface.[11]

$$PbO + H^+ \rightleftharpoons PbOH^+ \quad (1)$$

$$PbOH^+ + e^- \longrightarrow PbO—H_{ads} \quad (2)$$

$$PbO—H_{ads} + PbO—H_{ads} + e^- \longrightarrow PbO + H_2 \quad (3)$$

$$PbO—H_{ads} + CO_2 + e^- \longrightarrow PbO + HCOO^- \quad (4)$$

The proposed mechanism for Bismuth electrode in contrast, involves (1) reduction of a proton to an adsorbed hydrogen atom at a bare metallic site at the electrode surface, (2) an

electrochemical reaction of the surface hydrogen either with another surface hydrogen to form H_2 *via* the Volmer reaction or with CO_2 and a proton to form formate as shown in **Equations 5** to **7** with both reduction of H^+ to H_2 and the reduction of CO_2 to formate occurring at metallic bismuth sites at the electrode surface.

$$Bi^0 + H^+ + e^- \rightleftharpoons Bi^0—H_{ads} \quad (5)$$

$$Bi^0—H_{ads} + Bi^0—H_{ads} \longrightarrow 2Bi^0 + H_2 \quad (6)$$

$$Bi^0—H_{ads} + CO_2 + e^- \longrightarrow Bi^0 + HCOO^- \quad (7)$$

These studies inspired our interest to investigate the non-aqueous electrochemistry of these post-transition metal derivatives of the monosubstituted Keggin POMs. POMs are historically known to show a diverse redox chemistry.[14-16] And understanding the redox properties of the post-transition metal derivatives of monosubstituted Keggin POMs in acetonitrile could lead to their potential application as electrocatalysts for CO_2 reduction based on **Scheme 7.1**. In this regard, the electrochemistry in acetonitrile of a series of post-transition metal mono-substituted POMs, $(TBA)_4[ClSn^{IV}PW_{11}O_{39}]$ (**$PW_{11}SnCl$**); $(TBA)_4[(HO)Sn^{IV}PW_{11}O_{39}]$ (**$PW_{11}SnOH$**); $(TBA)_5[Sn^{II}PW_{11}O_{39}]$ (**$PW_{11}Sn$**); $(TBA)_5[Pb^{II}PW_{11}O_{39}]$ (**$PW_{11}Pb$**); $(TBA)_4[Sb^{III}PW_{11}O_{39}]$ (**$PW_{11}Sb$**) and $(TBA)_4[Bi^{III}PW_{11}O_{39}]$ (**$PW_{11}Bi$**) in relation to the well-known $(TBA)_3[PW_{12}O_{40}]$ (**PW_{12}**), $(TBA)_4[H_3PW_{11}O_{39}]$ (**$PW_{11}H_3$**) and $(TBA)_6[NaPW_{11}O_{39}]$ (**$PW_{11}Na$**) are discussed herein.

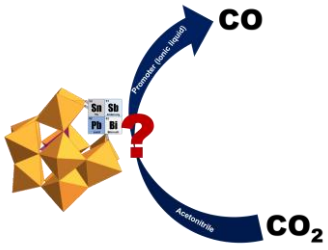

Scheme 7.1. Possible application of post-transition metal substituted POMs in the reduction of CO_2 to CO.

7.2 Results and Discussion

7.2.1 Cyclic voltammograms of $(TBA)_3[PW_{12}O_{40}]$ and $(TBA)_4H_3[PW_{11}O_{39}]$

Figure 7.1 shows three reduction peaks (E_{pc}) for $(TBA)_3[PW_{12}O_{40}]$ in acetonitrile at -0.328, -0.852 and -1.560 V vs. SCE and three oxidation peaks (E_{pa}) at -1.464, -0.776 and -0.256 V vs.

SCE associated with three reversible processes. The redox waves for $(TBA)_4H_3[PW_{11}O_{39}]$ in acetonitrile as expected were shifted to more negative potential values. This has been attributed to the increase in the overall negative charge of the polyanion, $(TBA)_4H_3[PW_{11}O_{39}]$.[9,17] The first redox couple of $(TBA)_4H_3[PW_{11}O_{39}]$ appeared at a half wave potential of -0.828 V vs. SCE with a separation of 75 mV. Two other redox couples at -1.356 V with a separation of 117 mV and -1.572 V vs. SCE with a separation of 99 mV were observed for $(TBA)_4H_3[PW_{11}O_{39}]$ within the potential range studied.

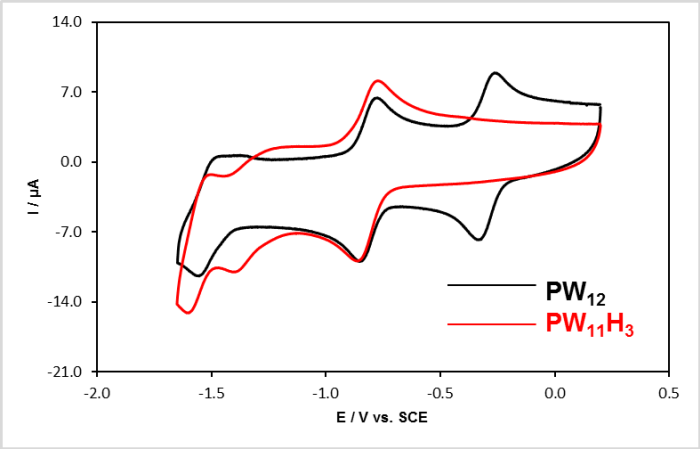

Figure 7.1. Cyclic voltammograms of PW_{12} (black) and $PW_{11}H_3$ (red) in acetonitrile + 0.2 M $TBAClO_4$; POM concentrations, 0.82 mM (PW_{12}) and 0.72 mM ($PW_{11}H_3$). Scan rate 100 mV.s^{-1}. Glassy carbon working electrode; Pt wire auxiliary electrode; SCE reference electrode.

7.2.2 Cyclic voltammograms of $(TBA)_4H_3[PW_{11}O_{39}]$ and $(TBA)_6[NaPW_{11}O_{39}]$

In contrast to $(TBA)_4H_3[PW_{11}O_{39}]$, which exhibited four reduction peaks (E_{pc}) at -0.87, -1.42, -1.62 and -2.19 V vs. SCE and five oxidation peaks (E_{pa}) at -0.79, -0.88, -1.31, -1.52 and -1.99 V vs. SCE, $(TBA)_6[NaPW_{11}O_{39}]$ in acetonitrile only showed two reduction peaks (E_{pc}) at -1.58 and -2.31 V vs. SCE and two oxidations peaks (E_{pa}) at -1.40 and -2.01 V vs. SCE (see **Figure 7.2**). The CV of $(TBA)_6[NaPW_{11}O_{39}]$ was generally not well defined and no concrete reason is available yet as to why this is. But it might be linked to the sodium in the lacuna. $(TBA)_6[NaPW_{11}O_{39}]$ was earlier (Chapter 3) observed to degrade easily in the presence of protons and might exhibit similar behavior with electrons. However, the observed waves for $(TBA)_6[NaPW_{11}O_{39}]$ were generally shifted to more negative potentials than those of $(TBA)_4H_3[PW_{11}O_{39}]$ possibly due to the presence of protons in $(TBA)_4H_3[PW_{11}O_{39}]$ and the higher overall negative charge of $(TBA)_6[NaPW_{11}O_{39}]$.[9]

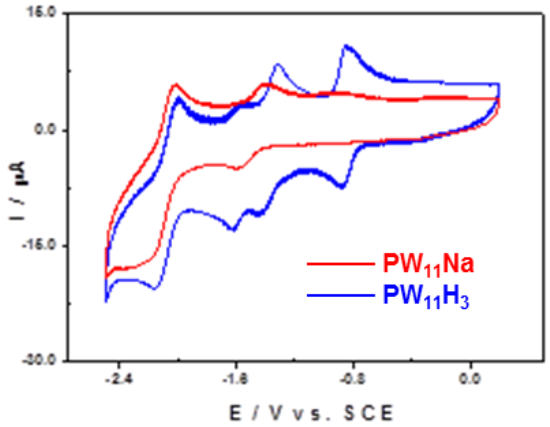

Figure 7.2. Cyclic voltammograms of $PW_{11}Na$ (red) and $PW_{11}H_3$ (blue) in acetonitrile + 0.2 M $TBAClO_4$; POM concentration, 0.72 mM. Scan rate 100 $mV.s^{-1}$. Glassy carbon working electrode; Pt wire auxiliary electrode; SCE reference electrode.

7.2.3 Cyclic voltammograms of $(TBA)_4H_3[PW_{11}O_{39}]$ and $(TBA)_5[PbPW_{11}O_{39}]$

Only two reduction waves were observed for $(TBA)_5[PbPW_{11}O_{39}]$ in acetonitrile within the scan range studied and these were shifted to more negative potentials (E_{pc} = -0.99 V and -1.72 V vs. SCE), thus indicating that $(TBA)_4H_3[PW_{11}O_{39}]$ was more readily reduced than $(TBA)_5[PbPW_{11}O_{39}]$ probably due to the lower overall negative charge of -4 in $(TBA)_4H_3[PW_{11}O_{39}]$ i.e. $H_3[PW_{11}O_{39}]^{4-}$ vs. $[PbPW_{11}O_{39}]^{5-}$. This agrees with the observations of Couto *et al*.[18] No waves attributable to redox processes involving Pb were observed within the scan region (**Figure 7.3**).

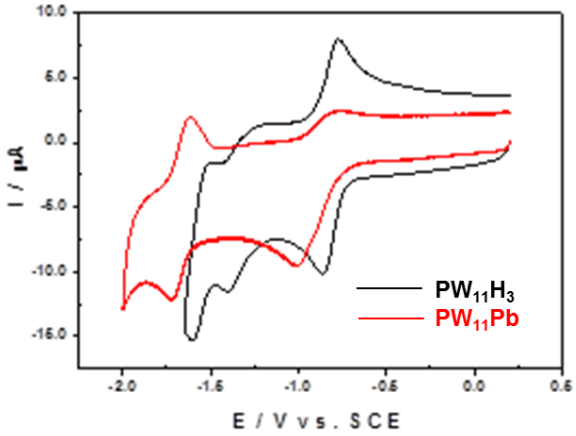

Figure 7.3. Cyclic voltammograms of $PW_{11}H_3$ (black) and $PW_{11}Pb$ (red) in acetonitrile + 0.2 M $TBAClO_4$; POM concentrations, 0.72 mM ($PW_{11}H_3$) and 0.45 mM ($PW_{11}Pb$). Scan rate 100 $mV.s^{-1}$. Glassy carbon working electrode; Pt wire auxiliary electrode; SCE reference electrode.

7.2.4 Cyclic voltammograms of $(TBA)_4H_3[PW_{11}O_{39}]$, $(TBA)_4[ClSnPW_{11}O_{39}]$ and $(TBA)_4[(HO)SnPW_{11}O_{39}]$

Figure 7.4 shows a similar pattern for the first redox waves of $(TBA)_4H_3[PW_{11}O_{39}]$, $(TBA)_4[ClSnPW_{11}O_{39}]$ and $(TBA)_4[(HO)PW_{11}O_{39}]$ in acetonitrile with the waves of $(TBA)_4[(L)SnPW_{11}O_{39}]$ (L = Cl; OH) shifted to more negative potentials. The order of reduction peak potentials (E_{pc}) for the sole wave observed under these experimental conditions was $(TBA)_4H_3[PW_{11}O_{39}]$ less negative than $(TBA)_4[ClSnPW_{11}O_{39}]$, which was less negative than $(TBA)_4[(HO)SnPW_{11}O_{39}]$ suggesting both heteroatom and ligand effects on the redox potentials. As in the case of Pb, no redox wave was observed for Sn within the scan region. This is consistent with the observations of Pope.[17]

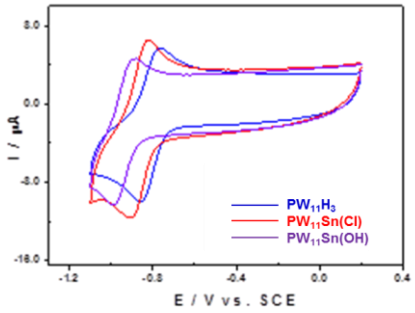

Figure 7.4. Cyclic voltammograms of $PW_{11}H_3$ (blue) $PW_{11}Sn(Cl)$ (red) and $PW_{11}Sn(OH)$ (purple) in acetonitrile + 0.2 M $TBAClO_4$; POM concentrations, 0.72 mM $[PW_{11}H_3]$, 0.44 mM $[PW_{11}Sn(Cl)]$ and 0.43 mM $[PW_{11}Sn(OH)]$. Scan rate 100 $mV.s^{-1}$. Glassy carbon working electrode; Pt wire auxiliary electrode; SCE reference electrode.

7.2.5 Cyclic voltammograms of $(TBA)_4H_3[PW_{11}O_{39}]$, $(TBA)_4[SbPW_{11}O_{39}]$ and $(TBA)_4[BiPW_{11}O_{39}]$

The first reduction peak of $(TBA)_4[SbPW_{11}O_{39}]$ in acetonitrile was observed at E_{pc} = -1.00 V vs. SCE while an oxidation peak was observed at E_{pa} = -0.16 V vs. SCE. (**Figure 7.5A)**. The peaks were irreversible and the reduction potential occurred at a more negative potential than was observed for $(TBA)_4H_3[PW_{11}O_{39}]$. In contrast to the CVs of $(TBA)_4H_3[PW_{11}O_{39}]$, $(TBA)_5[PbPW_{11}O_{39}]$, $(TBA)_4[ClSnPW_{11}O_{39}]$ and $(TBA)_4[(HO)SnPW_{11}O_{39}]$, no well-defined redox waves that could be assigned to the tungsten addenda were observed. A further irreversible oxidation peak at E_{pa} = 0.99 V vs. SCE and reduction peak at 0.059 V vs. SCE (**Figure 7.5C**) was observed upon scanning to a more positive potential. It is not clear why no well-defined tungsten redox waves were observed as the tungsten cage was expected to be more readily reduced than the antimony heterometal based on standard redox potentials.[19] However, the

CVs might suggest an initial irreversible reduction of Sb^{3+} to Sb^{0}, oxidation of Sb^{0} to Sb^{3+} and further oxidation to Sb^{5+}. This might result from decomposition of the POM to give Sb^{3+} ions which then undergoes the redox processes in solution. The CVs of $(TBA)_4[SbPW_{11}O_{39}]$ and $(TBA)_4[BiPW_{11}O_{39}]$ (**Figure 7.6**) showed a similar redox pattern with the first reduction potential of $(TBA)_4[BiPW_{11}O_{39}]$ (E_{pc} = -1.17 V vs. SCE) occurring at a more negative potential than $(TBA)_4[SbPW_{11}O_{39}]$ (E_{pc} = -1.00 V vs. SCE). Furthermore, $(TBA)_4[BiPW_{11}O_{39}]$ did not show a further oxidation of Bi^{3+} as was seen in $(TBA)_4[SbPW_{11}O_{39}]$ within the scan region.

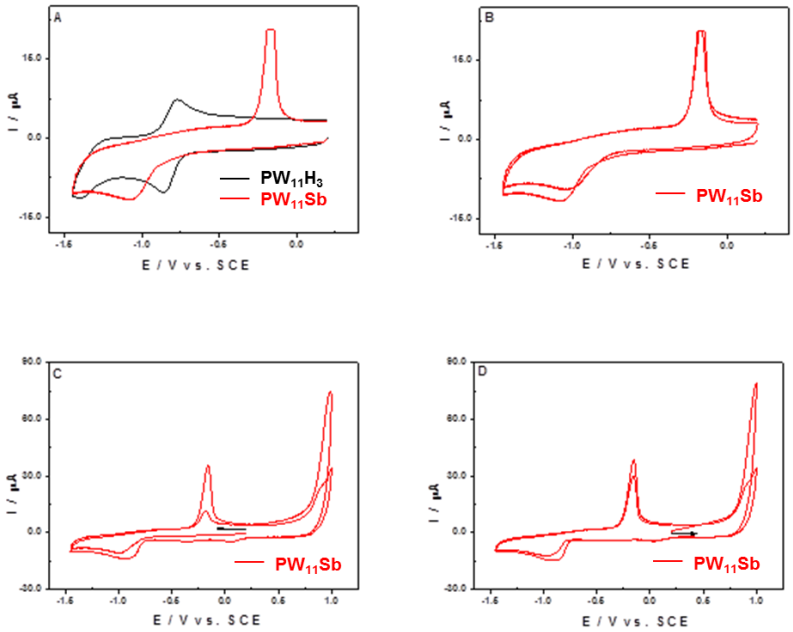

Figure 7.5. Cyclic voltammograms in acetonitrile + 0.2 M $TBAClO_4$ of (A) $PW_{11}Sb$ (red) and $PW_{11}H_3$ (black) (B) $PW_{11}Sb$ after 2 cycles (C) $PW_{11}Sb$ after 2 cycles starting with the cathodic side and (D) $PW_{11}Sb$ after 2 cycles starting with the anodic side; POM concentrations, 0.72 mM (PW_{11}), 0.42 mM ($PW_{11}Sb$). Scan rate 100 $mV.s^{-1}$. Glassy carbon working electrode; Pt wire auxiliary electrode; SCE reference electrode.

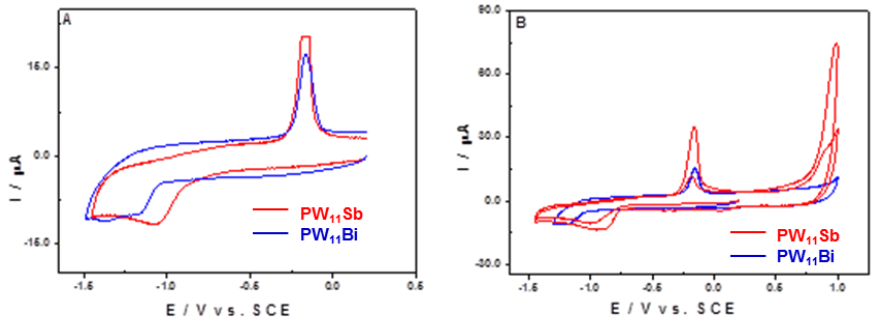

Figure 7.6. Cyclic voltammograms of $PW_{11}Sb$ (red) and $PW_{11}Bi$ (blue) in acetonitrile + 0.2 M $TBAClO_4$; POM concentrations, 0.42 mM ($PW_{11}Sb$), 0.44 mM ($PW_{11}Bi$). Scan rate 100 $mV.s^{-1}$. Glassy carbon working electrode; Pt wire auxiliary electrode; SCE reference electrode.

7.2.6 Cyclic voltammograms of $(TBA)_5[Sn^{II}PW_{11}O_{39}]$, $(TBA)_5[Pb^{II}PW_{11}O_{39}]$ and $(TBA)_4[(HO)Sn^{IV}PW_{11}O_{39}]$

$(TBA)_5[Sn^{II}PW_{11}O_{39}]$ in acetonitrile showed three redox waves at -0.98, -1.44 and -2.12 V vs. SCE with separations of 72, 80 and 128 mV respectively. These were assigned to quasi-reversible processes associated with the tungsten addenda. An irreversible oxidation peak (E_{pa}) at 1.12 V vs. SCE was assigned to the oxidation of Sn(II) to Sn(IV) while a reduction peak (E_{pc}) at 0.68 V vs. SCE was assigned to the subsequent reduction of Sn(IV) back to Sn(II) (see **Figure 7.7**). It is worth noting that no such peaks associated with reduction or oxidation of heterometals were observed for $(TBA)_5[PbPW_{11}O_{39}]$ and $(TBA)_4[(HO)SnPW_{11}O_{39}]$ (**Figure 7.8**).

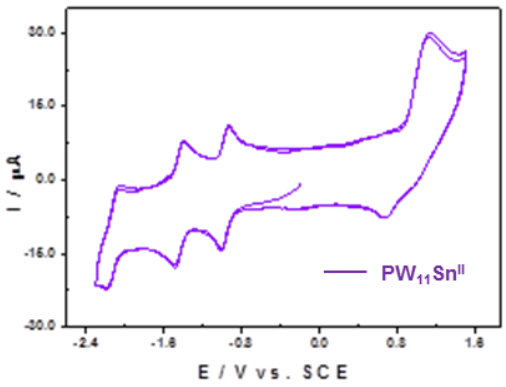

Figure 7.7. Cyclic voltammograms of $PW_{11}Sn^{II}$ in acetonitrile + 0.2 M $TBAClO_4$; POM concentration, 0.70 mM. Scan rate 100 $mV.s^{-1}$. Glassy carbon working electrode; Pt wire auxiliary electrode; SCE reference electrode.

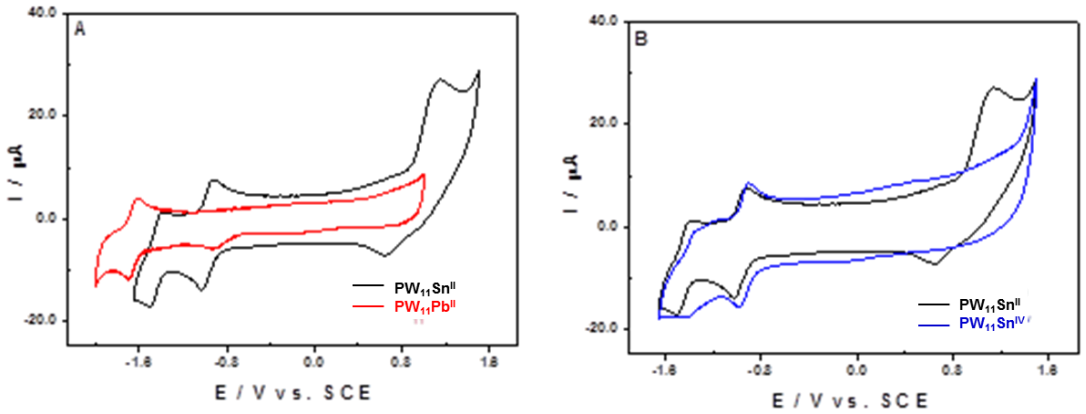

Figure 7.8. Cyclic voltammograms of (A) $PW_{11}Sn^{II}$ (black) and $PW_{11}Pb^{II}$ (red) and (B) $PW_{11}Sn^{II}$ (black) and $PW_{11}Sn^{IV}(OH)$(blue) in acetonitrile + 0.2 M $TBAClO_4$; POM concentrations, 0.70 mM ($PW_{11}Sn^{II}$), 0.45 mM ($PW_{11}Pb$) and 0.43 mM [$PW_{11}Sn(OH)$]. Scan rate 100 $mV.s^{-1}$. Glassy carbon working electrode; Pt wire auxiliary electrode; SCE reference electrode.

Table 7.1. Redox potentials of parent Keggin, unsubstituted lacunary and mono-substituted Heterometallic POMs

Sample	Ec (V)		Ea (V)		$E_{1/2}$ (V)	E_{pc} - E_{pa} (mV)
PW_{12}	E_{pc} (1)	-0.328	E_{pa} (1)	-0.256	-0.292	72
	E_{pc} (2)	-0.852	E_{pa} (2)	-0.776	-0.814	76
	E_{pc} (3)	-1.560	E_{pa} (3)	-1.464	-1.512	96
	E_{pc} (4)	-2.072	E_{pa} (4)	-1.960	-2.016	112
$PW_{11}H_3$	E_{pc} (1)	-0.865	E_{pa} (1)	-0.790 & -0.880	-0.828 & -0.873	75 & 15
	E_{pc} (2)	-1.423	E_{pa} (2)	-1.306	-1.365	117
	E_{pc} (3)	-1.621	E_{pa} (3)	-1.522	-1.572	99
	E_{pc} (4)	-2.191	E_{pa} (4)	-1.990	-2.094	201
$ClSnPW_{11}$	E_{pc} (1)	-0.904	E_{pa} (1)	-0.822	-0.863	82
	E_{pc} (2)	-1.326	E_{pa} (2)	-1.128	-1.227	198
	E_{pc} (3)	-1.466	E_{pa} (3)	-1.478	-1.472	12
$HOSnPW_{11}$	E_{pc} (1)	-1.012	E_{pa} (1)	-0.888	-0.950	124
	E_{pc} (2)	-1.474	E_{pa} (2)	-1.324	-1.399	150
$NaPW_{11}$	E_{pc} (1)	-1.582	E_{pa} (1)	-1.402	-1.492	180
	E_{pc} (2)	-2.305	E_{pa} (2)	-2.014	-2.160	291
$Pb^{II}PW_{11}$	E_{pc} (1)	-0.988	E_{pa} (1)	-0.808	-0.898	180
	E_{pc} (2)	-1.717	E_{pa} (2)	-1.615	-1.666	102
$Sn^{II}PW_{11}$	E_{pc} (1)	-1.012	E_{pa} (1)	-0.940	-0.976	72
	E_{pc} (2)	-1.484	E_{pa} (2)	-1.404	-1.444	80
	E_{pc} (3)	-2.192	E_{pa} (3)	-2.064	-2.128	128
	E_{pc} (Sn)	0.676	E_{pa}(Sn)	1.120		
$SbPW_{11}$	E_{pc} (1)	-0.997	E_{pa} (1)	-0.163		
			E_{pa} (2)	0.992		
$BiPW_{11}$	E_{pc} (1)	-1.171	E_{pa}	-0.172		
	E_{pc} (2)	-1.37				
	E_{pc} (3)	-1.651				

Supporting electrolyte: 0.2 M $TBAClO_4$. Scan rate 100 $mV.s^{-1}$. Glassy carbon working electrode, Pt wire auxiliary electrode, SCE reference electrode.

7.3 Conclusions

The electrochemical studies in MeCN have shown that the tungstate cage of the lacunary POM $(TBA)_4H_3[PW_{11}O_{39}]$ was more readily reduced than the heterometallic POMs ($[MPW_{11}O_{39}]^{n-}$; M = Na^+, Pb^{2+}, Sn^{2+}, Sn^{4+}, Bi^{3+}, Sb^{3+}). The redox potentials associated with the tungsten cage were observed to be influenced by the nature of the heterometallic group and tend to increase to more negative values with increase in overall negative charge of the polyanions. No heterometal redox processes were observed for $(TBA)_4[(HO)Sn^{IV}PW_{11}O_{39}]$ and $(TBA)_5[PbPW_{11}O_{39}]$ while redox waves for Sn^{2+}/Sn^{4+} were observed for $(TBA)_5[Sn^{II}PW_{11}O_{39}]$ within the potential range studied. Additionally, the waves observed in the CVs of $(TBA)_4[SbPW_{11}O_{39}]$ and $(TBA)_4[BiPW_{11}O_{39}]$ seem to suggest decomposition of the POMs to give Sb^{3+} and Bi^{3+} ions.

REFERENCES

1. O. A. Kholdeeva, *Top. Catal.*, 2006, **40**, 229-243.
2. D. L. Long, R. Tsunashima and L. Cronin, *Angew Chem Int Ed Engl*, 2010, **49**, 1736-1758.
3. M. T. Pope and A. Mueller, *Angew. Chem. Int. Ed. Engl.*, 1991, **30**, 34 - 48.
4. A. Müller, L. Dloczik, E. Diemann and M. T. Pope, *Inorg. Chim. Acta.*, 1997, **257**, 231-239.
5. M. Sadakane and M. Higashijima, *Dalton Trans.*, 2003, 659-664.
6. M. Sadakane and E. Steckhan, *J. Mol. Catal. A: Chem.*, 1996, **114**, 221-228.
7. M. S. Balula, J. A. Gamelas, H. M. Carapuca, A. M. V. Cavaleiro and W. Schlindwein, *Eur. J. Inorg. Chem.*, 2004, 619-628.
8. M. Sadakane and E. Steckhan, *Chem. Rev.*, 1998, **98**, 219-238.
9. S. Wenliang, L. Huizhang, K. Jilie, X. Gaoyang and D. Jiaqi, *J. Electroanal. Chem.*, 1997, **437**, 67-76.
10. J. Medina-Ramos, R. C. Pupillo, T. P. Keane, J. L. DiMeglio and J. Rosenthal, *J. Am. Chem. Soc.*, 2015, **137**, 5021-5027.
11. J. E. Pander, M. F. Baruch and A. B. Bocarsly, *ACS Catal.*, 2016, **6**, 7824-7833.
12. Y. Chen and M. W. Kanan, *J. Am. Chem. Soc.*, 2012, **134**, 1986-1989.
13. Z. M. Detweiler, J. L. White, S. L. Bernasek and A. B. Bocarsly, *Langmuir*, 2014, **30**, 7593-7600.
14. M. T. Pope, *Heteropoly and Isopoly oxometalates* Springer-Verlag Berlin, New York, 1983.
15. P. Souchay, *Ions Mineraux Condenses*, Masson, Paris, 1969.
16. I. Kozhevnikov, *Catalysis by Polyoxometalates*, John Wiley and Sons Ltd, England, 2002.
17. G. S. Chorghade and M. T. Pope, *J. Am. Chem. Soc.*, 1987, **109**, 5134-5138.
18. F. A. R. S. Couto, A. M. V. Cavaleiro, J. D. Pedrosa de Jesus and J. E. J. Simão, *Inorg. Chim. Acta*, 1998, **281**, 225-228.
19. P. Vany´sek, Electrochemical Series, http://www.smauro.it/chimica_fisica/Dati%20Termodinamici/Electrochemical%20Series.).

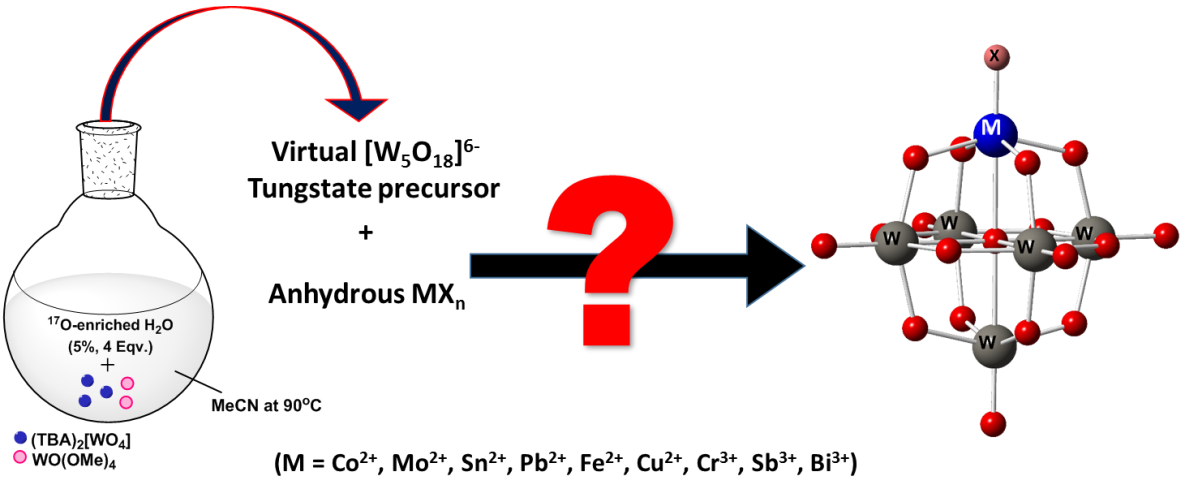

Chapter 8

Studies on Lindqvist-type Polyoxotungstates

This chapter discusses attempts to extend the non-aqueous hydrolytic aggregation approach developed in the Errington group to Lindqvist-type POM derivatives of the series $[(L)MW_5O_{18}]^{n-}$ (M = Co^{2+}, Mo^{2+}, Sn^{2+}, Pb^{2+}, Fe^{2+}, Cu^{2+}, Cr^{3+}, Sb^{3+}, Bi^{3+}) *via* reactions between the 'virtual' pentatungstate anion, 'W_5O_{18}' and anhydrous metal salts.

8. Studies on Lindqvist-type Polyoxotungstates

8.1 Introduction

In a series of papers, the Errington group described approaches hinged on metal alkoxide hydrolysis as routes to a range of heterometallic Lindqvist-type polyoxometalates $[M_2W_4]$ and $[MW_5]$ with reactive $[MX]^{n+}$ heterometal sites.[1-7] An advantage of these methods is the provision of a versatile platform to new ^{17}O-enriched species for detailed and systematic reactivity studies. These methods, for instance have been applied in the synthesis of tin-, titanium- and zirconium-substituted polyanion, according to **Equations 8.1**, **8.2**, **8.3** and **8.4** and non-aqueous reactivity studies[5,6,8,9] have resulted in derivatives of these POMs providing useful insights into the assembly and properties of these metal oxide clusters. The method has also been applied in the preparation of the 'virtual' pentatungstate anion, $[W_5O_{18}]^{6-}$ based on **Equation 8.5** and reactions between this anion and $[Co(MeCN)_4(H_2O)_2](BF_4)_2$ or $CoCl_2$ have yielded $[(CoW_5O_{18}H)_2]^{6-}$.[7] This triggered our interest on reactions between $[W_5O_{18}]^{6-}$ and salts of other +2 and +3 cations.

$$3\,[WO_4]^{2-} + 7\,WO(OMe)_4 + 2\,Sn(O^tBu)_4 + 17\,H_2O \longrightarrow 2\,[(MeO)SnW_5O_{18}]^{3-} + 8\,{}^tBuOH + 26\,MeOH \quad (8.1)$$

$$3\,[WO_4]^{2-} + 7\,WO(OMe)_4 + 2\,Ti(OMe)_4 + 17\,H_2O \longrightarrow 2\,[(MeO)TiW_5O_{18}]^{3-} + 34\,MeOH \quad (8.2)$$

$$3\,[WO_4]^{2-} + 5\,WO(OMe)_4 + 4\,Ti(OMe)_4 + 15\,H_2O \longrightarrow 2\,[(MeO)Ti_2W_4O_{16}]^{3-} + 30\,MeOH \quad (8.3)$$

$$3\,[WO_4]^{2-} + 7\,WO(OMe)_4 + 2\,Zr(O^nPr)_4 \xrightarrow[(ii)\ MeOH]{(i)\ 17\,H_2O} 2\,[\{(MeO)ZrW_5O_{18}\}_2]^{6-} + 8\,{}^nPrOH + 26\,MeOH \quad (8.4)$$

$$3\,[WO_4]^{2-} + 2\,WO(OMe)_4 + 4\,H_2O \longrightarrow [W_5O_{18}]^{6-} + 8\,MeOH \quad (8.5)$$

Thus the first part of this chapter discusses the synthesis, structure and reactivity of $[\{CH_3C(O)NH_2\}CoW_5O_{17}(OMe)]^{3-}$. Subsequent sections present attempts to prepare the

quadruple bonded Mo≡Mo anion, $[(Mo^{II}W_5O_{18})_2]^{8-}$ and other derivatives of $[(L)MW_5O_{18}]^{n-}$ (M = Sn^{2+}, Pb^{2+}, Fe^{2+}, Cu^{2+}, Cr^{3+}, Sb^{3+}, Bi^{3+}) *via* reactions between the 'virtual' pentatungstate anion, 'W_5O_{18}' and anhydrous metal salts.

8.2 Results and Discussion

8.2.1 Synthesis, structure and reactivity of $(TBA)_3[\{CH_3C(O)NH_2\}CoW_5O_{17}(OMe)]$

8.2.1.1 Synthesis

Attempts to prepare $[LCoW_5O_{18}]^{4-}$ (L = MeCN) *via* **Equation 8.6** at elevated temperatures (90 ^oC) resulted in hydrolysis of MeCN solvent and isolation of $(TBA)_3[\{CH_3C(O)NH_2\}CoW_5O_{17}(OMe)]$(see characterization below). Previous work had led to the isolation and characterization of the protonated dimer $[(CoW_5O_{18}H)_2]^{6-}$.[7] However, as shown by FT-IR spectroscopy (**Figure 8.1**), no hydrolysis of MeCN was observed when the reactions were repeated at room temperature (25 ^oC) in MeCN and at 90 ^oC in DMSO. And several attempts to crystallize the products were not successful.

$$[W_5O_{18}]^{6-} + CoCl_2 \xrightarrow[MeCN]{90\ ^oC} [(MeCN)CoW_5O_{18}]^{4-} + 2Cl^- \qquad (8.6)$$

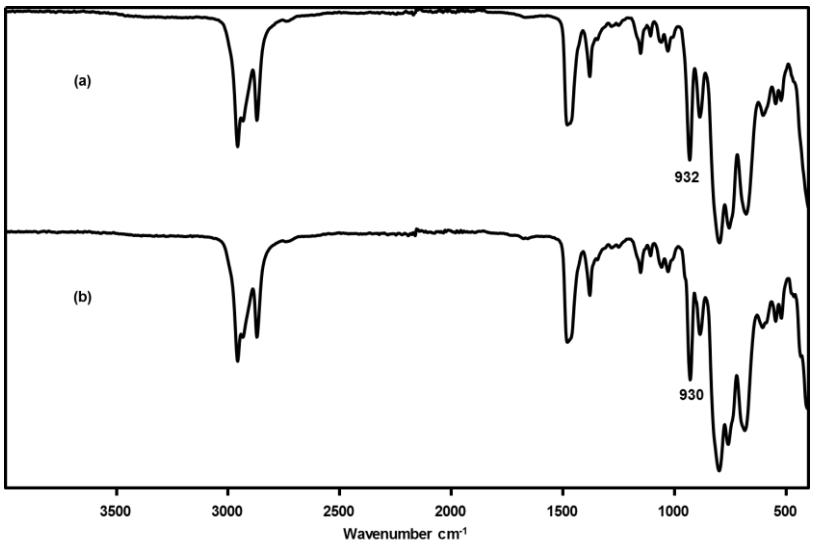

Figure 8.1. FT-IR Spectra of products from reactions between $(TBA)_6[W_5O_{18}]$ and $CoCl_2$ (a) in MeCN at 25 ^oC and (b) in DMSO at 90 ^oC.

8.2.1.2 X-ray crystal structure of $[\{CH_3C(O)NH_2\}CoW_5O_{17}(OMe)]^{3-}$

Purple XRD quality single crystals were formed after about 4 weeks of slow diffusion of diethyl ether vapour into a purple acetonitrile solution of the sample. The polyanion crystallized in a monoclinic space group (I 2/a)[see **Appendix** (**Table A8.1**) for crystallographic data and **Section 10.2.6** for refinement method]. The X-ray crystal structure shown in **Figure 8.2** shows the acetamide ligand in the polyanion to be bonded to Co(II) *via* oxygen and hydrogen-bonded to a CoOW bridging oxygen. The proton-acceptor (H4D---O1) distance is 2.10 Å (typically less than 2.5 Å) and the angle defined by the hydrogen-acceptor-donor atoms (N4—H4D—O1) is 155.3 º (typically between +/- 90 and 180º).[10] The presence of the bridging methoxido ligand is similar to the protonated CoOW observed in $[(py)CoW_5O_{18}H]^{3-}$,[7] and of the bridging Ti(μ-OMe)Ti in $[(MeO)_3Ti_2W_4O_{16}]^{3-}$.[11] This is a demonstration of the bi-functionality of $[MW_5O_{18}]^{n-}$ POMs, which contain both a Lewis acidic heterometal site and basic MOW oxygens, with potential implications for their application as bi-functional catalysts. The Lewis acidic site is also similar to oxide-supported metal sites in heterogeneous catalysts.[12,13] The longest Co—O distance, 2.220 (4) Å was between Co1 and the central oxygen (O18) followed by 2.123 (4) Å between Co1 and O2 which is bonded to a methoxyl group whilst the smallest Co—O distance, 2.046 (4) Å was between Co1 and O19 (the oxygen of the acetamide CO group bonded to Co1). The bond length between tungsten atoms and the central oxygen (O18) was between 2.307 (4) Å (W2—O18) and 2.386 (4) Å (W4—O18). The W4—O18 bond length was the highest tungsten—oxygen distance whilst the *trans*-W5—O17 had the least bond length of 1.713 (4) Å compared with the four equatorial tungstens (W1 to W4). The terminal W=O bond length of 1.713 (4) to 1.735 (4) Å was in the range of other $[(X)MW_5O_{18}]^{3-}$ polyanions (~1.709 Å for $[\{CoW_5O_{18}H\}_2]^{6-}$). W2—O2—Co1 had the smallest bond angle of 105.69(16) º compared with those of other equatorial tungstens, which were all similar. W1—O1—Co1 was 109.41(17) º, W3—O3—Co1 was 109.69 (19) º and W4—O4—Co1 was 109.51(18) º. The reduction in W2—O2—Co1 bond angle is likely due to the attached methoxido group at O2. Five butyl chains across two of the tetrabutyl ammonium counterions were disordered over two positions. The occupancies of the two parts were allowed to refine with isotropic atom treatment. Upon convergence, the occupancies were fixed before anisotropy was introduced to the model. There are four

relatively large residual electron density peaks close to tungsten atoms but the pattern of this residual density is not consistent with whole-molecule disorder.

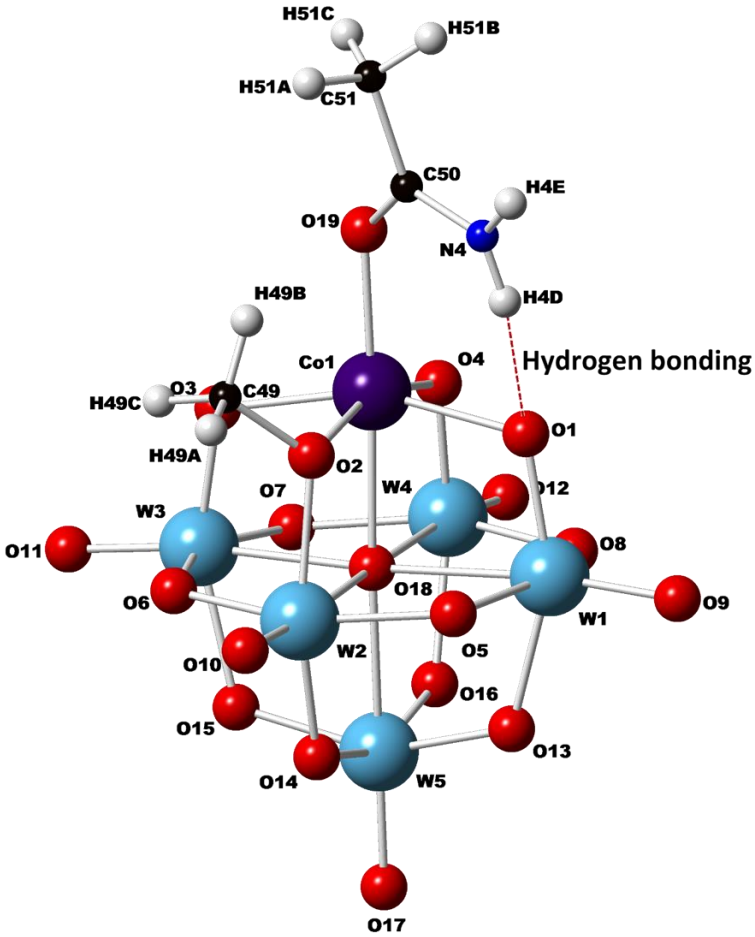

Figure 8.2. A ball and stick model of X-ray crystal structure of [{$CH_3C(O)NH_2$}$CoW_5O_{17}(OMe)]^{3-}$ anion.

8.2.1.3 FT-IR spectrum of $(TBA)_3$[{$CH_3C(O)NH_2$}$CoW_5O_{17}(OMe)$]

Figure 8.3 presents the FT-IR spectrum of $(TBA)_3$[{$CH_3C(O)NH_2$}$CoW_5O_{17}(OMe)$]. The spectrum is very similar to those reported for $[(py)CoW_5O_{18}H]^{3-}$ and $[(CoW_5O_{18}H)_2]^{6-}$ except for the acetamide bands at 3267, 3092 (ν_{NH}) and 1663 cm^{-1} (ν_{CO}) and a weak band at 2820 cm^{-1} assigned to the ν_{CH} of the OMe group. Weak bands in the 2860-2800 cm^{-1} IR region are characteristic of methoxido group.[14] The terminal W=O vibration at 933 cm^{-1} compares well with those of $[(py)CoW_5O_{18}H]^{3-}$ at 935 cm^{-1} and $[(CoW_5O_{18}H)_2]^{6-}$ at 933 cm^{-1} but is lower than that of the unsubstituted $[W_6O_{19}]^{2-}$ (974 cm^{-1}). This is expected because of the higher overall polyanion charge of $(TBA)_3$[{$CH_3C(O)NH_2$}$CoW_5O_{17}(OMe)$].

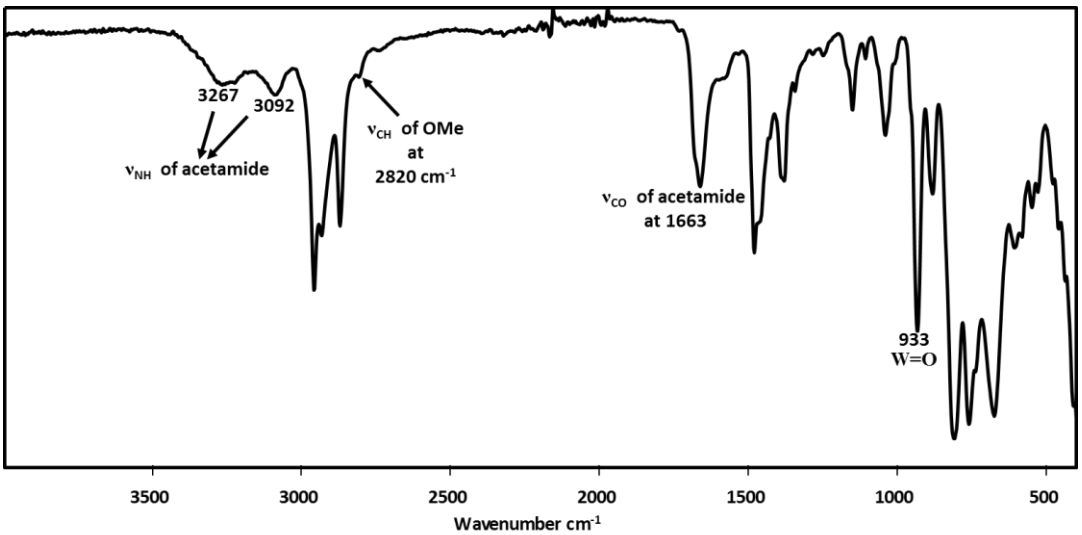

Figure 8.3. FT-IR Spectrum of [{$CH_3C(O)NH_2$}CoW_5O_{17}(OMe)]$^{3-}$

8.2.1.4 Cyclic voltammetry

The CV of $(TBA)_3$[{$CH_3C(O)NH_2$}CoW_5O_{17}(OMe)] from 0.2 V to -1.65 V [**Figure 8.4 (a)**] showed an ill-defined redox couple at E_{pc} = -0.970 and E_{pa} = -0.876 V vs SCE. This was assigned to tungsten reduction and oxidation. Scanning to more positive potential [**Figure 8.4 (b)**] gave an irreversible redox couple assigned to Co^{2+} (E_{pc} = 0.471 and E_{pa} = 1.308 V vs. SCE). No attempt was made to determine the number of electrons involved in the process.

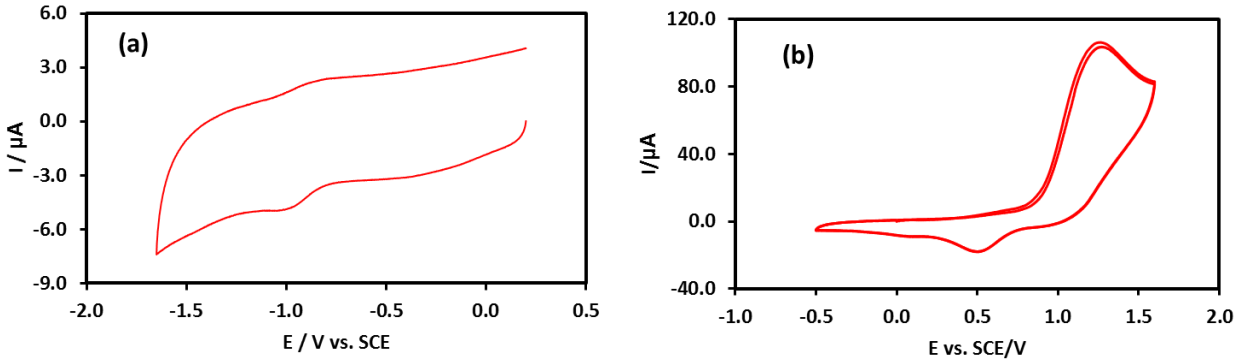

Figure 8.4. CVs of $(TBA)_3$[{$CH_3C(O)NH_2$}CoW_5O_{17}(OMe)] in acetonitrile + 0.2 M $TBAClO_4$ (a) V_1 = -1.65 V; V_2 = Pass and (b) V_1 = 1.6 V; V_2 = -0.5 V; POM concentration, 1.75 mM. Scan rate 100 mV.s^{-1}. Working electrode, glassy carbon; auxiliary electrode, Pt wire; reference electrode, SCE.

Table 8.1. Redox potentials of $(TBA)_3$[{$CH_3C(O)NH_2$}CoW_5O_{17}(OMe)]

Sample	Ec (V)		Ea (V)	
CoW_5	Epc (1)	-0.970	E_{pa} (1)	-0.876
	E_{pc} (Co)	0.471	E_{pa} (Co)	1.308

Supporting electrolyte: 0.2 M $TBAClO_4$. Scan rate 100 mV.s^{-1}. Working electrode, glassy carbon; auxiliary electrode, Pt wire; reference electrode, SCE.

8.2.1.5 DFT calculations

DFT calculations done in collaboration with the Poblet group at URV, Tarragona revealed high spin Co(II) to be 16 kcal/mol more stable than low spin Co(II), thus indicating a quartet spin density where the three open shell electrons are localized over Co orbitals. Additionally, the calculations reproduced the geometry of the structure very well with the observed hydrogen bond length 2.09 Å consistent with the calculated value of 1.80 Å whilst the observed acetamide Co-O bond length of 2.04 Å compares well with the calculated 2.07 Å (see **Figure 8.5**).

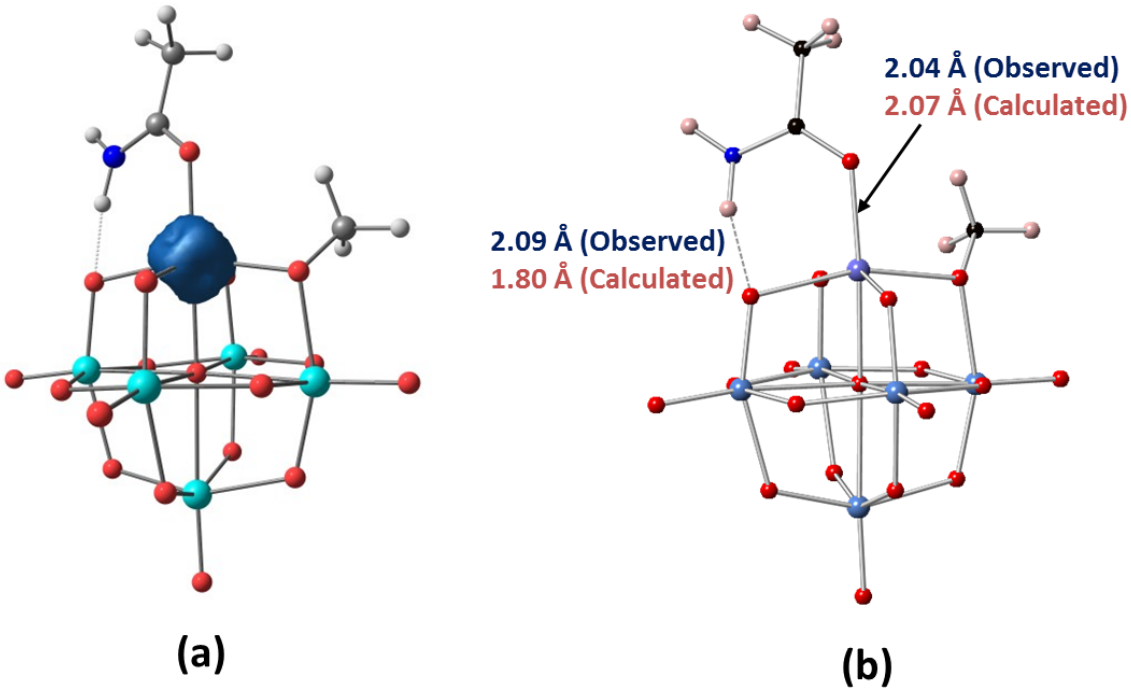

Figure 8.5. (a) Quartet spin density model and (b) calculated geometry of $(TBA)_3[\{CH_3C(O)NH_2\}CoW_5O_{17}(OMe)]$.

8.2.1.6 UV-Vis spectroscopy

The UV-Vis spectrum of $(TBA)_3[\{CH_3C(O)NH_2\}CoW_5O_{17}(OMe)]$ (**Figure 8.6**) showed peaks at 482 nm (ε = 62, 500 L $mol^{-1}cm^{-1}$) and 511 nm (ε = 47, 500 L $mol^{-1}cm^{-1}$) which are similar to those observed for $Co(NO_3)_2$ (480 and 511 nm)[15] and a Co^{2+} nitrogen complex (480 nm)[16] and were assigned to metal-to-ligand charge transfer (MLCT) transitions.[17] Thus further confirming the acetamide adduct. A broad shoulder from 545 to 640 nm, which was not assigned was also observed.

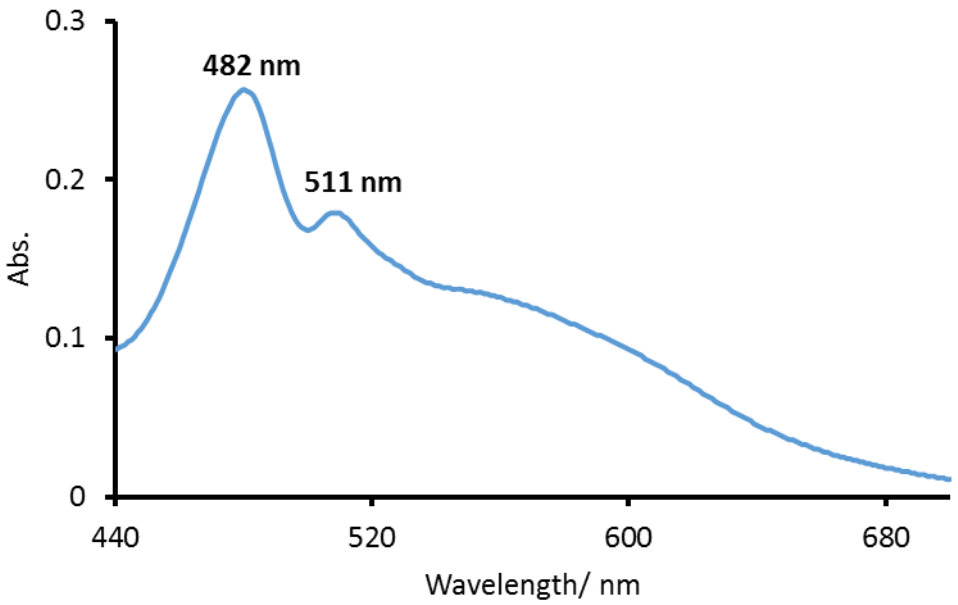

Figure 8.6. UV-Vis spectrum of 4x10^{-3} mM of (TBA)$_3$[{CH$_3$C(O)NH$_2$}CoW$_5$O$_{17}$(OMe)] in MeCN.

8.2.2 Attempted preparation of Mo≡Mo bonded (TBA)$_8$[(Mo^{II}W$_5$O$_{18}$)$_2$]

An attempt to prepare the quadruply bonded Mo≡Mo anion, [(Mo^{II}W$_5$O$_{18}$)$_2$]$^{8-}$ *via* **Equation 8.7** resulted in an immediate change in colour from blue to dark brownish green. The isolated product obtained after allowing the solution to stir for 16 h was characterized by FT-IR (see **Figure 8.7**) and Single crystal XRD (see **Figure 8.8**) as the one-electron reduced polyanion, (TBA)$_3$[W$_6$O$_{19}$].

$$2[W_5O_{18}]^{6-} + [Mo_2(NCCH_3)]_8(ax\text{-}CH_3CN)_{0.5}[BF_4]_4 \xrightarrow[MeCN]{RT} [(MoW_5O_{18})_2]^{8-} + 4[BF_4]^- \quad (8.7)$$

The FT-IR spectrum (**Figure 8.7**) showed that the terminal W=O vibration was reduced to 949 from 974 cm^{-1} for the unreduced polyanion, (TBA)$_2$[W$_6$O$_{19}$] due to increase in the overall polyanion charge by -1. Whilst crystallographic data showed that there are three tetrabutylammonium cations per polyanion [see **Figure 8.8** for crystal structure and **Appendix** (**Table A8.2**) for crystallographic data], which is further confirmation of an overall charge of -3 due to the addition of one electron to the POM. The average terminal W=O bond length of 1.718 Å compares well with those of other Lindqvist polyanions with an overall charge of -3 (e.g. ~1.709 Å for [{CoW$_5$O$_{18}$H}$_2$]$^{6-}$ and 1.713 (4) to 1.735 (4) Å for [[CH$_3$C(O)NH$_2$]CoW$_5$O$_{17}$(OMe)]$^{3-}$) but is longer than those of [W$_6$O$_{19}$]$^{2-}$ (1.69 Å) further supporting the higher charge on (TBA)$_3$[W$_6$O$_{19}$].

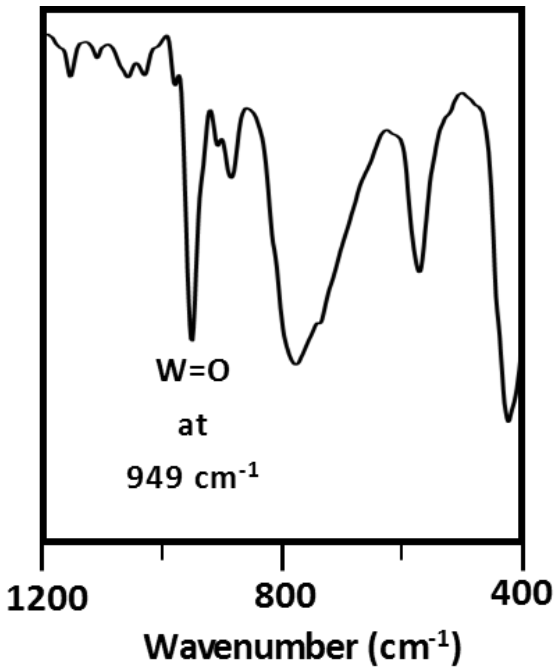

Figure 8.7. FT-IR Spectrum of the product from the reaction between $(TBA)_6[W_5O_{18}]$ and $[Mo_2(NCCH_3)_8(ax\text{-}CH_3CN)_{0.5}][BF_4]_4$ within the region 1200 – 400 cm^{-1}

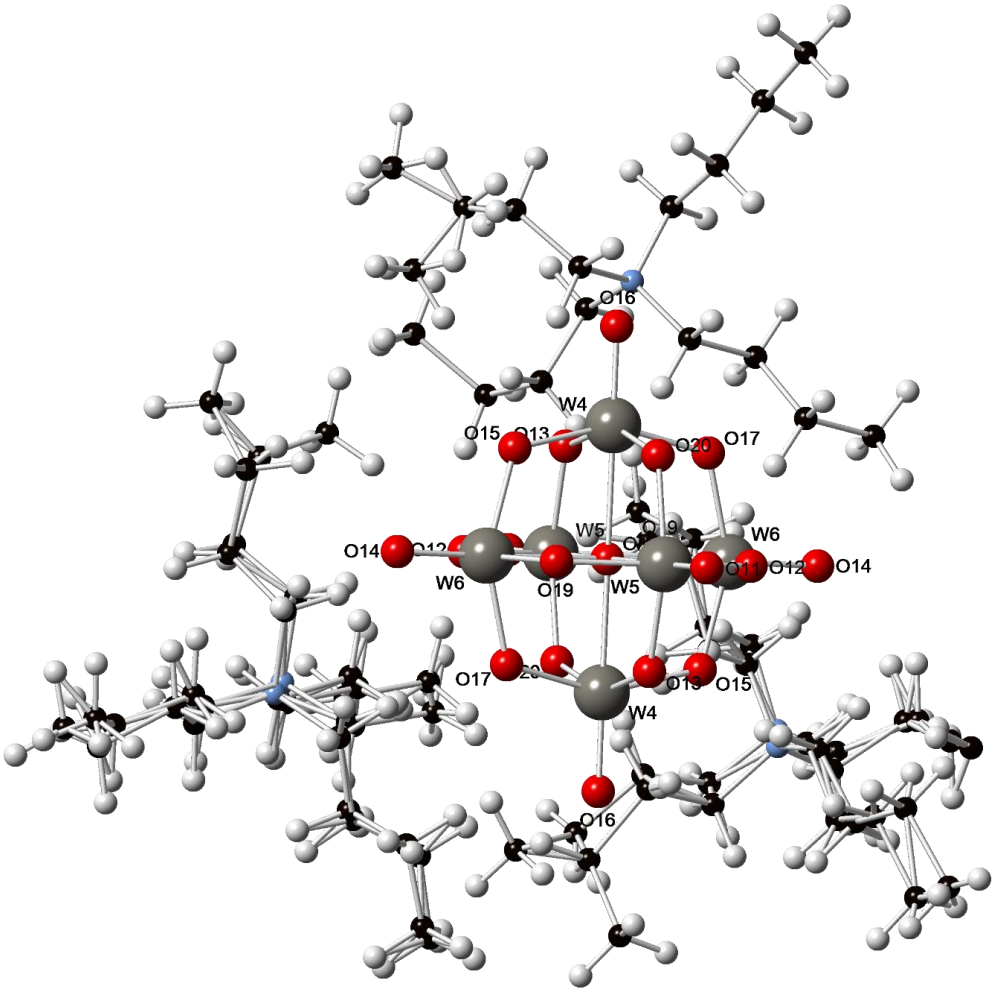

Figure 8.8. Ball and stick model of crystal structure of product from the reaction between $(TBA)_6[W_5O_{18}]$ and $[Mo_2(NCCH_3)_8(ax\text{-}CH_3CN)_{0.5}][BF_4]_4$ showing the one-electron reduced polyanion, $(TBA)_3[W_6O_{19}]$ with three TBA cations.

8.2.3 Attempted preparation of $(TBA)_4[Sn^{II}W_5O_{18}]$

Treatment of $[W_5O_{18}]^{6-}$ with $SnCl_2$ based on **Equation 8.8** gave an immediate change in colour to dark orange and the solution was allowed to stir at room temperature for 16 h.

$$[W_5O_{18}]^{6-} + SnCl_2 \xrightarrow[MeCN]{RT} [Sn^{II}W_5O_{18}]^{4-} + 2\,Cl^- \qquad (8.8)$$

The ^{119}Sn NMR spectrum of the product [**Figure 8.9 (a)**] showed a major peak (~71%), at -651 ppm with $^2J_{Sn\text{-}W}$ of 58 Hz in addition to a peak assigned to $[(MeO)SnW_5O_{18}]^{3-}$ at -650 ppm and a yet to be assigned peak at -625 ppm. Though the ^{17}O NMR spectrum (**Figure 8.10**) showed peaks for several species, the major terminal W=O resonance at 708 ppm and μ_6-O

resonance at -7.1 ppm are consistent with a higher overall charge than the $[(L)SnW_5O_{18}]^{3-}$ series (L = MeO, HO). For instance, $[(MeO)SnW_5O_{18}]^{3-}$ has terminal W=O peaks at 721 and 684 ppm and μ_6-O at 17.4 ppm while $[(HO)SnW_5O_{18}]^{3-}$ has terminal W=O peaks at 719 and 683 ppm and μ_6-O at 17.2 ppm.[18,19] Also peaks assigned to SnOW at 480 ppm and WOW at 415 and 372 ppm in the ^{17}O NMR spectrum were shifted downfield than values for $[(MeO)SnW_5O_{18}]^{3-}$ which are SnOW at 397 and WOW at 384 and 365 ppm (see **Figure 8.10**). This is also consistent with the higher charge proposed for the major product. The terminal W=O FT-IR vibration at 941 cm^{-1} (see **Table 8.2**) which is lower than that of $[(MeO)SnW_5O_{18}]^{3-}$ and $[(HO)SnW_5O_{18}]^{3-}$ (951 cm^{-1})[18,19] and $(TBA)_2[W_6O_{19}]$ (974 cm^{-1}) is further support of the higher overall charge of the product. When the solution was left to stand for 1 week, **Figure 8.9 (b)** shows that the species at -651 ppm had disappeared with the appearance of peaks assigned to $[(HO)SnW_5O_{18}]^{3-}$ at 633 ppm and $[(\mu\text{-}O)SnW_5O_{18}]^{6-}$ at -667 ppm and two unassigned peaks at -540 and -663 ppm. Addition of water to this solution gave only $[(HO)SnW_5O_{18}]^{3-}$ (67%) and an unassigned broadened peak at 687 ppm (33%). Overall, these results can be interpreted as possibly the formation of the unstable $[Sn^{II}W_5O_{18}]^{4-}$, which readily undergoes oxidation and hydrolysis in the presence of MeOH and/or H_2O to form tin (IV) products. The ability of Sn(II) to undergo oxidation in the presence of H_2O even in the rigorous absence of oxygen has been shown.[20] Also, the Keggin analogue, $[Sn^{II}PW_{11}O_{39}]^{5-}$ discussed in **Chapters 3** and **6** was observed to be similarly unstable in solution. It is also worth mentioning that $[Sn^{II}W_5O_{18}]^{4-}$ might be expected to associate and possibly protonate as was observed for $[(Co^{II}W_5O_{18}H)_2]^{6-}$,[7] and these would result in a complex ^{17}O NMR spectrum due to lower symmetry.

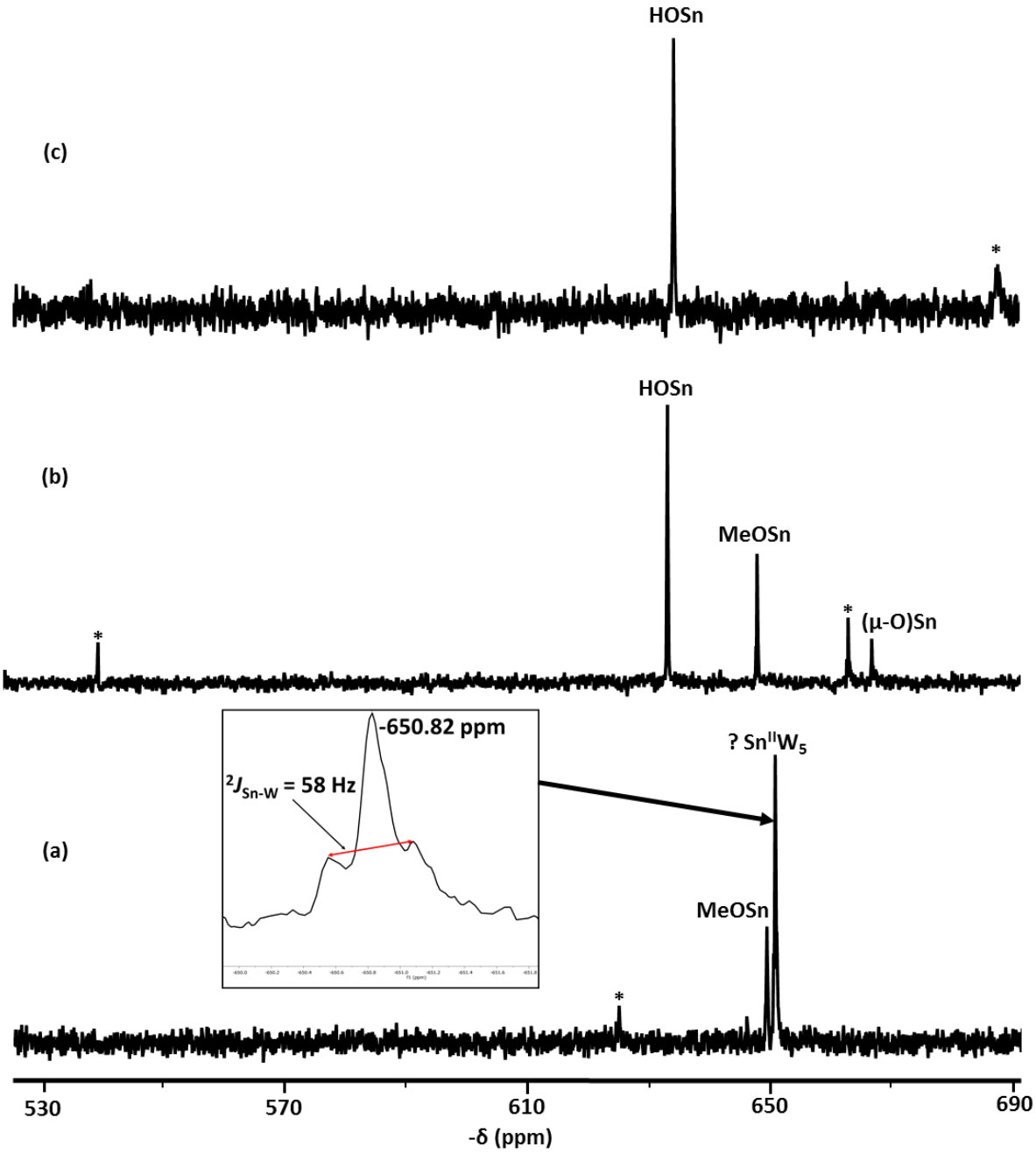

Figure 8.9. ^{119}Sn NMR spectra of the products from the reaction between $(TBA)_6[W_5O_{18}]$ and 1 mole-equivalent of $SnCl_2$ in CD_3CN (a) after stirring at room temperature for 16 h (b) after being in solution for 1 week and (c) (b) plus H_2O. Peaks marked asterisk were not assigned. Inset is expansion of peak at -650.82 showing Sn-W coupling.

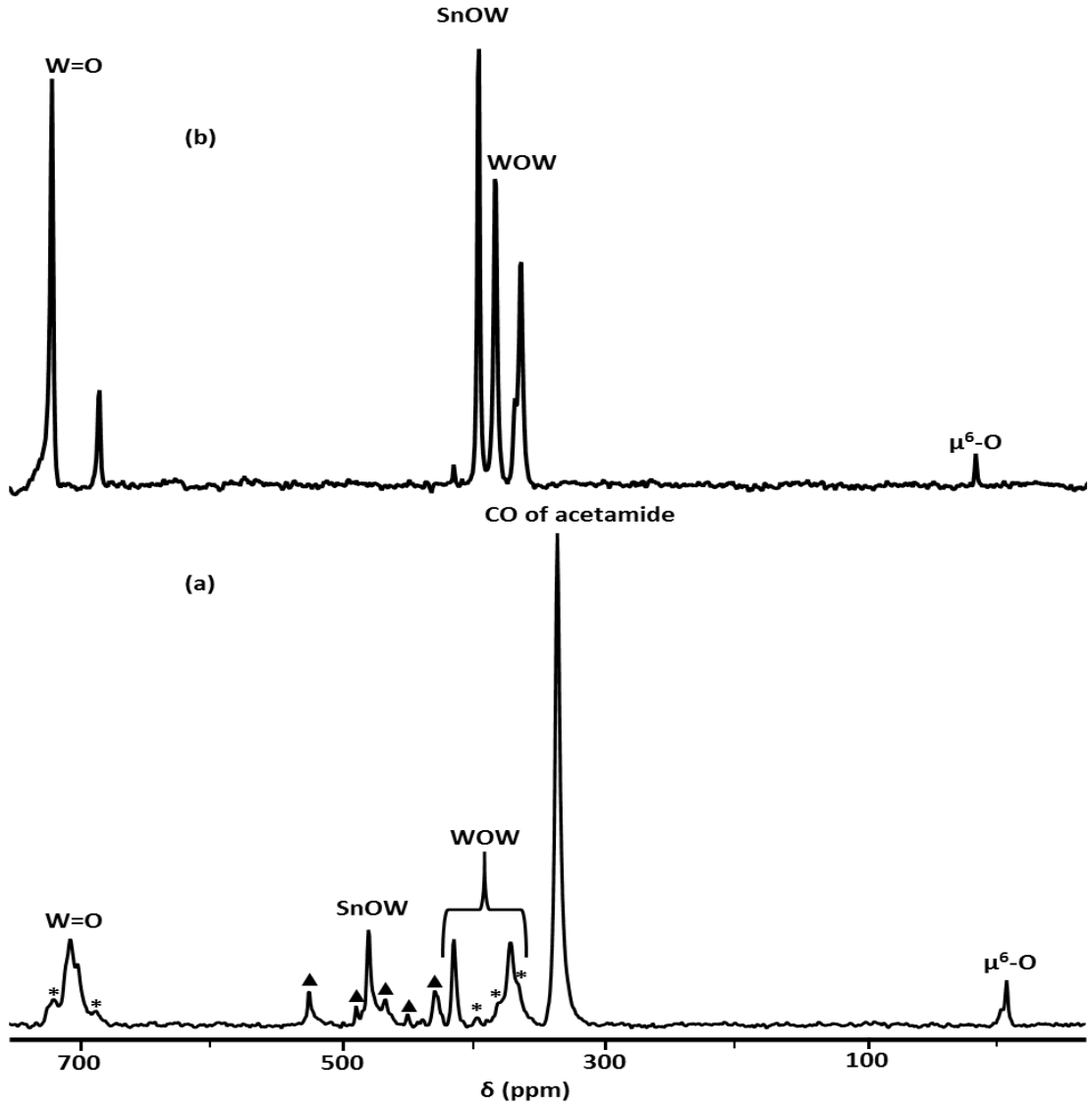

Figure 8.10. ^{17}O NMR spectra of (a) the products from the reaction between $(TBA)_6[W_5O_{18}]$ and 1 mole-equivalent of $SnCl_2$ after stirring at room temperature for 16 h and (b) $(TBA)_3[(MeO)SnW_5O_{18}]$. Peaks with asterisks are assigned to $(TBA)_3[(MeO)SnW_5O_{18}]$ whilst peaks with ▲ are unassigned species.

8.2.4 Attempted preparation of $(TBA)_4[Pb^{II}W_5O_{18}]$

Reaction between $[W_5O_{18}]^{6-}$ and $PbCl_2$ based on **Equation 8.9** in a mixture of MeCN/DMSO resulted in an instant colour change to brown, which became cloudy after stirring at room temperature for 16 h. After filtering off the pale solid, which was characterized as $(TBA)_2[W_6O_{19}]$, FT-IR analysis on the soluble product showed a terminal W=O vibration of 936 cm^{-1} (**Table 8.2**) which was around values expected for a polyanion charge of -3 or -4. Attempts to crystallize the product were not successful and no attempt was made to record an ^{17}O NMR spectrum because of the presence of DMSO in the solvent.

$$[W_5O_{18}]^{6-} + PbCl_2 \xrightarrow[MeCN/DMSO]{RT} [Pb^{II}W_5O_{18}]^{4-} + 2\,Cl^- \quad (8.9)$$

Table 8.2. FT-IR and ^{17}O NMR parameters of the products of reactions of the virtual 'W_5O_{18}' and a range of metal salts

Metal salt/ polyanions	FT-IR band (cm^{-1})		^{17}O NMR δ (ppm)			
	W=O	W-O-W	W=O	MOW	WOW	μ^6-O
$CoCl_2$	935	882, 806,	1038, 904, 750,	651, 581, 529,	367	
$SnCl_2$	941	880, 803	708, 702	480, 415, 371	336	-7
$PbCl_2$	936	879, 812				
$FeCl_2$	939, 901	884, 858, 803				
$CuCl_2$	932	878, 805,	731, 693 (broad)	440	337	-
$Cr(THF)Cl_3$	942	881, 803				
$SbCl_3$	947	878, 798,	779, 763, 752, 722, 716, 710	417, 400	383, 337	-4.15, -7.28
$BiCl_3$	943	878, 800	727, 720, 704	452, 434, 518	337	-8.67?
$[(MeO)Sn^{IV}W_5O_{18}]^{3-}$	960, 951	790, 749	720 – 684	395	383, 363	17.4
$[(MeO)Ti^{IV}W_5O_{18}]^{3-}$	948	779	720	533	389, 380	-63
$[W_6O_{19}]^{2-}$	974		776		416	

8.2.5 Attempted preparation of $(TBA)_4[ClFe^{II}W_5O_{18}]$

Treatment of $[W_5O_{18}]^{6-}$ with $FeCl_2$ in MeCN/DMSO was expected to follow **Equation 8.10** and an instant colour change from brownish to reddish brown was observed. FT-IR spectrum of the product obtained after stirring for 16 h showed a terminal W=O vibration at 901 and 939 cm^{-1} suggestive of an overall polyanion charge of -4 or -5. No attempt was made to run an ^{17}O NMR whilst crystallization efforts were not successful.

$$[W_5O_{18}]^{6-} + FeCl_2 \xrightarrow[MeCN/DMSO]{RT} [ClFe^{II}W_5O_{18}]^{5-} + Cl^- \quad (8.10)$$

8.2.6 Attempted preparation of $(TBA)_4[Cu^{II}W_5O_{18}]$

Reaction between an acetonitrile solution of $[W_5O_{18}]^{6-}$ and a dark brown solution of $CuCl_2$ in MeCN according to **Equation 8.11** resulted in a colour change to dark green and the solution was allowed to stir for 16 h. FT-IR spectrum of the product showed a terminal W=O vibration

at 932 cm^{-1} which is similar to values for the Co^{2+} polyanions. The ^{17}O NMR spectrum (**Figure 8.11**) showed a broadened terminal W=O resonances at 731 – 693 ppm due to the paramagnetic Cu^{2+} and peaks at 440 and 337 ppm assigned to CuOW and the CO of acetamide/WOW respectively. The peak for μ^6-O was not observed. Attempts to crystallize the product were not successful.

$$[W_5O_{18}]^{6-} + CuCl_2 \xrightarrow[MeCN]{RT} [Cu^{II}W_5O_{18}]^{4-} + 2Cl^- \quad (8.11)$$

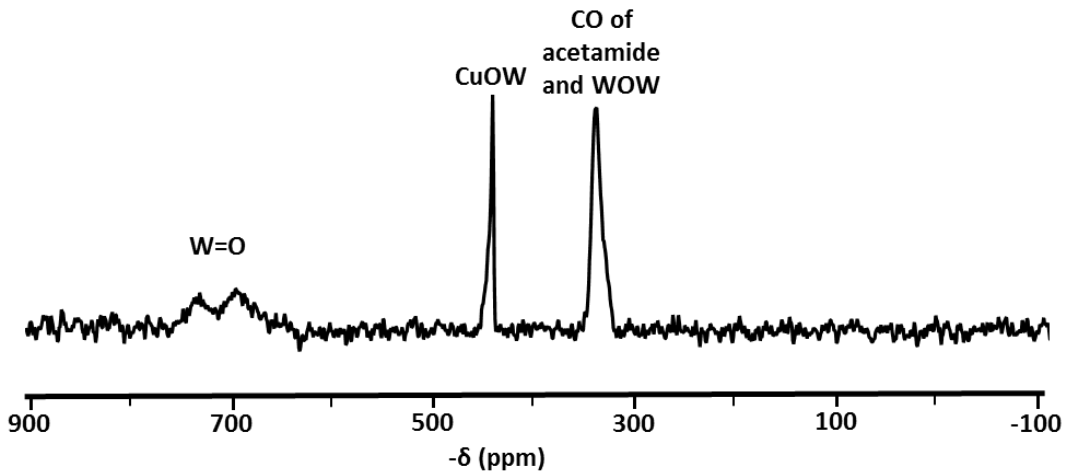

Figure 8.11. ^{17}O NMR spectrum of the product of the reaction between $(TBA)_6[W_5O_{18}]$ and $CuCl_2$ after stirring at room temperature for 16 h.

8.2.7 Attempted preparation of $(TBA)_4[ClCr^{III}W_5O_{18}]$

Reaction between an acetonitrile solution of $[W_5O_{18}]^{6-}$ and a pink solution of $Cr(THF)_3Cl_3$ in MeCN gave an instant colour change from pink to dark green and the reaction was expected to follow **Equation 8.12**. FT-IR spectrum of the product after stirring for 16 h showed a terminal W=O vibration at 942 cm^{-1} suggestive of a charge of -4. Attempts to crystallize the product however was not successful.

$$[W_5O_{18}]^{6-} + Cr(THF)_3Cl_3 \xrightarrow[MeCN]{RT} [ClCr^{III}W_5O_{18}]^{4-} + 2\ Cl^- + 3\ THF \quad (8.12)$$

8.2.8 Attempted preparation of $(TBA)_4[ClSb^{III}W_5O_{18}]$

Treatment of $[W_5O_{18}]^{6-}$ with $SbCl_3$ in MeCN gave an orange solution which was stirred for 16 h. The ^{17}O NMR spectrum (**Figure 8.12**) of the product showed a mixture of products including $[W_6O_{19}]^{2-}$. The central μ_6-O resonances (5, -3 and -6 ppm) in the ^{17}O NMR spectrum suggest formation of 3 species possibly based on **Equation 8.13**. While the terminal ^{17}O NMR resonances (721 and 709 ppm) suggest formation of polyanions of overall charge of -3 and/or -4. After filtering the solution to remove $[W_6O_{19}]^{2-}$, the FT-IR spectrum of the solid isolated from the filtrate gave a terminal W=O band at 947 cm^{-1}, which compares well with that of $[(MeO)TiW_5O_{18}]^{3-}$ (948 cm^{-1}) further supporting an overall charge of -3 or -4 for the polyanion (see **Table 8.2**).

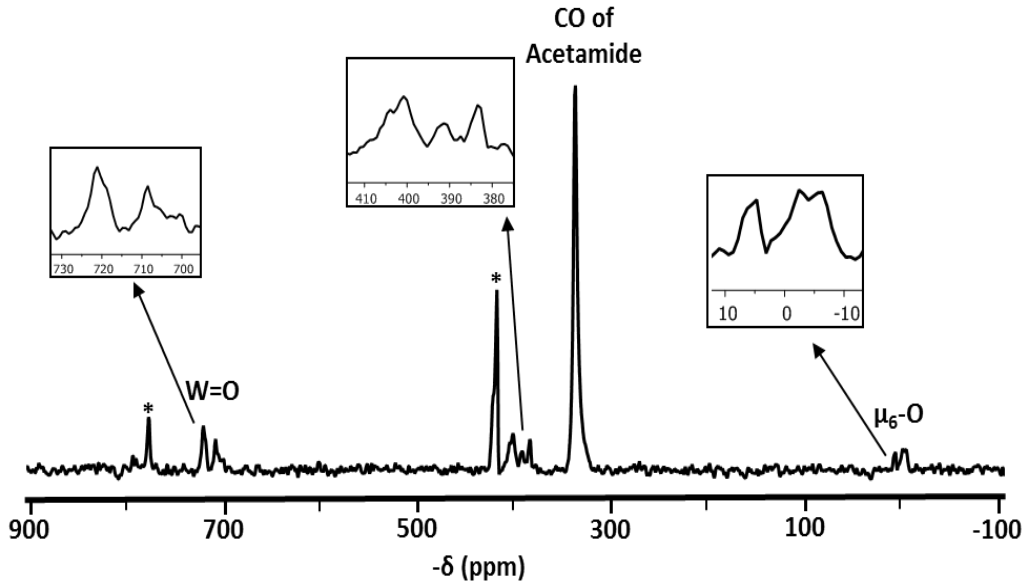

Figure 8.12. ^{17}O NMR spectrum of the product from the reaction between $(TBA)_6[W_5O_{18}]$ and $SbCl_3$ after stirring at room temperature for 16 h. Peaks asterisked are assigned to $[W_6O_{19}]^{2-}$.

$$[W_5O_{18}]^{6-} + SbCl_3 \xrightarrow[MeCN]{RT} [Cl_{3-x}Sb^{III}W_5O_{18}]^{(6-x)-} + x\ Cl^- \qquad (8.13)$$

8.2.9 Attempted preparation of $(TBA)_4[ClBi^{III}W_5O_{18}]$

As in the reaction involving $SbCl_3$, the product of the reaction between $[W_5O_{18}]^{6-}$ and $BiCl_3$ showed several species in the ^{17}O NMR spectrum (**Figure 8.13**) although no formation of

$[W_6O_{19}]^{2-}$ was observed. The observed W=O resonances were 721, 708 and 704 ppm whilst μ_6-O peaks were at 2, -1 and -8 ppm.

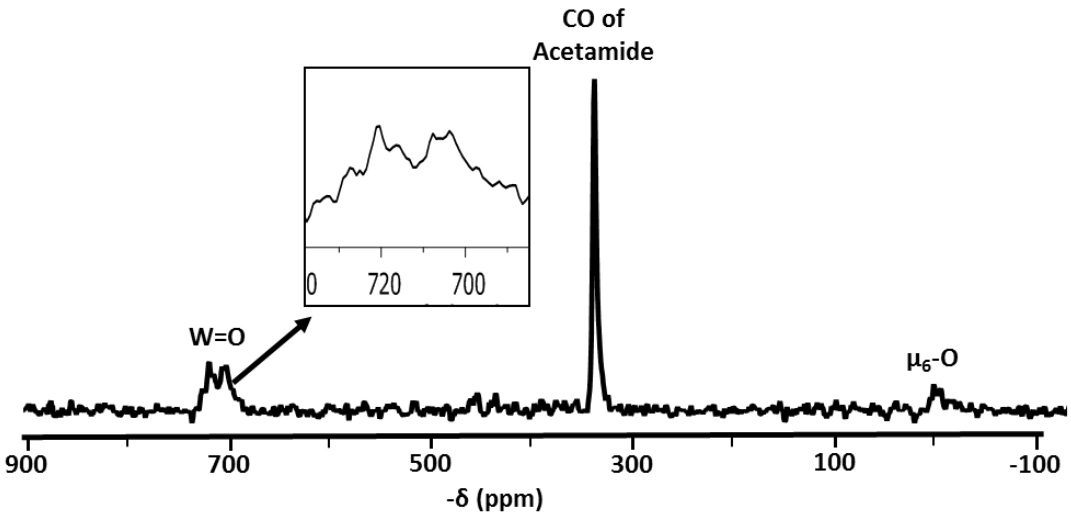

Figure 8.13. ^{17}O NMR spectrum of the product from the reaction between $(TBA)_6[W_5O_{18}]$ and $BiCl_3$ after stirring at room temperature for 16 h.

8.3 Conclusions

Although attempts to prepare derivatives of the Lindqvist-type POM, $[(L)MW_5O_{18}]^{n-}$ (M = Co^{2+}, Mo^{2+}, Sn^{2+}, Pb^{2+}, Fe^{2+}, Cu^{2+}, Cr^{3+}, Sb^{3+}, Bi^{3+}) *via* reactions of $[W_5O_{18}]^{6-}$ and metal salts were not as straight-forward as expected, this chapter has shown that spectroscopic data are consistent with formation of $[(L)MW_5O_{18}]^{n-}$ species based on terminal W=O FT-IR vibrations and ^{17}O NMR chemical shifts which suggest overall polyanion charge of -3 or -4 for the reaction products. However, in the majority of reactions, conditions used appear to promote acetonitrile hydrolysis, which resulted in the crystallographic characterization of $[\{CH_3C(O)NH_2\}CoW_5O_{17}(OMe)]^{3-}$ in reactions with $CoCl_2$. While the one-electron reduced polyanion, $(TBA)_3[W_6O_{19}]$ was isolated from the reaction involving $[Mo_2(NCCH_3)_8(ax\text{-}CH_3CN)_{0.5}][BF_4]_4$. Also, though unstable in solution, there was evidence for the formation of $[Sn^{II}W_5O_{18}]^{4-}$ in reactions with $SnCl_2$. Furthermore, reactions with $PbCl_2$, $SbCl_3$ and $BiCl_3$ were observed to give multiple species including $(TBA)_2[W_6O_{19}]$.

References

1. W. Clegg, M. R. J. Elsegood, R. J. Errington and J. Havelock, *J. Chem Soc., Dalton Trans.*, 1996, 681-690.
2. R. J. Errington, in *Polyoxometalate Chemistry: From Topology via Self-Assembly to Applications*, eds. M. T. Pope and A. Müller, Springer, Dordrecht, 2001, pp. 7-22.
3. R. J. Errington, in *NATO Sci. Ser., II*, eds. J. J. Borrás-Almenar, E. Coronado, A. Müller and M. Pope, Springer, Netherlands, 2003, vol. 98, ch. Polyoxometalate Molecular Science, pp. 55-78.
4. R. J. Errington, in *Comprehensive Coordination Chemistry II: From Biology to Nanotechnology*, ed. J. A. McCleverty, Meyer, T.J., Elsevier Ltd., Oxford, UK, 2003, vol. 2, pp. 759-773.
5. R. J. Errington, S. S. Petkar, P. S. Middleton, W. McFarlane, W. Clegg, R. A. Coxall and R. W. Harrington, *Dalton Trans.*, 2007, 5211-5222.
6. R. J. Errington, S. S. Petkar, P. S. Middleton, W. McFarlane, W. Clegg, R. A. Coxall and R. W. Harrington, *J. Am. Chem. Soc.*, 2007, **129**, 12181-12196.
7. R. J. Errington, G. Harle, W. Clegg and R. W. Harrington, *Eur. J. Inorg. Chem.*, 2009, 5240-5246.
8. R. J. Errington, S. S. Petkar and P. S. Middleton, Boston, MA, United States., 2007.
9. J. Errington, L. Coyle, G. Harle, B. Kandasamy and P. Middleton, Honolulu, HI, United States., 2010.
10. E. N. Baker and R. E. Hubbard, *Prog. Biophys. Mol. Biol.*, 1984, **44**, 97 - 179.
11. R. J. Errington, unpublished work.
12. M. P. Conley, M. F. Delley, F. Núñez-Zarur, A. Comas-Vives and C. Copéret, *Inorg. Chem.*, 2015, **54**, 5065-5078.
13. M. F. Delley, F. Nunez-Zarur, M. P. Conley, A. Comas-Vives, G. Siddiqi, S. Norsic, V. Monteil, O. V. Safonova and C. Coperet, *Proc. Natl. Acad. Sci. U. S. A.*, 2014, **111**, 11624-11629.
14. I. A. Degen, *Appl. Spectrosc.*, 1968, **22**, 164-166.
15. M. J. Sever and J. J. Wilker, *Dalton. Trans.*, 2004, 1061-1072.
16. D. Basu, S. Mazumder, J. Niklas, H. Baydoun, D. Wanniarachchi, X. Shi, R. J. Staples, O. Poluektov, H. B. Schlegel and C. N. Verani, *Chem. Sci.*, 2016, **7**, 3264-3278.
17. M. T. Weller and N. A. Young, *Characterisation Methods in Inorganic Chemistry*, Oxford University Press, Oxford, 2017.
18. B. Kandasamy, PhD Thesis, University of St. Andrews, 2011.
19. B. Kandasamy, C. Wills, W. McFarlane, W. Clegg, R. W. Harrington, A. Rodriguez-Fortea, J. M. Poblet, P. G. Bruce and R. J. Errington, *Chem. Eur. J.*, 2012, **18**, 59-62.
20. H. G. Langer and R. F. Bogucki, *J. Inorg. Nucl. Chem.*, 1967, **29**, 495-502.

Chapter 9

General Conclusions

This chapter features milestones achieved and provides a general conclusion to the findings of the thesis. Additionally, it highlights possible areas for further studies.

9. General Conclusions

9.1 Milestones achieved

9.1.1 Synthesis and characterization of ^{17}O-enriched $(TBA)_6[NaPW_{11}O_{39}]$

^{17}O-enriched $(TBA)_6[NaPW_{11}O_{39}]$ was efficiently prepared *via* a non-aqueous route developed at Newcastle and was characterized by FT-IR, Multinuclear NMR (^{1}H, ^{17}O, ^{31}P and ^{183}W), ESI-MS and single crystal XRD. The POM, which was shown to be very sensitive to protonation is a potential starting material to a series of ^{17}O-enriched heterometallic POMs for detailed and systematic reactivity studies.

9.1.2 Non-aqueous studies of substitution into $(TBA)_6[NaPW_{11}O_{39}]$

Reactions between $(TBA)_6[NaPW_{11}O_{39}]$ and metal salts were shown to be a convenient route to ^{17}O-enriched heterometallic POMs of the series, $[(L)MPW_{11}O_{39}]^{n-}$ (M = Sn^{2+}, Pb^{2+}, Bi^{3+}, Sb^{3+}, Sn^{4+}, Ti^{4+}). These ^{17}O-enriched heterometallic POMs can serve as models for mechanistic studies using ^{17}O NMR technique in homogenous and heterogeneous processes such as catalysis and sensing. They can also provide experimental basis for extending available theoretical models for predicting ^{17}O NMR chemical shifts for a wide variety of POMs.

9.1.3 ^{17}O enrichment of monosubstituted heterometallic Keggin POMs

Using $(TBA)_4[ClSn^{IV}PW_{11}O_{39}]$ and $(TBA)_4[(HO)Sn^{IV}PW_{11}O_{39}]$, which are resistant to hydrolysis, it was shown that post-enrichment of the polyoxometalate cage was not possible by treatment with ^{17}O-enriched water even at 80 ^{o}C for up to 72 h. This emphasises the importance of the enriched $(TBA)_6[NaPW_{11}O_{39}]$ as a convenient route in the non-aqueous synthesis of ^{17}O-enriched heterometallic POMs.

9.1.4 Synthesis of tin- and titanium-monosubstituted Keggin POM derivatives

To the best of our knowledge, the readily-hydrolysable, tin-substituted POMs, $(TBA)_4[(CH_3O)SnPW_{11}O_{39}]$ and $(TBA)_8[(\mu\text{-}O)(SnPW_{11}O_{39})_2]$ were successful prepared for the first time and characterized by FT-IR, multinuclear NMR (^{17}O, ^{31}P, ^{119}Sn and ^{183}W) and solid state NMR.

Although much work has been published on $(TBA)_5[Ti^{IV}PW_{11}O_{40}]$, $(TBA)_4[(L)Ti^{IV}PW_{11}O_{39}]$ (L = CH_3O; HO) and $(TBA)_8[(\mu\text{-}O)(TiPW_{11}O_{39})_2]$, this work has successfully demonstrated that in DMSO, the previously reported unstable $(TBA)_4[(HO)TiPW_{11}O_{39}]$ can exist in solution for up to 3 months without condensing.

9.1.5 Hydrolysis of $(TBA)_4[(CH_3O)M^{IV}PW_{11}O_{39}]$ (M = Sn and Ti)

$(TBA)_4[(CH_3O)Sn^{IV}PW_{11}O_{39}]$ was shown to hydrolyse faster (~3 mins) than $(TBA)_4[(CH_3O)Ti^{IV}PW_{11}O_{39}]$ in acetonitrile. The faster hydrolysis rate of $(TBA)_4[(CH_3O)SnPW_{11}O_{39}]$ is attributed to the more ionic character in the Sn—OCH_3 bond than in Ti—OCH_3. The greater covalency in the Ti—O bond results from the availability of Ti 3d orbitals for π-bonding with oxygen. This is absent in the Sn—O bond. While the hydrolytic products of $(TBA)_4[(CH_3O)Ti^{IV}PW_{11}O_{39}]$ are $(TBA)_4[(HO)TiPW_{11}O_{39}]$ and $(TBA)_8[(\mu\text{-}O)(TiPW_{11}O_{39})_2]$, hydrolysis of $(TBA)_4[(CH_3O)Sn^{IV}PW_{11}O_{39}]$ resulted in only $(TBA)_4[(HO)Sn^{IV}PW_{11}O_{39}]$. Also, POM concentration and solvent were shown to affect the rate of hydrolysis of $(TBA)_4[(CH_3O)Ti^{IV}PW_{11}O_{39}]$. The hydrolysis was observed to be faster in DMSO yielding only $(TBA)_4[(HO)Ti^{IV}PW_{11}O_{39}]$ as product. Additionally, alcohol-alkoxide exchange studies provided more support for the higher moisture-sensitivity of the tin-POM compared to the titanium analogue.

9.1.6 Dimerization of $(TBA)_4[(HO)M^{IV}PW_{11}O_{39}]$ (M = Sn and Ti)

In contrast to $(TBA)_4[(HO)Ti^{IV}PW_{11}O_{39}]$, which condenses readily at room temperature in acetonitrile, $(TBA)_4[(HO)SnPW_{11}O_{39}]$ did not condense at room temperature in solution for up to 1 month. At elevated temperatures, typically ~120 ^oC, in the presence of a water-scavenging agent, such as DCC or when volatiles were removed under reduced pressure, condensation did take place.

9.1.7 Hydrolysis of $(TBA)_4[(Cl)M^{IV}PW_{11}O_{39}]$ (M = Sn and Ti)

In the presence of a 1000-fold excess of H_2O, $(TBA)_4[ClTiPW_{11}O_{39}]$ was observed to hydrolyse more readily than $(TBA)_4[ClSnPW_{11}O_{39}]$ to give $(TBA)_4[(HO)TiPW_{11}O_{39}]$ and $(TBA)_8[(\mu\text{-}O)(TiPW_{11}O_{39})_2]$ whilst $(TBA)_4[ClSnPW_{11}O_{39}]$ hydrolysis gave only $(TBA)_4[(HO)Sn^{IV}PW_{11}O_{39}]$.

9.1.8 DFT calculations

Calculations on the hydrolysis and condensation of $[(MeO)M^{IV}PW_{11}O_{39}]^{4-}$ anions (M = Ti, Sn) proposed a concerted mechanism for formation of the hydroxido derivatives, with a lower activation energy for the tin anion and greater stability for $[(HO)SnPW_{11}O_{39}]^{4-}$, which is consistent with the faster hydrolysis rate observed for the tin compound and the ease of isolation of $(TBA)_4[(HO)SnPW_{11}O_{39}]$. The preferred condensation reaction pathways predicted for both hydroxido anions involve nucleophilic attack by the OH group of one $[(HO)M^{IV}PW_{11}O_{39}]^{4-}$ anion at the heterometal M of an adjacent anion with subsequent hydrogen transfer and elimination of a water molecule. The pathways for Ti and Sn were observed to differ slightly in that an extra transition state for the initial Sn–O bond formation was found in the case of the $[(HO)Sn^{IV}PW_{11}O_{39}]^{4-}$ anion, while hydrogen transfer and loss of water was found to occur in a second step. Similar values were obtained for the highest energy transition state in each of these condensation reactions, but the titanium oxo-bridged product $[(\mu\text{-}O)(TiPW_{11}O_{39})_2]^{8-}$ was predicted to be significantly more stable than the tin analogue. Again, this is consistent with the experimental observations, where it was more difficult to prepare pure samples of $(TBA)_8[(\mu\text{-}O)(SnPW_{11}O_{39})_2]$ than of $(TBA)_8[(\mu\text{-}O)(TiPW_{11}O_{39})_2]$.

9.1.9 Chemical reduction of $(TBA)_4[(L)Sn^{IV}PW_{11}O_{39}]$ ($L = Cl^-, HO^-$)

Spectroscopic evidence (^{119}Sn and ^{31}P NMR spectroscopy) as well as the colour of the product showed that treatment of $(TBA)_4[(L)Sn^{IV}PW_{11}O_{39}]$ (L = Cl, HO) with $NaBH_4$ resulted in the reduction of the tin heteroatom from +4 to +2 oxidation state rather than the tungsten cage as was observed during electrochemical reduction.

9.1.10 Protonation of tin- and titanium-substituted Keggin POMs

Spectroscopic studies provided evidence for protonation at TiOW sites in $[(CH_3O)TiPW_{11}O_{39}]^{4-}$ and an initial protonation at ROSn before subsequent proton migration to SnOW sites in $[(HO)SnPW_{11}O_{39}]^{4-}$ suggesting that $Ti^{IV}OW$ is more basic than $Sn^{IV}OW$ in $[(RO)M^{IV}PW_{11}O_{39}]^{4-}$. Protonation of $[ClM^{IV}PW_{11}O_{39}]^{4-}$ (M = Sn, Ti) was shown to result in several species, presumably *via* proton attack at M^{IV}-O-W sites whereas protonation of both TiOW and TiOTi sites was observed in $[(\mu\text{-}O)(TiPW_{11}O_{39})_2]^{8-}$.

9.1.11 Investigation of possible metal binding sites in $[(\mu\text{-}O)(TiPW_{11}O_{39})_2]^{8-}$

Preliminary results presented in this thesis provide evidence for metal binding at Ti-O-W and TiOTi sites in reactions between $[(\mu\text{-}O)(TiPW_{11}O_{39})_2]^{8-}$ and $AgBF_4$, $[Co(CH_3CN)_4(H_2O)_2][BF_4]_2$, $SbCl_3$ and $SnCl_4$ whilst reactions between $[(\mu\text{-}O)(TiPW_{11}O_{39})_2]^{8-}$ and $SnCl_2$, $FeCl_2$, $BiCl_3$ and $(CH_3)_2SnCl_2$ appear to proceed *via* metal binding at only TiOW sites of the POM. Additionally, reactions involving $SbCl_3$, $SnCl_4$ and $TiCl_4$ were shown to give varying amounts of chlorinated products. These results suggest that $[(\mu\text{-}O)(TiPW_{11}O_{39})_2]^{8-}$ is sufficiently basic to act as a potential 'pincer' ligand opening up avenues for new POM-supported reactivity studies.

9.1.12 Protonation of post-transition metal substituted Keggin POMs

This thesis has provided evidence suggesting protonation of the MOW sites in the post-transition metal substituted polyanions, $[M^{II}PW_{11}O_{39}]^{5-}$ (Sn, Pb) and $[M^{III}PW_{11}O_{39}]^{4-}$ (M = Sb and Bi).

9.1.13 Non-aqueous studies on $(TBA)_5[M^{II}PW_{11}O_{39}]$ (Sn, Pb)

$[Sn^{II}PW_{11}O_{39}]^{5-}$ was shown to readily undergo oxidative addition with Br_2 and I_2 producing halogenated tin(IV) products whereas $[Pb^{II}PW_{11}O_{39}]^{5-}$ was only oxidized by Br_2. Furthermore, electron transfer was observed to $[PMo_{12}O_{40}]^{3-}$ from $[Sn^{II}PW_{11}O_{39}]^{5-}$ but not from $[Pb^{II}PW_{11}O_{39}]^{5-}$.

9.1.14 Electrochemical behaviour of post-transition metal substituted Keggin POMs

It has been shown that the tungstate cage of the lacunary POM, $(TBA)_4H_3[PW_{11}O_{39}]$ was more readily reduced than the heterometallic POMs ($[MPW_{11}O_{39}]^{n-}$; M = Na^+, Pb^{2+}, Sn^{2+}, Sn^{4+}, Bi^{3+}, Sb^{3+}) and the heteroatoms (Na, Pb, Sn, Bi and Sb) and ligands (Cl^- and HO^-) were observed to influence the reduction potentials of the POMs. No redox processes associated with the heterometals were observed for $(TBA)_4[(HO)Sn^{IV}PW_{11}O_{39}]$ and $(TBA)_5[PbPW_{11}O_{39}]$ whereas redox waves for Sn^{2+}/Sn^{4+} were observed for $(TBA)_5[Sn^{II}PW_{11}O_{39}]$ within the potential range studied. Additionally, the waves observed in the CVs of $(TBA)_4[SbPW_{11}O_{39}]$

and $(TBA)_4[BiPW_{11}O_{39}]$ seem to suggest decomposition of the POMs to give Sb^{3+} and Bi^{3+} ions.

9.1.15 Studies on Lindqvist-type POMs

Although attempts to prepare derivatives of the Lindqvist-type POM, $[(L)MW_5O_{18}]^{n-}$ (M = Co^{2+}, Mo^{2+}, Sn^{2+}, Pb^{2+}, Fe^{2+}, Cu^{2+}, Cr^{3+}, Sb^{3+}, Bi^{3+}) *via* reactions between the 'virtual' pentatungstate anion, $[W_5O_{18}]^{6-}$ and metal salts were not as straight-forward as expected, acetonitrile hydrolysis in reactions involving $CoCl_2$ resulted in the formation of $[[CH_3C(O)NH_2]CoW_5O_{17}(OMe)]^{3-}$ which was characterised by X-ray crystallography, FT-IR and UV-Vis spectroscopy. The one-electron reduced polyanion, $(TBA)_3[W_6O_{19}]$ was isolated from a reaction involving $[Mo_2(NCCH_3)_8(ax\text{-}CH_3CN)_{0.5}][BF_4]_4$. Evidence was obtained for the formation of $[Sn^{II}W_5O_{18}]^{4-}$ in reactions involving $SnCl_2$ while reactions involving $PbCl_2$, $SbCl_3$ and $BiCl_3$ were observed to give multiple species including $(TBA)_2[W_6O_{19}]$.

9.2 Suggestions for further studies

The following are suggested as viable areas for further studies:

i. Optimization of reactions between $(TBA)_6[NaPW_{11}O_{39}]$ and noble metal salts as a route to ^{17}O-enriched noble metal substituted POMs for systematic protonation studies.

ii. Extension of theoretical studies on ^{17}O NMR chemical shifts to a wider range of Keggin POMs based on the new data presented in this thesis.

iii. More studies to fully harness the potential of the tin-substituted POMs as catalysts.

iv. Further attempts to obtain crystals for structural characterisation of products from reactions between $[(\mu\text{-}O)(TiPW_{11}O_{39})_2]^{8-}$ and electrophiles in order to better understand the bonding involved.

v. More detailed studies of the electrochemistry of the post-transition metal substituted Keggin POMs.

vi. Investigation of possible electrocatalytic activity of $[Sn^{II}PW_{11}O_{39}]^{5-}$ and $[MPW_{11}O_{39}]^{4-}$ ($M = Bi^{3+}$, Sb^{3+}) for CO_2 reduction.

Chapter 10

Experimental

This chapter describes the experimental details including materials, instrumentation and methods (synthesis and reactivity study) employed in carrying out the research work discussed in this thesis.

10. Experimental

10.1. General procedures, solvents and reagents

Most of the materials handled in the course of this research work were air-sensitive so all manipulations were carried out under dry, oxygen-free nitrogen using standard Schlenk techniques, or in a glove-box fitted with a recirculation system. Filtration of air-sensitive samples were *via* cannula filter sticks constructed using a PTFE sleeving as described elsewhere.[1] In some cases, the use of plastic syringes was avoided to prevent introduction of plasticizers into the sample while metal spatulas and cannulas were not used to prevent reduction of organic polyanion derivatives in solution. Because of the air-sensitive nature of some of the compounds handled, solvents were pre-dried over and distilled from appropriate drying agents [see **Appendix (Table A10.1)]** before storing over activated 3Å molecular sieves. The sieves were activated by heating at 290 ^{o}C under vacuum for ~24 h. All reagents were purchased commercially from Sigma Aldrich, Fisher Scientific, Alfa Aesar, Acros Organics, Fluka Chemika or Mersen and used without further purification [see **Appendix (Table A10.2)**] for details of chemicals, grades and suppliers). The compounds: $(TBA)_2[WO_4]$,[2] $WOCl_4$,[3] $WO(OMe)_4$,[3] $(TBA)_3[PMo_{12}O_{40}]$,[4] $(TBA)_3[PW_{12}O_{40}]$,[5] $Na_3[PW_{12}O_{40}].8H_2O$,[5] $Mo_2(O_2CCH_3)_4$,[6] $[Mo_2(NCCH_3)_8(ax\text{-}CH_3CN)_{0.5}][BF_4]_4$,[7] $Co(MeCN)_4(H_2O)_2][BF_4]_2$ and anhydrous metal chlorides[8] were prepared by literature methods.

10.2. Instrumentation

10.2.1. CHN elemental microanalysis

CHN microanalysis were performed using a Carlo Eba 1108 Elemental analyser controlled with CE Eager 200 software by a technician in the Analytical Lab, School of Chemistry, Newcastle University. Samples were vacuum-dried for 24 h before analysis and weighed using a certified Mettler MX5 Microbalance calibrated with Acetanilide Organic Analytical Standard. Batch No. 11853 with <0.3% confidence limit.

10.2.2. FT-IR spectroscopy

Fourier transform-Infrared spectra were recorded on a Bruker Alpha spectrometer fitted with a Platinum ATR module or a Varian 600 FTIR spectrometer fitted with a Diamond ATR (4000 – 400 cm^{-1}). Spectra were recorded for solid samples after vacuum drying for at least 2 h.

10.2.3. Multinuclear NMR spectroscopy

NMR spectra were recorded on Bruker Avance 7.05 Tesla 300 MHz, 9.40 Tesla 400 MHz, 11.75 Tesla 500 MHz or 16.44 Tesla 700 MHz spectrometers. Deuterated solvents (acetonitrile-D3, dimethylsuffoxide-D6, dichloromethane-D2, chloroform-D1, toluene-D8 or water-D2) (Cambridge Isotope Laboratories, Inc) were added to solutions of NMR samples to obtain deuterium lock signals. NMR solvents (except water-D2) were degassed on a Schlenk line and dried over activated 3Å molecular sieves for at least 3 days before use. Unless stated otherwise, measurements were made at ambient probe temperature (~295K) using 5-mm or 10-mm o.d. (for ^{183}W) screw capped spinning tubes. Relaxation delays were 30 s for ^{1}H, 1 s for ^{13}C, 0.0010 s for ^{17}O, 20 s for ^{31}P, 8 s for ^{119}Sn, 3 s for ^{183}W, 0.05 s for ^{195}Pt and 0.0010 s for ^{207}Pb [see **Appendix (Table A10.3)** for more parameters]. All chemical shifts were measured relative to external standards, 85% TMS (^{1}H and ^{13}C); D_2O (^{17}O); 85% H_3PO_4 (^{31}P), Me_4Sn 90% in C_6D_6 (^{119}Sn); 1 M Na_2WO_4 in D_2O (^{183}W); 1.2 M Na_2PtCl_6 in D_2O (^{195}Pt) and Me_4Pb + 5% C_6D_6 (^{207}Pb). Samples were prepared on the day of measurement and were analysed within 24 h of preparation except for ^{183}W NMR analyses which were run over weekends (~65 h). Typical concentrations of NMR samples were 0.01 M (^{1}H and ^{31}P); 0.03 M (^{13}C, ^{17}O, ^{119}Sn and ^{207}Pb) and 0.14 M (^{183}W). 2D ^{1}H EXSY experiments were run at 333K with a relaxation delay of 60 s and a mixing time of 250 ms for $(TBA)_4[(CH_3O)TiPW_{11}O_{39}]$ and at 298K with a relaxation delay of 60 s and a mixing time of 500 ms for $(TBA)_4[(CH_3O)SnPW_{11}O_{39}]$. For both samples, the offset was 2.5 ppm and the sweep width was 5.00 ppm. 2 scans per increment were obtained with a final matrix size of 2048 x 256 (F2 x F1), which was transformed to 4096 x 1024.

10.2.4. UV-Visible spectroscopy

UV-Vis spectra of $4x10^{-3}$ mM solutions of POMs in acetonitrile were recorded on a UV-1800 Shimadzu UV spectrophotometer using 1-cm quartz cells.

10.2.5. Electrospray ionization mass spectrometry (ESI-MS)

Measurements were carried out using a Bruker MaXis Impact instrument at the Cronin Group, University of Glasgow. The calibration solution used was Agilent ESI-L low concentration tuning mix solution, Part No. G1969-85000, enabling calibration between approximately 100 m/z and 2500 m/z. 25 μM solutions of samples were prepared in dry acetonitrile and introduced into the MS at a dry gas temperature of 180 °C. The ion polarity

for all MS scans recorded was negative, with the voltage of the capillary tip set at 4500 V, end plate offset at −500 V, funnel 1 RF at 400 Vpp and funnel 2 RF at 400 Vpp, hexapole RF at 200 Vpp, ion energy 5.0 eV, collision energy at 10 eV, collision cell RF at 1500 Vpp, transfer time at 100.0 µs, and the pre-pulse storage time at 10.0 µs. The dry gas (N_2) was set to 4.0 L/min and the nebuliser gas (N_2) was set to 0.3 Bar.

10.2.6. Single crystal X-ray diffraction analysis

X-ray diffraction data for all samples were collected on a Xcalibur Atlas Gemini ultra-diffractometer equipped with an Oxford Cryosystems CryostreamPlus open-flow N_2 cooling device at Newcastle X-ray crystallography services. Suitable crystals were selected and mounted on a cryoloop using Fomlin YR-1800 oil under nitrogen and data were collected using an Enhance Ultra (Cu) X-ray Source ($\lambda_{CuK\alpha}$ = 1.54184 Å) for $(TBA)_6[NaPW_{11}O_{39}]$, $(TBA)_3[(CH_3CONH_2)CoW_5O_{18}(CH_3)]$ and $Ce(NO_3)_6$ and an Enhance (Mo) X-ray Source ($\lambda_{MoK\alpha}$ = 0.71073 Å) for $(TBA)_3[W^{V}W^{VI}_5O_{18}]$. Cell refinement, data collection and data reduction were undertaken *via* the software CrysAlisPro.[9] For $(TBA)_6[NaPW_{11}O_{39}]$, $(TBA)_3[(CH_3CONH_2)CoW_5O_{18}(CH_3)]$ and $Ce(NO_3)_6$ intensities were corrected for absorption analytically using a multifaceted crystal model based on expressions derived by R.C. Clark & J.S. Reid,[10] whereas an empirical absorption correction using spherical harmonics was performed in the case of $(TBA)_3[W^{V}W^{VI}_5O_{18}]$.

All structures were solved using XT[11] and refined using XL[12] using the Olex2 graphical user interface.[13] All non-hydrogen atoms were refined anisotropically and hydrogen atoms were positioned with idealised geometry. For the hydrogen atoms the displacement parameters were constrained using a riding model. SADI and EADP restraints were applied as appropriate.

10.2.7. Cyclic voltammetry

Cyclic voltammograms were recorded at Laboratoire de Chimie Physique (LCP), Universite Paris-Sud, Orsay, France on a Versasat™ II potentiostat connected to a computer for data acquisition. Sample solutions were deaerated thoroughly for at least 30 min with pure argon and kept under a positive argon pressure during the experiments. A three compartment electrochemical cell was used. The side arms contained the saturated calomel reference electrode (SCE) and a platinum counter electrode with a surface area of approximately 1 cm^2. The reference and the counter electrodes were separated from the test solution by a fine and

medium porosity ceramic, respectively. The working electrode was a glassy carbon electrode (3 mm diameter, surface area ~7 mm^2). The glassy carbon rod was electrically connected to a copper wire with silver epoxy, encapsulated in epoxy resin and dried. The surface of the glassy carbon electrode was prepared by grinding with emery paper followed by polishing with 6, 3 and 1 µ diamond paste then abundantly rinsed with ultrapure water (milliQ grade with a resistance of 18.2 MΩ.cm), pure acetone, absolute ethanol and sonicated in absolute ethanol for 5 mins. Measurements were obtained with samples (0.45 – 0.70 mM) in acetonitrile + 0.2 M $TBAClO_4$ supporting electrolytes (5 ml) at 100 $mV.s^{-1}$ scan rate.

10.2.8. Computational studies

Static Density Functional Theory (DFT) calculations and Classical Molecular Dynamics (CMD) simulations were performed by the Quantum Chemistry Group at the Universitat Rovira i Virgili, Tarragona (Spain).

10.3. Protonation studies

Protonation studies were carried out with a 0.25 M solution of $HBF_4.Et_2O$ in MeCN. Fresh acid solutions were prepared prior to each experiment.

10.4. Preparation of reagents

0.03 M $SnCl_4$ in CH_3CN: $SnCl_4$ (0.35 ml) was dissolved in dry CH_3CN (50 ml) in a 100-ml volumetric flask in a glove box and made up to the 100 ml mark with more dry CH_3CN.

0.05 M $TiCl_4$ in CH_2Cl_2: $TiCl_4$ (0.55 ml) was dissolved in dry CH_2Cl_2 (50 ml) in a 100-ml volumetric flask in a glove box and made up to the 100 ml mark with more dry CH_2Cl_2.

0.1 M CH_3ONa in CH_3OH: CH_3ONa (0.54 g) was dissolved in dry CH_3OH (50 ml) in a 100-ml volumetric flask in a glove box and made up to the 100 ml mark with more dry CH_3OH. CH_3ONa was prepared by dissolving Na metal in excess CH_3OH under N_2 atmosphere and vacuum-drying the colourless solution for 4 h to obtain a white solid.

0.1 M $(NH_4)_2[Ce(NO_3)_6]$ in CH_3CN : $(NH_4)_2[Ce(NO_3)_6]$ (5.48 g) was dissolved in dry CH_3CN (50 ml) in a 100-ml volumetric flask in a glove box and made up to the 100 ml mark with more dry CH_3CN.

***0.25 M* $HBF_4.Et_2O$ *in* CH_3CN:** $HBF_4.Et_2O$ (0.34 ml) was dissolved in dry CH_3CN (5 ml) in a 10-ml volumetric flask in a glove box and made up to the 10 ml mark with more dry CH_3CN.

***0.24 M Ag*BF_4 *in* CH_3CN:** $AgBF_4$ (0.47 g) was dissolved in dry CH_3CN (5 ml) in a 10-ml volumetric flask in a glove box and made up to the 10 ml mark with more dry CH_3CN.

***0.26 M* $H_2NNH_2.HCl$ *in* CH_3CN:** $H_2NNH_2.HCl$ (0.178 g) was dissolved in dry CH_3CN (5 ml) in a 10-ml volumetric flask in a glove box and made up to the 10 ml mark with more dry CH_3CN.

0.25 M $NaOH_{(aq)}$: NaOH (0.1 g) was dissolved in H_2O (5 ml) in a 10-ml volumetric flask and made up to the 10 ml mark with more H_2O.

10.5. Experimental for Chapter 3

10.5.1. Preparation of $Mo_2(O_2CCH_3)_4$[6]

$Mo(CO)_6$ (4 g, 15.15 mmol) and a Teflon coated magnetic stirrer bar were placed in a 250 ml RB flask equipped with a condenser and a side arm. The contents were flushed with N_2 for 5 mins. Glacial acetic acid (150 ml, excess) and acetic anhydride (10 ml) were added under N_2 and the flask was fitted to the reflux condenser attached to a mineral oil bubbler. The mixture was refluxed for 12 h and allowed to cool for another 12 h before filtering with a Buchner funnel. The bright yellow solid obtained was washed with ethanol (10 ml x 3) and ether (10 ml x 3) and allowed to dry in air for 10 mins (**2.1 g, 65%**). The product was stored in a Schlenk flask under N_2.

10.5.2. Preparation of $[Mo_2(NCCH_3)_8(ax\text{-}CH_3CN)_{0.5}][BF_4]_4$[7]

$Mo_2(O_2CCH_3)_4$ (1.20 g, 2.80 mmol) was dissolved in a mixture of CH_3CN (20 ml) and CH_2Cl_2 (100 ml). To this vigorously stirring yellow solution was added $HBF_4.Et_2O$ (5.1 ml) which caused a colour change to a red solution. The solution was continuously stirred at room temperature and progressed through red to purple to blue-purple within 30 min of the acid addition. During this period, a large crop of bright blue-purple microcrystals precipitated from the reaction solution. The reaction mixture was then heated to reflux temperature and gently refluxed for 40 min before cooling to room temperature. The solution became less intensely blue as a result of product precipitation from solution. The supernatant liquid was decanted off and the solid was washed with CH_2Cl_2 (10 ml x 4) until the wash solution was clear. The product was

then washed with diethyl ether (10 ml x 3) and dried for 8 h at 35 ^{o}C (**2.06 g, 83 %**). The ^{1}H NMR and UV-Vis spectra of the product were recorded [see **Appendix** (**Figure A10.1** and **Figure A10.2**)]

10.5.3. Preparation of $(TBA)_3[PMo_{12}O_{40}]$

A literature procedure[4] was used with recrystallisation from acetonitrile rather than acetone. $Na_2MoO_4.2H_2O$ (29.04 g, 120 mmol) was dissolved in water (120 mL) to give a 1 M colourless solution. 1 M H_3PO_4 solution was made up by adding 85% H_3PO_4 (0.68 mL) to water (9.32 mL) and this was added to the molybdate solution. 1, 4-dioxane (100 mL) was added and the solution changed from colourless to cloudy before adding nitric acid (15.2 M, 15 mL) which turned the solution orange and then yellow after stirring for 5 min. TBABr (10.2 g, 31.6 mmol) was dissolved in water (10 mL) to give a colourless solution by gentle heating and this solution was added to the yellow solution with immediate formation of a yellow precipitate. The mixture was filtered and the solid was washed with water. The yellow solid was then boiled in water (100 mL) before filtering the solid with a Buchner funnel and washing with water, ethanol and diethyl ether. The solid was dried under vacuum over the weekend. The crude product was dissolved in acetonitrile (500 mL) by gentle heating and left to recrystallise. Yellow crystals formed after 12 h and were collected using a Buchner funnel. The crystals were transferred into a Schlenk flask and vacuum-dried for 1 h (**19.84 g, 78%**). **IR (4000 – 400 cm^{-1})**: 2966 (m), 2926 (m), 2868 (m), 2809 (w), 1490 (w), 1466 (m), 1378 (w), 1061 (s), 950 (w), 933 (w), 892 (m), 876 (m), 781 (s, br), 726 (s, br), 627 (w), 610 (w), 570 (w), 551 (w), 532 (w), 501 (w), 452 (w), 437 (w) **^{31}P NMR** (121.49 MHz, CD_3CN): δ (ppm), -3.82, line width fwhm = 1.9 Hz.

10.5.4. Preparation of $Na_3[PW_{12}O_{40}].8H_2O$[5]

$H_3PW_{12}O_{40}.xH_2O$ (60 g, 20.83 mmol) was dissolved in distilled H_2O (20 ml) in a 250 ml conical flask. NaCl (3.65 g, 62.5 mmol) was added and a white precipitate formed immediately. The precipitate was filtered with a Buchner funnel and the white solid was washed with minimum water (~5 ml), vacuum-dried in a Schlenk flask and weighed. The filtrate was concentrated to obtain more of the solid product. (**52.64 g, 82 %**). **IR (4000 – 400 cm^{-1}):** 3415 (m, br), 1616 (m), 1077 (s), 976 (s, sh), 918 (m), 796 (vs, br), 594 (m), 505 (s); **^{31}P NMR (**121.49 MHz, **CD_3CN):** δ (ppm), -15.35, line width fwhm = 3.25 Hz.

10.5.5. Preparation of $(TBA)_3[PW_{12}O_{40}]^5$

$H_3PW_{12}O_{40}.xH_2O$ (20 g, 6.94 mmol) was dissolved in distilled H_2O (5 ml) in a 250 ml conical flask. A concentrated aqueous solution of TBABr (6.72 g, 20.83 mmol) was added to the polyanion solution and a white precipitate formed immediately. The precipitate was filtered with a Buchner funnel and the white solid was washed with minimum water (~2 ml) and dried in air. The solid was recrystallised from hot acetonitrile and dried under vacuum to give colourless crystals. (**17.4 g, 70 %**). **IR (4000 – 400 cm^{-1}):** 2963 (m), 2934 (m), 2874 (m) 1469 (m), 1380 (w), 1077 (s), 971 (vs, sh), 891 (s), 791 (vs, br), 594 (s), 507 (s); **^{31}P NMR (**121.49 MHz, **CD_3CN):** δ (ppm), -15.35, line width fwhm = 3.64 Hz. $(TBA)_3[PW_{12}O_{40}]$ was enriched by stirring in minimum ^{17}O-enriched H_2O for 12 h at 80 ^oC. **^{17}O NMR** (54.23 MHz, **CH_3CN**): δ = 770, 432, 405 ppm.

10.5.6. Preparation of $(TBA)_6[NaPW_{11}O_{39}]$

$Na_3[PW_{12}O_{40}].8H_2O$ (20.69 g, 6.70 mmol) was dissolved in MeCN (60 ml) and cooled in a cryostat to -30 ^oC. 1 M methanolic TBAOH (40.17 ml, 40.17 mmol) was added gently with continuous stirring and the cloudy white solution was allowed to warm to room temperature and stirred for 12 h. The resulting solution was allowed to settle, filtered *via* a cannula filter stick and vacuum dried to give a sticky solid, which was washed with diethyl ether (40ml x 2) and vacuum dried again to obtain a white solid powder. The white solid was redissolved by gentle heating in MeCN (35 ml) to give a cloudy white solution, which was allowed to stand for 12 h before filtering the clear solution. Diethyl ether (~ 140 ml) was added to the solution and the cloudy solution was heated gently to obtain a clear solution, which was allowed to cool to room temperature before putting it in the freezer. White crystals formed after ~12 h were collected by filtering, washing with diethyl ether (20 ml) and vacuum drying. (**24.7 g, 89 %**). The crystals were enriched in ^{17}O by dissolving 20 g in MeCN (20 ml), adding 10 % ^{17}O-enriched H_2O (0.1 ml) and stirring at 80 ^oC for 12 h. The solution was allowed to cool to room temperature, vacuum-dried for 8 h, washed with diethyl ether (20 ml) and vacuum-dried again for 2 h to obtained white ^{17}O-enriched $(TBA)_6[NaPW_{11}O_{39}]$ solid (**20 g, 100%**). The enriched product was used as starting material in the preparation of a range of ^{17}O-enriched heterometallic Keggin POMs. Single crystal XRD quality crystals were obtained by slow diffusion of Et_2O vapour into a solution of 0.2 g of the white unenriched crystals in MeCN (1 ml) after adding 3 drops of DMSO. Colourless cubic crystals formed after about 6 weeks. Anal.

Calcd for $[(C_4H_9)_4N]_6[NaPW_{11}O_{39}]$: N, 2.02; C, 27.75; H, 5.24. Found: N, 2.14; C, 27.63; H, 5.88; **IR (4000 – 400 cm^{-1}):** 2958 (m), 2930 (m), 2869 (m), 1661(vw), 1480 (m), 1378 (w), 1152 (vw), 1106 (vw), 1070 (m), 1034 (m), 933 (s), 880 (m), 843 (s), 804 (s), 714 (vs, br), 589 (m), 504 (m), 431 (m), 409 (m); **^{31}P NMR (**161.83 MHz, CD_3CN**):** δ (ppm), -10.40, line width fwhm = 3.70 Hz, **^{1}H NMR** (399.78 MHz, CD_3CN): δ (ppm), 3.24 – 320, 1.69-1.61, 1.46-1.37 and 0.94 – 0.98 (TBA resonances); **^{17}O NMR** (67.84 MHz, CH_3CN): δ (ppm), 707 – 644 (6 peaks assigned to W=O), 438 – 433 (1 peak and a shoulder peak assigned to NaOW), 402 – 363 (2 broad peaks and a shoulder peak assigned to WOW); **^{183}W NMR** (20.84 MHz, CD_3CN): δ (ppm), -75.55 (2), -82.70 (2), -82.91 (2), -100.52 (1), -115.08 (2), -137.03 (2).

10.5.7. Preparation of $(TBA)_4[ClSnPW_{11}O_{39}]$

$(TBA)_6[NaPW_{11}O_{39}]$ (6 g, 1.44 mmol) was dissolved in MeCN (20 ml) in a Schlenk flask inside a glove box. 0.03 M $SnCl_4$ in MeCN (48 ml, 1.44 mmol) was added and the solution was stirred for 1 h. The cloudy white solution was allowed to settle and was then filtered *via* a cannula with subsequent washing and filtering of the original solution to improve product yield. The filtrate was vacuum-dried, washed with DCM (20 ml x 3) and re-vacuum dried to obtain 5.02g (92%) of crude product. The white solid was redissolved by heating in MeCN (50 ml) and allowed to stand overnight. Pale solid settled out and the top clear solution was filtered, concentrated to ~25 ml and allowed to crystallise. 2.94g of pure product was obtained. The mother liquor was concentrated and more product was crystalized. A total of 4.31 g (**79%**) of pure product was obtained after three crystallisation steps. Anal. Calcd for $[(C_4H_9)_4N]_4ClSnPW_{11}O_{39}$: C, 20.22; H, 3.81; N, 1.47. Found: C, 19.81; H, 3.81; N, 1.32. **IR (4000 – 400 cm^{-1}):** 2960 (m), 2934 (m), 2872 (m), 1482 (m), 1381 (w), 1079 (m), 1056 (m), 962 (s), 880 (m), 787 (vs, br), 702 (s), 658 (s) 593 (m), 513 (m), 434 (w), 412 (w); **^{31}P NMR** (161.83 MHz, CD_3CN): δ (ppm), -12.90, line width fwhm = 3.04 Hz [^{2}J(Sn-P) = 37 Hz]; **^{119}Sn NMR** (186.40 MHz, CD_3CN**):** δ (ppm), -578.08, line width fwhm = 7.15 Hz [^{2}J (^{119}Sn^{183}W$_A$) = 157 Hz; ^{2}J (^{119}Sn^{183}W$_F$) = 63 Hz, see **Figure 4.18** for labelling]; **^{17}O NMR** (54.20 MHz, CH_3CN): δ (ppm), 749 – 737 (3 peaks assigned to W=O), 429 – 372 (3 major peaks and 4 smaller peaks assigned to SnOW and WOW); **^{183}W NMR** (20.84 MHz, CD_3CN): δ (ppm), -76.78 (2), -91.41 (2), -108.35 (2), -114.80 (2), -130.65 (1), -174.49 (2).

10.5.8. Preparation of $(TBA)_4[ClTiPW_{11}O_{39}]$

$(TBA)_6[NaPW_{11}O_{39}]$ (5 g, 1.20 mmol) was dissolved in DCM (20 ml) in a Schlenk flask inside a glove box to give a clear colourless solution. 0.05 M $TiCl_4$ in DCM (24 ml, 1.20 mmol) was added and the clear solution immediately changed to yellow with precipitation of some pale solid. The solution was stirred for 1 h, allowed to settle and filtered. The solid was washed with DCM (30ml x 8) until the solution became clear. The solid was vacuum-dried, redissolved in MeCN (30ml) and allowed to stand for 1h. It was filtered *via* cannula filter stick and dried to obtain a crude product (3.89 g). Pure crystals were obtained by recrystallisation from hot MeCN (2.98 g, 67%). **IR (4000 – 400 cm^{-1}):** 2960 (m), 2934 (m), 2873 (m), 1482 (m), 1381 (w), 1152 (vw), 1071 (s), 962 (vs), 883 (s), 787 (vs, br), 594 (m), 504 (s), 472 (m), 431 (w), 412 (w); **^{31}P NMR** (161.83 MHz, CD_3CN): δ (ppm), -14.36, line width fwhm = 3.10 Hz; **^{17}O NMR** (54.20 MHz, CH_3CN): δ (ppm), 747 – 743 (2 peaks assigned to W=O), 585, 565 (2 sharp peaks assigned to TiOW), 427 – 386 (2 major broad peaks with shoulders and a minor peak assigned to WOW).

10.5.9. Preparation of $(TBA)_5[SnPW_{11}O_{39}]$

$TBA)_6[NaPW_{11}O_{39}]$ (6 g, 1.44 mmol) was dissolved in MeCN (30 ml) in a glove box. $SnCl_2$ (0.27 g, 1.44 mmol) was added and the colour changed instantly from colourless to deep orange-yellow to pale yellow. The solution was stirred for ~ 1 h before allowing it to settle for 4 h. The yellow solution was filtered, vacuum-dried, washed with EtOAc (20 ml x 3) and vacuum-dried for 2 h to obtain 4.97g of greenish-yellow solid. The solid was purified by dissolving in DCM (20 ml), allowing the solution to settle and filtering the clear greenish yellow solution before vacuum-drying for 4 h (**4.62 g, 80%)**. Anal. Calcd for $[(C_4H_9)_4N]_5SnPW_{11}O_{39}$: C, 23.97; H, 4.53; N, 1.75. Found: C, 24.03; H, 5.04; N, 1.68. **IR (4000 – 400 cm^{-1}):** 2958 (m), 2932 (m), 2871 (m), 1481 (m), 1379 (w), 1153(vw), 1097 (m), 1046 (m), 942 (s), 872 (m), 787 (vs, br), 681 (s), 660 (s) 594 (m), 509 (m), 485 (m), 432 (w), 411 (w); **^{31}P NMR** (121.49 MHz, CD_3CN): δ (ppm), -13.22, line width fwhm = 2.98 Hz; **^{119}Sn NMR** (111.89 MHz, CD_3CN)**:** δ (ppm), -684.38, line width fwhm = 14.97 Hz [^2J ($^{119}Sn^{183}W_A$) = 131 Hz; ^2J ($^{119}Sn^{183}W_F$) = 91 Hz, see **Figure 4.18** for labelling]; **^{17}O NMR** (54.20 MHz, CH_3CN): δ (ppm), 720 – 701 (3 peaks assigned to W=O), 527 – 522 (a broad peak with a shoulder assigned to SnOW), 426 – 379 (a sharp peak, and two broad peaks with shoulders assigned to WOW); **^{183}W NMR** (20.84 MHz, CD_3CN): δ (ppm), -62.78 (2), -96.30 (2), -106.06 (2), -106.89 (1), -115.94 (2), -127.17(2).

10.5.10. Preparation of $(TBA)_5[PbPW_{11}O_{39}]$

$(TBA)_6[NaPW_{11}O_{39}]$ (4 g, 0.963 mmol) was dissolved in MeCN (20 ml). $Pb(CH_3COO)_2.3H_2O$ (0.37 g, 0.963 mmol) was added with stirring and the clear solution became cloudy. The solution was stirred for 1 h before allowing it to settle for ~12 h. The top clear solution was filtered *via* cannula and vacuum-dried for 4 h. The white solid obtained was further washed with EtOAc (10 ml x 3) and diethyl ether (10 ml) before drying under vacuum for 4 h. (**3.14 g, 80 %)**. Anal. Calcd for $[(C_4H_9)_4N]_5PbPW_{11}O_{39}$: C, 23.46; H, 4.43; N, 1.71. Found: C, 24.11; H, 5.51; N, 1.77. **IR (4000 – 400 cm^{-1}):** 2958 (m), 2932 (m), 2871 (m), 1481 (m), 1379 (w), 1153(vw), 1083 (m), 1040 (m), 940 (s), 873 (m), 787 (vs, br), 687 (s), 665 (s) 592 (m), 507 (m), 481 (m), 431 (w), 410 (w); **^{31}P NMR** (121.49 MHz, CD_3CN): δ (ppm), -11.99, line width fwhm = 3.39 Hz; **^{207}Pb NMR** (104.58 MHz, CD_3CN)**:** δ (ppm), -355.52, line width fwhm = 3109 Hz; **^{17}O NMR** (54.20 MHz, CH_3CN): δ (ppm), 718 – 694 (3 peaks with a shoulder assigned to W=O), 566 (a sharp peak assigned to PbOW), 426 – 372 (three broad peak with a shoulder and a minor peak assigned to WOW); **^{183}W NMR** (20.84 MHz, CD_3CN): δ (ppm), -48.92 (2), -77.53 (2), -92.57 (2), -97.77(1), -116.18 (2), -129.90(2).

10.5.11. Preparation of $(TBA)_4[BiPW_{11}O_{39}]$

$(TBA)_6[NaPW_{11}O_{39}]$ (6 g, 1.44 mmol) was dissolved in MeCN (30 ml). $BiCl_3$ (0.46 g, 1.44 mmol) was added and the resulting cloudy solution was stirred for 1 h and allowed to settle for ~12 h. The top clear solution was filtered *via* cannula filter stick, vacuum-dried and washed with EtOAc (10 ml x 3) before vacuum-drying to obtain a white solid. (**4.97 g, 84 %)**. Anal. Calcd for $[(C_4H_9)_4N]_4BiPW_{11}O_{39}$: C, 19.94; H, 3.76; N, 1.45. Found: C, 19.83; H, 3.85; N, 1.53. **IR (4000 – 400 cm^{-1}):** 2959 (m), 2932 (m), 2872 (m), 1482 (m), 1380 (w), 1153(vw), 1084 (m), 1053 (m), 952 (s), 879 (m), 784 (vs, br), 594 (m), 513 (m), 431 (w), 410 (w); **^{31}P NMR** (121.49 MHz, CD_3CN): δ (ppm), -12.54, line width fwhm = 5.74 Hz; **^{17}O NMR** (54.20 MHz, CH_3CN): δ (ppm), 743 – 719 (1 major peak and 2 minor peaks assigned to W=O), 487 (a broad peak assigned to BiOW), 425 – 384 (two broad peaks with shoulders assigned to WOW); **^{183}W NMR** (20.84 MHz, CD_3CN): δ (ppm), -40.61 (2), -60.35(2), -92.49 (2), -102.31(1), -115.70 (2), -121.22 (2).

10.5.12. Preparation of $(TBA)_4[SbPW_{11}O_{39}]$

$(TBA)_6[NaPW_{11}O_{39}]$ (2 g, 0.48 mmol) was dissolved in MeCN (20 ml). $SbCl_3$ (0.11 g, 0.48 mmol) was added and the clear solution turn cloudy. The solution was stirred for 1 h and centrifuged (4200 rpm) for 15 min. The collected clear solution was vacuum-dried, washed with DCM (10

ml x 3) and vacuum-dried to obtain a white solid. (**1.13 g, 58 %)**. Anal. Calcd for $[(C_4H_9)_4N]_4SbPW_{11}O_{39}$: C, 20.40; H, 3.85; N, 1.49. Found: C, 17.83; H, 3.60; N, 1.35. **IR (4000 – 400 cm^{-1}):** 2959 (m), 2935 (m), 2872 (m), 1482 (m), 1381 (w), 1152(vw), 1101 (m), 1061 (m), 955 (s), 880 (m), 787 (vs, br), 597 (m), 516 (m), 430 (w), 406 (w); **^{31}P NMR** (161.83 MHz, CD_3CN): δ (ppm), -14.22, line width fwhm = 3.42 Hz; **^{17}O NMR** (54.20 MHz, CH_3CN): δ (ppm), 750 – 730 (4 peaks assigned to W=O), 427 – 384 (five peaks assigned to SbOW and WOW); **^{183}W NMR** (20.84 MHz, DMSO-d6): δ (ppm), -82.04 (2), -96.46(2), -105.00 (1), -111.88(2), -114.96 (2), -142.33 (2).

10.5.13. Preparation of $(TBA)_5[CoPW_{11}O_{39}]$

$(TBA)_6[NaPW_{11}O_{39}]$ (8.9 g, 2.14 mmol) was dissolved in MeCN (40ml) to give a clear solution. A solution of $[Co(H_2O)_6](NO_3)_2$ (0.62 g, 2.14 mmol) in MeCN (15ml) was added to the original solution with stirring to give a cloudy purple solution. The mixture was allowed to stir for 2 h and left to settle before filtering the pink solution *via* a cannula filter stick, which was vacuum-dried to give a pink solid. The solid was dissolved in DCM (35ml), washed five times with water (50ml), vacuum-dried for 4 h with gentle heating to give a green solid, which was redissolved in DCM (10ml) to give a green solution and a pale precipitate. The dark green solution was filtered *via* a cannula filter stick and the filtrate was vacuum dried to give green solid (**4.97g, 58.86%**). **IR (4000 – 400 cm^{-1}):** 2958(m), 2871(m), 1482(m), 1379(w), 1153 (vw), 1065 (s), 946 (s), 873(s), 792 (vs), 729(s), 689(s), 590(m), 511(m), 488(m), 408(m); **^{31}P NMR** (121.53 MHz, CD_2Cl_2): δ (ppm), 273.23, line width fwhm = 210 Hz; (121.53 MHz, CD_3CN): δ (ppm), 330.92, line width fwhm = 77.10 Hz.

10.5.14. Preparation of $(TBA)_5[NiPW_{11}O_{39}]$

$(TBA)_6[NaPW_{11}O_{39}]$ (4.87 g, 1.17 mmol) was dissolved in MeCN (30ml) to give a cloudy white solution. A green solution of $NiBr_2.3H_2O$ (0.31 g, 1.17 mmol) dissolved in MeCN (15ml) was transferred *via* cannula into the original solution. The light green solution was stirred for 3 h and allowed to settle overnight. It was filtered *via* a cannula filter stick, vacuum dried and dissolved in DCM (10ml). The resulting solution was washed five times with distilled water (50ml) and vacuum dried to give light green solid (**2.13g, 46.2%**). **IR(4000 – 400 cm^{-1}):** 2959(m), 2871(m), 1482(m), 1379(w), 1153(vw), 1062(s), 946(s), 875(s), 793(vs), 736(s), 696(s), 591(m), 510(m), 488(m), 433(m), 411(m); **^{31}P NMR** (121.49 MHz, CD_3CN): δ (ppm), -12.78, line width fwhm = 3.84 Hz.

10.5.15. Reaction between $(TBA)_6[NaPW_{11}O_{39}]$ and $[Mo_2(NCCH_3)_8(ax\text{-}CH_3CN)_{0.5}][BF_4]_4$

To a clear solution of $(TBA)_6[NaPW_{11}O_{39}]$ (1.0 g, 0.24 mmol) in MeCN (15 ml) was added a deep blue solution of $[Mo_2(NCCH_3)_8(ax\text{-}CH_3CN)_{0.5}][BF_4]_4$ (0.1 g, 0.12 mmol) in MeCN (5 ml) *via* cannula with washing with more MeCN (5 ml). The colour of the resultant solution changed to dark green. A ^{31}P NMR spectrum was recorded. The solution was allowed to stir for 12 h, vacuum-dried and washed with diethyl ether (10 ml x 3) and vacuum-dried to obtain a dark solid. **IR (4000 – 400 cm^{-1}):** 2961(m), 2934(m), 2873 (m), 1483(m), 1381(w), 1283(vw), 1152(vw), 1047 (s), 1036(s) 943(s, sh), 881(s), 853(m), 783(vs, br), 729(vs, br), 592(m), 510(s), 431(w).

10.5.16. Attempted preparation of $(TBA)_5[ClRh^{III}PW_{11}O_{39}]$

$(TBA)_6[NaPW_{11}O_{39}]$ (0.2 g, 0.05 mmol), $RhCl_3$ (0.012 g, 0.05 mmol) and DMSO (1 ml) were added to a 5-mm screw-capped NMR tube. The orange solution was heated at 120 ^oC for 5 h, 7, 12, 30, 36, 40, 58, 82 and 114 h with recording of the ^{31}P NMR spectra.

In a second experiment, $(TBA)_6[NaPW_{11}O_{39}]$ (0.2 g, 0.05 mmol), $RhCl_3$ (0.012 g, 0.05 mmol) and DMSO (1 ml) were added to a 5-mm screw-capped NMR tube. The orange solution was heated at 150 ^oC for 18.5 h and a ^{31}P NMR spectrum was recorded. The dark orange solution was transferred into a Schlenk flask, washed with diethyl ether (10 ml x 4) and vacuum-dried. The solid was redissolved in MeCN (5 ml), allowed to settle and filtered *via* cannula and pumped dry again to obtain an orange solid. The ^{31}P NMR spectrum was recorded.

10.5.17. Attempted preparation of $(TBA)_5[ClIr^{III}PW_{11}O_{39}]$

$(TBA)_6[NaPW_{11}O_{39}]$ (0.2 g, 0.05 mmol) was dissolved in DMSO (1 ml) in a 5-mm screw-capped NMR tube to give a clear solution. $IrCl_3$ (0.014 g, 0.05 mmol) was added and heated at 150 ^oC with the ^{31}P NMR spectra recorded after 0 min , 80 min, 18 h 10 min, 22 h 45 min, 40 h, 48 h, 65 h and 72 h. The solution was transferred into a Schlenk flask, vacuum-dried, washed with diethyl ethyl (5 ml x 5), dissolved in MeCN (10 ml), filtered *via* cannula filter stick and vacuum-dried again. The solid was dissolved in DCM (10 ml), filtered and vacuum-dried to get a dark solid. The ^{31}P NMR spectrum was recorded.

10.5.18. Attempted preparation of $(TBA)_4[ClIr^{IV}PW_{11}O_{39}]$

$(TBA)_6[NaPW_{11}O_{39}]$ (1.5 g, 0.36 mmol) was dissolved in DMSO (3 ml). $Na_2IrCl_6.xH_2O$ (0.2 g, 0.36 mmol, 35.37% Ir) was added and the colour of the solution changed from colourless to dark brown. The solution was heated at 150 ^oC with recording of the ^{31}P NMR spectra at 50 mins, 140 mins, 20 h, 24 h 15 mins, 27 h 20 mins and 44 h. A greenish yellow solution appeared after heating at 150 ^oC for 140 mins and the solution became dark green after 140 mins. The solution was triturated with Et_2O (10ml x 7) and vacuum dried. It was redissolved in DCM (5ml) and allowed to settle before filtering and vacuum-drying the dark blue solution. The dark solid was redissolved in MeCN (10ml), vacuum filtered and dried to give dark blue solid. (**0.23g, 23%**). The ^{31}P NMR spectrum of the product was recorded.

10.5.19. Attempted preparation of $(TBA)_4[ClPt^{IV}PW_{11}O_{39}]$

$(TBA)_6[NaPW_{11}O_{39}]$ (0.22 g, 0.053 mmol) was dissolved in DMSO (0.4 ml) in a 5-mm o.d. screw capped NMR tube to give a clear solution. Na_2PtCl_6 (0.03 g, 0.053 mmol) was added and the orange solution was heated at 100 ^oC with recording of the ^{31}P and ^{195}Pt NMR spectra after 10 min, 1, 3, 4 and 18 h. As a control spectra were also recorded with only Na_2PtCl_6 (0.03 g, 0.053 mmol) in DMSO.

In a second experiment, $(TBA)_6[NaPW_{11}O_{39}]$ (0.1 g, 0.24 mmol) was dissolved in DMSO (3 ml). Na_2PtCl_6 (0.11 g, 0.24 mmol) was added and the orange solution was heated at 100 ^oC for 5 h with recording of a ^{31}P NMR spectrum. The solution was then triturated with Et_2O (20 ml x 5), washed with EtOAc (20 ml x 2) and pumped dry. The solid was dissolved in DCM (15 ml) and the orange solution was filtered *via* a cannula filter-stick, vacuum-dried and redissolved in MeCN (15 ml). The solution was allowed to settle, filtered *via* a cannula filter-stick and vacuum-dried again before recording the ^{31}P and ^{195}Pt NMR spectra.

10.5.20. Attempted preparation of $(TBA)_4[(NO_3)Ce^{IV}PW_{11}O_{39}]$

$(TBA)_6[NaPW_{11}O_{39}]$ (0.5 g, 0.12 mmol) was dissolved in MeCN (5 ml). An orange solution of $(NH_4)_2[Ce(NO_3)_6]$ (1.2 ml, 0.1 M in MeCN, 0.12 mmol) was added and the solution turned cloudy green. The solution was stirred for 1 h and allowed to settle before recording a ^{31}P NMR spectrum. The solution was then allowed to stir for 18 h. After settling, it was filtered *via* cannula filter-stick and vacuum-dried before washing with EtOAc (10 ml x 3) and vacuum-dried again to obtain a greenish yellow solid. **IR(4000 – 400 cm^{-1}):** 2960(m), 2933(m) 2873(m),

1731(vw), 1483(m), 1380(w), 1305(m), 1153(w), 1106(m), 1049(m), 952(s), 880(m), 785(vs, br), 732(vs, sh), 592(m), 511(m); **^{31}P NMR** (121.49 MHz, CD_3CN): δ (ppm), -12.30, line width fwhm = 4.31 Hz.

10.5.21. Attempted preparation of $(TBA)_3[(dmso)Ce^{IV}PW_{11}O_{39}]$

$(TBA)_6[NaPW_{11}O_{39}]$ (0.5 g, 0.12 mmol) was dissolved in MeCN (10 ml). DMSO (0.35ml, 4.8 mmol) and orange solution of $(NH_4)_2[Ce(NO_3)_6]$ (1.2 ml, 0.1 M in MeCN, 0.12 mmol) were added and orange red precipitates formed immediately. The solution was stirred for 1 h and allowed to settle before recording a ^{31}P NMR spectrum. The top yellow solution was filtered *via* cannula filter-stick and vacuum-dried to obtain a sticky yellow mass, which was triturated with diethyl ether (10 ml x 10) and vacuum-dried to obtain a yellow solid. The IR and ^{31}P NMR spectra of the product were recorded. **IR(4000 – 400 cm^{-1}):** 3248(w, br), 2960(m), 2935(m), 2874(m), 1743(vw), 1487(m), 1430(m), 1321(vs), 1152(vw), 1048(m), 953(s), 882(m), 789(vs, br), 734(s, sh), 593(m), 514(m); **^{31}P NMR** (121.49 MHz, CD_3CN): δ (ppm), -12.34, line width fwhm = 2.97 Hz. Crystallisation was attempted by slow diffusion of diethyl ethyl vapour into an acetonitrile solution of the solid product.

10.5.22. Preparation of $(TBA)_{10}[Ce^{IV}(PW_{11}O_{39})_2]$

$(TBA)_6[NaPW_{11}O_{39}]$ (0.2 g, 0.048 mmol) was dissolved in MeCN (0.5 ml) in a screw-capped NMR tube. An orange solution of $(NH_4)_2[Ce(NO_3)_6]$ (0.24 ml, 01 M in MeCN, 0.024 mmol) was added and the clear colourless solution turned cloudy yellow. A ^{31}P NMR spectrum was recorded after vigorous shaking for 30 mins.

10.6. Experimental for Chapter 4

10.6.1. Preparation of $(TBA)_4[(CH_3O)SnPW_{11}O_{39}]$

$(TBA)_4[ClSnPW_{11}O_{39}]$ (1.71 g, 0.450 mmol) was dissolved in MeCN (15 ml). CH_3ONa (6.75 ml, 0.1 M solution in MeOH, 0.675 mmol, 1.5 eq) was added and the clear solution was allowed to stir for ~1 h. The solution was vacuum-dried to give a white solid, which was washed with DCM (10 ml x 3) and vacuum-dried again. The white solid was redissolved in MeCN (20 ml) and the cloudy solution was allowed to settle overnight, filtered before adding MeOH (10 ml). The clear solution was stirred for 5 min before vacuum-drying to give a white solid. (**1.15 g, 67%).** Anal. Calcd for $[(C_4H_9)_4N]_4CH_3OSnPW_{11}O_{39}$: C, 20.56; H, 3.90; N, 1.48. Found: C, 20.38;

H, 4.15; N, 1.17. **IR (4000 – 400 cm^{-1}):** 2958 (m), 2932 (m), 2871 (m), 2819 (w) assigned to OMe, 1482 (m), 1380 (w), 1077 (m), 1058 (m), 961 (s), 881 (m), 791 (vs, br), 708 (s), 662 (s) 592 (m), 552 (m), 511 (s), 434 (w); **^{1}H NMR** (500.15 MHz, CD_3CN): In addition to TBA resonances at 3.17−3.14, 1.68−1.61, 1.44−1.37, and 1.00−0.97, δ (ppm), 3.68 was observed for methoxyl protons with tin satellites [$^{3}J(^{1}H\text{-}^{119}Sn)$ = 81 Hz, $^{3}J(^{1}H\text{-}^{117}Sn)$ = 78 Hz]. The ratio of methoxyl protons to CH_2N protons was 1:13 (calculated 1:11); **^{13}C NMR** (176.07 MHz, CD_3CN)**:** δ (ppm), 53.82 [$^{2}J(^{13}C\text{-}^{117/119}Sn)$ = 39 Hz]. **^{31}P NMR** (121.49 MHz, CD_3CN/CH_3OH): δ (ppm), -12.66, line width fwhm = 2.96 Hz [^{2}J(Sn-P) = 37 Hz]; **^{119}Sn NMR** (186.40 MHz, CD_3CN/ CH_3OH)**:** δ (ppm), -622.09, line width fwhm = 1.45 Hz [^{2}J ($^{119}Sn^{183}W_A$) = 149 Hz; ^{2}J ($^{119}Sn^{183}W_F$) = 58 Hz, see **Figure 4.18** for labelling]; **^{17}O NMR** (54.20 MHz, CH_3CN/CH_3OH): δ (ppm), 745 – 731 (3 peaks assigned to W=O), 427 – 333 (1 well resolved and several unresolved peaks assigned to SnOW and WOW); **^{183}W NMR** (20.84 MHz, CD_3CN/CH_3OH): δ (ppm), -70.82 (2), -91.50 (2), -109.29 (2), -115.10 (2), -130.89 (1), -169.70 (2).

10.6.2. Preparation of $(TBA)_4[(HO)SnPW_{11}O_{39}]$

$(TBA)_4[CH_3OSnPW_{11}O_{39}]$ (0.65 g, 0.171 mmol) was dissolved in MeCN (15 ml). H_2O (7 µl, 0.389 mmol) was added and the mixture was stirred for ~ 30 min, vacuum dried for 5 h, washed with ether (20 ml x 3) and vacuum dried again before recording the weight of the crude product (**0.61 g, 92%).** The white solid was recrystallised from hot MeCN solution (0.47g, 72%). Anal. Calcd for $[(C_4H_9)_4N]_4HOSnPW_{11}O_{39}$: C, 20.32; H, 3.86; N, 1.48. Found: C, 20.36; H, 4.26; N, 1.27. **IR (4000 – 400 cm^{-1}):** 3639 (w) assigned to free OH, 2959 (w), 2934 (w), 2872 (w), 1482 (m), 1381 (w), 1077 (m), 1058 (m), 961 (s), 882 (m), 789 (vs, br), 705 (s), 661 (s), 591 (m), 512 (s), 434 (w), 411 (w); **^{1}H NMR** (300.13 MHz): In addition to TBA resonances at 3.18−3.12, 1.70−1.59, 1.46−1.33, and 1.01−0.96 in CD_3CN, δ (ppm), 1.98 was observed for hydroxyl proton with tin satellites [$^{2}J(^{1}H\text{-}^{119}Sn)$ = 48 Hz (It was not possible to obtain the integral ratio of the hydroxyl proton to CH_2N protons due to overlap with CD_3CN peaks). In addition to TBA resonances at 3.21−3.15, 1.58, 1.39−1.27, and 0.96−0.91 in DMSO-d6, δ (ppm), 3.98 was observed for hydroxyl proton with tin satellites $^{2}J(^{1}H\text{-}^{117/119}Sn)$ = 42 Hz]. The ratio of hydroxyl proton to CH_2N protons was 1:39 (calculated 1:32); **^{31}P NMR** (121.49 MHz, CD_3CN): δ (ppm), -12.60, line width fwhm = 3.96 Hz [^{2}J(Sn-P) = 34 Hz]; **^{119}Sn NMR** (186.40 MHz, CD_3CN)**:** δ (ppm), -600.24, line width fwhm = 11.58 Hz [^{2}J ($^{119}Sn^{183}W_A$) = 149 Hz; ^{2}J ($^{119}Sn^{183}W_F$) = 56 Hz, see **Figure 4.18** for labelling]; **^{17}O NMR** (54.20 MHz, CH_3CN): δ (ppm), 746 – 733 (3 peaks assigned to

W=O), 427 – 340 (6 peaks assigned to SnOW and WOW); **^{183}W NMR** (20.84 MHz, CD_3CN): δ (ppm), -76.42 (2), -90.43 (2), -108.70 (2), -114.08 (2), -128.65 (1), -175.17 (2).

10.6.3. Preparation of $(TBA)_4[(DO)SnPW_{11}O_{39}]$

$(TBA)_4[CH_3OSnPW_{11}O_{39}]$ (0.15 g, 0.04 mmol) was dissolved in MeCN (0.5 ml) to give a colourless solution. D_2O (2 ml, 111 mmol) was added and white precipitate formed immediately. The mixture was allowed to stir for ~ 1 h and vacuum dried. (**0.15 g, 100%**). **IR (4000 – 400 cm^{-1}):** 2958(w), 2934.39(w), 2872 (w), 2684 (vw) assigned to free OD, 1482 (m), 1381 (w), 1152.78 (s), 1078 (m), 1058 (m), 961 (s), 882 (s), 792 (vs, br), 710 (m), 665 (m), 591(m), 512(m), 433 (w), 412(w); **^{31}P NMR** (121.49 MHz, CD_3CN): δ (ppm), -12.60, line width fwhm = 2.87 Hz [^{2}J(Sn-P) = 34 Hz]; **^{119}Sn NMR** (186.40 MHz, CD_3CN)**:** δ (ppm), -599.824, line width fwhm = 19.82 Hz

10.6.4. Preparation of $(TBA)_8[(\mu\text{-}O)(SnPW_{11}O_{39})_2]$

$(TBA)_4[HOSnPW_{11}O_{39}]$ (0.54 g, 0.14 mmol) was dissolved in MeCN (10 ml). *N, N'*-Dicyclohexylcarbodiimide (DCC) (0.21 g, 0.99 mmol, 14 eq) was added and heated at ~120 ^{o}C for 48 h. The solution was allowed to cool to room temperature for 2 h, within which some colourless crystals came out of solution. The solution was then filtered *via* cannula filter stick, vacuum dried and washed with THF (15 ml X 6). It was vacuum dried for 1 h to obtain a white solid (**0.28 g, 52 %). IR (4000 – 400 cm^{-1}):** 2960 (m), 2932(m), 2872(m), 1482(m), 1379(w), 1153 (vw), 1065(s, sh), 959(vs), 882(s), 802(vs), 748(vs), 708(s), 663(s), 593(m), 495(m), 433(w), 411(w); **^{31}P NMR** (121.49 MHz, CD_3CN): δ (ppm), -12.64, line width fwhm = 3.16 Hz [^{2}J(Sn-P) = 28 Hz]. The product contained $(TBA)_4[ClSnPW_{11}O_{39}]$ impurity peak at -12.90 (3.3%) from the starting material and two other impurity peaks at -13.31 (7.9%) and -14.0 (1.4%), which were side products of the reaction and were yet to be assigned; **^{119}Sn NMR** (186.40 MHz, CD_3CN)**:** δ (ppm), -620.42, line width fwhm = 10.64 Hz [^{2}J ($^{119}Sn^{183}W_A$) = 164 Hz; ^{2}J ($^{119}Sn^{183}W_F$) = 67 Hz, see **Figure 4.18** for labelling]; **^{17}O NMR** (54.20 MHz, CH_3CN): δ (ppm), 740 – 732 (3 broad peaks assigned to W=O), 429 – 374 (3 broad peaks with a shoulder and a minor peak assigned to SnOW and WOW). The peak for SnOSn was not observed; **^{183}W NMR** (20.84 MHz, CD_3CN): δ (ppm), -82.48 (2), -89.69 (2), -109.39 (2), -114.66 (2), -127.06 (1), -182.18 (2).

10.6.5. Reaction between $(TBA)_4[(HO)SnPW_{11}O_{39}]$ and 4-$Bu^tC_6H_4O$

$(TBA)_4[HOSnPW_{11}O_{39}]$ (0.3 g, 0.079 mmol) was dissolved in MeCN (10 ml) to give a colourless solution. 4-tert-butylphenol (0.06 g, 0.40 mmol) was added and the mixture was heated at 90 ^oC with stirring for 18 h before vacuum drying. It was washed with toluene (20ml x 3), EtOAc (20ml x 2) and Ether (20 ml x 3) and vacuum dried to obtain 0.27 g of product. **IR (4000 – 400 cm^{-1}):** 2960 (w), 2873 (w), 1508 (w), 1482 (m), 1380 (w), 1250 (w), 1151 (vw), 1077 (m), 1056 (m), 962 (s), 882 (m), 785 (vs, br), 706 (s), 660 (s), 593 (m), 550 (m), 512 (s), 434 (w), 410 (w); **^{31}P NMR** (121.49 MHz, CD_3CN): δ (ppm), -12.82 (78.4%), line width fwhm = 3.34 Hz [^2J(Sn-P) = 36.86 Hz]. The product contained impurity peaks at -12.90 (11.7%) for $(TBA)_4[ClSnPW_{11}O_{39}]$from the starting material and at -12.60 (9.9%) for unreacted $(TBA)_4[(HO)SnPW_{11}O_{39}]$ or due to hydrolysis; **^{119}Sn NMR** (111.89 MHz, CD_3CN)**:** δ (ppm), -647.17, line width fwhm = 10.12 Hz; **^{1}H NMR (**300.13 MHz, CD_3CN**):** δ (ppm), 7.25, 7.24, 7.23, 7.22, 7.21, 7.20, 6.91, 6.90, 6.89, 6.88, 6.87, 6.77, 6.75, 6.74, 6.73, 6.72, 6.71, 3.18, 3.17, 3.15, 3.14, 3.13, 2.20, 2.15, 1.96, 1.94, 1.93, 1.92, 1.70, 1.67, 1.66, 1.65, 1.63, 1.62, 1.61, 1.59, 1.47, 1.44, 1.42, 1.39, 1.37, 1.35, 1.28 -1.26 (4-tert-butyl), 1.01, 0.99, 0.96. The ratio of aromatic protons to CH_2N protons is not reported because of the impurity (~20%) in the product, which will affect the ratio. **^{13}C NMR** (75.48 MHz, CD_3CN): δ (ppm), 126.38, 120.00, 117.88, 115.18, 58.93, 58.89, 58.85, 31.54, 31.38, 24.01, 19.97, 13.52, 1.73, 1.45, 1.18, 0.94, 0.90, 0.63, 0.35, 0.07.

10.6.6. Reaction between $(TBA)_4[(HO)SnPW_{11}O_{39}]$ and 3, 5-$Me_2C_6H_3O$

$(TBA)_4[HOSnPW_{11}O_{39}]$ (0.3g, 0.079 mmol) was dissolved in MeCN (10 ml) to give a colourless solution. 3, 5-dimethylphenol (0.049 g, 0.40 mmol) was added and the mixture was heated at 90 ^oC with stirring for 18 h before vacuum drying. It was washed with toluene (20ml x 3), EtOAc (20ml x 2) and Ether (20 ml x 3) and vacuum dried to obtain 0.25 g of product. **IR (4000 – 400 cm^{-1}):** 2960 (w), 2933 (w), 2873 (w), 1592 (w), 1482 (m), 1380 (w), 1315 (w), 1152 (w), 1077 (m), 1056 (m), 962 (s), 880 (m), 787 (vs, br), 706 (s), 663 (s), 593 (m), 512 (s), 434 (w), 410 (w); **^{31}P NMR** (121.49 MHz, CD_3CN): δ (ppm), -12.83 (87.4%), line width fwhm = 3.09 Hz [^2J(Sn-P) = 36.45 Hz]. The product contained impurity peaks at -12.90 (9.7%) for $(TBA)_4[ClSnPW_{11}O_{39}]$ from the starting material and at -12.60 (2.9%) from unreacted $(TBA)_4[(HO)SnPW_{11}O_{39}]$ or due to hydrolysis; **^{119}Sn NMR** (111.89 MHz, CD_3CN)**:** δ (ppm), -647.34, line width fwhm = 9.91 Hz [^2J ($^{119}Sn^{183}W_A$) = 157 Hz; ^2J ($^{119}Sn^{183}W_F$) = 67 Hz, see **Figure 4.18** for labelling]; **^{1}H NMR (**300.13

MHz, CD_3CN**):** δ (ppm), 6.68, 6.63, 6.51, 6.47, 6.42, 3.16, 3.15, 3.14, 3.12, 3.11, 2.33, 2.22, 2.21, 1.96, 1.96, 1.95, 1.94, 1.94, 1.93, 1.69, 1.66, 1.65, 1.64, 1.62, 1.61, 1.60, 1.58, 1.46, 1.43, 1.41, 1.38, 1.36, 1.34, 1.01, 1.01, 0.98, 0.96. The ratio of aromatic protons to CH_2N protons is not reported because of the impurity (~13%) in the product, which will affect the ratio. **^{13}C NMR** (75.48 MHz, CD_3CN): δ (ppm), 139.87, 121.95, 117.87, 113.40, 58.93, 58.90, 58.86, 23.99, 19.96, 13.50, 1.73, 1.45, 1.18, 0.90, 0.63, 0.35, 0.08.

10.6.7. Reaction between $(TBA)_4([(HO)SnPW_{11}O_{39}]$ and 2, 4, 6-Tri-$Bu^tC_6H_4O$

$(TBA)_4[HOSnPW_{11}O_{39}]$ (0.2 g, 0.053 mmol) was dissolved in MeCN/CD_3CN (1 ml) in an NMR tube to give a colourless solution. 2, 4, 6-tri-tetbutylphenol, $[(CH_3)_3C]_3C_6H_3OH$ (0.06 g, 0.229 mmol) was added and the mixture was heated gently to a clear orange solution and a ^{31}P NMR spectrum was recorded. It was subsequently heated at ~90 ^{o}C for 18 h and a ^{31}P NMR spectrum was recorded before transferring the solution into a Schlenk flask and vacuum drying. The solid washed with toluene (20ml x 3), EtOAc (20ml x 2) and Ether (20 ml x 3) and vacuum dried. The IR and NMR spectra of the product were recorded.

10.6.8. Preparation of $(TBA)_4[(CH_3O)TiPW_{11}O_{39}]$

The method of Knoth[14] was adopted with some modifications. $(TBA)_4[ClTiPW_{11}O_{39}]$ (4.30 g, 1.15 mmol) was dissolved in MeCN (40 ml) with gentle heating. CH_3ONa (15 ml, 0.1 M solution in MeOH, 1.5 mmol, 1.3 eq) was added and the solution was allowed to stir for ~1 h before vacuum drying. The resulting white solid was washed with DCM (15 ml x 3), dried, redissolved in MeCN (20 ml) and allowed to stand overnight. The clear top solution was filtered, vacuum dried for 2 h to give a white solid, which was recrystallise from MeCN. (**2.84 g, 66%**). **IR (4000 – 400 cm^{-1}):** 2959 (m), 2934 (m), 2872 (m), 2819 (vw) assigned to OMe, 1482 (m), 1381 (w), 1152 (vw), 1068 (s), 959 (vs), 882 (s), 784 (vs, br), 620 (m) 590 (m), 500 (s), 472 (m), 432 (w), 410 (m); **^{1}H NMR** (399.78 MHz, CD_3CN): In addition to TBA resonances at 3.18−3.14, 1.69−1.61, 1.46−1.37, and 1.00−0.97, δ (ppm), 4.31 was observed for methoxyl protons. The ratio of methoxyl protons to CH_2N protons was 1:12 (calculated 1:11); **^{31}P NMR** (161.83 MHz, CD_3CN): δ (ppm), -14.05, line width fwhm = 3.49 Hz; **^{17}O NMR** (54.23 MHz, CH_3CN): δ (ppm), 740 – 738 (2 peaks assigned to W=O), 559, 534 (2 peaks assigned to TiOW), 424 – 382 (2 major broad and a minor broad peaks assigned to WOW).

10.6.9. Preparation of $(TBA)_4[(HO)TiPW_{11}O_{39}]$

In MeCN: $(TBA)_4[(CH_3O)TiPW_{11}O_{39}]$ (0.1 g, 0.027 mmol) was dissolved in MeCN (10 ml). H_2O (1.0 ml, 54 mmol, 2000 eq) was added and the solution was allowed to stir for ~1 h and vacuum dried to give a white solid. The hydrolysis step was repeated 5 more times to obtain a white solid (**0.096 g, 96 %**). **IR (4000 – 400 cm^{-1}):** 3633 (w) assigned to free OH, 2959 (m), 2934 (m), 2872 (m), 1482 (m), 1381 (w), 1152 (vw), 1070 (s), 960 (vs), 884 (s), 791 (vs, br), 689 (m) 594 (m), 515 (s) 501 (s), 472 (m), 432 (w), 410 (m); **^{31}P NMR** (161.83 MHz, CD_3CN): δ (ppm), -14.14 (91.1%), line width fwhm = 3.25 Hz. The product contained two impurity peaks at -15.35 (3.3%) assigned to $(TBA)_4[ClTiPW_{11}O_{39}]$ from the starting material and at -14.08 (5.7%) due to some dimerization to $(TBA)_8[(\mu\text{-}O)(TiPW_{11}O_{39})_2]$; **^{17}O NMR** (54.23 MHz, CH_3CN): δ (ppm), 739 – 736 (2 peaks assigned to W=O), 559, 536 (2 sharp peaks assigned to TiOW), 424 – 401 (4 major and 1 minor broad peaks assigned to WOW). The spectrum showed minor impurity peaks at 771 and 433 ppm which were assigned to $(TBA)_3[PW_{12}O_{40}]$.

In DMSO: $(TBA)_4[(CH_3O)TiPW_{11}O_{39}]$ (1.6 g, 0.429 mmol) was dissolved in DMSO (15 ml). H_2O (2 ml, 110.9 mmol, 258.4 eq) was added and the solution was allowed to stir for ~1 h and vacuum dried for 4 h to remove volatiles (MeOH and H_2O). The resulting colourless solution was triturated with diethyl ether (30 ml x 12) to obtain a white solid **(1.32 g, 83 %**). **IR (4000 – 400 cm^{-1}):** 3633 (w) assigned to free OH, 2959 (m), 2934 (m), 2872 (m), 1482 (m), 1381 (w), 1152 (vw), 1070 (s), 960 (vs), 884 (s), 791 (vs, br), 689 (m) 594 (m), 515 (s) 501 (s), 472 (m), 432 (w), 410 (m); **^{1}H NMR** (399.78 MHz, DMSO-d_6): In addition to TBA resonances at 3.19−3.15, 1.61−1.54, 1.37−1.28, and 0.96−0.92, δ (ppm), 12.04 was observed for hydroxyl proton. The ratio of hydroxyl proton to CH_2N protons was 1:34 (calculated 1:32); **^{31}P NMR** (121.49 MHz, DMSO-d6): δ (ppm), -14.35 (96.7%), line width fwhm = 3.04 Hz. The product contained a minor impurity peak at -14.28 (3.3%) due to some dimerization to $(TBA)_8[(\mu\text{-}O)(TiPW_{11}O_{39})_2]$. This peak disappeared when the DMSO solution of the POM was allowed to stand for ~3 weeks. **^{183}W NMR** (20.84 MHz, CD_3CN): δ (ppm), -81.47 (2) (broaden peak, line width fwhm = 45 Hz), -90.74 (2), -94.58(1), -98.75 (2), -108.90 (2), -110.25 (2). The spectrum showed a minor impurity peak at 85.60 ppm which was assigned to $(TBA)_3[PW_{12}O_{40}]$.

10.6.10. Preparation of $(TBA)_4[(\mu\text{-}O)(TiPW_{11}O_{39})_2]$

$(TBA)_4[(MeO)TiPW_{11}O_{39})$ (5.2g, 1.40 mmol) was dissolved in MeCN (40 ml). H_2O (2 ml, 112 mmol, 80 eq) was added, stirred for 3 h and vacuum-dried to give a white solid. The hydrolysis

was repeated 3 more times and the resulting white solid was dissolved in MeCN (30 ml). Activated 3Å molecular sieves were added to the solution before allowing it to stand for ~2 d. The solution was filtered *via* cannula filter stick and vacuum-dried for 4 h to obtain a white solid (**4.86g, 94%**). The oxobridge in the POM was selectively enriched in a separate experiment by hydrolysis of unenriched $(TBA)_4[(MeO)TiPW_{11}O_{39}]$ with ~0.06 % ^{17}O-enriched H_2O. **IR (4000 – 400 cm^{-1}):** 2960 (m), 2933 (m), 2871 (m), 1478 (m), 1379 (w), 1154 (vw), 1065 (s, sh), 959 (vs), 882 (s), 792 (vs, br), 630 (vs, br), 591 (vs) 496 (s, br), 432 (w), 409 (m); **^{1}H NMR** (399.78 MHz, CD_3CN): In addition to TBA resonances at 3.18−3.14, 1.69−1.61, 1.46−1.37, and 1.00−0.97, δ (ppm), 4.31 was observed for methoxyl protons. The ratio of methoxyl protons to CH_2N protons was 1:12 (calculated 1:11); **^{31}P NMR** (161.83 MHz, CD_3CN): δ (ppm), -14.07, line width fwhm = 3.36 Hz; **^{17}O NMR** (54.23 MHz, CH_3CN): δ (ppm), 742 – 738 (2 peaks assigned to W=O), 712 (a sharp peak assigned to TiOTi), 572, 544 (2 sharp peaks assigned to TiOW), 423 – 404 (2 broad peaks with a shoulder assigned to WOW). **^{183}W NMR** (20.84 MHz, CD_3CN): δ (ppm), -89.91 (2), -91.44 (2), -92.22(1), -97.14 (2), -108.61 (2), -109.24 (2).

10.6.11. Hydrolysis of $(TBA)_4[(L)M^{IV}PW_{11}O_{39}]$ (M = Sn, Ti; L = CH_3O, Cl)

$(TBA)_4[(CH_3O)SnPW_{11}O_{39}]$: Hydrolysis of $(TBA)_4[(CH_3O)SnPW_{11}O_{39}]$ (0.05 g) in MeCN (0.8 ml) with 10 mole-equivalents (2.4 µl) of H_2O was monitored by ^1H and ^{31}P NMR spectroscopy.

$(TBA)_4[(CH_3O)TiPW_{11}O_{39}]$: Hydrolysis of $(TBA)_4[(CH_3O)TiPW_{11}O_{39}]$ (0.05 g) in MeCN (0.5 ml) with 10 (2.4 µl) and 50 (12.1 µl) mole-equivalent of H_2O respectively and in DMSO (0.5 ml) with 10 (2.4 µl) mole-equivalents of H_2O was monitored by ^1H and ^{31}P NMR spectroscopy.

$(TBA)_4[ClSnPW_{11}O_{39}]$: $(TBA)_4[ClSnPW_{11}O_{39}]$ (0.06g, 0.016 mmol) was dissolved in MeCN (1.5 ml). H_2O (0.25 ml, 14.3 mmol, 892 eq) was added and stirred for 2 h before recording a ^{31}P NMR spectrum. More H_2O (0.25 ml, 28.6 mmol, 1784 eq) was added stirred for 2 h and a ^{31}P NMR spectrum was recorded. The solution was allowed to stir for 3 d before recording a ^{31}P NMR spectrum again.

$(TBA)_4[ClTiPW_{11}O_{39}]$: $(TBA)_4[ClTiPW_{11}O_{39}]$ (0.12 g, 0.032 mmol) dissolved in MeCN (3 ml). H_2O (0.1 ml, 172 eq) was added with stirring for 1 h before recording a ^{31}P NMR spectrum. More H_2O [0.9 ml (a total of 1 ml, 1720 eq)] was added and the solution immediately became cloudy and then clear again after ~10 min. A ^{31}P NMR spectrum was recorded before vacuum drying

the solution to obtain a white solid. The IR and ^{31}P NMR spectra of the product were recorded again.

10.6.12. Dimerization of $(TBA)_4[(HO)TiPW_{11}O_{39}]$

The dimerization of $(TBA)_4[(HO)TiPW_{11}O_{39}]$ (0.02 M) in MeCN and DMSO was monitored by ^{31}P NMR spectroscopy.

10.6.13. Alcohol-alkoxide exchange studies

The alcohol-alkoxide exchange between $TBA)_4[(CH_3O)M^{IV}PW_{11}O_{39}]$ (M = Ti, Sn) and CH_3OH was invested using 2D EXSY and ^1H NMR spectroscopy. For 2D EXSY studies, ~0.02 M POM solutions in MeCN and MeOH (1.63µL - 5.3 µL, 3 - 10 eq) were used. For ^1H NMR ~0.02 M POM solutions in MeCN and CD_3OD (0.6 µL, 9 eq) were used.

10.6.14. Reduction of $(TBA)_4[(HO)SnPW_{11}O_{39}]$

Treatment with $NaBH_4$: To two 5-mm o.d. screw-capped NMR tubes (A and B) in a glove box was added $(TBA)_4[(HO)SnPW_{11}O_{39}]$ (0.05 g, 0.0132 mmol) and MeCN/CD_3CN (0.5 ml) to give clear solutions. To A was added $NaBH_4$ (0.5 mg 0.0132 mmol) and the tube was shaken vigorously before recording the ^{31}P and ^{119}Sn NMR spectra. To B was added $NaBH_4$ (0.5 mg 0.0132 mmol) and the tube was shaken vigorously and heated gently with a hot gun before recording a ^{31}P NMR spectrum.

Treatment with $H_2NNH_2.HCl$: $(TBA)_4[(HO)SnPW_{11}O_{39}]$ (0.05 g, 0.0132 mmol) and MeCN/CD_3CN (0.5 ml) were added to a 5-mm o.d. screw capped NMR tube in a glove box to give a clear solution. $H_2NNH_2.HCl$ (51 µl, 0.26 M in MeCN, 0.0132 mmol) was added and the tube was shaken vigorously before recording a ^{31}P NMR spectrum. The solution was heated at 50 ^oC for 2 h with recording of a ^{31}P NMR spectrum.

10.6.15. Reduction of $(TBA)_4[ClSnPW_{11}O_{39}]$

Treatment with $NaBH_4$: $(TBA)_4[ClSnPW_{11}O_{39}]$ (0.1 g, 0.0263 mmol) and MeCN/CD_3CN (0.9 ml) were added to a 5-mm o.d. screw capped NMR tube in a glove box to give a clear solution. $NaBH_4$ (1 mg 0.0263 mmol) was added and the tube was shaken vigorously before recording the ^{31}P and ^{119}Sn NMR spectra of the yellow solution.

Treatment with $H_2NNH_2.HCl$: $(TBA)_4[ClSnPW_{11}O_{39}]$ (0.1 g, 0.0263 mmol) and MeCN/CD_3CN (0.9 ml) were added to a 5-mm o.d. screw capped NMR tube in a glove box to give a clear solution. $H_2NNH_2.HCl$ (101 µl, 0.26 M in MeCN, 0.0263 mmol) was added and the tube was shaken vigorously before recording a ^{31}P NMR spectrum. The solution was heated at 50 ^oC for 2 h with recording of a ^{31}P NMR spectrum.

10.7. Experimental for Chapter 5

10.7.1. Reaction between $(TBA)_8[(\mu\text{-}O)(TiPW_{11}O_{39})_2]$ and $AgBF_4$

To two 5-mm o.d. screw-capped NMR tubes (A and B) in a glove box were added $(TBA)_8[(\mu\text{-}O)(TiPW_{11}O_{39})_2]$ (0.1 g, 0.014 mmol) and MeCN/CD_3CN (0.5 ml). Solutions of $AgBF_4$ in MeCN (60 µl, 0.24 M, 0.014 mmol, 1 eq) and (120 µl, 0.24 M, 0.028 mmol, 2 eq) were then added to A and B respectively and vigorously shaken for 30 mins before recording the NMR spectra (^{31}P and ^{17}O). The solutions were vacuum-dried, washed with $CHCl_3$ (5 ml x 3), vacuum-dried again before recording the IR spectrum of the white solids.

10.7.2. Reaction between $(TBA)_8[(\mu\text{-}O)(TiPW_{11}O_{39})_2]$ and $Co(MeCN)_4(H_2O)_2][BF_4]_2$

To a 5-mm o.d. screw-capped NMR tube in a glove box was added $(TBA)_8[(\mu\text{-}O)(TiPW_{11}O_{39})_2]$ (0.1 g, 0.014 mmol) and MeCN/CD_3CN (0.5 ml). $Co(MeCN)_4(H_2O)_2][BF_4]_2$ (6 mg, 0.014 mmol) was added and the resultant purple solution was vigorously shaken for 30 mins before recording the NMR spectra (^{31}P and ^{17}O). The solution was vacuum-dried, washed with $CHCl_3$ (5 ml x 3), vacuum-dried again before recording the IR spectrum of the purple solid.

10.7.3. Reaction between $(TBA)_8[(\mu\text{-}O)(TiPW_{11}O_{39})_2]$ and $Mo_2(MeCN)_{10}[BF_4)_4$

$(TBA)_8[(\mu\text{-}O)(TiPW_{11}O_{39})_2]$ (0.1 g, 0.014 mmol) and MeCN/CD_3CN (1.0 ml) were added to a Schlenk flask and cooled to -30 ^oC. $Mo_2(MeCN)_{10}[BF_4)_4$ (6 mg, 0.007 mmol) was dissolved in MeCN (1 ml) in a second Schlenk flask (B) to give a blue solution. Solution B was transferred into A and the colour gradually changed to green then dark brown within ~ 10 min as the solution warmed up to room temperature. The solution was concentrated before recording the NMR spectra (^{31}P and ^{17}O). The solution was then vacuum-dried before recording the IR spectrum of the dark brown solid.

10.7.4. Reaction between $(TBA)_8[(\mu\text{-}O)(TiPW_{11}O_{39})_2]$ and $SnCl_2$

To a 5-mm o.d. screw-capped NMR tube in a glove box was added $(TBA)_8[(\mu\text{-}O)(TiPW_{11}O_{39})_2]$ (0.1 g, 0.014 mmol) and MeCN/CD_3CN (0.5 ml). $SnCl_2$ (3 mg, 0.014 mmol) was added with immediate change in colour to yellow. The solution was vigorously shaken for 30 mins before recording the NMR spectra (^{31}P and ^{17}O). The solution was vacuum-dried, washed with $CHCl_3$ (5 ml x 3), vacuum-dried again before recording the IR spectrum of the yellow solid.

10.7.5. Reaction between $(TBA)_8[(\mu\text{-}O)(TiPW_{11}O_{39})_2]$ and $FeCl_2$

To a 5-mm o.d. screw-capped NMR tube in a glove box was added $(TBA)_8[(\mu\text{-}O)(TiPW_{11}O_{39})_2]$ (0.1 g, 0.014 mmol) and MeCN/CD_3CN (0.5 ml). $FeCl_2$ (2 mg, 0.014 mmol) was added and the resulting brown solution was vigorously shaken for 30 mins before recording the NMR spectra (^{31}P and ^{17}O). The solution was vacuum-dried, washed with $CHCl_3$ (5 ml x 3), vacuum-dried again before recording the IR spectrum of the brown solid.

10.7.6. Reaction between $(TBA)_8[(\mu\text{-}O)(TiPW_{11}O_{39})_2]$ and $BiCl_3$

To a 5-mm o.d. screw-capped NMR tube in a glove box was added $(TBA)_8[(\mu\text{-}O)(TiPW_{11}O_{39})_2]$ (0.1 g, 0.014 mmol) and MeCN/CD_3CN (0.5 ml). $BiCl_3$ (4.3 mg, 0.014 mmol) was added and the solution became slightly cloudy. It was vigorously shaken for 30 mins before recording the NMR spectra (^{31}P and ^{17}O). The solution was filtered, vacuum-dried, washed with $CHCl_3$ (5 ml x 3), vacuum-dried again before recording the IR spectrum of the white solid.

10.7.7. Reaction between $(TBA)_8[(\mu\text{-}O)(TiPW_{11}O_{39})_2]$ and $SbCl_3$

To a 5-mm o.d. screw-capped NMR tube in a glove box was added $(TBA)_8[(\mu\text{-}O)(TiPW_{11}O_{39})_2]$ (0.1 g, 0.014 mmol) and MeCN/CD_3CN (0.5 ml). $SbCl_3$ (3 mg, 0.014 mmol) was added and the solution became cloudy. It was vigorously shaken for 30 mins before recording the NMR spectra (^{31}P and ^{17}O). The solution was filtered, vacuum-dried, washed with $CHCl_3$ (5 ml x 3), vacuum-dried again before recording the IR spectrum of the white solid.

10.7.8. Reaction between $(TBA)_8[(\mu\text{-}O)(TiPW_{11}O_{39})_2]$ and $SnCl_4$

To a 5-mm o.d. screw-capped NMR tube in a glove box was added $(TBA)_8[(\mu\text{-}O)(TiPW_{11}O_{39})_2]$ (0.1 g, 0.014 mmol) and MeCN/CD_3CN (0.5 ml). $SnCl_4$ (1.6 µl, 0.014 mmol) was added and the solution was vigorously shaken for 30 mins before recording the NMR spectra (^{31}P and ^{17}O).

The solution was vacuum-dried, washed with $CHCl_3$ (5 ml x 3), vacuum-dried again before recording the IR spectrum of the white solid.

10.7.9. Reaction between $(TBA)_8[(\mu\text{-}O)(TiPW_{11}O_{39})_2]$ and $TiCl_4$

To a 5-mm o.d. screw-capped NMR tube in a glove box was added $(TBA)_8[(\mu\text{-}O)(TiPW_{11}O_{39})_2]$ (0.1 g, 0.014 mmol) and MeCN/CD_3CN (0.5 ml). $TiCl_4$ (1.5 µl, 0.014 mmol) was added and the solution was vigorously shaken for 30 mins before recording the NMR spectra (^{31}P and ^{17}O). The solution was vacuum-dried, washed with $CHCl_3$ (5 ml x 3), vacuum-dried again before recording the IR spectrum of the white solid.

10.7.10. Reaction between $(TBA)_8[(\mu\text{-}O)(TiPW_{11}O_{39})_2]$ and Me_2SnCl_2

To a 5-mm o.d. Schlenk flask in a glove box was added $(TBA)_8[(\mu\text{-}O)(TiPW_{11}O_{39})_2]$ (0.9 g, 0.122 mmol) and MeCN (5 ml). Me_2SnCl_2 (27 mg, 0.122 mmol) was added and the solution was stirred for 3 h. The solution was vacuum-dried, washed with $CHCl_3$ (10 ml x 3), vacuum-dried again before recording the NMR (^{1}H, ^{31}P, ^{17}O, ^{119}Sn and ^{183}W) and IR spectra of the white solid (**0.85 g, 99%**).

10.8. Experimental for Chapter 6

10.8.1. Reactivity of $(TBA)_5[SnPW_{11}O_{39}]$

Treatment with Br_2: $(TBA)_5[SnPW_{11}O_{39}]$ (0.5 g, 0.13 mmol) was dissolved in MeCN (10 ml). Br_2 (~0.1 ml, 2.02 mmol) was added and the colour changed to slightly dark yellow immediately. The solution was dried, washed with EtOAc (20 ml) and Ether (20 ml x 3), dried and crystallised from MeCN/Ether solution. **^{31}P NMR** (161.83 MHz, CD_3CN)**:** δ = -12.85 ppm [^{2}J(Sn-P) = 35 Hz]; **^{119}Sn NMR** (186.40 MHz, CD_3CN)**:** δ = -643.1 ppm [$^{2}J(^{119}Sn^{183}W_{1/2})$ = 170 Hz; $^{2}J(^{119}Sn^{183}W_{3/4})$ = 62 Hz].

Treatment with I_2: $(TBA)_5[SnPW_{11}O_{39}]$ (0.5 g, 0.13 mmol) was dissolved in MeCN (10 ml). I_2 (0.04 g, 0.15 mmol) was added and the colour changed to brown after shaking for 5 mins. The solution was dried, washed with EtOAc (20 ml x 3) and Ether (20 ml x 3), dried and crystallised from MeCN/Ether solution. **^{31}P NMR** (161.83 MHz, CD_3CN): δ = -12.77ppm [^{2}J(Sn-P) = 32 Hz]; **^{119}Sn NMR** (186.40 MHz, CD_3CN): δ = -812.76 ppm. The resolution of the spectrum did not allow for measurement of any Sn-W couplings.

Treatment with 1-bromobutane: $(TBA)_5[SnPW_{11}O_{39}]$ (0.5 g, 0.13 mmol) was dissolved in MeCN (10 ml). 1-bromobutane (0.1 ml, 7.14 mmol, XS) was added and the colour became lighter immediately. The solution was stirred for 1 h, dried in vacuum, washed with EtOAc (20 ml x 3) and Ether (20 ml x 3), dried and crystallised from MeCN/Ether solution. **^{31}P NMR** (161.83 MHz, CD_3CN): δ = -13.22ppm; **^{119}Sn NMR** (CD_3CN): δ = -684.33 ppm. The resolution of the spectrum did not allow for measurement of any Sn-W couplings.

Treatment with $(TBA)_3[PMo_{12}O_{40}]$: To three 5-mm o.d. screw-capped NMR tubes (A, B and C) were added $(TBA)_5[SnPW_{11}O_{39}]$ (0.1g, 0.025 mmol) for A and B and $(TBA)_5[SnPW_{11}O_{39}]$ (0.2g, 0.05 mmol) for C. DMSO-d_6 (0.5 ml) was added to each tube to give a clear yellow solution. To A was added $(TBA)_3[PMo_{12}O_{40}]$ (0.06 g, 0.025 mmol) with an immediate change in colour to dark green. The tube was vigorously shaken before recording the NMR spectra (^{31}P and ^{119}Sn). To B was added $(TBA)_3[PMo_{12}O_{40}]$ (0.12 g, 0.05 mmol) with immediate change in colour to dark green. The tube was shaken vigorously and the NMR spectra (^{31}P and ^{119}Sn) were recorded. To C was added $(TBA)_3[PMo_{12}O_{40}]$ (0.06 g, 0.025 mmol) and the tube was vigorously shaken before recording NMR spectra (^{31}P and ^{119}Sn) of the resulting dark blue solution.

Treatment with NaOMe: $(TBA)_5[SnPW_{11}O_{39}]$ (0.1 g, 0.025 mmol) and MeCN/CD_3CN (0.5 ml) were added to a 5-mm o.d. screw capped NMR tube in a glove box. NaOMe (1 eq, 0.1M in MeOH) was added and the tube was shaken vigorously for 30 min before recording a ^{31}P NMR spectrum. The solution was vacuum-dried and the NMR spectra (^{1}H, ^{31}P and ^{119}Sn) of the product were recorded.

Treatment with TBAOH: $(TBA)_5[SnPW_{11}O_{39}]$ (0.1 g, 0.025 mmol) and MeCN/CD_3CN (0.5 ml) were added to a 5-mm o.d. screw capped NMR tube in a glove box. TBAOH (25 µl, 1 M in MeOH, 1 eq) was added and a ^{31}P NMR spectrum was recorded.

Treatment with HCl: $(TBA)_5[SnPW_{11}O_{39}]$ (0.1 g, 0.025 mmol) and MeCN/CD_3CN (0.5 ml) were added to a 5-mm o.d. screw capped NMR tube in a glove box. HCl (0.25 ml, 0.1 M, 0.025 mmol) was added and the tube was shaken vigorously before recording a ^{31}P NMR spectrum.

10.8.2. Reactivity of $(TBA)_5[PbPW_{11}O_{39}]$

Treatment with Br_2: $(TBA)_5[PbPW_{11}O_{39}]$ (0.1 g, 0.024 mmol) and MeCN/CD_3CN (0.5 ml) were added to a 5-mm o.d. screw capped NMR tube in a glove box to give a clear solution. Br_2 (1.3 µl, 0.024 mmol) was added to give a yellow solution. The tube was vigorously shaken before recording the ^{31}P NMR spectrum. More Br_2 (xs) was added to give a reddish solution and the ^{31}P NMR spectrum was recorded.

Treatment with I_2: $(TBA)_5[PbPW_{11}O_{39}]$ (0.1 g, 0.024 mmol) and MeCN/CD_3CN (0.5 ml) were added to a 5-mm o.d. screw capped NMR tube in a glove box to give a clear solution. I_2 (18 mg, 0.072 mmol) was added and the tube was shaken vigorously before recording the ^{31}P NMR spectrum of the dark brown solution.

Treatment with $(TBA)_3[PMo_{12}O_{40}]$: To two 5-mm o.d. screw-capped NMR tubes (A and B) were added $(TBA)_5[PbPW_{11}O_{39}]$ (0.1g, 0.024 mmol) and DMSO-d_6 (0.5 ml). To A was added $(TBA)_3[PMo_{12}O_{40}]$ (0.061 g, 0.024 mmol) and the tube was vigorously shaken before recording the ^{31}P NMR spectra of the yellow solution. To B was added $(TBA)_3[PMo_{12}O_{40}]$ (0.12 g, 0.048 mmol) and the tube was shaken vigorously before recording the ^{31}P NMR spectrum of intense yellow solution.

10.8.3. Reactions of $(TBA)_4[MPW_{11}O_{39}]$ (M = Sb^{3+}, Bi^{3+}) and MeONa

Treatment of *$(TBA)_4[BiPW_{11}O_{39}]$ with MeONa:* $(TBA)_4[BiPW_{11}O_{39}]$ (0.12 g, 0.029 mmol) was dissolved in MeCN (5 ml). MeONa (0.15 ml, 0.2 M in MeOH) was added and stirred for 1 h before recording the ^{31}P NMR spectrum. The solution was allowed to stir for 12 h, vacuum-dried and the NMR spectra (^1H, ^{17}O and ^{31}P) were recorded.

Treatment of $(TBA)_4[SbPW_{11}O_{39}]$ with MeONa: $(TBA)_4[SbPW_{11}O_{39}]$ (0.08 g, 0.02 mmol) was dissolved in MeCN (3 ml). MeONa (0.1 ml, 0.2 M in MeOH) was added and stirred for 1 h before recording the ^{31}P NMR spectrum. The solution was allowed to stir for 12 h, vacuum-dried and the NMR spectra (^1H, ^{17}O and ^{31}P) were recorded.

10.9. Experimental for Chapter 8

10.9.1. Preparation of $Cr(THF)_3Cl_3$[8]

$CrCl_3.6H_2O$ (2.66 g, 10 mmol), THF (20 ml) and a magnetic stirrer bar were placed in a 100-ml, three-necked, round-bottom flask that was equipped with a condenser fitted with a drying tube. To the slurry at 25 ^oC, was added $(CH_3)_3SiCl$ (32 ml, 253 mmol) dropwise with stirring causing an evolution of heat and a change in colour from dark green to deep purple. The purple solid that precipitated was washed with hexane and vacuum-dried (**3.2 g, 85%**). The IR spectrum was recorded.

10.9.2. Preparation of $WOCl_4$[3]

$WO_3.H_2O$ (65.5g, 262.14mmol) was added to excess $SOCl_2$ (300ml) in a 1L round bottom flask to give a bright yellow suspension which changed to orange red after about an hour of reaction with the evolution of gas bubbles trapped with a KOH trap. The mixture was allowed to stir overnight at ~85 ^oC and the resulting dark red solution was vacuum dried with gentle heating. The crude product (20 – 30g) x 3 was transferred into a sublimation flask and sublimed under vacuum for 30 mins using an IR-Lamp. The sublimate was weighed and transferred into a sample bottle in a drybox. (**69.3 g, 78 %**).

10.9.3. Preparation of $WO(OMe)_4$[3]

$WOCl_4$ (17.22g, 50.40mmol) was dissolved at ~30 ^oC in THF (180ml) in one side of a double round bottom filter flask to give a red solution. MeOH (8.2m, 201.61mmol) was added and NH_3 gas was bubbled through the resulting yellow solution for 5 mins to give a white precipitate. N_2 was bubbled through the solution for 10mins to remove any excess NH_3 and the solution was allowed to settle for ~30mins before filtering under vacuum. The pale yellow filtrate was vacuum dried in a Schlenk flask. (**16.22g, 99 %**). **^{1}H NMR** (300.13 MHz, Toluene-D3): δ (ppm), 4.48, 4.35, 4.33 (in the ratio 2:1:1).

10.9.4. Preparation of $(TBA)_3[(CH_3CONH_2)Co^{II}W_5O_{18}(CH_3)]$

$(TBA)_2[WO_4]$ (1.90 g, 2.59 mmol) was dissolved in MeCN (10 ml) – Solution A. $WO(OMe)_4$ (0.56 g, 1.73 mmol) was dissolved in MeCN (10 ml) – Solution B. Solution B was transferred into A *via* cannula and washed with more MeCN (5 ml). The greenish yellow solution was heated at 90 ^oC for 90 min and the resultant orange solution was allowed to cool before adding H_2O

(62.5 µL) and heated overnight (~ 19 h) at 90 °C. After vacuum-drying all volatiles, the solution was washed with diethyl ether (20 ml x 2) and pumped dry to give an orange sticky solid, which was dissolved in MeCN (10 ml) to give a colourless solution with a slight orange tinge. A solution of blue $CoCl_2$ (0.11 g, 0.86 mmol) in MeCN (10 ml) was transferred into the initial colourless solution and the colour changed immediately to purple. The purple solution was allowed to stir overnight at room temperature (~ 16 h) before vacuum-drying to give purple solid. The solid was triturated with diethyl ether (20 ml x 4), pumped dry, redissolved in MeCN (2 ml) and set up for crystallisation by slow diffusion of diethyl ether vapour into the MeCN solution of the product. Pale solid settled at the bottom of the crystallisation tube after 8 h. After filtering off the solid, the purple filtrate was again set up for crystallisation by slow diffusion of diethyl ether vapour. Purple XRD quality single crystals formed after about 4 weeks. Anal. Calcd for $(TBA)_3[(CH_3CONH_2)Co^{II}W_5O_{18}(CH_3)]$: C, 29.63; H, 5.66; N, 2.71. Found: C, 34.75; H, 7.92; N, 3.69. **IR (4000 – 400 cm^{-1}):** 3267(w) and 3092(w) assigned to ν_{NH} of acetamide, 2959 (s), 2934 (m), 2872 (m), 2819 (vw) assigned to ν_{CH} of OMe, 1663(m) assigned to ν_{CO} of acetamide, 1481 (m), 1380 (m), 1345(w), 1151(w), 1107(vw), 1041 (w), 933 (s), 882 (m), 809(vs), 760(vs), 675 (vs), 608(m), 548(m), 528 (m), 451 (m).

10.9.5. Preparation of tungstate precursor "$(TBA)_6[W_5O_{18}]$" for attempted synthesis of $[MW_5O_{18}]^{n-}$ (M =Sn^{2+}, Pb^{2+}, Mo^{2+}, Ni^{2+}, Fe^{2+}, Cu^{2+}, Cr^{3+}, Bi^{3+}, Sb^{3+}).

$(TBA)_2[WO_4]$ (1.00 g, 1.37 mmol) was dissolved in MecN (10 ml) – Solution A. $WO(OMe)_4$ (0.30 g, 0.91 mmol) was dissolved in MeCN (10 ml) – Solution B. Solution B was transferred into A *via* cannula and washed with more MeCN (5 ml). The clear solution was heated at 90 °C for 90 min and the solution, which now had a slight orange tinge was allowed to cool before adding ^{17}O-enriched H_2O (32.8 µL, 1.82 mmol). After heating overnight (~ 16 h) at 90 °C, the solution was allowed to cool to room temperature before vacuum-drying to remove all volatiles and washed with diethyl ether (20 ml x 2) to give a sticky solid, which was used as the tungstate precursor for the attempted synthesis of $[MW_5O_{18}]^{n-}$ derivatives (described below), using the same amounts of $(TBA)_2WO_4$ and $WO(OMe)_4$ in all cases. Crystallisation was attempted for the products of all the reaction by slow diffusion of diethyl ether vapour into an acetonitrile solution of the product.

10.9.6. Attempted preparation of $(TBA)_4[Sn^{II}W_5O_{18}]$

The tungstate precursor was dissolved in MeCN (10 ml) and was transferred into a solution of $SnCl_2$ (0.058 g, 0.46 mmol) in MeCN (10 ml). The resulting dark orange solution was allowed to stir overnight at room temperature (~ 16 h) before vacuum-drying to give a sticky orange solid, which was triturated with diethyl ether (15 ml x 4) and pumped dry. The IR and NMR spectra (^{17}O and ^{119}Sn) of the product were recorded. The ^{119}Sn spectrum was recorded after allowing a solution of the product in MeCN to stand for 1 week in a Schlenk flask. 3 drops of H_2O was added to this solution and ^{119}Sn was recorded again.

10.9.7. Attempted preparation of $(TBA)_4[Pb^{II}W_5O_{18}]$

A solution of $PbCl_2$ (0.058 g, 0.46 mmol) in MeCN (10 ml) and 5 drops of DMSO was transferred into a solution of the tungstate precursor in MeCN (10 ml) and the colour changed immediately to brown. The solution was allowed to stir overnight at room temperature (~ 16 h) and the cloudy solution was allowed to settle, filtered and pumped dry. The sticky solid was triturated with diethyl ether (15 ml x 8) and dried. The IR and ^{17}O NMR spectra of the product were recorded.

10.9.8. Attempted preparation of $(TBA)_5[ClFe^{II}W_5O_{18}]$

A brownish solution of $FeCl_2$ (0.058 g, 0.46 mmol) in MeCN (10 ml) and 3 drops of DMSO was transferred into a solution of the tungstate precursor in MeCN (10 ml) and the colour changed immediately to reddish brown. The solution was allowed to stir overnight at room temperature (~ 16 h) and vacuum dried to give a sticky solid, which was triturated with diethyl ether (20 ml x 4) and dried. The IR and ^{17}O NMR spectra of the product were recorded.

10.9.9. Attempted preparation of $(TBA)_5[ClCu^{II}W_5O_{18}]$

$CuCl_2$ (0.062 g, 0.46 mmol) was dissolved in MeCN (10 ml) by gentle heating to give a dark brown solution. A clear solution of the tungstate precursor in MeCN (10 ml) was transferred into the dark brown solution with an immediate change in colour to dark green. The solution was allowed to stir overnight at room temperature (~ 16 h) and vacuum dried to give a sticky solid, which was triturated with diethyl ether (20 ml x 4) and pumped dry. The IR and ^{17}O NMR spectra of the product were recorded.

10.9.10. Attempted preparation of Mo≡Mo bonded $(TBA)_8[(Mo^{II}W_5O_{18})_2]$

A blue solution of $[Mo_2(NCCH_3)_8(ax\text{-}CH_3CN)_{0.5}][BF_4]_4$ (0.058 g, 0.46 mmol) in MeCN (10 ml) was transferred into a solution of the tungstate precursor in MeCN (10 ml) and the colour changed immediately to brownish dark green. The solution was stirred overnight at room temperature (~ 16 h) and allowed to settle, filtered and vacuum dried to give a solid, which was triturated with diethyl ether (20 ml x 4) and pumped dry. The IR and ^{17}O NMR spectra of the solid product were recorded. Dark XRD quality single crystals, which were characterized as the one-electron reduced $(TBA)_3[W_6O_{19}]$ were obtained by slow diffusion of diethyl ether vapour into a solution of the solid product in MeCN (1 ml) after about 2 weeks. **IR (4000 – 400 cm^{-1}):** 2959 (m), 2934 (m), 2873 (m), 1668(w), 1481 (s), 1380 (m), 1152(w), 1107(vw), 1056 (w), 1028(w) 977 (w), 949(vs), 906(m), 884(m), 776(vs, br), 570(s), 422(vs).

10.9.11. Attempted preparation of $(TBA)_4[ClCr^{III}W_5O_{18}]$

A clear solution of the tungstate precursor in MeCN (10 ml) was transferred *via* cannula into a pink solution of $Cr(THF)_3Cl_3$ (0.172 g, 0.46 mmol) in MeCN (10 ml). The resulting green solution was allowed to stir overnight at room temperature (~ 16 h) and vacuum dried to give a green solid, which was triturated with diethyl ether (20 ml x 4) and pumped dry. The IR spectrum was recorded.

10.9.12. Attempted preparation of $(TBA)_4[ClSb^{III}W_5O_{18}]$

A clear solution of the tungstate precursor in MeCN (10 ml) was transferred *via* cannula into a clear solution of $SbCl_3$ (0.105 g, 0.46 mmol) in MeCN (10 ml). The resulting orange solution was stirred overnight at room temperature (~ 16 h) and allowed to settle before filtering and vacuum drying to get a colourless solid, which was triturated with diethyl ether (20 ml x 4) and pumped dry. The IR and ^{17}O NMR spectra were recorded.

10.9.13. Attempted preparation of $(TBA)_4[ClBi^{III}W_5O_{18}]$

A clear solution of the tungstate precursor in MeCN (10 ml) was transferred *via* cannula into a clear solution of $BiCl_3$ (0.15 g, 0.46 mmol) in MeCN (10 ml). The colourless solution was stirred overnight at room temperature (~ 16 h) and vacuum dried to give a colourless solid, which was triturated with diethyl ether (20 ml x 4) and pumped dry. The IR and ^{17}O NMR spectra were recorded.

10.9.14. Attempted preparation of (TBA)[IW_5O_{18}]

$(TBA)_2[WO_4]$ (0.1 g, 0.14 mmol) and $WO(OMe)_4$ (0.4 g, 1.23 mmol) were dissolved in MeCN (10 ml) and the solution was heated at 90 ^oC for 90 min. The orange solution was allowed to cool and the colour became darker. The solution was transfer *via* cannula into a suspension of H_5IO_6 (0.07 g, 0.3 mmol) in MeCN (10 ml) and heated at 90 ^oC for 1 h before adding H_2O (33 µL, 1.82 mmol) and heating was continued overnight (~ 16 h). The resulting pale yellow solution was allowed to cool to room temperature and settle. Filter *via* cannula filter stick, vacuum-dried before recording the IR and ^{17}O NMR. The product was characterised as $(TBA)_6[W_6O_{19}]$.

References

1. R. J. Errington, *Advanced Practical Inorganic and Metalorganic Chemistry*, Blackie Academic & Professional, London, 1997.
2. T. M. Che, V. W. Day, L. C. Francesconi, C. M. F. Fredrich, W. G. Klemperer and W. Shum, *Inorg. Chem.* , 1985, **24**, 4055-4062.
3. William Clegg, R. John Errington, P. Kraxner and C. Redshaw, *J. Chem. Soc., Dalton Trans.*, 1992, 1431-1438.
4. C. Sanchez, J. Livage, J. P. Launay, M. Fournier and Y. Jeannin, *J. Am. Chem. Soc.*, 1982, **104**, 3194-3202.
5. R. L. Wingad, PhD Thesis, The University of Newcastle upon-Tyne, 1999.
6. T. A. Stephenson, E. Bannister and G. Wilkinson, *J. Chem. Soc.*, 1964, 2538-2541.
7. F. A. Cotton and K. J. Wiesinger, in *Inorg. Synth.*, John Wiley & Sons, Inc., 1992, vol. 29, pp. 134-137.
8. P. Boudjouk and J.-H. So, in *Inorg. Synth.*, John Wiley & Sons, Inc., 1992, vol. 29, ch. 3 - Transition Metal Co-ordination Compounds, pp. 108-111.
9. CrysAlisPro, *Rigaku Oxford Diffraction*.
10. R. C. Clark and J. S. Reid, *Acta Crystallogr. Sect. A*, 1995, **51**, 887-897.
11. G. Sheldrick, *Acta Crystallogr. Sect. A*, 2015, **71**, 3-8.
12. G. Sheldrick, *Acta Crystallogr. Sect. A*, 2008, **64**, 112-122.
13. O. V. Dolomanov, L. J. Bourhis, R. J. Gildea, J. A. K. Howard and H. Puschmann, *J. Appl. Crystallogr.*, 2009, **42**, 339-341.
14. W. H. Knoth, P. J. Domaille and D. C. Roe, *Inorg. Chem.*, 1983, **22**, 198-201.

Appendices

This section contains full NMR spectra, full ESI-MS spectra, expansions and simulated ESI-MS spectra of some assigned polyanions, simulated ^{119}Sn NMR spectra showing couplings to ^{31}P, ^{183}W and ^{1}H, crystallographic data and a brief curriculum vitae showing Skills acquired during my PhD, publications and participation in Conferences/Workshops/Symposia.

Appendix A3 – A10

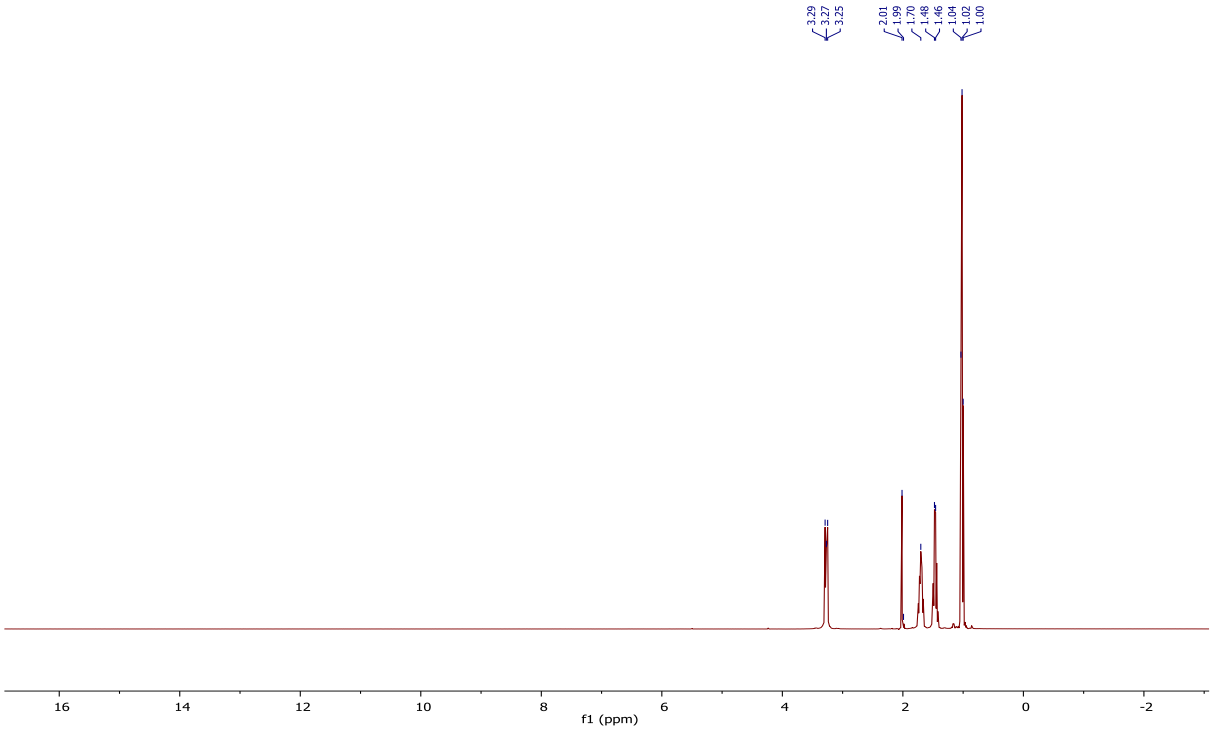

Figure A3.1. ^{1}H NMR spectrum of $(TBA)_6[NaPW_{11}O_{39}]$ in $CD_3CN/MeCN$.

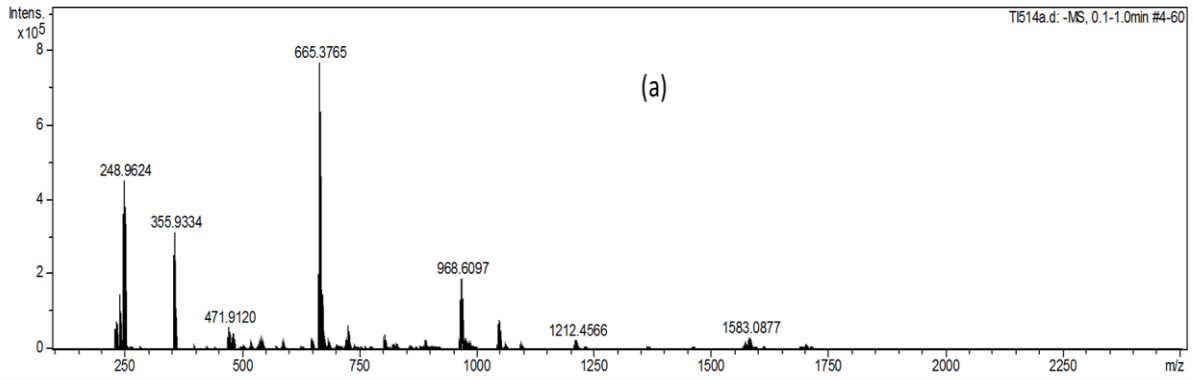

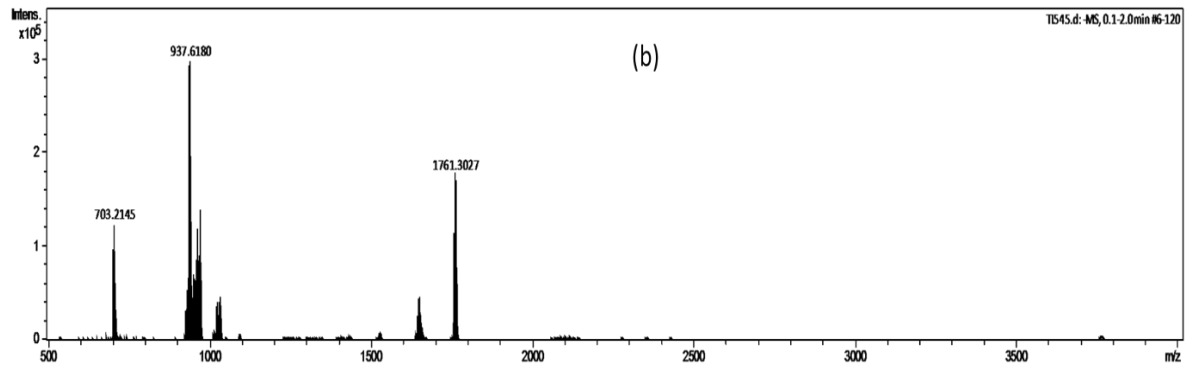

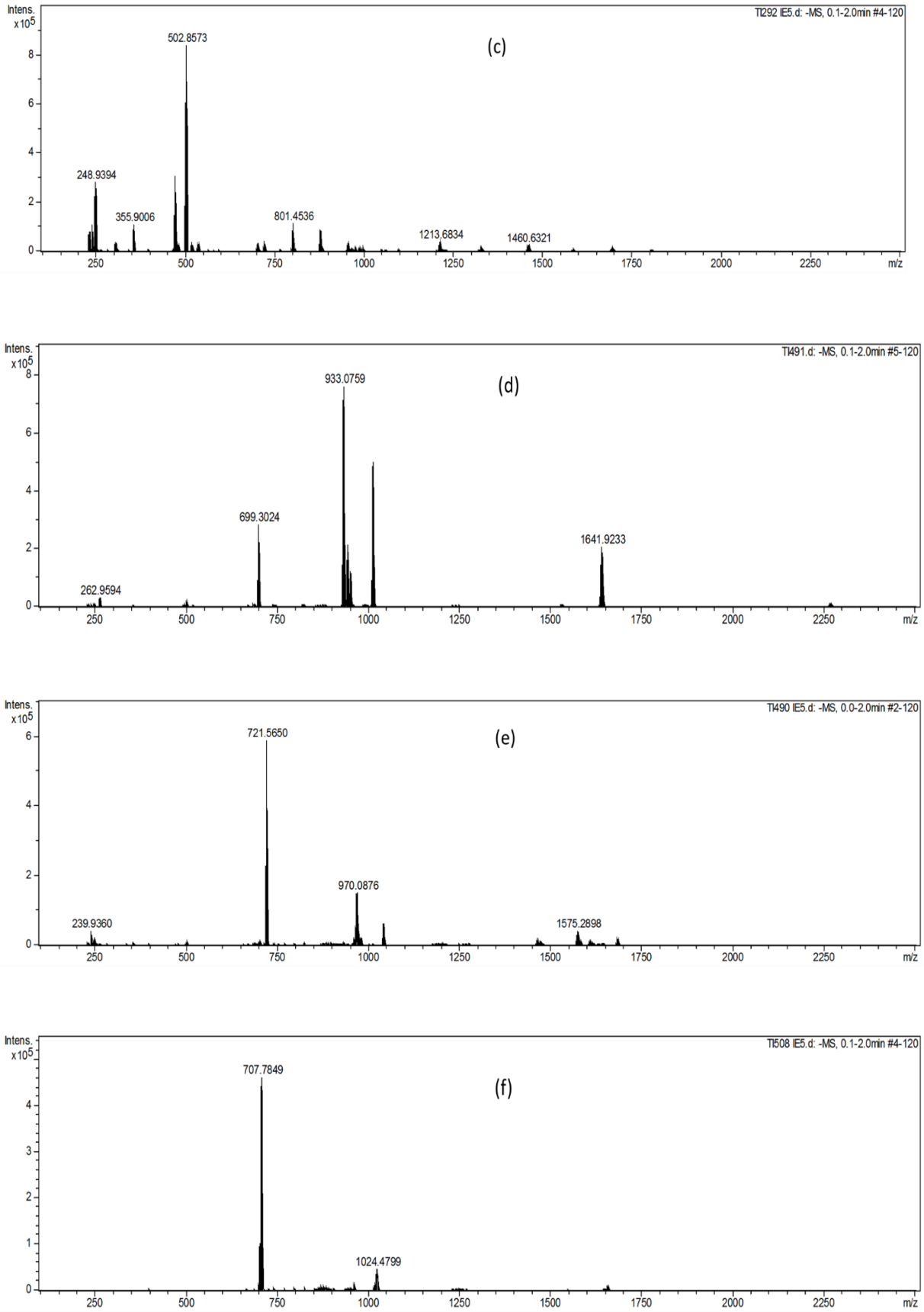

Figure A3.2. Full ESI-MS spectra of (a) $(TBA)_6[NaPW_{11}O_{39}]$ (b) $(TBA)_5[Sn^{II}PW_{11}O_{39}]$ (c) $(TBA)_5[Pb^{II}PW_{11}O_{39}]$ (d) $(TBA)_4[Sb^{III}PW_{11}O_{39}]$ (e) $(TBA)_4[Bi^{III}PW_{11}O_{39}]$ and (f) $(TBA)_4[ClSn^{IV}PW_{11}O_{39}]$.

(a) $[TBA_2HNaPW_{11}O_{39}]^{3-}$

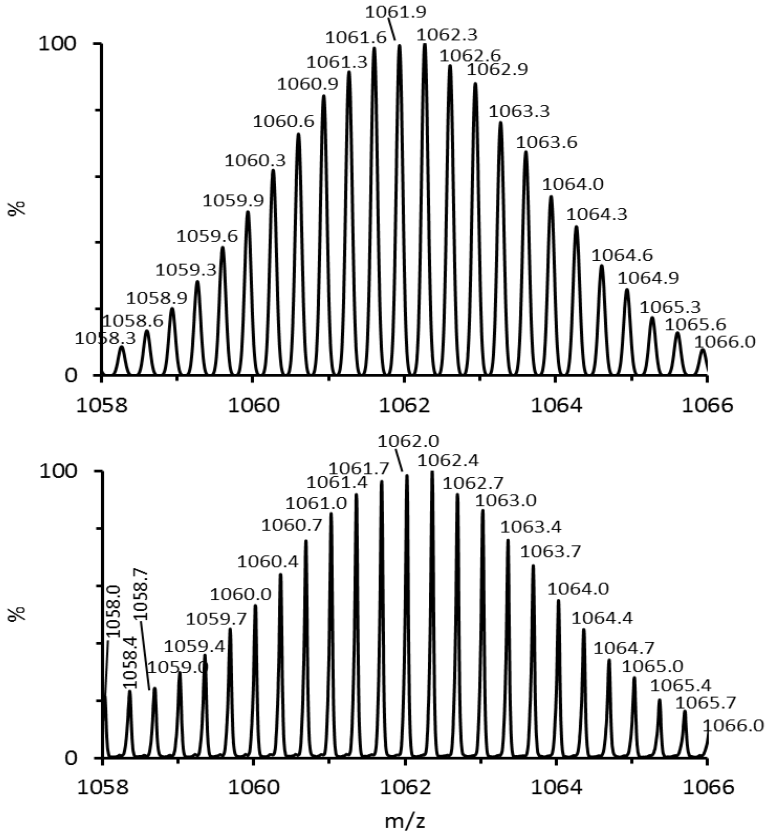

(b) $[TBA_3HNaPW_{11}O_{39}]^{2-}$

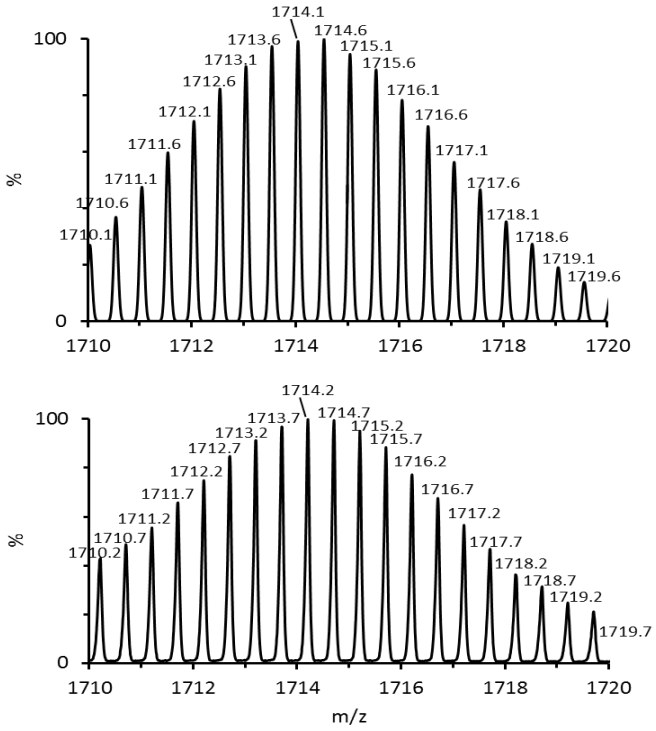

Figure A3.3. Simulations and expansions of some of the ESI-MS peaks assigned in Table 3.2 for $(TBA)_6[NaPW_{11}O_{39}]$. In each of parts (a) – (b), the simulated plot is shown above the experimental plot.

(a) $[H_2SnPW_{11}O_{39}]^{2-}$

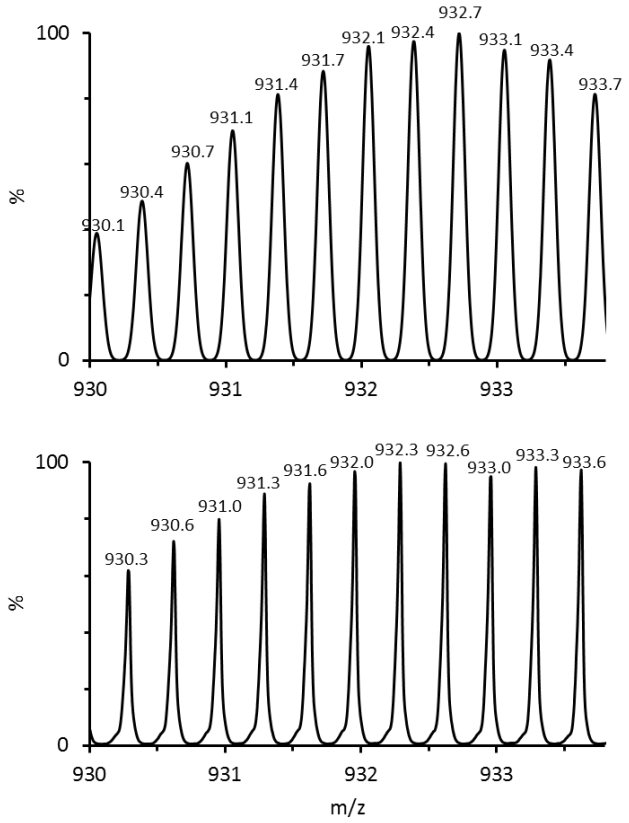

(b) $[TBAHSnPW_{11}O_{39}]^{3-}$

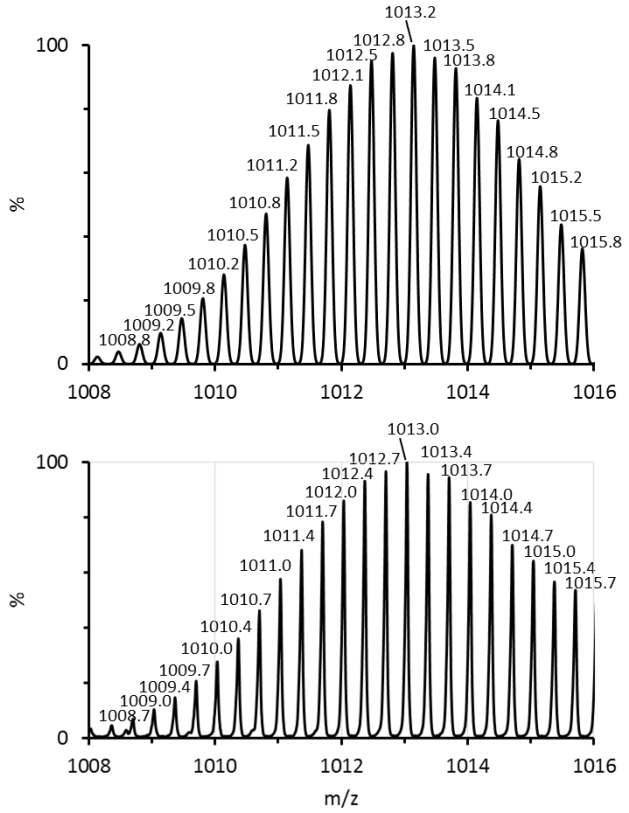

(c) $[TBA_3SnPW_{11}O_{39}]^{2-}$

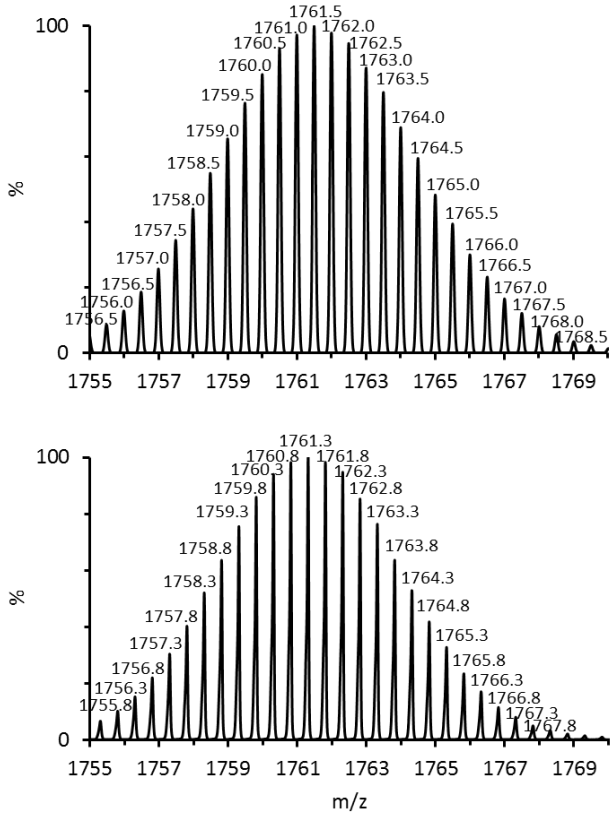

(d) $[TBA_4SnPW_{11}O_{39}]^{-}$

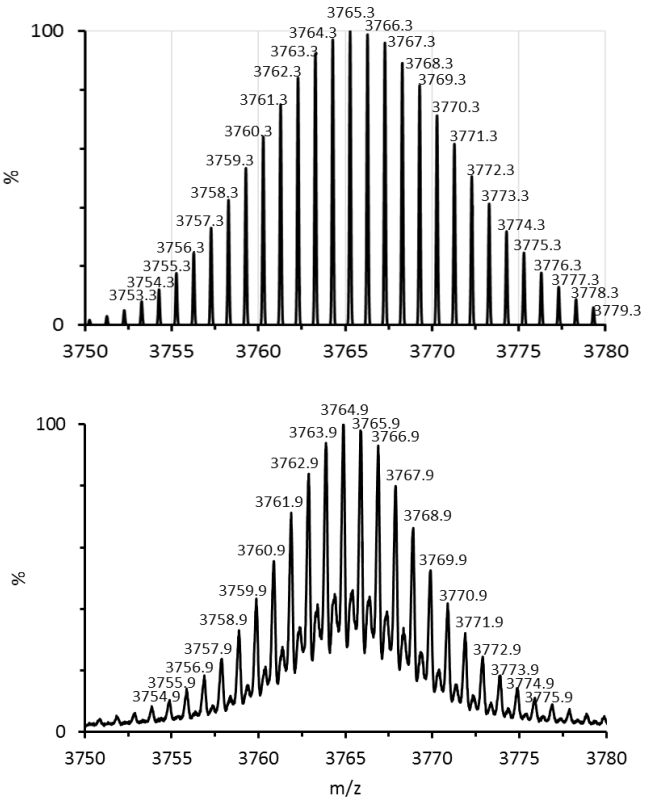

(e) $[TBA_2SnPW_{11}O_{39}]^{3-}$

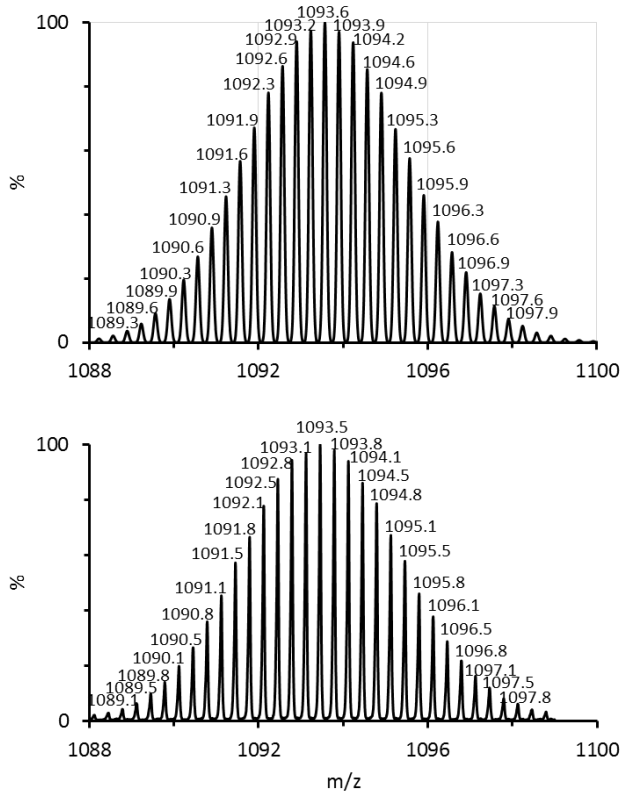

Figure A3.4. Simulations and expansions of some of the ESI-MS peaks assigned in Table 3.7 for $(TBA)_5[Sn^{II}PW_{11}O_{39}]$. In each of parts (a) – (e), the simulated plot is shown above the experimental plot.

(a) $[Na_2PbPW_{11}O_{39}]^{3-}$

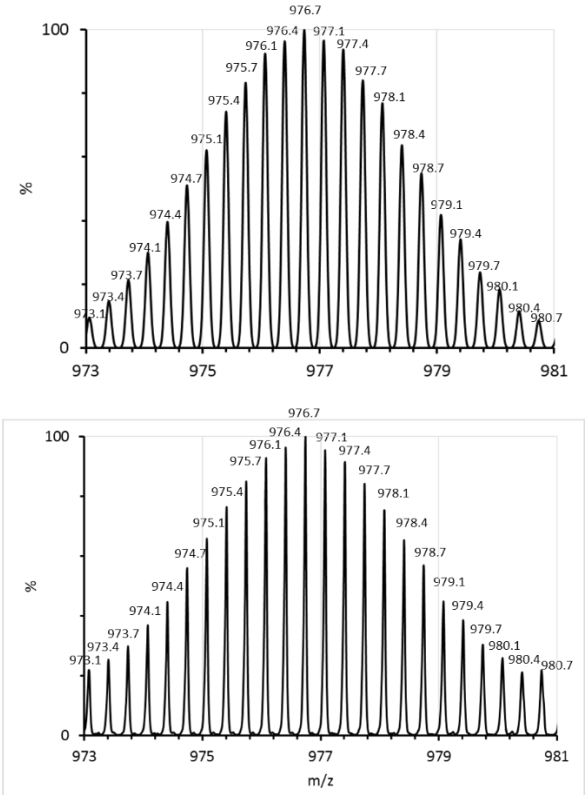

(b) $[TBA_2PbPW_{11}O_{39}]^{3-}$

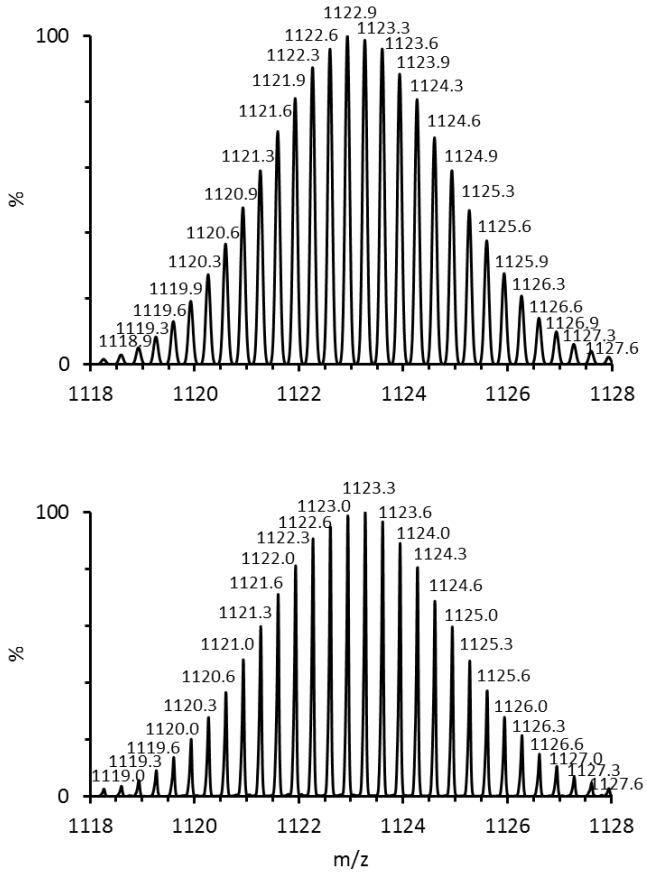

(c) $[Na_3PbPW_{11}O_{39}]^{2-}$

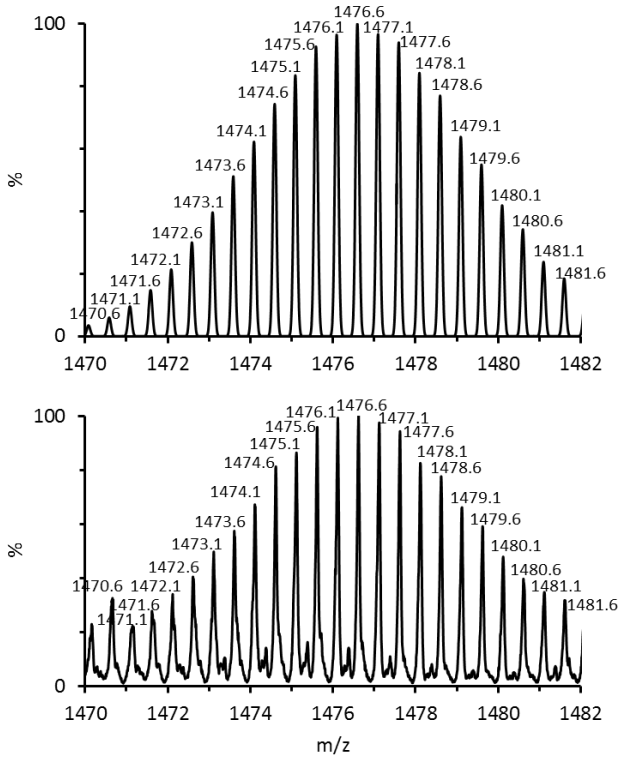

(d) $[TBAPbPW_{11}O_{39}]^{4-}$

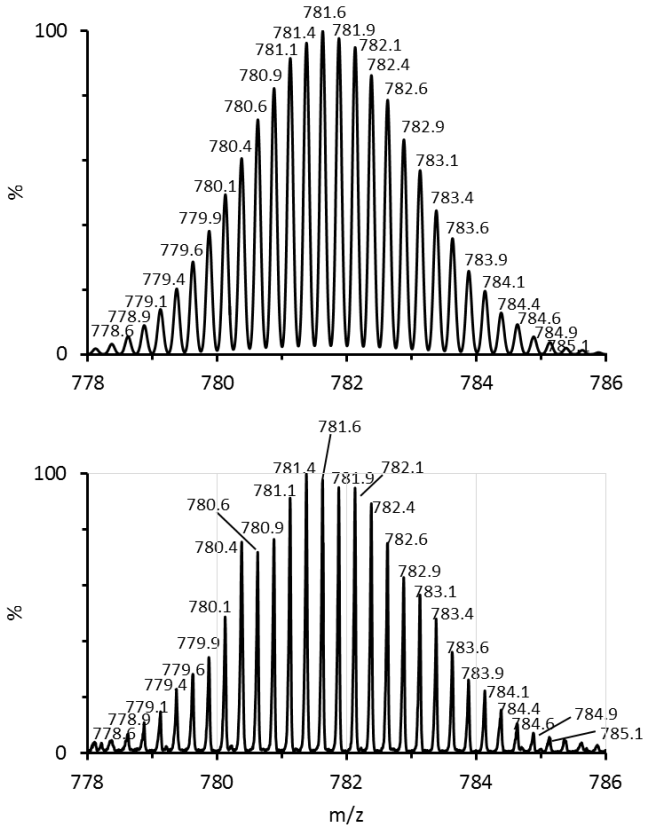

(e) $[HPbPW_{11}O_{39}]^{4-}$

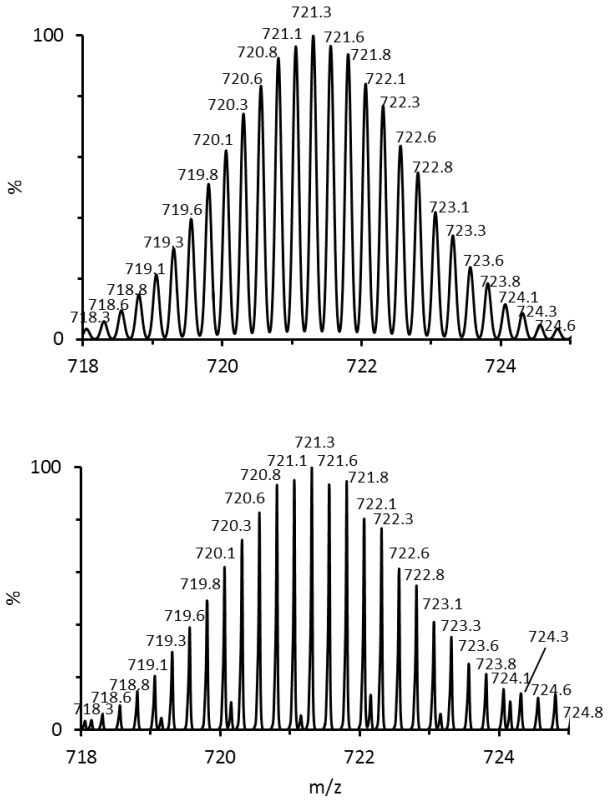

(f) $[TBAHPbPW_{11}O_{39}]^{3-}$

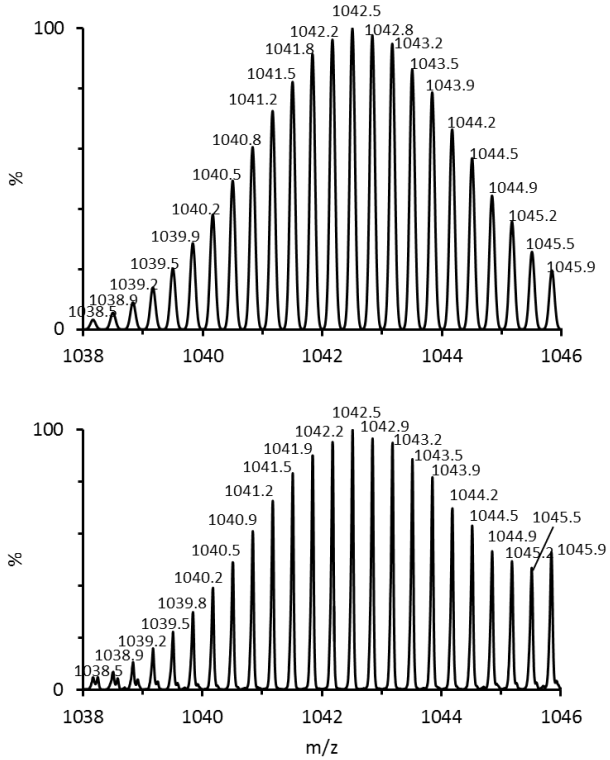

(g) $[TBA_3PbPW_{11}O_{39}]^{2-}$

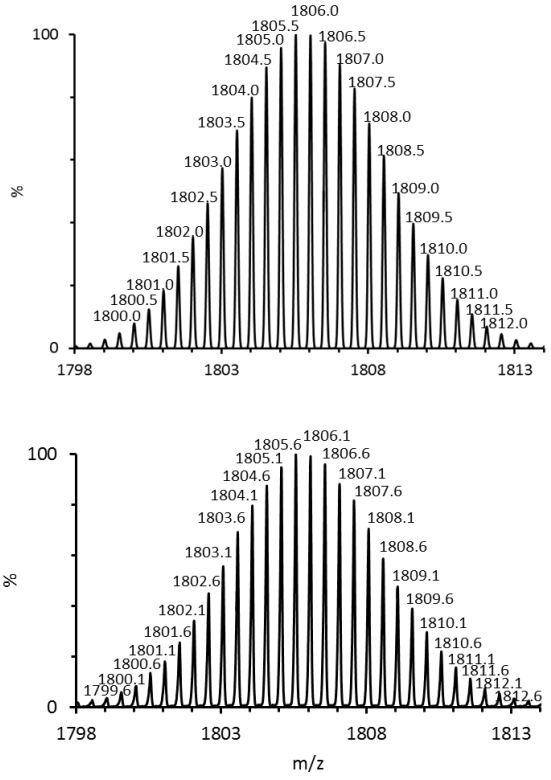

Figure A3.5. Simulations and expansions of some of the ESI-MS peaks assigned in Table 3.8 for $(TBA)_5[Pb^{II}PW_{11}O_{39}]$. In each of parts (a) – (g), the simulated plot is shown above the experimental plot.

(a) $[Sb^{III}PW_{11}O_{39}]^{4-}$

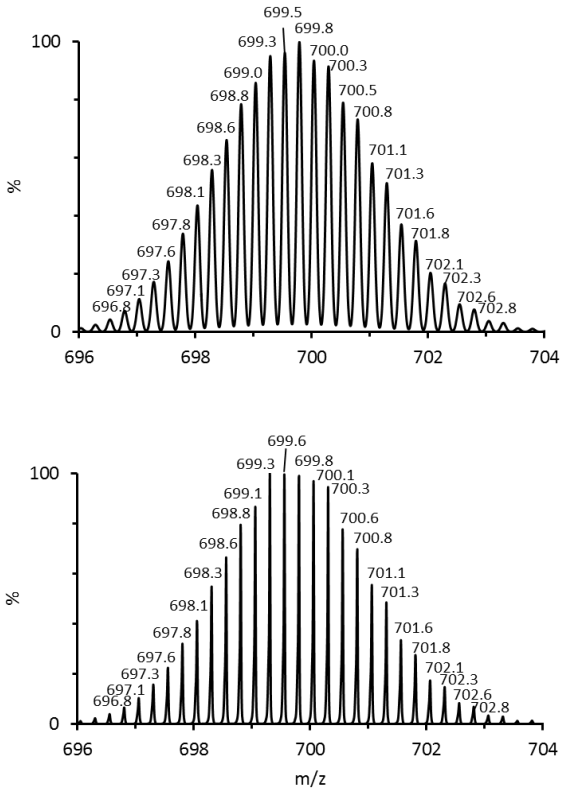

(b) $[HSb^{III}PW_{11}O_{39}]^{3-}$

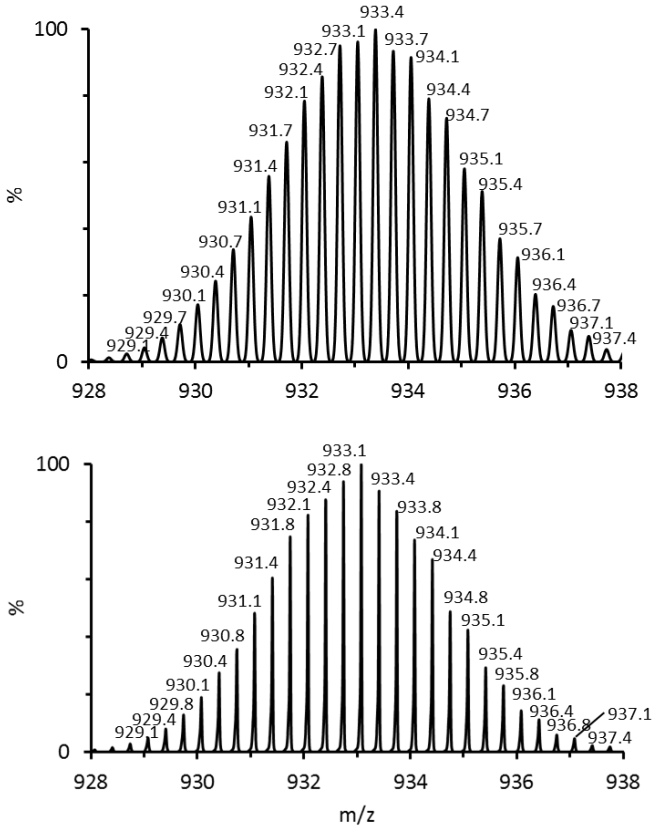

(c) $[TBASb^{III}PW_{11}O_{39}]^{3-}$

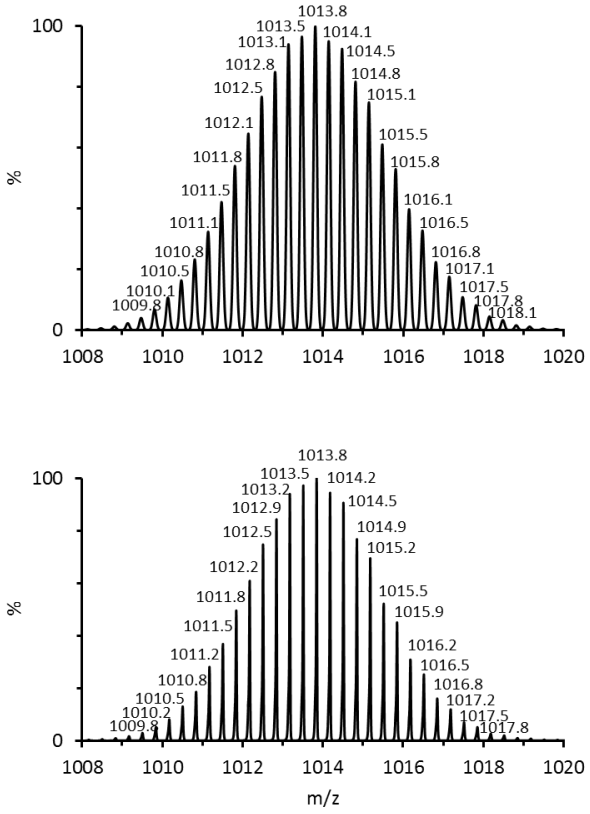

(d) $[TBA_2Sb^{III}PW_{11}O_{39}]^{2-}$

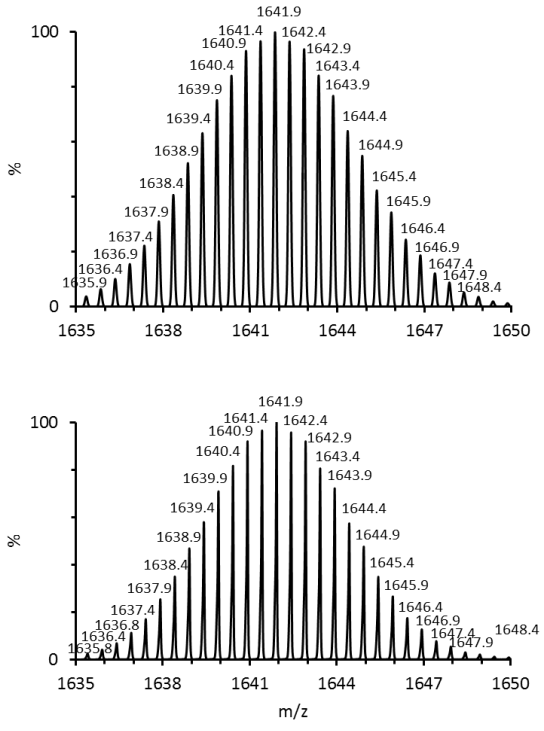

Figure A3.6. Simulations and expansions of some of the ESI-MS peaks assigned in Table 3.9 for $(TBA)_4[Sb^{III}PW_{11}O_{39}]$. In each of parts (a) – (d), the simulated plot is shown above the experimental plot.

(a) $[Bi^{III}PW_{11}O_{39}]^{4-}$

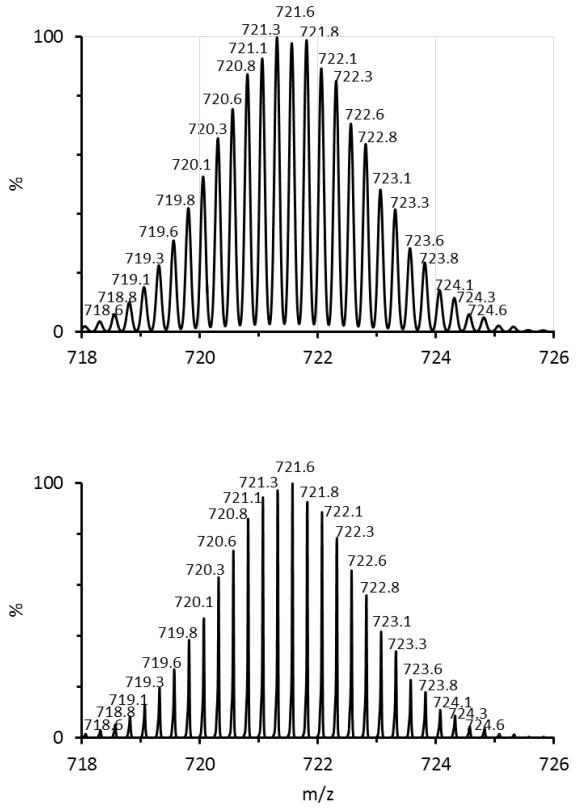

(b) $[HBi^{III}PW_{11}O_{39}]^{3-}$

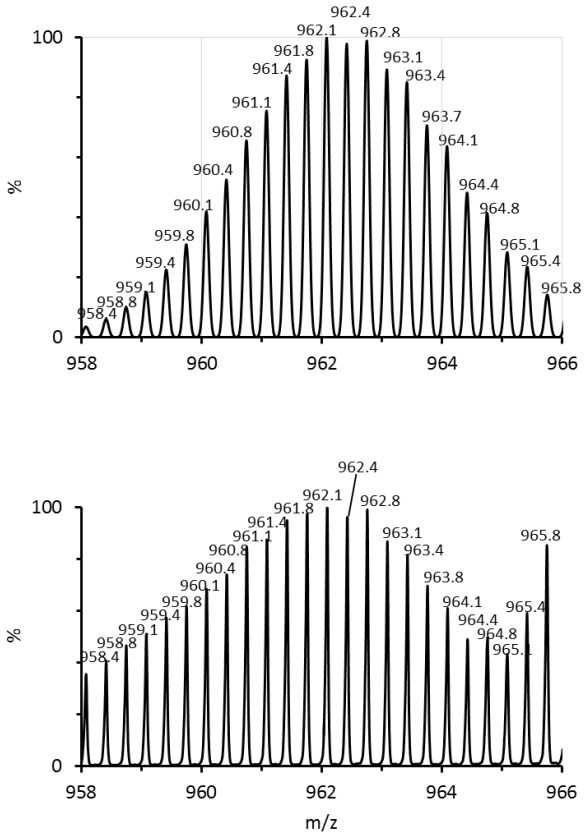

(c) $[NaBi^{III}PW_{11}O_{39}]^{3-}$

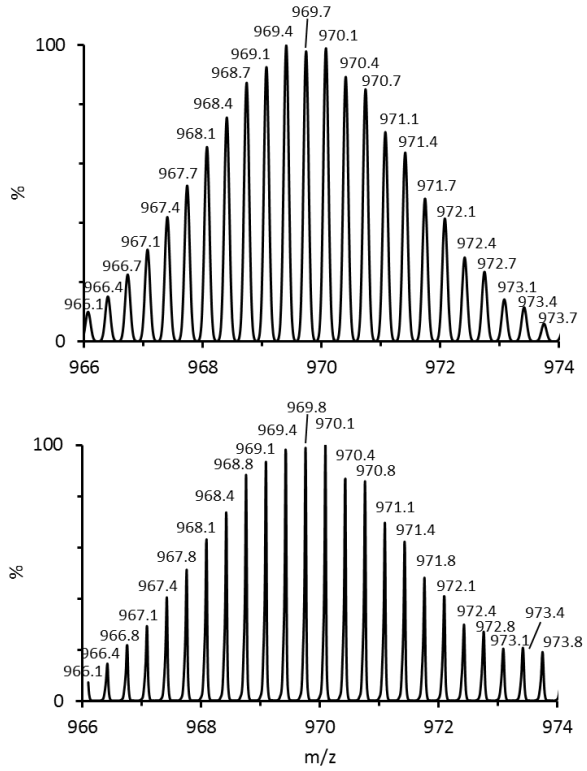

(d) $[TBABi^{III}PW_{11}O_{39}]^{3-}$

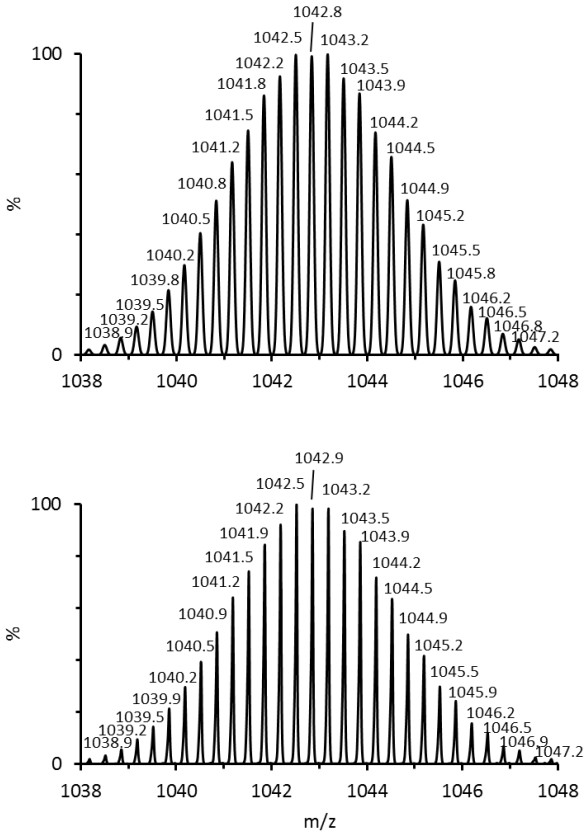

(e) $[TBA_2Bi^{III}PW_{11}O_{39}]^{2-}$

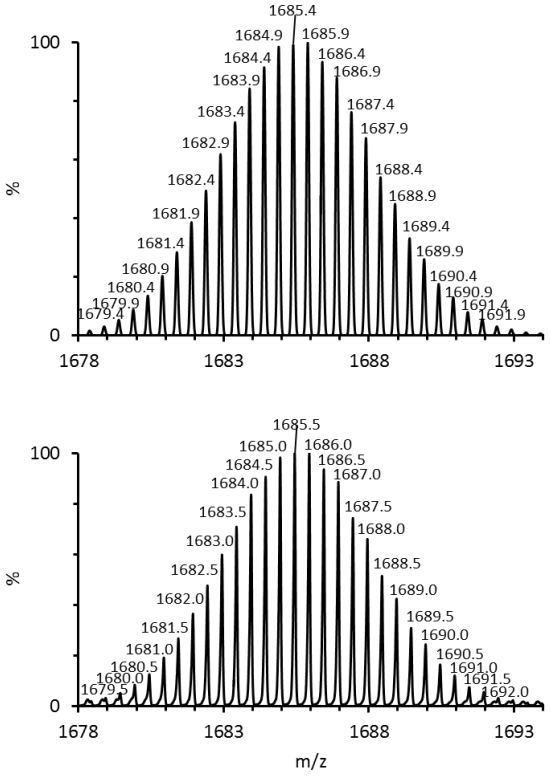

(f) $[Na_2Bi^{III}PW_{11}O_{39}]^{2-}$

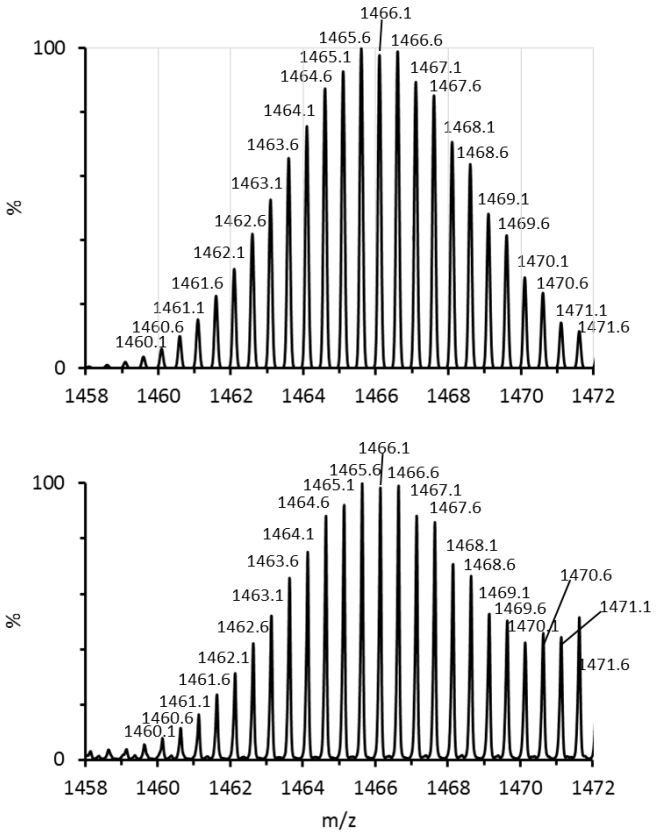

(g) $[TBANaBi^{III}PW_{11}O_{39}]^{2-}$

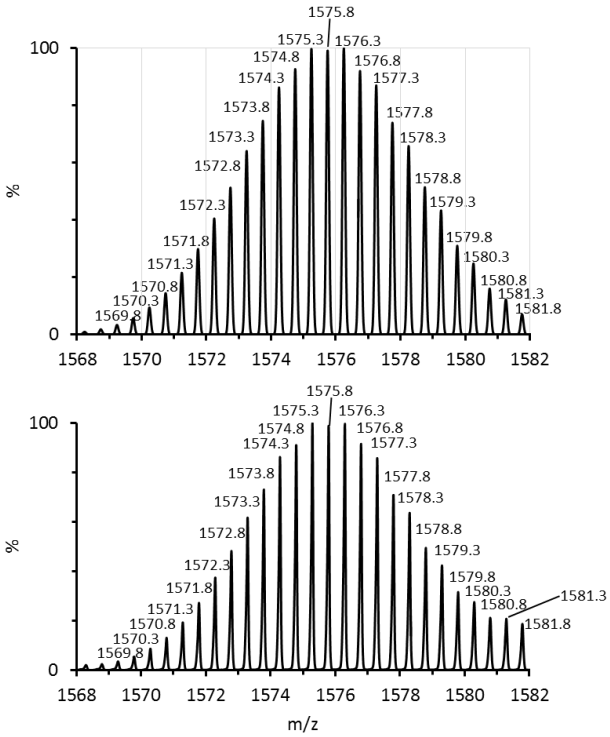

Figure A3.7. Simulations and expansions of some of the ESI-MS peaks assigned in Table 3.10 for $(TBA)_4[Bi^{III}PW_{11}O_{39}]$. In each of parts (a) – (g), the simulated plot is shown above the experimental plot.

(a) $[ClSnPW_{11}O_{39}]^{4-}$

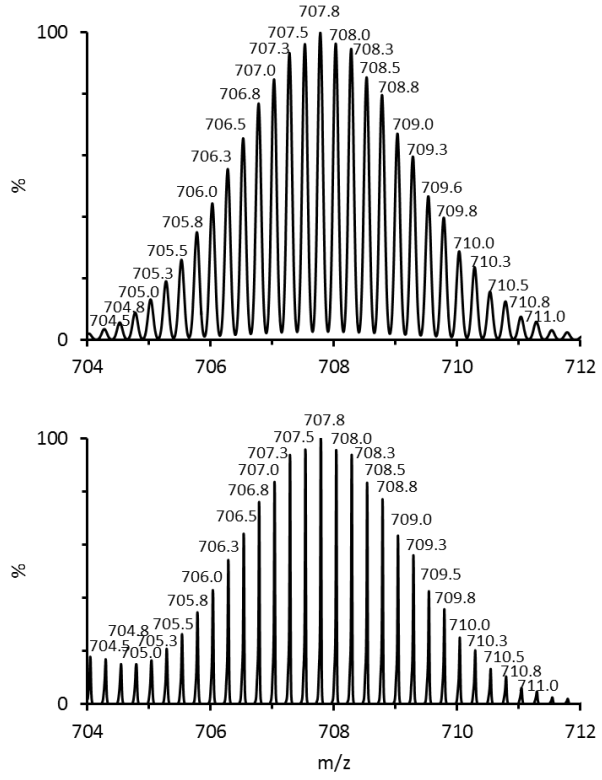

(b) $[TBAClSnPW_{11}O_{39}]^{3-}$

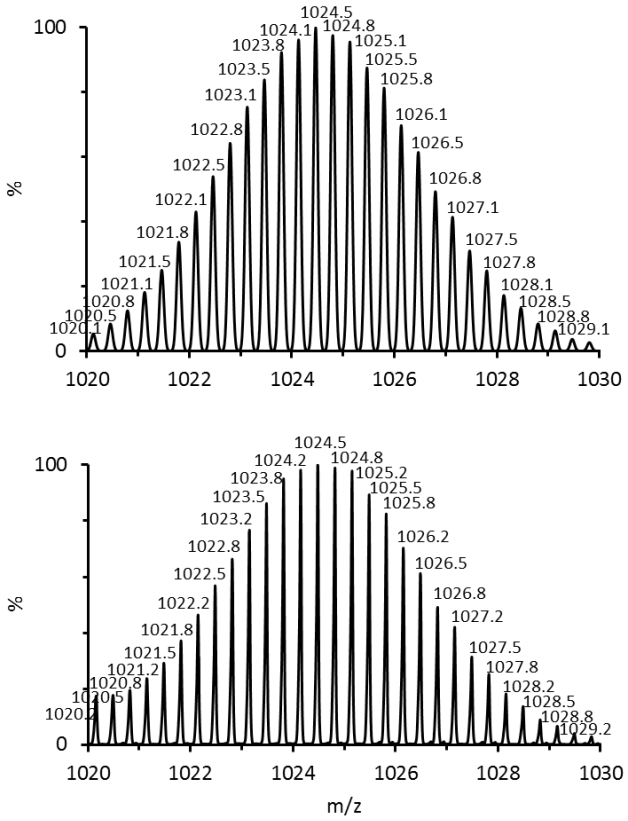

(c) $[TBA_2ClSnPW_{11}O_{39}]^{2-}$

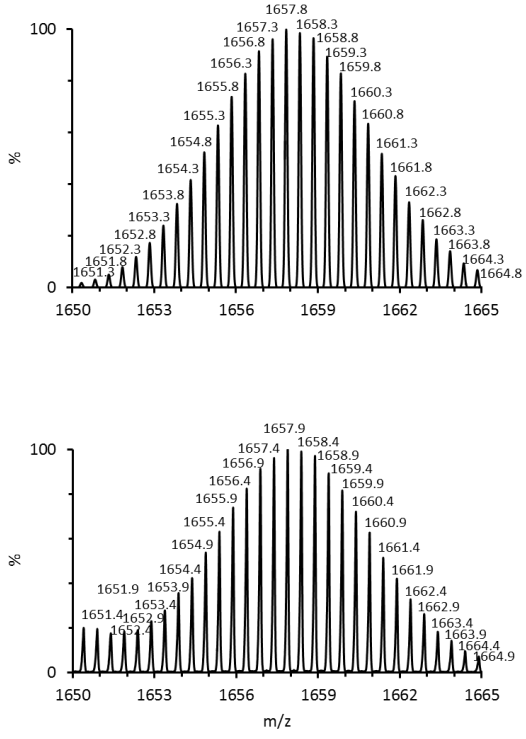

Figure A3.8. Simulations and expansions of some of the ESI-MS peaks assigned in Table 3.11 for $(TBA)_4[ClSn^{IV}PW_{11}O_{39}]$. In each of parts (a) – (c), the simulated plot is shown above the experimental plot.

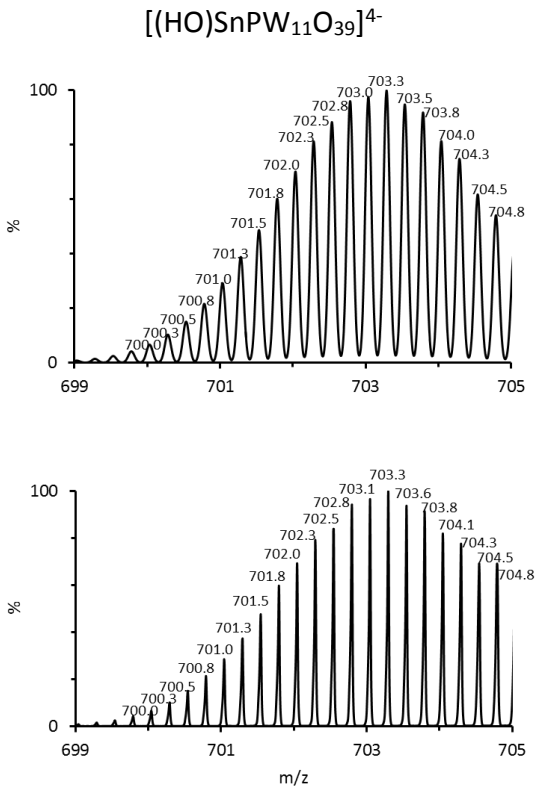

Figure A3.9. Simulations and expansions of some of the ESI-MS peaks assigned to $[(HO)Sn^{IV}PW_{11}O_{39}]^{4-}$ polyanion. The simulated plot is shown above the experimental plot.

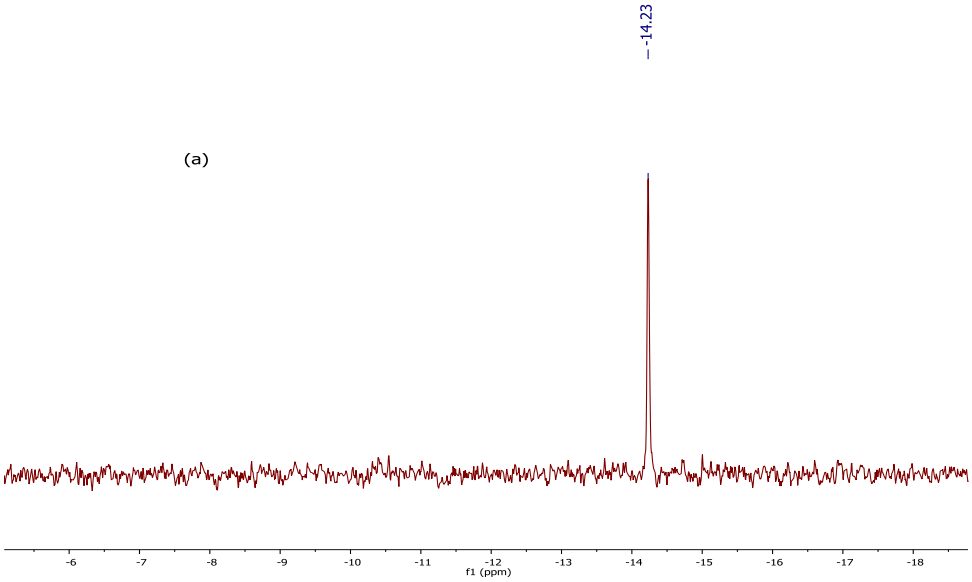

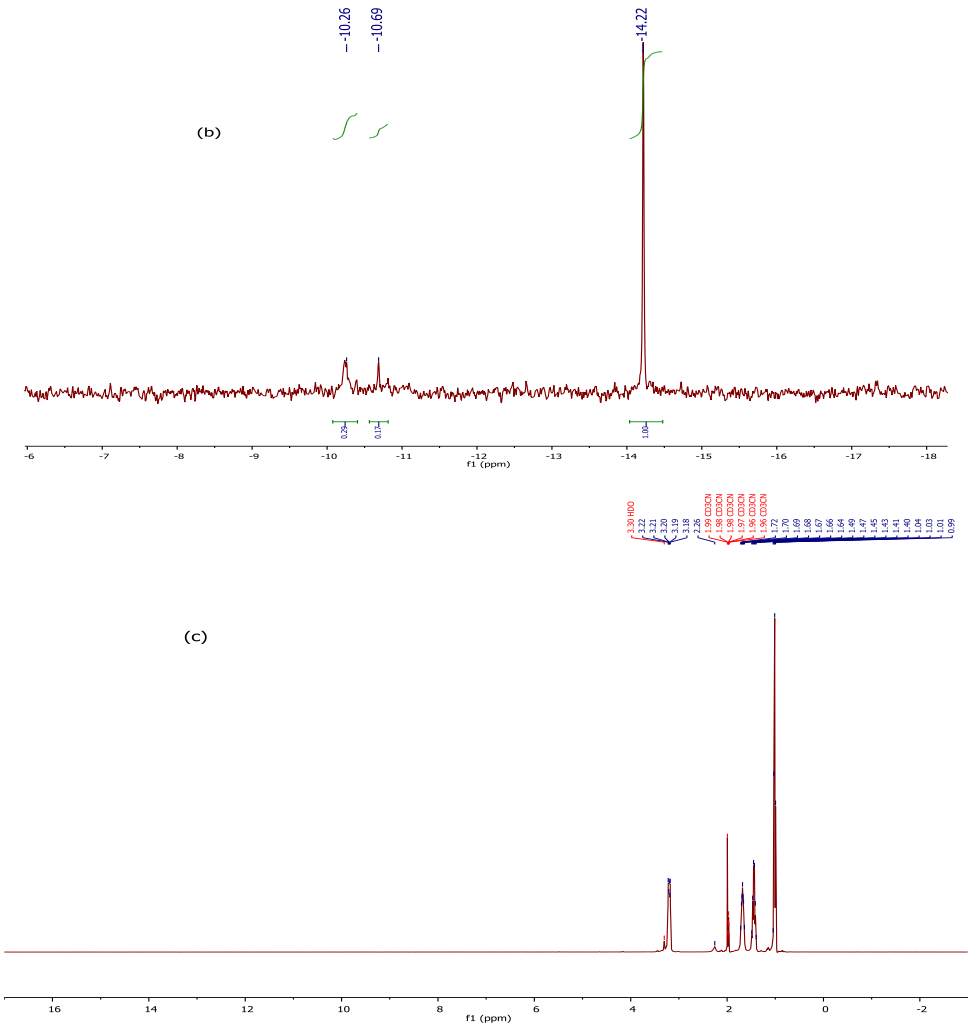

Figure A3.10. ^{31}P NMR spectra in MeCN/CD_3CN of (a) $[Sb^{III}PW_{11}O_{39}]^{4-}$ (b) vacuum-dried product of the reaction between $[Sb^{III}PW_{11}O_{39}]^{4-}$ and 1 mole-equivalent of methanolic MeONa and (c) ^{1}H NMR spectrum of vacuum-dried product of the reaction between $[Sb^{III}PW_{11}O_{39}]^{4-}$ and 1 mole-equivalent of methanolic MeONa.

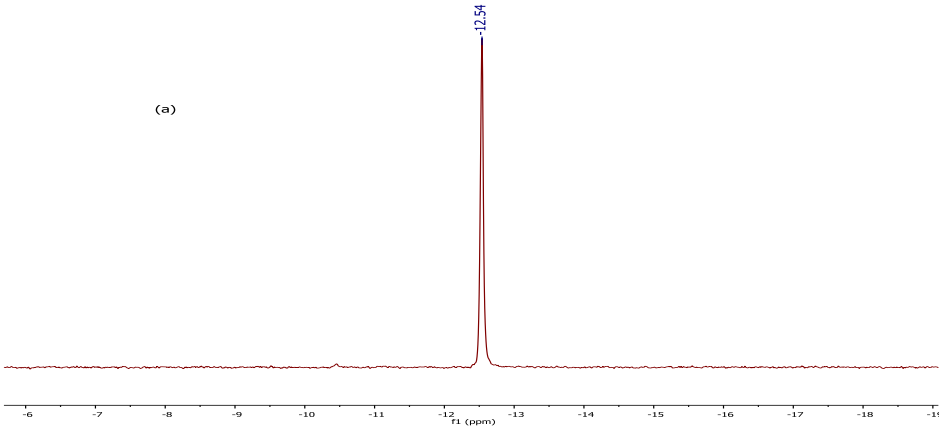

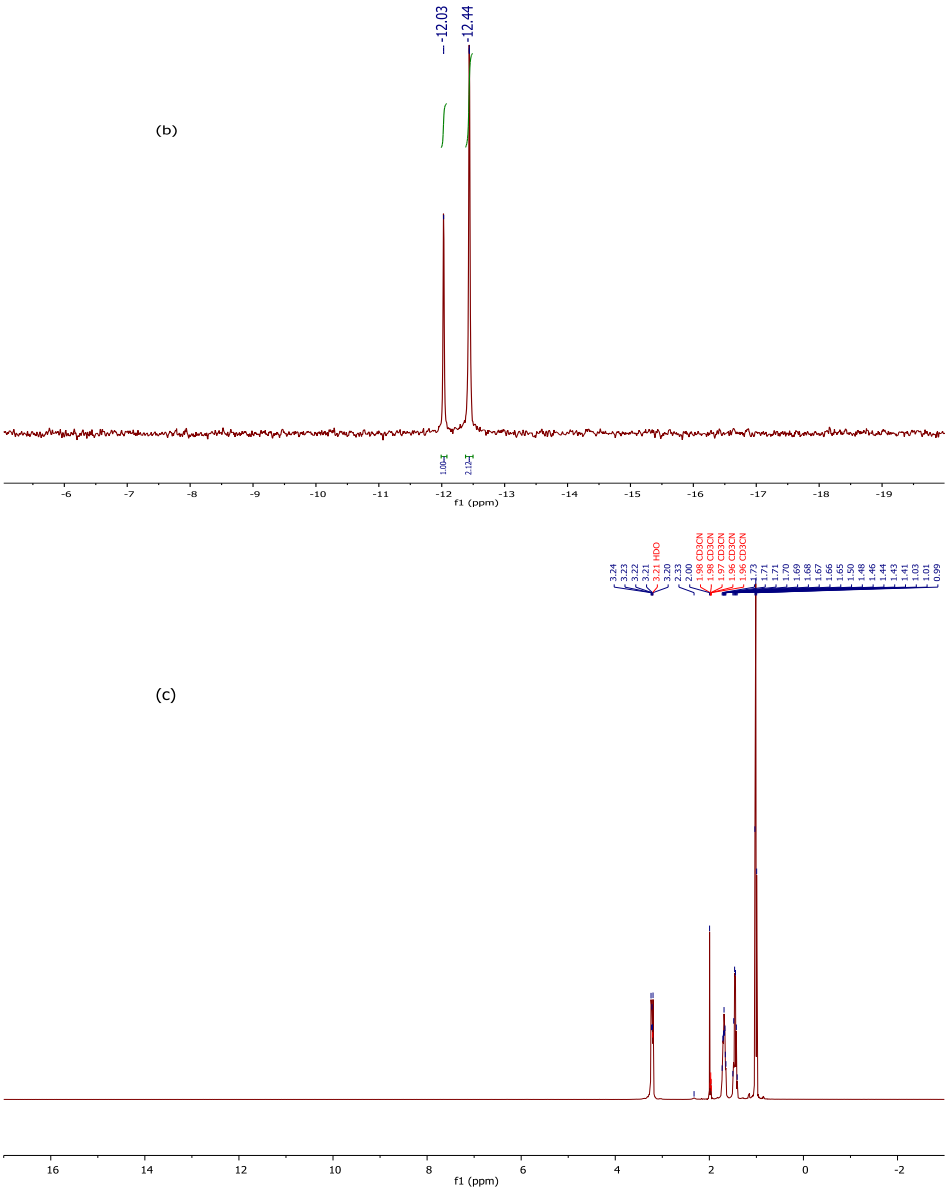

Figure A3.11. ^{31}P NMR spectra in MeCN/CD_3CN of (a) $[Bi^{III}PW_{11}O_{39}]^{4-}$ (b) vacuum-dried product of the reaction between $[Bi^{III}PW_{11}O_{39}]^{4-}$ and 1 mole-equivalent of methanolic MeONa and (c) ^{1}H NMR spectrum of vacuum-dried product of the reaction between $[Bi^{III}PW_{11}O_{39}]^{4-}$ and 1 mole-equivalent of methanolic MeONa.

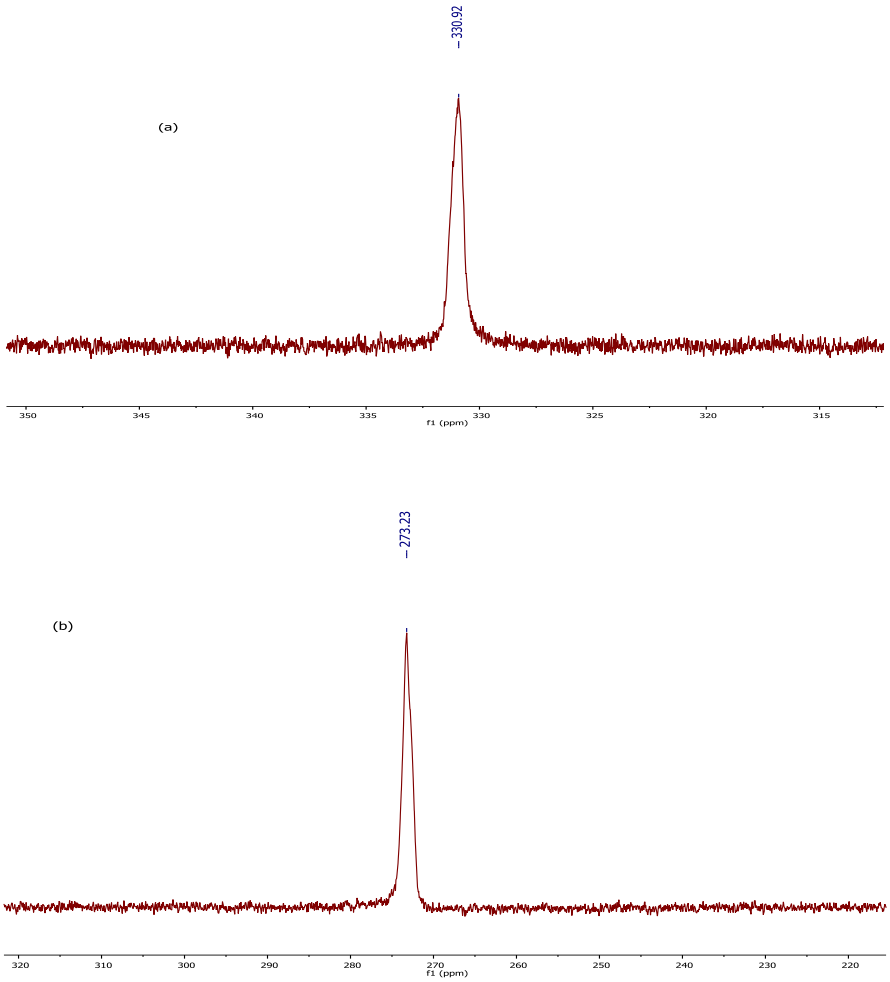

Figure A3.12. ^{31}P NMR spectra of (a) purple solution of $(TBA)_5[CoPW_{11}O_{39}]$ in MeCN/CD_3CN and (b) green solution of $(TBA)_5[CoPW_{11}O_{39}]$ in CD_2Cl_2/CH_2Cl_2.

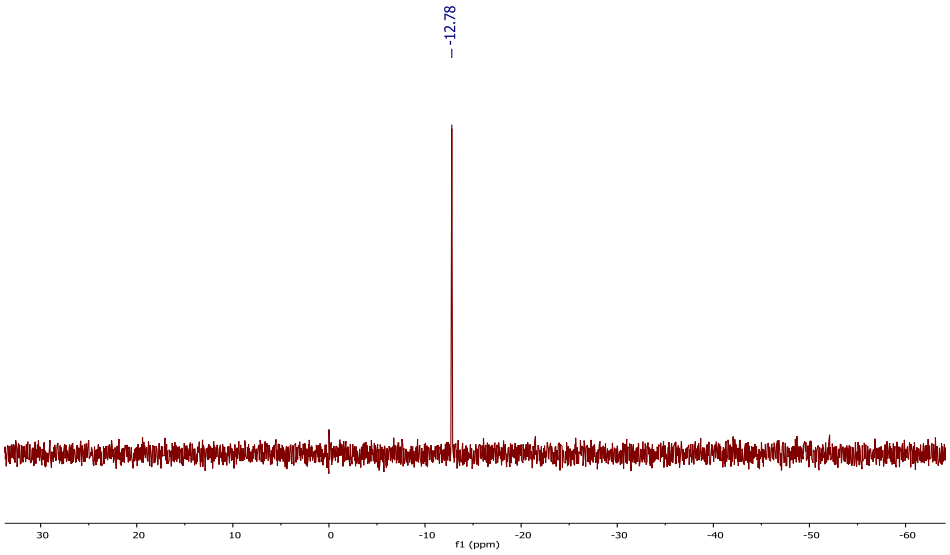

Figure A3.13. ^{31}P NMR spectrum of green solution of $(TBA)_5[NiPW_{11}O_{39}]$ in MeCN/CD_3CN.

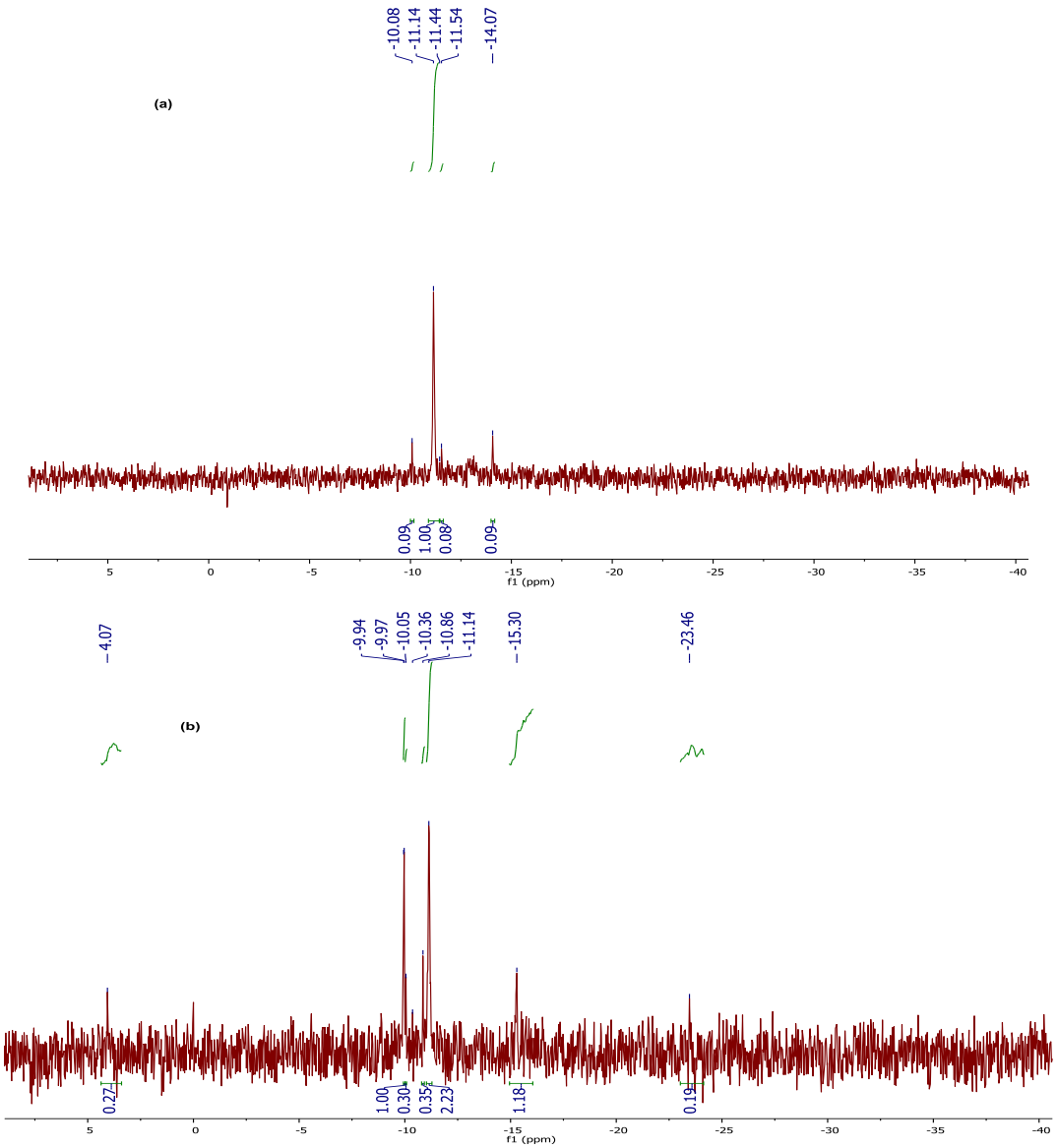

Figure A3.14. ^{31}P NMR spectra of the product of the reaction between $(TBA)_6[NaPW_{11}O_{39}]$ and ½ mole-equivalent of $[Mo_2(NCCH_3)_8(ax\text{-}CH_3CN)_{0.5}][BF_4]_4$ in MeCN at 22 °C (a) after ~30 mins and (b) after stirring the solution for 12 h.

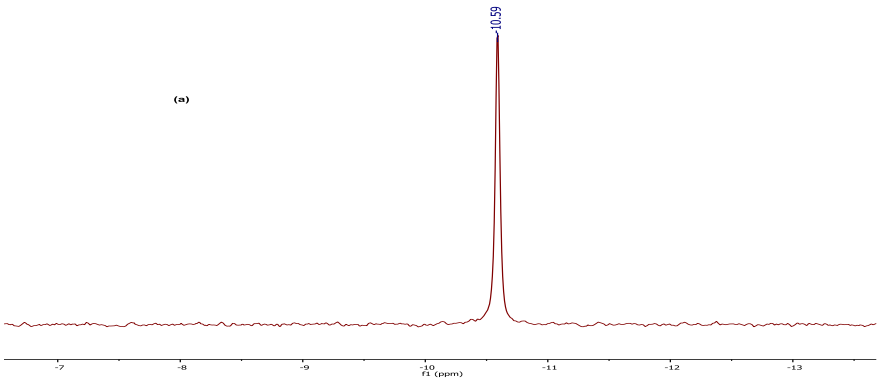

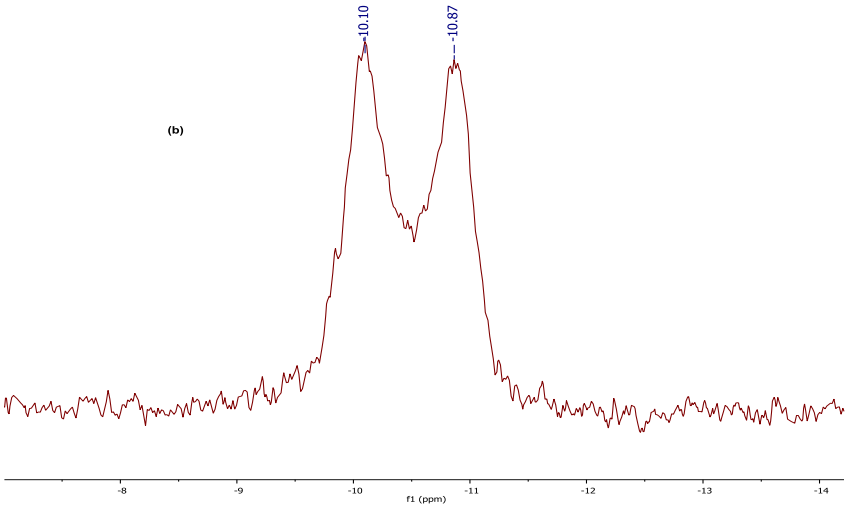
(b)
-10.10
-10.87
-8
-9
-10
-11
-12
-13
-14
f1 (ppm)

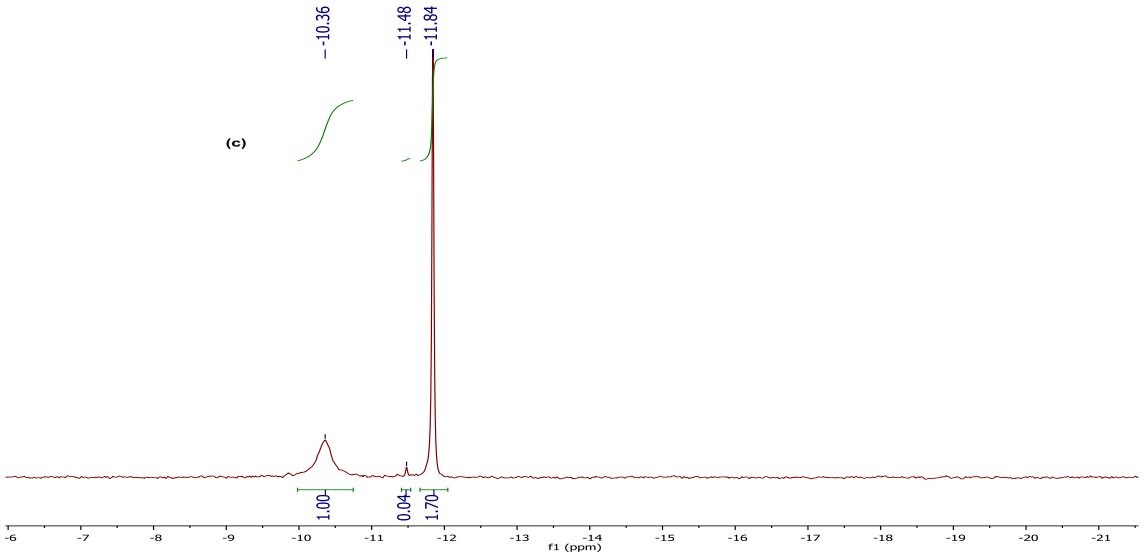
(c)
-10.36
-11.48
-11.84
1.00
0.04
1.70
-6
-7
-8
-9
-10
-11
-12
-13
-14
-15
-16
-17
-18
-19
-20
-21
f1 (ppm)

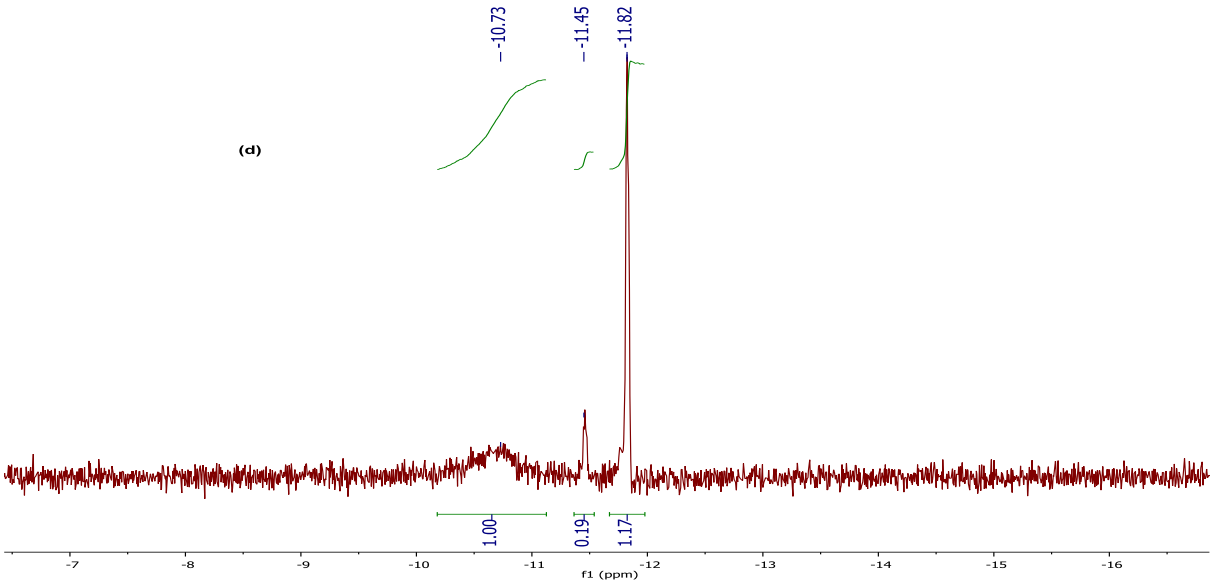
(d)
-10.73
-11.45
-11.82
1.00
0.19
1.17
-7
-8
-9
-10
-11
-12
-13
-14
-15
-16
f1 (ppm)

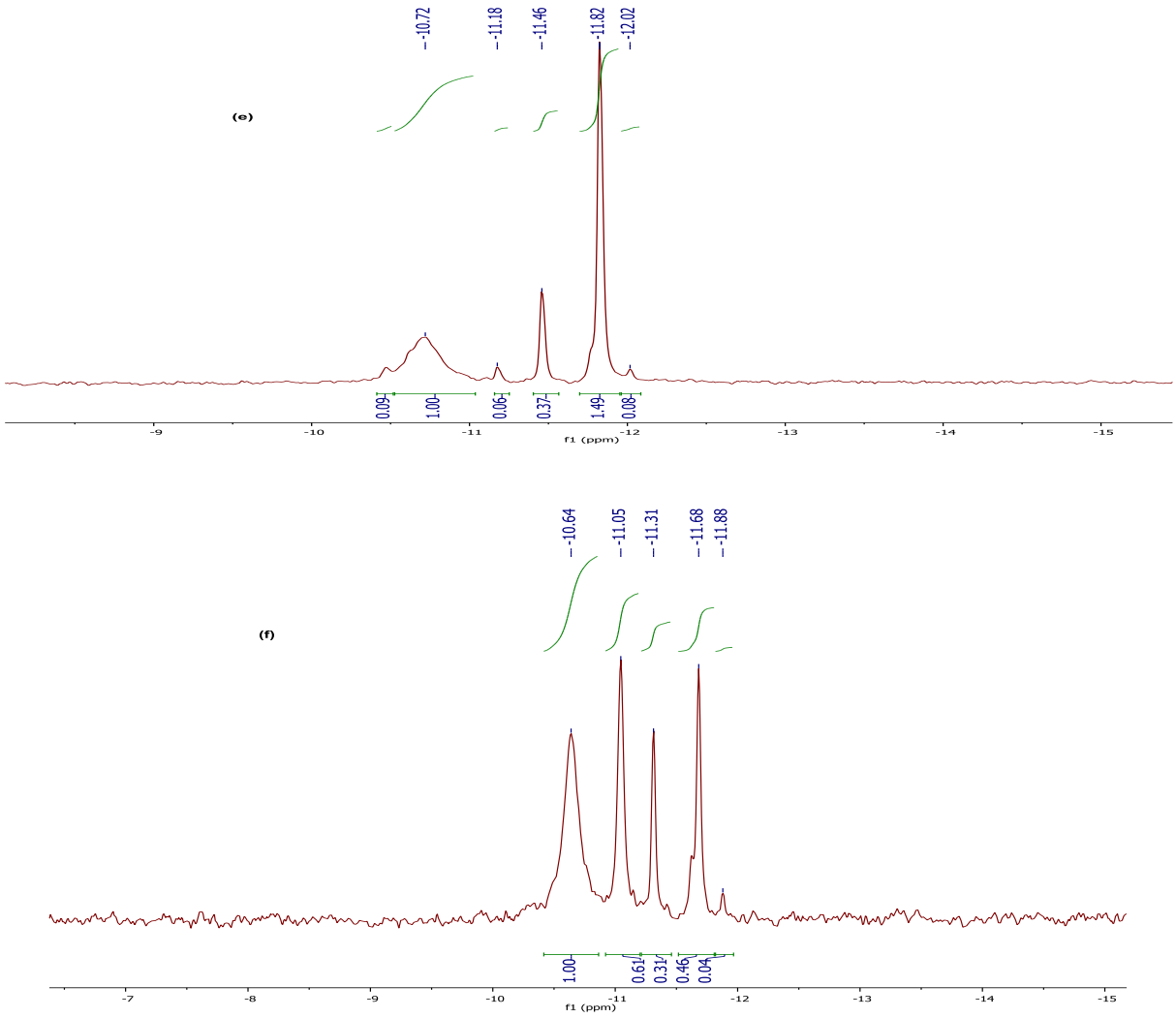

Figure A3.15. ^{31}P NMR spectra of (a) $(TBA)_6[NaPW_{11}O_{39}]$ in DMSO and the product of the reaction between $(TBA)_6[NaPW_{11}O_{39}]$ and 1 mole-equivalent of $RhCl_3$ in DMSO (b) after ~10 mins at 22 °C (c) after ~5 h at 120 °C (d) after 30 h at 120 °C (e) after 36 h at 120 °C and (f) after 82 h at 120 °C.

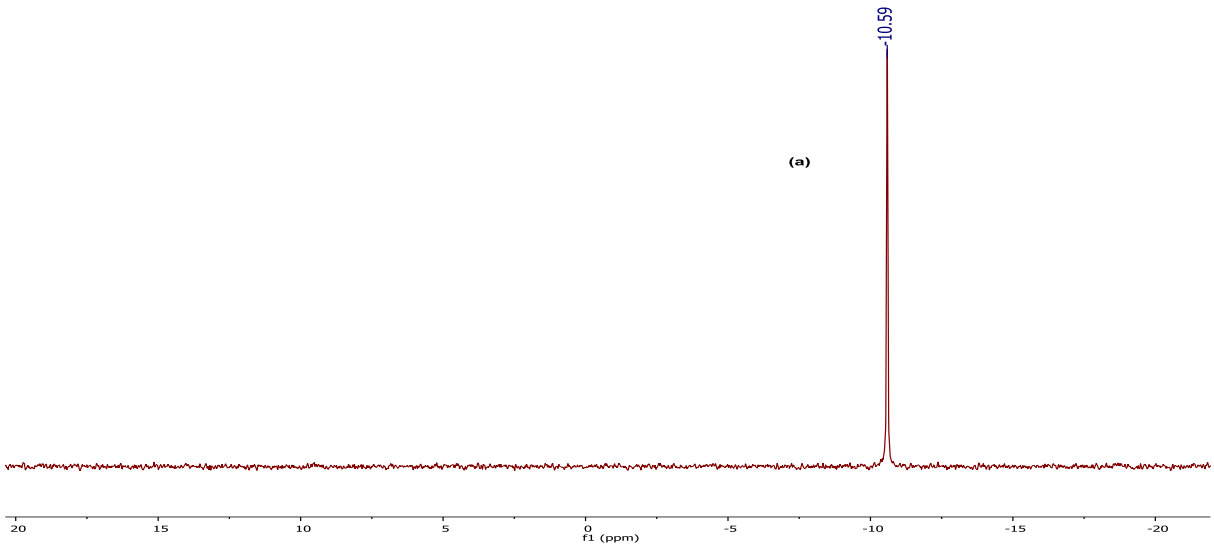

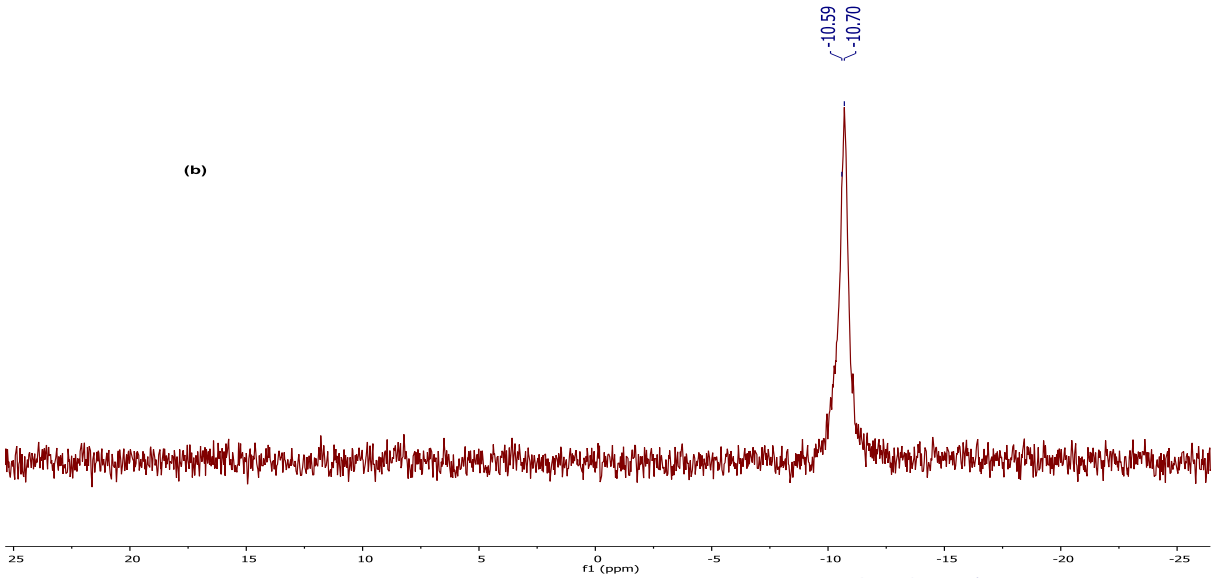
-10.59
-10.70
(b)
25 20 15 10 5 0 -5 -10 -15 -20 -25
f1 (ppm)

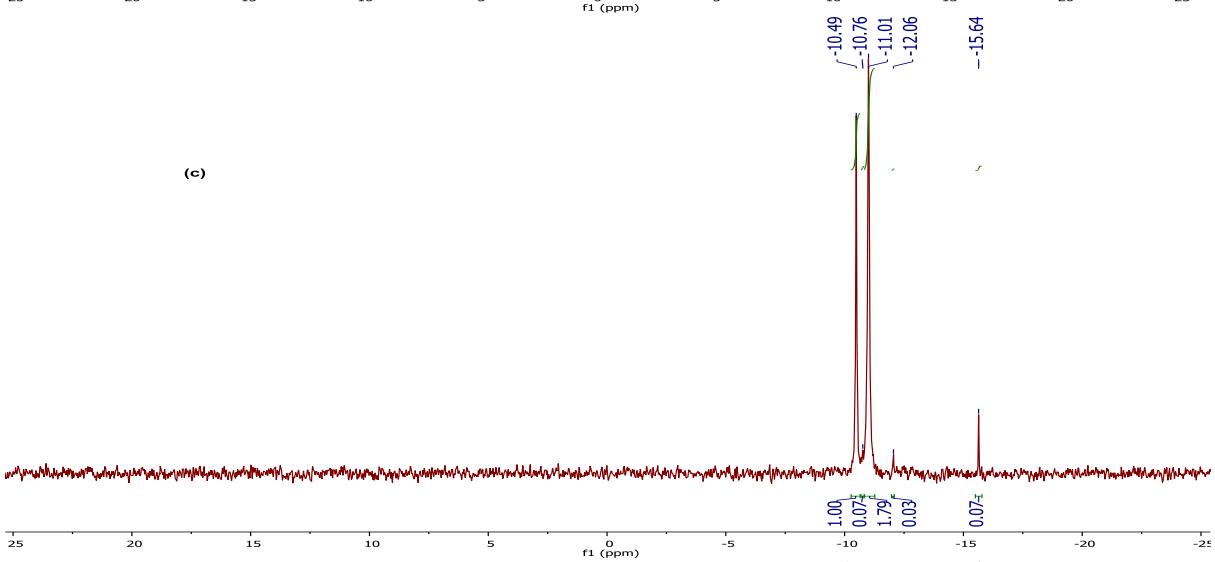
-10.49
-10.76
-11.01
-12.06
-15.64
(c)
1.00
0.07
1.79
0.03
0.07
25 20 15 10 5 0 -5 -10 -15 -20
f1 (ppm)

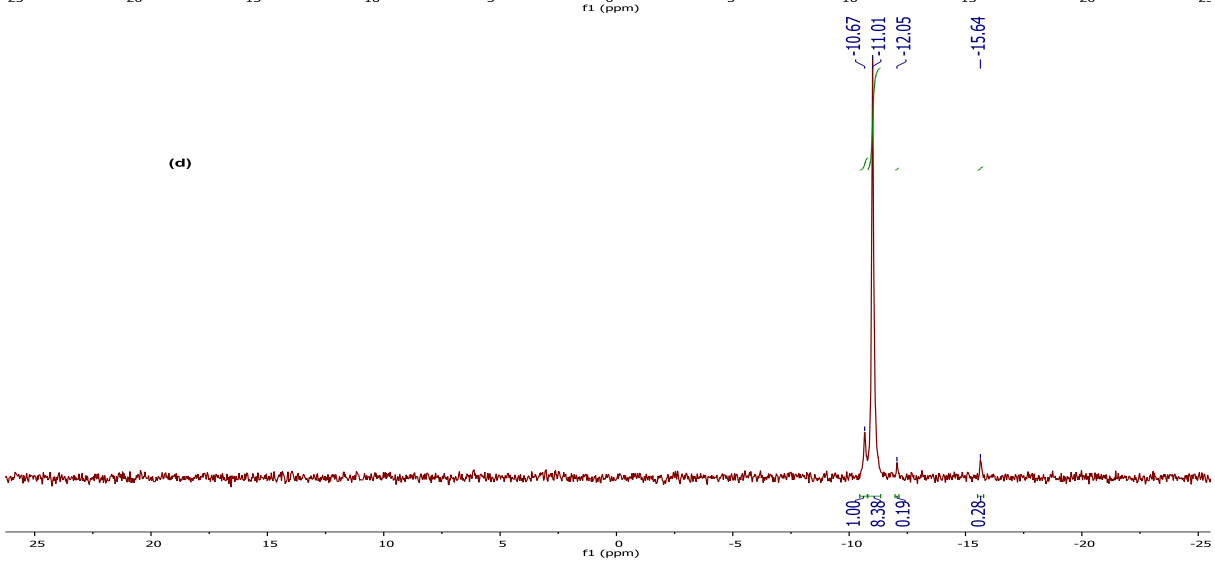
-10.67
-11.01
-12.05
-15.64
(d)
1.00
8.38
0.19
0.28
25 20 15 10 5 0 -5 -10 -15 -20
f1 (ppm)

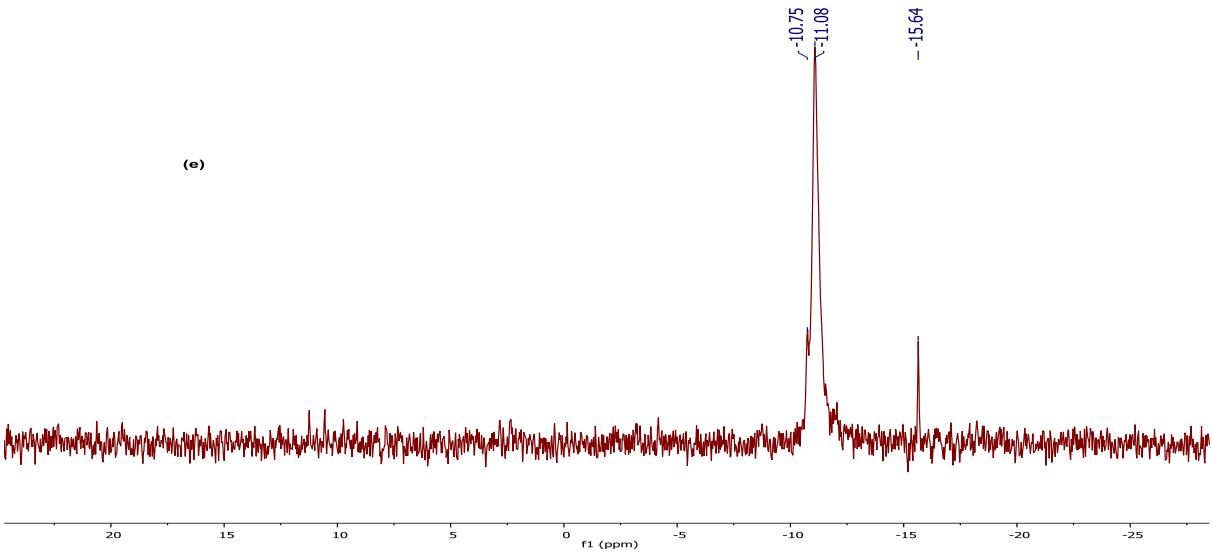

Figure A3.16. ^{31}P NMR spectra of (a) $(TBA)_6[NaPW_{11}O_{39}]$ in DMSO and the product of the reaction between $(TBA)_6[NaPW_{11}O_{39}]$ and 1 mole-equivalent of $IrCl_3$ in DMSO (b) after ~10 mins at 22 °C (c) after ~18 h at 150 °C (d) after 22 h at 150 °C (e) after 65 h at 150 °C.

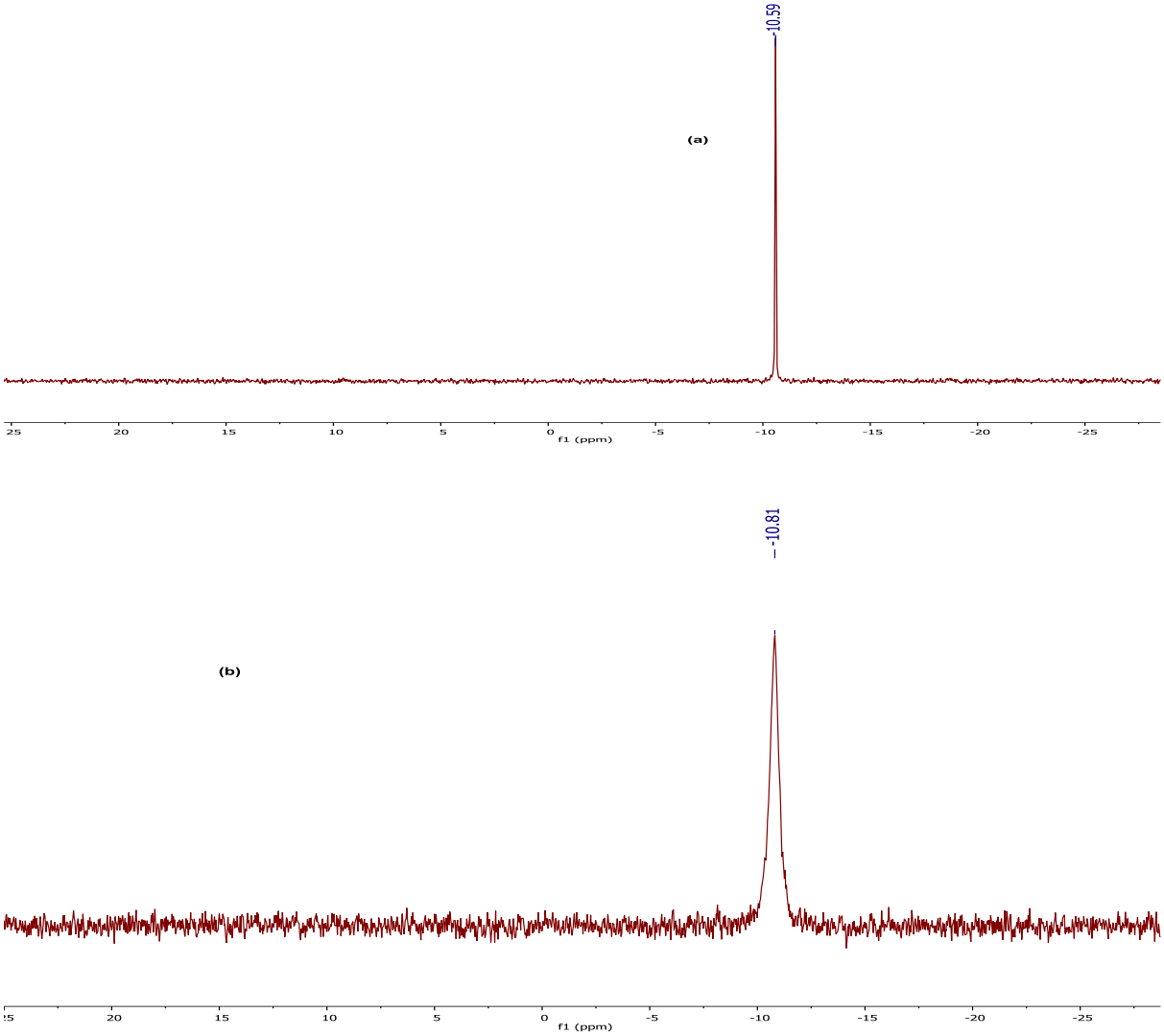

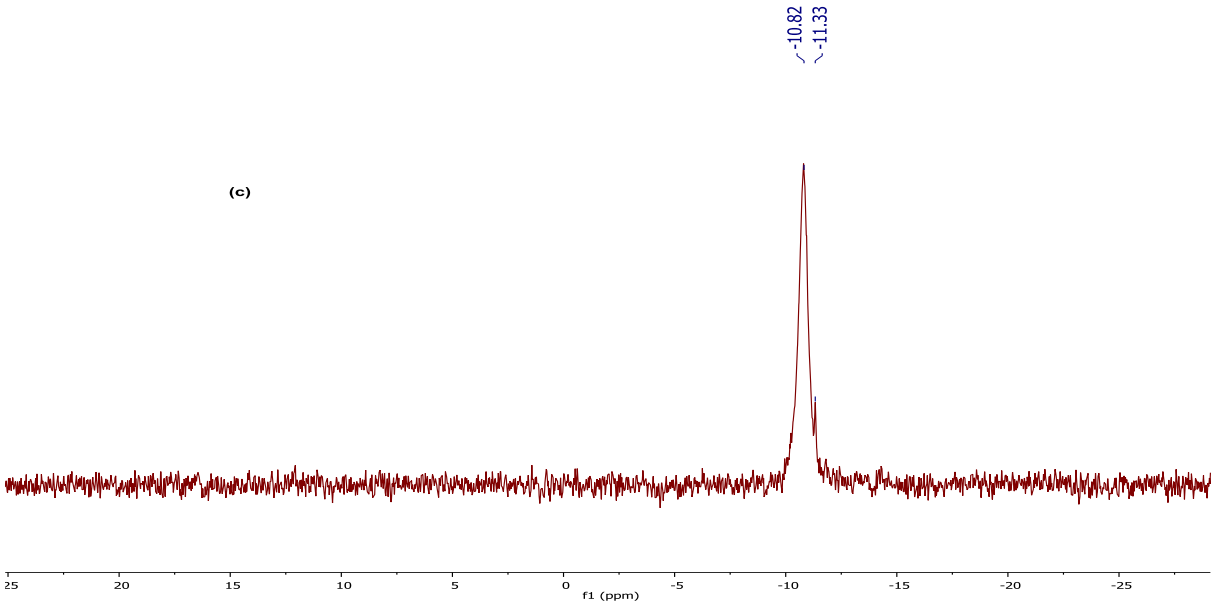
-10.82
-11.33
(c)
25 20 15 10 5 0 -5 -10 -15 -20 -25
f1 (ppm)

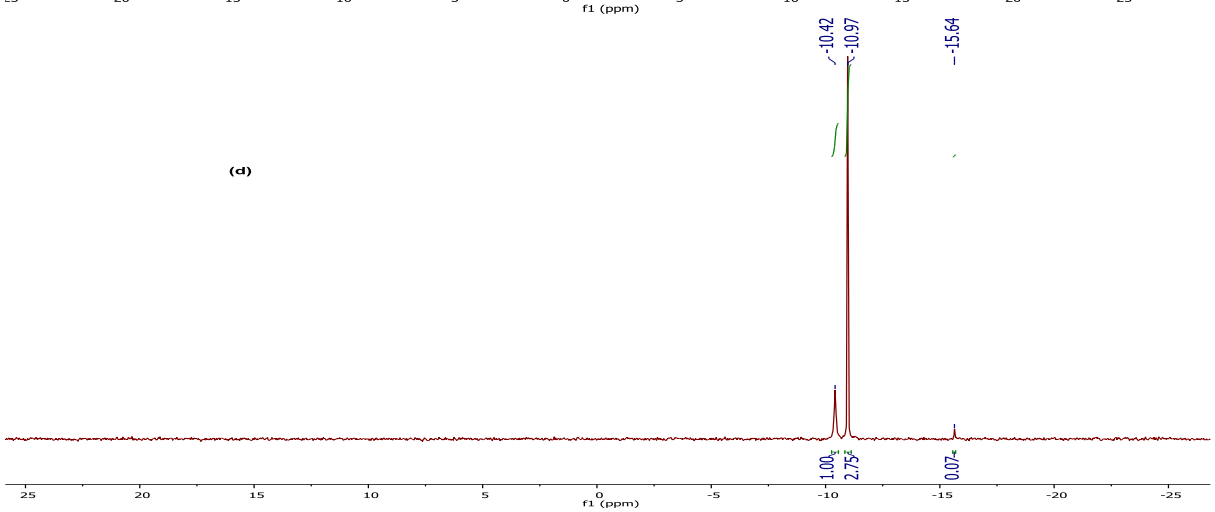
-10.42
-10.97
-15.64
(d)
1.00
2.75
0.07
25 20 15 10 5 0 -5 -10 -15 -20 -25
f1 (ppm)

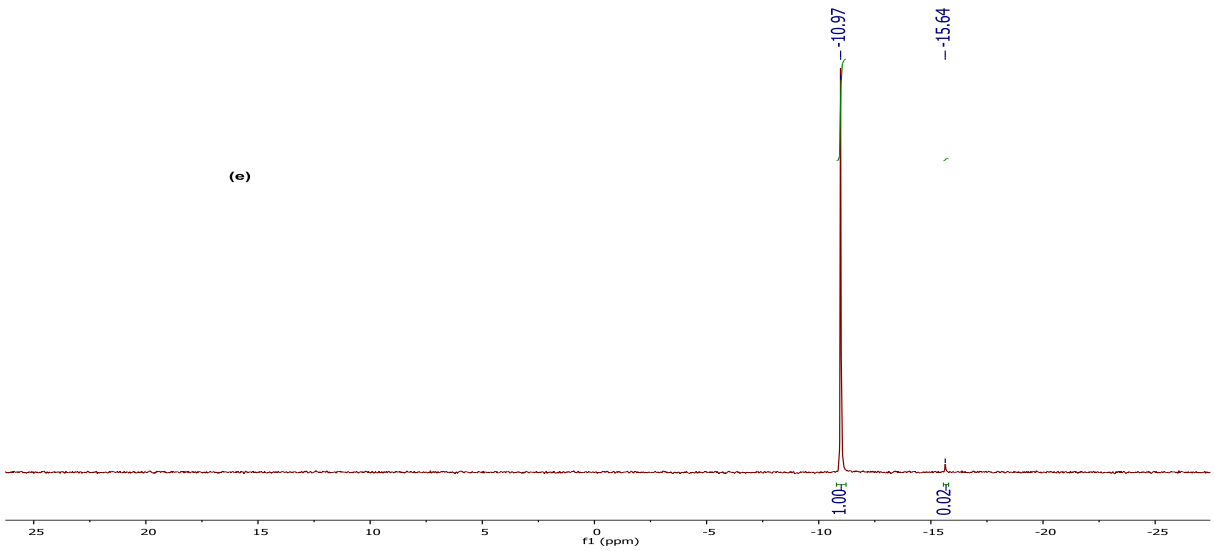
-10.97
-15.64
(e)
1.00
0.02
25 20 15 10 5 0 -5 -10 -15 -20 -25
f1 (ppm)

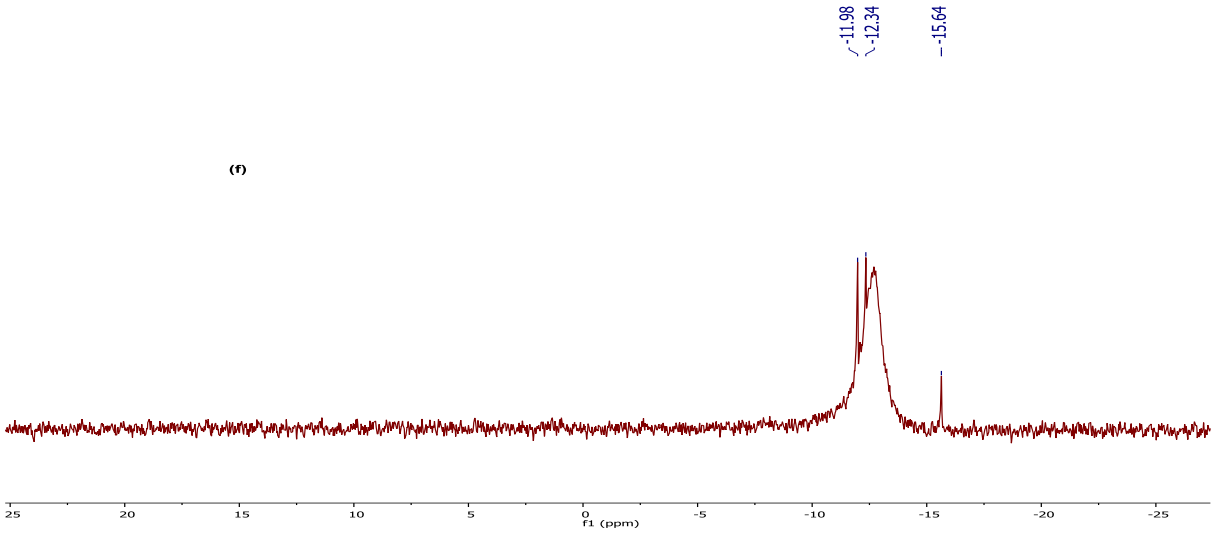

Figure A3.17. ^{31}P NMR spectra of (a) $(TBA)_6[NaPW_{11}O_{39}]$ in DMSO and the product of the reaction between $(TBA)_6[NaPW_{11}O_{39}]$ and 1 mole-equivalent of $Na_2IrCl_6.xH_2O$ in DMSO at 150 °C (b) after ~50 mins (c) after ~2 h (d) after 20 h (e) after 44 h and (f) mixture obtained after solution workup.

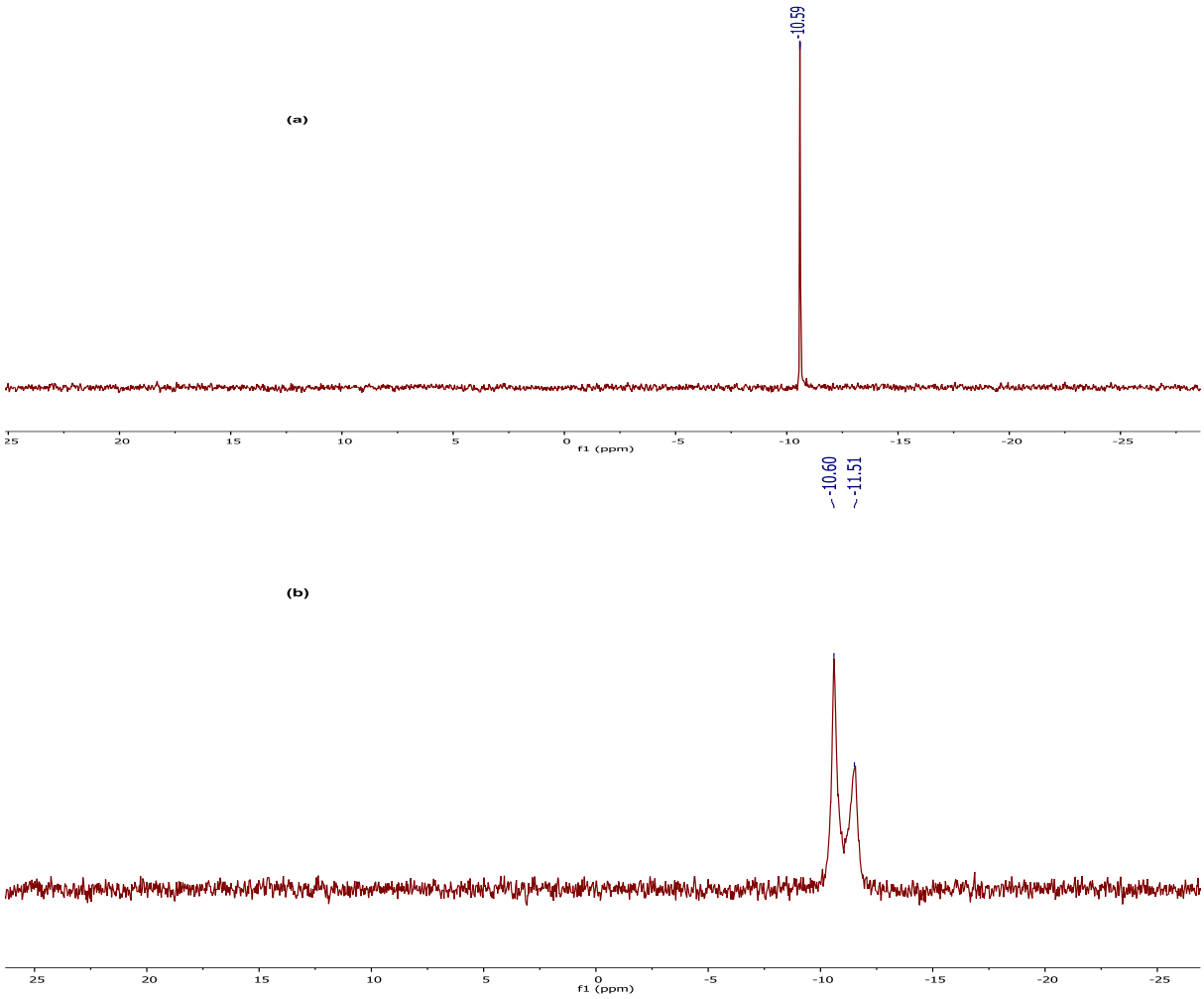

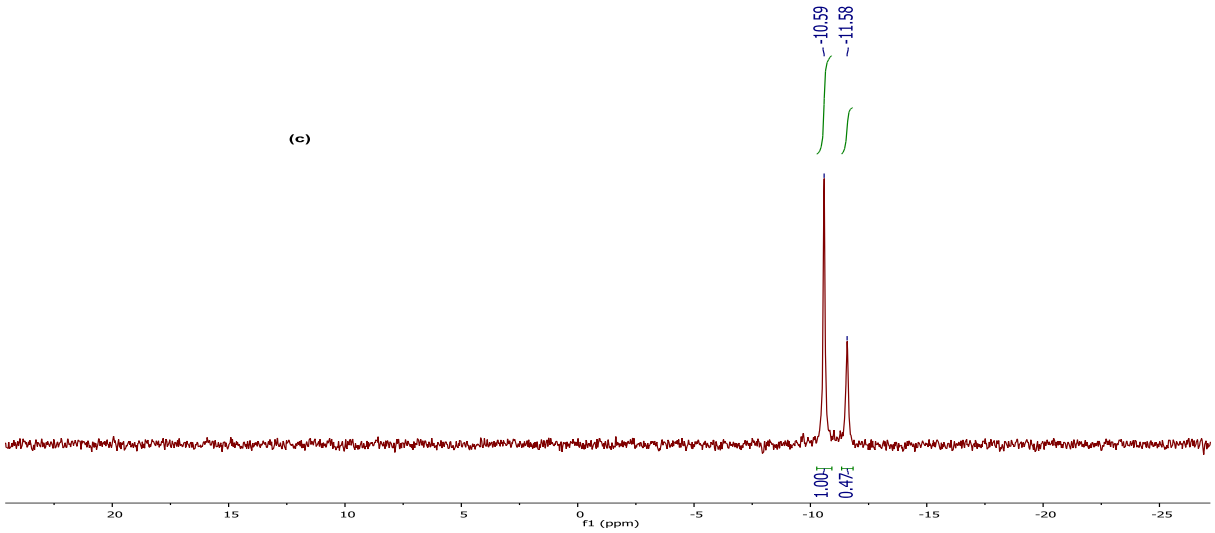
(c)
-10.59
-11.58
1.00
0.47
20
15
10
5
0
-5
-10
-15
-20
-25
f1 (ppm)

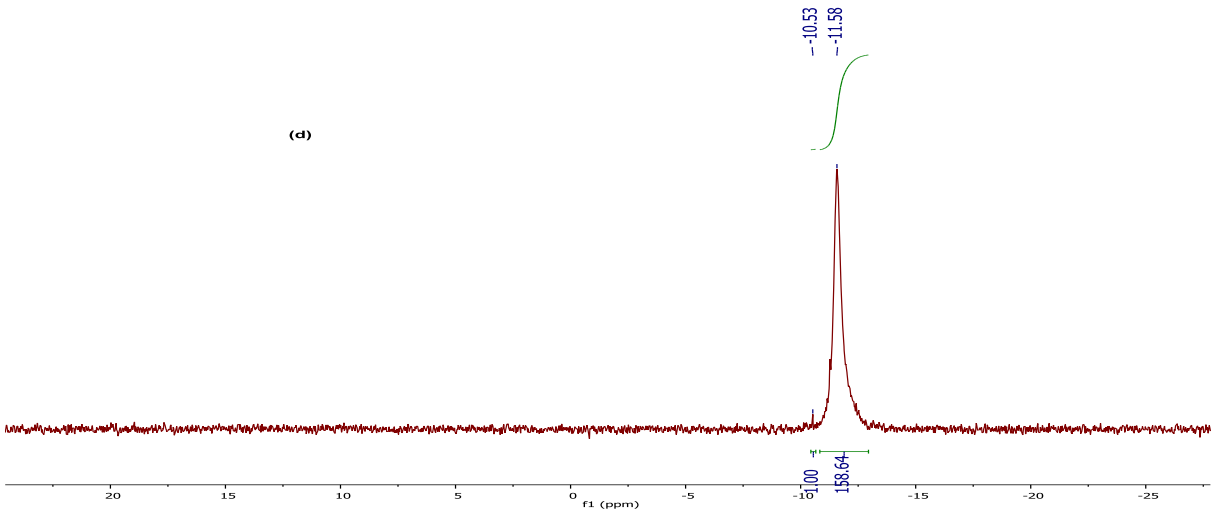
(d)
-10.53
-11.58
1.00
158.64
20
15
10
5
0
-5
-10
-15
-20
-25
f1 (ppm)

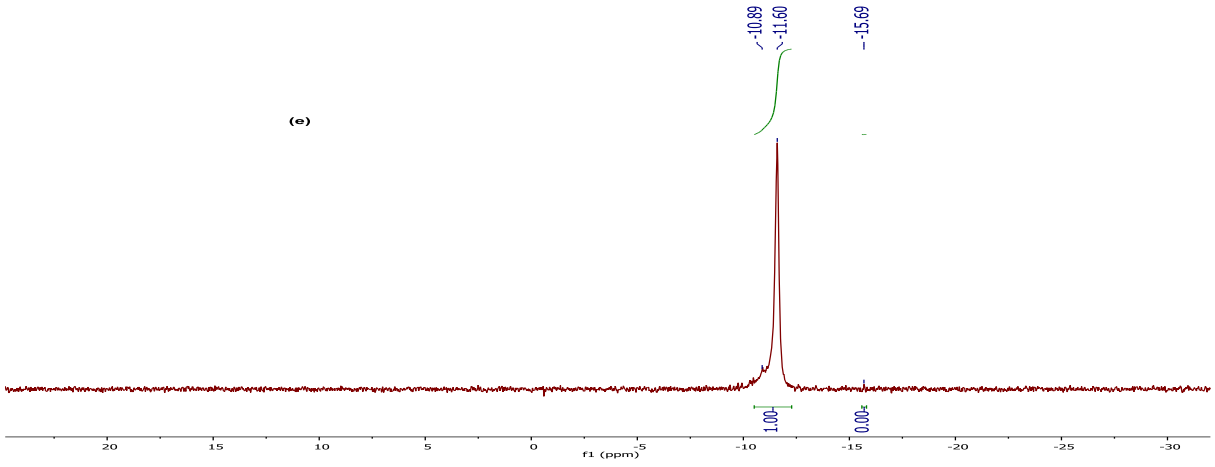
(e)
-10.89
-11.60
-15.69
1.00
0.00
20
15
10
5
0
-5
-10
-15
-20
-25
-30
f1 (ppm)

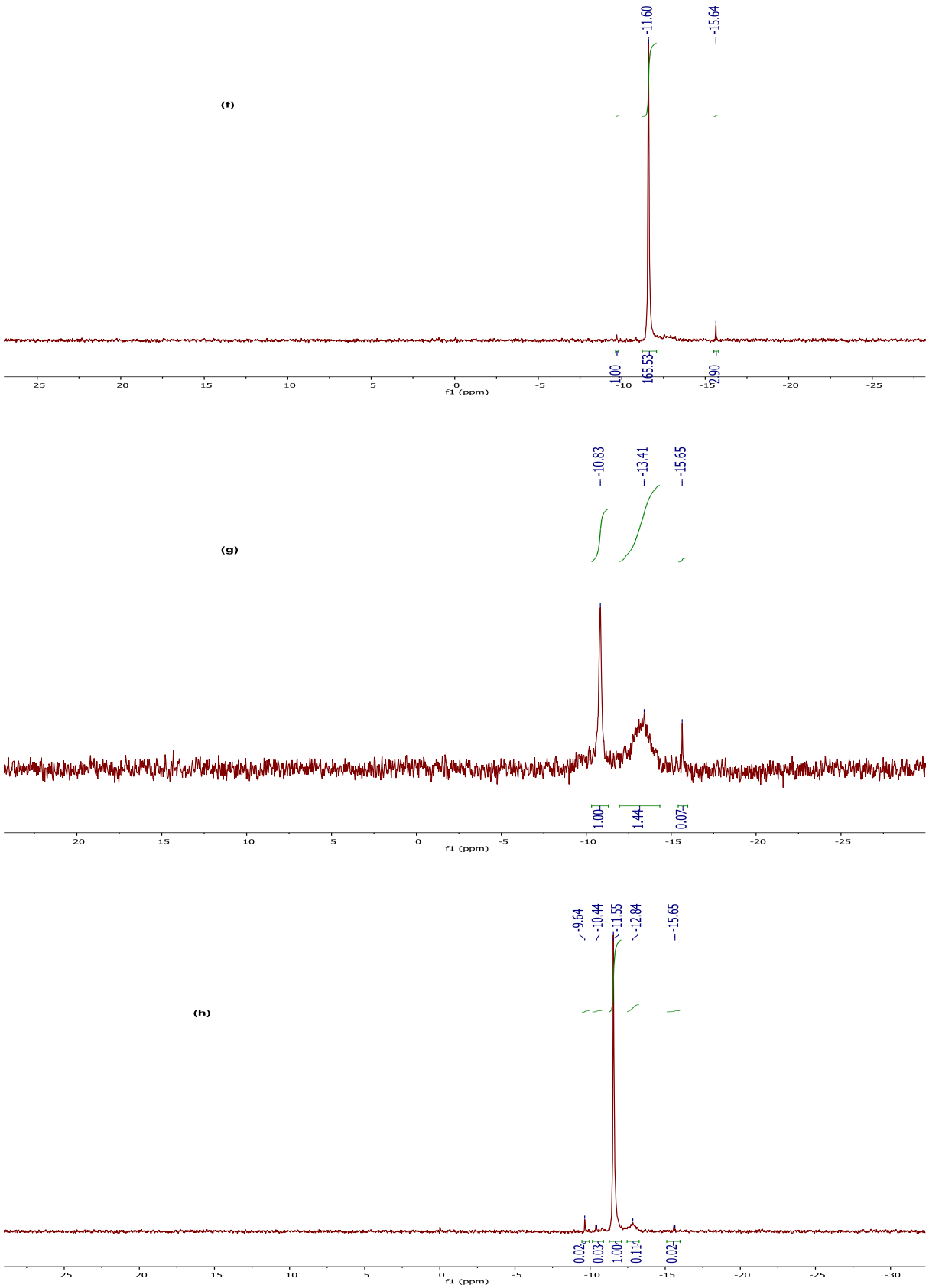

Figure A3.18. ^{31}P NMR spectra of (a) $(TBA)_6[NaPW_{11}O_{39}]$ in DMSO and the product of the reaction between $(TBA)_6[NaPW_{11}O_{39}]$ and 1 mole-equivalent of Na_2PtCl_6 in DMSO (b) after ~10 mins at 22 °C (c) after ~11 h at 22 °C (d) after heating at 100 °C for 1 h (e) after heating at 100 °C for 3 h (f) after heating at 100 °C for 4 h (g) after heating at 100 °C for 18 h and (h) the product of a second reaction between $(TBA)_6[NaPW_{11}O_{39}]$ and 1 mole-equivalent of Na_2PtCl_6 in DMSO after heating at 100°C for 5 h.

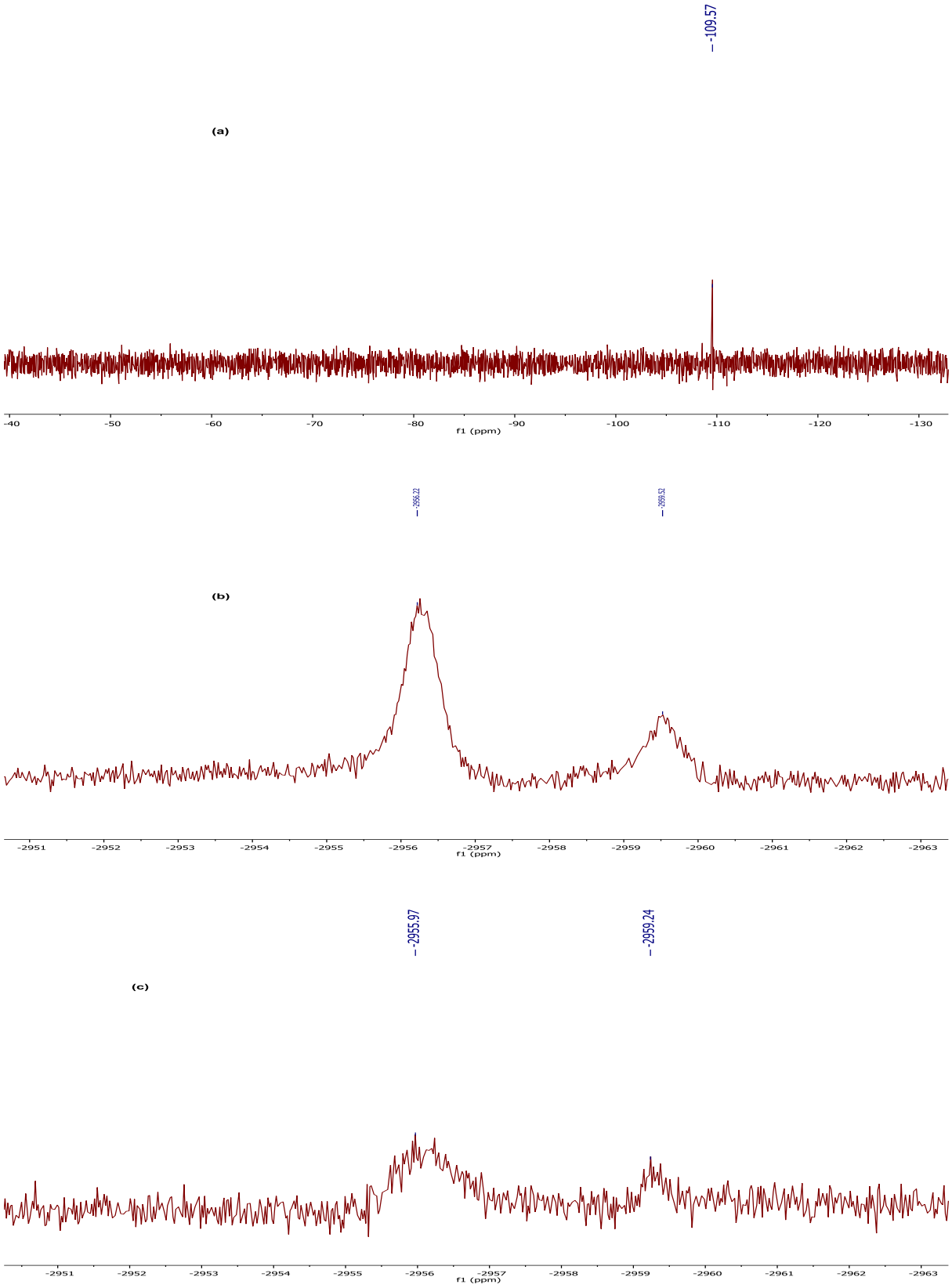

Figure A3.19. ^{195}Pt NMR spectra of (a) Na_2PtCl_6 in DMSO (b) the product of the reaction between $(TBA)_6[NaPW_{11}O_{39}]$ and 1 mole-equivalent of Na_2PtCl_6 in DMSO after 5 h at 150 ^oC and (c) Na_2PtCl_6 in DMSO after heating at 150 ^oC for 1 h.

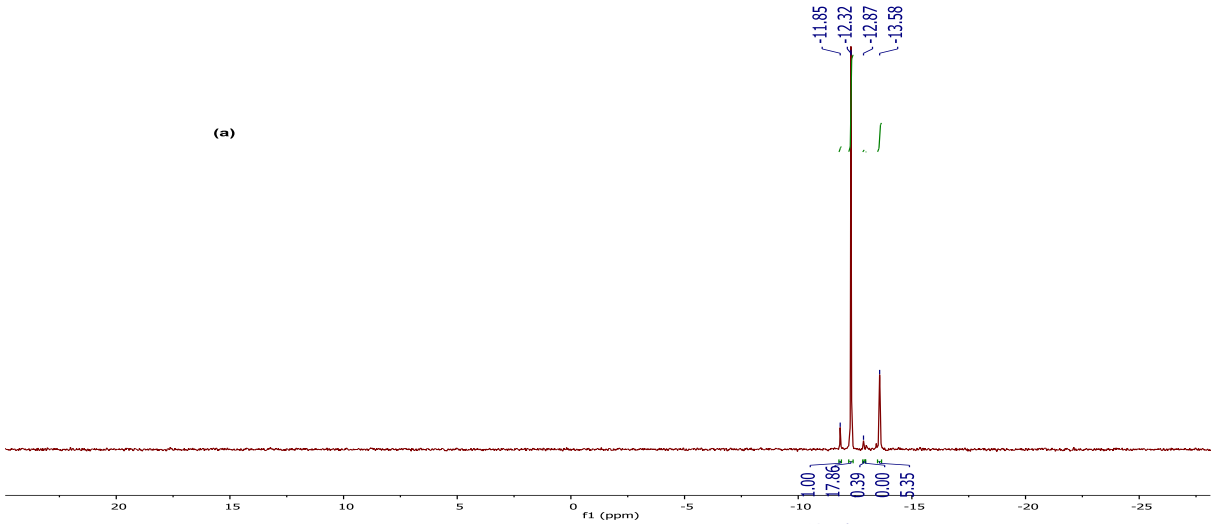
(a)
-11.85
-12.32
-12.87
-13.58
1.00
17.86
0.39
0.00
5.35
f1 (ppm)

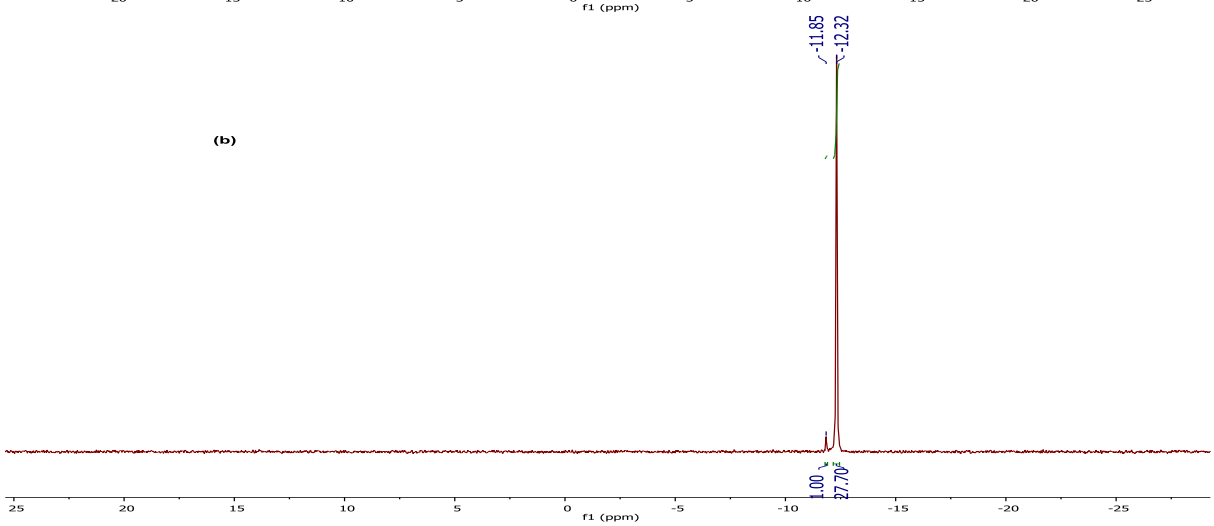
(b)
-11.85
-12.32
1.00
27.70
f1 (ppm)

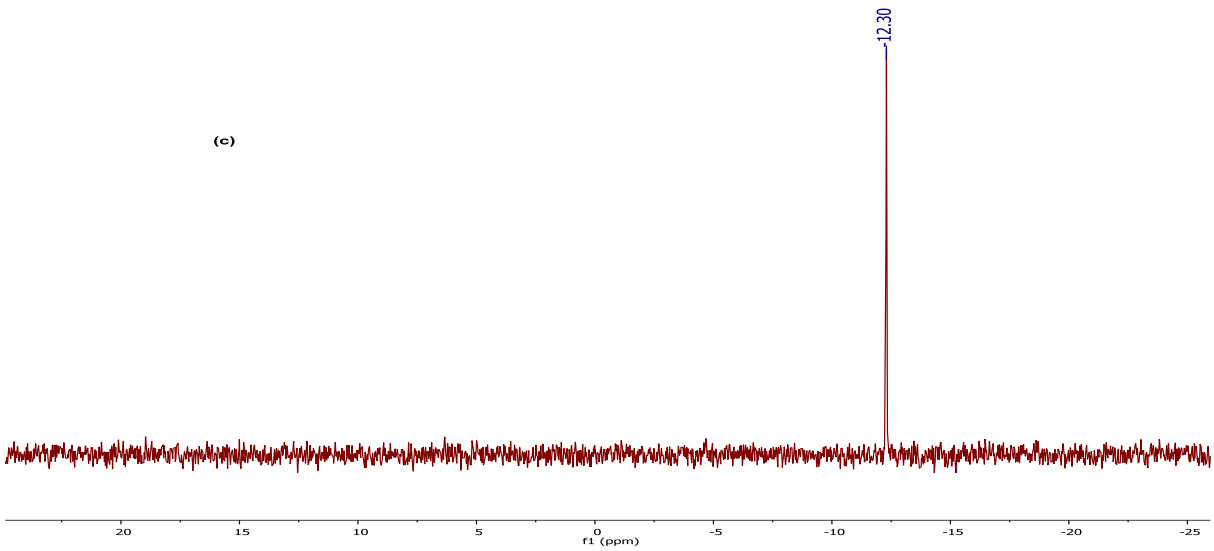
(c)
12.30
f1 (ppm)

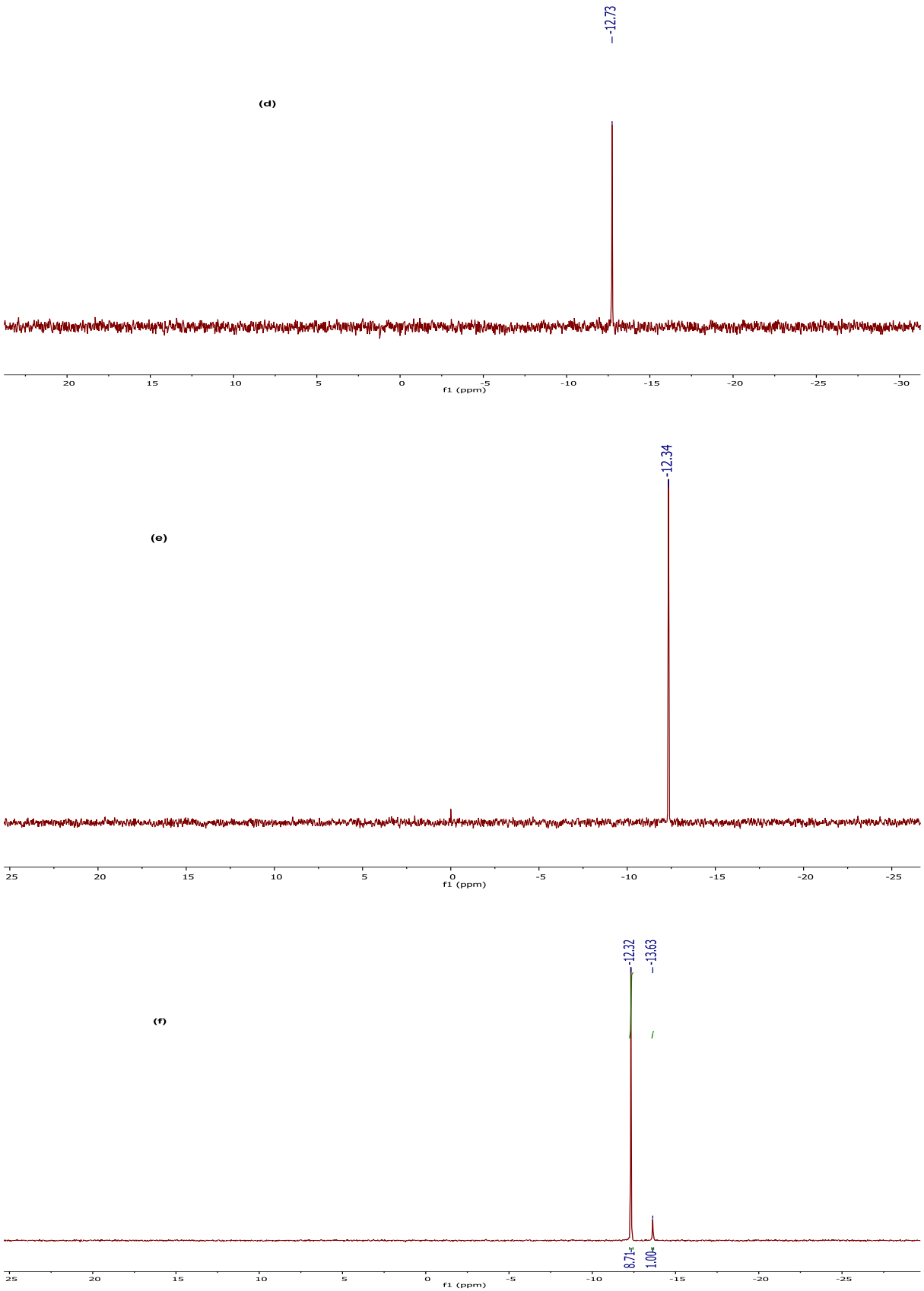

Figure A3.20. ^{31}P NMR spectra in MeCN at 22 °C of (a) reaction between $(TBA)_6[NaPW_{11}O_{39}]$ and 1 equivalent of $(NH_4)_2[Ce(NO_3)_6]$ after ~10 mins (b) after stirring for 18 h (c) isolated product of the reaction(d) product of a second reaction between $(TBA)_6[NaPW_{11}O_{39}]$, 1 mole-equivalent of $(NH_4)_2[Ce(NO_3)_6]$ and 4 mole-equivalents of

DMSO (e) isolated product of the reaction and (f) product of a third reaction between $(TBA)_6[NaPW_{11}O_{39}]$, ½ mole-equivalents of $(NH_4)_2[Ce(NO_3)_6]$.

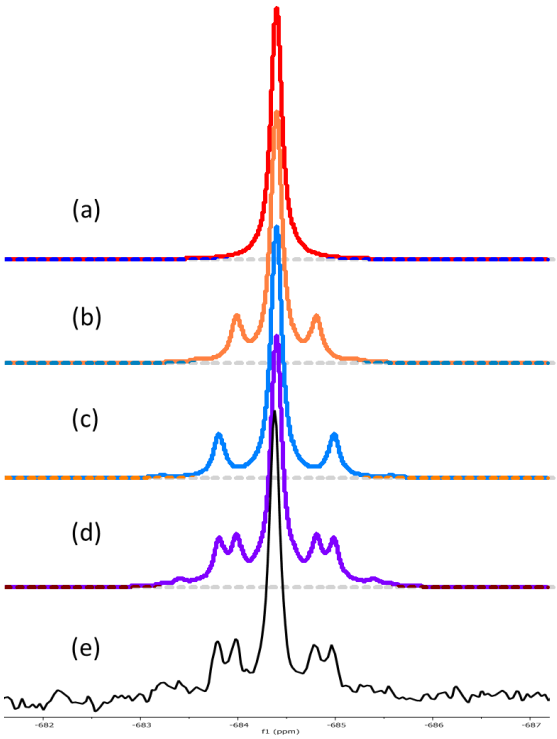

Figure A3.21. Simulations of ^{119}Sn NMR spectrum of $(TBA)_5[SnPW_{11}O_{39}]$ shown in Figure 3.8 (a) with decoupling of all tungstens (W_A and W_F) (b) with decoupling of only W_F (c) with decoupling of only W_A (d) without tungsten decoupling and (e) experimental ^{119}Sn NMR spectrum of $(TBA)_5[SnPW_{11}O_{39}]$.

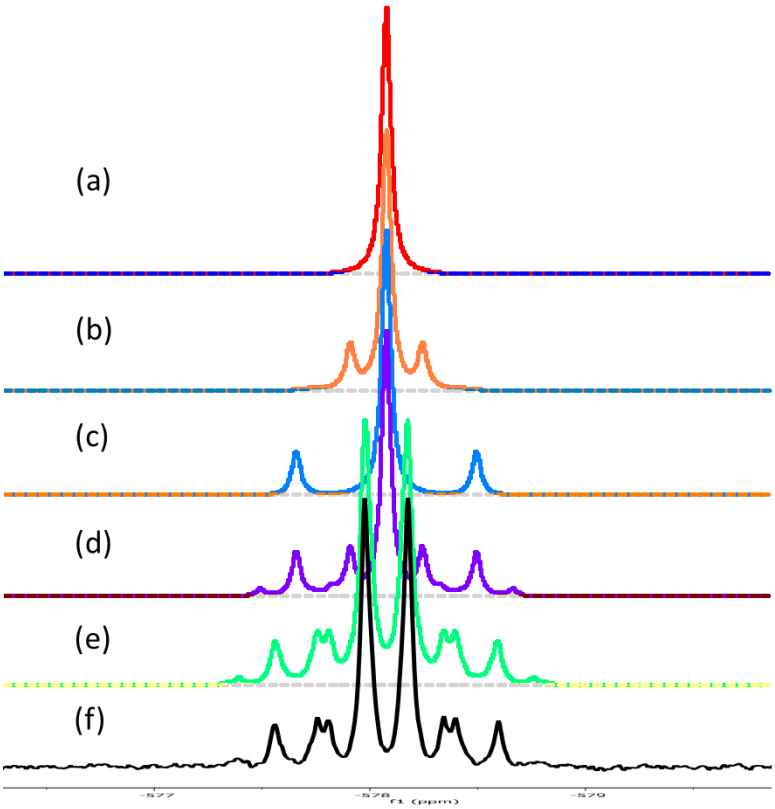

Figure A3.22. Simulations of ^{119}Sn NMR spectrum of $(TBA)_4[ClSnPW_{11}O_{39}]$ shown in Figure 3.14. (a) with decoupling of all tungstens (W_A and W_F) and phosphorus (b) with decoupling of only W_F and phosphorus (c) with decoupling of only W_A and phosphorus (d) with decoupling of phosphorus (e) without tungsten and phosphorus decoupling and (f) experimental ^{119}Sn NMR spectrum of $(TBA)_4[ClSnPW_{11}O_{39}]$.

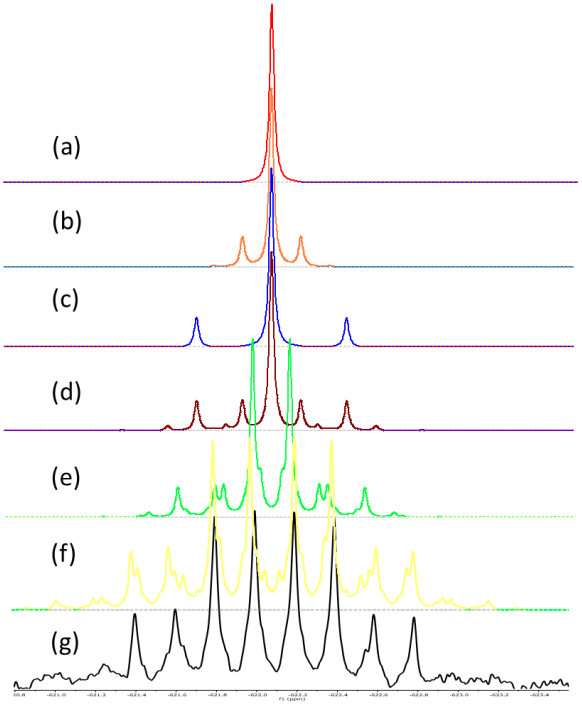

Figure A3.23. Simulations of ^{119}Sn NMR spectrum of $(TBA)_4[(MeO)SnPW_{11}O_{39}]$ shown in Figure 4.15 (b). (a) with decoupling of all tungstens (W_A and W_F), phosphorus and protons (b) with decoupling of only W_F , phosphorus and protons (c) with decoupling of only W_A, phosphorus and protons (d) with decoupling of phosphorus and protons (e) with decoupling of protons (f) without tungsten, phosphorus and proton decoupling and (g) experimental ^{119}Sn NMR spectrum of $(TBA)_4[(MeO)SnPW_{11}O_{39}]$. See tungsten labelling in Figure 4.18.

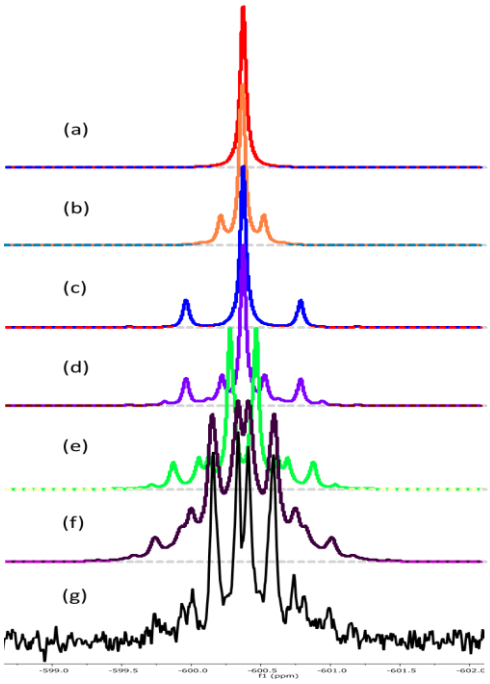

Figure A3.24. Simulations of ^{119}Sn NMR spectrum of $(TBA)_4[(HO)SnPW_{11}O_{39}]$ shown in Figure 4.15 (c). (a) with decoupling of all tungstens (W_A and W_F), phosphorus and proton (b) with decoupling of only W_F , phosphorus

and proton (c) with decoupling of only W_A, phosphorus and proton (d) with decoupling of phosphorus and proton (e) with decoupling of proton (f) without tungsten, phosphorus and proton decoupling and (g) experimental ^{119}Sn NMR spectrum of $(TBA)_4[(HO)SnPW_{11}O_{39}]$. See tungsten labelling in Figure 4.18.

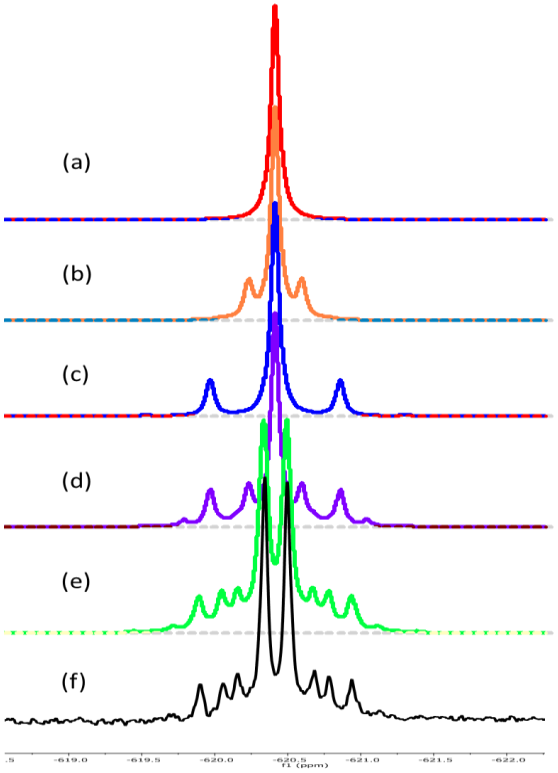

Figure A3.25. Simulations of ^{119}Sn NMR spectrum of $(TBA)_8[(\mu\text{-}O)(SnPW_{11}O_{39})_2]$ shown in Figure 4.15 (d). (a) with decoupling of all tungstens (W_A and W_F) and phosphorus (b) with decoupling of only W_F and phosphorus (c) with decoupling of only W_A and phosphorus (d) with decoupling of phosphorus (e) without tungsten and phosphorus decoupling and (f) experimental ^{119}Sn NMR spectrum of $(TBA)_8[(\mu\text{-}O)(SnPW_{11}O_{39})_2]$. See tungsten labelling in Figure 4.18.

(a) = $^{2}J[^{119}Sn\text{-}^{117}Sn]$ = 0 Hz

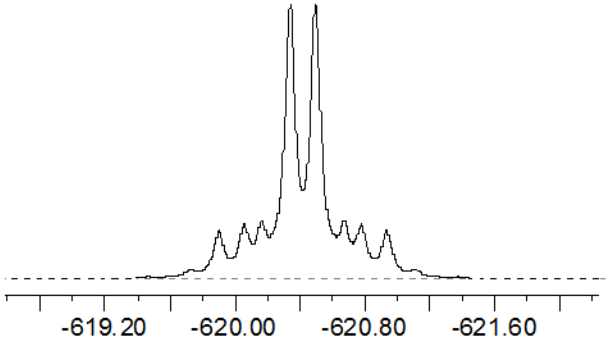

(b) = $^{2}J[^{119}Sn\text{-}^{117}Sn]$ = 10 Hz

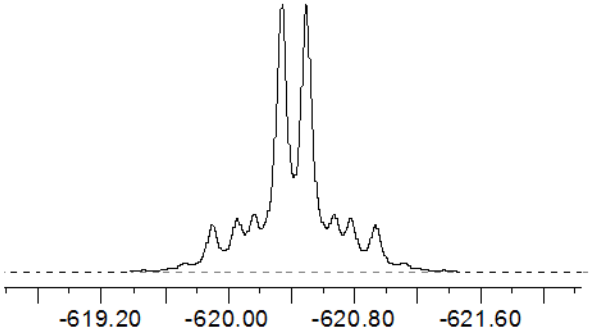

(c) = $^{2}J[^{119}Sn\text{-}^{117}Sn]$ = 20 Hz

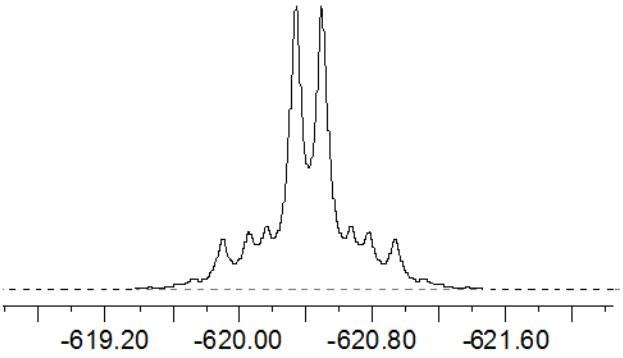

(d) = $^{2}J[^{119}Sn\text{-}^{117}Sn]$ = 30 Hz

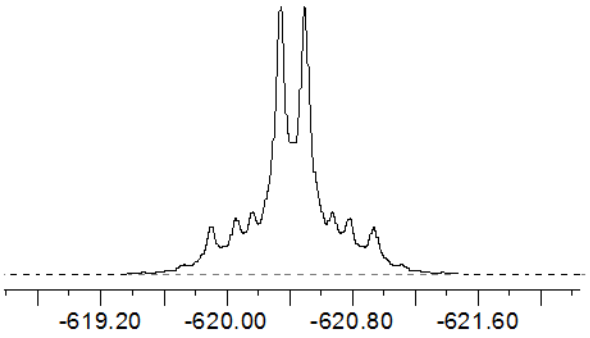

(e) = $^{2}J[^{119}Sn\text{-}^{117}Sn]$ = 40 Hz

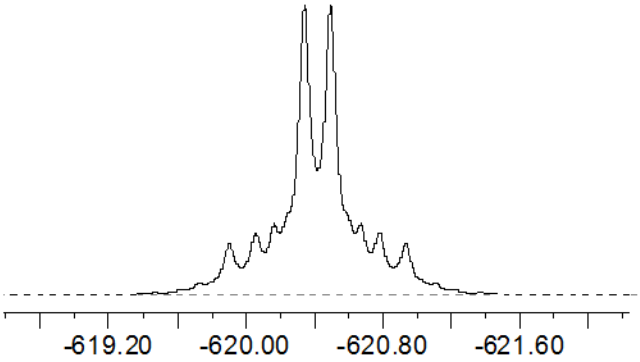

(f) = $^{2}J[^{119}Sn\text{-}^{117}Sn]$ = 50 Hz

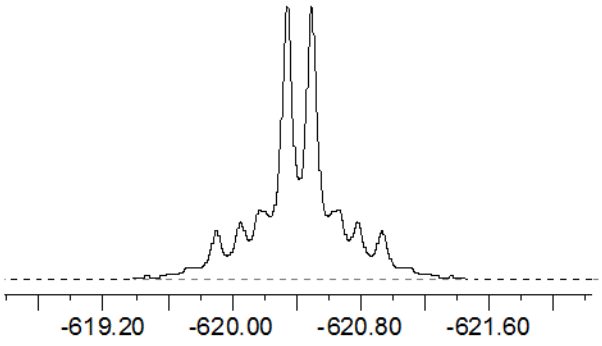

(g) = $^{2}J[^{119}Sn\text{-}^{117}Sn]$ = 60 Hz

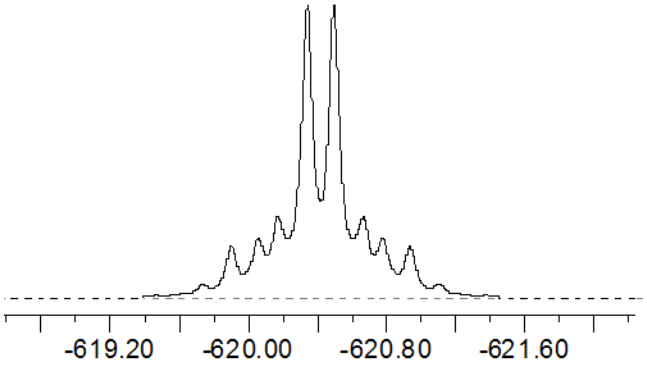

(h) = $^{2}J[^{119}Sn\text{-}^{117}Sn]$ = 70 Hz

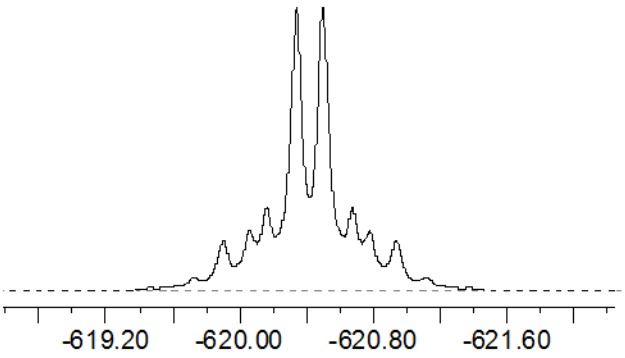

(i) = $^{2}J[^{119}Sn\text{-}^{117}Sn]$ = 80 Hz

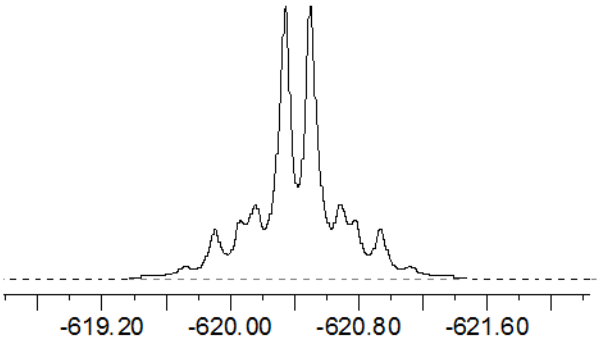

(j) = $^{2}J[^{119}Sn\text{-}^{117}Sn]$ = 90 Hz

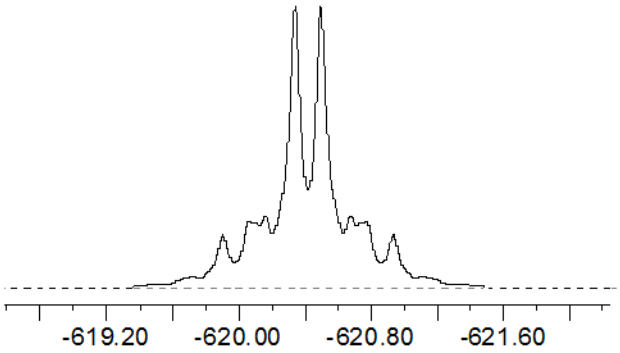

(k) = $^{2}J[^{119}Sn\text{-}^{117}Sn]$ = 100 Hz

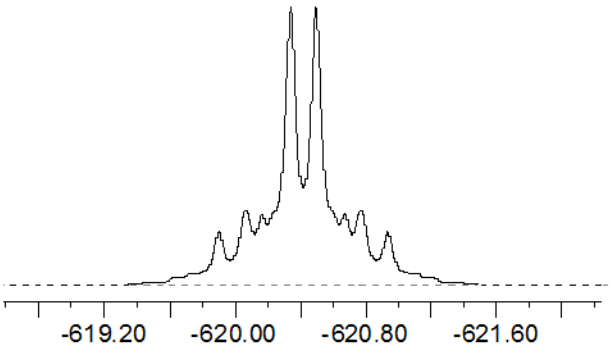

(l) = $^{2}J[^{119}Sn\text{-}^{117}Sn]$ = 110 Hz

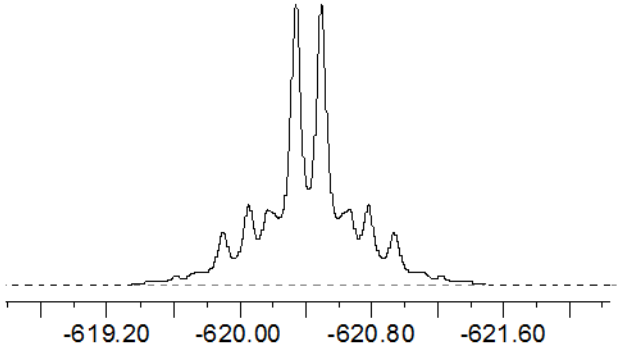

(m) = $^{2}J[^{119}Sn\text{-}^{117}Sn]$ = 120 Hz

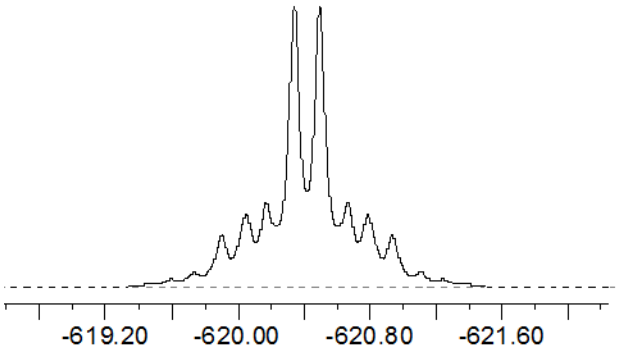

(n) = $^{2}J[^{119}Sn\text{-}^{117}Sn]$ = 130 Hz

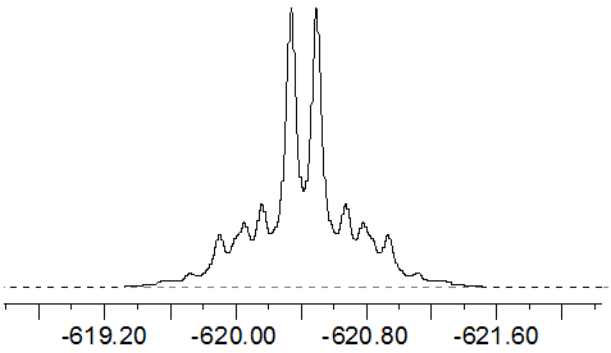

(o) = $^{2}J[^{119}Sn\text{-}^{117}Sn]$ = 140 Hz

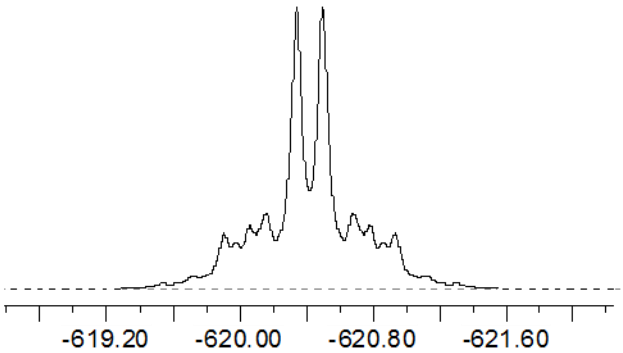

(p) = $^{2}J[^{119}Sn\text{-}^{117}Sn]$ = 150 Hz

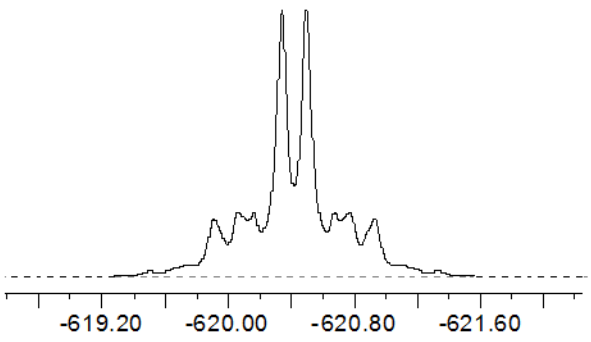

(q) = $^{2}J[^{119}Sn\text{-}^{117}Sn]$ = 160 Hz

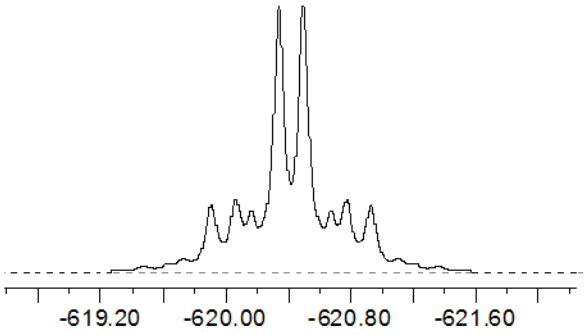

(r) = $^{2}J[^{119}Sn\text{-}^{117}Sn]$ = 170 Hz

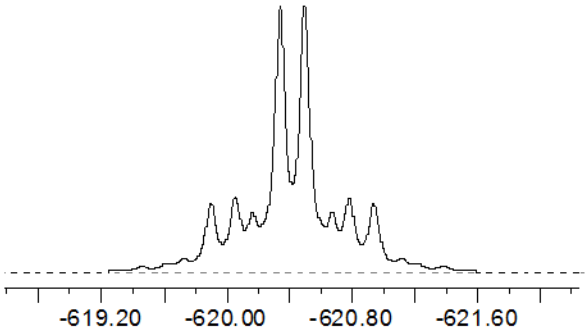

(s) = $^{2}J[^{119}Sn\text{-}^{117}Sn]$ = 180 Hz

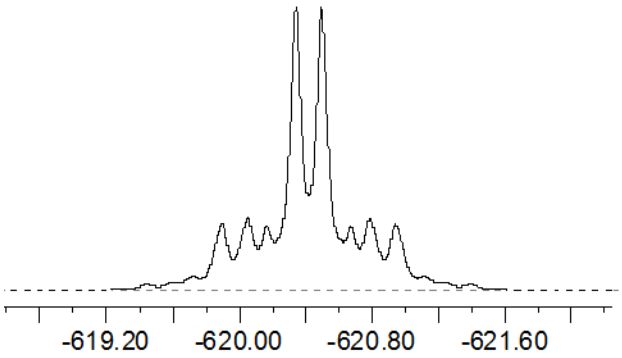

(t) = $^{2}J[^{119}Sn\text{-}^{117}Sn]$ = 190 Hz

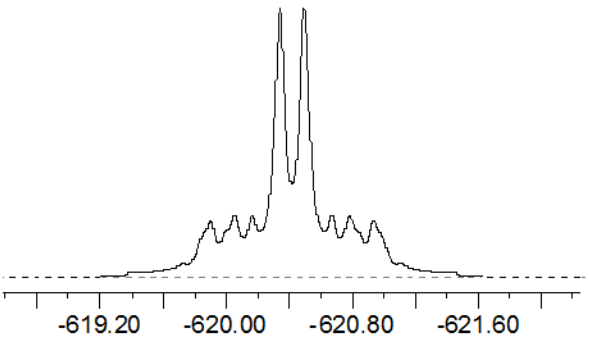

(u) = $^{2}J[^{119}Sn\text{-}^{117}Sn]$ = 200 Hz

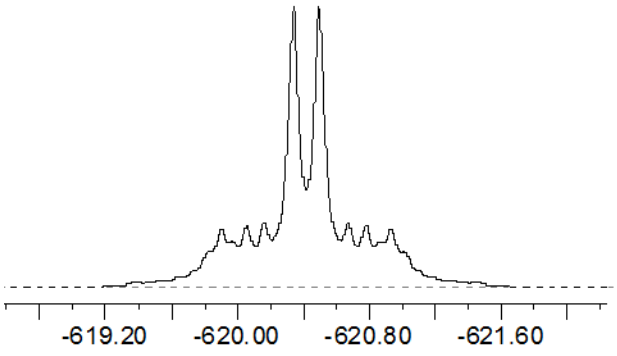

(v) = $^{2}J[^{119}Sn\text{-}^{117}Sn]$ = 210 Hz

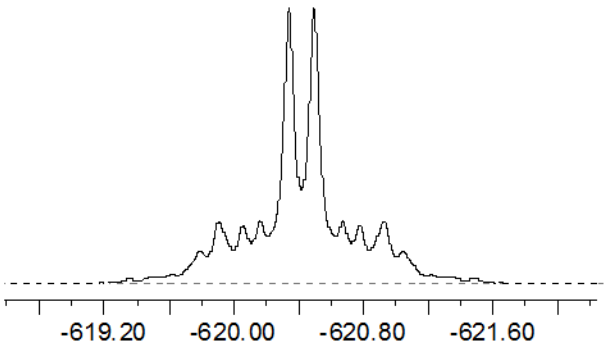

(w) = $^{2}J[^{119}Sn\text{-}^{117}Sn]$ = 220 Hz

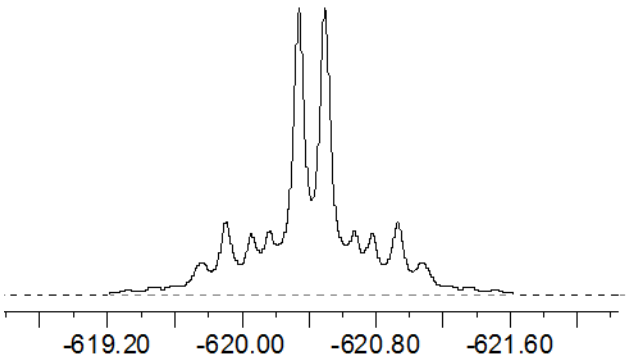

(x) = $^{2}J[^{119}Sn\text{-}^{117}Sn]$ = 230 Hz

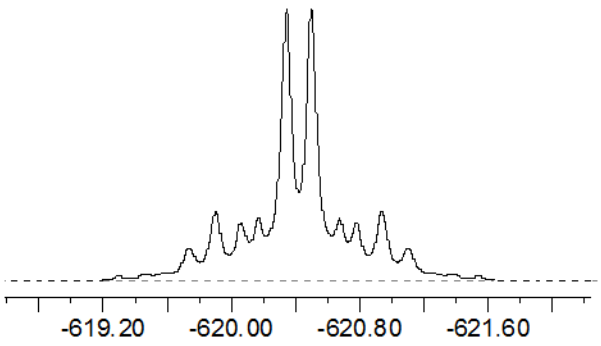

(y) = $^{2}J[^{119}Sn\text{-}^{117}Sn]$ = 240 Hz

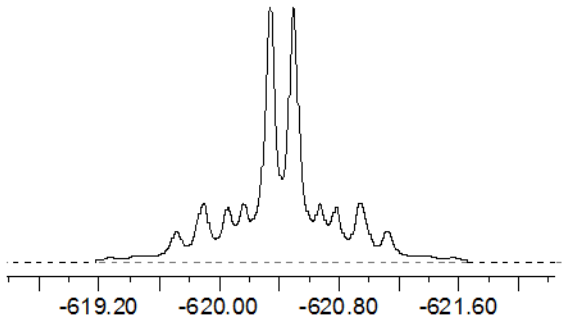

(z) = $^{2}J[^{119}Sn\text{-}^{117}Sn]$ = 250 Hz

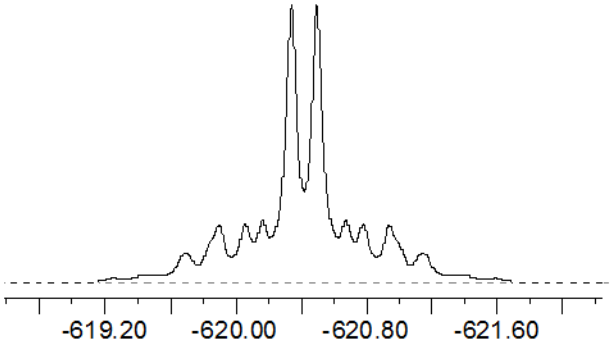

(aa) = $^{2}J[^{119}Sn\text{-}^{117}Sn]$ = 260 Hz

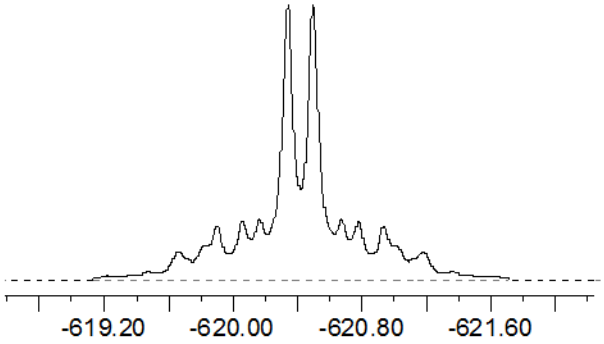

(bb) = $^{2}J[^{119}Sn\text{-}^{117}Sn]$ = 270 Hz

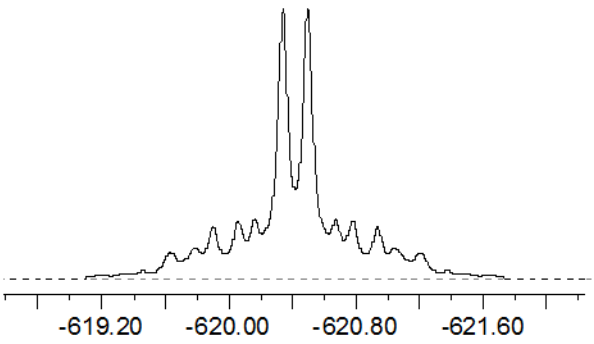

(cc) = $^{2}J[^{119}Sn\text{-}^{117}Sn]$ = 280 Hz

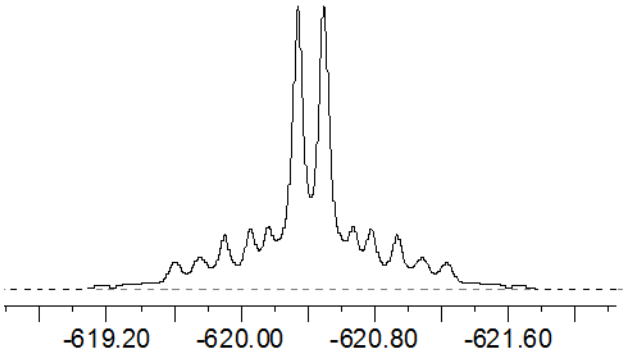

(dd) = $^{2}J[^{119}Sn\text{-}^{117}Sn]$ = 290 Hz

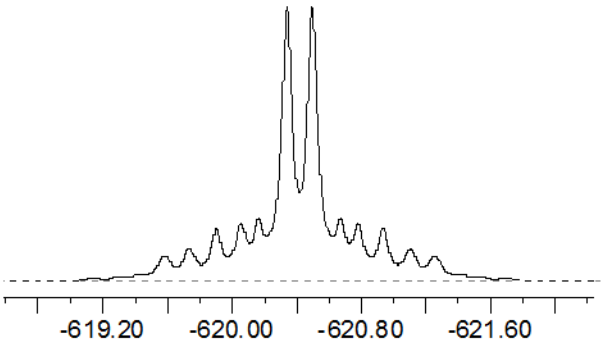

(ee) = $^{2}J[^{119}Sn\text{-}^{117}Sn]$ = 300 Hz

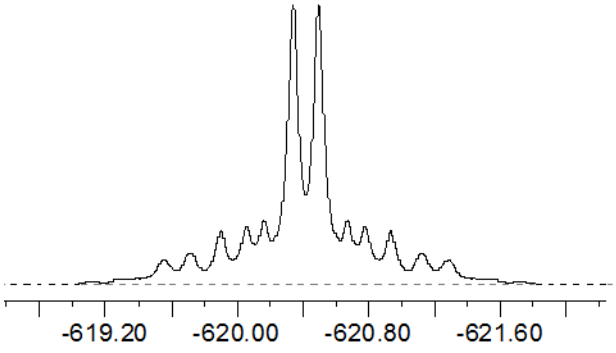

(ff) = $^{2}J[^{119}Sn\text{-}^{117}Sn]$ = 310 Hz

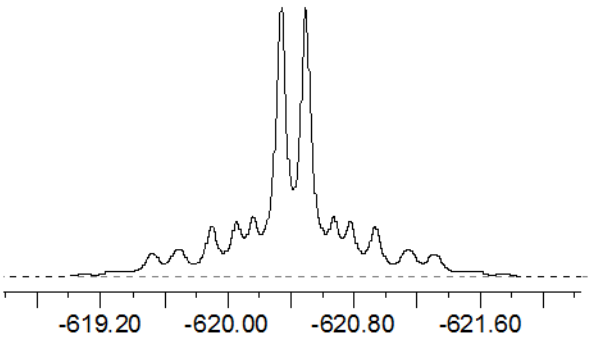

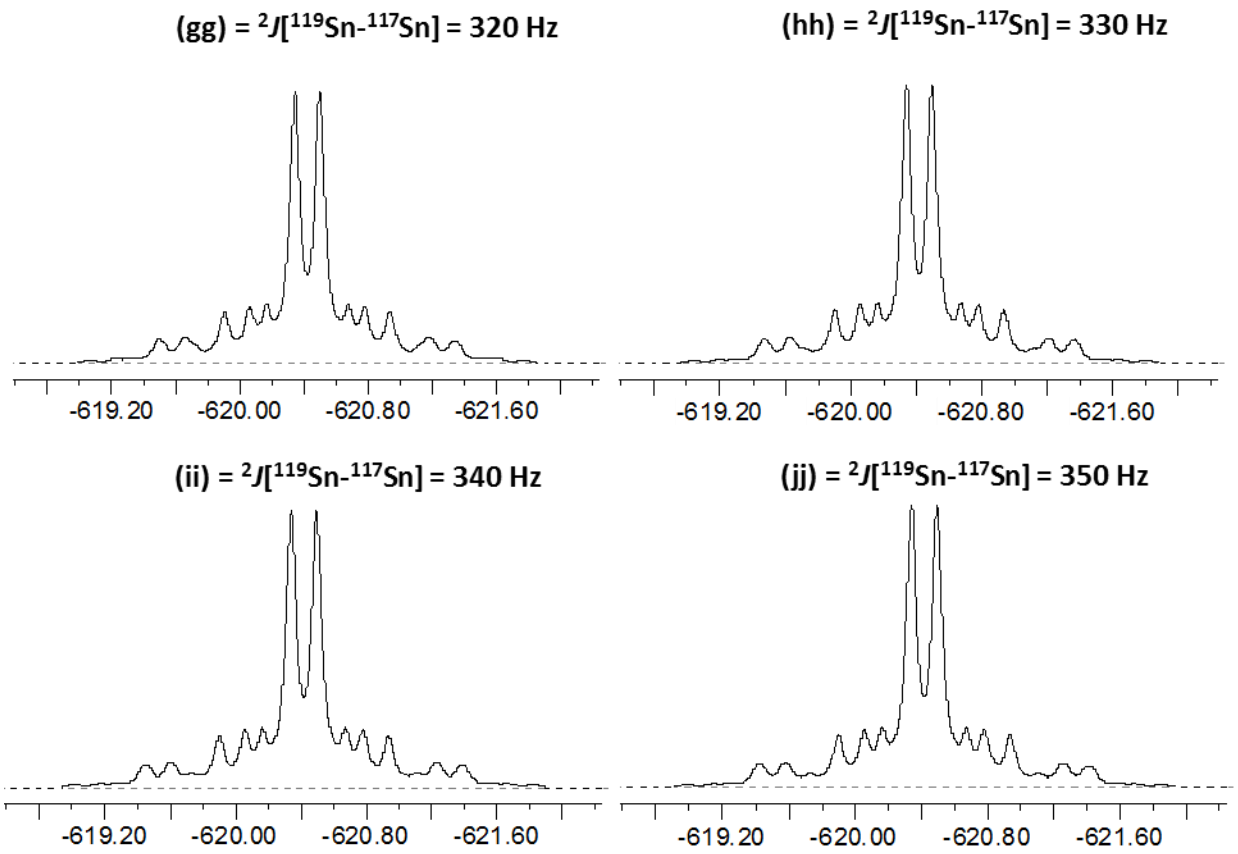

Figure A4.1. Simulated ^{119}Sn NMR spectra for $(TBA)_8[(\mu\text{-}O)(SnPW_{11}O_{39})_2]$ using obtained experimental NMR (^{31}P, ^{119}Sn and ^{183}W) parameters in Table 4.2 while varying $^{2}J(^{119}Sn\text{-}^{117}Sn)$ from 0 to 350 Hz.

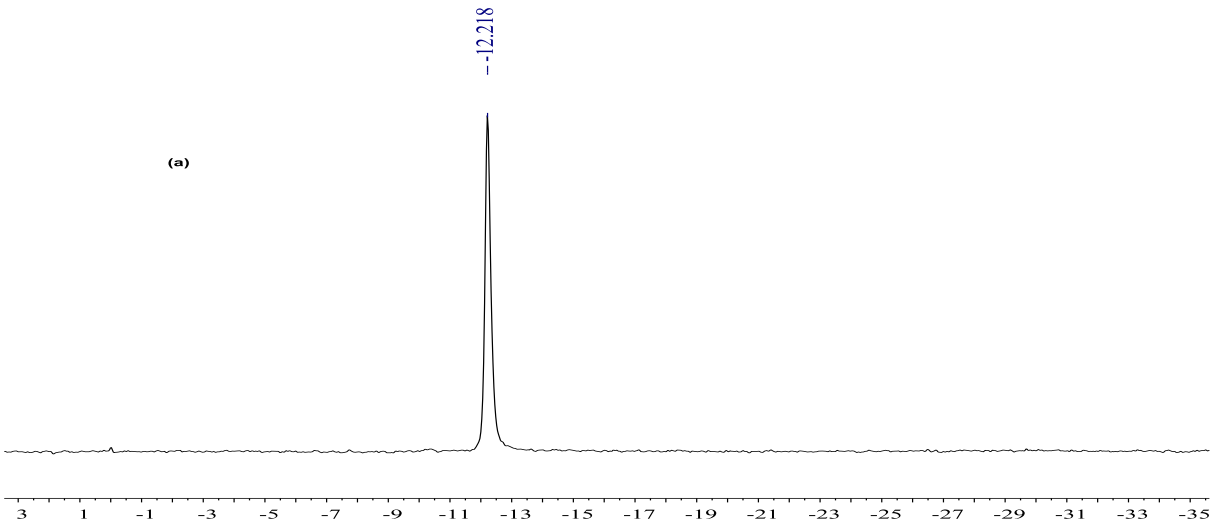

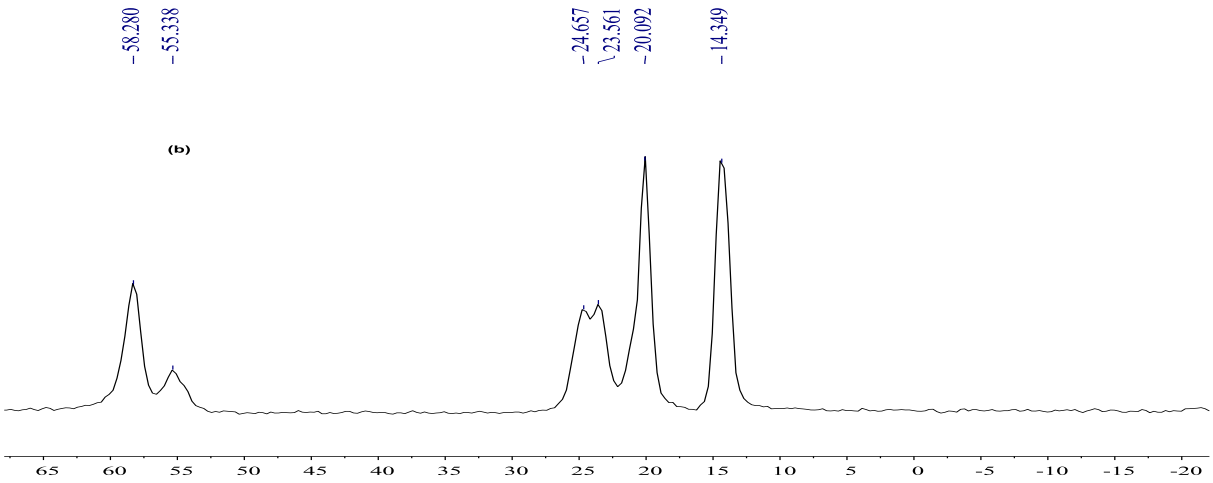

Figure A4.2. (a) ^{31}P and (b) ^{13}C solid state NMR spectra of $(TBA)_4[(MeO)SnPW_{11}O_{39}]$.

Table A8.1 (a). Crystal data and structure refinement for $[\{CH_3C(O)NH_2\}CoW_5O_{17}(OMe)]^{3-}$

Empirical formula	$C_{51}H_{116}CoN_4O_{19}W_5$
Formula weight	2067.65
Temperature/K	150.0(2)
Crystal system	monoclinic
Space group	I2/a
a/Å	24.9068(3)
b/Å	13.3603(2)
c/Å	41.3232(6)
α/°	90
β/°	97.6998(13)
γ/°	90
Volume/Å^3	13626.9(4)
Z	8
ρ_{calc}g/cm^3	2.016
μ/mm^{-1}	17.555
F(000)	7992.0
Crystal size/mm^3	0.22 × 0.15 × 0.08
Radiation	CuKα (λ = 1.54184)
2Θ range for data collection/°	6.96 to 135.26
Index ranges	-29 ≤ h ≤ 24, -15 ≤ k ≤ 16, -49 ≤ l ≤ 49
Reflections collected	50312
Independent reflections	12210 [R_{int} = 0.0515, R_{sigma} = 0.0409]
Data/restraints/parameters	12210/853/786
Goodness-of-fit on F^2	1.042
Final R indexes [I>=2σ (I)]	R_1 = 0.0292, wR_2 = 0.0623
Final R indexes [all data]	R_1 = 0.0404, wR_2 = 0.0678
Largest diff. peak/hole / e Å^{-3}	2.00/-1.37

Table A8.1 (b). Fractional Atomic Coordinates (×10^4) and Equivalent Isotropic Displacement Parameters (Å^2×10^3) for [{$CH_3C(O)NH_2$}$CoW_5O_{17}(OMe)]^{3-}$. U_{eq} is defined as 1/3 of of the trace of the orthogonalised U_{IJ} tensor.

Atom	*x*	*y*	*z*	U(eq)
W1	4485.4(2)	3983.6(2)	5838.0(2)	20.07(6)
W2	4754.4(2)	6406.1(2)	5929.1(2)	23.72(6)
W3	5798.4(2)	5856.3(2)	6478.0(2)	23.20(6)
W4	5484.5(2)	3451.1(2)	6419.8(2)	22.42(6)
W5	4547.5(2)	5092.4(2)	6571.7(2)	22.84(6)
Co1	5683.5(3)	4721.3(7)	5800.3(2)	19.98(18)
O1	5010.8(15)	3943(3)	5579.4(8)	24.0(8)
O2	5279.5(16)	6035(3)	5608.2(9)	27.6(8)
O3	6160.9(15)	5588(3)	6142.0(9)	26.3(8)
O4	5881.8(15)	3462(3)	6093.4(8)	23.9(8)
O5	4325.9(15)	5379(3)	5699.2(8)	23.6(8)
O6	5368.4(15)	6879(3)	6208.3(9)	27.1(8)
O7	5902.7(15)	4520(3)	6651.4(8)	24.7(8)
O8	4845.2(15)	3011(3)	6135.3(8)	22.9(8)
O9	3963.5(16)	3332(3)	5621.1(9)	29.1(9)
O10	4511.2(18)	7491(3)	5729.8(10)	36.4(10)
O11	6239.7(16)	6577(3)	6741.4(9)	34(1)
O12	5684.3(18)	2372(3)	6631.2(9)	36.1(10)
O13	4126.2(15)	4410(3)	6223.0(8)	23.2(8)
O14	4351.4(15)	6307(3)	6274.7(9)	28.1(8)
O15	5154.7(15)	5881(3)	6731.3(9)	28.6(9)
O16	4917.5(15)	3931(3)	6702.3(8)	26.2(8)
O17	4112.5(15)	5219(3)	6856.8(9)	31.7(9)
O18	5121.8(14)	4956(3)	6167.5(8)	22.2(7)
O19	6204.3(16)	4588(3)	5460.5(9)	29.6(9)
N1	4509.4(19)	2051(3)	7363.4(10)	22.0(9)
N2	5292(2)	10166(4)	5876.9(13)	38.5(12)
N3	7601.9(19)	4350(4)	6177.8(11)	30(1)
N4	5575(2)	4384(4)	5020.3(11)	36.0(12)
C1	4112(2)	2456(4)	7084.2(12)	25.3(11)
C2	4059(2)	1868(5)	6768.3(13)	30.9(13)
C3	3617(2)	2306(5)	6520.5(14)	32.1(13)
C4	3552(3)	1744(5)	6198.3(14)	39.2(15)
C5	5076(2)	2158(4)	7272.5(12)	25.7(11)
C6	5537(2)	1904(5)	7542.8(13)	30.2(12)
C7	6078(2)	1928(4)	7411.1(13)	28.3(12)
C8	6553(3)	1791(5)	7679.0(15)	37.1(14)
C9	4392(2)	960(4)	7429.1(12)	23.4(11)
C10	3817(2)	724(4)	7476.4(14)	29.1(12)

C11	3744(3)	-392(4)	7541.3(14)	31.9(13)
C12	3187(3)	-622(5)	7622.2(17)	41.3(15)
C13	4441(2)	2630(4)	7670.1(13)	26.5(11)
C14	4570(3)	3748(4)	7661.0(14)	33.8(13)
C15	4319(3)	4275(5)	7932.2(15)	38.3(14)
C16	3703(3)	4294(6)	7873(2)	54.3(19)
C17	5019(3)	10211(5)	6184.8(15)	38.2(14)
C18	4737(3)	9249(5)	6262.1(15)	40.8(15)
C19	4399(3)	9400(5)	6532.7(16)	41.7(15)
C20	4158(4)	8410(6)	6636.2(19)	59(2)
C21	5695(3)	9290(5)	5896.6(18)	46.0(16)
C22	6164(3)	9335(7)	6163(2)	58(2)
C23	6565(3)	8514(6)	6123(2)	62(2)
C24	7055(4)	8524(8)	6363(3)	81(3)
C25	5586(3)	11163(5)	5845.6(19)	47.9(16)
C29	4880(3)	9992(5)	5578.2(16)	45.5(15)
C33	7133(3)	3762(5)	6283.0(15)	37.7(14)
C37	7357(3)	5083(5)	5924.2(14)	36.8(13)
C45	7906(2)	4903(5)	6471.6(13)	28.7(12)
C46	7570(2)	5651(4)	6635.3(13)	28.9(12)
C47	7855(2)	5884(5)	6977.5(13)	31.8(13)
C48	7596(3)	6749(5)	7140.2(15)	39.5(15)
C49	5599(3)	6785(5)	5479.6(17)	43.5(16)
C50	6073(2)	4559(5)	5154.8(13)	30.9(13)
C51	6495(3)	4729(6)	4939.4(14)	43.6(17)
C26A	5841(5)	11200(10)	5523(3)	53(3)
C27A	6237(6)	12035(10)	5521(3)	59(3)
C28A	6512(6)	12093(13)	5217(3)	67(4)
C30A	4451(4)	10771(10)	5509(3)	40(3)
C31A	4182(7)	10680(20)	5158(3)	77(6)
C32A	3692(7)	11300(20)	5078(3)	92(8)
C34A	7267(12)	2990(19)	6541(6)	86(4)
C35A	7114(14)	1980(12)	6490(5)	76(5)
C36A	7150(20)	1340(30)	6785(12)	71(6)
C38A	7851(5)	5659(10)	5795(3)	37(3)
C39A	7643(6)	6259(11)	5497(3)	48(3)
C40A	7203(6)	6997(13)	5544(4)	54(3)
C41A	7984(6)	3545(10)	6088(4)	33(3)
C42A	7814(13)	2977(19)	5770(7)	67(4)
C43A	8155(10)	2038(17)	5758(6)	90(6)
C44A	7905(11)	1296(17)	5516(6)	115(6)
C26B	6022(8)	11360(20)	5641(5)	53(3)
C27B	5759(9)	11858(17)	5334(5)	59(3)

C28B	6199(10)	12060(20)	5108(5)	67(4)
C30B	4363(7)	10580(20)	5575(5)	40(3)
C31B	4039(12)	10540(40)	5238(6)	77(6)
C32B	3523(13)	11100(40)	5195(7)	92(8)
C34B	7285(13)	3070(20)	6569(7)	86(4)
C35B	7001(14)	2184(13)	6598(5)	76(5)
C36B	7260(20)	1440(30)	6836(13)	71(6)
C38B	7660(6)	5904(10)	5791(4)	37(3)
C39B	7315(7)	6551(12)	5542(4)	48(3)
C40B	7609(6)	7365(12)	5386(4)	54(3)
C41B	8033(6)	3816(11)	6007(4)	33(3)
C42B	7761(14)	3220(20)	5712(8)	67(4)
C43B	8120(11)	2403(16)	5614(6)	90(6)
C44B	8103(13)	1456(17)	5807(7)	115(6)

Table A8.1(c). Anisotropic Displacement Parameters ($Å^2×10^3$) for [{$CH_3C(O)NH_2$}$CoW_5O_{17}(OMe)$]$^{3-}$. The Anisotropic displacement factor exponent takes the form: $-2\pi^2[h^2a^{*2}U_{11}+2hka^*b^*U_{12}+\ldots]$.

Atom	U_{11}	U_{22}	U_{33}	U_{23}	U_{13}	U_{12}
W1	17.15(12)	27.88(12)	14.95(10)	-3.36(9)	1.27(8)	-0.71(10)
W2	22.70(14)	26.88(12)	20.93(11)	-0.94(9)	0.55(9)	0.56(10)
W3	15.05(12)	36.12(14)	18.21(10)	-7.62(9)	1.40(9)	-0.99(10)
W4	20.07(13)	32.84(13)	14.55(10)	2.20(9)	2.99(9)	4.33(11)
W5	15.12(12)	37.14(14)	16.87(10)	-6.95(9)	4.38(8)	-0.08(11)
Co1	15.9(4)	32.2(5)	12.3(3)	-1.3(3)	3.3(3)	-0.1(4)
O1	20.9(18)	33.8(19)	16.7(15)	-2.0(14)	0.5(13)	-2.2(16)
O2	28(2)	33.1(19)	21.4(16)	2.2(15)	3.5(15)	-3.4(16)
O3	16.8(18)	41(2)	21.6(16)	-0.8(15)	6.1(14)	1.2(16)
O4	16.7(18)	35(2)	20.2(15)	-1.4(14)	2.6(13)	4.6(16)
O5	16.8(18)	33.0(19)	19.0(15)	-2.1(14)	-4.5(14)	1.7(15)
O6	19.1(19)	31.3(19)	29.1(17)	-6.4(15)	-3.4(15)	-1.9(16)
O7	16.9(18)	38(2)	18.4(15)	-1.1(14)	0.6(14)	1.6(16)
O8	19.3(18)	30.4(18)	19.7(15)	-0.8(14)	5.7(14)	-1.2(15)
O9	23(2)	39(2)	24.9(17)	-6.6(16)	-0.4(15)	-8.5(17)
O10	38(2)	36(2)	33(2)	1.8(17)	-1.7(18)	5.3(19)
O11	22(2)	53(3)	26.8(18)	-14.5(18)	2.4(16)	-7.9(19)
O12	40(2)	46(2)	23.4(18)	9.9(17)	5.9(17)	8(2)
O13	15.6(18)	33.3(19)	20.9(15)	-5.8(14)	3.0(13)	-0.3(16)
O14	18.9(19)	33(2)	31.2(18)	-10.0(15)	0.2(15)	4.5(16)
O15	19.3(19)	45(2)	20.9(16)	-9.3(16)	-0.8(14)	0.5(17)
O16	20.5(19)	40(2)	17.8(15)	0.2(15)	2.8(14)	-2.3(16)
O17	16.9(19)	53(3)	25.6(18)	-11.4(17)	6.0(15)	-4.3(18)

O18	18.6(17)	33.1(18)	14.2(14)	-6.2(13)	-0.1(12)	3.2(15)
O19	21(2)	50(2)	17.4(15)	0.1(16)	2.7(14)	1.4(18)
N1	23(2)	26(2)	17.6(18)	3.1(16)	4.0(16)	0.9(18)
N2	43(3)	33(3)	42(3)	-5(2)	13(2)	6(2)
N3	20(2)	40(2)	30(2)	-11.0(18)	3.2(17)	-2(2)
N4	28(3)	62(3)	18(2)	1(2)	1.8(18)	5(2)
C1	23(3)	31(3)	22(2)	5(2)	3.1(19)	2(2)
C2	30(3)	39(3)	22(2)	1(2)	-1(2)	4(3)
C3	29(3)	37(3)	29(3)	2(2)	-2(2)	3(3)
C4	36(4)	52(4)	27(3)	-1(3)	-4(2)	8(3)
C5	25(3)	32(3)	20(2)	4(2)	3.4(19)	4(2)
C6	22(3)	44(3)	23(2)	6(2)	1(2)	-1(2)
C7	25(3)	32(3)	28(2)	1(2)	2(2)	0(2)
C8	26(3)	49(4)	36(3)	6(3)	-1(2)	4(3)
C9	27(3)	25(2)	19(2)	3.2(19)	5(2)	1(2)
C10	29(3)	29(3)	31(3)	-4(2)	9(2)	0(2)
C11	36(3)	31(3)	30(3)	-3(2)	8(2)	1(2)
C12	39(4)	39(3)	48(4)	1(3)	11(3)	-2(3)
C13	26(3)	31(3)	24(2)	-3(2)	6(2)	0(2)
C14	38(3)	33(3)	29(3)	-2(2)	1(2)	-2(3)
C15	44(4)	33(3)	36(3)	-7(2)	0(3)	4(3)
C16	46(4)	46(4)	71(5)	-15(4)	7(3)	10(3)
C17	38(3)	42(3)	35(3)	-8(2)	5(2)	-2(3)
C18	50(4)	40(3)	32(3)	-3(2)	6(3)	3(3)
C19	45(4)	45(3)	35(3)	-3(3)	4(3)	5(3)
C20	82(6)	52(4)	48(4)	0(3)	25(4)	-5(4)
C21	50(4)	41(3)	51(3)	-1(3)	21(3)	14(3)
C22	53(4)	63(5)	59(4)	4(4)	13(3)	26(4)
C23	49(4)	48(4)	91(6)	9(4)	21(4)	17(4)
C24	57(5)	84(7)	100(7)	8(6)	6(5)	35(5)
C25	48(4)	37(3)	61(4)	0(3)	17(3)	1(3)
C29	55(4)	45(3)	37(3)	-6(3)	10(3)	4(3)
C33	30(3)	46(3)	38(3)	-11(2)	9(2)	-14(3)
C37	33(3)	51(3)	25(2)	-5(2)	1(2)	-7(3)
C45	13(2)	45(3)	28(2)	-8(2)	1(2)	0(2)
C46	28(3)	33(3)	25(2)	-2(2)	3(2)	2(2)
C47	26(3)	42(3)	27(3)	-4(2)	4(2)	1(3)
C48	38(4)	45(3)	35(3)	-8(3)	5(3)	5(3)
C49	46(4)	39(3)	49(4)	9(3)	17(3)	-5(3)
C50	26(3)	49(3)	17(2)	3(2)	2.0(19)	5(3)
C51	28(3)	83(5)	20(2)	4(3)	4(2)	2(3)
C26A	51(6)	55(5)	55(5)	-6(5)	16(4)	-14(4)
C27A	74(6)	57(5)	48(4)	-10(4)	20(4)	-22(5)

C28A	79(9)	74(7)	51(6)	-14(6)	25(6)	-28(8)
C30A	43(5)	45(6)	32(5)	0(4)	9(4)	-2(5)
C31A	84(9)	101(11)	42(6)	-15(7)	-6(6)	31(10)
C32A	95(10)	121(15)	51(9)	-28(11)	-19(8)	49(13)
C34A	145(9)	55(5)	51(5)	1(4)	-15(5)	-40(5)
C35A	96(12)	57(5)	73(11)	4(6)	-4(8)	-25(6)
C36A	70(16)	60(7)	81(13)	9(8)	2(9)	-29(8)
C38A	37(6)	45(5)	32(3)	-4(4)	15(4)	4(4)
C39A	37(6)	60(6)	46(4)	9(4)	4(4)	-1(5)
C40A	43(5)	63(6)	57(6)	8(5)	8(4)	6(5)
C41A	24(4)	39(6)	38(6)	-7(5)	13(3)	-5(4)
C42A	30(6)	96(9)	78(8)	-53(8)	13(5)	-2(6)
C43A	53(6)	105(9)	113(12)	-69(9)	9(8)	12(8)
C44A	118(13)	104(10)	122(11)	-66(9)	9(9)	8(8)
C26B	51(6)	55(5)	55(5)	-6(5)	16(4)	-14(4)
C27B	74(6)	57(5)	48(4)	-10(4)	20(4)	-22(5)
C28B	79(9)	74(7)	51(6)	-14(6)	25(6)	-28(8)
C30B	43(5)	45(6)	32(5)	0(4)	9(4)	-2(5)
C31B	84(9)	101(11)	42(6)	-15(7)	-6(6)	31(10)
C32B	95(10)	121(15)	51(9)	-28(11)	-19(8)	49(13)
C34B	145(9)	55(5)	51(5)	1(4)	-15(5)	-40(5)
C35B	96(12)	57(5)	73(11)	4(6)	-4(8)	-25(6)
C36B	70(16)	60(7)	81(13)	9(8)	2(9)	-29(8)
C38B	37(6)	45(5)	32(3)	-4(4)	15(4)	4(4)
C39B	37(6)	60(6)	46(4)	9(4)	4(4)	-1(5)
C40B	43(5)	63(6)	57(6)	8(5)	8(4)	6(5)
C41B	24(4)	39(6)	38(6)	-7(5)	13(3)	-5(4)
C42B	30(6)	96(9)	78(8)	-53(8)	13(5)	-2(6)
C43B	53(6)	105(9)	113(12)	-69(9)	9(8)	12(8)
C44B	118(13)	104(10)	122(11)	-66(9)	9(9)	8(8)

Table A8.1 (d) Bond Lengths for [{$CH_3C(O)NH_2$}$CoW_5O_{17}(OMe)]^{3-}$.

Atom	**Atom**	**Length/Å**	**Atom**	**Atom**	**Length/Å**
W1	O1	1.798(4)	C1	C2	1.514(7)
W1	O5	1.976(4)	C2	C3	1.518(8)
W1	O8	1.925(4)	C3	C4	1.518(8)
W1	O9	1.714(4)	C5	C6	1.529(7)
W1	O13	2.009(4)	C6	C7	1.519(8)
W1	O18	2.340(3)	C7	C8	1.520(8)
W2	O2	2.044(4)	C9	C10	1.506(8)
W2	O5	1.911(4)	C10	C11	1.530(8)
W2	O6	1.896(4)	C11	C12	1.502(9)

W2	O10	1.735(4)	C13	C14	1.529(8)
W2	O14	1.857(4)	C14	C15	1.526(8)
W2	O18	2.307(4)	C15	C16	1.523(10)
W3	O3	1.791(4)	C17	C18	1.519(9)
W3	O6	1.984(4)	C18	C19	1.502(9)
W3	O7	1.929(4)	C19	C20	1.537(10)
W3	O11	1.732(4)	C21	C22	1.494(11)
W3	O15	2.029(4)	C22	C23	1.508(10)
W3	O18	2.314(3)	C23	C24	1.467(12)
W4	O4	1.776(4)	C25	C26A	1.553(12)
W4	O7	1.942(4)	C25	C26B	1.487(16)
W4	O8	1.939(4)	C29	C30A	1.492(12)
W4	O12	1.724(4)	C29	C30B	1.509(16)
W4	O16	2.052(4)	C33	C34A	1.488(14)
W4	O18	2.386(4)	C33	C34B	1.504(15)
W5	O13	1.899(3)	C37	C38A	1.604(12)
W5	O14	2.053(4)	C37	C38B	1.480(12)
W5	O15	1.888(4)	C45	C46	1.520(8)
W5	O16	1.848(4)	C46	C47	1.527(7)
W5	O17	1.713(4)	C47	C48	1.524(8)
W5	O18	2.347(3)	C50	C51	1.483(8)
Co1	O1	2.076(4)	C26A	C27A	1.491(14)
Co1	O2	2.123(4)	C27A	C28A	1.511(14)
Co1	O3	2.074(4)	C30A	C31A	1.521(12)
Co1	O4	2.093(4)	C31A	C32A	1.477(15)
Co1	O18	2.220(4)	C34A	C35A	1.410(18)
Co1	O19	2.043(4)	C35A	C36A	1.48(2)
O2	C49	1.426(7)	C38A	C39A	1.502(15)
O19	C50	1.262(6)	C39A	C40A	1.507(16)
N1	C1	1.515(6)	C41A	C42A	1.527(14)
N1	C5	1.515(7)	C42A	C43A	1.520(18)
N1	C9	1.517(7)	C43A	C44A	1.48(2)
N1	C13	1.514(6)	C26B	C27B	1.505(19)
N2	C17	1.522(8)	C27B	C28B	1.554(19)
N2	C21	1.538(8)	C30B	C31B	1.516(17)
N2	C25	1.535(9)	C31B	C32B	1.475(19)
N2	C29	1.513(9)	C34B	C35B	1.397(17)
N3	C33	1.518(8)	C35B	C36B	1.49(2)
N3	C37	1.502(8)	C38B	C39B	1.520(16)
N3	C45	1.532(7)	C39B	C40B	1.503(16)
N3	C41A	1.516(12)	C41B	C42B	1.538(15)
N3	C41B	1.536(12)	C42B	C43B	1.501(18)
N4	C50	1.310(8)	C43B	C44B	1.50(2)

Table A8.1(e). Bond Angles for [{$CH_3C(O)NH_2$}$CoW_5O_{17}(OMe)]^{3-}$.

Atom	Atom	Atom	Angle/˚	Atom	Atom	Atom	Angle/˚
O1	W1	O5	89.43(17)	W3	O7	W4	117.43(17)
O1	W1	O8	92.59(16)	W1	O8	W4	117.18(19)
O1	W1	O13	156.35(15)	W5	O13	W1	118.52(18)
O1	W1	O18	82.66(14)	W2	O14	W5	113.98(19)
O5	W1	O13	82.47(15)	W5	O15	W3	117.52(18)
O5	W1	O18	74.88(13)	W5	O16	W4	116.79(18)
O8	W1	O5	151.71(15)	W1	O18	W4	88.51(13)
O8	W1	O13	84.51(15)	W1	O18	W5	91.57(13)
O8	W1	O18	77.41(14)	W2	O18	W1	91.08(12)
O9	W1	O1	103.60(17)	W2	O18	W3	91.01(13)
O9	W1	O5	102.63(17)	W2	O18	W4	178.75(19)
O9	W1	O8	104.28(18)	W2	O18	W5	89.65(12)
O9	W1	O13	99.85(17)	W3	O18	W1	175.98(18)
O9	W1	O18	173.34(16)	W3	O18	W4	89.47(11)
O13	W1	O18	73.79(13)	W3	O18	W5	91.88(11)
O2	W2	O18	79.72(14)	W5	O18	W4	89.19(12)
O5	W2	O2	82.34(16)	Co1	O18	W1	87.93(11)
O5	W2	O18	76.85(14)	Co1	O18	W2	94.40(13)
O6	W2	O2	86.66(16)	Co1	O18	W3	88.48(13)
O6	W2	O5	153.22(16)	Co1	O18	W4	86.76(13)
O6	W2	O18	77.21(15)	Co1	O18	W5	175.93(19)
O10	W2	O2	96.19(18)	C50	O19	Co1	126.0(4)
O10	W2	O5	103.13(18)	C1	N1	C5	108.2(4)
O10	W2	O6	102.27(19)	C1	N1	C9	111.0(4)
O10	W2	O14	103.56(19)	C5	N1	C9	110.0(4)
O10	W2	O18	175.88(18)	C13	N1	C1	108.7(4)
O14	W2	O2	160.06(17)	C13	N1	C5	111.8(4)
O14	W2	O5	90.42(16)	C13	N1	C9	107.2(4)
O14	W2	O6	91.76(17)	C17	N2	C21	110.4(5)
O14	W2	O18	80.55(15)	C17	N2	C25	107.9(5)
O3	W3	O6	89.57(17)	C25	N2	C21	110.4(6)
O3	W3	O7	92.65(17)	C29	N2	C17	111.0(5)
O3	W3	O15	156.71(16)	C29	N2	C21	107.0(5)
O3	W3	O18	82.62(15)	C29	N2	C25	110.1(6)
O6	W3	O15	82.79(16)	C33	N3	C45	109.9(4)
O6	W3	O18	75.43(14)	C33	N3	C41B	120.1(7)
O7	W3	O6	151.90(15)	C37	N3	C33	106.3(5)
O7	W3	O15	84.23(17)	C37	N3	C45	110.5(5)
O7	W3	O18	77.08(14)	C37	N3	C41A	120.1(7)
O11	W3	O3	104.77(18)	C37	N3	C41B	103.1(8)
O11	W3	O6	102.70(19)	C45	N3	C41B	106.6(8)

O11	W3	O7	103.79(19)	C41A	N3	C33	103.6(7)
O11	W3	O15	98.37(17)	C41A	N3	C45	106.0(8)
O11	W3	O18	172.45(16)	C2	C1	N1	116.3(5)
O15	W3	O18	74.18(13)	C1	C2	C3	110.7(5)
O4	W4	O7	92.95(16)	C2	C3	C4	112.5(5)
O4	W4	O8	92.18(16)	N1	C5	C6	115.5(4)
O4	W4	O16	157.68(16)	C7	C6	C5	110.4(4)
O4	W4	O18	82.99(15)	C6	C7	C8	112.2(5)
O7	W4	O16	81.62(15)	C10	C9	N1	115.7(5)
O7	W4	O18	75.10(14)	C9	C10	C11	111.3(5)
O8	W4	O7	149.77(16)	C12	C11	C10	111.9(5)
O8	W4	O16	82.40(14)	N1	C13	C14	115.6(5)
O8	W4	O18	76.01(14)	C15	C14	C13	109.0(5)
O12	W4	O4	103.85(19)	C16	C15	C14	113.1(5)
O12	W4	O7	105.40(19)	C18	C17	N2	114.4(5)
O12	W4	O8	102.21(19)	C19	C18	C17	111.3(6)
O12	W4	O16	98.46(18)	C18	C19	C20	111.7(6)
O12	W4	O18	173.05(17)	C22	C21	N2	116.6(6)
O16	W4	O18	74.69(14)	C21	C22	C23	110.6(7)
O13	W5	O14	82.13(15)	C24	C23	C22	115.0(8)
O13	W5	O18	75.53(14)	N2	C25	C26A	110.8(7)
O14	W5	O18	75.82(14)	C26B	C25	N2	126.3(12)
O15	W5	O13	150.32(16)	C30A	C29	N2	116.0(7)
O15	W5	O14	83.31(16)	C30B	C29	N2	114.2(10)
O15	W5	O18	75.89(14)	C34A	C33	N3	117.2(12)
O16	W5	O13	91.24(16)	C34B	C33	N3	114.8(11)
O16	W5	O14	155.15(16)	N3	C37	C38A	106.6(6)
O16	W5	O15	91.22(17)	C38B	C37	N3	124.2(7)
O16	W5	O18	79.33(14)	C46	C45	N3	115.3(4)
O17	W5	O13	103.48(17)	C45	C46	C47	109.3(5)
O17	W5	O14	102.21(19)	C48	C47	C46	113.0(5)
O17	W5	O15	104.81(17)	O19	C50	N4	122.3(6)
O17	W5	O16	102.62(19)	O19	C50	C51	119.1(5)
O17	W5	O18	177.87(17)	N4	C50	C51	118.6(5)
O1	Co1	O2	86.31(15)	C27A	C26A	C25	112.1(9)
O1	Co1	O4	88.04(15)	C26A	C27A	C28A	114.7(10)
O1	Co1	O18	79.97(14)	C29	C30A	C31A	109.9(9)
O2	Co1	O18	80.12(14)	C32A	C31A	C30A	114.6(11)
O3	Co1	O1	159.12(15)	C35A	C34A	C33	121.8(16)
O3	Co1	O2	89.57(15)	C34A	C35A	C36A	116.3(19)
O3	Co1	O4	89.17(15)	C39A	C38A	C37	109.4(10)
O3	Co1	O18	79.17(14)	C38A	C39A	C40A	114.9(11)
O4	Co1	O2	160.72(15)	N3	C41A	C42A	116.8(13)

O4	Co1	O18	80.74(14)	C43A	C42A	C41A	110.4(13)
O19	Co1	O1	101.75(15)	C44A	C43A	C42A	112.9(16)
O19	Co1	O2	97.34(16)	C25	C26B	C27B	106.7(15)
O19	Co1	O3	99.07(15)	C26B	C27B	C28B	108.7(15)
O19	Co1	O4	101.86(16)	C29	C30B	C31B	109.8(14)
O19	Co1	O18	176.88(17)	C32B	C31B	C30B	116.1(17)
W1	O1	Co1	109.41(17)	C35B	C34B	C33	120.8(16)
W2	O2	Co1	105.69(16)	C34B	C35B	C36B	117(2)
C49	O2	W2	120.6(4)	C37	C38B	C39B	113.7(11)
C49	O2	Co1	117.4(4)	C40B	C39B	C38B	115.9(12)
W3	O3	Co1	109.69(19)	N3	C41B	C42B	110.1(17)
W4	O4	Co1	109.51(18)	C43B	C42B	C41B	112.1(14)
W2	O5	W1	117.13(17)	C44B	C43B	C42B	114.1(18)
W2	O6	W3	116.3(2)				

Table A8.1 (f). Hydrogen Bonds for [{$CH_3C(O)NH_2$}$CoW_5O_{17}(OMe)$]$^{3-}$.

D	H	A	d(D-H)/Å	d(H-A)/Å	d(D-A)/Å	D-H-A/°
N4	H4D	O1	0.88	2.10	2.921(6)	155.3
N4	H4E	O5[1]	0.88	2.22	3.033(6)	153.9

[1]1-X,1-Y,1-Z

Table A8.1 (g). Torsion Angles for [{$CH_3C(O)NH_2$}$CoW_5O_{17}(OMe)$]$^{3-}$.

A	B	C	D	Angle/˚	A	B	C	D	Angle/˚
Co1	O19	C50	N4	-15.9(9)	C5	N1	C9	C10	-171.8(4)
Co1	O19	C50	C51	164.0(5)	C5	N1	C13	C14	56.4(6)
O2	W2	O6	W3	-82.2(2)	C5	C6	C7	C8	173.8(5)
O2	W2	O14	W5	9.1(6)	C9	N1	C1	C2	-53.3(6)
O5	W1	O1	Co1	76.33(18)	C9	N1	C5	C6	-65.7(6)
O5	W2	O6	W3	-16.6(5)	C9	N1	C13	C14	177.1(5)
O5	W2	O14	W5	77.3(2)	C9	C10	C11	C12	174.3(5)
O6	W2	O14	W5	-76.0(2)	C13	N1	C1	C2	-171.0(5)
O6	W3	O3	Co1	-76.97(19)	C13	N1	C5	C6	53.3(6)
O7	W3	O3	Co1	75.01(19)	C13	N1	C9	C10	66.4(6)
O7	W4	O4	Co1	-74.40(19)	C13	C14	C15	C16	-68.6(7)
O8	W1	O1	Co1	-75.45(19)	C17	N2	C21	C22	-62.9(8)
O8	W4	O4	Co1	75.80(19)	C17	N2	C25	C26A	-176.0(8)
O9	W1	O1	Co1	179.19(19)	C17	N2	C25	C26B	162.0(11)
O10	W2	O6	W3	-177.8(2)	C17	N2	C29	C30A	60.4(9)
O10	W2	O14	W5	-179.1(2)	C17	N2	C29	C30B	41.5(15)

O11	W3	O3	Co1	-180.0(2)	C17	C18	C19	C20	-174.3(6)
O12	W4	O4	Co1	178.94(19)	C21	N2	C17	C18	-55.6(7)
O13	W1	O1	Co1	6.8(5)	C21	N2	C25	C26A	63.3(9)
O13	W5	O15	W3	-22.4(5)	C21	N2	C25	C26B	41.3(13)
O13	W5	O16	W4	74.5(2)	C21	N2	C29	C30A	-179.1(7)
O14	W2	O6	W3	77.9(2)	C21	N2	C29	C30B	162.0(14)
O14	W5	O13	W1	84.2(2)	C21	C22	C23	C24	177.1(8)
O14	W5	O15	W3	-83.4(2)	C25	N2	C17	C18	-176.4(6)
O14	W5	O16	W4	0.7(5)	C25	N2	C21	C22	56.4(8)
O15	W3	O3	Co1	-6.5(6)	C25	N2	C29	C30A	-59.1(9)
O15	W5	O13	W1	22.9(5)	C25	N2	C29	C30B	-78.0(15)
O15	W5	O16	W4	-76.0(2)	C25	C26A	C27A	C28A	178.3(12)
O16	W4	O4	Co1	0.6(5)	C25	C26B	C27B	C28B	-179.2(18)
O16	W5	O13	W1	-71.8(2)	C29	N2	C17	C18	62.9(7)
O16	W5	O15	W3	72.3(2)	C29	N2	C21	C22	176.2(7)
O17	W5	O13	W1	-175.1(2)	C29	N2	C25	C26A	-54.7(9)
O17	W5	O15	W3	175.7(2)	C29	N2	C25	C26B	-76.7(13)
O17	W5	O16	W4	178.6(2)	C29	C30A	C31A	C32A	170.3(18)
O18	W1	O1	Co1	1.50(17)	C29	C30B	C31B	C32B	-179(4)
O18	W2	O6	W3	-2.01(18)	C33	N3	C37	C38A	-176.5(7)
O18	W2	O14	W5	0.72(17)	C33	N3	C37	C38B	170.6(9)
O18	W3	O3	Co1	-1.60(17)	C33	N3	C45	C46	-60.2(7)
O18	W4	O4	Co1	0.19(16)	C33	N3	C41A	C42A	73(2)
O18	W5	O13	W1	6.85(18)	C33	N3	C41B	C42B	53.2(19)
O18	W5	O15	W3	-6.42(19)	C33	C34A	C35A	C36A	-166(4)
O18	W5	O16	W4	-0.57(17)	C33	C34B	C35B	C36B	165(4)
N1	C1	C2	C3	175.3(5)	C37	N3	C33	C34A	-178.8(16)
N1	C5	C6	C7	173.7(5)	C37	N3	C33	C34B	-172.5(18)
N1	C9	C10	C11	-179.9(4)	C37	N3	C45	C46	56.7(7)
N1	C13	C14	C15	162.4(5)	C37	N3	C41A	C42A	-45(2)
N2	C17	C18	C19	-170.2(5)	C37	N3	C41B	C42B	-64.7(18)
N2	C21	C22	C23	-171.7(7)	C37	C38A	C39A	C40A	56.4(17)
N2	C25	C26A	C27A	-166.2(10)	C37	C38B	C39B	C40B	-176.9(13)
N2	C25	C26B	C27B	99.6(18)	C45	N3	C33	C34A	-59.2(17)
N2	C29	C30A	C31A	162.4(13)	C45	N3	C33	C34B	-52.9(18)
N2	C29	C30B	C31B	167(3)	C45	N3	C37	C38A	64.3(8)
N3	C33	C34A	C35A	-123(3)	C45	N3	C37	C38B	51.4(10)
N3	C33	C34B	C35B	-149(3)	C45	N3	C41A	C42A	-171(2)
N3	C37	C38A	C39A	169.1(9)	C45	N3	C41B	C42B	178.8(17)
N3	C37	C38B	C39B	-178.9(10)	C45	C46	C47	C48	170.9(5)
N3	C45	C46	C47	161.6(5)	C41A	N3	C33	C34A	53.7(18)
N3	C41A	C42A	C43A	-165(2)	C41A	N3	C37	C38A	-59.5(11)
N3	C41B	C42B	C43B	-159(2)	C41A	N3	C45	C46	-171.6(7)

C1	N1	C5	C6	172.9(5)	C41A	C42A	C43A	C44A	162(3)
C1	N1	C9	C10	-52.1(6)	C41B	N3	C33	C34B	71(2)
C1	N1	C13	C14	-62.9(6)	C41B	N3	C37	C38B	-62.2(12)
C1	C2	C3	C4	179.5(5)	C41B	N3	C45	C46	168.1(8)
C5	N1	C1	C2	67.5(6)	C41B	C42B	C43B	C44B	83(3)

Table A8.1 (h). Hydrogen Atom Coordinates (Å×10^4) and Isotropic Displacement Parameters (Å^2×10^3) for [{$CH_3C(O)NH_2$}CoW_5O_{17}(OMe)]$^{3-}$.

Atom	***x***	***y***	***z***	**U(eq)**
H4D	5319	4282	5144	43
H4E	5497	4368	4806	43
H1A	3751	2493	7158	30
H1B	4222	3148	7038	30
H2A	3973	1162	6812	37
H2B	4408	1882	6678	37
H3A	3703	3015	6481	39
H3B	3269	2289	6612	39
H4A	3261	2049	6048	59
H4B	3463	1043	6236	59
H4C	3892	1777	6103	59
H5A	5124	2857	7202	31
H5B	5108	1720	7083	31
H6A	5541	2392	7723	36
H6B	5477	1229	7631	36
H7A	6116	2577	7301	34
H7B	6085	1391	7247	34
H8A	6890	1746	7581	56
H8B	6503	1175	7800	56
H8C	6573	2363	7828	56
H9A	4487	556	7244	28
H9B	4634	746	7627	28
H10A	3571	923	7279	35
H10B	3717	1116	7663	35
H11A	3808	-779	7346	38
H11B	4017	-605	7725	38
H12A	2916	-421	7439	62
H12B	3125	-253	7819	62
H12C	3156	-1342	7661	62
H13A	4679	2325	7855	32
H13B	4063	2551	7714	32
H14A	4967	3850	7692	41

H14B 4420	4031	7446	41
H15A 4438	3931	8142	46
H15B 4456	4971	7952	46
H16A 3581	4627	7665	81
H16B 3566	4660	8051	81
H16C 3564	3606	7866	81
H17A 5295	10379	6372	46
H17B 4748	10758	6161	46
H18A 4504	9013	6064	49
H18B 5013	8726	6327	49
H19A 4101	9872	6459	50
H19B 4625	9701	6723	50
H20A 3921	8125	6451	89
H20B 3948	8534	6816	89
H20C 4452	7939	6708	89
H21A 5493	8663	5923	55
H21B 5840	9246	5685	55
H22A 6031	9264	6377	69
H22B 6344	9994	6159	69
H23A 6382	7861	6136	74
H23B 6674	8568	5902	74
H24A 7272	9117	6329	121
H24B 7268	7919	6338	121
H24C 6952	8541	6584	121
H25A 5874	11245	6034	57
H25B 5326	11723	5849	57
H25C 5298	11659	5775	57
H25D 5739	11353	6071	57
H29A 5076	9940	5386	55
H29B 4702	9340	5603	55
H29C 5047	10169	5381	55
H29D 4790	9270	5564	55
H33A 6878	4245	6361	45
H33B 6940	3428	6088	45
H33C 6857	4241	6340	45
H33D 6965	3360	6095	45
H37A 7120	5562	6021	44
H37B 7137	4727	5742	44
H37C 7197	4679	5734	44
H37D 7049	5400	6014	44
H45A 8054	4401	6636	34
H45B 8217	5261	6399	34
H46A 7207	5370	6649	35

H46B 7526	6274	6505	35
H47A 7849	5279	7115	38
H47B 8239	6050	6964	38
H48A 7659	7375	7028	59
H48B 7756	6796	7370	59
H48C 7205	6632	7128	59
H49A 5362	7309	5375	65
H49B 5805	6483	5318	65
H49C 5851	7077	5657	65
H51A 6515	5445	4891	65
H51B 6402	4356	4735	65
H51C 6846	4498	5049	65
H26A 6026	10557	5494	64
H26B 5550	11283	5337	64
H27A 6519	11961	5712	71
H27B 6047	12675	5545	71
H28A 6241	12021	5023	100
H28B 6780	11554	5220	100
H28C 6694	12741	5209	100
H30A 4614	11444	5547	48
H30B 4176	10684	5660	48
H31A 4449	10876	5011	92
H31B 4084	9974	5113	92
H32A 3544	11205	4848	138
H32B 3420	11108	5217	138
H32C 3785	12011	5115	138
H34A 7666	2999	6600	104
H34B 7110	3222	6736	104
H35A 7344	1681	6338	92
H35B 6735	1963	6381	92
H36A 6799	1316	6865	107
H36B 7422	1621	6956	107
H36C 7261	663	6731	107
H38A 8028	6109	5968	44
H38B 8124	5169	5741	44
H39A 7504	5791	5320	57
H39B 7951	6628	5425	57
H40A 7150	7457	5358	82
H40B 7307	7377	5745	82
H40C 6865	6635	5559	82
H41A 8036	3053	6269	40
H41B 8341	3859	6075	40
H42A 7427	2791	5755	81

H42B 7859	3413	5582	81
H43A 8516	2227	5702	109
H43B 8208	1723	5977	109
H44A 7732	1646	5321	173
H44B 7633	905	5611	173
H44C 8186	846	5455	173
H26C 6194	10719	5588	64
H26D 6304	11795	5758	64
H27C 5590	12496	5389	71
H27D 5472	11422	5220	71
H28D 6032	12045	4880	100
H28E 6481	11549	5145	100
H28F 6360	12724	5158	100
H30C 4450	11286	5636	48
H30D 4146	10299	5737	48
H31C 4268	10805	5079	92
H31D 3960	9832	5182	92
H32D 3347	11025	4970	138
H32E 3285	10834	5345	138
H32F 3594	11810	5242	138
H34C 7671	2894	6570	104
H34D 7263	3469	6769	104
H35C 6938	1863	6380	92
H35D 6642	2356	6660	92
H36D 7262	1690	7059	107
H36E 7635	1317	6795	107
H36F 7058	806	6811	107
H38C 7961	5614	5688	44
H38D 7822	6334	5974	44
H39C 7136	6111	5367	57
H39D 7026	6865	5650	57
H40D 7366	7660	5205	82
H40E 7927	7082	5304	82
H40F 7724	7884	5548	82
H41C 8245	3356	6163	40
H41D 8284	4315	5934	40
H42C 7420	2922	5766	81
H42D 7667	3681	5525	81
H43C 8012	2248	5380	109
H43D 8498	2651	5639	109
H44D 7727	1302	5834	173
H44E 8317	1543	6023	173
H44F 8254	905	5692	173

Table A8.1 (i) Atomic Occupancy for [{$CH_3C(O)NH_2$}CoW_5O_{17}(OMe)]$^{3-}$.

Atom	***Occupancy***	**Atom**	***Occupancy***	**Atom**	***Occupancy***
H25A	0.6432	H25B	0.6432	H25C	0.3568
H25D	0.3568	H29A	0.6432	H29B	0.6432
H29C	0.3568	H29D	0.3568	H33A	0.5121
H33B	0.5121	H33C	0.4879	H33D	0.4879
H37A	0.5121	H37B	0.5121	H37C	0.4879
H37D	0.4879	C26A	0.6432	H26A	0.6432
H26B	0.6432	C27A	0.6432	H27A	0.6432
H27B	0.6432	C28A	0.6432	H28A	0.6432
H28B	0.6432	H28C	0.6432	C30A	0.6432
H30A	0.6432	H30B	0.6432	C31A	0.6432
H31A	0.6432	H31B	0.6432	C32A	0.6432
H32A	0.6432	H32B	0.6432	H32C	0.6432
C34A	0.5121	H34A	0.5121	H34B	0.5121
C35A	0.5121	H35A	0.5121	H35B	0.5121
C36A	0.5121	H36A	0.5121	H36B	0.5121
H36C	0.5121	C38A	0.5121	H38A	0.5121
H38B	0.5121	C39A	0.5121	H39A	0.5121
H39B	0.5121	C40A	0.5121	H40A	0.5121
H40B	0.5121	H40C	0.5121	C41A	0.5121
H41A	0.5121	H41B	0.5121	C42A	0.5121
H42A	0.5121	H42B	0.5121	C43A	0.5121
H43A	0.5121	H43B	0.5121	C44A	0.5121
H44A	0.5121	H44B	0.5121	H44C	0.5121
C26B	0.3568	H26C	0.3568	H26D	0.3568
C27B	0.3568	H27C	0.3568	H27D	0.3568
C28B	0.3568	H28D	0.3568	H28E	0.3568
H28F	0.3568	C30B	0.3568	H30C	0.3568
H30D	0.3568	C31B	0.3568	H31C	0.3568
H31D	0.3568	C32B	0.3568	H32D	0.3568
H32E	0.3568	H32F	0.3568	C34B	0.4879
H34C	0.4879	H34D	0.4879	C35B	0.4879
H35C	0.4879	H35D	0.4879	C36B	0.4879
H36D	0.4879	H36E	0.4879	H36F	0.4879
C38B	0.4879	H38C	0.4879	H38D	0.4879
C39B	0.4879	H39C	0.4879	H39D	0.4879
C40B	0.4879	H40D	0.4879	H40E	0.4879
H40F	0.4879	C41B	0.4879	H41C	0.4879
H41D	0.4879	C42B	0.4879	H42C	0.4879
H42D	0.4879	C43B	0.4879	H43C	0.4879

H43D 0.4879	C44B 0.4879	H44D 0.4879
H44E 0.4879	H44F 0.4879	

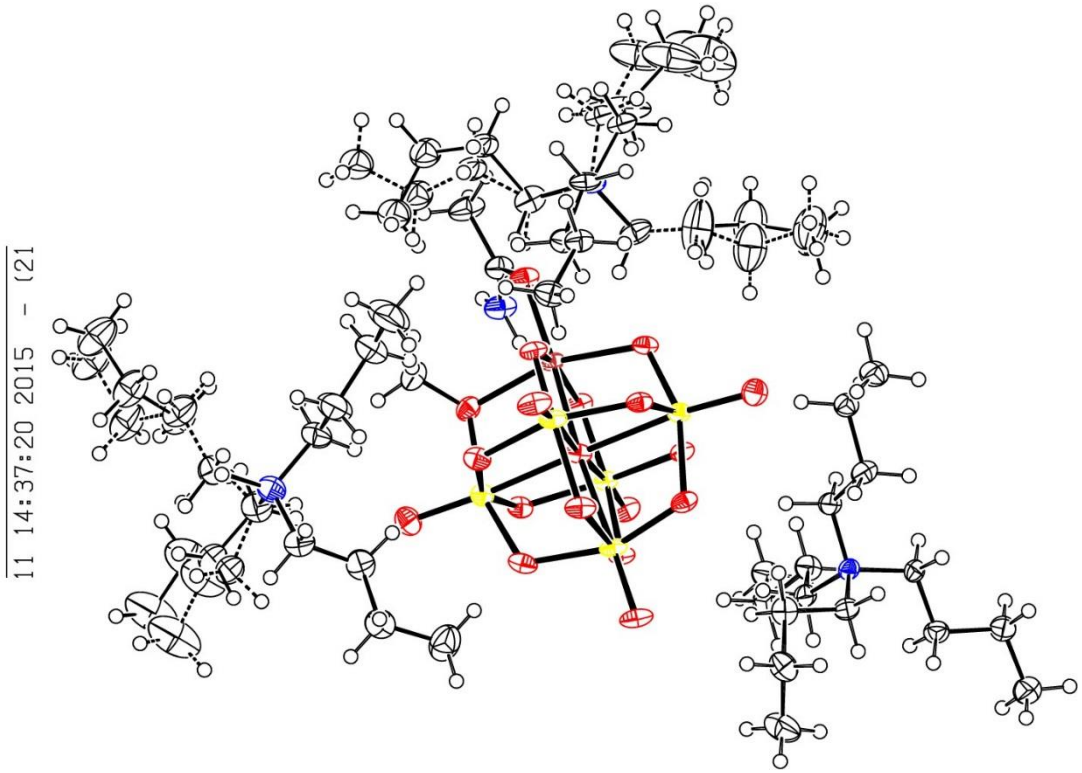

Figure A8.1. ORTEP structural diagram for [{$CH_3C(O)NH_2$}$CoW_5O_{17}(OMe)$]$^{3-}$

Table A8.2 (a). Crystal data and structure refinement for $(TBA)_3[W_6O_{18}]$

Empirical formula	$C_{96}H_{216}N_6O_{38}W_{12}$
Formula weight	4268.94
Temperature/K	150.0(2)
Crystal system	monoclinic
Space group	$P2_1/c$
a/Å	24.1107(4)
b/Å	16.9969(3)
c/Å	16.6482(2)
α/°	90
β/°	97.9997(15)
γ/°	90
Volume/Å^3	6756.18(19)
Z	2
ρ_{calc}g/cm^3	2.098
μ/mm^{-1}	10.236
F(000)	4052.0
Crystal size/mm^3	0.22 × 0.2 × 0.12
Radiation	MoKα (λ = 0.71073)

2Θ range for data collection/°	5.876 to 52.744
Index ranges	-30 ≤ h ≤ 29, -21 ≤ k ≤ 21, -20 ≤ l ≤ 19
Reflections collected	53208
Independent reflections	13631 [R_{int} = 0.0554, R_{sigma} = 0.0570]
Data/restraints/parameters	13631/721/750
Goodness-of-fit on F^2	1.069
Final R indexes [I>=2σ (I)]	R_1 = 0.0457, wR_2 = 0.0884
Final R indexes [all data]	R_1 = 0.0732, wR_2 = 0.0988
Largest diff. peak/hole / e $Å^{-3}$	1.76/-1.31

Table A8.2 (b). Fractional Atomic Coordinates (×10⁴) and Equivalent Isotropic Displacement Parameters (Å²×10³) for $(TBA)_3[W_6O_{18}]$. U_{eq} is defined as 1/3 of the trace of the orthogonalised U_{IJ} tensor.

Atom	*x*	*y*	*z*	U(eq)
W1	584.2(2)	3909.0(2)	4998.9(2)	27.54(10)
W2	-25.5(2)	4830.9(2)	6381.5(2)	26.95(9)
W3	781.4(2)	5814.6(2)	5289.5(2)	28.68(10)
W4	4368.1(2)	4413.2(3)	3997.5(2)	39.42(12)
W5	4433.2(2)	4657.9(3)	5973.8(2)	40.16(12)
W6	5481.1(2)	3816.3(3)	5216.3(2)	39.72(12)
O1	1019(3)	3108(4)	4997(4)	35.5(15)
O2	443(3)	3985(3)	6110(3)	26.5(13)
O3	1098(2)	4786(3)	5232(3)	27.4(13)
O4	-42(3)	4710(4)	7397(3)	34.3(15)
O5	608(2)	5519(3)	6345(3)	24.0(12)
O6	1354(3)	6403(4)	5506(4)	40.1(16)
O7	650(2)	5794(3)	4120(3)	26.4(13)
O8	0	5000	5000	19.7(16)
O9	-495(2)	5737(3)	6117(3)	21.0(12)
O10	153(2)	6532(3)	5251(3)	24.8(13)
O11	4019(3)	4398(4)	6693(4)	43.7(17)
O12	4931(3)	3764(4)	5956(4)	37.1(15)
O13	4034(2)	4243(4)	4973(4)	36.3(15)
O14	5825(3)	2933(4)	5366(4)	44.1(17)
O15	4879(3)	3569(4)	4357(4)	39.5(15)
O16	3898(3)	3976(4)	3262(4)	43.4(17)
O17	5898(2)	4529(4)	5980(3)	31.3(14)
O18	5000	5000	5000	29.9(18)
O19	4153(2)	5671(4)	5608(4)	36.4(15)
O20	4942(2)	4808(4)	3412(4)	33.6(15)
N1	577(3)	8041(4)	3201(4)	31.8(16)
N2	2430(3)	4272(6)	4291(5)	44.7(19)
N3B	4133(14)	7250(20)	2050(20)	75(4)
C37B	3830(20)	6520(20)	2280(20)	74(5)

C38B	3610(50)	5960(50)	1580(30)	71(5)
C39B	3340(30)	5260(30)	1880(30)	66(6)
C40B	3080(30)	4740(30)	1210(40)	80(7)
C33B	3716(18)	7860(30)	1620(20)	77(5)
C34B	3330(30)	8240(50)	2140(30)	102(7)
C35B	2920(30)	8770(50)	1600(40)	104(7)
C36B	2540(40)	9290(50)	2050(50)	127(10)
C45B	4420(18)	7580(20)	2840(20)	83(6)
C46B	4780(30)	8300(40)	2770(20)	124(11)
C47B	5040(30)	8590(30)	3660(30)	135(10)
C48B	5560(20)	9150(30)	3670(30)	152(11)
C41B	4570(20)	7050(30)	1500(20)	76(4)
C42B	4990(30)	6450(40)	1780(30)	91(6)
C43B	5340(30)	6260(40)	1080(40)	114(9)
C44B	5760(50)	5530(60)	1350(60)	168(17)
C1	961(4)	7386(6)	3001(6)	37(2)
C2	1181(4)	7455(6)	2211(6)	41(2)
C3	1592(6)	6828(8)	2101(8)	76(4)
C4	1835(6)	6862(8)	1325(8)	72(4)
C5	55(4)	8082(5)	2580(5)	33(2)
C6	-295(4)	7345(6)	2512(7)	42(2)
C7	-831(5)	7418(7)	2019(9)	75(4)
C8	-1203(6)	6725(8)	2035(9)	75(4)
C9	418(4)	7875(6)	4046(5)	38(2)
C10	-2(5)	8425(7)	4323(6)	46(3)
C11	97(6)	8543(7)	5241(6)	55(3)
C12	-333(6)	9043(7)	5544(7)	63(3)
C13	868(4)	8836(6)	3194(6)	37(2)
C14	1405(5)	8934(7)	3746(7)	58(3)
C15	1648(6)	9740(8)	3734(9)	74(4)
C16	2158(8)	9873(13)	4313(12)	134(7)
C17	2746(4)	5018(6)	4268(6)	44(2)
C18	2446(4)	5775(7)	4403(7)	52(3)
C19	2834(5)	6461(7)	4392(8)	59(3)
C20	2557(6)	7229(8)	4481(10)	85(4)
C21	2279(5)	4101(8)	5126(7)	54(3)
C22	2763(5)	4020(10)	5796(7)	72(4)
C23	2564(6)	3698(10)	6569(8)	89(4)
C24	2386(8)	2762(12)	6483(11)	123(6)
C25	2796(4)	3633(7)	4033(7)	52(2)
C26	2575(6)	2795(8)	4007(10)	78(4)
C27	3008(7)	2226(10)	3803(11)	97(4)
C29	1875(4)	4311(7)	3719(6)	49(3)

C30	1917(4)	4433(7)	2838(6)	51(3)
C31	1336(4)	4597(8)	2381(7)	60(3)
C32	1338(6)	4657(9)	1483(7)	75(4)
C28B	2927(16)	1400(20)	3880(20)	111(7)
C28A	3363(14)	2076(19)	4530(20)	111(7)
N3A	4302(8)	7196(12)	2050(12)	75(4)
C37A	3994(12)	6494(15)	2342(14)	74(5)
C38A	3600(30)	6060(30)	1682(16)	71(5)
C39A	3259(14)	5457(15)	2027(18)	66(6)
C40A	2990(14)	4899(18)	1400(20)	80(7)
C33A	3886(10)	7839(17)	1694(15)	77(5)
C34A	3485(17)	8120(30)	2240(19)	102(7)
C35A	3086(17)	8720(30)	1780(20)	104(7)
C36A	2640(20)	9060(30)	2260(30)	127(10)
C45A	4674(10)	7496(14)	2792(13)	83(6)
C46A	5008(15)	8240(20)	2650(16)	124(11)
C47A	5439(16)	8435(19)	3442(18)	135(10)
C48A	5954(14)	7857(17)	3600(20)	152(11)
C41A	4654(12)	6938(17)	1397(14)	76(4)
C42A	5058(17)	6300(20)	1610(18)	91(6)
C43A	5291(16)	6030(20)	830(20)	114(9)
C44A	5720(30)	5310(30)	1040(30)	168(17)

Table A8.2(c). Anisotropic Displacement Parameters ($Å^2×10^3$) for $(TBA)_3[W_6O_{18}]$. The Anisotropic displacement factor exponent takes the form: $-2\pi^2[h^2a^{*2}U_{11}+2hka^*b^*U_{12}+\ldots]$.

Atom	**U_{11}**	**U_{22}**	**U_{33}**	**U_{23}**	**U_{13}**	**U_{12}**
W1	35.6(2)	25.7(2)	21.74(19)	-0.67(15)	5.24(16)	1.48(16)
W2	39.3(2)	26.96(19)	14.85(18)	0.07(14)	4.78(15)	-1.21(16)
W3	32.9(2)	29.1(2)	24.4(2)	-6.06(15)	5.40(16)	-7.30(16)
W4	25.9(2)	63.5(3)	27.3(2)	-4.15(19)	-1.75(16)	0.78(19)
W5	26.4(2)	66.1(3)	27.9(2)	1.4(2)	3.44(17)	2.9(2)
W6	28.9(2)	58.9(3)	30.6(2)	-0.27(19)	1.29(17)	6.5(2)
O1	47(4)	30(3)	31(4)	0(3)	10(3)	8(3)
O2	42(3)	23(3)	15(3)	2(2)	4(2)	8(2)
O3	30(3)	28(3)	24(3)	-4(2)	2(2)	-4(2)
O4	54(4)	38(4)	11(3)	2(2)	7(3)	3(3)
O5	29(3)	28(3)	14(3)	-2(2)	1(2)	-3(2)
O6	37(3)	44(4)	42(4)	-16(3)	15(3)	-12(3)
O7	37(3)	22(3)	22(3)	-3(2)	9(2)	-7(3)
O8	32(4)	19(3)	9(3)	-3(3)	6(3)	-2(3)
O9	32(3)	21(3)	11(3)	-2(2)	7(2)	-3(2)

O10	37(3)	18(3)	21(3)	-4(2)	10(2)	-3(2)
O11	29(3)	68(5)	34(4)	3(3)	4(3)	0(3)
O12	30(3)	54(4)	27(3)	1(3)	1(2)	2(3)
O13	24(3)	56(4)	29(3)	0(3)	2(2)	-1(3)
O14	34(4)	55(4)	43(4)	4(3)	0(3)	4(3)
O15	32(3)	60(4)	26(3)	-4(3)	0(2)	1(3)
O16	34(3)	68(5)	26(3)	-4(3)	-7(3)	-4(3)
O17	20(3)	52(4)	22(3)	1(3)	2(2)	4(3)
O18	24(4)	48(4)	17(4)	-3(3)	2(3)	3(3)
O19	21(3)	58(4)	30(3)	-2(3)	3(3)	7(3)
O20	27(3)	49(4)	23(3)	-3(3)	-3(2)	3(3)
N1	47(4)	29(3)	21(3)	13(3)	7(3)	10(3)
N2	26(4)	73(5)	33(4)	11(3)	0(3)	-9(3)
N3B	102(10)	81(6)	40(5)	22(4)	5(6)	-15(7)
C37B	105(12)	79(6)	38(6)	20(5)	7(7)	-18(8)
C38B	87(10)	87(9)	39(7)	12(6)	10(7)	-10(8)
C39B	80(13)	70(11)	51(11)	3(7)	24(7)	2(11)
C40B	72(16)	103(12)	71(15)	-21(9)	33(10)	-5(13)
C33B	103(11)	82(7)	48(7)	27(5)	12(7)	-14(8)
C34B	138(15)	103(12)	73(11)	40(9)	39(11)	10(10)
C35B	130(15)	98(11)	87(15)	36(11)	33(11)	6(12)
C36B	153(16)	110(20)	120(20)	37(15)	59(16)	14(13)
C45B	109(13)	94(8)	45(6)	16(5)	5(8)	-24(9)
C46B	170(20)	122(12)	76(10)	27(9)	-8(12)	-69(15)
C47B	190(20)	111(13)	88(11)	26(10)	-26(13)	-73(15)
C48B	190(20)	101(14)	150(20)	37(12)	-35(13)	-74(15)
C41B	91(9)	91(9)	44(6)	17(5)	3(6)	-17(7)
C42B	97(10)	94(11)	81(13)	16(9)	3(8)	-10(9)
C43B	107(14)	133(19)	104(17)	-10(12)	20(13)	-13(14)
C44B	160(20)	170(20)	170(30)	10(20)	40(30)	30(20)
C1	46(5)	32(4)	33(4)	9(3)	9(4)	11(4)
C2	45(5)	42(5)	36(5)	1(4)	8(4)	5(4)
C3	99(9)	77(8)	60(7)	22(6)	37(7)	47(7)
C4	93(10)	69(9)	63(7)	11(6)	38(7)	30(8)
C5	46(4)	27(4)	26(4)	7(3)	4(3)	11(3)
C6	48(5)	34(5)	46(6)	3(4)	11(4)	3(4)
C7	64(6)	51(7)	100(10)	13(6)	-23(6)	-1(5)
C8	65(7)	60(7)	96(11)	-3(7)	-4(7)	-1(6)
C9	48(5)	47(5)	19(4)	14(3)	7(4)	12(4)
C10	60(6)	52(6)	26(4)	8(4)	9(4)	16(5)
C11	93(8)	42(6)	28(5)	1(4)	6(5)	11(6)
C12	102(9)	56(7)	33(6)	0(5)	14(6)	10(6)
C13	51(5)	36(4)	22(4)	4(3)	2(4)	7(3)

C14	66(6)	63(6)	40(6)	11(5)	-10(5)	-5(5)
C15	80(8)	69(7)	69(8)	-11(6)	2(6)	-18(6)
C16	112(11)	169(17)	110(13)	-20(12)	-23(10)	-44(11)
C17	22(4)	66(5)	42(6)	13(4)	0(4)	-1(3)
C18	30(5)	72(5)	52(7)	14(4)	1(5)	8(4)
C19	41(6)	65(6)	70(8)	12(5)	5(5)	10(4)
C20	68(9)	74(7)	114(12)	11(7)	14(8)	22(6)
C21	40(5)	79(8)	44(4)	16(4)	4(4)	-5(5)
C22	37(6)	137(11)	42(5)	22(6)	0(4)	-2(6)
C23	70(9)	145(12)	51(6)	28(7)	10(6)	-3(8)
C24	136(16)	149(12)	82(11)	37(9)	6(11)	-21(10)
C25	33(5)	70(5)	50(6)	3(4)	-2(4)	-9(4)
C26	73(8)	74(6)	86(10)	3(6)	8(7)	-18(5)
C27	88(9)	82(7)	118(12)	-12(8)	1(8)	-4(6)
C29	23(4)	78(7)	42(4)	14(4)	-4(3)	-12(4)
C30	33(5)	74(8)	43(5)	12(5)	-2(4)	-17(5)
C31	38(5)	93(9)	45(5)	23(5)	-4(4)	-22(5)
C32	71(8)	102(11)	47(6)	18(6)	-9(5)	-32(8)
C28B	107(12)	83(8)	134(14)	-11(8)	-13(10)	-5(8)
C28A	107(12)	83(8)	134(14)	-11(8)	-13(10)	-5(8)
N3A	102(10)	81(6)	40(5)	22(4)	5(6)	-15(7)
C37A	105(12)	79(6)	38(6)	20(5)	7(7)	-18(8)
C38A	87(10)	87(9)	39(7)	12(6)	10(7)	-10(8)
C39A	80(13)	70(11)	51(11)	3(7)	24(7)	2(11)
C40A	72(16)	103(12)	71(15)	-21(9)	33(10)	-5(13)
C33A	103(11)	82(7)	48(7)	27(5)	12(7)	-14(8)
C34A	138(15)	103(12)	73(11)	40(9)	39(11)	10(10)
C35A	130(15)	98(11)	87(15)	36(11)	33(11)	6(12)
C36A	153(16)	110(20)	120(20)	37(15)	59(16)	14(13)
C45A	109(13)	94(8)	45(6)	16(5)	5(8)	-24(9)
C46A	170(20)	122(12)	76(10)	27(9)	-8(12)	-69(15)
C47A	190(20)	111(13)	88(11)	26(10)	-26(13)	-73(15)
C48A	190(20)	101(14)	150(20)	37(12)	-35(13)	-74(15)
C41A	91(9)	91(9)	44(6)	17(5)	3(6)	-17(7)
C42A	97(10)	94(11)	81(13)	16(9)	3(8)	-10(9)
C43A	107(14)	133(19)	104(17)	-10(12)	20(13)	-13(14)
C44A	160(20)	170(20)	170(30)	10(20)	40(30)	30(20)

Table A8.2(d). Bond Lengths for $(TBA)_3[W_6O_{18}]$.

Atom	Atom	Length/Å	Atom	Atom	Length/Å
W1	O1	1.718(6)	N3B	C33B	1.55(2)

W1	O2	1.932(5)	N3B	C45B	1.51(2)
W1	O3	1.942(6)	N3B	C41B	1.54(2)
W1	O8	2.3289(4)	C37B	C38B	1.54(3)
W1	O9[1]	1.935(5)	C38B	C39B	1.48(2)
W1	O10[1]	1.920(6)	C39B	C40B	1.49(2)
W2	O2	1.920(6)	C33B	C34B	1.50(3)
W2	O4	1.708(5)	C34B	C35B	1.54(3)
W2	O5	1.931(6)	C35B	C36B	1.55(3)
W2	O7[1]	1.935(6)	C45B	C46B	1.53(3)
W2	O8	2.3272(3)	C46B	C47B	1.60(3)
W2	O9	1.926(5)	C47B	C48B	1.57(4)
W3	O3	1.915(6)	C41B	C42B	1.47(3)
W3	O5	1.928(5)	C42B	C43B	1.55(3)
W3	O6	1.703(6)	C43B	C44B	1.62(3)
W3	O7	1.929(6)	C1	C2	1.489(13)
W3	O8	2.3337(4)	C2	C3	1.485(15)
W3	O10	1.939(6)	C3	C4	1.492(16)
W4	O13	1.933(6)	C5	C6	1.506(13)
W4	O15	1.931(7)	C6	C7	1.437(15)
W4	O16	1.718(6)	C7	C8	1.483(17)
W4	O17[2]	1.912(6)	C9	C10	1.499(13)
W4	O18	2.3224(4)	C10	C11	1.527(13)
W4	O20	1.921(6)	C11	C12	1.484(16)
W5	O11	1.719(7)	C13	C14	1.489(14)
W5	O12	1.938(7)	C14	C15	1.490(17)
W5	O13	1.938(6)	C15	C16	1.47(2)
W5	O18	2.3346(4)	C17	C18	1.509(15)
W5	O19	1.918(7)	C18	C19	1.496(16)
W5	O20[2]	1.926(6)	C19	C20	1.483(17)
W6	O12	1.933(6)	C21	C22	1.504(15)
W6	O14	1.717(7)	C22	C23	1.535(17)
W6	O15	1.937(6)	C23	C24	1.65(2)
W6	O17	1.933(6)	C25	C26	1.519(17)
W6	O18	2.3252(4)	C26	C27	1.50(2)
W6	O19[2]	1.939(6)	C27	C28B	1.43(4)
O7	W2[1]	1.935(6)	C27	C28A	1.40(3)
O8	W1[1]	2.3289(4)	C29	C30	1.497(14)
O8	W2[1]	2.3272(3)	C30	C31	1.523(14)
O8	W3[1]	2.3337(4)	C31	C32	1.499(16)
O9	W1[1]	1.935(5)	N3A	C37A	1.521(18)
O10	W1[1]	1.920(6)	N3A	C33A	1.55(2)
O17	W4[2]	1.912(6)	N3A	C45A	1.510(19)
O18	W4[2]	2.3224(4)	N3A	C41A	1.53(2)

O18	W5[2]	2.3346(4)	C37A	C38A	1.54(3)
O18	W6[2]	2.3252(4)	C38A	C39A	1.48(2)
O19	W6[2]	1.939(6)	C39A	C40A	1.49(2)
O20	W5[2]	1.926(6)	C33A	C34A	1.50(2)
N1	C1	1.514(12)	C34A	C35A	1.53(3)
N1	C5	1.516(12)	C35A	C36A	1.55(3)
N1	C9	1.536(11)	C45A	C46A	1.53(2)
N1	C13	1.524(12)	C46A	C47A	1.60(3)
N2	C17	1.481(13)	C47A	C48A	1.58(4)
N2	C21	1.514(13)	C41A	C42A	1.47(2)
N2	C25	1.499(14)	C42A	C43A	1.55(3)
N2	C29	1.532(12)	C43A	C44A	1.62(3)
N3B	C37B	1.51(2)			

Table A8.2(e). Bond Angles for $(TBA)_3[W_6O_{18}]$.

Atom	Atom	Atom	Angle/˚	Atom	Atom	Atom	Angle/˚
O1	W1	O2	104.1(3)	W2[1]	O8	W2	180.0
O1	W1	O3	103.7(3)	W2	O8	W3	90.044(13)
O1	W1	O8	179.7(2)	W2[1]	O8	W3	89.956(13)
O1	W1	O9[1]	103.3(3)	W2[1]	O8	W3[1]	90.044(13)
O1	W1	O10[1]	103.7(3)	W2	O8	W3[1]	89.956(13)
O2	W1	O3	87.1(2)	W3[1]	O8	W3	180.000(18)
O2	W1	O8	76.02(16)	W2	O9	W1[1]	116.8(3)
O2	W1	O9[1]	152.5(2)	W1[1]	O10	W3	117.2(3)
O3	W1	O8	75.97(17)	W6	O12	W5	117.1(3)
O9[1]	W1	O3	86.3(2)	W4	O13	W5	116.9(3)
O9[1]	W1	O8	76.52(16)	W4	O15	W6	116.6(3)
O10[1]	W1	O2	87.3(2)	W4[2]	O17	W6	117.2(3)
O10[1]	W1	O3	152.6(2)	W4[2]	O18	W4	180.0
O10[1]	W1	O8	76.65(16)	W4	O18	W5	90.186(15)
O10[1]	W1	O9[1]	86.4(2)	W4	O18	W5[2]	89.814(15)
O2	W2	O5	87.3(2)	W4[2]	O18	W5	89.814(15)
O2	W2	O7[1]	86.3(2)	W4[2]	O18	W5[2]	90.186(15)
O2	W2	O8	76.27(16)	W4[2]	O18	W6[2]	90.166(15)
O2	W2	O9	153.0(2)	W4	O18	W6	90.166(15)
O4	W2	O2	103.8(3)	W4[2]	O18	W6	89.834(15)
O4	W2	O5	103.4(3)	W4	O18	W6[2]	89.834(15)
O4	W2	O7[1]	103.7(3)	W5	O18	W5[2]	180.0
O4	W2	O8	179.8(3)	W6[2]	O18	W5	89.737(15)
O4	W2	O9	103.2(3)	W6	O18	W5	90.263(15)
O5	W2	O7[1]	152.9(2)	W6[2]	O18	W5[2]	90.263(16)

O5	W2	O8	76.35(16)	W6	O18	$W5^2$	89.737(16)
$O7^1$	W2	O8	76.55(16)	$W6^2$	O18	W6	180.0
O9	W2	O5	87.1(2)	W5	O19	$W6^2$	117.0(3)
O9	W2	$O7^1$	86.7(2)	W4	O20	$W5^2$	117.4(3)
O9	W2	O8	76.73(15)	C1	N1	C5	111.0(7)
O3	W3	O5	86.9(2)	C1	N1	C9	107.7(6)
O3	W3	O7	86.7(2)	C1	N1	C13	110.8(7)
O3	W3	O8	76.35(17)	C5	N1	C9	110.1(7)
O3	W3	O10	152.5(2)	C5	N1	C13	107.1(6)
O5	W3	O7	152.7(2)	C13	N1	C9	110.1(7)
O5	W3	O8	76.24(16)	C17	N2	C21	112.3(9)
O5	W3	O10	85.7(2)	C17	N2	C25	106.7(7)
O6	W3	O3	103.3(3)	C17	N2	C29	110.8(8)
O6	W3	O5	103.4(3)	C21	N2	C29	106.2(7)
O6	W3	O7	103.8(3)	C25	N2	C21	110.5(9)
O6	W3	O8	179.5(3)	C25	N2	C29	110.5(8)
O6	W3	O10	104.2(3)	C37B	N3B	C33B	110.9(17)
O7	W3	O8	76.51(17)	C37B	N3B	C41B	110.9(16)
O7	W3	O10	87.7(2)	C45B	N3B	C37B	105.3(14)
O10	W3	O8	76.19(16)	C45B	N3B	C33B	110.6(17)
O13	W4	O18	76.65(18)	C45B	N3B	C41B	110.1(18)
O15	W4	O13	87.2(3)	C41B	N3B	C33B	109.0(14)
O15	W4	O18	76.71(19)	N3B	C37B	C38B	116.5(17)
O16	W4	O13	102.9(3)	C39B	C38B	C37B	111.4(18)
O16	W4	O15	103.2(3)	C38B	C39B	C40B	112.7(19)
O16	W4	$O17^2$	103.3(3)	C34B	C33B	N3B	115.4(17)
O16	W4	O18	179.6(2)	C33B	C34B	C35B	107.9(18)
O16	W4	O20	103.9(3)	C34B	C35B	C36B	115(2)
$O17^2$	W4	O13	86.8(3)	N3B	C45B	C46B	115.0(18)
$O17^2$	W4	O15	153.4(3)	C45B	C46B	C47B	108.8(19)
$O17^2$	W4	O18	76.72(17)	C48B	C47B	C46B	114(3)
$O17^2$	W4	O20	87.0(3)	C42B	C41B	N3B	117.7(19)
O20	W4	O13	153.2(3)	C41B	C42B	C43B	109(2)
O20	W4	O15	86.7(3)	C42B	C43B	C44B	110(2)
O20	W4	O18	76.58(17)	C2	C1	N1	116.1(7)
O11	W5	O12	103.3(3)	C3	C2	C1	112.2(9)
O11	W5	O13	103.8(3)	C2	C3	C4	115.4(10)
O11	W5	O18	179.4(3)	C6	C5	N1	114.6(7)
O11	W5	O19	103.8(3)	C7	C6	C5	114.9(9)
O11	W5	$O20^2$	103.8(3)	C6	C7	C8	114.8(11)
O12	W5	O18	76.17(19)	C10	C9	N1	115.6(7)
O13	W5	O12	86.3(3)	C9	C10	C11	111.8(9)
O13	W5	O18	76.26(18)	C12	C11	C10	113.3(10)

O19	W5	O12	152.9(3)		C14	C13	N1	117.1(8)
O19	W5	O13	86.7(3)		C13	C14	C15	113.8(10)
O19	W5	O18	76.72(18)		C16	C15	C14	115.3(14)
O19	W5	O20[2]	87.7(3)		N2	C17	C18	117.9(8)
O20[2]	W5	O12	86.4(3)		C19	C18	C17	110.5(9)
O20[2]	W5	O13	152.4(3)		C20	C19	C18	113.3(10)
O20[2]	W5	O18	76.18(18)		C22	C21	N2	116.0(9)
O12	W6	O15	87.2(3)		C21	C22	C23	110.7(10)
O12	W6	O18	76.5(2)		C22	C23	C24	112.3(13)
O12	W6	O19[2]	153.1(3)		N2	C25	C26	118.0(10)
O14	W6	O12	103.2(3)		C27	C26	C25	111.0(12)
O14	W6	O15	102.4(3)		C28B	C27	C26	121(2)
O14	W6	O17	104.8(3)		C28A	C27	C26	106(2)
O14	W6	O18	178.9(2)		C30	C29	N2	116.3(8)
O14	W6	O19[2]	103.7(3)		C29	C30	C31	109.4(9)
O15	W6	O18	76.5(2)		C32	C31	C30	112.3(10)
O15	W6	O19[2]	86.7(3)		C37A	N3A	C33A	111.0(14)
O17	W6	O12	87.1(3)		C37A	N3A	C41A	110.2(13)
O17	W6	O15	152.8(3)		C45A	N3A	C37A	105.3(11)
O17	W6	O18	76.26(18)		C45A	N3A	C33A	110.8(14)
O17	W6	O19[2]	86.5(3)		C45A	N3A	C41A	110.6(15)
O19[2]	W6	O18	76.57(19)		C41A	N3A	C33A	109.0(11)
W2	O2	W1	117.6(3)		N3A	C37A	C38A	115.4(12)
W3	O3	W1	117.6(3)		C39A	C38A	C37A	112.1(14)
W3	O5	W2	117.4(3)		C38A	C39A	C40A	112.5(14)
W3	O7	W2[1]	117.0(3)		C34A	C33A	N3A	115.8(13)
W1	O8	W1[1]	180.0		C33A	C34A	C35A	108.7(15)
W1	O8	W3	90.091(13)		C34A	C35A	C36A	115.0(18)
W1[1]	O8	W3[1]	90.091(13)		N3A	C45A	C46A	114.6(14)
W1[1]	O8	W3	89.909(13)		C45A	C46A	C47A	110.0(16)
W1	O8	W3[1]	89.909(13)		C48A	C47A	C46A	114(2)
W2[1]	O8	W1	89.906(13)		C42A	C41A	N3A	117.1(14)
W2[1]	O8	W1[1]	90.094(13)		C41A	C42A	C43A	108.5(16)
W2	O8	W1[1]	89.906(13)		C42A	C43A	C44A	109(2)
W2	O8	W1	90.094(13)					

[1]-X,1-Y,1-Z; [2]1-X,1-Y,1-Z

Table A8.2(f). Torsion Angles for $(TBA)_3[W_6O_{18}]$.

A	B	C	D	Angle/˚	A	B	C	D	Angle/˚
N1	C1	C2	C3	174.8(10)	C13	N1	C5	C6	-179.0(8)

N1	C5	C6	C7	170.9(10)	C13	N1	C9	C10	64.2(11)
N1	C9	C10	C11	-147.8(9)	C13	C14	C15	C16	175.8(14)
N1	C13	C14	C15	-177.1(10)	C17	N2	C21	C22	-59.9(14)
N2	C17	C18	C19	177.7(9)	C17	N2	C25	C26	179.5(10)
N2	C21	C22	C23	-169.4(12)	C17	N2	C29	C30	61.0(13)
N2	C25	C26	C27	-175.4(12)	C17	C18	C19	C20	177.2(11)
N2	C29	C30	C31	-170.4(10)	C21	N2	C17	C18	-66.1(11)
N3B	C37B	C38B	C39B	178(6)	C21	N2	C25	C26	57.3(13)
N3B	C33B	C34B	C35B	-176(5)	C21	N2	C29	C30	-176.9(11)
N3B	C45B	C46B	C47B	178(4)	C21	C22	C23	C24	71.3(17)
N3B	C41B	C42B	C43B	173(4)	C25	N2	C17	C18	172.7(9)
C37B	N3B	C33B	C34B	69(5)	C25	N2	C21	C22	59.0(14)
C37B	N3B	C45B	C46B	177(5)	C25	N2	C29	C30	-57.0(13)
C37B	N3B	C41B	C42B	-55(5)	C25	C26	C27	C28B	170(2)
C37B	C38B	C39B	C40B	174(7)	C25	C26	C27	C28A	82(2)
C33B	N3B	C37B	C38B	74(7)	C29	N2	C17	C18	52.4(12)
C33B	N3B	C45B	C46B	-63(5)	C29	N2	C21	C22	178.9(12)
C33B	N3B	C41B	C42B	-177(5)	C29	N2	C25	C26	-59.9(13)
C33B	C34B	C35B	C36B	-173(8)	C29	C30	C31	C32	-175.1(11)
C45B	N3B	C37B	C38B	-166(7)	N3A	C37A	C38A	C39A	-172(3)
C45B	N3B	C33B	C34B	-47(6)	N3A	C33A	C34A	C35A	-177(3)
C45B	N3B	C41B	C42B	61(5)	N3A	C45A	C46A	C47A	-173(3)
C45B	C46B	C47B	C48B	161(6)	N3A	C41A	C42A	C43A	170(3)
C41B	N3B	C37B	C38B	-47(7)	C37A	N3A	C33A	C34A	55(3)
C41B	N3B	C33B	C34B	-169(5)	C37A	N3A	C45A	C46A	-177(3)
C41B	N3B	C45B	C46B	57(5)	C37A	N3A	C41A	C42A	-55(3)
C41B	C42B	C43B	C44B	-174(7)	C37A	C38A	C39A	C40A	-165(4)
C1	N1	C5	C6	59.9(10)	C33A	N3A	C37A	C38A	62(4)
C1	N1	C9	C10	-174.9(9)	C33A	N3A	C45A	C46A	-57(3)
C1	N1	C13	C14	-57.2(11)	C33A	N3A	C41A	C42A	-177(3)
C1	C2	C3	C4	-179.6(12)	C33A	C34A	C35A	C36A	179(4)
C5	N1	C1	C2	61.6(11)	C45A	N3A	C37A	C38A	-178(4)
C5	N1	C9	C10	-53.6(11)	C45A	N3A	C33A	C34A	-62(3)
C5	N1	C13	C14	-178.5(9)	C45A	N3A	C41A	C42A	61(3)
C5	C6	C7	C8	-172.7(11)	C45A	C46A	C47A	C48A	72(4)
C9	N1	C1	C2	-177.8(9)	C41A	N3A	C37A	C38A	-59(4)
C9	N1	C5	C6	-59.3(10)	C41A	N3A	C33A	C34A	176(3)
C9	N1	C13	C14	61.8(11)	C41A	N3A	C45A	C46A	64(3)
C9	C10	C11	C12	-176.3(10)	C41A	C42A	C43A	C44A	-178(4)
C13	N1	C1	C2	-57.3(11)					

Table A8.2(g). Hydrogen Atom Coordinates (Å×10^4) and Isotropic Displacement Parameters (Å^2×10^3) for (TBA)$_3$[W$_6$O$_{18}$].

Atom	*x*	*y*	*z*	U(eq)
H37A	3507	6690	2542	89
H37B	4087	6223	2681	89
H38A	3339	6242	1181	85
H38B	3930	5795	1297	85
H39A	3055	5431	2207	79
H39B	3629	4953	2233	79
H40A	2909	4289	1440	120
H40B	2793	5040	862	120
H40C	3367	4563	888	120
H33A	3932	8277	1388	93
H33B	3485	7592	1158	93
H34A	3550	8550	2574	123
H34B	3120	7829	2396	123
H35A	2685	8437	1202	124
H35B	3145	9118	1283	124
H36A	2298	9611	1652	190
H36B	2310	8957	2346	190
H36C	2771	9640	2426	190
H45A	4658	7161	3128	100
H45B	4130	7715	3188	100
H46A	4553	8728	2481	149
H46B	5088	8172	2451	149
H47A	4745	8877	3902	162
H47B	5148	8126	4000	162
H48A	5698	9299	4235	228
H48B	5861	8865	3448	228
H48C	5458	9617	3350	228
H41A	4366	6866	969	91
H41B	4770	7535	1390	91
H42A	4804	5963	1937	110
H42B	5240	6643	2259	110
H43A	5555	6731	968	137
H43B	5082	6124	585	137
H44A	5975	5418	906	252
H44B	6010	5675	1837	252
H44C	5538	5070	1454	252
H1A	1283	7358	3439	44
H1B	755	6882	3004	44
H2A	865	7425	1764	49
H2B	1362	7975	2182	49

H3A	1407	6311	2134	92
H3B	1903	6857	2557	92
H4A	1535	6802	867	109
H4B	2108	6437	1314	109
H4C	2021	7370	1284	109
H5A	-180	8525	2722	40
H5B	167	8199	2042	40
H6A	-82	6922	2283	51
H6B	-355	7180	3063	51
H7A	-771	7515	1452	90
H7B	-1025	7885	2204	90
H8A	-1004	6250	1900	113
H8B	-1539	6797	1637	113
H8C	-1312	6668	2578	113
H9A	268	7333	4050	45
H9B	764	7894	4445	45
H10A	-383	8211	4162	55
H10B	20	8940	4052	55
H11A	102	8022	5509	66
H11B	470	8787	5395	66
H12A	-354	9551	5262	95
H12B	-233	9129	6128	95
H12C	-698	8781	5441	95
H13A	940	8942	2633	44
H13B	605	9245	3334	44
H14A	1681	8551	3589	70
H14B	1342	8809	4306	70
H15A	1735	9847	3180	88
H15B	1360	10124	3847	88
H16A	2286	10416	4262	201
H16B	2075	9785	4866	201
H16C	2451	9508	4198	201
H17A	2879	5052	3733	52
H17B	3081	4984	4683	52
H18A	2122	5841	3972	62
H18B	2303	5754	4932	62
H19A	3148	6401	4838	70
H19B	2992	6459	3874	70
H20A	2275	7323	4007	128
H20B	2838	7650	4523	128
H20C	2375	7223	4972	128
H21A	2033	4529	5273	65
H21B	2059	3607	5097	65

H22A	2941	4540	5912	87
H22B	3046	3660	5622	87
H23A	2239	4009	6690	107
H23B	2868	3761	7030	107
H24A	2082	2697	6032	185
H24B	2261	2583	6987	185
H24C	2710	2450	6378	185
H25A	3154	3643	4404	62
H25B	2881	3766	3484	62
H26A	2465	2658	4541	94
H26B	2237	2757	3596	94
H27A	3065	2329	3235	117
H27B	3364	2359	4148	117
H27C	2829	1732	3582	117
H27D	3223	2455	3394	117
H29A	1669	3814	3774	58
H29B	1648	4744	3901	58
H30A	2076	3958	2614	61
H30B	2168	4883	2774	61
H31A	1079	4169	2494	72
H31B	1192	5095	2582	72
H32A	967	4822	1221	112
H32B	1431	4143	1270	112
H32C	1618	5045	1372	112
H28A	2928	1261	4449	166
H28B	3229	1115	3664	166
H28C	2566	1248	3567	166
H28D	3572	2555	4702	166
H28E	3625	1655	4439	166
H28F	3138	1915	4947	166
H37C	3773	6677	2765	89
H37D	4275	6114	2600	89
H38C	3345	6447	1374	85
H38D	3822	5807	1299	85
H39C	2966	5720	2291	79
H39D	3502	5158	2449	79
H40D	2770	4511	1659	120
H40E	2742	5190	989	120
H40F	3279	4628	1147	120
H33C	4103	8296	1540	93
H33D	3667	7632	1191	93
H34C	3694	8373	2728	123
H34D	3270	7674	2416	123

H35C	2893	8463	1280	124
H35D	3310	9160	1602	124
H36D	2401	9435	1919	190
H36E	2404	8633	2422	190
H36F	2822	9331	2744	190
H45C	4940	7074	2996	100
H45D	4438	7608	3219	100
H46C	4748	8684	2520	149
H46D	5215	8152	2184	149
H47C	5580	8977	3393	162
H47D	5236	8421	3919	162
H48D	6199	8017	4091	228
H48E	5820	7320	3662	228
H48F	6165	7877	3135	228
H41C	4395	6774	912	91
H41D	4863	7402	1242	91
H42C	4872	5849	1842	110
H42D	5368	6481	2019	110
H43C	5485	6479	609	137
H43D	4979	5866	417	137
H44D	5871	5144	552	252
H44E	6033	5481	1452	252
H44F	5528	4869	1260	252

Table A8.2(h). Atomic Occupancy for $(TBA)_3[W_6O_{18}]$.

Atom	***Occupancy***	**Atom**	***Occupancy***	**Atom**	***Occupancy***
N3B	0.359	C37B	0.359	H37A	0.359
H37B	0.359	C38B	0.359	H38A	0.359
H38B	0.359	C39B	0.359	H39A	0.359
H39B	0.359	C40B	0.359	H40A	0.359
H40B	0.359	H40C	0.359	C33B	0.359
H33A	0.359	H33B	0.359	C34B	0.359
H34A	0.359	H34B	0.359	C35B	0.359
H35A	0.359	H35B	0.359	C36B	0.359
H36A	0.359	H36B	0.359	H36C	0.359
C45B	0.359	H45A	0.359	H45B	0.359
C46B	0.359	H46A	0.359	H46B	0.359
C47B	0.359	H47A	0.359	H47B	0.359
C48B	0.359	H48A	0.359	H48B	0.359
H48C	0.359	C41B	0.359	H41A	0.359
H41B	0.359	C42B	0.359	H42A	0.359

H42B 0.359	C43B 0.359	H43A	0.359
H43B 0.359	C44B 0.359	H44A	0.359
H44B 0.359	H44C 0.359	H27A	0.4725
H27B 0.4725	H27C 0.5275	H27D	0.5275
C28B 0.4725	H28A 0.4725	H28B	0.4725
H28C 0.4725	C28A 0.5275	H28D	0.5275
H28E 0.5275	H28F 0.5275	N3A	0.641
C37A 0.641	H37C 0.641	H37D	0.641
C38A 0.641	H38C 0.641	H38D	0.641
C39A 0.641	H39C 0.641	H39D	0.641
C40A 0.641	H40D 0.641	H40E	0.641
H40F 0.641	C33A 0.641	H33C	0.641
H33D 0.641	C34A 0.641	H34C	0.641
H34D 0.641	C35A 0.641	H35C	0.641
H35D 0.641	C36A 0.641	H36D	0.641
H36E 0.641	H36F 0.641	C45A	0.641
H45C 0.641	H45D 0.641	C46A	0.641
H46C 0.641	H46D 0.641	C47A	0.641
H47C 0.641	H47D 0.641	C48A	0.641
H48D 0.641	H48E 0.641	H48F	0.641
C41A 0.641	H41C 0.641	H41D	0.641
C42A 0.641	H42C 0.641	H42D	0.641
C43A 0.641	H43C 0.641	H43D	0.641
C44A 0.641	H44D 0.641	H44E	0.641
H44F 0.641			

Table A10.1. Solvent and drying agents.

Solvent	**Pre-drying agent**	**Distilled from**
Acetonitrile, dichloromethane (DCM) and chloroform	Calcium hydride	Calcium hydride
Diethyl ether	Sodium wire	Benzophenone/ sodium wire
Toluene, tetrahydrofuran (THF) and hexane	Sodium wire	9-fluorenone/ sodium wire
Methanol and ethanol	3A molecular sieves	magnesium methoxide
Dimethylsulphoxide (DMSO)	3A molecular sieves	-

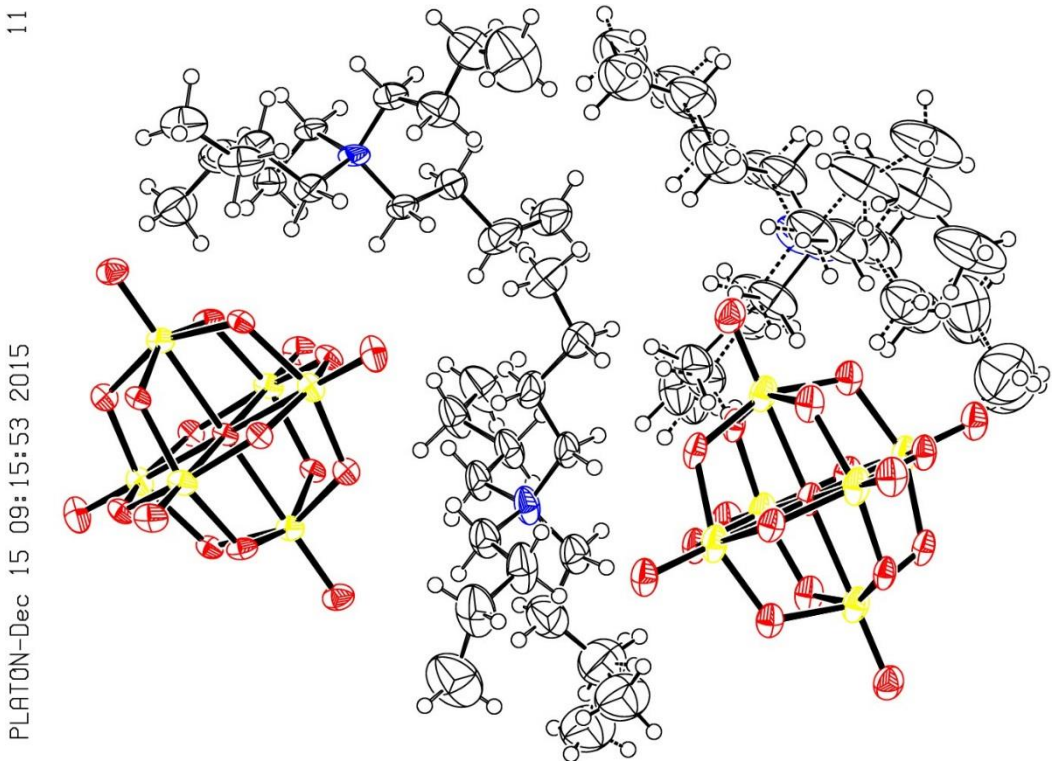

Figure A8.2. ORTEP structural diagram for $(TBA)_3[W_6O_{18}]$

Table A10.2. List of Reagents and Suppliers.

Reagents	Formula	Purity	Grade	Supplier
Absolute ethanol	CH_3CH_2OH	-	AR	Fischer Scientific
Acetone	CH_3COCH_3	-	GPR	Fischer Scientific
Industrial Methylated Spirit (IMS)	CH_3CH_2OH	-	GPR	Fischer Scientific
Acetonitrile (MeCN)	CH_3CN	99.8%	-	Acros Organic.
Tetrabutyl ammonium perchlorate	$[CH_3(CH_2)_3]_4N(ClO_4)$	-	-	Fluka Chemika
Glassy carbon rod (3mm diameter)	-	-	-	Mersen
Fomlin (Perfluoropolyether)YR -1800	-	-	-	Alfa Aesar
Phosphotungstic acid hydrate	$H_3PW_{12}O_{40}.xH_2O$	-	RG	Sigma-Aldrich
Sodium chloride	NaCl	-	ACSR	EMD Millipore Corp.
Tetrabutylammonium hydroxide 1 M in Methanol	$[CH_3(CH_2)_3]_4NOH$	-		Sigma-Aldrich
Diethyl ether	$(CH_3CH_2)_2O$		AR	Fischer Scientific
Tin (IV) chloride	$SnCl_4$	98%	LR	BDH Chemicals

Dichloromethane (DCM)	CH_2Cl_2	-	LR	Fischer Scientific
Sodium metal sticks in liquid paraffin	Na	-	SLR	Fischer Scientific
N, N'-Dicyclohexylcarbodiimide (DCC)	$C_6H_{11}N=C=NC_6H_{11}$	99 %	LR	Sigma-Aldrich
Tetrahydrofuran (THF)	C_4H_8O	-	LR	Fischer Scientific
4-tert-Butylphenol	$(CH_3)_3CC_6H_4OH$	≥99 %	-	Aldrich
Toluene	$C_6H_5CH_3$	99.8%	-	Sigma
Ethyl acetate	$CH_3COOC_2H_5$		LR	Fischer Scientific
3, 5-dimethylphenol	$(CH_3)_2C_6H_3OH$	≥99 %	-	Aldrich
2, 4, 6-tri-tert-butylphenol	$[(CH_3)_3C]_3C_6H_2OH$	98%	-	Aldrich
Hydrazine monohydrochloride	$H_2NNH_2.HCl$	97%	-	Aldrich
Methanol	CH_3OH	-	LR	Fischer Scientific
Titanium (IV) chloride	$TiCl_4$	99.99%		Acros Organics
Dimethyl sulfoxide	$(CH_3)_2SO$	≥99.5%	LR	Sigma-Aldrich
3A molecular sieves, pellets, 1.6 mm	-	-	-	Sigma-Aldrich (Fluka)
Tin(II) chloride	$SnCl_2$	99%		Aldrich
Lead acetate trihydrate	$Pb(CH_3COO)_{2.}3H_2O$	99+ %	ACSR	Aldrich
Bismuth (III) chloride	$BiCl_3$	-	-	Strem Chemicals
Antimony (III) chloride	$SbCl_3$	≥99.9%		Aldrich
Cobalt (II) hexaaqua trioxonitrate (V)	$[Co(H_2O)_6](NO_3)_2$	-	-	
Acetic acid (Glacial)	CH_3COOH	≥99.79	ACSR	Sigma-Adrich
Tetrabutylammonium tribromide	$TBABr_3$	98%	-	Aldrich
Styrene oxide		97+ %	-	Acros Organics
Nickel (II) bromide trihydrate	$NiBr_2.3H_2O$	≥98 %	-	Aldrich
Ammonium cerium (IV) nitriate	$(NH_4)_2[Ce(NO_3)_6]$	≥ 99.9%		Aldrich
Sodium hexachloroirridate (IV)	$Na_2IrCl_6.xH_2O$			Johnson Matthey
Irridium (III) chloride	$IrCl_3$	55.83%		Johnson Matthey
Rhodium (III) chloride	$RhCl_3$	41.61%		Johnson Matthey
Sodium hexachloroplatinate (IV)	Na_2PtCl_6	37.21%		Johnson Matthey
Potassium hexahydroxyl palatinate (IV)	$K_2Pt(OH)_6$	51.37%		Johnson Matthey
Tetrafluoroboric acid diethyl ether complex	$HBF_4.Et_2O$	-		Aldrich

Deionized water	H_2O			
^{17}O-enriched water	$H_2{}^{17}O$	10 %		Goss Scientific
Silver tetrafluoroborate	$AgBF_4$	98%		Sigma-Aldrich
Iron (II) chloride	$FeCl_2$	98%		Aldrich
Dimethyl tin dichloride	$(CH_3)_2SnCl_2$	-	-	Lancaster Synthesis
Chloroform	$CHCl_3$	≥99%	RG	Sigma-Aldrich
Sodium hydroxide	NaOH	≥98%	RG	Sigma-Aldrich
Hydrochloric acid	HCl	35%	ACSR	Sigma-Aldrich
Bromine	Br_2	≥99.5%	AR	BDH Chemicals
Iodine	I_2	≥99.8%	ACSR	Sigma-Aldrich
I-bromobutane	$CH_3(CH_{2)2}Br$	-	-	BDH Chemicals
p-tolyl isocyanate	$CH_3C_6H_4NCO$	-	-	Acros Organics
D-lactide				
Molybdenum hexacarbonyl	$Mo(CO)_6$	98%	-	Aldrich
Tetrabutylammoniun chloride	$[CH_3(CH_2)_3]_4NCl$	≥ 97.5%	-	Aldrich
Sodium borohydride	$NaBH_4$		-	Avocado
Cobalt (II) chloride	$CoCl_2$	≥98%	-	Aldrich
Lead (II) chloride	$PbCl_2$	98%	-	Aldrich
Copper (II) chloride	$CuCl_2$	99.99%	-	Aldrich
Nickel (II) chloride	$NiCl_2$	98%	-	Aldrich
Tetrabutylammonium bromide	$[CH_3(CH_2)_3]_4NBr$	99+%	-	Acros Organics
Tellurium (IV) chloride	$TeCl_4$	99%	-	Aldrich

AR- Analytical reagent; LR – Laboratory reagent; SLR – Standard laboratory reagent; ACSR – American Chemical Society reagent grade; RG – Reagent grade

Table A10.3. NMR frequencies and pulse width.

Nuclei	Bruker Avance Spectrometer	Frequency (MHz)	Pulse width (µs) (90° flip angle)	Relaxation delay (s)	Number of Scans
^1H	7.05 T 300 MHz	300.132	13.25	30	1 – 8
	9.40 T 400 MHz	399.78	6.3		
	11.75 T 500 MHz	500.15	10.00		
^{13}C	7.05 T 300 MHz				
	16.44 T 700 MHz	176.07	12.00	1	
^{17}O	9.40 T 400 MHz	54.20	10.00	0.0010	10240 - 50000
	11.75 T 500 MHz	67.84	14.00		
^{31}P	7.05 T 300 MHz	121.49	10.40	20	1 - 32
	9.40 T 400 MHz	161.83	9.10		
^{119}Sn	7.05 T 300 MHz	111.89	11.00	8	1024 – 5000

	9.40 T 400 MHz	149.04	9.80		
	11.75 T 500 MHz	186.40	12.00		
^{183}W	11.75 T 500 MHz	20.84	30.00	3	
^{195}Pt	9.40 T 400 MHz	85.94	9.00	0.05	17974
^{207}Pb	11.75 T 500 MHz	104.58	12.00	0.0010	1568643

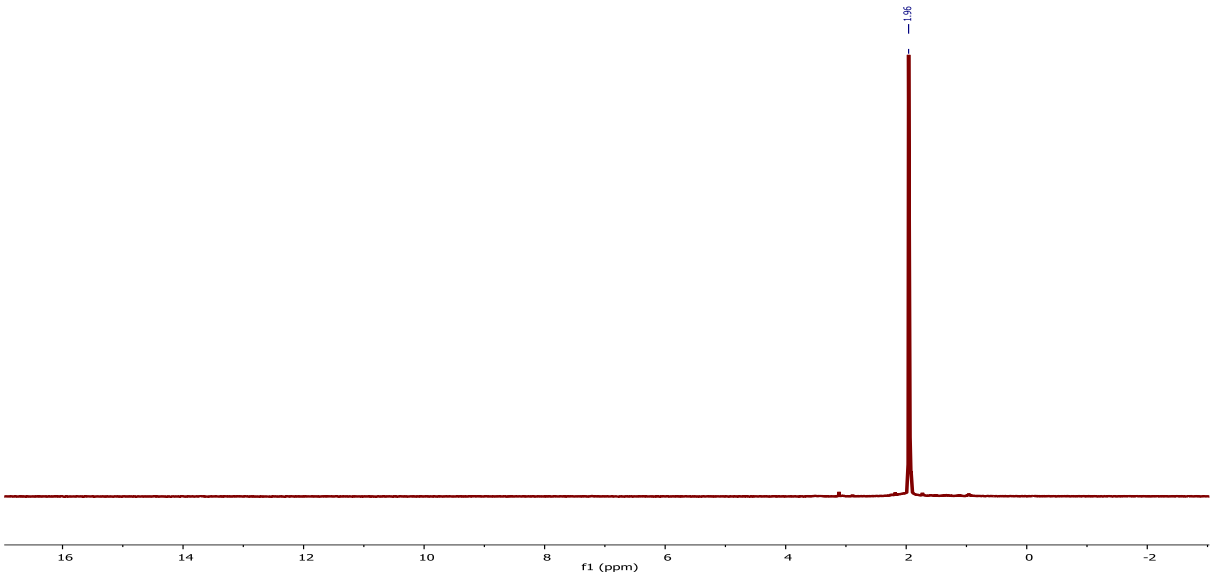

Figure A10.1. ^{1}H NMR spectrum of $[Mo_2(NCCH_3)_8(ax\text{-}CH_3CN)_{0.5}][BF_4]_4$.

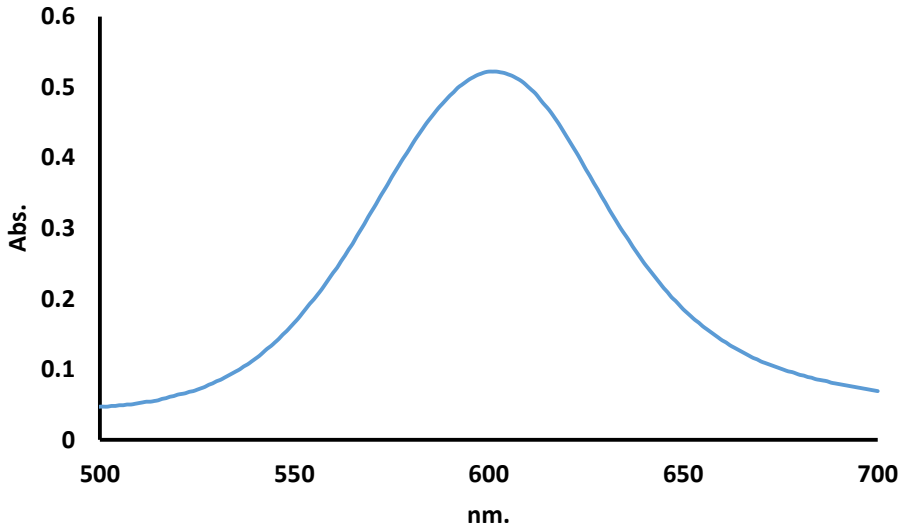

Figure A10.2. UV-Vis spectrum of $[Mo_2(NCCH_3)_8(ax\text{-}CH_3CN)_{0.5}][BF_4]_4$.

CURRICULUM VITAE

PERSONAL DATA

SURNAME:	Izuagie
FIRST NAME:	Thompson
PLACE AND DATE OF BIRTH:	Kano/8th September, 1983
SEX:	Male
NATIONALITY:	Nigerian
HOBBIES:	Reading, Travelling and Swimming
E-mail:	tomyi2012@yahoo.com, t.izuagie@newcastle.ac.uk
CURRENT CONTACT ADDRESS:	Room 1.30, First Floor, Bedson Building, School of Chemistry, Newcastle University upon Tyne NE1 7RU, UK.
PERMANENT CONTACT ADD.:	Department of Chemistry, Sokoto State University, P. M. B. 2134, Sokoto, Sokoto State, Nigeria.

EDUCATION HISTORY (Name of Schools with dates)

- Newcastle University, Newcastle Upon Tyne, UK — 2013 to date
- Newcastle University, Newcastle Upon Tyne, UK — 2014 to 2016
- Usmanu Danfodiyo University, Sokoto — 2010 – 2012
- Usmanu Danfodiyo University, Sokoto — 2003 – 2007

ACADEMIC QUALIFICATIONS WITH DATES:

- PhD Chemistry (FT) — In View
- PG Cert. in Adv. Stud. in Aca. Practice (CASAP) — 2016
- M.Sc. in Applied Chemistry — 2012
- B.Sc. Hons. Chemistry (**2nd Class Upper Division**) — 2007

TEACHING EXPERIENCE:

Designation	Institution	Nature of Duty	Dates
Student demonstrator	Newcastle University, UK	Teaching	2014 to 2017
Lecturer II	Sokoto State University, Sokoto	Teaching& Research	2013 till date
Lecturer II	The Polytechnic of Sokoto State	Teaching& Research	2012 to 2013
Lecturer III	The Polytechnic of Sokoto State	Teaching& Research	2009 to 2012
NYSC : Part time (Subject Teacher)	Department for Higher Education, Sokoto State Extra-Mural Classes Programme	Teaching	2009 to 2010
Computer Instructor	Niceday Computer Academy	Teaching	2002 – 2006

SPECIAL SKILLS ACQUIRED FROM WORKSHOPS/TRAININGS

I. Handling and Manipulation of Air-sensitive compounds
II. Synthesis of Polyoxometalates and other Metalo-organic compounds.
III. Experience with standard characterization techniques including FT-IR, ESI-MS, CV, UV-Vis, XRD and Multinuclear NMR Spectroscopy
IV. The Use of ChemDraw, MestReNova, Opus, Varian, Crystal maker, Olex2 and other data manipulation software
V. Electrochemical and electrocatalytic skills
VI. Adsorption and Characterization of nanoporous materials
VII. Making of Nano and 2D Materials
VIII. Flow Chemistry Techniques
IX. Effective Research Proposal and Scientific Writing Skills for Publication
X. Skills on Science Outreach
XI. Webpage design

MEMBERSHIP OF PROFESSIONAL ORGANIZATIONS

i.	D2 Fellow UK Higher Education Academy (FHEA)	2016
ii.	Member Royal Society of Chemistry (MRSC)	2014
iii.	Member American Chemical Society (MACS)	2014
iv.	Member Chemical Society of Nigeria (MCSN)	2010
v.	Member Institute of Chartered Chemists of Nigeria (MICCON)	2010
vi.	Member Science Association of Nigeria (MSAN)	2010

COMMUNITY SERVICE

- **Peer Mentor** – MSc Students, School of Chemistry, Newcastle University, Newcastle upon Tyne, UK. – 2015.

PUBLICATIONS

i. R. John Errington, **Thompson Izuagie**, Paul G. Waddell, *CSD Communication*, 2015: 10.5517/cc1jn89r.
ii. R. John Errington, Balamurugan Kandasamy, Daniel Lebbie and **Thompson Izuagie** (2017). Alkoxido-Derivatised Lindqvist and Keggin Type Polyoxometalates. In: *Structure and Bonding*. Springer, Berlin, Heidelberg.
iii. Daniel Lebbie, Balamurugan Kandasamy, **Thompson Izuagie**, Magda Pascual-Borras, Corinne Wills, Josep M. Poblet and R. John Errington (2017). Mechanistic aspects of alcoholysis, hydrolysis and condensation of alkoxido-derivatised polyoxometalates: comparative reactivities of Lindqvist-type {MW5} and Keggin-type {MPW11} anions (M = Ti, Sn). *In Preparation*.
iv. **Thompson Izuagie** and R. John Errington (2017). Non-aqueous substitution into $[NaPW_{11}O_{39}]^{6-}$: a suitable route to ^{17}O-enriched monosubstituted heterometallic Keggin POMs for systematic protonolysis studies. *In Preparation*.

PRESENTATIONS AT CONFERENCES/WORKSHOPS/SEMINARS/SYMPOSIA:

i. **T. Izuagie,** I. M. Mbomekalle, P. de Oliveira and R. J. Errington (2016). Non-aqueous synthesis and electrochemical behaviour of post-transition metal substituted Keggin Polyoxotungstates. A poster presented at the 4th FMOCS-PoCheMoN – Frontiers in Metal Oxide Clusters Science Symposium joined to the Polyoxometalates Chemistry for Molecular Nanoscience COST Action 1203 Annual meeting, held in Newcastle, UK, July, 10th to 14th, 2016.

ii. **Thompson Izuagie** and R. John Errington (2016). Non-aqueous strategy to a range of tin-substituted polyoxotungstates. A Poster presented at Dalton 2016 Conference, held on 29th to 31st March, 2016 at the University of Warwick, UK.

iii. **Thompson Izuagie,** Kate Phipps and R. John Errington (2015). Rational studies on heavier group-14 mono-substituted keggin polyoxometalates: insights into redox properties and ligand metathesis. A Poster presented at the 1st Chemistry in Energy (1st CEC) Conference, held on 20th to 22nd July, 2015 at Edinburgh Conference Centre, Heriot Watt University, Edinburgh, Scotland.

iv. **Thompson Izuagie** and R. John Errington (2015). Systematic chemistry on a range of tin-substituted Keggin Polyoxometalates. An oral presentation at the Universities of Scotland Inorganic Chemistry Conference (USIC 2015), held on 2nd to 3rd July, 2015 at the Institute of Chemical Sciences, Heriot Watt University, Edinburgh, Scotland.

v. **Thompson Izuagie** (2015). Targeted non-aqueous approach to a range of substituted monolacunary Keggin polyoxotungstates. An oral talk at the PG Short Talks, held on 6th March, 2015 at Faraday Room, School of Chemistry, Bedson Building, Newcastle University, Newcastle upon Tyne, UK.

vi. **Thompson Izuagie**, Rebecca Gould and R. J. Errington (2014). Non-aqueous Studies of Substitution into $[NaPW_{11}O_{39}]^{6-}$. A poster presented at the 3rd FMOCS-PoCheMoN – Frontiers in Metal Oxide Clusters Science Symposium joined to the Polyoxometalates Chemistry for Molecular Nanoscience COST Action 1203 Annual meeting, held in Maffliers, France, July, 12th to 15th, 2014.

CONFERENCES/WORKSHOPS/SEMINARS/SYMPOSIA/SCHOOLS ATTENDED

I. **Participant/Member Local Organising Committee** – 4th FMOCS-PoCheMoN – Frontiers in Metal Oxide Clusters Science Symposium joined to the Polyoxometalates Chemistry for Molecular Nanoscience COST Action CM1203 Annual meeting, held in Newcastle, UK, July, 10th to 14th, 2016.

II. **COST-Action CM1203 STSM Visit** to the Electrochemistry and Photoelectrochemistry Group of Prof. Pedro de Oliveira and Dr. Israel Mbomekalle, Universite Paris-Sud, Orsay Cedex, France.

III. **Participant** – Dalton 2016 Conference, held on 29th to 31st March, 2016 at the University of Warwick, UK.

IV. **Participant** – 1st Chemistry in Energy (1st CEC) Conference, held on 20th to 22nd July, 2015 at Edinburgh Conference Centre, Heriot Watt University, Edinburgh, Scotland.

V. **Participant** – Universities of Scotland Inorganic Chemistry Conference (USIC 2015), held on 2nd to 3rd July, 2015 at Institute of Chemical sciences, Heriot Watt University, Edinburgh, Scotland.

VI. **Participant** – Royal Society of Chemistry early evening symposium: on Analytical Science in Art held at Northumbria University, Newcastle upon Tyne, UK on Thursday, 14th May, 2015.

VII. **Participant** – 5th Annual Chemical Nanoscience Symposium, held at School of Chemistry, Bedson Building, Newcastle University, Newcastle upon Tyne, UK on 26th March, 2015.

VIII. **Participant** – RSC North East Regional Meeting 2015, held at the Biscuit Factory, Newcastle upon Tyne, UK on 22th January, 2015.

IX. **Participant** – VII European School on Molecular Nanoscience (ESMoINa2014), in Gandia, Span, 26th to 31st October, 2014.

X. **Participant** – 4th Northern Sustainable Chemistry (NORSC) PG Symposium, held at the University of Huddersfield, UK, 23rd October, 2014.

XI. **Participant** – Northern Universities Postgraduate Symposium 2014, held at the University of Sheffield, UK, 12th September, 2014.

XII. **Participant** – Universities of Scotland Inorganic Conference 2014, held at Sir Charles Wilson Building, University Avenue, University of Glasgow, UK, 4th and 5th September, 2014.

XIII. **Participant** – 3rd FMOCS-PoCheMoN – Frontiers in Metal Oxide Clusters Science Symposium joined to the Polyoxometalates Chemistry for Molecular Nanoscience COST Action CM1203 Annual meeting, held in Maffliers, France, July, 12th to 15th, 2014.

XIV. **Participant** – 4th Annual Chemical Nanoscience Symposium, held at Research Beehive, Newcastle University, Newcastle upon Tyne, UK on 2th April, 2014.

XV. **Participant** – Advanced Training Workshop on Flow Chemistry, held at the Faraday Room, Bedson Building, Newcastle University upon Tyne, UK on 27th March, 2014.

XVI. **Participant** – Scottish Dalton Meeting held on 19th March, 2014 at the School of Chemistry, University of St. Andrews, Scotland, UK.

XVII. **Participant** – Advanced Training Workshop on Anerobic Technics, held at the Faraday Room, Bedson Building, Newcastle University upon Tyne, UK on 3rd March, 2014.

XVIII. **Participant** – The 34th Annual General Meeting of the RSC Newcastle and North East Coast Local Section, tagged: Chemistry of Beer Production on Thursday, 27th February, 2014 at Northumbria University, Newcastle, UK.

XIX. **Participant** – Workshop on Reaxys held at Hope Cluster (Room 161), Robinson Library, Newcastle University upon Tyne, UK on 26th February, 2014.

XX. **Participant** – Workshop on Scifinder, held at Hope PC Cluster, Level 1, Robinson Library, Newcastle University upon Tyne, UK on 12th February, 2014.

XXI. **Participant** – Workshop on Science Outreach, held at Culture Lab, Newcastle University upon Tyne, UK on 30th January, 2014.

XXII. **Participant** – A one-day Metrohm Seminar organised by Metrohm, UK Ltd on Wednesday, 15th January, 2014 at Northumbria University, Newcastle, UK.

XXIII. **Participant** – Seminar Being a Specialist in a Complex World, held at Room 1.03, 1st Floor, Armstrong Building, Newcastle University upon Tyne, UK on 19th November, 2013.